C

Cadmium

Monica Vasiliu and David A. Dixon
Department of Chemistry, University of Alabama,
Tuscaloosa, AL, USA

Element Data
Atomic Symbol: Cd
Atomic Number: 48
Atomic Weight: 112.411
Isotopes and Abundances: ^{106}Cd 1.25%, ^{108}Cd 0.89%, ^{110}Cd 12.51%, ^{111}Cd 12.81%, ^{112}Cd 24.13%, ^{113}Cd 12.22%, ^{114}Cd 28.72%, ^{116}Cd 7.47%
1 Atm Melting Point: 594.1 K
1 Atm Boiling Point: 1038 K
Common Valences: +2, +1
Ionic Radii: (+II) 103 ppm, (+I) 114 ppm
Pauling Electronegativity: 1.69
First Ionization Energy: 867.8 kJ/mol
Chondritic (CI) Abundance: 686 ppb
Silicate Earth Abundance: 0.04 ppm
Crustal Abundance: 0.11 ppm
Seawater Abundance: 0.11 ppb
Core Abundance: 0.15 ppm

Properties

Cadmium (Emsley 1991, 2001; Anthoni 2006; Anders and Grevesse 1989; McDonough 2005) is a lustrous, silvery-white metal with a bluish tinge on the surface and tarnishes in air. It is very ductile and malleable and is soft enough to be cut with a knife. Cadmium is soluble in acids but not in alkaline solutions. In many ways, cadmium is similar to zinc but forms more complex compounds.

Cadmium was not considered to be radioactive until 1970 when, as a surprise, ^{113}Cd was shown to be an α-emitter with a very long half-life (9×10^{15} years). The consequence of this radioactivity is negligible as only one atom is lost per minute in a 10 g piece of cadmium metal.

History and Use

At the beginning of the 1800s, apothecaries made zinc oxide by heating a naturally occurring form of zinc carbonate called cadmia, also named calamine. Sometimes the resulting product was yellow instead of being pure white. And Friedrich Stromeyer of Göttingen University traced the discoloration to a component in the mineral that he could not identify. In 1817, he separated a brown oxide, purified unknown element, and named it cadmium after the mineral from which it came. Karl Meissner in Halle, and Karl Karsten in Berlin, working on the same problem, reported their discovery of cadmium 1 year later. A significant amount of research led to the conclusion that cadmium is present in all zinc ores but has no effect on the performance of zinc compounds. Cadmium was partly removed when zinc metal was smelted because cadmium is more volatile than zinc and was lost in the atmosphere.

Cadmium is a poison and is known to cause birth defects and cancers so its use is more limited. Around 80% of the cadmium that is produced is used in rechargeable Ni-Cd batteries. These batteries are slowly being phased out and replaced with nickel hydride batteries. The remainder of the cadmium is mainly used for pigments (yellow, orange, and red), coatings, and plating and as stabilizers for plastics.

Cadmium films about 0.05 mm thick were used to electroplate steel to protect it against corrosion. It is still used today to protect critical components of airplanes and oil platforms. Cadmium absorbs neutrons and is used in rods in nuclear reactors to control atomic fission.

Geochemical Behavior

Cadmium is naturally occurring in the Earth's crust and always occurs in combination with zinc. The only mineral containing significant quantities of cadmium is greenockite (cadmium sulfide). It is also present is small amounts in sphalerite (ZnS) in which CdS is a significant up to 3% impurity. Almost all commercially produced cadmium is obtained as a by-product of zinc, lead, or copper extractions and refining.

Naturally, a cadmium is released into the environment with half being released into rivers through weathering rocks and some released into the air by forest fires and volcanoes. The remainder of the released cadmium is from human activities including manufacturing. In some cases, cadmium is washed onto soil used to grow crops and to feed animals.

Biological Utilization and Toxicity

Cadmium is toxic, carcinogenic, and teratogenic. On average the human intake is 0.05 mg/day, but it accumulates and stays in the body for around 30 years; the human body stores about 50 mg of cadmium.

Before the dangers of cadmium were fully understood, welders and some other metal workers were at risk of becoming ill. For example, in 1966 welders working on the Severn Road Bridge in England became ill from breathing cadmium fumes.

Although it has not been proven, there are suggestions that cadmium could be essential for some species, as it can stimulate metabolism. Marine organisms absorb cadmium rapidly so that little cadmium is found in the surface layers of the oceans.

Cadmium can never be totally excluded from the diet and can be found in food like offal, shellfish, and rice. Some fungi such as the mushroom *Amanita muscaria* and other food crops (lettuce, spinach, cabbage, and turnip) have the ability to absorb cadmium. Smoking adds to the body burden because tobacco plants absorb it as well.

Cross-References

References

Anders E, Grevesse N (1989) Abundances of the elements: meteoritic and solar. Geochim Cosmochim Acta 53:197–214. http://meteorites. wustl.edu/goodstuff/chondritic_abundances.htm

Anthoni JF (2006) The chemical composition of seawater. http://www. seafriends.org.nz/oceano/seawater.htm

Emsley J (1991) The elements, 2nd edn. Clarendon Press, Oxford

Emsley J (2001) Nature's building blocks an A-Z guide to the elements. Oxford University Press, Oxford

McDonough WF (2005) Compositional model for the earth's core. In: Carlson RW (ed) The mantle and core. Elsevier, Oxford, pp 547–568. http://www.knowledgedoor.com/2/elements_handbook/element_abundances_in_the_earth_s_core.html

Caesium

Gray E. Bebout
Department of Earth and Environmental Sciences, Lehigh University, Bethlehem, PA, USA

Element Data
Atomic Symbol: **Cs**
Atomic Number: **55**
Atomic Weight: 132.90545 u
Isotopes and Abundances: ^{133}Cs, ~100%
1 Atm Melting Point: 28.5 °C
1 Atm Boiling Point: 670.8 °C
Common Valences: 1+
Ionic Radii: 12-fold: 188 pm
Pauling Electronegativity: 0.79
First Ionization Energy: 375.4 kJ/mol
Chondritic (CI) Abundance: 0.188 ppm
Silicate Earth Abundance: 7.7 ppb
Crustal Abundance: 2 ppm
Seawater Abundance: 2 nmol/kg
Core Abundance: ~0

Properties

Caesium, a reactive silvery-gold metal belonging to the group IA on the periodic table, is one of the alkali elements and considered as a "lithophile" element as defined by Goldschmidt. Caesium, atomic number 55, has a standard atomic weight of 132.90545 and an electronic configuration of [Xe]6 s^1. The lone 6 s electron is relatively easily removed; this first ionization potential of Cs is 375.4 kJ/mol. Caesium is highly ionic in character and the ionic radius of Cs^{1+} is

188 pm in 12-fold coordination. Caesium has a 1 atm melting point of 28.5 °C. Caesium has only one naturally occurring isotope, the stable ^{133}Cs. However, there are 40 known isotopes of Cs, with atomic masses of 112–151. The longest-lived radioisotope of Cs is ^{135}Cs, with a half-life of 2.3 million years. All but three of the other radioisotopes of Cs have half-lives of less than 2 weeks, many of them well under 1 h.

Caesium nearly always is bonded by electrostatic forces as Cs^{+1} with various anions and it is, in general, highly soluble in aqueous solutions, for example, during weathering and in the oceans. Caesium, with an ionic radius similar to that of K^+, tends to show geochemical behavior similar to that of K^+ and therefore in silicate rocks to occur in greatest concentrations in K-rich minerals such as illite (a clay mineral), muscovite and biotite (both micas; phengite is a Si-rich muscovite), and alkali feldspars. Concentrations of Cs in silicate minerals are ordinarily at trace levels in the ppm range, commonly lower than 100 ppm but in some rocks as high as 100 s of ppm (see, for example, the ion microprobe analyses of coexisting metamorphic minerals in Bebout et al. 2007, 2013). In the crust, it is a main constituent in nonabundant minerals such as pollucite, a tectosilicate (zeolite group mineral), and lepidolite (a Li-rich mica), both found in Li-rich pegmatites.

History and Uses

Caesium was discovered, along with Rb, by Gustav Kirchhoff and Robert Bunsen in 1860 by spectroscopic study of mineral waters. Its name derives from the Latin *caesius*, meaning sky blue, referring to the color of its emission spectrum. "Caesium" is the name adopted by the International Union of Pure and Applied Chemistry while the American Chemical Society uses "Cesium," which is also common usage in North America. Nonradioactive Cs is used in drilling fluids in the oil industry (the largest current use) and also in atomic clocks and various electronics applications.

The radioactive isotope ^{137}Cs has been used as a tracer in hydrologic studies, in applications similar to those of ^{3}H; both of these isotopes are produced largely by nuclear testing. With the initiation of nuclear testing in 1945, Cs isotopes were released into the atmosphere where it is absorbed readily into solution and is returned to the surface of the earth as a component of radioactive fallout. ^{137}Cs is a particularly dangerous fission product because of its high yield during fission, moderate half-life (30.17 years), high-energy decay pathway, and chemical reactivity. Because of these properties, ^{137}Cs is a major contributor to the total radiation released during nuclear accidents. Despite its prevalence in spent nuclear fuel and nuclear waste, ^{137}Cs is extremely rare. Its half-life is too short for it to persist

from natural fission sources, and on earth it is a synthetic isotope only, presently showing decline in concentration in surface reservoirs due to the cessation of major nuclear bomb testing.

Abundances

The solar system abundance of Cs is estimated at 0.371 Atoms/10^6 Si; (Lodders et al. 2009), based on study of meteorites. The bulk Earth Cs concentration is believed to be 0.035 ppm (McDonough 2003) and Hofmann and White (1982) estimated a concentration of 7.7 ppb in the primitive mantle. Seawater contains 2 nmol/kg of Cs and shows concentrations as high as 368 nmol/kg of seawater in seafloor hydrothermal fluids (Palmer and Edmond 1989). Caesium concentration in the continental crust is estimated as being near 2 ppm, with greater amounts (4.9 ppm) concentrated in the more felsic upper continental crust (Rudnick and Gao 2014) and 2.2 and 0.3 ppm concentrations in the middle and lower continental crust, respectively. Fresh NMORB contains $\sim$0.01 ppm and is enriched by up to $\sim$20X during seafloor alteration (see Bebout 2014 and references therein), with Cs enrichments showing strong correlation with enrichments of K and Rb (see Bebout 2014). Seafloor sediments can contain far greater concentrations of Cs, with the GLOSS (global subducting sediment) composition containing $\sim$3.5 ppm or about 350X the concentration in fresh NMORB (see Plank 2014).

General Behavior in Fluid/Melt-Mineral Systems

Caesium is commonly thought of as belonging to the group of large-ion lithophile elements (LILE), along with K, Rb, Sr, and Ba, and showing the most similarity in behavior with K and Rb. It shows strong incompatibility during melting in the mantle and is partitioned into basaltic melts. Its great tendency to partition into fluids and melts is reflected in its tendency to be enriched in late-stage differentiation products in more felsic igneous systems. Economically important Cs deposits are commonly in pegmatitic systems reflecting this late-stage differentiation. During metamorphism of sedimentary rocks, Cs concentrations are largely governed by reactions involving phyllosilicates capable of housing this element as highly coordinated atoms in interlayer sites. However, Cs has shown some tendency to become mobilized in H_2O-rich fluids, during devolatilization reactions, to a greater extent than other LILE and charged molecules residing in these sites (e.g., K^+, Rb^+, and NH_4^+ see Bebout et al. 1999, 2007). Although significant loss of Cs to fluids can occur during low- to medium-grade metamorphism, and during

partial melting reactions, significant fractions of the protolith Cs can be retained even during partial melting, including those that result in destabilization of its preferred mineral host, the micas. Caesium, on the average, shows somewhat greater tendency than K^+ and Rb^+ to be mobilized into aqueous fluids and depleted in devolatilizing rocks, thus whole-rock Rb/Cs and K/Cs can be strongly increased by devolatilization (see the discussion of Rb and Cs on Earth by McDonough et al. 1992; also see Rudnick and Gao 2014). In seafloor basaltic rocks, Cs concentrations are enriched along with K during hydrothermal alteration and, as for metasedimentary rocks, strongly influenced in their behavior by the abundance of potassic mineral phases, particularly the clays and micas.

Subduction Zone Cycling of Caesium

Subduction of Cs, along with Rb^+ and NH_4^+ is strongly tied to the stability and reactions involving K-rich micas such as phengite (Si-rich muscovite). In subduction zones with typical relatively "cool" thermal structure, much of the LILE inventory in both sedimentary and basaltic rocks could be retained to depths beneath volcanic arcs (and perhaps beyond, into the deeper mantle; see Bebout et al. 2013). Figure 1 illustrates the strong dependence of Cs retention in subducted sediments on the thermal structure of the subduction zone. On this figure, whole-rock (Fig. 1a; data from Bebout et al. 1999) and phengite (Fig. 1b; data obtained using an ion microprobe; see Bebout et al. 2007) Rb/Cs are plotted against metamorphic grade in the Catalina Schist paleo-accretionary complex, exposed on Santa Catalina Island, California. From the left to the right on this diagram, rocks experienced increasingly warmer P-T paths during their subduction into this evolving paleo-margin (all at pressures of ~8–11 kb, corresponding to ~24–33 km depths). The increase in Rb/Cs, with increasing grade, is associated with loss of Cs at relatively constant Rb concentration.

Caesium enrichments in volcanic lavas are one characteristic of these rocks believed to reflect additions to mantle-wedge melting regions by aqueous fluids or silicate melts derived in subducting slabs (Elliott 2003). In Fig. 2 (from Bebout 2014), element concentrations in arc volcanic rocks and in mid-ocean ridge basalts are normalized to concentrations in the primitive Earth mantle. High- and ultrahigh-pressure metamorphic rocks, representing deeply subducted oceanic slab sections (oceanic crust and overlying sediment), contain a complementary record of Cs release, mobility during devolatilization reactions, and metasomatic enrichment in metabasaltic and metaultramafic rocks (Bebout 2014).
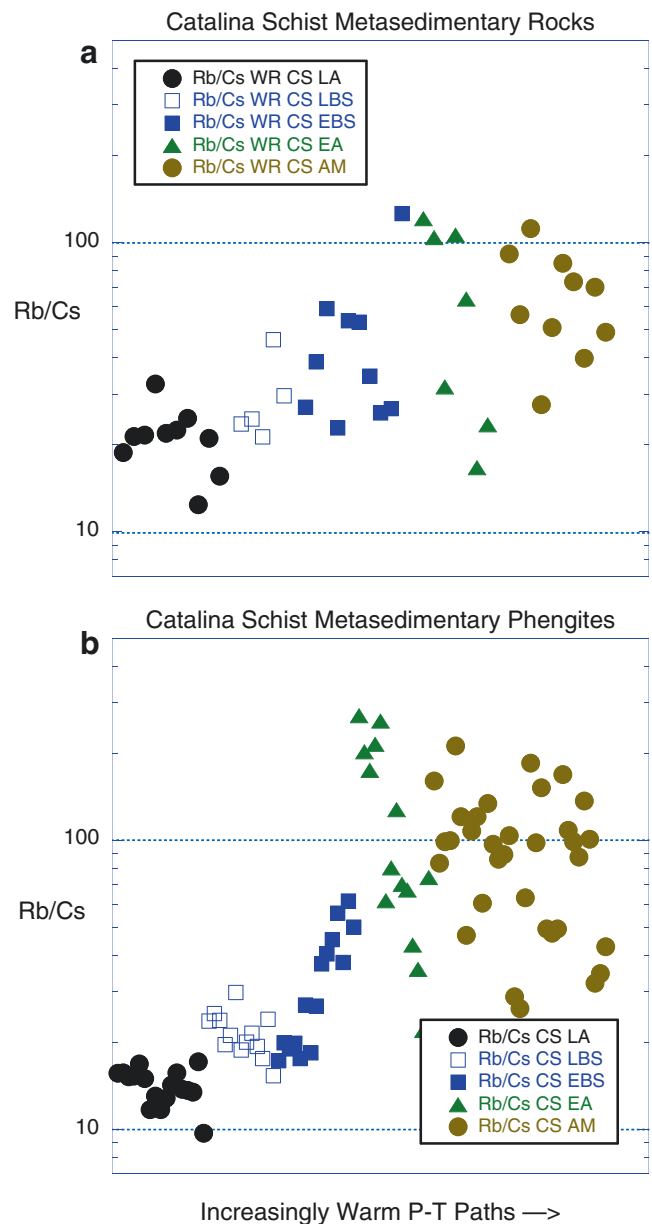
Caesium, Fig. 1 Ratio of Rb to Cs concentration in whole-rock samples (**a**) and phengites (siliceous white micas; **b**) in subduction-zone-metamorphosed sedimentary rocks in the Catalina Schist (from Bebout et al. 1999, 2007). From *left* to *right* on this diagram, the metamorphic units experienced increasingly higher-temperature P-T paths during prograde metamorphism in the evolving paleo-subduction zone (*LA* lawsonite-albite, *LBS* lawsonite blueschist, *EBS* epidote blueschist, *EA* epidote amphibolite, *AM* amphibolite). Bebout et al. (2007) presented Cs and Rb concentrations in all coexisting minerals in these samples, demonstrating the strong partitioning of both elements into phengite. Also showing whole-rock (and phengite) losses was (**B**), which like Cs is highly concentrated in the micas. In these rocks, Ba^{+2} also is strongly concentrated in the phengite (at considerably higher concentrations of 1000 s of ppm) but does not show evidence of loss across this range in grade

Caesium, Fig. 2 Chemical characteristics of subduction zone outputs: erupted lavas. Data are normalized to primitive mantle from Hofmann (1988). Data for arc basalt outputs are from Elliott (2003). Note the large enrichments in Cs in arc lavas, relative to mid-ocean ridge basalts, accompanied by enrichments in Rb and Ba. These enrichments are generally attributed to additions to mantle-wedge arc magma source regions by hydrous fluids or silicate melts derived in subducting slabs and overlying sediments
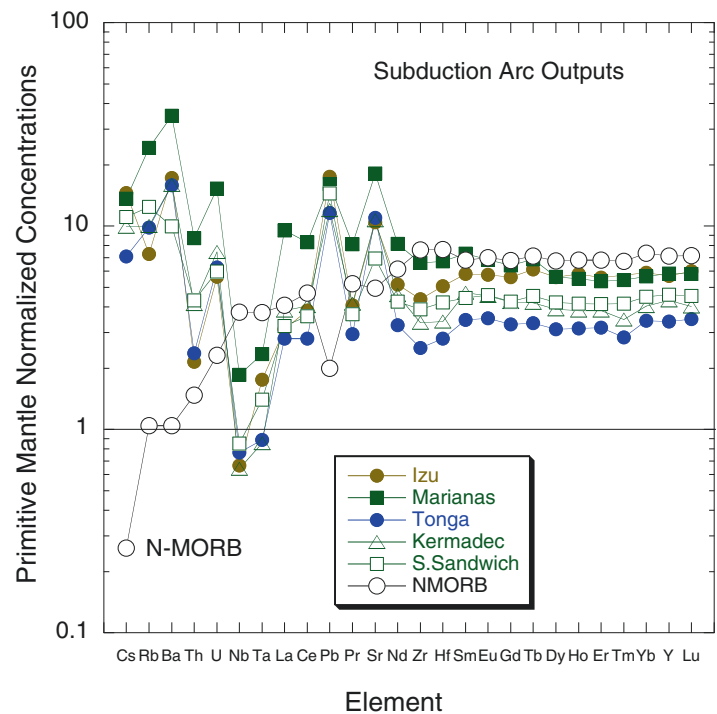
Caesium Behavior During Partial Melting in the Continental Crust

Partial melting in the continental crust shows a tendency to similarly disrupt the Rb/Cs of metasedimentary rocks, as related to the preferential loss of Cs, relative to Rb, during partial melting. Figure 3a shows the apparent effect of partial melting reactions (at pressures of 4–8 kb; corresponding to ~12–24 km depths) on Rb and Cs concentrations, and Rb/Cs, in the Ivrea Zone, Italy (data from Bea and Montero 1999). Figure 3b shows the change in the concentrations of the two elements, and Rb/Cs, as related to a series of partial melting reactions experienced at pressures of 2–4 kb (corresponding to ~6–12 depths) and now exhibited in Zones 1–3 at Mt. Stafford, Australia (from Palya et al. 2011). Rubidium shows only very modest change but Cs shows considerable loss, producing the increase in Rb/Cs. In such rocks, partial melting reactions can be driven by infiltration by H_2O-rich fluids (H_2O-saturated melting) or can involve partial or complete breakdown of hydrous mineral phases such as the micas, the latter in many cases the dominant mineral hosts for both Rb and Cs. In rocks experiencing complete mica breakdown, these elements can be partly retained in feldspars, particularly the alkali feldspars. A combination of devolatilization and partial melting, and ascent of relatively low Rb/Cs felsic magmas to shallow levels, likely contributes to the elevated Rb/Cs of middle and lower continental crust, ~30 and ~37,

respectively, as compared with the Rb/Cs of upper continental crust (~17; see Rudnick and Gao 2014).

Biological Utilization and Toxicity

Caesium has no biological role, although it can to some extent replace potassium in the body because of the chemical similarity of the two elements and can be uptaken by plants affected by potassium nutrition (White and Broadley 2000; Fujiwara 2013). Ingestion of any caesium compound is in general to be avoided; however, it is unlikely that humans would be exposed to enough [133]Cs to experience health effects that can be related to this stable isotope. Because of the similarity in behavior of caesium with potassium, the radioactive isotopes [134]Cs and [137]Cs (present in the biosphere in small amounts as a result of radiation leaks) are very toxic. Both isotopes emit beta radiation and gamma radiation. [137]Cs is also used in some medical applications (e.g., brachytherapy).

Summary

Caesium, of interest to researchers in many scientific fields, shows strong similarity in behavior with potassium but also some intriguing differences in behavior compared with this
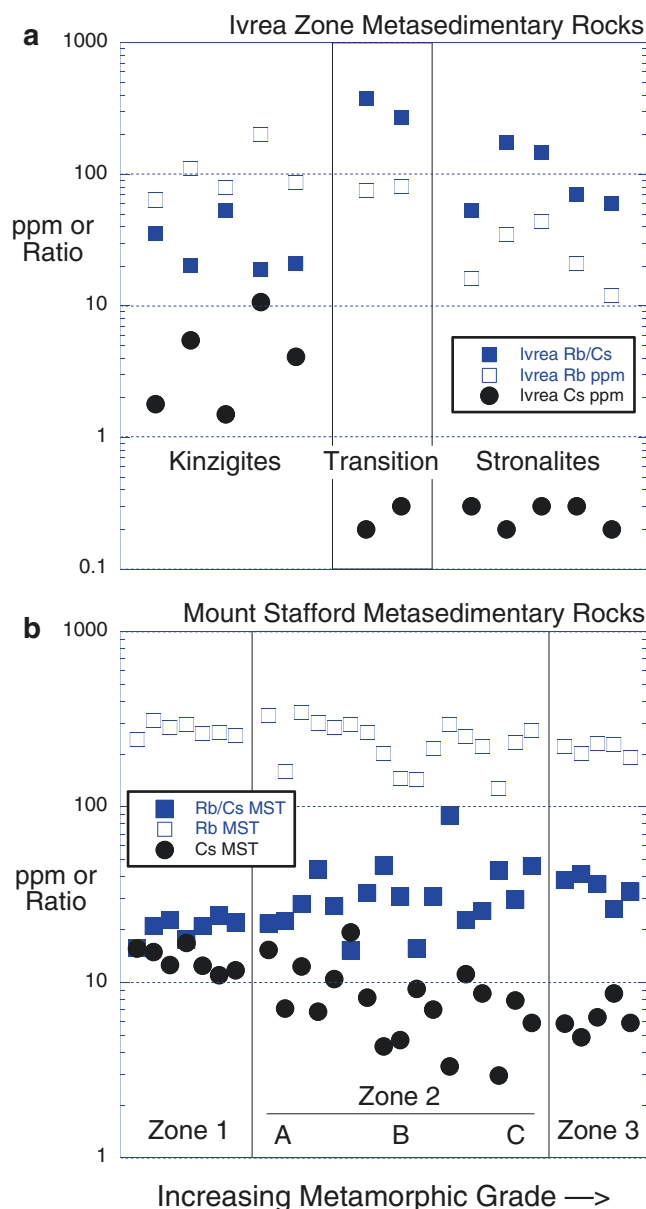
Caesium, Fig. 3 Caesium and Rb concentrations, and Rb/Cs, in whole-rock metasedimentary samples experiencing partial melting reactions at middle to deep levels of the continental crust. (**a**) Data for migmatites of the Ivrea Zone, Italy (Val Strona di Omegna), investigated by Bea and Montero (1999). (**b**) Data for metasedimentary rocks exposed at Mt. Stafford (North-Central Australia), from Palya et al. (2011). On both diagrams, metamorphic grade increases from left to right (see the labeled zones described in detail by Bea and Montero (1999), and Palya et al. 2011)

and other LILE. It is a trace element in most environments of interest to humans, but it serves as an extremely useful tracer of a large number of processes in the hydrosphere, biosphere, and lithosphere. Because of the hazards associated with radioactive ^{137}Cs, caesium receives attention in not only the scientific community but also from the medical community and more broadly in society.

Cross-References

▶ Clay Minerals
▶ Earth's Continental Crust
▶ Fluid–Rock Interaction
▶ Geochemical Classification of Elements
▶ Hydrothermal Alteration
▶ Large-Ion Lithophile Elements
▶ Metamorphic Reactions and Processes
▶ Partial Melting
▶ Radioactivity
▶ Rubidium
▶ Subduction Zone Geochemistry

References

Bea F, Montero P (1999) Behavior of accessory phases and redistribution of Zr, REE, Y, Th, and U during metamorphismand partial melting ofmetapelites in the lower crust: an example from the Kinzigite formation of Ivrea-Verbano, NW Italy. Geochim Cosmochim Acta 63:1133–1153

Bebout GE (2014) 4.20. Chemical and isotopic cycling in subduction zones. In: Rudnick RL (ed) Treatise on geochemistry: the crust, vol 4, 2nd edn. Elsevier, Amsterdam, pp 703–747

Bebout GE, Ryan JG, Leeman WP, Bebout AE (1999) Fractionation of trace elements during subduction-zone metamorphism: impact of convergent margin thermal evolution. Earth Planet Sci Lett 171:63–81

Bebout GE, Bebout AE, Graham CM (2007) Cycling of B, Li, and LILE (K, Cs, Rb, Ba, Sr) into subduction zones: SIMS evidence from micas in high-P/T metasedimentary rocks. Chem Geol 239:284–304

Bebout GE, Agard P, Kobayashi K, Moriguti T, Nakamura E (2013) Devolatilization history and trace element mobility in deeply subducted sedimentary rocks: SIMS evidence from Western Alps HP/UHP suites. Chem Geol 342:1–20

Elliott T (2003) Tracers of the slab. In: Eiler J (ed) Inside the subduction factory, Geophysical Monograph, vol 138. American Geophysical Union, Washington, DC, pp 23–45

Fujiwara T (2013) Cesium uptake in rice: possible transporter, distribution, and variation, Chapter 4. In: Nakanishi TM, Tanoi K (eds) Agricultural implications of the Fukushima nuclear accident. Springer, New York, pp 29–35

Hofmann AW (1988) Chemical differentiation of the earth: the relationship between mantle, continental crust, and oceanic crust. Earth Planet Sci Lett 90:297–314

Hofmann AW, White WM (1982) Ba, Rb, and Cs in the Earth's mantle. Z Naturforsch A 38(2):256–266

Lodders K, Palme H, Gail HP (2009) Abundances of the elements in the solar system, Chapter 4.4. In: Trümper JE (ed) Landolt Börnstein, new series, vol VI/4B. Springer, Berlin/Heidelberg/New York, pp 560–630

McDonough WF (2003) Compositional model for the Earth's core. In: Carlson RW (ed) Treatise on geochemistry: the mantle and core, vol 2, 1st edn. Elsevier, Amsterdam, pp 547–568

McDonough WF, Sun S-S, Ringwood AE, Jagoutz E, Hofmann AW (1992) Potassium, rubidium, and caesium in the Earth and Moon and the evolution of the mantle of the Earth. Geochim Cosmochim Acta 56:1001–1012

Palmer MR, Edmond JM (1989) Cesium and rubidium in submarine hydrothermal fluids: evidence for recycling of alkali elements. Earth Planet Sci Lett 95:8–14

Palya AP, Buick IS, Bebout GE (2011) Storage and mobility of nitrogen in the continental crust: evidence from partially melted meta-sedimentary rocks at Mount Stafford, North-Central Australia. Chem Geol 281:211–226

Plank T (2014) 4.17. The chemical composition of subducting sediments. In: Rudnick RL (ed) Treatise on geochemistry: the crust, vol 4, 2nd edn. Elsevier, Amsterdam, pp 607–629

Rudnick RL, Gao S (2014) 4.1. Composition of the continental crust. In: Rudnick RL (ed) Treatise on geochemistry: the crust, vol 4, 2nd edn. Elsevier, Amsterdam, pp 1–51

White PJ, Broadley MR (2000) Mechanisms of caesium uptake by plants. New Phytol 147:241–256
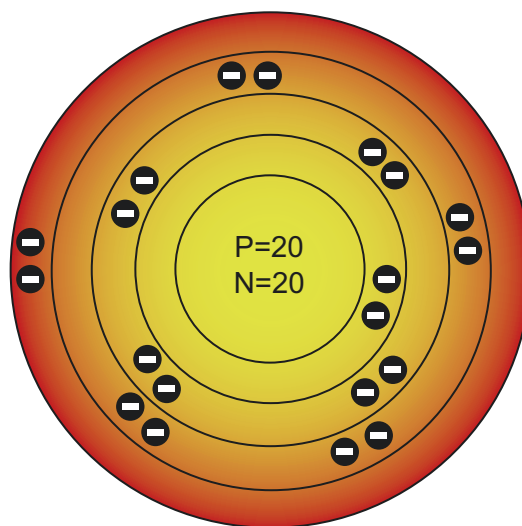
Calcium

Christophe Lécuyer
Laboratoire de Géologie de Lyon, LGL-TPE, CNRS UMR 5276, Université Claude Bernard Lyon 1 and Institut Universitaire de France, Lyon, France

Element Data
Atomic Symbol: Ca
Atomic Number: 20
Atomic Weight: 40.078(4)
Isotopes and Abundances: ^{40}Ca, 96.941(156)%; ^{42}Ca, 0.647(23)%; ^{43}Ca, 0.135(10)%; ^{44}Ca, 2.086(110)%; ^{48}Ca, 0.187(21)%
1 Atm Melting Point: 840 °C
1 Atm Boiling Point: 1,484 °C
Common Valences: +2
Ionic Radii: 6-fold: 114 pm
Pauling Electronegativity: 1.00
First Ionization Potential: 589.83 kJ.mol^{-1}
Chondritic (CI) Abundance: 9,110 ppm (59,820 atoms/10^6 Si)
Silicate Earth Abundance: 25,300 ppm
Crustal Abundance: 41,500 ppm
Seawater Abundance: 412 to 420 ppm
Core Abundance: ~0

Properties

Calcium is a metal (alkaline earth) with a silvery color and a cubic crystal structure. This element belongs to group 2 and period 4 of the periodic table (Fig. 1). Calcium has 25 known isotopes of which 5 are stable (source of data: National Institute of Standards and Technology: http://www.nist.gov/pml/data/comp.cfm).

Calcium, Fig. 1 Schematic illustration of the atomic configuration of ^{40}Ca

Geochemists measure the relative variations in the ^{44}Ca/^{40}Ca of terrestrial and extraterrestrial materials that result mainly from chemical equilibrium and kinetic effects. Some of this variation also results from the β decay of ^{40}K (decay constant = 4.962×10^{-10} year^{-1}) to ^{40}Ca (Dickin 2005). For example, ^{40}K–^{40}Ca measurements were performed to quantify the contribution of crustal silicates to the marine calcium cycle (Caro et al. 2010).

The electron configuration of calcium is $1s^2 2s^2 2p^6 3s^2 3p^6 4s^2$, while its valence state is +2, forming ionic bonds with nonmetal elements. Its nonbonded atomic radius is 197 pm; its covalent radius is 174 pm, along with a strong electronegativity of 1.00 on the Pauling scale and an electron affinity of 2.369 kJ.mol^{-1} (Coursey et al. 2010; Haynes 2015). Calcium has a density of 1,550 kg.m^{-3} at 20 °C. Calcium salts are more or less soluble in water; indeed, at 25 °C, the solubility products of calcite (trigonal $CaCO_3$), aragonite (orthorhombic $CaCO_3$), gypsum ($CaSO_4.2H_2O$), anhydrite ($CaSO_4$), and antarcticite ($CaCl_2.6H_2O$) are $10^{-8.48}$, $10^{-8.34}$, $10^{-4.58}$, $10^{-4.36}$, and $10^{-4.09}$, respectively. Hydroxyapatite, the biomineral constituting the skeleton of vertebrates, has a much lower solubility product of $10^{-54.45}$ (Fig. 2). Calcium is also characterized by a specific heat capacity of 653 J.kg^{-1}.K^{-1}.

History and Use

The name calcium originates from the Latin word "calx" that means "the ashy remaining substance after burning," i.e., the "lime." In nature, calcium does not occur in its elemental form but bounds to oxygen or halogens (fluorite CaF_2). Calcium compounds, such as quick lime (CaO), slaked

Calcium, Fig. 2 Crystal lattice of hydroxyapatite. Atomic symbols: *Yellow* calcium, *dark gray* carbon, *red* oxygen, *white* hydrogen, *purple* phosphorus
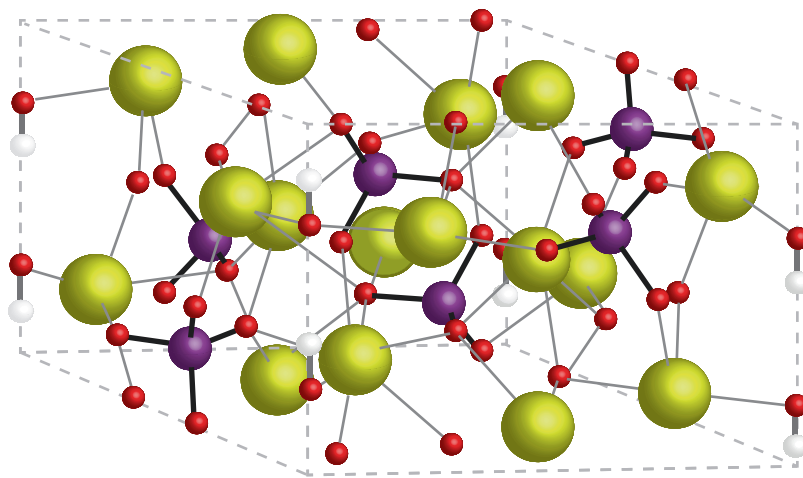
lime (Ca(OH)$_2$), limestone (CaCO$_3$), gypsum (CaSO$_4$.2H$_2$O), anhydrite (CaSO$_4$), and hydroxyapatite (Ca$_5$(PO$_4$)$_3$(OH)), have all been known and used by human beings for several thousands of years. The Romans heated calx (limestone) to produce a decarbonation reaction leaving calcium oxide as the solid residue. While gypsum is a common component of wallboard for buildings and concrete for the construction of highways and bridges, it has also been used for centuries in the field of fine arts. Alabaster, which is the translucent variety of gypsum, is a sought-after mineral used for ornamental stonework and sculptures. Anhydrite is commonly used to produce industrial sulfuric acid.

Despite the use of calcium compounds for centuries, the element calcium was not isolated and identified until electricity was under control. Calcium as a metal species was first isolated by Sir Humphry Davy (1808). Calcium forms alloys with magnesium, aluminum, copper, and lead. Calcium bromide (CaBr$_2$), a white powder, has many uses and is present in fire retardants, drilling fluids, cooling agents in freezing mixtures, food preservatives, and medication for the treatment of anxiety. Quicklime (CaO) is, for example, used in water purification devices for drinking water production. Calcium favors the growth of symbiotic and nonsymbiotic nitrogen-fixing bacteria, which are critical for the growth of legumes.

Natural Abundance

Calcium is a lithophile element according to Goldschmidt's classification (Goldschmidt 1926); it is one of the most important rock-forming element (after Si, Al, and Na) at the Earth's surface with a crustal abundance of 41,500 ppm. Several minerals, rare to common, contain from ≈8 to 40 mol% of Ca (Table 1).

CI meteorites contain 9,110 ppm on average (Palme et al. 2014). In most chondrites, calcium is hosted by diopside (CaMgSi$_2$O$_6$), chlorapatite (Ca$_5$(PO4)$_3$Cl), and merrillite (Ca$_9$Na(Mg,Fe) (PO$_4$)$_7$) and also occurs in minor amounts in feldspars or orthopyroxene. Despite the strong lithophile

Calcium, Table 1 Molar content of calcium in the most common of Earth's crust minerals and biominerals

Mineral	Chemical formula	Ca mol%
Calcite, aragonite	CaCO$_3$	40.04
Dolomite	CaMg (CO$_3$)$_2$	21.73
Anhydrite	CaSO$_4$	29.44
Gypsum	CaSO$_4$.2H$_2$O	25.47
Anorthite	CaAl$_2$Si$_2$O$_8$	14.41
Wollastonite	CaSiO$_3$	34.50
Diopside	CaMgSi$_2$O$_6$	18.51
Hydroxyapatite	Ca$_5$(PO$_4$)$_3$(OH)	07.98
Fluorite	CaF$_2$	51.33
Antarcticite	CaCl$_2$.6H$_2$O	26.67

property of calcium as mentioned above, it may occur as sulfides such as oldhamite ((Ca,Mg,Fe)S) in the reduced sulfide-rich enstatite chondrites. It is also worth noting that calcite, dolomite, and gypsum have been observed in Cl and C2 chondrites.

Of special interest are the calcium-aluminum-rich inclusions (CAIs), considered to belong to the first solid grains that condensed in the nebular disc surrounding the protosun. Pb-Pb dating of these CAIs indicates that they formed 4,568.2 My ago, the oldest age obtained for any solar system object so far (Bouvier and Wadhwa 2010).

Palme and O'Neill (2014) have estimated the upper primitive mantle CaO content at 3.78 wt%. Mid-ocean ridge basalts contain between 11.39 and 11.46 wt% of CaO according to measurements of fresh basaltic glass (Gale et al. 2013; White and Klein 2014). Wedepohl (1995) calculated that the CaO content of the bulk continental crust is close to 5.5 wt‰. The upper continental crust contains an average CaO concentration of 3.59 ± 0.2 wt% (Rudnick and Gao 2005).

Seawater calcium abundance is in the range 412–420 ppm; consequently it is the fifth most abundant element after Cl,

Na, Mg, and S (Bruland et al. 2014) dissolved in seawater (O_2 gas excluded). The calcium content increases from the ocean surface down to depths of 2,000–3,000 m and then decreases again down to the seafloor (de Villiers 1998). The calcium content was found to be closely related to carbonate alkalinity according to the temperature and pH dependence of calcium carbonate solubility in seawater. However, de Villiers (1998) observed that the deep ocean contains higher amounts of dissolved calcium than predicted by the thermodynamics of calcium carbonate dissolution. The Ca excess occurring at these intermediate depths could correspond to the calcium contribution from hydrothermal systems located at the axis of mid-ocean ridges (de Villiers 1998).

Dissolved calcium abundance and its rather homogeneous distribution in seawater are related to its relative high residence time close to 1 My. Consequently Ca is considered as a "conservative" element in seawater.

The world's average polluted river water contains 14.7 ppm of calcium, with anthropogenic contributions corresponding to 9% of the total concentration. The main non-anthropogenic calcium fluxes to rivers result from the dissolution of calcium and magnesium carbonates ($\approx$70% of the total flux), evaporites such as gypsum or anhydrite ($\approx$10% of the total flux), and Ca-feldspars or Ca-pyroxenes hosted by basaltic or ultrabasic rocks ($\approx$20% of the total flux).

Most lakes contain from a few ppm to a few dozens of ppm of dissolved calcium. The highly alkaline saline Mono Lake, USA, has only a $[Ca^{2+}] \approx 6$ mg.L^{-1} for a pH of 9.8 and a salinity S of 81 g.L^{-1} (Domagalski et al. 1990). Acid lakes are generally characterized by higher concentrations of dissolved calcium, typically in the range 50–100 ppm (Lake Ontario, Canada).

Geochemical Cycling

The long-term (My scale) calcium geochemical cycle is basically defined by four reservoirs, which are (1) the upper continental crust, (2) the marine biomass made of calcifying organisms, (3) the marine sediments, and (4) the oceanic crust. Connecting fluxes are contributed by (1) the rivers; (2) the dissolution and precipitation of sediments (carbonates and sulfates); (3) the primary production of calcifying organisms with the most important planktonic producers being the coccolithophores, the foraminifera, and the euthecosomatous pteropods (Fabry et al. 2008); and (4) the seawater-basalt interactions associated with hydrothermal activity located at mid-ocean ridges.

The two net input Ca fluxes to the oceans are the river and hydrothermal fluxes. The first one is obtained by multiplying the world river flux (3.74×10^{16} kg of water per year) by the average river Ca content of 14.7 ppm, which gives a calcium flux of 5.5×10^{11} kg.$year^{-1}$. The second flux corresponds to the release of dissolved calcium at mid-ocean ridges during the hydrothermal alteration of clinopyroxene (diopside; $(Ca, Mg)Si_2O_6$) into amphibole (tremolite; $Ca_2Mg_5(Si_8O_{22})(OH)_2$) (6) and Ca-plagioclase (anorthite; $CaAl_2Si_2O_8$) into Na-plagioclase (albite; $NaAlSi_3O_8$).

This hydrothermal flux was estimated close to 1×10^{11} kg of Ca per year (Alt et al. 1986; Bednarz and Schmincke 1989). Consequently, the total input flux to the oceans is about 6.5×10^{11} kg.$year^{-1}$.

Assuming that the calcium geochemical cycle is close to steady state, output fluxes from the oceans to other solid reservoirs should more or less balance the net input flux estimated above. A first output flux is the precipitation of calcium carbonate in the tensile fractures that develop in the oceanic crust during its off-axis cooling.

Alt and Teagle (1999) calculated a flux of about 1.4×10^{11} kg Ca.$year^{-1}$. A second flux corresponds to the subduction of sediments that operates at a rate of 0.5 km^3.$year^{-1}$ with a present-day carbon content of 8,200 ppm. These data allow the calculation of an average carbon flux of 1.2×10^{10} kg.$year^{-1}$. The biogenic contribution to this C flux is evaluated at 15% of the total sedimentary flux, thus corresponding to a Ca flux of 1.7×10^{11} kg Ca.$year^{-1}$.

Consequently, the difference between the net input and output flux is 3.4×10^{11} kg Ca.$year^{-1}$. Such an apparent "missing output Ca flux" could be explained by the oceanic primary productivity involving the calcifying organisms. Indeed, the dissolution of carbonated skeletons from dead organisms does not match the rate of calcification in the oceans. According to Langer et al. (1997), the total present-day $CaCO_3$ production in the world oceans is 3.27×10^{12} kg.$year^{-1}$, which corresponds to a flux of 1.31×10^{12} kg Ca.$year^{-1}$. A part of this flux could have contributed to the progressive integration of carbonates into the upper continental crust through the accumulation of carbonates in passive margins. The amount of Ca trapped into carbonates (limestones and dolomites) (Taylor and McLennan 1985) was estimated close to 1.8×10^{20} kg Ca. The apparent "missing output flux of Ca" from the oceans could be thus explained by the storage of carbonates in passive margins during the last 530 My ($\approx$ the Phanerozoic) at a rate of 3.4×10^{11} kg of Ca.$year^{-1}$.

It is also worthy to note that the budget of Ca^{2+} in the oceans is linked to the carbon cycle through the dissolution and precipitation (8) of carbonates. One mole of carbon is trapped during carbonate precipitation, but one mole is released as CO_2. The dissolution of $CaCO_3$ tends to buffer the pH of the oceans when atmospheric pCO_2 is rising.

Strong connections operate between Earth's climate modes and geochemical cycles. Such relationships are evidenced by secular variations in seawater chemistry over the Phanerozoic, which have been recorded in the composition of marine evaporites (halite) and biogenic carbonates

such as corals and foraminifera. The "greenhouse" climatic conditions of both Jurassic and Cretaceous were characterized by low molar Mg/Ca ratios ($\approx$1) that favored the precipitation of calcitic cements (the so-called "calcite" seas), while the "icehouse" Tertiary has been a period of high Mg/Ca ratios (from 3 to 5) that produced inorganic aragonite cements in the so-called "aragonite" seas (Gothmann et al. 2015).

On the continents, massive precipitation of calcium carbonates (travertines) may occur associated with geothermal waters. In most cases, geothermal waters originate from meteoric waters that infiltrate the continental crust through fissures and cracks and that are heated up at the contact of magma chambers beneath volcanoes or slowly cooling plutonic rocks such as granites. Carbonate precipitation then occurs as a result of the degassing of carbon dioxide when calcium concentrations higher than 100 mg.L^{-1}.

Biological Utilization and Toxicity

Calcium is of primordial importance for the growth of skeletons of many invertebrates (e.g., mollusks, foraminifera, coccolithophores, corals, bryozoans) and all vertebrates. Calcium ions are the most important messengers between cells in living organisms. Calcium oxalates, such as weddellite (Ca(C_2O_4).2(H_2O)) and whewellite (Ca(C_2O_4).(H_2O)), are present in soils and play an important role in the availability of nutrients to plant roots (Graustein et al. 1977).

In the oceans, phytoplankton developed the remarkable ability to regulate the concentration of Ca^{2+} in the intracellular cytosol. Over geological times, most taxonomic groups were thus able to cope with variations in seawater chemistry (Müller et al. 2015). For example, coccolithophores were abundant during the Cretaceous, a warm period most likely characterized by high levels in seawater dissolved calcium abundance (Müller et al. 2015).

Calcifying marine organisms is commonly considered to be highly sensitive to a decrease in oceanic pH because calcification rates are expected to decrease. However, in situ observations, laboratory experiments, and paleontological records indicate that numerous marine organisms are capable of adjusting their physiological functions to deal with an increase in seawater acidity (Findlay et al. 2009). For example, McCulloch et al. 2012) have shown that cold-water scleractinian corals have a strong resilience to oceanic acidification.

Calcium is the most abundant of the metallic elements in the human body. The average adult body contains about 1 kg of calcium, 99% of which is located in the hydroxyapatite mineral constituting the skeleton. While old bone is regularly eliminated by osteoclasts, new bone is mineralized by osteoblasts in fibroblasts that secrete and mineralize the bone matrix. The mineralized extracellular matrix is mainly composed of type I collagen and osteocalcin (a noncollagenous protein), matrix Gla protein, osteopontin, bone sialoprotein, bone morphogenetic proteins (BMPs), transforming growth factor-beta (TGF-β), and hydroxyapatite.

If calcium is crucial for living organisms including human beings, intake of calcium in excess may provoke arterial calcification and may also increase the risk of cardiovascular diseases in elderly persons. Even healthy kidneys have a restricted capability for eliminating excessive calcium derived from the diet. So high calcium intakes in adults should be avoided since they have relatively limited or no positive consequences for bone mineral density (Anderson and Klemmer 2013).

Summary

This lithophile element is one of the most important rock-forming elements of the Earth. The budget of Ca^{2+} in the oceans is linked to the carbon cycle through dissolution and precipitation of $CaCO_3$.

Calcium is a critical component of skeletons of many invertebrates and all vertebrates, and its ions are the most important messengers between cells, resulting in Ca being the most abundant of the metallic elements in the human body.

Cross-References

▶ Acid–Base Reactions
▶ Alkali and Alkaline Earth Metals
▶ Carbonate Minerals and the CO2-Carbonic Acid System
▶ Calcium Isotopes
▶ Carbon Cycle
▶ Carbonate Compensation Depth
▶ Carbonate Minerals and the CO2-Carbonic Acid System
▶ Carbonate Compensation Depth
▶ Chondrites
▶ Geochemical Thermodynamics
▶ Lithophile Elements
▶ Ocean Biochemical Cycling and Trace Elements
▶ Refractory Inclusions in Chondritic Meteorites
▶ Solubility
▶ Sulfate Minerals

References

Alt JC, Teagle DA (1999) The uptake of carbon during alteration of ocean crust. Geochim Cosmochim Acta 63:1527–1535
Alt JC, Honnorez J, Laverne C, Emmermann R (1986) Hydrothermal alteration of a 1 km section through the upper oceanic crust, Deep Sea Drilling Project Hole 504B: mineralogy, chemistry and evolution of

seawater-basalt interactions. J Geophys Res Solid Earth 91:10309–10335

Anderson JJ, Klemmer PJ (2013) Risk of high dietary calcium for arterial calcification in older adults. Forum Nutr 5:3964–3974

Bednarz U, Schmincke HU (1989) Mass transfer during sub-seafloor alteration of the upper Troodos crust (Cyprus). Contrib Mineral Petrol 102:93–101

Bouvier A, Wadhwa M (2010) The age of the Solar System redefined by the oldest Pb–Pb age of a meteoritic inclusion. Nat Geosci 3:637–641

Bruland KW, Middag R, Lohan MC (2014) 8.2 – controls of trace metals in seawater A2 – Holland, Heinrich D. In: Turekian KK (ed) Treatise on geochemistry, 2nd edn. Elsevier, Oxford, pp 19–51

Caro G, Papanastassiou DA, Wasserburg GJ (2010) ^{40}K-^{40}Ca isotopic constraints on the oceanic calcium cycle. Earth Planet Sci Lett 296:124–132

Coursey JS, Schwab DJ, Tsai JJ, Dragoset RA (2010) Atomic weights and isotopic compositions. National Institute of Standards and Technology, Gaithersburg

Davy H (1808) The Bakerian lecture: on some new phenomena of chemical changes produced by electricity, particularly the decomposition of the fixed alkalies, and the exhibition of the new substances which constitute their bases; and on the general nature of alkaline bodies. Phil Trans R Soc London 98:1–44

de Villiers S (1998) Excess dissolved Ca in the deep ocean: a hydrothermal hypothesis. Earth Planet Sci Lett 164:627–641

Dickin AP (2005) Radiogenic isotope geology. Cambridge University Press, Cambridge. 492 pp

Domagalski JL, Eugster HP, Jones BF (1990) Trace metal geochemistry of Walker, Mono, and Great Salt Lakes. Fluid-Miner Interactions 2:315–353

Fabry VJ, Seibel BA, Feely RA, Orr JC (2008) Impacts of ocean acidification on marine fauna and ecosystem processes. ICES J Mar Sci 65:414–432

Findlay HS, Wood HL, Kendall MA, Spicer JI, Twitchett RJ, Widdicombe S (2009) Calcification, a physiological process to be considered in the context of the whole organism. Biogeosci Discuss 6:2267–2284

Gale A, Dalton CA, Langmuir CH, Su Y, Schilling J-G (2013) The mean composition of ocean ridge basalts. Geochem Geophys Geosyst 14(3):489–518

Goldschmidt VM (1926) Geochemische Verteilungsgesetze der Elemente. VII: Die Gesetze der Krystallochemie. Skrifter Norske Videnskaps Akad, Oslo, (I) Mat. Natur. K1, Oslo

Gothmann AM, Stolarski J, Adkins JF, Schoene B, Dennis KJ, Schrag DP, Mazur M, Bender ML (2015) Fossil corals as an archive of secular variations in seawater chemistry since the Mesozoic. Geochim Cosmochim Acta 160:188–208

Graustein WC, Cromack K, Sollins P (1977) Calcium oxalate: occurrence in soils and effect on nutrient and geochemical cycles. Science 198:1252–1254

Haynes WM (2015) CRC handbook of chemistry and physics, 95th edn. CRC Press & Taylor and Francis, Boca Raton

Langer MR, Silk MT, Lipps JH (1997) Global Ocean carbonate and carbon dioxide production; the role of reef Foraminifera. J Foram Res 27:271–277

McCulloch M, Trotter J, Montagna P, Falter J, Dumbar R, Freiwald A, Försterra G, López Correa M, Maier C, Rüggeberg A, Taviani M (2012) Resilience of cold-water scleractinian corals to ocean acidification: boron isotopic systematics of pH and saturation state up-regulation. Geochim Cosmochim Acta 87:21–34

Müller MN, Barcelos e Ramos J, Schulz KG, Riebesell U, Kazmierczak J, Gallo F, Mackinder L, Li Y, Nesterenko PN, Trull TW, Hallegraeff GM (2015) Phytoplankton calcification as an effective mechanism to prevent cellular calcium poisoning. Biogeosci Discuss 12:6493–6501

Palme H, O'Neill HSC (2014) 3.1 – Cosmochemical estimates of mantle composition. In: Turekian HDHK (ed) Treatise on geochemistry, 2nd edn. Elsevier, Oxford, pp 1–39

Palme H, Lodders K, Jones A (2014) 2.2 – solar system abundances of the elements A2. In: Holland HD, Turekian KK (eds) Treatise on geochemistry, 2nd edn. Elsevier, Oxford, pp 15–36

Rudnick RL, Gao S (2005) Composition of the continental crust. In: Rudnick RL (ed) Treatise on geochemistry, The crust, vol 3. Elsevier-Pergamon, Oxford, pp 1–64

Taylor SR, McLennan SM (1985) The continental crust: its composition and evolution. An examination of the geochemical record preserved in sedimentary rocks. Blackwell Scientific Publications, Oxford. 312 pp

Wedepohl KH (1995) The composition of the continental crust. Geochim Cosmochim Acta 59:1217–1232

White WM, Klein EM (2014) 4.13 – composition of the oceanic crust. In: Holland HD, Turekian KK (eds) Treatise on geochemistry, 2nd edn. Elsevier, Oxford, pp 457–496

C

Calcium Isotopes

Juraj Farkaš

Department of Earth Sciences, School of Physical Sciences, University of Adelaide, Adelaide, South Australia, Australia
Department of Geochemistry, Czech Geological Survey, Prague, Czech Republic
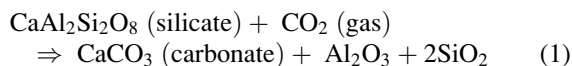
Introduction

Calcium (Ca) is the fifth most abundant element and dissolved ion, respectively, in the Earth's crust and the oceans. Ca is also an essential nutrient for marine and terrestrial organisms where it regulates metabolic processes (i.e., calcium homeostasis) as well as the production of skeletal structures (i.e., bones and calcitic shells). Importantly, Ca has six naturally occurring isotopes (^{40}Ca, ^{42}Ca, ^{43}Ca, ^{44}Ca, ^{46}Ca, and ^{48}Ca), where ^{40}Ca is the most abundant and also produced by the radioactive decay of potassium ^{40}K with a half-life of ~1.277 billion years (Byr). Due to its numerous isotopes and a high mobility in near-surface environments, Ca represents a valuable tracer for earth system processes and biogeochemical pathways. The isotope studies of Ca are thus relevant for a better understanding of global elemental cycles and mutual interactions between lithosphere, hydrosphere, and biosphere. In this contribution, we present the stable Ca isotope variations as delta values ($\delta^{44/40}$Ca, in per mil) normalized to NIST 915a; and the radiogenic ^{40}Ca isotope anomalies are expressed as epsilon units (ϵCa, in parts per ten thousand).

The global biogeochemical cycle of Ca is tightly linked to other major elemental cycles, including the global carbon (C) cycle, which is facilitated through processes such as continental weathering, hydrothermal exchange at

Calcium Isotopes, Fig. 1 A schematic diagram showing the links between the global Ca and C cycles in the earth surface environments, including the main sources and sinks of Ca^{2+} and CO_3^{2-} ions in the modern oceans (Modified after Husson et al. 2015)
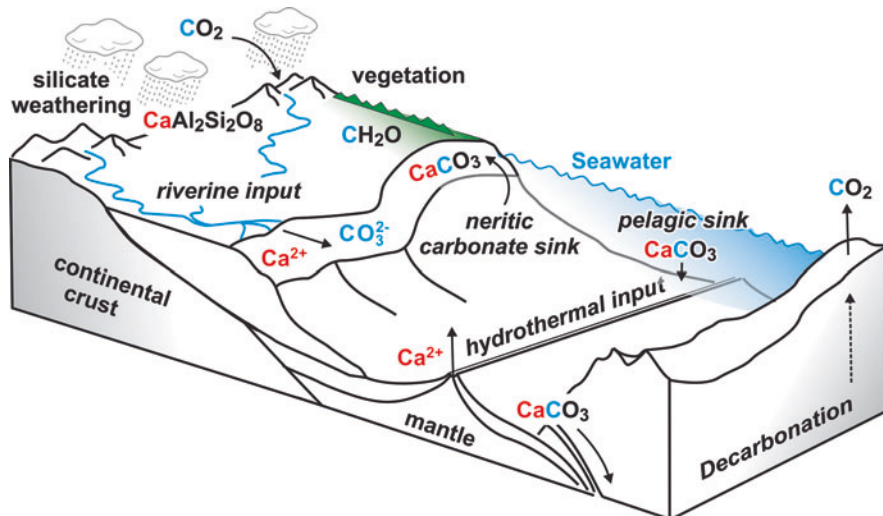
mid-ocean ridges, and/or the formation and deposition of marine carbonates (see Fig. 1). The majority of Ca delivered to the oceans by rivers is primarily derived from the dissolution of continental crust, which contains Ca-bearing carbonate and silicate minerals, expressed by simplified chemical formulas $CaCO_3$ and $CaAl_2Si_2O_8$, respectively. Although carbonates are more soluble, it is the dissolution of silicates that consumes carbon dioxide (CO_2) from the atmosphere, which in turn regulates the Earth's climate over geological time, according to the following simplified reaction (cf., Berner and Berner 1997):

$$CaAl_2Si_2O_8 \text{ (silicate)} + CO_2 \text{ (gas)}$$
$$\Rightarrow CaCO_3 \text{ (carbonate)} + Al_2O_3 + 2SiO_2 \quad (1)$$

A reversed process of this reaction is the "decarbonation" of limestones in the subduction zones, where the increasing temperature decomposes carbonate minerals and liberates CO_2 gas which can be then reintroduced back into the atmosphere via volcanic systems (see Fig. 1). The tight coupling between the global Ca and C cycles in terrestrial and marine environments highlights the importance of Ca isotope studies for a better understanding of the global C cycle and its role in the modulation of atmospheric CO_2 levels.

Stable Calcium Isotope Variations and Global Ca Cycle

The stable, or mass-dependent, isotope fractionation of Ca in nature is expressed as delta (δ) notation based on the measured isotope ratios of $^{44}Ca/^{40}Ca$ (or alternatively also $^{44}Ca/^{42}Ca$) in a sample relative to a standard, according to the following relation:

$$\delta^{44/40}Ca = \left(\frac{\left(^{44}Ca/^{40}Ca\right)_{sample}}{\left(^{44}Ca/^{40}Ca\right)_{standard}} - 1 \right) \cdot 10^3 \quad (2)$$

where the reported delta values ($\delta^{44/40}Ca$) are in "per mil" (‰, parts per thousand), and here normalized to a standard NIST 915a. The recent compilation of $\delta^{44/40}Ca$ values from major geological and biological reservoirs (Fantle and Tipper 2014) shows an overall range of about 4 ‰ for various terrestrial and marine samples (see Fig. 2; n > 2600 measurements), where the isotopically heaviest Ca reservoir on Earth is the ocean water ($\delta^{44/40}Ca \approx 1.9$ ‰). In contrast, the isotopically lightest Ca is associated with vegetation (i.e., terrestrial plants) and/or biologically precipitated marine carbonates (i.e., calcitic and aragonitic shells). This points to a critical role of organisms and the biosphere in fractionating the stable Ca isotopes in the Earth's surface environments, due to a preferential incorporation of lighter Ca isotopes by plants and animals, which is a common feature of the stable isotope systems of other bioessential elements including carbon (Hoefs 2015). Nevertheless, pure abiotic processes such as (i) the inorganic precipitation of $CaCO_3$ and $CaSO_4$ minerals due to an oversaturation of natural waters, and/or (ii) the adsorption of dissolved Ca^{2+} ions on clays and exchangeable sites of particles can also lead to a significant fractionation of stable Ca isotopes at low temperatures (Fantle and Tipper 2014 and references therein).

The magnitude of stable Ca isotope fractionation in nature diminishes with an increasing temperature (being proportional to $1/T^2$ at high temperatures), and thus igneous silicate Ca reservoirs exhibit much narrower range of $\delta^{44/40}Ca$ values (about 2 ‰) compared to marine carbonates and/or the organically complexed Ca (see Fig. 2). Nevertheless, recent studies of Ca isotope fractionation in high-temperature
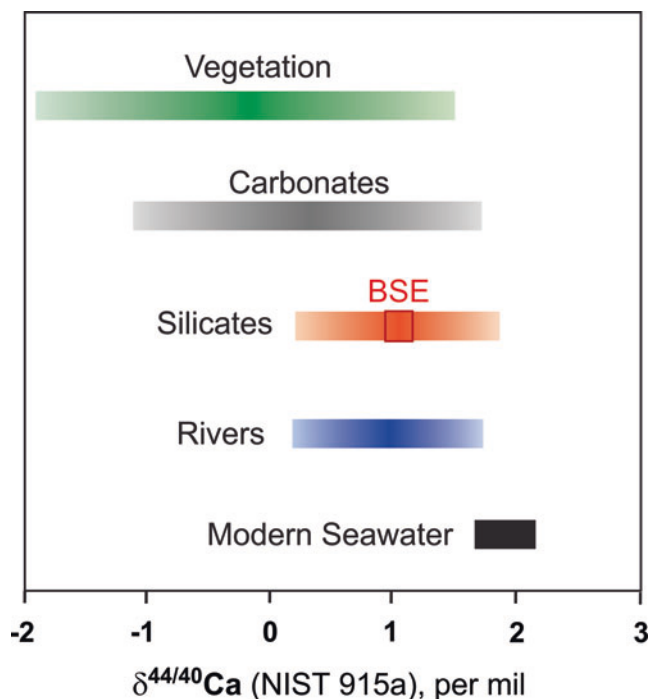
Calcium Isotopes, Fig. 2 A compilation of the published Ca isotope data from terrestrial samples (more than 2600 measurements) presented on a common delta scale: $\delta^{44/40}$Ca relative to NIST 915a (Modified after Fantle and Tipper 2014). *BSE* Bulk Silicate Earth (After Huang et al. 2010)

mantle xenolithes and bulk mafic rocks (cf., DePaolo 2004; Huang et al. 2010).

Apart from the unanticipated and relatively large (up to 0.8 ‰) high-temperature fractionation of Ca isotopes in the Earth's mantle, another intriguing and currently unresolved aspect of the terrestrial Ca isotope cycle is the fact the mean $\delta^{44/40}$Ca signature of the global riverine Ca flux of about 0.9 ‰ overlaps with that of the silicate Ca reservoir ($\delta^{44/40}$Ca of ~1 ‰) but is systematically higher than the mean $\delta^{44/40}$Ca of carbonates ($\delta^{44/40}$Ca of ~0.6 ‰; Fantle and Tipper 2014). This finding is unexpected considering that previous studies suggested that the majority (>75%) of Ca in the global riverine flux should be derived from carbonates (Gaillardet et al. 1999; Berner and Berner 2012). Hence, one would expect that the mean $\delta^{44/40}$Ca signature of the global riverine flux to be much lower and closer to carbonate sources, i.e., somewhere between 0.6 and 0.7 ‰, based on a simple isotope mass-balance constraints using available data (cf., Fantle and Tipper 2014). Accordingly, either the current estimates of silicate vs. carbonate contributions of Ca to the global riverine flux are incorrect (i.e., the silicate-derived Ca contribution is underestimated), or there is an ongoing fractionation of Ca isotopes during the weathering and transport of Ca^{2+} ions that shifts the riverine $\delta^{44/40}$Ca to higher values relative to those observed in the source rocks (Fantle and Tipper 2014).

geological settings revealed systematic behavior of the $\delta^{44/40}$Ca proxy in certain igneous rocks and silicate minerals (Schiller et al. 2016 and references therein). Specifically, there is a general coupling between Ca isotopes and Ca and Mg contents in ultramafic rocks (i.e., dunite, peridotite, komatiite), where $\delta^{44/40}$Ca values become higher (i.e., heavier) with decreasing CaO and increasing MgO contents, but such trend has not been documented for felsic and mafic rocks (Schiller et al. 2016 and references therein). Complementary to this isotopically heavy Ca source in ultramafic rocks is the isotopically light Ca present in serpentinized slab mantle rocks, suggesting that perhaps dehydration of slab-mantle serpentinite can produce fluids with high $\delta^{44/40}$Ca that could be then imparted to ultramafic rocks via metasomatisms (Schiller et al. 2016 and references therein). Moreover, the Ca isotope analysis of mineral separates from mantle xenoliths and/or granitic rocks revealed systematic differences in $\delta^{44/40}$Ca signatures of individual minerals, which have been interpreted to reflect either a high temperature equilibrium isotope fractionation or isotope effects generated by igneous differentiation processes (Schiller et al. 2016 and references therein). Overall, the average $\delta^{44/40}$Ca of silicate rocks is close to 1 ‰, which is also our best estimate for the Ca isotope composition of the *bulk silicate Earth* (BSE), the latter constrained by the analysis of mineral separates from

Radiogenic Calcium Isotopes in Geological Reservoirs

The radiogenic, or mass independent, isotope variation of ^{40}Ca in nature is expressed as an epsilon (ε) notation in parts per ten thousand (10^4), relative to the Earth's mantle reservoir, according to the following relation (Marshall and DePaolo 1982):

$$\varepsilon_{Ca} = \left[\left(^{40}Ca/^{n}Ca\right)_{sample} / \left(^{40}Ca/^{n}Ca\right)_{mantle} - 1 \right] \cdot 10^4 \quad (3)$$

where n is 44 or 42, and the Ca isotope ratios of sample and mantle are after an "internal normalization" following an exponential law for the correction of an instrumental fractionation during the isotope analysis. The radiogenic isotope of calcium, ^{40}Ca, is the product of radioactive decay of potassium ^{40}K, with a half-life of 1.277 billion years; however, only about 89.5% of the ^{40}K decay results in the production of ^{40}Ca and the remaining 10.5% produce ^{40}Ar. Due to the relatively short half-life of ^{40}K compared to the age of the Earth, minerals and rock that crystallized in Precambrian and had high initial K/Ca ratios (e.g., the continental crust containing K-rich minerals like potassium feldspar and biotite) can accumulate significant amount of the radiogenic ^{40}Ca over time, thus yielding positive epsilon ε_{Ca} values.

The potential of a radiogenic ε_{Ca} tracer for the earth system evolution studies has been explored by Kreissig and Elliott (2005) to distinguish between two possible end-member scenarios for the early crustal growth (i.e., "steady-state" vs. "continuous" growth models) and concluded that Ca isotope data provide little support for the "steady-state" model. However, this study also found that the radiogenic Ca isotope proxy is not a robust tracer of crustal growth due to its sensitivity to secondary processes such as potassium metasomatism and/or the Ca isotope exchange during metamorphic events. More recent studies, performed both in laboratory (Ryu et al. 2011) and natural settings (Farkaš et al. 2011; Hindshaw et al. 2011), applied the ε_{Ca} proxy to investigate the weathering processes in granitic rocks and the associated release of a radiogenic ^{40}Ca from K-rich minerals (i.e., feldspar and biotite), with implications for mineral weathering, soil formation, and the sources of bioavailable Ca^{2+} for plants at base-poor granitic sites.

Future Directions in Ca Isotope Research

Aside from the abovementioned problem regarding the unexpectedly high $\delta^{44/40}Ca$ in the global riverine flux, compared to what is anticipated based on the estimates of carbonate vs. silicate partitioning of Ca in the world's rivers (Fantle and Tipper 2014), there are also unresolved issues related to the interpretation of Ca isotope variability observed in igneous rocks (Schiller et al. 2016 and references therein) and marine sedimentary archives (Fantle and Tipper 2014); the latter relevant for the reconstructions of past changes in the oceanic Ca cycle. Numerous studies aimed to constrain the Ca isotope evolution of seawater over different time intervals (e.g., Heuser et al. 2005; Farkaš et al. 2007; Payne et al. 2010; Blättler et al. 2011), using various marine archives such as bulk carbonate sediments, calcitic shells, marine barite, and phosphate. As pointed out by Fantle and Tipper (2014), such different approaches and recording phases have led to some conflicting results and uncertainties in terms of the reconstructed $\delta^{44/40}Ca$ evolution of the past seawater. Since then, more work has been done on Ca isotopes in the marine Ca cycle, particularly with the emphasis on "deep times" including Paleozoic and Neoproterozoic (e.g., Blättler and Higgins 2014; Kasemann et al. 2014; Du Vivier et al. 2015; Husson et al. 2015; Farkaš et al. 2016), yet the uncertainty with respect to the reconstructed $\delta^{44/40}Ca$ of paleo-seawater remains, and thus a more systematic research towards a better understanding of a marine $\delta^{44/40}Ca$ proxy in different mineral archives and depositional environments (e.g., *open* vs. *restricted* settings) is currently of a high priority. First pioneering studies addressing these issues have been recently performed, specifically Holmden et al. (2012a) investigated the effects of submarine groundwater (SGD) and a

"local elemental cycling" on the marine $\delta^{44/40}Ca$ proxy in a modern shallow-lagoon environment; and Hinojosa et al. (2012) utilized a "multiple-archive" approach (i.e., based on marine carbonates and phosphates) to constrain the Ca isotope composition of paleo-seawater. More work following these directions is needed, including laboratory-controlled precipitation and culturing experiments (cf., Tang et al. 2008), to realize the full potential of the Ca isotope proxy for the paleooceanographic and earth system evolution studies.

Finally, due to the different residence times of Ca and C in the oceans (i.e., 10^6 vs. 10^5 years, respectively), the marine $\delta^{44/40}Ca$ and $\delta^{13}C$ proxies are expected to respond differently to perturbations in the oceanic Ca and C cycles, assuming that these occurred in an "open ocean" settings (cf., Holmden et al. 2012b; Farkaš et al. 2016). Hence, any positive or negative $\delta^{13}C$ excursion recorded in marine archives should recover much faster compared to a time needed for the recovery of a possible accompanying $\delta^{44/40}Ca$ excursion, due to an order of magnitude longer residence time of Ca in the oceans compared to C. Accordingly, future detail studies that will use a coupled $\delta^{44/40}Ca$ and $\delta^{13}C$ proxy approach might help to clarify if the observed C isotope excursions in marine carbonates are indeed an evidence of past changes in the *global* marine C cycle, or rather reflect diagenetic and/or *local* scale processes. The latter involving a locally enhanced bioproductivity and/or a mixing of different water masses (e.g., seawater, groundwater) and carbonate sediments (i.e., facies migration) within a basin, linked to eustatic sea-level fluctuations (cf., Holmden et al. 2012b; Husson et al. 2015; Farkaš et al. 2016).

Advances in Ca Isotope Analysis

Analytical challenges associated with a precise and accurate measurements of stable and radiogenic Ca isotopes have been recognized by the community for decades (cf., Boulyga 2010; Fantle and Tipper 2014), and it was really the development of a new generation of mass spectrometers (both TIMS and MC ICP MS) over the last ca. 10–15 years which opened up the possibilities to fully explore the research potential of Ca isotopes. Although, most of the instrumental and analytical issues are now resolved and well understood, the main limitation for a rapid expansion of the field of the Ca isotope biogeochemistry lies in the relatively time-consuming sample preparation (i.e., chemical purification of Ca) and the necessity for a longer analytical runs (i.e., ca. 1.5 h for TIMS). Fortunately, recent advances in semiautomated sample purification systems (cf., Romaniello et al. 2015; Husson et al. 2015) promise to significantly speed up this sample preparation step, thus allowing a higher and more efficient sample throughput, and possibly also a more rapid expansion of the field in the near future.

Summary and Conclusions

Calcium is the fifth most abundant element in the Earth's crust, and due to its numerous isotopes (^{40}Ca, ^{42}Ca, ^{43}Ca, ^{44}Ca, ^{46}Ca, and ^{48}Ca), it is also a valuable isotope tracer in many geological and biological systems. The natural variations in the Ca isotope composition can be produced by either mass-depended fractionation processes (i.e., $\delta^{44/40}Ca$ and $\delta^{44/42}Ca$ variations) or via a radioactive decay of potassium ^{40}K, which generates radiogenic ^{40}Ca isotopes (i.e., ε_{Ca} variations). Thus far, available studies documented approximately 4 per mil variation in $\delta^{44/40}Ca$ in different terrestrial and marine samples, where the largest anomalies towards light Ca are produced due to a biological cycling of Ca both on land (i.e., plants, vegetation) and in the oceans (i.e., marine carbonates). In contrast, the isotopically heaviest Ca reservoir on Earth is the ocean water, which is thus complementary to the isotopically light Ca accumulated in marine carbonates. Relatively large Ca isotope variations (>0.5 per mil) have been documented in terrestrial igneous rocks, including ocean island basalts, granites, and mantle-derived rocks; thus implying that Ca isotopes can be also significantly fractionated during high-temperature processes.

Importantly, the biogeochemical cycle of Ca on Earth is tightly linked with the global C cycle and therefore the atmospheric CO_2, via processes such as continental weathering of carbonate/silicate rocks, hydrothermal reactions at mid-ocean ridges and off-axis centers, and the precipitation of shallow- and deep-water marine carbonates. Future detail Ca isotope studies on marine carbonate archives could thus help to better understand the functioning of the global C cycle and the origin of C isotope anomalies recorded in marine carbonate sediments.

Cross-References

▶ Alkali and Alkaline Earth Metals
▶ Calcium
▶ Carbonate Minerals and the CO_2-Carbonic Acid System
▶ Carbon Cycle
▶ Carbon Isotopes
▶ Geochronology and Radiogenic Isotopes
▶ Stable Isotope Geochemistry

References

Berner RA, Berner EK (1997) Silicate weathering and climate. In: Ruddiman WF (ed) Tectonic uplift and climate change. Plenum Press, New York, pp 313–327

Berner RA, Berner EK (2012) Global environment: water, air, and geochemical cycles. Princeton University Press, Princeton, p 488

Blättler CL, Higgins JA (2014) Calcium isotopes in evaporites record variations in Phanerozoic seawater SO_4 and Ca. Geology 42:711–714

Blättler CL, Jenkyns HC, Reynard LM, Henderson GM (2011) Significant increases in global weathering during Oceanic Anoxic Events 1a and 2 indicated by calcium isotopes. Earth Planet Sci Lett 309:77–88

Boulyga SF (2010) Calcium isotope analysis by mass spectrometry. Mass Spectrom Rev 29:685–716

DePaolo DJ (2004) Calcium isotopic variations produced by biological, kinetic, radiogenic and nucleosynthetic processes. Rev Mineral Geochem 55:255–288

Du Vivier ADC, Jacobson A, Lehn G, Selby D, Hurtgen MT, Sageman BB (2015) Ca isotope stratigraphy across the Cenomanian-Turonian OAE 2: links between volcanism, seawater geochemistry, and the carbonate fractionation factor. Earth Planet Sci Lett 416:121–131

Fantle MS, Tipper ET (2014) Calcium isotopes in the global biogeochemical Ca cycle: implications for development of a Ca isotope proxy. Earth Sci Rev 129:148–177

Farkaš F, Böhm F, Wallmann K, Blenkinsop J, Eisenhauer A, van Geldern R, Munnecke A, Voigt S, Veizer J (2007) Calcium isotope record of Phanerozoic oceans: implications for chemical evolution of seawater and its causative mechanisms. Geochim Cosmochim Acta 71:5117–5134

Farkaš J, Déjeant A, Novák M, Jacobsen SB (2011) Calcium isotope constraints on the uptake and sources of Ca^{2+} in a base-poor forest: a new concept of combining stable ($\delta^{44/42}Ca$) and radiogenic (εCa) signals. Geochim Cosmochim Acta 75:7031–7046

Farkaš J, Frýda J, Holmden C (2016) Calcium isotope constraints on marine carbon cycle and $CaCO_3$ deposition during the late Silurian (mid-Ludfordian) positive d13C excursion. Earth Planet Sci Lett. (in press). https://doi.org/10.1016/j.epsl.2016.06.038

Gaillardet J, Dupre B, Louvat P, Allegre CJ (1999) Global silicate weathering and CO_2 consumption rates deduced from the chemistry of large rivers. Chem Geol 159:3–30

Heuser A, Eisenhauer A, Böhm F, Wallmann K, Gussone N, Pearson PN, Nägler TF, Dullo WC (2005) Calcium isotope ($\delta^{44/40}Ca$) variations of Neogene planktonic foraminifera. Paleoceanography 20:PA2013

Hindshaw RS, Reynolds B, Wiederhold JG, Bourdon B (2011) Calcium isotopes in a proglacial weathering environment: Damma Glacier, Switzerland. Geochim Cosmochim Acta 75:106–118

Hinojosa JL, Brown ST, Chen J, DePaolo DJ, Paytan A, Shen SZ, Payne JL (2012) Evidence for end-Permian Ocean acidification from calcium isotopes in biogenic apatite. Geology 40:743–746

Hoefs J (2015) Stable isotope geochemistry. Springer, Berlin, p 389

Holmden C, Papanastassiou DA, Blanchon P, Evans S (2012a) $\delta^{44/40}Ca$ variability in shallow water carbonates and the impact of submarine groundwater discharge on Ca-cycling in marine environments. Geochim Cosmochim Acta 83:179–194

Holmden C, Panchuk K, Finney S (2012b) Tightly coupled records of Ca and C isotope changes during the Hirnantian glaciation event in an epeiric sea settings. Geochim Cosmochim Acta 98:94–106

Huang S, Farkaš J, Jacobsen SB (2010) Calcium isotope fractionation between clinopyroxene and orthopyroxene from mantle peridotites. Earth Planet Sci Lett 292:337–344

Husson JM, Higgins JA, Maloof AC, Schoene B (2015) Ca and Mg isotope constraints on the origin of Earth's deepest $\delta^{13}C$ excursion. Geochim Cosmochim Acta 160:243–266

Kasemann SA, Pogge von Strandmann PAE, Prave AR, Fallick AE, Elliott T, Hoffmann KH (2014) Continental weathering following a Cryogenian glaciation: evidence from calcium and magnesium isotopes. Earth Planet Sci Lett 396:66–77

Kreissig K, Elliott T (2005) Ca isotope fingerprints of early crust-mantle evolution. Geochim Cosmochim Acta 69:165–176

C

Marshall BD, DePaolo DJ (1982) Precise age determinations and petrogenetic studies using K-Ca method. Geochim Cosmochim Acta 46:2537–2545

Payne JL, Turchyn AV, Paytan A, DePaolo DJ, Lehrmann DJ, Yu M, Wei J (2010) Calcium isotope constraints on the end-Permian mass extinction. Proc Natl Acad Sci 107:8543–8548

Romaniello SJ, Field MP, Smith HB, Gordon GW, Kim MH, Anbar AD (2015) Fully automated chromatographic purification of Sr and Ca for isotopic analysis. J Anal At Spectrom 30:1906–1912

Ryu JS, Jacobson AD, Holmden C, Lundstrom C, Zhang Z (2011) The major ion, $\delta^{44/40}Ca$, $\delta^{44/42}Ca$, and $\delta^{26}Mg$ geochemistry of granite weathering at pH = 1 and T = 25° C: power-law processes and the relative reactivity of minerals. Geochim Cosmochim Acta 75:6004–6026

Schiller M, Gussone N, Wombacher F (2016) High temperature geochemistry and cosmochemistry. In: Calcium stable isotope geochemistry. Springer, Berlin/Heidelberg

Tang J, Dietzel M, Böhm F, Köhler SJ, Eisenhauer A (2008) Sr^{2+}/Ca^{2+} and $^{44}Ca/^{40}Ca$ fractionation during inorganic calcite formation: II. Ca isotopes. Geochim Cosmochim Acta 72:3733–3745

Calorimetry

Masaki Akaogi
Department of Chemistry, Gakushuin University, Tokyo, Japan

Definition

In major areas in Earth Science, particularly geochemistry, petrology, and mineralogy, one of fundamental theoretical frameworks is thermodynamics which is expressed by thermodynamic functions: Gibbs energy, Helmholtz energy, enthalpy, entropy, heat capacity, etc. Calorimetry means experiments to measure heat changes which lead to the thermodynamic quantities. A calorimeter is an instrument used to measure the heat change associated with change of a substance. The heat change at a constant pressure is equal to enthalpy change. Calorimetric measurements are generally divided into two categories (Sorai 2004). The first one is measurement of heat capacity, and the second is measurement of heat of reaction.

Heat Capacity Measurement

The heat capacity is defined as absorbed heat energy divided by the associated temperature change in a substance, and customarily two different heat capacities are defined, C_p and C_v, relating to temperature change at constant pressure and to that at constant volume, respectively. The heat capacity is a function of intrinsic energy related to atomic motion or lattice vibration of the substance. At a temperature range between near 0 K and about room temperature, C_p is measured using adiabatic calorimetry and thermal relaxation calorimetry. The standard entropy at 298.15 K ($S^0_{298.15}$) of a pure crystalline substance is obtained by integrating C_p/T with T between 0 and 298.15 K. A latent heat of transition is also measured in the heat capacity measurement. For C_p measurement at temperature above room temperature, two methods can be adopted: differential scanning calorimetry up to about 2000 K and high-temperature drop calorimetry up to about 2500 K. Among the above techniques, the adiabatic calorimetry is most accurate but requires a sample of at least several grams, as well as in the high-temperature drop calorimetry. Instruments for differential scanning calorimetry and thermal relaxation calorimetry are commercially available and need a sample of only about 10–20 mg, though the methods are somewhat less accurate than the other two methods. However, it is generally not feasible to get a large amount of natural homogeneous samples or to synthesize pure materials of several grams, particularly at high pressure and high temperature.

Reaction Calorimetry

The second method of calorimetry used in Earth Science is reaction calorimetry, which is generally solution calorimetry to measure heat associated with dissolution of a substance in a solvent at a constant pressure, mostly atmospheric pressure. The experimental solution calorimetry is divided into two types: hydrofluoric acid solution calorimetry and high-temperature oxide melt solution calorimetry. In the former measurement, a sample is dissolved in HF at around 323 K, and in the latter a sample is dissolved in oxide melt such as lead borate and sodium molybdate at 1000–1100 K, in order to measure heat of solution of a substance. The heats of formation, transition, and reaction are calculated from the measured heats using thermochemical cycles. The heats of mixing of solid solutions and of glasses and heat associated with order-disorder transition can also be measured. Oxide melt solution calorimetry needs a sample of only several to several 10 mg and is widely used to various inorganic compounds including silicate minerals, metal oxides, hydrous phases, high-pressure phases, nanomaterials, etc.

Summary

Measurements of heat capacity and heat of reaction are fundamental experimental techniques to obtain the important thermodynamic quantities. A limited number of laboratories perform calorimetric measurements because the methods are specialized. For minerals and related inorganic substances of

geochemical, petrological, and mineralogical interests, calorimetrically measured data and derived data from them are summarized in several publications (e.g., Robie and Hemingway 1995; Navrotsky 1997, 2014).

Cross-References

- ▶ Enthalpy
- ▶ Entropy
- ▶ Equilibrium
- ▶ Free Energy
- ▶ Geochemical Thermodynamics
- ▶ Geothermometry and Geobarometry
- ▶ Heat Capacity
- ▶ Phase Equilibria

References

Navrotsky A (1997) Progress and new directions in high temperature calorimetry revisited. Phys Chem Minerals 24:222–241

Navrotsky A (2014) Progress and new directions in calorimetry: a 2014 perspective. J Am Ceram Soc 97:3349

Robie RA, Hemingway BS (1995) Thermodynamic properties of minerals and related substances at 298.15 K and 1 bar (10^5 Pascals) pressure and at higher temperatures. US Geol Surv 2131: 461pp

Sorai M (2004) Comprehensive handbook of calorimetry and thermal analysis. Wiley, London, 534 pp

Carbon

Adrian Jones
Department of Earth Sciences, University College London, London, UK

Element Data
Atomic Symbol: C
Atomic Number: 6
Atomic Weight: 12.0107
Isotopes and Abundances: ^{12}C: ~98.89%, ^{13}C: ~1.11%, ^{14}C ~10^{-12}
Atm Melting Point*: 3550 °C
1 Atm Boiling Point*: 4492 °C (101 kPa)
Common Valences: −4, 0, +2, +4
Ionic Radii: 30 pm (4+)
Pauling Electronegativity: 2.5
First Ionization Energy: 1086 kJmol^{-1}

(continued)

Chondritic (CI) Abundance: 3.65 wt%
Silicate Earth Abundance: 50–500 ppm
Crustal Abundance: ~1800 ppm
Seawater Abundance: ~28 ppm
Core Abundance: unknown 0.2–2%

C

Properties

Carbon has three isotopes, two are stable ^{12}C (98.89%) and ^{13}C (1.11%) plus a radioactive isotope ^{14}C (~10^{-12}). The systematics of carbon isotopes yield important information about their environments and are discussed separately (Cross reference #1). ^{12}C is the standard which defines mass number 12 containing 6 protons, 6 neutrons, and 6 electrons.

The melting point of carbon is extremely high and varies with pressure*; in a carbon arc, it sublimes above ~5,530 °C, which is higher in temperature than any known metal. Consequently, carbon may have been the first element to condense from gas to solid in the protoplanetary nebula as nanodiamond or graphite, although oxidized forms are also abundant in the universe. The ability of hydrocarbons to bond with themselves is known as catenation and leads to more complex forms, such as cyclohexane, or even benzene. Hydrocarbons are hydrophobic. Some are abundant in the solar system as sampled widely in primitive undifferentiated meteorites like chondrites (Sephton 2002). Carbon-rich lakes of methane occur on Titan, and polycyclic aromatic hydrocarbons (PAHs) are abundant in nebulae. In carbonaceous chondrites, the average carbon abundance is 3.65 wt%, whereas in the bulk Earth estimates for carbon vary from 50 to 500 (Zhang and Zindler 1993; Marty 2012) and much of Earth's carbon from ~0.2 to 2 wt%, maybe in the core (Wood et al. 2013).

History and Use

Carbon (*from* Latin *carbo* meaning charcoal or coal), the element with atomic number 6, is the fourth most abundant element in the universe but is less abundant in the *differentiated* Earth. Carbon occurs naturally in pure elemental form, the two most famous crystalline allotropes of carbon are diamond (cubic, density 3.51 gcm^{-3}), the hardest known mineral, and graphite (hexagonal, density 2.266 gcm^{-3}), one of the softest and most refractory substances known. Other carbon allotropes of native carbon include crystalline lonsdaleite, chaoite, fullerenes, and graphene, plus several noncrystalline forms of glassy ("vitreous") carbon, nanofoam ("carbon aerogel"), and carbine (Hazen et al. 2013, Table 1).

In diamond, each carbon atom is bonded to four adjacent carbon atoms in tetrahedral coordination, with a C─C distance of ~1.54 A$^{\circ}$, and C─C─C angles close to ideal 109.5°. This tetrahedral covalent bonding configuration reflects the hybridization of one 2 s and three 2p orbitals from each carbon atom to form four sp^3 orbitals. The framework structure of diamond leads to its superlative physical and chemical properties, including being the hardest known material (10 on *Moh's scale of hardness*). The absence of conduction electrons make diamond an insulator, yet paradoxically it is an excellent thermal conductor with ~five times better thermal conductivity than copper, which some jewellers can detect by touch. Diamond forms naturally at depths on Earth below ~150 km and is stable to temperatures and pressures greater than at the centre of the Earth (Oganov et al. 2013).

The optical properties of diamond feature the widest transparency of all known solids, extending from the UV (225 nm) to the far infrared, even at very high temperatures and radiation intensities. The combination of unique properties, including hardness and brilliance, have led to its preeminence as a gemstone. The best diamond gemstones are graded for qualities of the "four c's"; cut, color, clarity (absence of inclusions), and carat weight. One carat equals 1/5 g. The main impurity in "Type I" natural diamond is nitrogen, trapped in the lattice as single atoms, aggregates or clusters capable of changing color toward yellow and brown. The specific nitrogen residency in diamond provides a useful way of categorizing diamond, with nitrogen-free "Type II" diamond being the rarest (Cartigny 2005). A nitrogen-induced optical absorption in diamond around 270 nm has been identified in interstellar clouds. Diamond formed by shock during hypervelocity impact cratering usually contains the hexagonal polymorph called lonsdaleite, as at the 35 Ma Popigai impact crater in Siberia (Jones et al. 2016).

Since the 1950s, diamond synthesized at high pressures and temperatures (HPHT) replicates all of the mechanical properties of natural diamond suitable for industrial uses, but usually with different absorption and luminescence lines inherited from nickel and cobalt-rich metal solvents. Diamond can also be grown dynamically from low-pressure gas by chemical vapor deposition (CVD).

"Carbonado" is a variety of black or dark polycrystalline diamond, which is slightly porous, found only in Brazil and the Central African Republic, and possibly of nonterrestrial origin (Garai et al. 2006).

In graphite, graphene, fullerenes, and several types of amorphous and glassy carbon, the carbon atoms are covalently bonded in planar three-coordination, with typical C─C distances of ~1.42 A$^{\circ}$, and C─C─C angles close to 120°. This trigonal coordination results from hybridization of carbon electrons where the 2 s orbital mixes with two 2p orbitals to form three sp^2 orbitals. Graphite is formed of electronically neutral, monatomic flat carbon layers, which bonds through relatively weak van der Waals attractions between the layers, separated by 3.41 A$^{\circ}$. The layered structure leads to highly orientation-dependent or anisotropic properties and the weak interlayer bonding leads to uses as a lubricant and as pencil "lead." Graphite is highly refractory and its very high-temperature stability, >4,800 K, make it useful as a heater or in nuclear reactors as a neutron moderator.

Individual one atom-thick two-dimensional carbon layers when meticulously separated are known as graphene, a pure carbon allotrope ~200 times stronger than steel, with unique electronic and mechanical properties (Geim and Novoselov 2007) that can produce lightweight composite structures which can be transparent, flexible, and yet impermeable even to helium.

Geochemical Behavior

Carbon shows remarkable chemical flexibility with the ability to bond to itself and with more than 80 other elements, most commonly in 2-, 3-, and 4-coordination. Carbon has oxidation numbers ranging from −4 to +4 and can behave as a cation, as an anion, and as a neutral species in mineral phases with a spectacular variety of crystal structures, chemical bonding, and physical and chemical properties (Hazen et al. 2013). Carbon occurs in solids, liquids, and gases in variable amounts throughout the Earth, from the atmosphere and oceans to the crust-mantle and core, as both a major element and trace element. Carbon on Earth also moves, and is fundamental to life, it belongs to the boundary matter between living and nonliving matter, and is central to the science of organic chemistry. Carbon transforms and moves between near-surface reservoirs in the *carbon cycle* (Berner 2004) and carbon also moves deep below the surface through rocks over geological timescales, as studied by the Deep Carbon Observatory (https://deepcarbon.net) extending the biosphere on Earth to the deep subsurface (Colwell and D'Hondt 2013; Schrenk et al. 2013). Evidence for the connection between the Earth's conventional *carbon cycle* and the *deep carbon cycle* is provided in the form of volcanic degassing, where volatile gases deliver carbon as CO_2 to the atmosphere, and subducting plates return solid carbon back into the mantle; the carbon flux of this geological process is enormous but slow and is globally estimated to be largely in balance (Kelemen and Manning 2015).

Carbon Minerals

By far the most abundant carbon minerals in the Earth's crust are carbonates, whose crystal structures incorporate $(CO_3)^{2-}$ anions, with an equilateral triangle of oxygen atoms around the central carbon atom. Most C─O bond distances are

between 1.21 and 1.30 A^O, and O—C—O angles are ~120°. Two types of rhombohedral carbonates, calcite and dolomite (CaMg(CO$_3$)$_2$), account for at least 90% of crustal carbon as massive sedimentary and metamorphic formations (Reeder 1983). In the calcite structure (CaCO$_3$), each Ca^{2+} cation is coordinated to six (CO$_3$)$^{2-}$ groups and each (CO$_3$)$^{2-}$ group is coordinated to six Ca^{2+} cations.

Calcite appears most commonly in sedimentary rocks where it occurs as the principal mineral of limestone, and as natural cement in siliceous sandstone and shales. In the present day, calcite is deposited within shallow marine settings, but the distributions of carbonate minerals have varied through Earth history, principally as a consequence of evolving feedback between the geosphere and biosphere (Hazen et al. 2008). Calcite is also common in metamorphic rocks such as marble and calcareous gneiss. Calcite and other carbonate minerals also crystallize in unusual carbonate-rich igneous volcanic rocks called carbonatites (Jones et al. 2013). Approximately 200 of the ~300 known carbonate minerals also include water in their structure. These include mixed anionic forms such as carbonate sulfates, carbonate silicates, and carbonate phosphates. The common copper carbonates are also hydrous including highly colored varieties like green malachite and blue azurite, which form in the oxidized zones of copper deposits.

Carbides, such as cohenite (Fe, Co, Ni)$_3$C, are refractory materials formed where carbon bonds to a less electronegative element, represented by ~10 different naturally occurring minerals. These are scarce in the Earth's crust, but familiar from meteorites and may represent a significant volume fraction of carbon in Earth's deep interior especially the core (Wood et al. 2013).

Organic Carbon and Energy

Carbon forms a variety of minerals which incorporate organic molecules into their structure, including organic molecular crystals, carbon minerals with organic anions, clathrate silicates, and clathrate hydrates. These can have both biological and nonbiological origins. The water-based clathrates are also known as gas hydrates or clathrate hydrates, and are remarkable compounds which form at low temperatures (<0 °C) and elevated pressures (>6 MPa). They are widely distributed around the globe in deep-offshore marine environments and have attracted growing interest because of their enormous potential for methane-based energy. The unnamed main form of "methane ice," which occurs in oceans and deep permafrost regions, is a large cubic 3D H$_2$O framework with two types of cages partially filled with methane (CH$_4$) molecules holding on average ~0.17 moles of methane per mole of water, with a density close to 0.9 gcm^{-3} (Max 2003).

A major category of carbon materials concerns carbon deposits in the crust, which are related to energy resources, namely coal and hydrocarbons. Coals are combustible sedimentary rocks derived from organic matter and are composed primarily of carbon, plus other volatile elements like hydrogen, oxygen, sulfur, and nitrogen. The sequence of coal formation by *carbonization* occurs over long geological timescales, accompanied by burial, increasing in grade from peat to lignite, then subbituminous coal, bituminous coal, and finally anthracite. Mature coal deposits sometimes hold unusual crystalline hydrocarbon phases and other organic materials (Sephton and Hazen 2013).

Deep deposits of hydrocarbons represent perhaps the most economically important component of the deep carbon cycle. Most are considered to have a purely biological origin, but there are some challenges to this paradigm, which include similar methane-rich hydrocarbons observed to form in ultramafic rocks like serpentinites (Schrenk et al. 2013), suggesting that alternative nonbiogenic pathways to form hydrocarbon gas deposits are also possible.

Conventional natural oil and gas resources reside in sedimentary basins, and the hydrocarbons of interest consist entirely of carbon and hydrogen, forming a large number of organic compounds. Their empirical formulae differ between types of gaseous hydrocarbons in the series of linear structured hydrocarbons; the amount of bonded hydrogen decreases in the series of alkanes, alkenes, and alkynes, with self-bonding of carbon preventing saturation of the hydrocarbon by the formation of double or triple bonds. Liquid components of petroleum include a complex mixture primarily of linear and cyclic hydrocarbons from C$_3$ to C$_{10}$, as well as numerous other molecular species, while solid hydrocarbons include such broad categories as paraffin waxes (typically from C$_{18}$ to C$_{40}$).

Summary

Carbon (atomic number 6) is the fourth most abundant element in the solar system. Its abundance on Earth is much less well known. It exists everywhere in the atmosphere and oceans, through the crust and mantle in the deep subsurface all the way to the core. A major global concerted effort is underway (the *Deep Carbon Observatory*) to quantify the reservoirs and fluxes of carbon below the surface, to find out how deep life can exist on our planet, and to evaluate how all this additional carbon impacts, if at all, on the measurable and observable *carbon cycle*.

Diamond is the most spectacular form of native elemental carbon. Used since ancient times as a gemstone, not only does it have brilliant optical properties and unmatched hardness, but sophisticated advances in synthesis, including low-pressure chemical vapor deposition (Roy 1987), are leading
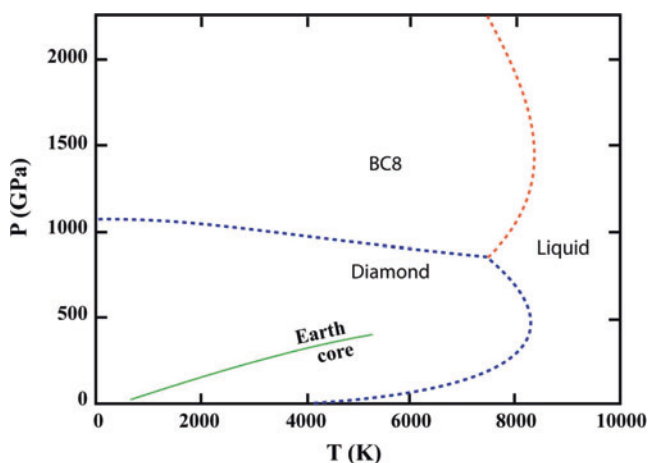
Carbon, Fig. 1 Phase diagram for elemental carbon at high temperatures and pressures

to new uses of diamond in industry. Diamond is also at the forefront of experimental research into defining the limits of extreme pressure and temperature. Two opposing diamonds are used to generate very high static pressures in the megabar range a small experimental device called a "diamond anvil cell," permitting simultaneous heating by laser to thousands of degrees (Lazor et al. 1992). Diamond is the deepest known mineral from Earth, and may also be the oldest, but it is currently impossible to date. By contrast 1-atom thick-layered carbon, graphene, was only isolated in 2004 and is emerging as an important industrial material.

Carbon exists in many forms on Earth, not just as allotropes some of which like diamond are actually rare, but also as hundreds of inorganic minerals and organic compounds or hydrocarbons. Dispersed carbon may also be present deep in the Earth as a nonstoichiometric component in high-pressure silicate minerals and dissolved as CO_2 in silicate melts (Ni and Keppler 2013).

Carbon is essential to life on Earth and can exist in gaseous, liquid, and solid forms. Its mobility in dissolved aqueous fluids is particularly important, not only in the oceans and hydrosphere but in the way tectonic plates are subducted at plate boundaries over geological time (Fig. 1).

Cross-References

References

Berner RA (2004) The phanerozoic carbon cycle. Oxford University Press, Oxford, 158 pp

Cartigny P (2005) Stable isotopes and the origin of diamond. Elements 1:79–84

Colwell FS, D'Hondt S (2013) Nature and extent of the deep biosphere. In: Hazen RM, Jones AP, Baross JA (eds) Carbon in Earth. Review in mineral and geochemistry, vol 75, pp 547–574

Garai J, Haggerty SE, Rekhi S, Chance M (2006) Infrared absorption investigations confirm the extraterrestrial origin of carbonado diamonds. Astrophys J 653:L153–L156

Geim AK, Novoselov KS (2007) The rise of graphene. Nat Mater 6:181–191

Hazen RM, Papineau D, Bleeker W, Downs RT, Ferry JM, McCoy TJ, Sverjensky DA, Yang H (2008) Mineral evolutions. Am Mineral 93:1693–1720

Hazen RM, Downs RT, Jones AP, Kah L (2013) Carbon mineralogy and crystal chemistry. In: Hazen RM, Jones AP, Baross JA (eds) Carbon in Earth. Review in mineral and geochemistry, vol 75, pp 7–46

Jones AP, McMillan PF, Salzmann CG, Alvaro M, Nestola F, Prencipe M, Dobson D, Hazael R, Moore M (2016) Structural characterisation of natural diamond shocked to 60 GPa; implications for earth and planetary sciences. Lithos 265:214–221

Jones AP, Genge M, Carmody L (2013) Carbonate melts and carbonatites. In: Hazen RM, Jones AP, Baross JA (eds) Carbon in Earth. Review in mineralogy and Geochemistry, vol 75, pp 289–322

Kelemen PB, Manning CE (2015) Reevaluating carbon fluxes in subduction zones, what goes down, mostly comes up. Proc Natl Acad Sci 112:E3997–E4006

Lazor P, Shen G, Saxena SK (1992) Laser-heated diamond anvil cell experiments at high pressure: melting curve of nickel up to 700 kbar. Phys Chem Miner 20:86–90

Marty B (2012) The origins and concentrations of water, carbon, nitrogen and noble gases on earth. Earth Planet Sci Lett 313–314:56–66

Max MD (2003) Natural gas hydrate in oceanic and permafrost environments. Kluwer Academic, Dordrecht

Ni H, Keppler H (2013) Carbon in silicate melts. In: Hazen RM, Jones AP, Baross JA (eds) Carbon in Earth. Review in mineral and geochemistry, vol 75, pp 251–287

Oganov AR, Hemley RJ, Hazen RM, Jones AP (2013) Structure, bonding, and mineralogy of carbon at extreme conditions. In: Hazen RM, Jones AP, Baross JA (eds) Carbon in Earth. Review in mineral and geochemistry, vol 75, pp 47–77

Reeder RJ (ed) (1983) Carbonates: mineralogy and chemistry. Reviews in Mineralogy, vol 11

Roy R (1987) Diamonds at low pressure. Nature 325:17–18

Schrenk MO, Brazelton WJ, Lang SQ (2013) Serpentinization, carbon, and deep life. In: Hazen RM, Jones AP, Baross JA (eds) Carbon in Earth. Review in mineral and geochemistry, vol 75 pp 575–606

Sephton MA (2002) Organic compounds in carbonaceous chondrites. Nat Prod Rep 19:292–311

Sephton MA, Hazen RM (2013) On the origins of deep hydrocarbons. In: Hazen RM, Jones AP, Baross JA (eds) Carbon in Earth. Review in mineral and geochemistry, vol 75, pp 449–465

Wood BJ, Li J, Shahar A (2013) Carbon in the core: its influence on the properties of core and mantle. In: Hazen RM, Jones AP, Baross JA (eds) Carbon in Earth. Review in mineral and geochemistry, vol 75, pp 231–250

Zhang YZ, Zindler A (1993) Distribution and evolution of carbon and nitrogen in earth. Earth Planet Sci Lett 117:331–345

Carbon Cycle

Elizabeth A. Canuel[1] and Amber K. Hardison[2]
[1]Department of Physical Science, Virginia Institute of Marine Science, College of William & Mary, Gloucester Point, VA, USA
[2]Marine Science Institute, The University of Texas at Austin, Port Aransas, TX, USA
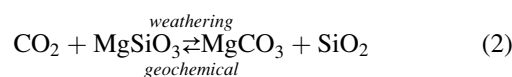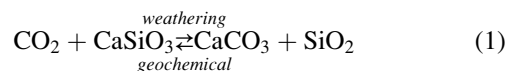
Definition

The biochemical and geochemical cycling of the organic and inorganic forms of carbon through Earth processes is referred to as the global carbon cycle. The carbon cycle considers the flow of carbon across four reservoirs: atmosphere; continental, including the biosphere, freshwaters, and soils; ocean; and geosphere (Fig. 1). Processes influencing the transfer of carbon between reservoirs occur over short (active) and long (geologic) timescales. The global carbon cycle is closely linked to the cycles of other elements (e.g., oxygen, nitrogen, phosphorus, and sulfur) because of the important role these elements play in biological and geological processes. Studies of the carbon cycle encompass contemporary, historical, and geologic timescales. Analyses of the rock and sediment records aim to understand how the carbon cycle has varied in the past in response to global transformations and earth system cycles and provide useful analogues for understanding future change. Ice cores provide a record of atmospheric concentrations of carbon dioxide (CO_2) and methane (CH_4) over the past 400,000 years. Interest in the carbon cycle has grown in recent decades due to increasing concentrations of atmospheric CO_2 from anthropogenic combustion of fossil fuels and associated effects on global climate change.

Inorganic Carbon

The main reservoirs of inorganic carbon in the Earth's crust are sedimentary rocks, which hold ~60,000,000 Pg (1 Pg = 10^{15} g) (Hedges and Keil 1995). This oxidized carbon occurs primarily as carbonate minerals (calcite and dolomite) in limestones (80%) and shales (14%) (Hunt 1996). These rock reservoirs are isolated from surficial processes by deep burial and only affect biological cycles on geologic

timescales. In contrast, surficial reservoirs, although considerably smaller in size, are more dynamic on biological timescales. The largest of these "active" reservoirs is dissolved inorganic carbon (DIC) in seawater (~40,000 PgC) (Hedges and Keil 1995). Approximately 25% of all marine DIC is stored in the upper kilometer of ocean above the permanent thermocline (Hedges 1992) with most exchange between the atmosphere and ocean taking place in the mixed layer (25–200 m). DIC is also stored in the deep ocean, and exchange between the deep ocean carbon pool and the atmosphere through the process of upwelling occurs at ~1,000 year timescales. Other major reservoirs of inorganic carbon at the Earth's surface include soil carbonates (1,100 PgC) and atmospheric CO_2 (828 PgC).

At geologic timescales, inorganic carbon is transferred between the geosphere and atmosphere by geochemical (weathering) and geothermal (tectonic) processes (Eqs. 1 and 2). Rock weathering produces dissolved bicarbonate (HCO_3^-), which is delivered to the ocean by rivers and groundwater where it is precipitated as calcium carbonate ($CaCO_3$) and other carbonate minerals. There is a positive feedback between weathering and tectonics because subduction processes cause the outgassing of CO_2 from the mantle, thereby increasing atmospheric CO_2 and temperature. Tectonic processes also increase weathering by increasing the amount of land available to weathering through uplift and mountain building. These processes are summarized in the following equations with the forward reaction described on top and the reverse reaction on the bottom:

$$CO_2 + CaSiO_3 \underset{geochemical}{\overset{weathering}{\rightleftarrows}} CaCO_3 + SiO_2 \qquad (1)$$

$$CO_2 + MgSiO_3 \underset{geochemical}{\overset{weathering}{\rightleftarrows}} MgCO_3 + SiO_2 \qquad (2)$$

Organic Carbon

Organic carbon (OC) is present in both living and nonliving systems and ultimately fuels all of Earth's biogeochemical processes. Understanding the formation, cycling, and preservation of OC is essential for understanding the cycling of all bio-elements between living and nonliving reservoirs, the formation of economically important petroleum and coal deposits, and predicting how human activity may change the natural balance of these systems.
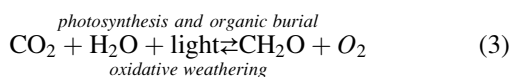
Much of the OC formed during photosynthesis or by chemosynthetic autotrophs is decomposed by heterotrophic organisms. Heterotrophic processes occur in the water column of marine and aquatic environments, as well as in sediments, soils, and rocks. Organic matter (OM) diagenesis
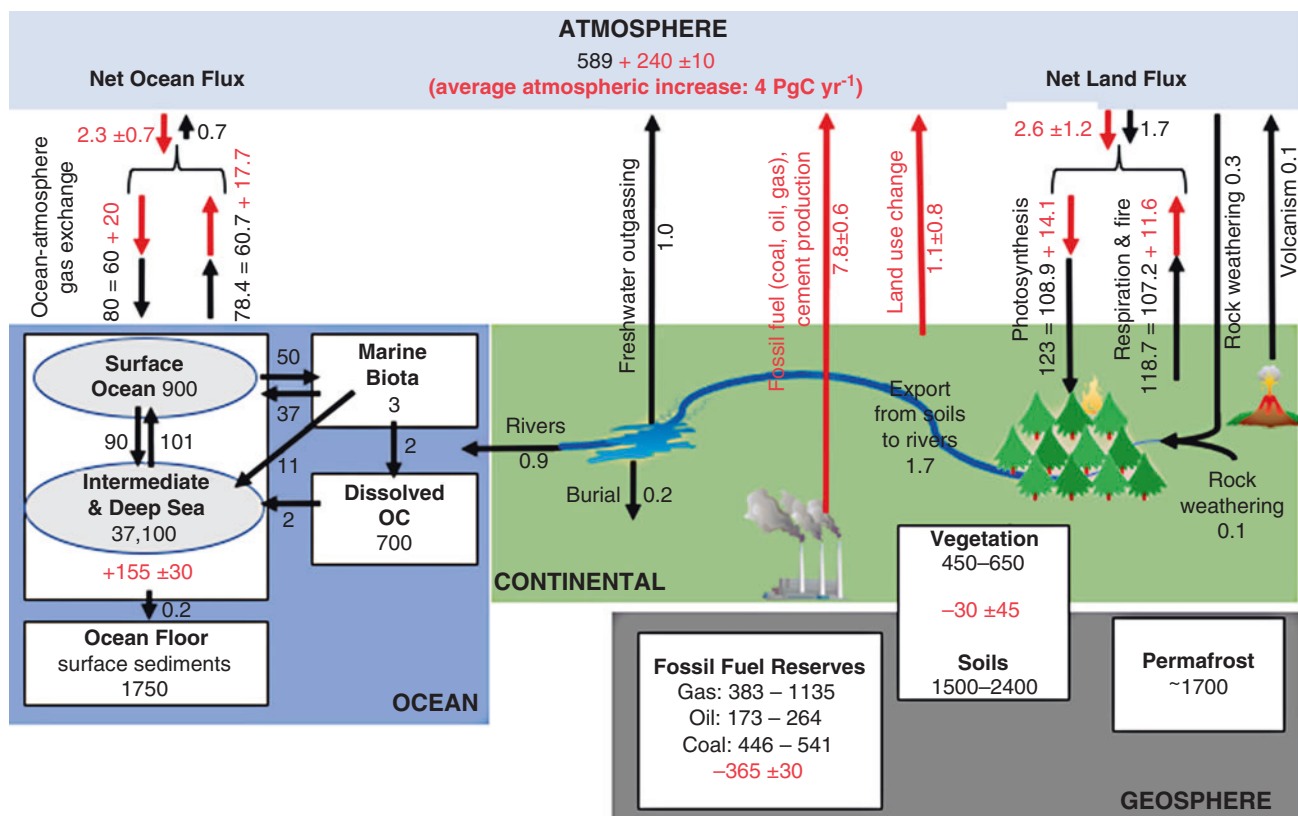
Carbon Cycle, Fig. 1 Simplified schematic of the global carbon cycle, with a focus on the relatively fast-cycling reservoirs. *Numbers* represent reservoir mass, also called "carbon stocks" in PgC and annual carbon exchange fluxes (in PgC year^{-1}). *Numbers* and *arrows* indicate reservoir mass and exchange fluxes estimated for the time prior to the Industrial Era (~1750). *Red* reservoir numbers denote cumulative changes of anthropogenic carbon over the Industrial Period 1750–2011. *Red arrows* and *numbers* indicate annual anthropogenic fluxes averaged from 2000 to 2009. By convention, a positive cumulative change means that a reservoir has gained carbon since 1750. Unless otherwise specified, these values pertain to total C, while values in the text are provided for organic and inorganic C pools (Figure adapted from Ciais et al. (2013) and references therein. *Symbols* courtesy of Integration and Application Network, University of Maryland Center for Environmental Science (ian.umces.edu/imagelibrary/))

occurs under low temperature (<50 °C) and low pressure and primarily through biological processes that occur in surface sediments. The OC preserved following diagenesis is subject to further alteration by the processes of catagenesis and metagenesis, which occur at higher temperatures and pressures and lead to the formation of petroleum and natural gas.

$$\underset{\textit{oxidative weathering}}{\overset{\textit{photosynthesis and organic burial}}{CO_2 + H_2O + light \rightleftarrows CH_2O + O_2}} \qquad (3)$$

The major fluxes between organic pools are driven by marine and terrestrial primary production (Fig. 1). The active (surficial) pools of OC include soil humus, land and marine plant tissue, seawater dissolved OC (DOC), and surface marine sediments (Hedges and Keil 1995). Photosynthesis, the harvesting of light energy to convert inorganic carbon to reduced (organic) forms in the tissue of plants, is the primary mode of primary production. However, chemosynthesis by microbial organisms, which uses chemical energy rather than

sunlight, is also important. The fixation of carbon by plants over the Earth's history accounts for the oxygen in the atmosphere; thus the cycles of carbon and oxygen are closely linked over geologic time. In fact, to maintain current atmospheric oxygen levels, rapid cycling of carbon in the surficial pools is required. These pools exchange on relatively short timescales (10^2–10^4 years). In contrast, OC that remains in the sedimentary system cycles slowly (~10^8 year). Over geologic time, sedimentary reservoirs only become exchangeable through uplift, followed by oxidative weathering of OC by exposure to the atmosphere (Eq. 3).

Global gross primary production on land (123 PgC year^{-1}) is dominated by nonwoody plant tissues such as leaves, grasses, and herbaceous plants (Schlesinger 1997). The highest gross terrestrial production and storage as biomass occurs in the tropics (56%), while polar regions are considerably less productive (0.5%; Taube 1992). Forests are the most productive continental biomes; deserts and tundra are the least productive, reflecting global patterns of temperature and

precipitation. Marine primary productivity (~50 PgC year^{-1}) is dominated by open water (pelagic) phytoplankton productivity because open water constitutes ~75% of the total ocean area. However, when normalized to area, coastal and upwelling areas together account for nearly two-thirds of the total oceanic productivity because a greater supply of nutrients is available to support phytoplankton in these areas. Other primary producers along the coasts (i.e., seagrass, marsh plants, macroalgae, mangroves) provide locally important sources of OC (Canuel and Hardison 2016).

Delivery of OC (as dissolved and particulate fractions) from the land to coastal marine environments by rivers accounts for 0.4 PgC year^{-1} (Meybeck 1982). However, there remains considerable uncertainty in the ability to adequately quantify carbon exchange from land to the coastal ocean and in understanding the processes influencing the fate of terrigenous carbon in coastal sediments (Hedges and Keil 1995). Generally, the total annual riverine OC load to the ocean is proportional to annual total river flow, which is dominated by a small set of rivers that transport the bulk of the freshwater from land to sea (Schlesinger 1997). However, seasonal and annual/interannual variations in hydrology as well as large events such as storms and hurricanes influence the input, dispersion, and cycling of sediment OM in coastal environments, thus making it difficult to trace terrigenous OM. In addition, molecular and isotopic evidence suggests that OC in seawater and marine sediments is marine, rather than terrestrial, in source, suggesting that remineralization of terrestrial material must occur in rivers prior to delivery to the coastal ocean (Cole et al. 2007) or in the marine environment. Eaolian (air) OC flux from the land to the sea approximates 0.1 Pg C year^{-1}, but this estimate remains uncertain (Zafiriou et al. 1985).

Organic Matter Preservation and Geologic Processes

Only ~0.1% of global net primary production (NPP) is ultimately preserved within sediments; however, it is this OC that eventually becomes part of the sedimentary record and available to be transformed into fossil fuels. The remaining 99.9% of global NPP is remineralized to inorganic carbon, nutrients, and water. Remineralization represents a sink for oxygen, linking the global cycles of OC and oxygen. Microfauna, bacteria, and fungi (on land) are responsible for the breakdown of OM.

The rates and extent of decomposition are influenced by environmental, biological, and physical factors. There must be a sufficient supply of labile OM to be degraded, and the depth-integrated rate of OM remineralization in marine sediments correlates closely with carbon flux to the sediment surface (Henrichs 1993). Interestingly, the fraction of OC that is *not* remineralized is also highly correlated with the carbon flux to the sediment surface. Thus, the efficiency of OM decomposition appears to be lower in systems that receive the highest input of OC compared to systems with lower accumulation rates (Henrichs and Reeburgh 1983). Second, like most metabolic processes, decomposition rates are proportional to temperature, resulting in global patterns of decomposition rates (e.g., higher degradation rates in the tropics than in tundra systems) (Schlesinger 1997). Oxygen is also a controlling factor for decomposition. Recent evidence suggests that oxygen exposure time rather than oxygen concentration may be an important determinant of the extent to which OM is decomposed (Hartnett et al. 1998).

Physical and chemical "protection" of OM also plays a key role in controlling preservation. Protection by binding to inorganic ions, clays, and organic residues decreases the surface area of OM that is exposed to bacteria for degradation. This protection or encapsulation of OM explains why compounds that appear to be labile, or readily available for decomposition, have been found in sedimentary OC deposits. Preservation of OC occurs predominantly in anoxic marine sediments. More than 80% of preserved OC is located in deltaic-shelf environments associated with fine-grained sediments (Berner 1982), which supports the physical or chemical protection model since these sediments provide the most potential surface area with which OM can bind. This has likely been true for millions of years, as current petroleum deposits are found in areas that were formerly coastal, fine-grained sediments. Major depositional environments include lacustrine environments (open, closed lakes), peat swamps and coal, and continental margins, enclosed or silled basins, and the Black Sea (Hedges and Keil 1995).

Sedimentary rocks are the largest geologic reservoir of OC and make up ~99.5% of the total global OC. Sedimentary OC occurs primarily as kerogen, coal beds, and petroleum reservoirs, which ultimately come from biogenic processes or sources. Kerogen is amorphous, highly insoluble particulate OM that is thought to form by two pathways – selective preservation and geopolymerization – both of which occur under low temperature and pressure conditions. Petroleum, naturally occurring fluids (liquid and gases) that evolve from kerogen, is formed primarily from the remains of microbes (algae and bacteria) although some types of petroleum are formed from higher plants. In contrast, coal is a solid and is formed from the remains of higher plants. The most common type of coals, humic coals, is formed through the processes of peatification and coalification, which involve both biological and geochemical processes. The OC in ancient sedimentary rocks provides these economically important fossil fuels as well as a molecular record of life, which has allowed the construction of evolutionary trees and an understanding of the geologic timing of past events and the response of natural systems to tectonic, environmental, and biological change.

Summary

The global carbon cycle involves exchange of OC between surface and subsurface (buried) reservoirs on timescales of less than 1 year to millions of years. These fluxes are driven by the production and cycling of OC through biological, physical, and geological processes. The global OC cycle is intimately linked with other global cycles and is sensitive to human-induced perturbations. In 2016, concentrations of atmospheric CO_2 (~400 ppm) and CH_4 (1,834 ppb) reached a new milestone in human history, and the last time the Earth experienced atmospheric concentrations of CO_2 that were this high was during the Pliocene (~3 million years ago). Understanding changes in the size and composition of carbon reservoirs and changes in these reservoirs through space and time is essential for predicting Earth system responses to anthropogenic activities as well as responses in the associated cycles of other biologically important elements.

Cross-References

- ▶ Anthropogenic CO_2
- ▶ Atmospheric Evolution
- ▶ Biogeochemistry
- ▶ Coal
- ▶ Diagenesis
- ▶ Geochemistry
- ▶ Kerogen
- ▶ Nitrogen Cycle
- ▶ Organic Geochemistry
- ▶ Organic Matter Degradation and Preservation
- ▶ Oxygen
- ▶ Peat
- ▶ Petroleum
- ▶ Soils
- ▶ Sulfur Cycle

References

Berner RA (1982) Burial of organic carbon and pyrite sulfur in the modern ocean: its geochemical and environmental significance. Am J Sci 282:451–473

Canuel EA, Hardison AK (2016) Sources, ages, and alteration of organic matter in estuaries. Annu Rev Mar Sci 8:409–434

Ciais P, Sabine C, Bala G, Bopp L, Brovkin V, Canadell J, Chhabra A, DeFries R, Galloway J, Heimann M, Jones C, Le Quéré C, Myneni RB, Piao S, Thornton P (2013) Carbon and other biogeochemical cycles. In: Stocker TF, Qin D, Plattner G-K, Tignor M, Allen SK, Boschung J, Nauels A, Xia Y, Bex V, Midgley M (eds) Climate change 2013: the physical science basis, Contribution of Working Group I to the Fifth Assessment Report of the Intergovernmental Panel on Climate Change. Cambridge University Press, Cambridge, UK

Cole JJ, Prairie YR, Caraco NF, McDowell WH, Tranvik LJ, Striegl RG, Duarte CM, Kortelainen P, Downing JA, Middelburg JJ, Melack J (2007) Plumbing the global carbon cycle: integrating inland waters into the terrestrial carbon budget. Ecosystems 10:171–184

Hartnett HE, Keil RG, Hedges JI, Devol AH (1998) Influence of oxygen exposure time on organic carbon preservation in continental margin sediments. Nature 391:572–574

Hedges JI (1992) Global biogeochemical cycles: progress and problems. Mar Chem 39:67–93

Hedges JI, Keil RG (1995) Sedimentary organic matter preservation: an assessment and speculative synthesis. Mar Chem 49:81–115

Henrichs SM (1993) Early diagenesis of organic matter: the dynamics (rates) of cycling of organic compounds. In: Engel MH, Macko SA (eds) Organic geochemistry. Plenum Press, New York, pp 101–117

Henrichs SM, Reeburgh WS (1983) Anaerobic mineralization of marine sediment organic matter: rates and the role of anaerobic processes in the oceanic carbon economy. Geomicrobiology 5:191–237

Hunt JM (1996) Petroleum geochemistry and geology, 2nd Edition. W.H. Freeman and Company, New York

Meybeck M (1982) Carbon, nitrogen, and phosphorus transport by world rivers. Am J Sci 282:401–450

Schlesinger WH (1997) Biogeochemistry: an analysis of global change. Academic Press, San Diego, CA

Taube M (1992) Evolution of matter and energy. In: P. Craig and O. Hutzinger (eds) The Natural Environment and the Biogeochemical Cycles, Springer-Verlag, New York, pp 200

Zafiriou OC, Gagosian RB, Peltzer ET, Alford JB, Loder T (1985) Air-to-sea fluxes of lipids at Enewetak Atoll. Geophys Res 90(D1):2409–2423

Carbon Isotopes

Thomas Wagner[1], Clayton R. Magill[1] and Jens O. Herrle[2]
[1]Lyell Centre for Marine and Earth Science and Technology, Heriot-Watt University, Edinburgh, UK
[2]Institute of Geosciences, Goethe University Frankfurt, Frankfurt, Germany

Synonyms

$^{13}C/^{12}C$ ratios; Carbon isotope stratigraphy; Stable carbon isotopes

Definition

The stable carbon isotopes ^{12}C and ^{13}C comprise 98.89% and 1.11% respectively of the carbon on Earth (Craig 1953). Measurements of these isotopes are expressed as ratios to the more common ^{12}C in a sample ($^{13}C/^{12}C$) and reported in the $\delta^{13}C$ notation relative to the Vienna Pee Dee Belemnite (VPDB) standard in per mil (Coplen 1996). There is also an unstable nuclide – radiocarbon (^{14}C) – that is much rarer, with a natural abundance of ~1 part per trillion (Chanton et al. 2014).

Introduction and Main Applications

The stable carbon isotopes measured on the carbonate and organic carbon fractions in sediments or carbonate tests from planktonic and benthic organisms and molecular compounds (biomarkers) isolated from them are classical proxies in marine sciences. This chapter focusses on main applications of carbon isotopes in marine and climate sciences, which include reconstructions of the global carbon cycle, chemostratigraphy, tracing of water masses, and surface water productivity in the modern and past ocean, reconstructing early life, and likewise are relevant to applied forensic applications in numerous archaeological (sub)disciplines.
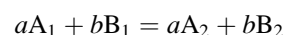
Carbon Isotopes

Isotopes are atoms with the same number of protons but different numbers of neutrons. Traditional nomenclature denotes isotopic species as $^{A}_{Z}E$, in which Z is the element's atomic number (e.g., number of protons) and A is the mass number (i.e., sum of protons and neutrons). For example, carbon atoms always contain six protons ($n = 6$), but this atom can contain either six, seven, or eight neutrons ($m = 12$, 13, or 14, respectively). With this in mind, the characteristic atomic weight for any particular atom is the average of the relative mass contributions of the atom's isotopic species, which for carbon is equal to 12.0107 (Coplen 1996).

Isotopic Nomenclature and Fractionation Mechanisms

Selective relative enrichment (discrimination) of discrete isotopic species, such as ^{12}C and ^{13}C, between compounds or coexisting phases (e.g., gaseous vs. aqueous carbon dioxide) is called "fractionation." There are two main important types of isotope fractionation – equilibrium and kinetic. Equilibrium isotope fractionation occurs via isotopic exchange when there is a relative separation (discrimination) of isotopes between substances in chemical equilibrium as a result of the reduction in vibrational (zero point) energy when a more massive isotope (e.g., ^{13}C) is substituted for a less massive isotope (e.g., ^{12}C). As such, isotopic exchange reactions occur if the isotope distribution of two or more substances changes, with no change in reactants or products. In contrast, kinetic fractionation is the consequence of rate dependent, incomplete, or nonreversible reactions, such as distillation ("rain out") and biology processes (Chen and Marcus 2005). In such systems, reaction dynamics are sensitive to atomic mass in one or more of the reactants. For instance, products show disproportional incorporation of lighter isotopes compared with reactants because molecules with the heavier isotope form stronger bonds and have higher dissociation energies compared with molecules with lighter isotopes (Fig. 1a, b). Thus, the energy required to achieve molecular dissociation is much lower for ^{12}C–^{12}C bonds compared with ^{13}C–^{12}C bonds (Matsson et al. 2005).

Isotopic exchange reactions are well described by generic equilibrium dynamics:

$$a\text{A}_1 + b\text{B}_1 = a\text{A}_2 + b\text{B}_2$$

Here, subscripts 1 and 2 represent the respective abundances of the light and heavy isotopic species of substances A and B, such that the equilibrium constant for such a reaction would be:

$$K = \frac{\left(\text{A}_2 / \text{A}_1\right)^a}{\left(\text{B}_2 / \text{B}_1\right)^b}$$
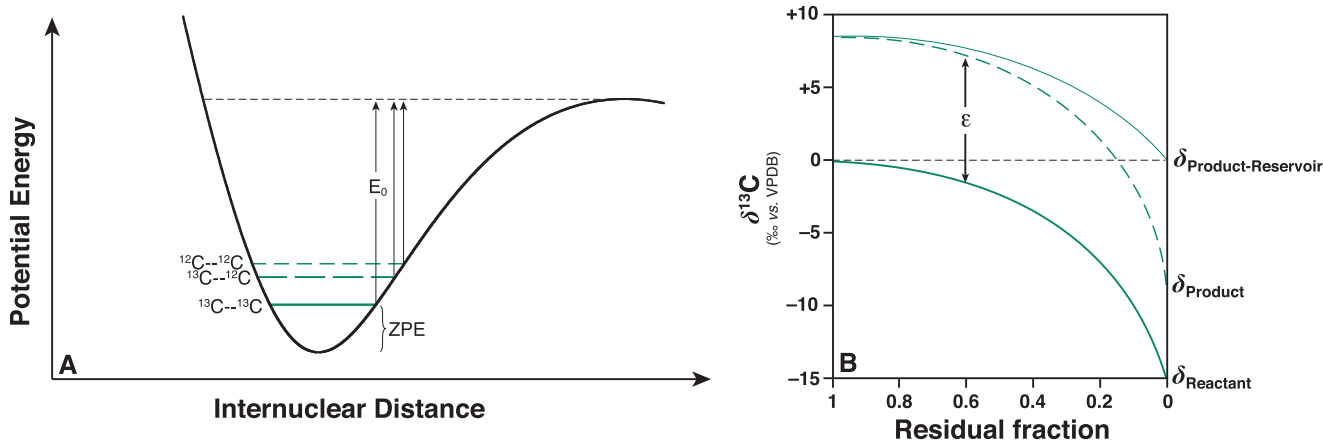
Carbon Isotopes, Fig. 1 (**a**) Schematic potential energy curve for the interaction of two carbon atoms in a stable molecule or amid two molecules in a solid/liquid. (**b**) Coeval $\delta^{13}C$ values of two discrete substances as a function of the residual fraction of the reactant for a Rayleigh process. ZPE (E_0) = Zero point energy

According to statistical mechanics, the equilibrium constant can be expressed by partition functions (Q) of these respective substances:

$$K = \frac{\left(Q_{A_2}/Q_{A_1}\right)}{\left(Q_{B_2}/Q_{B_1}\right)}$$

Accordingly, partition functions are defined by:

$$Q = \sum_i \left[g_i \, e^{\left(-E_i/kT\right)} \right]$$

where associated functions are summed for every potential level (E_i), g_i is equal to statistical weight of different i^{th} levels, k is the Boltzmann constant, and T is temperature in Kelvin (Stern et al. 1968).

The fractionation factor α mathematically describes isotopic discrimination, where $\alpha = R_A/R_B$. R is the isotopic ratio of interest (e.g., $^{13}C/^{12}C$), and A and B are discrete compounds or phases. The equilibrium constant (K) is related to the fractionation factor (α) by the equation $\alpha = K^{1/n}$, where n equals the number of atoms exchanged. For isotope exchange reactions involving a single atom, $K = \alpha_{A-B}$. As an example, consider exchange of ^{13}C and ^{12}C between carbon dioxide and Ca-carbonate:

$$^{13}CO_2 + Ca^{12}CO_3 <--->\ ^{12}CO_2 + Ca^{13}CO_3$$

This reaction would have an isotopic fractionation factor for aragonite equal to (Emrich et al. 1970).

$$\alpha_{CaCO_3-CO_2} = \frac{\left(\frac{^{13}C}{^{12}C}\right)_{CaCO_3}}{\left(\frac{^{13}C}{^{12}C}\right)_{CO_2}} = +10.63 \ (\text{at } 25^*C).$$

For calcite, which is common in many marine settings, the isotopic fractionation factors will be different (Romanek et al. 1992; Turner 1982).

Based on available experiments and theoretical data, $\alpha_{CaCO3-CO2}$ can be calculated from ambient temperature with the equation (Horita 2014):

$$10^3 \ln \alpha_{CaCO_3-CO_2} = -1.637 \left(\frac{10^6}{T^2}\right) + 7.290$$

Note that the addition of 10^3 is convenient for conversion of fractionations into more customary per mil (‰) deviations, which are straightforward to compare with conventional delta (δ) values vis-à-vis epsilon values:

$$\varepsilon_{CaCO_3-CO_2} = 10^3(\alpha_{CaCO_3-CO_2} - 1) = 10^3 \left(R_B/R_A - 1\right)$$

Delta (δ) notation is defined by the equation:

$$\delta_{SA}(‰) = 10^3 \left(\frac{(R_{SA} - R_{ST})}{R_{ST}}\right)$$

where R is the isotope ratio and subscripts SA and ST represent sample and standard respectively.

Carbon isotope ratio measurements are compared to an international isotopic reference material called Vienna Peedee Belemnite (VPDB) with an R equal to 0.011237 (Coplen 1996). As such, a sample substance's measured $^{13}C/^{12}C$ ratio is used to calculate stable carbon isotope values ($\delta^{13}C$):

$$\delta^{13}C_{Sample} = 10^3 \left(\frac{\left(\frac{^{13}C}{^{12}C}\right)_{Sample} - \left(\frac{^{13}C}{^{12}C}\right)_{VPDB}}{\left(\frac{^{13}C}{^{12}C}\right)_{VPDB}} \right)$$

In conjunction with the epsilon equation above, the stable carbon isotopic fractionation (α) between two substances can be calculated (c.f., Table 1):

$$\alpha_{A-B} = R_B/R_A = \left(\delta^{13}C_A + 1000\right)/\left(\delta^{13}C_B + 1000\right)$$

$$\approx \delta^{13}C_A - \delta^{13}C_B = \Delta\delta^{13}C_{A-B}$$

Carbon Isotopic Measurements

Isotope ratio mass spectrometry (IRMS) provides measurements of the absolute abundance of stable carbon isotopes in natural or synthetic materials. Over the last few decades, advances in IRMS instrumentation now allow for accurate and highly precise stable carbon isotope measurements of bulk and molecular samples. Further, recent IRMS

Carbon Isotopes, Table 1 Comparison of $\delta^{13}C$, $\Delta\delta^{13}C_{A-B}$, α_{A-B}, and $1000 \ln \alpha_{A-B}$ values of two discrete materials with different ^{13}C abundances

$\delta^{13}C_A$	$\delta^{13}C_B$	$\Delta^{13}C_{A-B}$	α_{A-B}	$10^3 \ln \alpha_{A-B}$
−20.0	0	−20.0	0.980	−20.2
−10.0	0	−10.0	0.990	−10.1
−5.0	0	−5.0	0.995	−5.0
−1.0	0	−1.0	0.999	−1.0
0	0	0	1.000	0
1.0	0	1.0	1.001	1.0
5.0	0	5.0	1.005	5.0
10.0	0	10.0	1.010	9.9
10.0	1.0	9.0	1.009	10.9
10.0	−1.0	11.0	1.011	8.9

technologies now support coupled instrumental techniques, which are configured to incorporate a range of differing peripheral (front-end) techniques such as elemental analysis (EA, Muccio and Jackson 2009), gas chromatography (GC; Sessions 2006), and high performance liquid chromatography (HPLC, Godin et al. 2007). Ultimately, these peripheral techniques use oxidation to convert diverse carbon compounds into carbon dioxide for IRMS detection (*c.f.*, Sessions 2006; Muccio and Jackson 2009). Following gasification, samples are compared to a reference gas calibrated with recognized international isotope reference materials (Table 2). This approach thus normalizes measured (raw) $\delta^{13}C$ values to a common reference scale shared between laboratories worldwide.

Current theoretical sensitivities of IRMS for combustion-interface carbon isotope measurements are about 0.025 nmol for samples with natural ^{13}C distribution abundances, although realized detection thresholds are much higher at 1–5 nmol (~50 ng of typical hydrocarbons [Sessions 2006]) for on-column injections. Precision of $\delta^{13}C$ values measured from samples with >5 nmol C is presently ca. 0.1–0.3‰ (1σ standard deviation). Comprehensive review of IRMS instrumentation and techniques are well beyond the scope of this chapter. The reader is directed toward recent literature

**Carbon Isotopes, Table 2** Reported $\delta^{13}C$ values of NBS-reference materials against VPDB

Ref.	Material	$\delta^{13}C$
NBS-18	Carbonatite	−5.0
NBS-19	Marble	+1.9
NBS-20	Limestone	−1.1
NBS-21	Graohite	−28.1
NBS-22	0il	−30.0

reviews (c.f., Brand 2004; Sessions 2006; Muccio and Jackson 2009) and other contributions in this encyclopedia.

Distribution of Carbon Isotopes in Nature

Stable carbon isotopic compositions are widely used as geochemical proxies to reconstruct changes in the global carbon cycle. Two main carbon reservoirs exist, the reduced biogenic organic carbon reservoir (organic matter) and the oxidized carbonate reservoir, covering a wide range of stable carbon isotopic signatures from less than −100‰ to greater than 10‰, depending on the carbon source (Figs. 2 and 3). The lowest $\delta^{13}C$ values are related to microbially produced methane (CH_4) (Grossman et al. 2002) in, e.g., gas-hydrate bearing sediments along continental slopes and related carbonate biohermes, marine seep systems, and Arctic permafrost (e.g., Claypool and Kvenvolden 1983; Whiticar 1999, and references therein). The highest values (>10‰) occur in dissolved inorganic carbon (DIC) associated with methanogenesis (Claypool and Kaplan 1974; Hudson 1977).

Differences in the organic carbon isotopic composition ($\delta^{13}C_{org}$), both at the bulk and the molecular level, are controlled by complex biosynthetic pathways, including the fractionation during the production of biomass, e.g., photosynthesis, in the marine and the terrestrial biosphere (e.g., Degens et al. 1968). Bulk organic carbon from terrestrial C3 plants, the most common type of vegetation on Earth, is lower in $\delta^{13}C$ with mean values of about −27‰. Bulk $\delta^{13}C_{org}$ values for marine algae scatter around −21‰. Terrestrial vegetation from arid climate zones utilizing the C4 and Crassulacean Acid Metabolism (CAM) photosynthetic pathway, mainly Savannah grasslands,
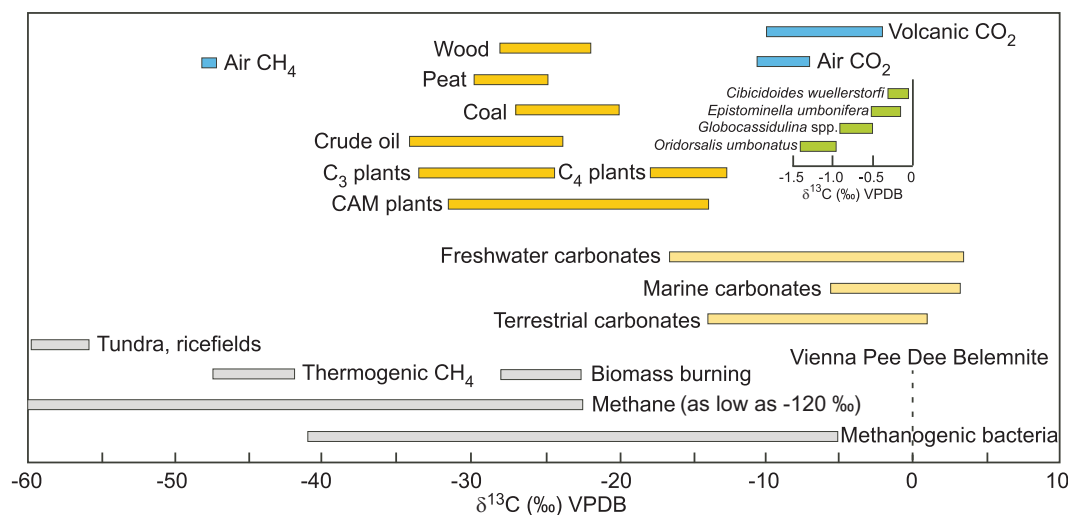
Carbon Isotopes, Fig. 2 Variations in stable carbon isotope ratios for different organic and inorganic sources in the modern environment and in sediments (Modified from Schidlowski and Aharon 1992; Wefer and Berger 1991)
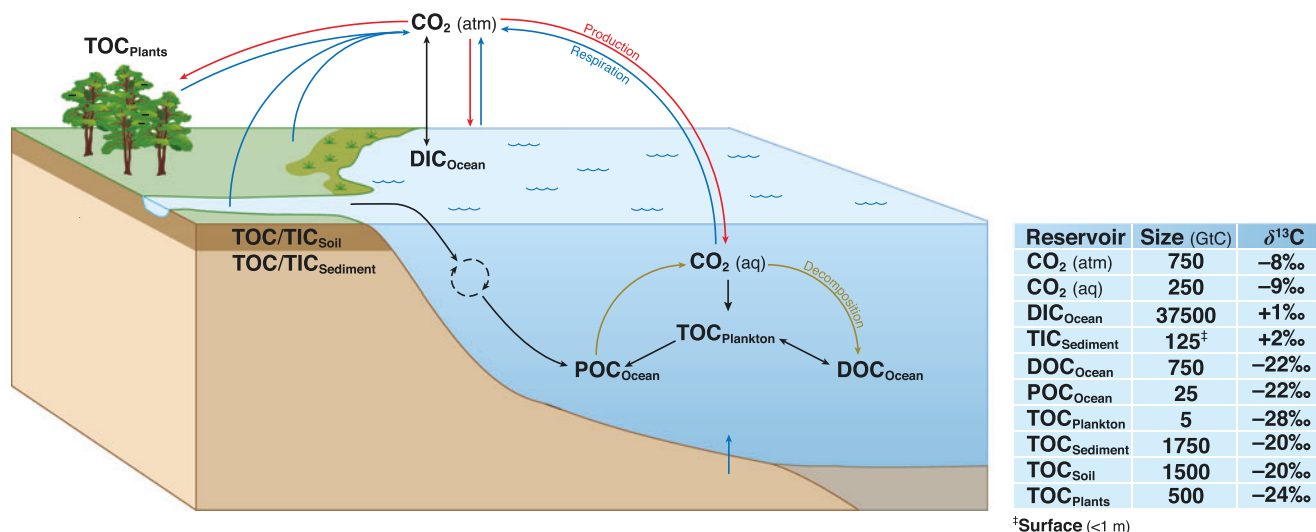
Carbon Isotopes, Fig. 3 Carbon cycle dynamics along the land-river-ocean continuum (modified from Canuel et al. 2012). Average $\delta^{13}C$ values, reservoir sizes, and fluxes are also shown for reference (Siegenthaler and Sarmiento 1993; Hedges et al. 1997; Rabouille et al. 2001)

shows averaged bulk $\delta^{13}C_{org}$ values of about $-12‰$. Within all these organisms, at the molecular scale, most lipids are ^{13}C–depleted (lower $\delta^{13}C$ values) as compared to starch ($\Delta\delta^{13}C_{Starch–Lipid} = 6.0‰$), sugars ($\Delta\delta^{13}C_{Sugar–Lipid} = 5.5‰$), proteins ($\Delta\delta^{13}C_{Protein–Lipid} = 5.0‰$), and therefore bulk biomass ($\Delta\delta^{13}C_{Bulk–Lipid} = 4.0‰$), as a consequence of biochemical (enzymatic) differences during production and transport through an organism (Hobbie and Werner 2004; Bowling et al. 2008).

Carbon Isotopes and the Emergence of Life

Physiochemical and biological processes create distinctive carbon isotopic signatures in biogenic material that trace the occurrence of life. In consequence, $^{13}C/^{12}C$ variations in sedimentary geologic archives are often used to reconstruct the origin(s) and evolution of life because of its characteristic discrimination against heavier isotopes. For instance, numerous studies adopt $\delta^{13}C$ values of fossil organic matter (kerogen) in sedimentary rocks to resolve the antiquity of life as we understand it based on remarkably persistent kinetic isotope effects associated with enzymatic carboxylation reactions (e.g., photosynthetic assimilation via ribulose bisphosphate carboxylase) as compared to inorganic carbon species, such as carbon dioxide and (bi)carbonate (Schidlowski and Aharon 1992; Havig et al. 2017).

Other disciplines, including paleontology and archeological fields, similarly utilize characteristic carbon isotopic discriminations imparted by plants and higher animal-derived biomass in order to more fully understand the evolution of life and behavior. For example, many previous studies interpret

$\delta^{13}C$ values of dental bioapatite derived from early humans with respect to vegetable versus meat-based dietary preferences during our species' evolution (Cerling et al. 2011; Sponheimer et al. 2013; Loftus et al. 2016). These same values also create an explicit link between our ancestors and their environments, which then can be contextualized by plant lipid $\delta^{13}C$ analyses of the matrix across an archeological horizon in order to shed light on community patterns, resource use, and (pre)historical behavior (Magill et al. 2016). The analysis of biochemical "residues" similarly provide new dimensions in archeological investigations of diverse materials, such as pottery (potsherds), soils, sediments, and biogenic remains in order to link lipid residues with their organic and environmental sources (Dudd and Evershed 1998; Dunne et al. 2016). Thus, combined bulk and molecular analyses are especially powerful because they can disentangle source-specific inputs within otherwise complex mixtures of lipids.

Carbon Isotopes in Shallow Seawater

The dissolved inorganic carbon (DIC) $\delta^{13}C$ of seawater ($\delta^{13}C_{DIC}$) is dynamically coupled to the global carbon cycle via the partitioning of the main carbon reservoirs between the ocean, atmosphere, and terrestrial biosphere (Fig. 3). $\delta^{13}C_{DIC}$ is not uniform in the modern ocean, nor constant over time (e.g., Sundquist and Visser 2004). The global seawater $\delta^{13}C_{DIC}$ composition is mainly controlled by three processes: photosynthesis, microbial decay of algal organic matter, and physical fractionation during gas exchange at the air-sea interface (Broecker and Maier-Reimer 1992). Marine surface

water is generally enriched in ^{13}C because photosynthesis of marine phytoplankton favors the light ^{12}C over the heavy ^{13}C, leading to lower $\delta^{13}C$ values for organic matter ($\delta^{13}C_{org}$) relative to ambient seawater $\delta^{13}C_{DIC}$ (Garlick 1974). This process is limited by the availability of nutrients, in particular nitrate and phosphate (Broecker and Peng 1982).

Most marine organisms exhibit $\delta^{13}C$ values in their carbonate shells, which were formed not in full equilibrium relative to ambient seawater (Fig. 1). The reason for this is manifold but metabolic effects, including the photosynthetic activity of algal symbionts, kinetic fractionation tied to growth rates, and carbonate ion concentrations are critical (McConnaughy 1989; Rohling and Cook 1999). These effects, together with species-specific differences, are summarized as 'vital effects' (e.g., Wefer and Berger 1991). Intriguingly, previous studies suggest that, if these vital effects are corrected for, isotopic mass-balance calculations can be used for reconstructions of biophysical factors, such as the concentration and the composition of Earth's atmospheric carbon dioxide (e.g., alkenones; Pagani 2014).

In most places, modern sea surface waters $\delta^{13}C_{DIC}$ is about 2–3‰ heavier than the deep-water values of about 0‰ due to biological activity in the photic zone (Kroopnick 1985; Raven and Falkowski 1999; Sarmiento and Gruber 2006). In addition, changes of the $\delta^{13}C_{DIC}$ in the ocean are influenced by increasing anthropogenic pCO_2 causing a decline in the ^{13}C content of DIC relative to ^{12}C – a phenomenon called the "Suess effect" (Keeling 1979; Quay et al. 1992).

Remineralization of organic matter and nutrients within thermocline subsurface water recycle isotopically light ^{12}C. Due to upwelling and wind-mixing of shallow waters, this light ^{12}C and nutrient-rich subsurface water can be remobilized back into the surface waters thereby stimulating primary productivity and influencing the carbon isotopic composition of calcareous shells (e.g. Broecker and Peng 1982).

## Tracing of Seawater Masses, Surface Water Productivity, and Ecology

The $\delta^{13}C_{DIC}$ in water is widely used as a tracer for seawater masses. Although changes in surface water productivity and mixing influence $\delta^{13}C_{DIC}$, other processes, including water mass formation, respiration, ocean circulation, and vital effects, determine the $\delta^{13}C_{DIC}$ value and therefore can be used as tracers for water masses (e.g., Ravelo and Hillarie-Marcel 2007). Deep water captures the $\delta^{13}C$ signature from its surface water sources. North Atlantic Deep Water (NADW) has therefore relatively high $\delta^{13}C$ values (~1.11‰) whereas Antarctic Bottom Water (ABW) is relatively low (~0.4‰), reflecting the major differences in surface water $\delta^{13}C_{DIC}$ in both high latitude source regions

(Kroopnick 1985). Variations in deep water $\delta^{13}C$ can, therefore, be used to trace the history of deep water currents. This approach is also referred to as "aging" of deep water (Rohling and Cook 1999), where the relative age of deep water provides a measure for ocean circulation.

The $\delta^{13}C$ difference between shallow and deep dwelling planktic foraminifera ($\Delta\delta^{13}C$) provides a well-established proxy for thermocline productivity and the depth of the shallow water mixed layer (e.g., Wefer et al. 1999). Increasing $\Delta\delta^{13}C$ values reflect more stratified surface water masses due to increasing contrasts between shallow and deep waters, and vice versa. A comparable approach is used to reconstruct productivity via changes in benthic foraminifera $\Delta\delta^{13}C$ of epifaunal and infaunal species (Zahn et al. 1986). Here, the $\delta^{13}C$ differences are mainly controlled by pore water geochemical gradients and the intensity of organic matter degradation, the latter being a function of organic matter supply (flux) to the sea floor (McCorkle et al. 1990). Large $\Delta\delta^{13}C$ values represent less organic matter flux, and thus less primary productivity, and vice versa. Benthic foraminifera $\Delta\delta^{13}C$ gradients can, however, be biased by the variability in new production of organic matter (fresh phytodetritus), which influences the stable isotope signal. This effect, constrained by variable primary productivity and organic matter fluxes at seasonal time scales, is referred to as the "Phytodetritus" or "Mackensen effect" (Mackensen et al. 1993). Furthermore, the carbon and oxygen isotopic composition of calcite tests of planktic foraminifera is used for reconstructing depth habitats and thus the ecology of extant and extinct species (e.g., Pearson et al. 1993).

Chemostratigraphy and Carbon Isotope Excursions (CIE)

The history of the global carbon cycle and climate through time is preserved in the carbon isotope record of marine and terrestrial sediments (Fig. 4). The application of organic and inorganic carbon isotope ratios as chemical fingerprints for stratigraphic correlations was pioneered in the late 1970s with the studies of Berger et al. (1978), Weissert et al. (1979), and Scholle and Arthur (1980), more recently summarized in Weissert et al. (2008), Saltzman and Thomas (2012), Wendler (2013), and Jarvis et al. (2015). The most robust Phanerozoic archives of marine carbon isotope signatures are from individual pristine preserved fossils and bulk carbonate from marine sediments (e.g., Joachimski and Buggisch 1993; Veizer et al. 1999; Grossman et al. 2008; Saltzman and Thomas 2012, and references therein). Carbon isotope fluctuations of several per mil are also reported from hemipelagic sediments, shallow water carbonates, and terrestrial sediments. Due to multiple local influences, however, they may differ in their absolute isotope values and ranges from their
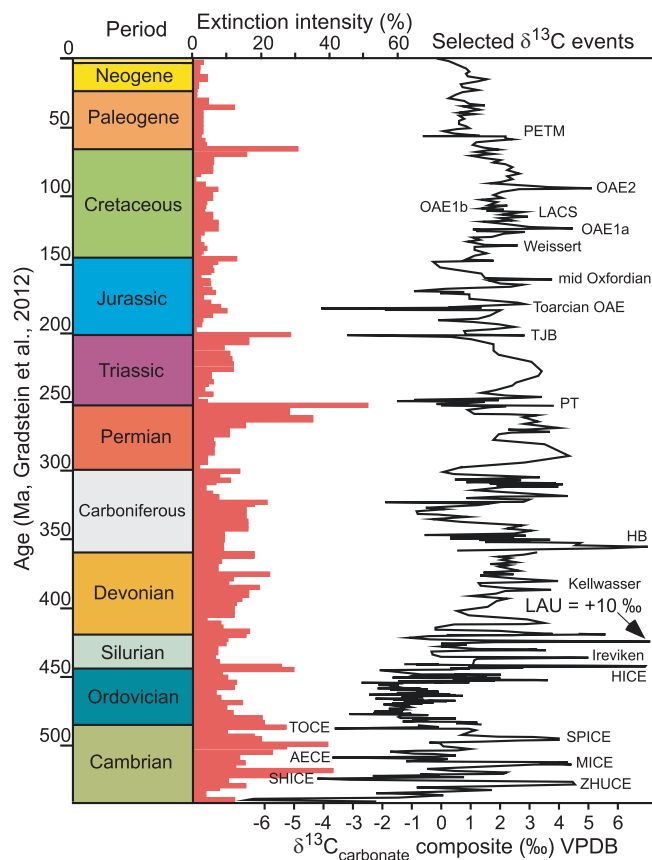
Carbon Isotopes, Fig. 4 Phanerozoic carbon isotope record, extinction events, and selected global events (CIEs) based on Gradstein et al. (2012) and references therein, Caplan and Bustin (1999), Munnecke et al. (2003), Wagner et al. (2007), Korte and Kozur (2010), and McAnena et al. (2013). Extinction intensity represents the fraction of genera that are present in each interval of time but do not exist in the following interval (Modified after Rohde and Muller (2005) and Sepkoski (2002). *PETM* Paleocene Eocene Thermal Maximum, *OAE* Oceanic Anoxic Events, *LACS* Late Aptian Cold Snap, *TJB* Triassic Jurassic Boundary, *PT* Perm-Trias Event, *HB* Hangenberg Event, *LAU* Lau Event, *HICE* Hirnantian Event, *TOCE* Top Cambrian Excursion, *SPICE* Steptoean Event, *MICE* Mingxinsi Event, *AECE* Archaeocyathids Event, *SHICE* Shiyantou Event, *ZHUCE* Zhujiaqing Event

corresponding pelagic sediment records, complicating their use in stratigraphic correlation across wider areas (Weissert and Breheret 1991; Saltzman and Thomas 2012; Jarvis et al. 2015).

The long-term trend in Earth's climate is interrupted by series of transient events, identified by distinct positive or negative carbon isotope excursions, CIEs (Fig. 4). These CIEs, combined with longer trends in the global carbon isotope record, are used in chemostratigraphy to identify chemical events (e.g., Zachos et al. 2001; Weissert et al. 1998), which can be correlated within and across shallow, hemipelagic, and pelagic marine and the terrestrial environments (e.g., Gröcke et al. 1999; Herrle et al. 2004). Well-documented examples of CIEs representing major perturbations of the global carbon cycle are reported from, e.g., the

Mesozoic-Paleogene greenhouse (Paleocene–Eocene thermal maximum PETM, Early Jurassic and Cretaceous Oceanic Anoxic Events, OAEs, Jenkyns 2003), and the Paleozoic (Saltzman and Thomas 2012, Fig. 4). In contrast to the large Paleozoic fluctuations of >10‰, the Mesozoic and Cenozoic amplitudes are with >2‰ much smaller. Many CIEs coincide with widespread environmental perturbations including severe and short-term global warming (hyperthermal events), ocean acidification, shoaling of the carbonate compensation depth (CCD), enhanced marine organic carbon burial linked to widespread ocean anoxia, major crisis or extinction of biota on land and in the ocean, and sudden shifts in Earth's hydrological cycle and climate (e.g., Leckie 2009; Stanley 2010; Beerling and Woodward 2001). Understanding how the Earth system responded to and recovered from these past extreme events remains a major focal point of Earth Sciences, adding to the discussion on anthropogenically induced global warming (Stanley 2010).

The magnitude of 2 to >10‰ and rapidity of CIEs in the Phanerozoic, combined with evidence for massive environmental change, has stimulated intense interdisciplinary research about the underlying trigger and feedback mechanisms. Positive CIEs are reported for multimillion to orbital time scales and are, among other possible mechanisms (Fig. 4), commonly associated with periods of globally enhanced marine carbon burial, leading to the concept of Oceanic Anoxic Events (Schlanger and Jenkyns 1976, Scholle and Arthur 1980) and global cooling (e.g., Kuypers et al. 1999). Recent studies, combining geochemical with biotic data and biogeochemical modeling, have shown that global cooling can cause perturbations to marine ecosystems and biogeochemical cycles at scales comparable to those associated with global warming (McAnena et al. 2013). Sharp negative CIEs, either isolated within the chemostratigraphic record or in combination with positive CIEs, have been recorded throughout the Phanerozoic sedimentary record (e.g., Saltzman and Thomas 2012) and have become a focal point for Earth System research. Negative CIEs have been related to a large number of mechanisms, including rapid dissociation of metastable marine methane hydrate, build-up and release of isotopically "light" carbon in stratified epicontinental seas, thermogenic release of methane related to the placement of volcanic dykes into coal-bearing strata or thermal maturation of other organic-rich sediments, extensive biomass burning, mobilization of labile carbon pools from terrestrial permafrost, ventilation of marine dissolved organic carbon, and others (for further information on mechanisms see, e.g., Cohen et al. 2007; deConto et al. 2012). Correlations of smaller magnitudes of >1.0‰ within less than 100 kyrs have been successfully used in regional epicontinental settings of the late Cretaceous (Menegatti et al. 1998; Herrle et al. 2004; Jarvis et al. 2015). In contrast to the large amplitudes, the factors controlling small scale variations of <0.5‰ are far less understood. Among

others, coccolith distribution and depletion in marl−limestone alternations, diagenetic effects of pore waters, sedimentation, and cementation have been identified to play a role (Jarvis et al. 1988, 2015; Mitchell et al. 1997).

Processes Limiting the Use of C within Chemostratigraphy

Major processes affecting the absolute values in both organic and inorganic matter are surface water productivity (Arthur et al. 1988), input of organic matter from land (Jarvis et al. 2015), remineralization in the water column (Sinninghe Damste and Köster 1998), mineralogy, and carbonate and organic composition of the sediments (cements, carbonate producers such as calcareous nannofossils composition and abundances; Beltran et al. 2007; Jarvis et al. 2015), early and late diagenetic processes (Mitchell et al. 1997; Allan and Matthews 1982; and Immenhauser et al. 2003), CO_2 (Kump and Arthur 1999), and sea-level changes (Jenkyns 1996). Furthermore, it has been shown that mineralogy can impact on carbon isotopic stratigraphy (e.g., Swart 2008). Paired organic and inorganic carbon isotope records might help overcome this problem (Menegatti et al. 1998; Jarvis et al. 2015). Parallel shifts, in both organic and inorganic carbon isotopes, are often a robust signal in different marine records as it is documented for example for the early Aptian carbon isotope event. For this event, a consistent >4–6‰ shift is observed in organic and inorganic carbon isotopes from shallow marine Cretaceous Arctic marsh records and subtropical pelagic and shallow marine records (Menegatti et al. 1998; Herrle et al. 2015).

Besides the chemical and physical alteration of the carbon isotope signals, the impact of orbital forcing on the carbon cycle, which is most dominant within the 400 kyr cycle in the Cenozoic and Mesozoic $\delta^{13}C$ records (Pälike et al. 2006; Gale et al. 2011), can make correlations difficult if major $\delta^{13}C$ shifts of >2‰ are absent. Thus, instead of correlating single peaks, longer intervals (>0.5–1 Ma) are needed to be studied together with biostratigraphic and/or chronostratigraphic makers (Herrle et al. 2004). The absolute $\delta^{13}C$ values might be obscured but the form and shape of isotope profiles are a robust feature in many long- and short-term records (Herrle et al. 2015; Jarvis et al. 2015). Thus, using longer records, the form and the shape are the basis for a reliable high-resolution chemostratigraphic approaches (Jarvis et al. 2015).

Conclusions

Stable carbon isotopes are commonly used for a wide range of applications in marine sciences and climate research. Applications include reconstructions of the global carbon cycle including short-term perturbations, chemostratigraphy, and tracing of water masses and surface water productivity in the modern and past ocean. The development of carbon isotopes at the bulk sediment, foraminifera shell, and compound-specific (molecular) level, especially when combined with complementary evidence from biota, nutrients, ocean chemistry and redox, and modeling, has opened new pathways to unravel the complex interplay between fluctuations of main carbon pools between the atmosphere, the living biosphere, and carbon buried in the sediments, and their interactions with and impact on global climate at multiple temporal and spatial scales.

Cross-References

▶ Anthropogenic CO_2
▶ Archeological Geochemistry
▶ Biogenic Methane
▶ Biogeochemistry
▶ Carbon
▶ Carbon Cycle
▶ Carbonate Compensation Depth
▶ Carbonate Minerals and the CO_2-Carbonic Acid System
▶ Coal
▶ Compound-Specific Isotope Analysis
▶ Diagenesis
▶ Dissolved Organic Matter (DOM)
▶ Gas Chromatography–Mass Spectrometry (GC–MS)
▶ Gas Hydrates
▶ Gas Source Mass Spectrometry (GS-MS)
▶ Marine Sediment
▶ Ocean Biochemical Cycling and Trace Elements
▶ Ocean Salinity, Major Elements, and Thermohaline Circulation
▶ Organic Geochemistry
▶ Organic Matter Degradation and Preservation
▶ Organics: Sources and Depositional Environments
▶ Oxygen Isotopes
▶ Paleoenvironments
▶ Paleoproductivity
▶ Stable Isotope Geochemistry

References

Allan J, Matthews R (1982) Isotope signatures associated with early meteoric diagenesis. Sedimentology 29:797–817

Arthur MA, Dean WE, Pratt LM (1988) Geochemical and climatic effects of increased marine organic carbon burial at the Cenomanian/Turonian boundary. Nature 335:714–717

Beerling DJ, Woodward FI (2001) Vegetation and the terrestrial carbon cycle: modelling the first 400 million years. Cambridge University Press, Cambridge, UK

Beltran C, de Rafélis M, Minoletti F, Foucault A, Renard M, Sicre MA, Ezat U (2007) Coccolith δ18O and alkenone records in middle Pliocene orbitally-controlled deposits: high frequency temperature and salinity variations of sea surface water. Geochem Geophys Geosyst 8. https://doi.org/10.1029/2006GC001483

Berger WH, Killingley JS, Vincent E (1978) Stable isotopes in deep-sea carbonates: box core ERDC-92, west equatorial Pacific. Oceanol Acta 1:203–216

Bowling DR, Pataki DE, Randerson JT (2008) Carbon isotopes in terrestrial ecosystem pools and CO_2 fluxes. New Phytol 178(1):24–40

Brand WA (2004) Mass spectrometer hardware for analyzing stable isotope ratios. Handbook of stable isotope analytical techniques 1:835–856

Broecker WS, Maier-Reimer E (1992) The influence of air and sea exchange on the carbon isotope distribution in the sea. Glob Biogeochem Cycles 6:315–320

Broecker WS, Peng T-H (1982) Tracers in the sea. Eldigio Press, Palisades

Canuel EA, Cammer SS, McIntosh HA, Pondell CR (2012) Climate change impacts on the organic carbon cycle at the land-ocean interface. Ann Rev Earth Planet Sci 40:685–711

Caplan ML, Bustin RM (1999) Devonian-carboniferous Hangenberg mass extinction event, widespread organic-rich mudrock and anoxia: causes and consequences. Palaeogeogr Palaeoclimatol Palaeoecol 148:187–207

Chanton J, Zhao T, Rosenheim BE, Joye S, Bosman S, Brunner C, Yeager KM, Diercks AR, Hollander D (2014) Using natural abundance radiocarbon to trace the flux of petrocarbon to the seafloor following the Deepwater horizon oil spill. Environ Sci Technol 49(2):847–854

Chen WC, Marcus RA (2005) On the theory of the CO+ OH reaction, including H and C kinetic isotope effects. J Chem Phys 123(9):094307

Cerling TE, Mbua E, Kirera FM, Manthi FK, Grine FE, Leakey MG, Sponheimer M, Uno KT (2011) Diet of Paranthropus boisei in the early Pleistocene of East Africa. Proc Natl Acad Sci 108(23):9337–9341

Claypool GE, Kaplan IR (1974) The origin and distribution of methane in marine sediments. In: Kaplan IR (ed) Natural gases in marine sediments, Springer, New York, pp 99–139

Claypool GE, Kvenvolden KA (1983) Methane and other hydrocarbon gases in marine sediment. Annu Rev Earth Planet Sci 11(1):299–327

Cohen AS, Coe AL, Kemp DB (2007) The late Paleocene-early Eocene and Toarcian (early Jurassic) carbon-isotope excursions: a comparison of their timescales, associated environmental changes, causes and consequences. J Geol Soc London 164:1093–1108

Coplen TB (1996) New guidelines for the reporting of stable hydrogen, carbon and oxygen isotope ratio data. Geochim Cosmochim Acta 60:3359–3360

Craig H (1953) The geochemistry of the stable carbon isotopes. Geochim Cosmochim Acta 3:53–92

Damsté JSS, Köster J (1998) A euxinic southern North Atlantic Ocean during the Cenomanian/Turonian oceanic anoxic event. Earth Planet Sci Lett 158(3):165–173

DeConto R, Galeotti S, Pagani M, Tracy D, Schaefer K, Zhang T, Pollard D, Beerling DJ (2012) Past extreme warming events linked to massive carbon release from thawing permafrost. Nature 484:87–92

Degens ET, Guillard RRL, Sackett WM, Hellebust JA (1968) Metabolic fractionation of carbon isotopes in marine plankton. I. Temperature and respiration experiments. Deep-Sea Res 15:1–9

Dudd SN, Evershed RP (1998) Direct demonstration of milk as an element of archaeological economies. Science 282:1478–1481

Dunne J, Mercuri AM, Evershed RP, Bruni S, di Lernia S (2016) Earliest direct evidence of plant processing in prehistoric Saharan pottery. Nature Plants 3:16194

Emrich K, Ehhalt DH, Vogel JC (1970) Carbon isotope fractionation during the precipitation of calcium carbonate. Earth Planet Sci Lett 8(5):363–371

Gale AS, Bown PR, Caron M, Crampton J, Crowhurst SJ, Kennedy WJ, Petrizzo MR, Wray DS (2011) The uppermost Middle and Upper Albian succession at the Col de Palluel, Hautes-Alpes, France: an integrated study (ammonites, inoceramid bivalves, planktonic foraminifera, nannofossils, geochemistry, stable oxygen and carbon isotopes, cyclostratigraphy). Cretaceous Res 32:59–130

Garlick GD (1974) The stable isotopes of oxygen, carbon, and hydrogen in the marine environment. In: Goldberg ED (ed) The Sea, vol 5. Wiley, New York, pp 393–425

Gradstein FM, Ogg JG, Schmitz M, Ogg G (2012) The Geological Time Scale. Elsevier, Amsterdam

Godin JP, Fay LB, Hopfgartner G (2007) Liquid chromatography combined with mass spectrometry for ^{13}C isotopic analysis in life science research. Mass Spectrom Rev 26(6):751–774

Grossman EL, Cifuentes LA, Cozzarelli IM (2002) Anaerobic methane oxidation in a landfill-leachate plume. Environ Sci Technol 36(11):2436–2442

Grossman EL, Yancey TE, Jones TE, Bruckschen P, Chuvashov B, Mazzullo SJ, Mii HS (2008) Glaciation, aridification, and carbon sequestration in the Permo-Carboniferous: the isotopic record from low latitudes. Palaeogeogr Palaeoclimatol Palaeoecol 268:222–233

Gröcke DR, Hesselbo SP, Jenkyns HC (1999) Carbon-isotope composition of lower cretaceous fossil wood: ocean-atmosphere chemistry and relation to sea-level change. Geology 27:155–158

Havig JR, Hamilton TL, Bachan A, Kump LR (2017) Sulfur and carbon isotopic evidence for metabolic pathway evolution and a four-stepped Earth system progression across the Archean and Paleoproterozoic. Earth Sci Rev https://doi.org/10.1016/j.earscirev.2017.06.014

Hedges JI, Keil RG, Benner R (1997) What happens to terrestrial organic matter in the ocean? Org Geochem 27(5):195–212

Herrle JO, Kößler P, Friedrich O, Erlenkeuser H, Hemleben C (2004) High-resolution carbon isotope records of the Aptian to lower Albian from SE France and the Mazagan plateau (DSPD site 545): a stratigraphic tool for paleocanographic and paleobiologic reconstruction. Earth Planet Sci Lett 218:149–161

Herrle JO, Schröder-Adams CJ, Davis W, Pugh AT, Galloway JM, Fath J (2015) Mid-Cretaceous high Arctic stratigraphy, climate, and oceanic anoxic events. Geology 43(5):403–406

Hobbie E, Werner RA (2004) Intramolecular, compound-specific, and bulk carbon isotope patterns in C3 and C4 plants: a review and synthesis. New Phytol 161(2):371–385

Hoefs J (2009) Stable isotope geochemistry, vol 6. Springer, Berlin

Horita J (2014) Oxygen and carbon isotope fractionation in the system dolomite–water–CO_2 to elevated temperatures. Geochim Cosmochim Acta 129:111–124

Hudson J (1977) Stable isotopes and limestone lithification. J Geol Soc 133:637–660

Immenhauser A, Della Porta G, Kenter JAM, Bahamonde JR (2003) An alternative model for positive shifts in shallow-marine carbonate $\delta^{13}C$ and $\delta^{18}O$. Sedimentology 50:953–959

Jarvis I, Trabucho-Alexandre J, Gröcke DR, Ulicny D, Laurin J (2015) Intercontinental correlation of organic carbon and carbonate stable isotope records: evidence of climate and sea-level change during the Turonian (Cretaceous). The Depositional Record 1:53–90

Jarvis I, Carson GA, Cooper MKE, Hart MB, Leary PN, Tocher BA, Horne D, Rosenfeld A (1988) Microfossil assemblages and the Cenomanian – Turonian (late Cretaceous) oceanic anoxic event. Cretaceous Res 9:3–103

Jenkyns HC (1996) Relative sea-level change and carbon isotopes: data from the Upper Jurassic (Oxfordian) of central and Southern Europe. Terra Nova 8:1365–3121

Jenkyns HC (2003) Evidence for rapid climate change in the Mesozoic-Palaeogene greenhouse world. Phil Trans R Soc Lond, Series A 361:1885–1916

Joachimski MM, Buggisch W (1993) Anoxic events in the late Frasnian – causes of the Frasnian-Famennian faunal crisis? Geology 21:675–678

Keeling CD (1979) The Suess effect: ^{13}Carbon-^{14}Carbon interrelations. Environ Int 2:229–300

Korte C, Kozur HW (2010) Carbon–isotope stratigraphy across the Permian-Triassic boundary: a review. J Asian Earth Sci 39:215–235

Kroopnick P (1985) The distribution of ^{13}C of ΣCO_2 in the world oceans. Deep-Sea Res 32:5784

Kump LR, Arthur MA (1999) Interpreting carbon-isotope excursions: carbonates and organic matter. Chem Geol 161(1–3):181–198

Kuypers MMM, Pancost R, Shinninghe Damsté JS (1999) A large and abrupt fall in atmospheric CO_2 concentration during Cretaceous times. Nature 399:342–345

Leckie M (2009) Seeking a better life in the plankton. Proc Natl Acad Sci 106(34):14183–14184

Loftus E, Roberts P, Lee-Thorp JA (2016) An isotopic generation: four decades of stable isotope analysis in African archaeology. Azania 51 (1):88–114

Mackensen A, Hubberten HW, Bickert T, Fischer G, Fütterer DK (1993) The ^{13}C in benthic foraminiferal tests of Fontbotia wuellerstorfi (Schwager) relative to the ^{13}C of dissolved inorganic carbon in southern ocean deep water: implications for glacial ocean circulation models. Paleoceanography 8:587–610

Magill CR, Ashley GM, Domínguez-Rodrigo M, Freeman KH (2016) Dietary options and behavior suggested by plant biomarker evidence in an early human habitat. Proc Natl Acad Sci 113(11):2874–2879

Matsson O, Dybala-Defratyka A, Rostkowski M, Paneth P, Westaway KC (2005) A theoretical investigation of α-carbon kinetic isotope effects and their relationship to the transition-state structure of SN2 reactions. J Org Chem 70(10):4022–4027

McAnena A, Flogel S, Hofmann P, Herrle JO, Griesand A, Pross J, Talbot HM, Rethemeyer J, Wallmann K, Wagner T (2013) Atlantic cooling associated with a marine biotic crisis during the mid-cretaceous period. Nat Geosci 6:558–561

McConnaughy T (1989) ^{13}C and ^{18}O disequilibrium in biological carbonates: I. Patterns. Geochim Cosmochim Acta 53:151–162

McCorkle DC, Keigwin LD, Corliss BH, Emerson SR (1990) The influence of microhabitats on the carbon isotopic composition of deep-sea benthic foraminifera. Paleoceanography 5:161–185

Menegatti AP, Weissert H, Brown RS, Tyson RV, Farrimond P, Strasser A, Caron M (1998) High-resolution δ^{13}C stratigraphy through the early Aptian 'Livello Selli' of the alpine Tethys. Paleoceanography 13:530–545

Mitchell SF, Ball JD, Crowley SF, Marshall JD, Paul CRC, Veltkamp C (1997) Isotope data from cretaceous chalks and foraminifera: environmental or diagenetic signals? Geology 25:691–694

Muccio Z, Jackson GP (2009) Isotope ratio mass spectrometry. Analyst 134(2):213–222

Munnecke A, Samtleben C, Bickert T (2003) The Ireviken event in the lower Silurian of Gotland, Sweden – relation to similar Palaeozoic and Proterozoic events. Palaeogeogr Palaeoclimatol Palaeoecol 195:99–124

Pagani M (2014) 12.13 biomarker-based inferences of past climate: the Alkenone pCO_2 proxy. Treatise on Geochemistry. Elsevier, Oxford, pp 361–378

Pälike H, Norris RD, Herrle JO, Wilson PA, Coxall HK, Lear CH, Shackleton NJ, Tripati AK, Wade BS (2006) The heartbeat of the Oligocene climate system. Science 314:1894–1898

Pearson PN, Shackleton NJ, Hall MA (1993) Stable isotope paleoecology of middle Eocene planktonic foraminifera and integrated isotope stratigraphy, DSDP site 523, South Atlantic. J Foramin Res 23:123–140

Quay PD, Tilbrook B, Wong CS (1992) Oceanic uptake of fossil fuel CO_2: Carbon-13 evidence. Science 256:74–79

Rabouille C, Mackenzie FT, Ver LM (2001) Influence of the human perturbation on carbon, nitrogen, and oxygen biogeochemical cycles in the global coastal ocean. Geochim Cosmochim Acta 65 (21):3615–3641

Ravelo A, Hillarie-Marcel C (2007) The use of oxygen and carbon isotopes of foraminifera in paleoceanography. In: Hillarie-Marcel C, de Vernal A (eds) Proxies in late Cenozoic paleoceanography, Developments in marine geology, vol 1. Elsevier, Amsterdam, pp 735–764

Raven JA, Falkowski PG (1999) Oceanic sink for atmospheric CO_2. Plant Cell Environ 22(6):741–755

Rohde RA, Muller RA (2005) Cycles in fossil diversity. Nature 434:209–210

Rohling EJ, Cook S (1999) Stable oxygen and carbon isotopes on foraminiferal carbonate shells. In: Gupta BKS (ed) Modern Foraminifera. Kluwer, Dordrecht, pp 239–258

Romanek CS, Grossman EL, Morse JW (1992) Carbon isotopic fractionation in synthetic aragonite and calcite: effects of temperature and precipitation rate. Geochim Cosmochim Acta 56(1):419–430

Saltzman MR, Thomas E (2012) Carbon isotope stratigraphy. In: Gradstein FM, Ogg JG, Schmitz M, Ogg G (eds) The Geological Time Scale, vol 1. Elsevier, Amsterdam, pp 207–232

Sarmiento JL, Gruber N (2006) Ocean Biogeochemical Dynamics. Princeton University Press, Princeton, p 503

Schidlowski M. Aharon P., 1992. Carbon cycle and carbon isotopic record: geochemical impact of life over 3.8 Ga of earth history. In: Schidlowski, M. et al., Early organic evolution: implications for energy and mineral resources. Springer, Berlin: 147–175

Schlanger SO, Jenkyns HC (1976) Cretaceous oceanic anoxic events: causes and consequences. Geol Mijnb 55:179–184

Scholle PA, Arthur MA (1980) Carbon-isotope fluctuations in cretaceous pelagic limestones: potential stratigraphic and petroleum exploration tool. AAPG Bull 64:67–87

Sepkoski JJ (2002) A compendium of fossil marine animal genera. Bull Am Paleontol 363:560

Sessions AL (2006) Isotope-ratio detection for gas chromatography. J Sep Sci 29(12):1946–1961

Siegenthaler U, Sarmiento JL (1993) Atmospheric carbon dioxide and the ocean. Nature 365(6442):119–125

Sponheimer M, Alemseged Z, Cerling TE, Grine FE, Kimbel WH, Leakey MG, Lee-Thorp JA et al (2013) Isotopic evidence of early hominin diets. Proc Natl Acad Sci 110(26):10513–10518

Stanley SM (2010) Relation of Phanerozoic stable isotope excursions to climate, bacterial metabolism, and major extinctions. Proc Natl Acad Sci 107:19185–19189

Stern MJ, Spindel W, Monse EU (1968) Temperature dependences of isotope effects. J Chem Phys 48(7):2908–2919

Sundquist ET, Visser K (2004) The geologic history of the carbon cycle. Treatise in. Geochemistry 8:425–472

Swart PK (2008) Global synchronous changes in the carbon isotopic composition of carbonate sediments unrelated to changes in the global carbon cycle. Proc Natl Acad Sci 105:13741–13745

Turner JV (1982) Kinetic fractionation of carbon-13 during calcium carbonate precipitation. Geochim Cosmochim Acta 46(7):1183–1191

Veizer J, Ala D, Azmy K, Bruckschen P, Buhl D, Bruhn F, Carden GAF, Diener A, Ebneth S, Godderis Y, Jasper T, Korte C, Pawellek F, Podlaha O, Strauss H (1999) $^{87}Sr/^{86}Sr$, $\delta^{13}C$ and $\delta^{18}O$ evolution of Phanerozoic seawater. Chem Geol 161:37–57

C

Wagner T, Wallmann K, Herrle JO, Hofmann P, Stüsser I (2007) Consequences of moderate 25,000 year lasting emission of light CO_2 into the mid-Cretaceous ocean. Earth Planet Sci Lett 259:200–211

Wefer G, Berger WH (1991) Isotope paleontology: growth and composition of extant calcareous species. Mar Geol 100:207–248

Wefer G, Berger WH, Bijma J, Fischer G (1999) Clues to ocean history: a brief overview of proxies. In: Fischer G, Wefer G (eds) Use of proxies in paleoceanography. Springer, Berlin, p 68

Weissert H, Bréhéret JG (1991) A carbonate carbon-isotope record from Aptian-Albian sediments of the Vocontian trough (SE France). Bull Soc Geol Fr 162(6):1133–1140

Weissert H, Joachimski M, Sarnthein M (2008) Chemostratigraphy. Newsl Stratigr 42:145–179

Weissert H, Lini A, Föllmi KB, Kuhn O (1998) Correlation of early Cretaceous carbon isotope stratigraphy and platform drowning events: a possible link? Palaeogeogr Palaeoclimatol Palaeoecol 137:189–203

Weissert H, McKenzie JA, Hochuli P (1979) Cyclic anoxic event in the early Cretaceous Tethys ocean. Geology 7:147–151

Wendler I (2013) A critical evaluation of carbon isotope stratigraphy and biostratigraphic implications for late Cretaceous global correlation. Earth-Sci Rev 126:116–146

Whiticar MJ (1999) Carbon and hydrogen isotope systematics of bacterial formation and oxidation of methane. Chem Geol 161(1):291–314

Zachos J, Pagani M, Sloan L, Thomas E, Billups K (2001) Trends rhythms, and aberrations in global climate 65 Ma to present. Science 292:689–693

Zahn R, Winn K, Sarnthein M (1986) Venthic foraminiferal ^{13}C and accumulation rates of organic carbon: Uvigerina peregrine group and Cibicidoides wuellerstorfi. Paleoceanography 1:27–42

Carbonate Compensation Depth

Ryan J. Woosley
Department of Ocean Science, University of Miami, Rosenstiel School of Marine and Atmospheric Sciences, Miami, FL, USA

Definition

Calcifying organisms in the surface supply $CaCO_3$ to deep waters when they die, and their tests or shells fall through the water column. As a result of respiration, increasing pressure, and decreasing temperature, waters become increasingly undersaturated with respect to $CaCO_3$ with depth, allowing the tests to dissolve more readily. The depth in the water column at which the rate of calcium carbonate supplied from the surface equals the rate of dissolution is called the carbonate compensation depth (CCD). If the sea floor lies above the CCD, these $CaCO_3$ tests can accumulate in the sediments; if the sea floor lies below the CCD, $CaCO_3$ will be absent from the sediments. In this way, the CCD can be thought of as a "snowline" marking the separation between carbonate-rich sediments and carbonate-deficient sediments.

This gives rise to an alternative definition of CCD as the depth at which the carbonate content of the sediments is 0% by weight. This is a more practical definition because measuring the carbonate content of sediments is much easier than measuring rates of supply and dissolution in the water column.

There are actually at least two different CCDs because there are two common crystalline polymorphs of $CaCO_3$ produced in the surface. Pteropods (cone-shaped mollusks) secrete the more soluble form, aragonite, while foraminifera (zooplankton) and coccolithophores (phytoplankton) secrete the more stable form, calcite. The aragonite compensation depth (ACD) is typically about 3,000 m shallower than the calcite compensation depth (Morse and Mackenzie 1990). Studies generally focus on the calcite compensation depth because it marks the complete dissolution of carbonates from the sediments. The system is further complicated by high-magnesium calcites, which are actually more soluble than aragonite, can also be produced as a by-product of osmoregulation (Woosley et al. 2012), and likely begin to dissolve shallower in the water column; however, very little is known about their contribution to the carbon cycle.

Factors Controlling CCD

The depth of the CCD is mainly controlled by two factors: the degree of undersaturation with respect to calcite or aragonite and the flux of $CaCO_3$ debris from the surface. The saturation state (Ω) is the ratio of the ion concentration product ($[Ca^{2+}][CO_3^{2-}]$) to the apparent solubility constant and represents how close the water is to thermodynamic equilibrium. Surface waters are generally supersaturated ($\Omega > 1$). The degree of supersaturation decreases with depth as a result of decreases in the solubility of the minerals with increasing pressure and decreasing temperature, as well as increased total CO_2 from remineralization of organic matter, until the water reaches saturation ($\Omega = 1$), a depth called the saturation horizon. Below the saturation horizon, the saturation state continues to decrease and the waters become undersaturated ($\Omega < 1$), allowing $CaCO_3$ to dissolve. At some depth at or below the saturation horizon, there is a rapid increase in the rate of dissolution; this is called the lysocline. Below the lysocline, the percent of $CaCO_3$ found in sediments decreases rapidly until the CCD is reached. The saturation horizon, lysocline, and CCD are shown schematically in Fig. 1. In a thermodynamically controlled ocean, the depth of the saturation horizon, lysocline, and CCD would all be very similar. But because the kinetics of $CaCO_3$ dissolution are complex and nonlinear, the lysocline and CCD can be 200–1000 m deeper than the saturation horizon. The majority of dissolution occurs at the sediment-water interface because $CaCO_3$

Carbonate Compensation Depth, Fig. 1 A schematic showing the relationship between the saturation horizon, lysocline, and carbonate compensation depth (CCD) in the ocean. The location of the three levels varies by location as a result of differences in $CaCO_3$ production at the surface and the degree of undersaturation at depth
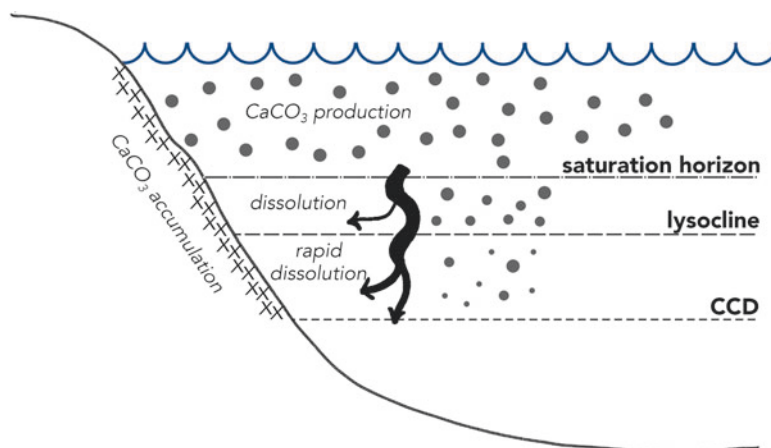
particles generally fall through the water column faster than they can dissolve. There is some evidence of dissolution above the aragonite saturation horizon, which is thought to be dissolution of high-magnesium calcites.

## Spatiotemporal Variability

The position of the CCD varies spatially as the result of differences in the magnitude and type of production at the surface and saturation state at depth. Specifically, the CCD is deeper in the Atlantic (~5,000 m) than in the Pacific and Indian (~3,500–4,500 m) due to a lower saturation state in the subsurface Pacific and Indian as a result of higher total CO_2 concentrations from organic matter remineralization. The CCD is also deeper in the tropics due to high productivity in the surface resulting in a higher flux of $CaCO_3$ to the deep and shallower near the continental margins due to increased organic matter remineralization decreasing the saturation state.

The position of the CCD also varies greatly (~2,000 m) over geologic time scales. This variability has major implications for the global carbon cycle because it determines how much carbon is stored long term (millions of years) in deep-sea sediments and how much is actively cycled through the ocean, atmosphere, and biosphere (~1,000-year time scales).

Buffering Anthropogenic CO_2

Currently, the uptake of anthropogenic CO_2 by the oceans is resulting in a decrease in pH and CO_3^{2-} concentration, a process termed ocean acidification. These changes to the inorganic carbon system cause the saturation horizon, and in turn the lysocline and CCD, to shoal. Lowering of the saturation state in the surface ocean may also lead to a decrease in $CaCO_3$ production at the surface and thus reduce the supply

of $CaCO_3$ to sediments, causing the CCD to shoal. If the CCD shoals, carbonate sediments that were formally below the CCD will become exposed to corrosive waters and begin to dissolve. The dissolution of $CaCO_3$ consumes CO_2 according to the following reaction:

$$CO_2 + H_2O + CaCO_3 \rightarrow Ca^{2+} + 2HCO_3^-. \quad (1)$$
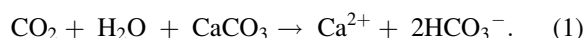
This reaction reflects the "neutralizing capacity" of the deep ocean by increasing the alkalinity (or buffering capacity) and will play a major role in returning atmospheric CO_2 concentrations to "natural" levels once fossil fuel burning ceases (Morse and Mackenzie 1990). However, this re-equilibration will take thousands of years (Broecker and Takahashi 2011).

Cross-References

▶ Biological Pump
▶ Calcium
▶ Carbonate Minerals and the CO2-Carbonic Acid System
▶ Dolomite and Dolomitization
▶ Earth's Oceanic Crust
▶ Fluid–Rock Interaction
▶ Organic Geochemistry

References

Broecker WS, Takahashi T (2011) Neutralization of fossil fuel CO_2 by marine calcium carbonate. In: Archer D, Pierrehumbert R (eds) The warming papers: the scientific Foundation for the climate change forecast. Wiley-Blackwell, Oxford, UK, pp 341–353

Morse JW, Mackenzie FT (1990) Geochemistry of sedimentary carbonates. Elsevier, Amsterdam, p 707

Woosley RJ, Millero FJ, Grosell M (2012) The solubility of fish-produced high magnesium calcite in seawater. J Geophys Res 117: C04018. https://doi.org/10.1029/2011JC007599

Carbonate Minerals and the CO$_2$-Carbonic Acid System

Abraham Lerman[1] and Fred T. Mackenzie[2]
[1]Department of Earth and Planetary Sciences, Northwestern University, Evanston, IL, USA
[2]Department of Oceanography, School of Ocean and Earth Science and Technology, University of Hawai'i at Manoa, Honolulu, HI, USA

Definition

Carbonic acid, H$_2$CO$_3$, forms from the dissolution of CO$_2$ in water and plays a key role in weathering, biological production, formation and deposition of sediments, and the carbon cycle. Carbonate minerals, primarily calcite, aragonite, and dolomite precipitating from these solutions, constitute the second most abundant class of sedimentary rocks.

Introduction

Carbonate rocks, consisting mainly of the minerals calcite (CaCO$_3$) and dolomite [CaMg(CO$_3$)$_2$], are the second most abundant class of sedimentary rocks, after terrigenous clastics, on land and on the ocean floor. The widespread occurrence of carbonate rocks in the geologic record is attributable to the following factors:

1. CO$_2$ gas has a relatively high solubility in water, higher than molecular oxygen and nitrogen.
2. CO$_2$ hydrolyzes in water, making the bicarbonate and carbonate anions (discussed in more detail in section "CO$_2$-Carbonic Acid-Carbonate System and Seawater") that react with divalent and monovalent metals.
3. Among the divalent cations, calcium combined with the carbonate anion makes a solid of low solubility.

Calcium is the fifth and carbon the 15th most abundant elements in the Earth's crust, and their presence in natural waters accounts for the formation of mineral CaCO$_3$ by inorganic and biogenic processes in many environments.

Twenty-seven carbonate minerals are listed in Table 1 to provide the reader with an appreciation of the wide variety of minerals in this mineral group. In terms of their abundance, calcites with Mg in their structure (Ca$_{1-x}$Mg$_x$CO$_3$) and aragonite (CaCO$_3$) are more abundant in the extant younger sedimentary mass, whereas dolomite and nearly pure calcite are more abundant in the geologically older sequences. Figure 1 shows the mass of calcite and dolomite in the preserved 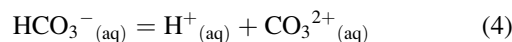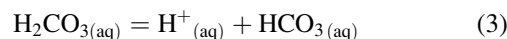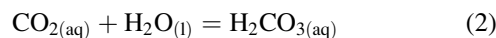sedimentary carbonate mass. A long-standing and unresolved geologic problem is how much of the extant dolomite in the sedimentary record is of primary origin, that is, a direct precipitate from seawater, and how much is secondary formed from alteration of calcite and aragonite. Some scientists have proposed that both the calcite/dolomite preserved mass distribution and the original composition of inorganic and biogenic calcite and aragonite phases have varied cyclically during the Phanerozoic (the past 545 Ma) reflecting major changes in seawater composition during this eon (see, e.g., Mackenzie and Andersson 2013).

Ca-carbonates are primarily inorganic and biogenic products of the marine environment. CaCO$_3$ is a first precipitate in an evaporative sequence of seawater, and later precipitates are Na and K chlorides and sulfates. In continental waters, however, the anions HCO$_3^-$ and CO$_3^{2-}$ are usually more abundant than Cl$^-$ and SO$_4^{2-}$, and the minerals precipitating are the various carbonates of Na, as shown in Table 1. Much of the information in this article is based on the books by Morse and Mackenzie (1990), Mackenzie and Lerman (2006), and Mackenzie and Andersson (2013).

CO$_2$-Carbonic Acid-Carbonate System and Seawater

This section presents some of the basic physical-chemical relationships relevant to understanding the behavior of CO$_2$ in aqueous solution in the Earth's surface environments. Readers are referred to the books by Broecker and Peng (1982), Morse and Mackenzie (1990), Mackenzie and Lerman (2006), Zeebe and Wolf-Gladrow (2001), and Millero (2013) for a detailed development of the subject material.

Dissolution and Dissociation of CO$_2$ in Water: Dissolution of carbon dioxide in water is the first step that enables photosynthetic production of organic matter in aqueous environments, precipitation of carbonate minerals from aqueous solutions, and chemical weathering of the Earth's crust and sediments. Carbon dioxide dissolves in water and reacts with it producing negatively charged bicarbonate and carbonate ions. In pure water the electrical charges are balanced by the hydrogen ion or in natural or experimental more complex aqueous solutions by other metal cations and the hydrogen ion. Dissolution and dissociation of the gaseous species CO$_2$(g) in water are represented by the following reactions:

$$CO_{2(g)} = CO_{2(aq)} \tag{1}$$

$$CO_{2(aq)} + H_2O_{(l)} = H_2CO_{3(aq)} \tag{2}$$

$$H_2CO_{3(aq)} = H^+_{(aq)} + HCO_{3\,(aq)} \tag{3}$$

$$HCO_3^-_{(aq)} = H^+_{(aq)} + CO_3^{2+}_{(aq)} \tag{4}$$

Carbonate Minerals and the CO$_2$-Carbonic Acid System, Table 1 Carbonate minerals[a,b]

	Mineral	Composition	Occurrence[b]
1	Calcite	$Ca_{1-x}Mg_xCO_3$, $0 \leq x \leq 0.25$	A major rock-forming mineral in sedimentary environments. Calcite is a common constituent of sedimentary rocks, limestone in particular, much of which is formed from the shells of dead marine organisms. Approximately 10% of sedimentary rock is limestone. Calcite is the primary mineral in metamorphic marble. It also occurs as a vein mineral in deposits from hot springs, and it occurs in caverns as stalactites and stalagmites. Calcite may also be found in volcanic or mantle-derived rocks such as carbonatites, kimberlites, or rarely in peridotites. Calcite is often the primary constituent of the shells of marine organisms, e.g., plankton (such as coccoliths and planktonic foraminifera), the hard parts of red algae, some sponges, brachiopods, echinoderms, some serpulids, most bryozoa, and parts of the shells of some bivalves (such as oysters and rudists) The largest documented single crystal of calcite originated from Iceland, measured $7 \times 7 \times 2$ m and $6 \times 6 \times 3$ m and weighed about 250 t
2	Aragonite	$CaCO_3$	Aragonite is the high pressure polymorph of calcium carbonate. As such, it occurs in high pressure metamorphic rocks such as those formed at subduction zones. Aragonite and calcite precipitate in hot springs as travertine deposits. Aragonite forms naturally in almost all mollusk shells, and as the calcareous endoskeleton of warm- and cold-water corals (Scleractinia). Several serpulids have aragonitic tubes. In some mollusks, such as pteropods, the entire shell is aragonite; in others, aragonite forms only discrete parts of a bimineralic shell (aragonite plus calcite). The nacreous layer of the aragonite fossil shells of some extinct ammonites forms an iridescent material called ammolite. Aragonite also forms in the ocean and in caves as inorganic precipitates called marine cements and speleothems, respectively. Aragonite is not uncommon in serpentinites where high Mg in pore solutions apparently inhibits calcite growth and promotes aragonite precipitation
3	Vaterite	$CaCO_3$	Vaterite occurs in mineral springs, organic tissue, gallstones, and urinary calculi. Vaterite can be produced as the first mineral deposits repairing natural or experimentally induced shell damage in some aragonite-shelled mollusks (e.g., gastropods). Subsequent shell deposition occurs as aragonite
4	Ikaite	$CaCO_3 \cdot 6H_2O$	At the Ikka Fjord, Greenland, Ikaite, occurs in spectacular towers growing out of the fjord floor toward the surface water, where they are naturally truncated by waves. The Ikaite towers are created as the result of a groundwater seep, rich in carbonate and bicarbonate ions, entering the fjord bottom. Ikaite has also been reported as occurring in high-latitude marine sediments in Antarctica, Sea of Okhotsk, and Saanich Inlet, British Columbia, Canada. In addition it has been reported in a deep sea fan off the Congo. The most recent occurrence has been reported by Dieckmann et al. (2008). Ikaite directly precipitates in sea ice in the Weddell Sea and throughout fast ice off Adélie Land, Antarctica
5	Monohydrocalcite	$CaCO_3 \cdot H_2O$	Monohydrocalcite has been observed in air conditioning systems, and in moonmilk deposits in caves, both probably formed from spray of carbonate-rich fluids. It is well known in Robe on the Limestone Coast of South Australia as a component of beach sands of Lake Fellmongery and Lake Butler, where it is believed to be formed from algal spume. Other lacustrine deposits include Lake Issyk-Kul, Lake Kivu, and Solar Lake, Sinai
6	Magnesite	$MgCO_3$	Magnesite occurs as veins in and an alteration product of ultramafic rocks, serpentinite, and other magnesium-rich rock types in both contact and regional metamorphic terrains. Magnesite is also present within the regolith above ultramafic rocks as a secondary carbonate within soil and subsoil, where it is deposited as a consequence of dissolution of magnesium-bearing minerals by carbon dioxide within groundwater
7	Barringtonite	$MgCO_3 \cdot 2H_2O$	Found with nesquehonite on the surfaces of olivine basalts
8	Nesquehonite	$MgCO_3 \cdot 3H_2O$	Bases of stalactites and incrustations, the remainder of which consisted of lansfordite. Anthracite coal deposit
9	Lansfordite	$MgCO_3 \cdot 5H_2O$	Small stalactites attached to carbonaceous shale
10	Pokrovskite	$MgCO_3 \cdot Mg(OH)_2 \cdot 0.5H_2O$	Alteration of ultramafic bodies of dunite and serpentinite
11	Artinite	$MgCO_3 \cdot Mg(OH)_2 \cdot 3H_2O$	Artinite is found along with hydromagnesite and other minerals as a low-temperature alteration product as veinlets or crusts in serpentinized ultrabasic rocks
12	Hydromagnesite	$4MgCO_3 \cdot Mg(OH)_2 \cdot 4H_2O$	Associated with the weathering products of magnesium containing minerals such as serpentine or brucite. It occurs as incrustations and vein or fracture fillings in ultramafic rocks and serpentinites. It occurs in hydrothermally altered dolomite and marble. It commonly appears in caves as speleothems and "moonmilk," deposited from water that has seeped through magnesium-rich rocks. It is the most common cave carbonate after calcite and aragonite
	Giorgiosite	$4MgCO_3 \cdot Mg(OH)_2 \cdot 4$–$6H_2O$	In white powdery crusts on lava

Carbonate Minerals and the CO₂-Carbonic Acid System, Table 1 (continued)

	Mineral	Composition	Occurrence[b]
13	Dypingite	$4MgCO_3 \cdot Mg(OH)_2 \cdot 5H_2O$	Alteration product in serpentines
14	Strontianite	$SrCO_3$	Strontianite is an uncommon low-temperature hydrothermal mineral formed in veins in limestone, marl, and chalk, and in geodes and concretions. It occurs rarely in hydrothermal metallic veins but is common in carbonatites
15	Witherite	$BaCO_3$	Witherite forms in low-temperature hydrothermal environments
16	Siderite	$FeCO_3$	Siderite is commonly found in hydrothermal veins and is associated with barite, fluorite, galena, and others. It is also a common diagenetic mineral in shales and sandstones, where it sometimes forms concretions, which can encase three-dimensionally preserved fossils. In sedimentary rocks, siderite commonly forms at shallow burial depths and its elemental composition is often related to the depositional environment of the enclosing sediments https://en.wikipedia.org/wiki/Lagoon
17	Dolomite	$CaMg(CO_3)_2$ or $Ca_{0.5}Mg_{0.5}CO_3$	A major sedimentary rock-forming mineral. Modern dolomite formation has been found to occur under anaerobic conditions in supersaturated saline lagoons. Vast deposits of dolomite are present in the geological record, but the mineral is relatively rare in modern environments
18	Ankerite	$Ca(Fe,Mg)(CO_3)_2$	Ankerite occurs with siderite in metamorphosed ironstones and sedimentary banded iron formations. It also occurs in carbonatites. In sediments it occurs as authigenic, diagenetic minerals and as a product of hydrothermal deposition
19	Natron	$Na_2CO_3 \cdot 10H_2O$	Geologically, the mineral natron and the historical natron are formed as transpiro-evaporite minerals, i.e., crystallizing during the drying up of salt lakes rich in sodium carbonate. The sodium carbonate is usually formed by absorption of carbon dioxide from the atmosphere by a highly alkaline, sodium-rich lake brine. Pure deposits of sodium carbonate decahydrate are rare, due to the limited temperature stability of this compound and due to the fact that the absorption of carbon dioxide usually produces mixtures of bicarbonate and carbonate in solution
20		$Na_2CO_3 \cdot 7H_2O$	*No known occurrences in nature*
21	Thermonatrite	$Na_2CO_3 \cdot H_2O$	As efflorescences on soil in arid regions and in saline lakes
22	Natrite	Na_2CO_3	Locally abundant in deep drill holes in pegmatites occurring in differentiated alkaline massifs, in sodalite xenoliths associated with an intrusive alkalic gabbro-syenite complex
23	Nahcolite	$NaHCO_3$	In lava tunnels. It occurs as a hot spring and saline lake precipitate or efflorescence, in differentiated alkalic massifs, in fluid inclusions as a daughter mineral phase, and in evaporite deposits
24	Wegscheiderite	$Na_2CO_3 \cdot 3NaHCO_3$	As a replacement of trona in a lacustrine deposit. Lacustrine deposits
25	Trona	$Na_2CO_3 \cdot NaHCO_3 \cdot 2H_2O$	Trona is found in alkaline saline lakes. Trona also occurs in magmatic environments, where it forms by autometasomatic reactions of late-magmatic fluids or supercritical fluid-melt mixtures with earlier crystallized rocks
26	Pirssonite	$Na_2CO_3 \cdot CaCO_3 \cdot 2H_2O$	Lacustrine clay beds. In oil shales; in sediments of a salt pan
27	Gaylussite	$Na_2CO_3 \cdot CaCO_3 \cdot 5H_2O$	Forms as an evaporite from alkali lacustrine waters. Also occurs rarely as veinlets in alkalic igneous rocks

[a]Morse and Mackenzie (1990), Mackenzie and Andersson (2013), Railsback (2002)
[b]Anthony et al. (1997–2003), Mindat (1993–2016), and Wikipedia articles by mineral name https://en.wikipedia.org/wiki/[mineralname]

Although aqueous uncharged CO_2 can include the species $H_2CO_{3(aq)}$, this species constitutes only a small fraction, about 1/400, of CO_2 in solution. As such the use of either $CO_{2(aq)}$ or $H_2CO_{3(aq)}$ for all of the aqueous species CO_2 is acceptable without a loss of meaning or accuracy (Millero 2013).

For each of the mass action Eqs. 1, 2, 3, and 4, one can write a thermodynamic equilibrium constant, using H_2CO_3* to represent both undissociated aqueous carbon species in solution – $H_2CO_{3(aq)}$ and $CO_{2(aq)}$ – which have values at 25 °C and 1 atm total pressure as follows (Morse and Mackenzie 1990):

$$K_o = \{H_2CO_3{}^*\}/P_{CO2} = 10^{-1.47} \quad (5)$$

$$K_1 = \{H^+\}\{HCO_3{}^-\}/\{H_2CO_3{}^*\} = 10^{-6.34} \quad (6)$$

$$K_2 = \{H^+\}\{CO_3{}^{2-}\}/\{HCO_3{}^-\} = 10^{-10.33} \quad (7)$$

where curly brackets designate thermodynamic activities of the chemical species (dimensionless quantities), and P_{CO2} is the partial pressure of CO_2, taken as an ideal gas and replacing its fugacity that is also dimensionless. The activities are also denoted as, for example, a_{H^+}, for the activity of the hydrogen ion, and a_{ion} for other species.

The activities of aqueous species and solids are referred to a standard state, chosen as a normal temperature and pressure

Carbonate Minerals and the CO₂-Carbonic Acid System, Fig. 1 Period-averaged preserved (extant) mass distribution of calcite and dolomite and mass ratio of calcite/dolomite through Phanerozoic time (After Mackenzie and Morse (1992))

carbon chemical species, have different values, and are functions of salinity as well as temperature and pressure. As an example, for an average seawater salinity of 35‰ and at a temperature of 25 °C and a total pressure of 1 bar (= ~1 atm), the stoichiometric constants and their values corresponding to Eqs. 5, 6, and 7 are Morse and Mackenzie (1990)

$$K'_0 = [H_2CO_3^*]/P_{CO2} = 2.84 \times 10^{-2} \qquad (8)$$

$$K'_1 = [H^+][HCO_3]/[H_2CO_3^*] = 1.39 \times 10^{-6} \qquad (9)$$

$$K'_2 = [H^+][CO_3^2]/[HCO_3] = 1.19 \times 10^{-9} \qquad (10)$$

where brackets denote concentrations of the chemical species in mol per 1 kg seawater.

Dissolved Inorganic Carbon: Because of the formation of the aqueous ions HCO_3^- and CO_3^{2-} from CO_2 in solution, the total concentration of dissolved inorganic carbon is the sum of all the inorganic carbon species, $CO_{2(aq)}$, HCO_3^-, and CO_3^{2-}. This parameter is termed dissolved inorganic carbon, to distinguish it from dissolved organic compounds, and it is usually denoted as ΣCO₂ or DIC:

$$DIC = CO_{2(aq)} + HCO_3^- + CO_3^{2-}. \qquad (11)$$

The relative distribution of DIC chemical species is commonly shown as a function of pH in a plot known as a Bjerrum diagram (Fig. 2). The individual values of the three fractions of DIC (CO_2 plus H_2CO_3 as CO_2, HCO_3^- and CO_3^{2-}) are shown in the figure for different sets of conditions, as a function of the solution pH, between pH = 2 and 12, at two temperatures of 5 and 25 °C, and 1 bar total pressure and for seawater $S = 35‰$ and 1 and 300 bar total pressure. In a very dilute solution of zero ionic strength (Fig. 2a), HCO_3^- is the dominant DIC species over the pH range from roughly 6.5 to slightly more than 10. This is the range in pH of many natural waters. In addition, in dilute waters, lower temperature favors relatively higher concentrations of undissociated CO_2 and lower concentrations of the carbonate anion, CO_3^{2-}; that is, the equal concentration points of 50% shift to the left, toward lower pH values.

The effects of salt concentration and pressure on the distribution of the dissolved carbon species are shown in Fig. 2b. Notice first that HCO_3^- is still by far the dominant species in seawater over its pH range of slightly above 7 (deep ocean waters) to slightly above 8 (surface ocean waters). In addition, at 5 and 25 °C, the effect of a mean seawater salinity of 35‰ on the abundance of the various DIC species is pronounced: from a dilute solution of salinity 0–35‰, the abundance of the bicarbonate ion, HCO_3^-,

(NTP) of 25 °C and 1 atm pressure, usually replaced by 298 K and 1 bar. Pure solids and solutes have an activity of 1 in a standard state. For solutes it is a 1 m (molal) solution, such that at infinite dilution the activity coefficient of the solute is equal to one. Thus, mass action equations written in terms of equilibrium constants are expressed as activities of the chemical species of interest and are a function of only pressure and temperature.

Because of the difficulties in determining the values of activity coefficients in seawater or compositional modifications of such, another standard state has been developed, that of the composition of seawater at the salinity $S = 35‰$ (g dissolved solids in 1 kg of solution; however, S in seawater is now taken as a dimensionless number because it is measured using a salinometer, which is based on electrical conductivity), 25 °C, and 1 atm total pressure. Thus for calculations of seawater CO_2-carbonic acid system chemistry, "apparent" or stoichiometric constants have been adopted and these vary with pressure, temperature, *and* composition (salinity). In seawater the mass action equations and the CO_2-carbonic acid system stoichiometric equilibrium constants (K-primes) have a similar formulation as the thermodynamic constants, but the expressions are written in terms of the concentrations of the dissolved inorganic

Carbonate Minerals and the CO$_2$-Carbonic Acid System, Fig. 2 Bjerrum diagram showing (**a**) Fractional concentrations of dissolved inorganic carbon species in pure water (salinity $S = 0‰$) as a function of pH at 5° and 25 °C. (**b**) Fractional concentrations of dissolved inorganic carbon species in seawater ($S = 35‰$) at 5 and 25 °C at atmospheric pressure, and at a pressure of 300 bar (After Mackenzie and Lerman (2006))
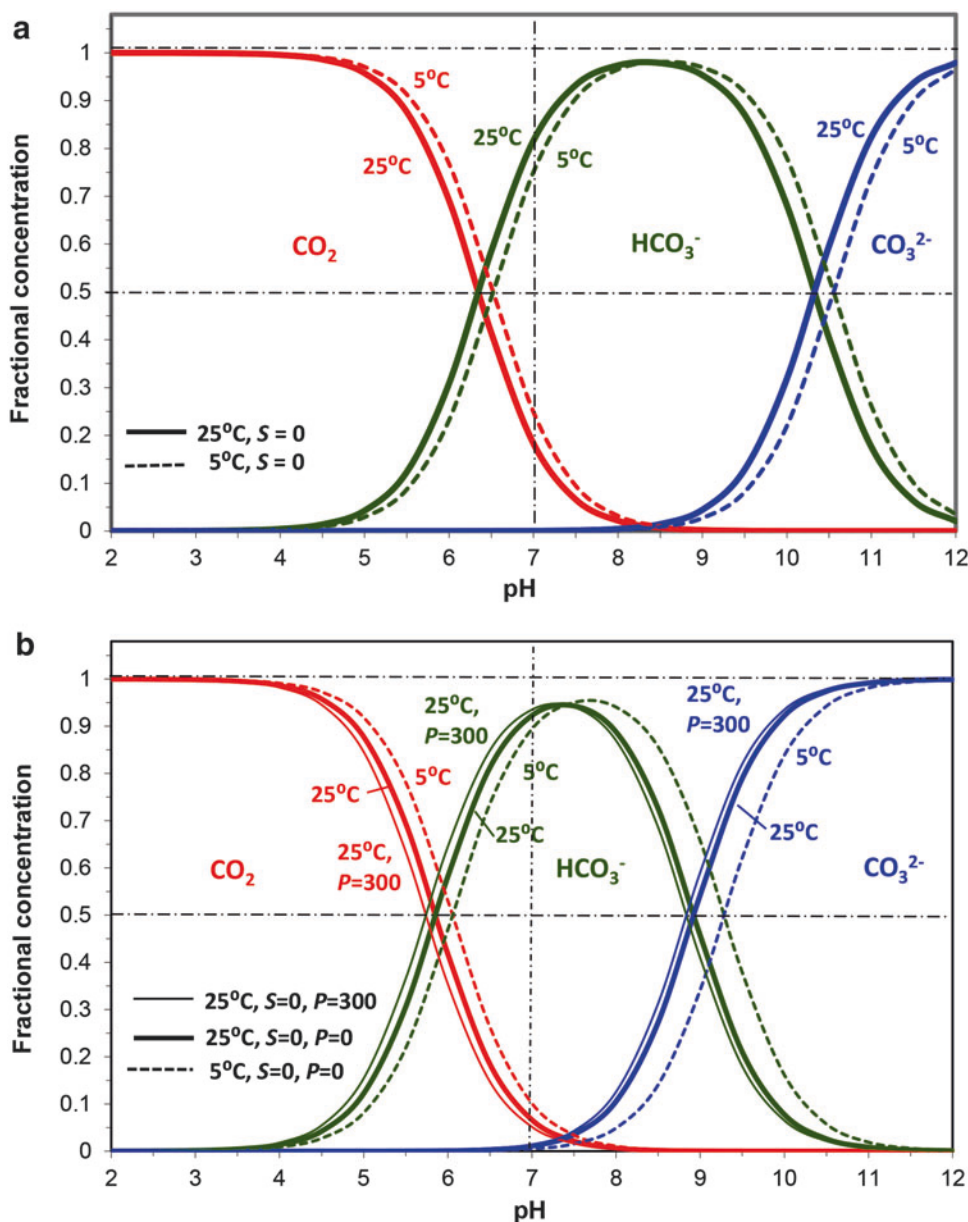
decreases at the expense of the other two species of $CO_{2(aq)}$ and $CO_3{}^{2-}$. However, the effect of pressure is small at a mean ocean water salinity of 35‰: a total pressure increase from atmospheric to 300 bars of pressure has only a small effect on the shift in the relative abundance of the DIC chemical species.

Total Alkalinity: One other variable of the CO$_2$-carbonic acid system that is important to seawater carbon chemistry is that of total alkalinity. For seawater, the difference between the charges of the conservative cations and anions is equal to the algebraic sum of the charges of the H$^+$-dependent ions, and this difference is called the total alkalinity of the solution, denoted [TA]:

$$2[Ca^{2+}] + 2[Mg^{2+}] + [Na^+] + [K^+] - [Cl^-] - 2[SO_4{}^{2-}]$$
$$= [HCO_3{}^-] + 2[CO_3{}^{2-}] + [B(OH)_4{}^-] + [OH^-] - [H^+]$$

$$(12)$$

and for the major species in seawater that contribute to the total alkalinity:

$$[TA] = [HCO_3{}^-] + 2[CO_3{}^{2-}] + [B(OH)_4{}^-]$$
$$+ [OH^-] - [H^+].$$

$$(13)$$

The determination of TA and DIC in ocean waters is a powerful tool to use to trace water masses in the ocean and to obtain estimates of primary productivity and the dissolution

and precipitation of carbonate minerals. Also if the values of these two variables are known, the pH and pCO_2 of seawater can be calculated. Alternatively, the pH can be measured in solution instead of being calculated.

Saturation State: It is also possible to write reactions and equilibrium constants for the solution (dissolution) and precipitation of minerals in aqueous solutions. The carbonate minerals are especially important minerals found in the ocean as the skeletons and tests of marine organisms and as cements in marine sediments. Calcite (hexagonal $CaCO_3$), aragonite (orthorhombic $CaCO_3$), and dolomite [hexagonal $CaMg(CO_3)_2$] are important marine minerals. The latter mineral is not found in great abundance in modern environmental settings, but it is an important carbonate mineral found in ancient rocks deposited in the marine environment (Fig. 1). The mass action equation for both calcite and aragonite is written

$$CaCO_3 = Ca^{2+} + CO_3{}^{2-}, \qquad (14)$$
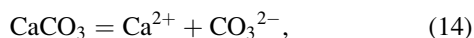
and at 25 °C and 1 atm total pressure, the thermodynamic equilibrium constants are

$$K_{cal} = \{Ca^{2+}\}\{CO_3{}^{2-}\} = 10^{-8.46} \qquad (15)$$

and

$$K_{arag} = \{Ca^{2+}\}\{CO_3{}^{2-}\} = 10^{-8.3} \qquad (16)$$

and in seawater of $S = 35‰$ under the same P and T conditions

$$K'_{cal} = [Ca^{2+}][CO_3{}^{2-}] = 10^{-6.37} \qquad (17)$$

and

$$K'_{arag} = [Ca^{2+}][CO_3{}^{2-}] = 10^{-6.19}. \qquad (18)$$

Despite the two minerals having the same composition, they differ in their atomic structure, and thus the K values for the two minerals differ. These K values basically represent the solubilities of the two minerals. The larger K value for aragonite than for calcite implies that aragonite is a more soluble mineral than calcite and is unstable relative to calcite under the environmental conditions specified above. However for these minerals to dissolve, the aqueous solution in which the minerals are bathed must be undersaturated with respect to the two minerals. This implies that the product of the activities or concentrations of Ca^{2+} and $CO_3{}^{2,-}$, termed the ion activity product (*IAP*) or ion concentration product (*ICP*), respectively, in the solution must be smaller than the K values for the minerals; that is, the ratio of *IAP/K* or *ICP/K′* must be <1. In general, in a solution at equilibrium, $\Omega = 1$:

$$\Omega = IAP/K \text{ or } ICP/K' = 1 \text{ at saturation.} \qquad (19)$$

In a supersaturated solution $\Omega > 1$, and in an undersaturated solution, $\Omega < 1$.

Both calcite and aragonite contain other elements in minor or trace amounts, and this affects their solubilities. Strontium is especially important in aragonite and magnesium in calcite. Indeed Mg can be so plentiful in biogenically and inorganically produced calcite that a special term has been applied to the calcites containing more than about 4 wt.% Mg, the magnesian calcites, that generally have greater solubilities than pure calcite, and for some magnesian calcite compositions, even than aragonite. The general mass action equation and thermodynamic equilibrium constant for calcites with Mg in them is written as

$$Ca_{(1-x)}Mg_x(CO_3) = (1-x)Ca^{2+} + xMg^{2+}$$
$$+ CO_3{}^{2-} \qquad (20)$$
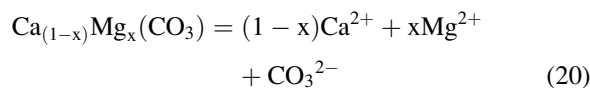
and

$$K_{Mg-calcite} = \{Ca^{2+}\}^{(1-x)}\{Mg^{2+}\}^{(x)}\{CO_3{}^{2-}\} \qquad (21)$$

where x is the mole fraction of $MgCO_3$.

For dolomite the mass action equation is

$$CaMg(CO_3)_2 = Ca^{2+} + Mg^{2+} + 2CO_3{}^{2-} \qquad (22)$$
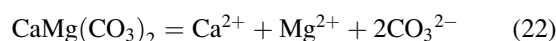
and

$$K_{dol} = \{Ca^{2+}\}\{Mg^{2+}\}\{CO_3{}^{2-}\}^2 = \sim 10^{-17}. \qquad (23)$$

To our knowledge the K', that is, the stoichiometric constant, for dolomite has never been determined experimentally in seawater because of the difficulty in doing experiments involving this phase at low temperatures due to its slow reactivity in aqueous solution.

Thermodynamic and Thermophysical Data for Major Carbonate Minerals

This section discusses a number of fundamental thermophysical and thermodynamic data for the major sedimentary carbonate minerals calcite, aragonite, dolomite, and magnesite that are germane to their occurrences on Earth. Table 2 gives the molecular mass of each mineral, its molar volume, and density at ambient conditions (25 °C and 1 atm total pressure, rounded to 298 K and 1 bar). Also given are the coefficients of volume expansion as a function of temperature $\alpha_V = (1/V)(\partial V/\partial T)_P$ K^{-1}, and the coefficient of isothermal compressibility $\beta_T = -(1/V)(\partial V/\partial P)_T$ bar^{-1}.

Carbonate Minerals and the CO₂-Carbonic Acid System, Table 2 Thermophysical data for four carbonate minerals

Mineral phase	Molecular mass	V_0[a]	ρ[a]	α_V			β_T			β_{ad}[i]
	(g/mol)[a]	(cm³/mol)	(g/cm³)	T range (K)	(K⁻¹)	Ref.	P range (kbar)	(bar⁻¹)	Ref.	(bar⁻¹)
CaCO₃ calcite	100.09	36.93	2.71	293–873	1.88E–05	[b]	2–12	1.39E–06	[d]	1.36E–06
				297–1,173	3.80E–06	[c]				
CaCO₃ aragonite	100.09	34.15	2.93	293–673	6.22E–05	[c]		1.55E–06	[d]	
				293–673	5.53E–05	[b]		1.45E–06	[e]	
CaMg(CO₃)₂ dolomite	184.40	64.34	2.87	297–973	2.28E–05	[c]		1.22E–06	[d]	1.05E–06
MgCO₃ magnesite	84.31	28.02	3.01	297–773	1.82E–05	[c]	0–60	8.71E–07	[f]	8.77E–07
							0–80	8.77E–07	[g]	
							0–20	6.83E–07	[h]	

[a]Robie and Hemingway (1995), density ρ from V and gram-formula mass of mineral
[b]Skinner (1966, p. 82)
[c]Fei (1995, p. 32)
[d]Birch (1966)
[e]Liu et al. (2005)
[f]Zhang and Reeder (1999)
[g]Ross (1997)
[h]Redfern et al. (1993)
[i]Bass (1995, p. 49)

The coefficient of adiabatic compressibility in Table 2 β_{ad} $= -(1/V)(\partial V/\partial P)_{ad}$ is related to β_T by the relationship β_{ad} $= \beta_T C_V/C_P$ bar⁻¹, where C_V and C_P are heat capacities of the mineral at constant volume and pressure, respectively, in J mol K⁻¹. Heat capacities at constant pressure, C_P, are given in Table 3 for different temperatures. Heat capacity at constant volume, C_V, is calculated from the thermodynamic relationship $C_P - C_V = TV\alpha_V^2/\beta_T$, where all the parameters are as defined above, and the ratios C_P/C_V for each mineral at different temperatures are given in Table 3.

The essential thermodynamic data that are needed for computation of mineral equilibria above the standard conditions of $T = 298$ K and $P = 1$ bar are summarized in Table 3 for temperatures from 298 to 900 K at 1 bar total pressure. The Gibbs standard free energy of formation of a mineral is designated $\Delta G_{T,1}$ (kJ/mol) and molar volume is $V_{T,1} = V_{0,1}$ $[1 + \alpha_V(T - 298)]$(cm³/mol), where the coefficient of thermal expansion α is given in Table 3.

The equilibrium constant of a reaction, log K, is defined in terms of the Gibbs standard free energy change for the reaction, $\Delta G_{r\,T,1} = \Delta G_{T,1}$ (products) – $\Delta G_{T,1}$ (reactants), as

$$\log K_{T,P=1} = -\frac{\Delta G_{rT,1}}{2.3RT} \quad (24)$$

where ΔG in kJ mol⁻¹ and $R = 8.314 \times 10^{-3}$ kJ mol⁻¹ K⁻¹.

For solids at higher pressures, by integration of Eq. 24,

$$\log K_{T,P} - \log K_{T,1} = -\frac{\Delta V_{rT,1}(P-1)}{2.3RT} \quad (25)$$

where the values of $V_{T,1}$ of the individual minerals are given in Table 3, P is pressure in bars, and the gas constant $R = 83.14$ cm³ bar mol⁻¹ K⁻¹. If isothermal compressibility β_T of the reacting phases needs to be taken into account at pressures in the megabar range, then Eqs. 24 and 25 become:

$$\left(\frac{\partial \log K}{\partial P}\right)_T = -\frac{1}{2.3RT}\left(\frac{\partial \Delta G_{rT,1}}{\partial P}\right)_T = -\frac{\Delta V_{rT,1}(1-\beta_T P)}{2.3RT} \quad (26)$$

$$\log K_{T,P} - \log K_{T,1} = -\frac{\Delta V_{rT,1}}{2.3RT}\left((P-1) - \frac{\beta_T(P^2-1)}{2}\right) \quad (27)$$

Carbonate Mineral Stability in the System CaCO₃-MgCO₃

Determination of the univariant temperature-CO₂ curve for the calcite-dolomite-magnesite system was made by Harker and Tuttle (1955) at high to moderate temperatures and pressures. The order of decomposition with increasing temperature was shown to be magnesite, dolomite, and calcite. The location of the calcite-dolomite and dolomite-magnesite solvi along the CaCO₃-MgCO₃ binary join (Fig. 3) was established through the collective work of a number of investigators (e.g., Graf and Goldsmith 1955; Goldsmith and Heard 1961). The top of the calcite-dolomite solvus was located by Goldsmith and Heard (1961) at 1,075 °C, giving a composition of Ca₀.₅₇.₅Mg₀.₄₂.₅CO₃, a slightly calcium-rich phase. Note in Fig. 3 that the composition of calcite in terms of its Mg

Carbonate Minerals and the CO₂-Carbonic Acid System, Table 3 Thermodynamic data for four carbonate minerals at $298.15 \leq T \leq 900$ K and $P = 1$ atm (≈ 1 bar). $\Delta G_{T,1}$ and C_p from Robie and Hemingway (1995). Others as explained in the text

T (K)	$\Delta G_{T,1}$ (kJ mol⁻¹)				C_p J mol⁻¹ K⁻¹				$V_{T,1}$ cm³ mol⁻¹				C_p/C_v			
	cal	arag	dol	mag	cal	arag	dol	mag	cal	arag	dol	mag	cal	arag	dol	mag
298.15	−1128.5	−1127.4	−2161.30	−1029.5	83.47	82.31	157.51	76.09	36.93	34.15	64.34	28.02	1.035	1.323	1.046	1.044
300	−1128.0	−1126.9	−2160.30	−1029.0	83.82	82.55	158.06	76.44	37.14	34.79	64.78	28.17	1.035	1.332	1.046	1.044
400	−1101.6	−1100.2	−2105.70	−1000.9	97	92.67	183.54	90.57	37.21	35.00	64.93	28.22	1.041	1.425	1.053	1.050
500	−1075.6	−1073.6	*−2051.50*	−973.0	104.55	99.8	201.89	99.92	37.28	35.21	65.07	28.27	1.047	1.534	1.061	1.057
600	−1049.9	−1047.3	−1997.70	−945.3	109.88	105.76	215.66	107.38	37.35	35.42	65.22	28.33	1.055	1.657	1.070	1.064
700	−1024.4	−1021.2	−1944.40	−917.9	114.16	111.17	226.65	113.96	37.42	35.64	65.37	28.38	1.062	1.794	1.078	1.071
800	−999.0	−995.0	−1891.40	−890.7	117.88	116.28	236.08	120.06	37.49	35.85	65.51	28.43	1.069	1.948	1.086	1.078
900	−973.8	−969.1	−1838.70	−863.7	121.18	121.22	244.73	125.88	37.55	36.06	65.66	28.48	1.076	2.120	1.095	1.084
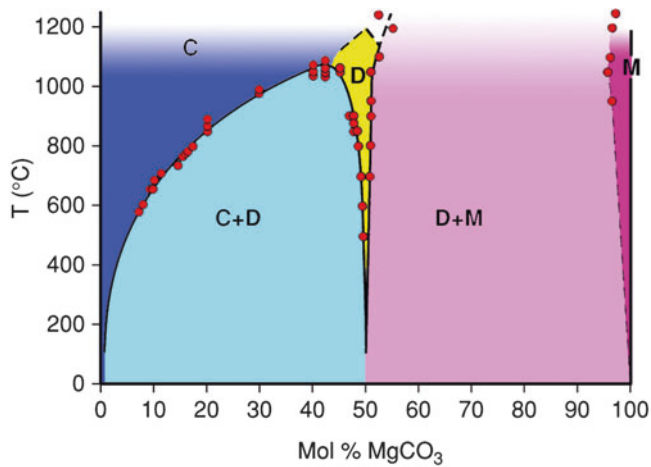
Carbonate Minerals and the CO₂-Carbonic Acid System, Fig. 3 Subsolvus relationships for the CaCO₃-MgCO₃ join. The top of the calcite-dolomite immisibility gap occurs at 1075 ºC. At this temperature, the phase composition is Ca₅₇.₅Mg₄₂.₅(CO₃)₂. *Dotted line* represents limit of detectable ordering in the dolomite structure. *C* calcite, *M* magnesite, and *D* dolomite (After Graf and Goldsmith (1958) and Goldsmith and Heard (1961); figure modified in Mackenzie and Andersson (2013))

Carbonate Minerals and the CO₂-Carbonic Acid System, Fig. 4 Free energy change of the reaction calcite + magnesite = dolomite with increasing T and P

content at the Earth's surface temperature and pressure in equilibrium with dolomite contains only a couple of mol% Mg in solid solution. All calcites containing more Mg than this are unstable relative to nearly pure calcite CaCO₃. Calcium-rich, somewhat disordered dolomite, protodolomite, is commonly found in younger sediments and, with aging of the rock, progressively converts to a stoichiometric dolomite with distinct ordering (Land 1985).

From the Earth's surface and down the *P-T* gradient, dolomite is a more stable phase than calcite and magnesite. This is illustrated in Fig. 4 for the free energy of the reaction

$$CaCO_3 + MgCO_3 = CaMg(CO_3)_2,$$
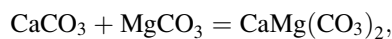
where the value of $\Delta G_{r\,T,P}$ is <0, indicating that the dolomite phase is more stable than the two reactant phases (data in Table 3).

Stability of the Calcites: Calcites constitute major and very important biogenic and inorganic constituents of modern marine sediments, Pleistocene, and older rocks as skeletal clasts and cements. These phases can contain up to 25 mol% MgCO₃, and higher Mg content phases have been produced in the laboratory and observed sparingly in nature. Calcites with more than a few percent MgCO₃ are usually referred to as magnesian calcites or magnesium calcites (Mg calcites). Generally, for the same MgCO₃ content, calcites comprising the skeletons and tests of organisms have greater concentrations of sodium, sulfate, water, hydroxide, and bicarbonate and tend to have larger cell volumes and greater carbonate anion and cation positional disorder in their structure than natural or synthetic mineral phases. Chemical and microstructural heterogeneities especially characterize biogenic magnesian calcites, and dislocations and plane defects are common in their crystals. All of these characteristics may affect the thermodynamic and kinetic properties and reactivity of these phases in aqueous solution.

The solubility of calcites depends on their MgCO$_3$ content, in addition to other chemical constituents, and environmental parameters. The solubility of calcites can be expressed as a function of their MgCO$_3$ content and the ion activity product (*IAP*) of a solution in equilibrium with the solid (Plummer and Mackenzie 1974):

$$Ca_{1-x}Mg_xCO_3 = (1-x)Ca^{2+} + xMg^{2+} + CO_3^{2-} \quad (28)$$
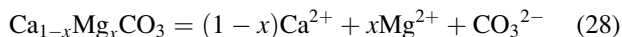
$$IAP_{calcite} = K_{sp} = \{Ca^{2+}\}^{1-x}\{Mg^{2+}\}^x\{CO_3^{2-}\}, \quad (29)$$

where curly brackets in the latter expression denote the *activities* of the ions in aqueous solution, *x* is the mole fraction of MgCO$_3$ in the solid, and K_{sp} is the solubility product. For pure calcite, the mole fraction of MgCO$_3$ is zero. The generalized trend in solubility with MgCO$_3$ content of calcite phases at 25 °C and 1 atm total pressure appears reasonably well defined (Fig. 5) owing to the work of Plummer and Mackenzie (1974), Thorstenson and Plummer (1977), Walter and Morse (1984), Bischoff et al. (1987, 1993), and Busenburg and Plummer (1989). Bertram et al. (1991) have made estimates of the change in solubility with temperature demonstrating that as with pure calcite, the magnesian calcites have retrograde solubility (solubility decreases with increasing temperature).

The *thermodynamic solubility product* of pure calcite at 25 °C and 1 atm is about $10^{-8.46}$. The solubilities of the compositions of other calcites with Mg in them expressed in terms of IAP exhibit a minimum of around two mole percent MgCO$_3$, beyond which their solubility increases nearly linearly with increasing MgCO$_3$ content. There appear to be three recognizable trends in the solubility-composition data: one for abiotic solids that are well crystallized, compositionally homogeneous, and chemically pure (Fig. 5, curve 3), and the other for biogenic phases and abiotic solids that exhibit substantial lattice defects, carbonate positional disorder, and substitution of such foreign ions as sulfate and sodium (Fig. 5, curve 2). The third solubility-composition curve is that of Plummer and Mackenzie (1974) for biogenic materials subjected to minimal cleaning procedures in the laboratory before use in dissolution experiments designed to determine the solubilities of these phases (Fig. 5, curve 1). This curve may best reflect the effective solubility of the biogenic magnesian calcites in nature as a function of MgCO$_3$ content. It is this latter curve that is most used by scientists today when they report the saturation state of an aqueous solution with respect to a Mg-calcite composition.

Biogenic and some abiotic calcites are unstable in aqueous solutions relative to synthetic phases of similar MgCO$_3$ content. Their solubilities differ by roughly 0.15 pIAP units (pIAP = −log IAP), or about 4.6 kJ mol^{-1} (1.1 kcal mol^{-1}). This difference arises because of physical and chemical differences between the two types of solids. The complex microarchitecture, greater positional disorder of the CO$_3^{2-}$ anion group, and chemical impurity of the biogenic phases and some biogenic calcites result in higher solubilities of these solids. It is likely that the solubility-composition curve 3 for pure, compositionally homogeneous, and structurally well-ordered calcite phases represents the true metastable equilibrium solubility of magnesian calcites in aqueous solution at 25 °C and 1 atm.

Stability of Aragonite: The most abundant naturally occurring orthorhombic carbonate is aragonite, the dimorph of calcite. At near Earth surface pressure and temperature, aragonite is found as the biogenic component of many common invertebrate skeletons, as sediments derived from the physical and biological disintegration and erosion of these skeletons, as cements in modern marine sediments and Neogene limestones, in some carbonate cave deposits and travertine precipitated by hot springs, and often as a replacement mineral in igneous and metamorphic rocks and ore deposits (Speer 1983; Table 1). Although aragonite has larger cation sites, the phase is denser than calcite and hence is stable relative to calcite at elevated pressure and temperature (Fig. 6). The solubility product of aragonite at 25 °C and 1 atm is about $10^{-8.30}$. Aragonites exhibit only limited solid solution, primarily with Pb and Sr. Plumbian aragonites with up to 2.5 mol% are common, and strontian aragonites occurring in hot springs may contain up to 14 mol% SrCO$_3$ (Speer 1983). The limited solid solution of Sr is of importance because of the fact that the degree of
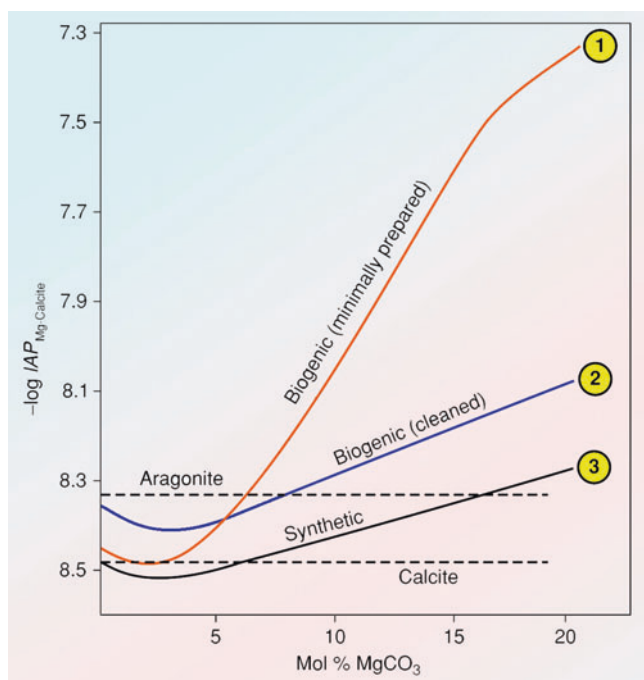
Carbonate Minerals and the CO$_2$-Carbonic Acid System, Fig. 5 Solubility of the magnesian calcites as a function of the MgCO$_3$ in the phase. See text for further explanation (After Bischoff et al. (1993); figure modified in Mackenzie and Andersson (2013))
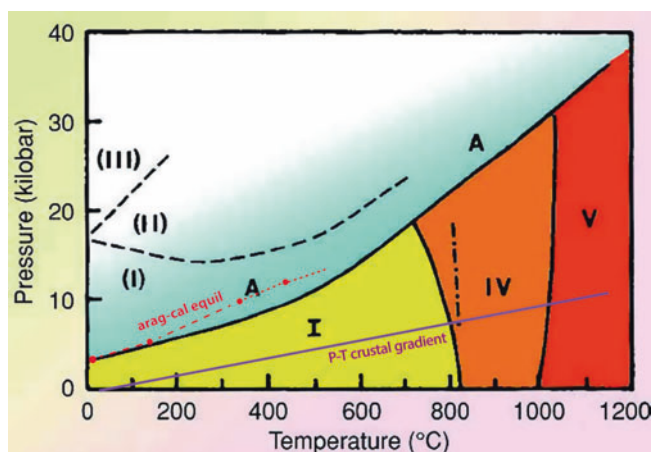
Carbonate Minerals and the CO$_2$-Carbonic Acid System, Fig. 6 Stability fields of aragonite and different polymorphs of calcite as a function of temperature and pressure. *A* aragonite, *I* through IV: calcite polymorphs with metastable fields shown by parentheses; *dash-dot line* at 800°C represents aragonite-calcite transition encountered on experimental cooling runs; *solid line* at lower temperature represents transition encountered on experimental heating runs (After Carlson (1980); figure modified in Mackenzie and Andersson (2013)). Calcite is the stable phase along the *P-T* gradient in Earth's crust. An equilibrium between aragonite and calcite, as shown by the *red dashed line*, would require pressures higher than those along the *P-T* gradient

solid solution varies among different groups of organisms having aragonitic shells, and the Sr content of some skeletal species has been used to obtain the Sr/Ca ratio or the temperature of the water from which the organism precipitated its skeleton.

Because aragonite is unstable relative to calcite at near Earth surface pressures and temperatures, with time and changes in environmental conditions, such as exposure to meteoric waters or burial in the subsurface, abiotic and biogenic aragonite can be converted to calcite or dolomite. Thus the original texture of the aragonite can be altered and the chemical and isotopic information contained in the phase lost. Rocks older than Neogene contain very little aragonite because of diagenetic reactions that lead to leaching of the components of the phase from the rock or its recrystallization to another mineral. Scant aragonite has been found in rocks as old as Pennsylvanian in age. The recrystallization process can lead to a loss of information concerning the environment of formation of a biogenic or abiotic aragonitic precipitate.

Stability of Dolomite: The mineral dolomite is a major constituent of especially ancient carbonate rocks. Dolomite was named in honor of Dieudonné Dolomieu (also known as Déodat Dolomieu), a geologist who worked in the Pyrenees and Alps in the eighteenth century and first described the mineral's characteristics and occurrence. Dolomite is distinguished from calcite and the other rhombohedral carbonates by its stoichiometry. Ideal dolomite has equal numbers of Ca and Mg atoms, and the Ca and Mg are segregated in distinct

lattice planes. These planes are oriented normal to the *c*-axis, each alternating with *c*-normal trigonal CO$_3$ groups that are also in essentially planar orientation. For geologists, dolomite has been the center of an unending debate regarding its mode of formation in surface environments, its past abundance relative to other sedimentary carbonates, and its overall significance in the geologic record (e.g., Land 1985; Machel and Mountjoy 1986; Hardie 1987; McKenzie 1991; Mackenzie and Morse 1992; McKenzie and Vasconcelos 2009). The stability relations for dolomite in the CaCO$_3$-MgCO$_3$ system are shown in Fig. 4. In many aqueous solutions, including seawater, the solution is found to be oversaturated with respect to dolomite, but the phase does not spontaneously precipitate. This conundrum is probably at least in part a result of the kinetics of the dolomite precipitation reaction, which are very slow due to the difficulty in forming such a well-ordered phase from solution at near Earth surface *T* and *P*. Arvidson and Mackenzie (1997, 1999) have shown experimentally that increases in temperature and saturation state of a solution with respect to dolomite increase the rate of precipitation of dolomite. Field data tend to support the experimental observations since most unequivocal *primary* dolomite forming in the modern marine environment and that which is observed in the rock record has formed from compositionally modified seawater solutions with higher dolomite saturation states and at warmer temperatures than the global mean average of today.

Importance of Reaction of Calcium Silicate, Calcium Carbonate, and CO$_2$ in Earth History

The connection between the world of silicate minerals in the Earth's igneous crust and the sedimentary carbonates is represented by the reaction

$$CaSiO_3 + CO_2 = CaCO_3 + SiO_2, \qquad (30)$$

where CaSiO$_3$ is a shorthand notation for the silicate minerals containing the 1st (O), 2nd (Si), and 5th (Ca) most abundant elements by mass in the Earth's crust, CO$_2$ is gas, and the products are solid calcite and amorphous silica which recrystallizes to quartz with time. The reaction was introduced by Urey (1952), and it was known as the Urey reaction until Berner and Maasch (1996) produced evidence that the chemist and mining engineer Jacques-Joseph Ebelmen thought of this reaction in 1845–1847. Since then, the name has been deservedly changed to the Ebelmen-Urey reaction.

After the Earth had formed and was still hot, all the volatiles occurred as gases in the primordial atmosphere at about 700 K – above the critical temperature of water of 647.14 K and other gases, atmospheric pressure was 342 bar, comprising mostly H$_2$O, CO$_2$, N$_2$, HCl, and H$_2$S
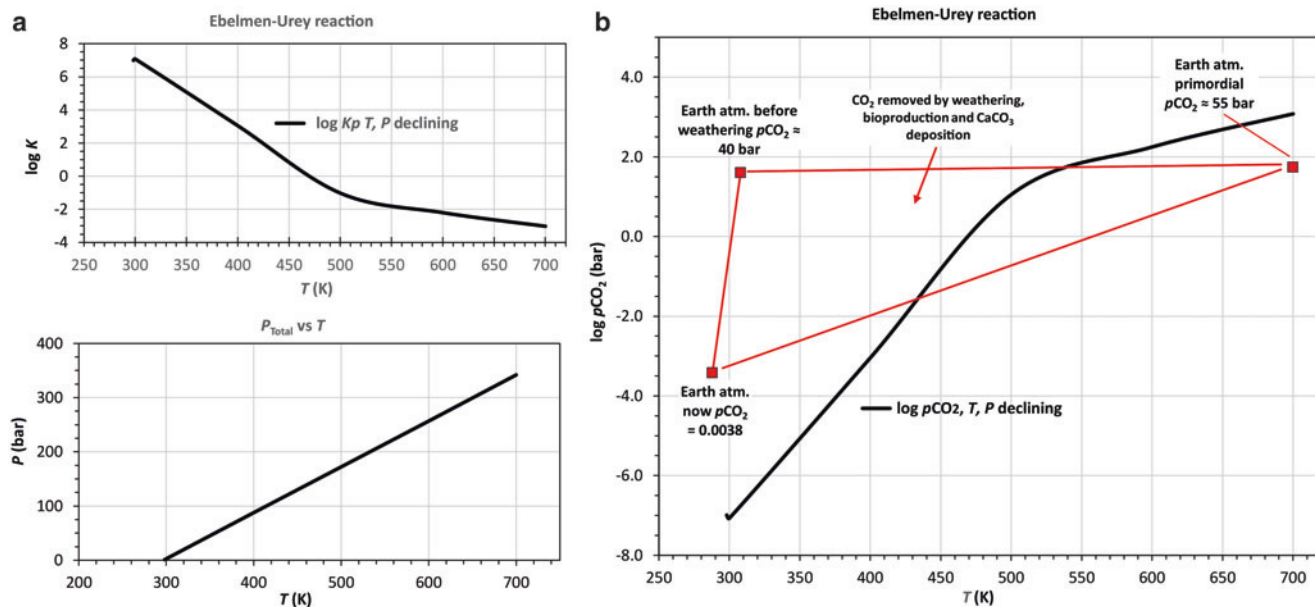
Carbonate Minerals and the CO₂-Carbonic Acid System, Fig. 7 (**a**) $\log K$ of reaction (30) at decreasing T (K), and P (bar). (**b**) Model decrease of atmospheric pressure P (bar) with decreasing temperature T (K). (**c**) p_{CO_2} from Eq. 31 calculated for atmospheric

pressure P (bar) and T (K) decreasing as shown in (**b**). The triangular section of CO₂ decrease on the cooling Earth from Mackenzie and Lerman (2006)

(Mackenzie and Lerman 2006). As the Earth cooled, water condensed to liquid, and CO₂ and other gases dissolved in the primordial ocean. Subsequently, the weathering reactions, deposition of limestone, and biological production and burial of organic matter have further reduced the atmospheric CO₂ content. Two paths of the depletion of the atmosphere in CO₂ are schematically shown in Fig. 7 where they are compared to p_{CO_2} from the equilibrium constants of reaction (30):

$$\log K_{T,P} = \frac{a_{CaCO_3}\, a_{SiO_2}}{a_{CaSiO_3}\, p_{CO_2}} \tag{31}$$

where a are the activities of pure solids ($a > 1$ at $P > 1$ bar) and p_{CO2} is partial pressure of CO₂ ideal gas.

Log $K_{T,P}$ for reaction (30) at the T and P values of the crustal geothermal-geobaric gradient were computed from the data of Robie and Hemingway (1995), such as those cited in Table 3. For solids CaSiO₃ (wollastonite), CaCO₃ (calcite), and SiO₂ (glass), the molar volume change in the reaction, $\Delta V_{solid,T,P}$ is as given in (Eq. 27), using α_V (K⁻¹) and β_T (bar⁻¹) from Table 3. At the highest point of $T = 700$ K and $P = 342$ bar, the solid activities are: $a_{CaSiO_3} = 1.27, a_{CaCO_3} = 1.25$, and $a_{SiO_2} = 1.17$. For the solids, the volume change of the reaction is small, $\Delta V_{solids\,T,P} = 24$–$25$ cm³ mol⁻¹. Much bigger volume change is associated with the reactant CO₂ that decreases from 24,666 cm³ mol⁻¹ at 298.15 K, 1 bar, to 178 cm³ mol⁻¹ at

700 K, 342 bar (NIST 2016). The equilibrium constant at a higher pressure is

$$\log K_{T,P} = \log K_{T,P=1}$$
$$- \left(\frac{V_{sil} + V_{cal} - V_{wol} - V_{CO_2}}{2.303RT} \right)_{T,P}$$
$$\times (P - 1) \tag{32}$$

where V (cm³ mol⁻¹) is molar volume at the temperature and pressure shown and gas constant $R = 83.14$ cm³ bar mol⁻¹ K⁻¹.

The relationships in Fig. 7c indicate that p_{CO_2} in the earlier Earth's atmosphere was lower than the equilibrium value of reaction (30–32) at the temperature above about 550 K. As the Earth cooled below 530–430 K, the equilibrium value of p_{CO_2} should be smaller that the atmospheric value. Under these conditions reaction (30) could be driven to the right and Ca-silicate converted to carbonate.

Accretion of the Earth, according to different models, might have lasted about 40 million years (Hanks and Anderson 1969; Wood et al. 2006). If life on Earth existed as early as 3.9 billion years B.P., the temperature of the atmosphere was likely to be below 50 °C or 325 K. This would imply that 325 K in Fig. 7c was reached some 600 million years after Earth's accretion, and most of the removal of atmospheric CO₂ by biological production and CaCO₃ formation occurred over a very long time stretch of Earth's history. In all, in the course of Earth's history 2.85×10^{20} kg CO₂ were removed

Carbonate Minerals and the CO$_2$-Carbonic Acid System, Table 4 Precipitation and dissolution rates of three major carbonate minerals

Precipitation $R_p = k_p(\Omega - 1)n$ (Zhong and Mucci 1989)	Rate constant (k) (μmol m–2 h − 1)	Reaction order (n)
1. Calcite	$10^{-0.20}$	2.80
2. 15 mol% Mg-calcite	$10^{-0.20}$	2.80
3. Aragonite	$10^{1.00}$	2.36
Dissolution $R_d = k_d(1 - \Omega)n$ (Walter and Morse 1985)	Rate constant (k) (μmol g–1 h–1)	
5. Calcite	$10^{2.82}$	2.86
6. 15 mol% Mg-calcite	$10^{2.62}$	3.34
7. Aragonite	$10^{2.89}$	2.48

from the atmosphere, leaving there 0.001% of the original mass, including the anthropogenic additions.

Carbonate Mineral Dissolution and Precipitation Rates

The relationships between the dissolution (R_d) and precipitation (R_p) rates of calcite, Mg-calcite, and aragonite at 25 °C in seawater are summarized in Table 4.

The dissolution rate is also a function of the pH. When a mineral dissolves in a partly closed system, such as in sediment pore water, of initially $\Omega < 1$, the solution can approach $\Omega = 1$ as dissolution progresses and the dissolution rate slows down. Mean dissolution rate $\overline{R}_d$ in the interval between the initial $\Omega < 1$ and final $\Omega = 1$ is:

$$\overline{R}_d = \frac{1}{1 - \Omega} \int_\Omega^1 k(1 - \Omega')^n d\Omega' = \frac{k(1 - \Omega)^n}{n + 1} \quad \mathrm{\mu mol\ g^{-1}h^{-1}}$$

(33)

The rates of dissolution of several carbonate minerals at 25 °C as function of pH are shown in Fig. 8. It should be noted that the rates are a strong function of pH, and that aragonite has the fastest dissolution rate and magnesite the slowest. There is also a considerable variation in the dissolution rate of the biogenic CaCO$_3$ phases (Fig. 9). The taxonomic nature of the carbonate-secreting organism evidently affects the crystal structure of the skeleton and hence its dissolution rate. Even though red algae particles of a Mg-calcite composition of ~20 mol% MgCO$_3$ are more soluble than the aragonitic green algal *Halimeda* sp., the rate of dissolution of the *Halimeda* is about 67% faster than that of the red algae. Pickett and Anderrson (2015) studied the dissolution rates of various biogenic Mg calcites in natural seawater at elevated pCO$_2$ values. They found that the rates increased with increasing Mg content, and that the relative dissolution rates were observed to be a function of both Mg content and
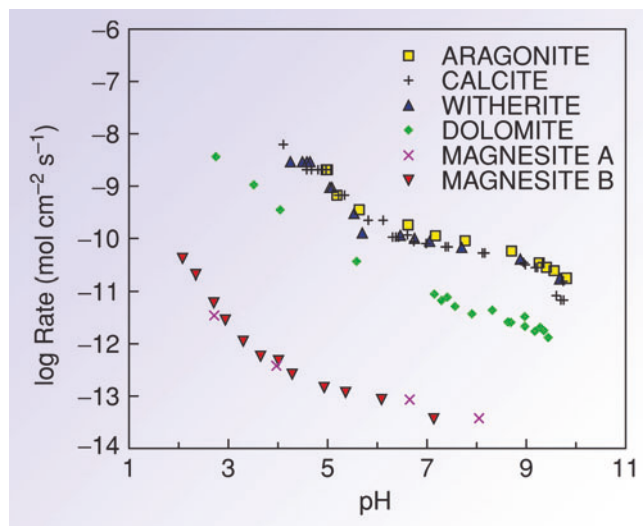
Carbonate Minerals and the CO$_2$-Carbonic Acid System, Fig. 8 Logarithmic rates of dissolution of several important carbonate minerals in distilled water at 25 °C and 1 atm as a function of pH. Notice the slower rates of dissolution for dolomite and especially magnesite. Also that aragonite dissolves faster than calcite (After Chou et al. (1989); figure modified in Mackenzie and Andersson (2013))
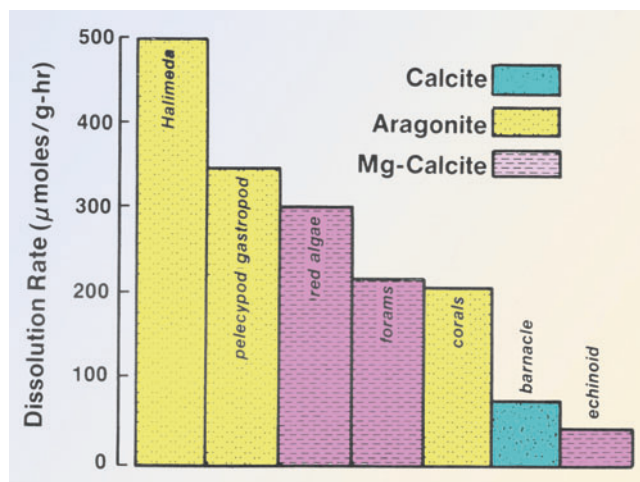
Carbonate Minerals and the CO$_2$-Carbonic Acid System, Fig. 9 Dissolution rates of disintegrated skeletons of various marine organisms of different carbonate mineralogies (After Walter and Morse (1985); figure modified in Mackenzie and Andersson (2013))

microstructure (surface area). Measured rates of dissolution increased with increasing pCO$_2$ treatment for all substrates and ranged from 2.5 to 18 umol g^{-1} h^{-1}.

CO$_2$-Carbonic Acid-Carbonate System of Ocean Waters

Discussion of the CO$_2$-carbonic acid-carbonate system of seawater is a treatise in itself (see, e.g., Broecker and Peng

1982; Andersson 2014). Here we look at two important aspects of the system in ocean water so the reader can gain an impression of the variables involved and their distribution and an appreciation of application of knowledge of the system to a major environmental problem, that of ocean acidification (OA).

Saturation State of Central Pacific Ocean Water Column: Surface ocean water is generally supersaturated with respect to the minerals aragonite and calcite (CaCO$_3$). Deeper-ocean waters are undersaturated with respect to aragonite and calcite, and the saturation depth is shallower for aragonite than that for calcite because aragonite is more soluble and hence $K'_{\text{arag}} > K'_{\text{cal}}$. The decrease in the degree of saturation with increasing depth is primarily due to an increase in CO$_2$ concentration due to bacterial decomposition of sinking organic matter and concomitant decrease in the CO$_3{}^{2-}$-ion concentration at the lower temperature of deep water and an increase in the value of K'_{cal} and K'_{arag} with increasing pressure. The depth where supersaturation changes to undersaturation varies among the major oceans (deepest in the Atlantic, shallower in the Indian, and shallowest in the Pacific oceans) and with latitude and location within an ocean (Broecker and Peng 1982; Morse and Mackenzie 1990).

Figure 10 shows generalized depth profiles of temperature, calcite and aragonite saturation states, dissolved inorganic carbon (DIC), total alkalinity, and dissolved calcium in waters of the Central Pacific. Notice the rapid decline with increasing depth of the degree of saturation of ocean water with respect to aragonite and calcite down to a depth of about 500 m and then the slow but steady decline to greater depths (Fig. 10b). The saturation depth of the more soluble aragonite is at about 500 m and that of calcite is at 3,000 m. The undersaturation of ocean waters at depth with respect to carbonate phases (Fig. 10b) accounts for the dissolution of CaCO$_3$ particles settling from the surface ocean layer and the return of calcium and total alkalinity to solution in this pump-like process. The increase in DIC with depth is mainly due to the microbial-mediated oxidation of organic matter sinking through the water column and at greater depth, the dissolution of CaCO$_3$.

It is of interest at this point to obtain a feel for how fast CaCO$_3$ dissolves in ocean waters and how quickly a hypothetical state of carbonate saturation in the oceanic water column might be reached. For the entire 5,500-m water column of Fig. 10, the average values of the degree of saturation are $\Omega_{\text{cal}} = 1.5$ and $\Omega_{\text{ar}} = 0.95$. However, below the saturation depth of 500 m for aragonite, the picture is very different: $\Omega_{\text{ar}} = 0.685$ from 500 to 5,500 m. To raise the degree of saturation with respect to aragonite to $\Omega_{\text{ar}} = 1.0$ within this depth range, total alkalinity (TA, Fig. 10c) would have to increase by a factor of 1.5. Equating this increase in TA as due to dissolution of CaCO$_3$ in ocean-floor carbonate sediments, the mass of the dissolved CaCO$_3$ would be 620 kg CaCO$_3$/m^2 or 21 cm/m^2 of solid CaCO$_3$. The mean rate of

aragonite dissolution, using Eq. 7 in Table 4 for $\Omega_{\text{ar}} = 0.685$ and $\overline{R}_d$ from Eq. 33, is 6.91×10^{-3} kg yr^{-1}. The time to dissolve the mass of aragonite of 620 kg m^{-2} is

$$t = \frac{\text{Mass CaCO}_3 \text{ dissolved}}{\text{Dissolution rate}} = \frac{620 \text{ kg m}^{-2}}{6.91 \times 10^{-3} \text{kg year}^{-1}}$$
$$\approx 90,000 \text{ year} \tag{34}$$

The preceding calculation assumes that Ω_{ar} rises in the course of aragonite dissolution from 0.685 to 1. The turnover time of the global ocean is much shorter $\geq 1,000$ years, and this may assure that the undersaturation value is maintained at 0.685, making the dissolution rate in Eq. 33 faster. Therefore the time of dissolution of 620 kg aragonite/m^2 in Eq. 34, needed for the theoretical saturation, would be considerably shorter, about 26,000 years. If the dissolution rates determined in the laboratory (Table 4) hold in the ocean, the mass of CaCO$_3$ that is needed to bring the entire water column to saturation with respect to aragonite would be smaller than, or comparable to, the thickness of CaCO$_3$ deposited over such periods of time at an estimated rate of about 3 cm/10^4 years (Hay et al. 1988).

Ocean Acidification: Carbon dioxide is one of the concentration variables in the definition of DIC, where DIC = HCO$_3{}^-$ + CO$_3{}^{2-}$ + CO$_2$ (Eq. 11). CO$_2$ exchange between surface ocean water and the atmosphere is mainly controlled by the partial pressure difference of gaseous CO$_2$ between surface waters and the atmosphere and an exchange coefficient that is mainly a function of wind speed. Carbon dioxide is naturally exchanged between seawater and the atmosphere by physical factors and biological productivity that draws down CO$_2$ and respiration that produces CO$_2$, determining whether surface seawater acts as a source or sink of CO$_2$. Prior to the eighteenth century, the oceans appear to have been a net source of CO$_2$ that eventually was consumed in plant productivity on land (Lerman et al. 2011; Mackenzie et al. 2011). With the burning of fossil fuels of coal, oil, and gas and land use changes (mainly deforestation), the situation was reversed. CO$_2$ emissions to the atmosphere from these anthropogenic activities led to accumulation of CO$_2$ in the atmosphere, and in the early part of the twenty-first century, storage of 26% of the anthropogenic CO$_2$ emissions in ocean waters (Fig. 11). This has led to the second problem of anthropogenic CO$_2$ emissions – the first being global climate change – that of ocean acidification (OA).

As CO$_2$ from anthropogenic emissions of CO$_2$ have been absorbed by ocean waters, the pH has decreased, and consequently the CO$_3{}^{2-}$ anion has decreased in concentration leading to a reduction in the carbonate saturation state of surface seawater:

$$2CO_2 + CO_3{}^{2-} + 2H_2O = 3HCO_3{}^- + H^+ \tag{35}$$
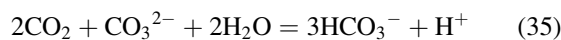
Carbonate Minerals and the CO$_2$-Carbonic Acid System, Fig. 10 Central Equatorial Pacific, W168.75°, S0° (WOCE Section P15S/14S, NOAA CGC-96, 6 March 1996, http://cdiac.ornl.gov/oceans/RepeatSections/clivar_p15s.html). Water depths calculated from pressure (Chapman 2006). (**a**) Temperature. (**b**) Degree of calcite and aragonite saturation (Ω) from *T-S-P* and carbonate-system parameters (Zeebe and Wolf-Gladrow 2001). (**c**) Dissolved inorganic carbon (DIC) and total alkalinity (TA). (**d**) Ca^{2+} concentration

C
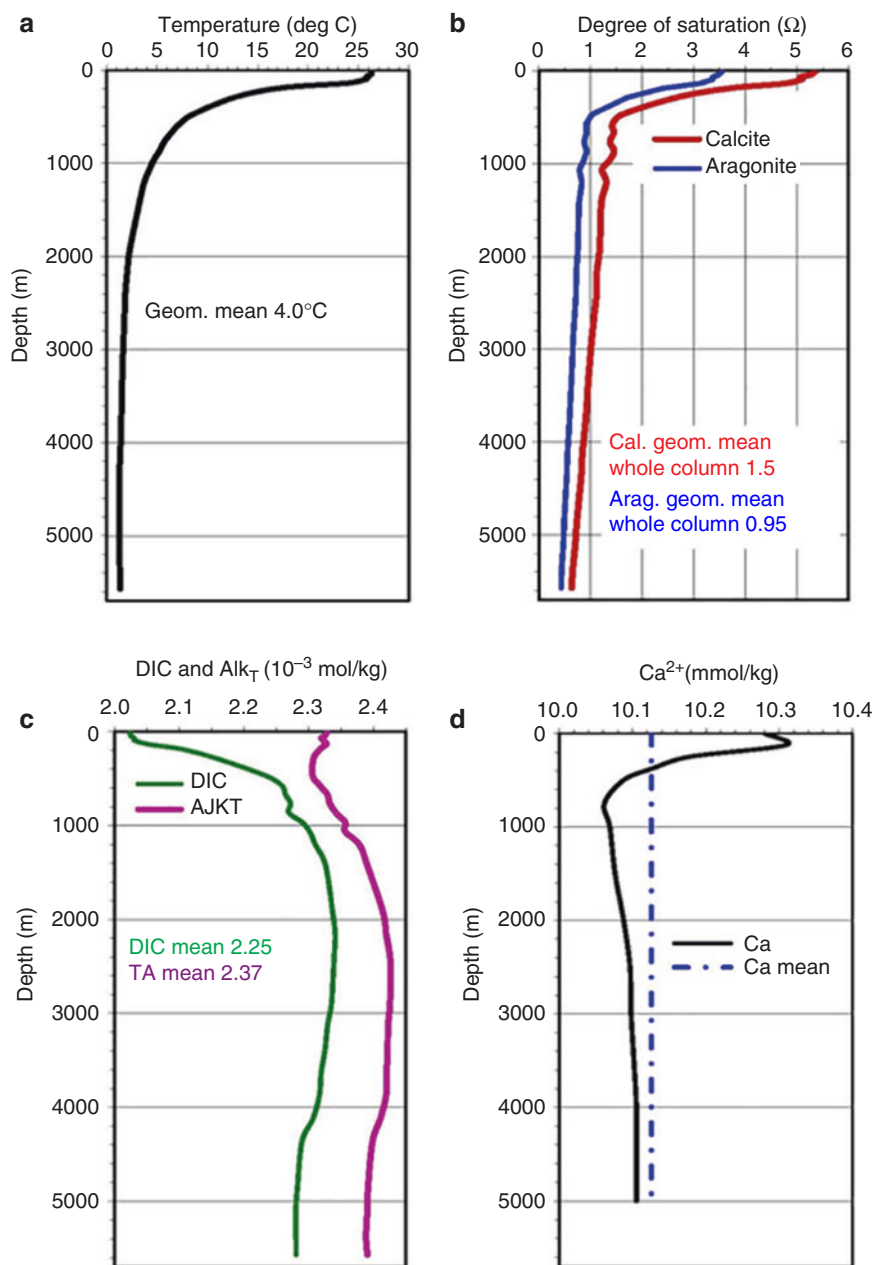
Figure 12 shows the depth to which anthropogenic CO$_2$ has penetrated the oceans integrated over the time period 1800–1994. Notice in particular the "hot spot" of penetration in the high North Atlantic where North Atlantic deep water forms and sinks.

Experimental work and direct observations (e.g., Sabine et al. 2004; references in the legend of Fig. 11) have shown that lowering of the pH of seawater decreases the rate of calcification of a skeletal organism. This has been observed for pelagic and benthic foraminifera, coralline red algae, and of most concern, hermatypic corals, among others. In a world affected by OA, there is much concern for coral reefs and other carbonate ecosystems of the world as skeletal organisms' ability to calcify will be diminished. Also, with lowered seawater pH, particles produced by the disintegration of organism shells and tests will be more susceptible to dissolution in the more acidic seawater. It is possible that because of these two effects of anthropogenic CO$_2$ uptake by surface ocean waters, coral reefs will cease to accrete, and there will be net loss of CaCO$_3$ from their structural edifices. This implies potential loss of these structures as refuges for fish, barriers to storm surges, sources of beach sand, and an aesthetic environment for all to appreciate.
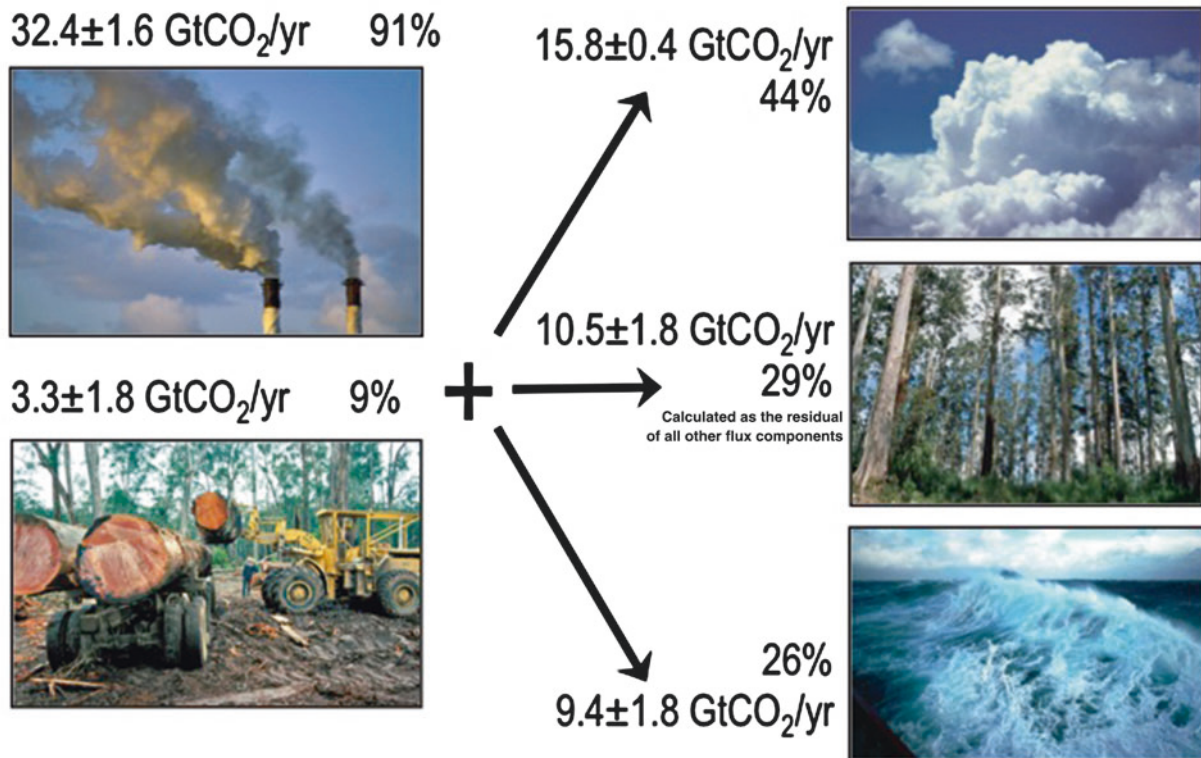
Carbonate Minerals and the CO$_2$-Carbonic Acid System, Fig. 11 Fate of anthropogenic CO$_2$ emissions from the fossil fuels of coal, oil, and gas and that of land use changes (deforestation). The sinks are the atmosphere, ocean waters, and by difference the land. Fossil-fuels have a lower ^{13}C/^{12}C ratio than CO$_2$ in the preindustrial atmosphere and their emissions dilute it (After Le Quere et al. (2015); see "Isotopes in Carbonates in Interpretation of Earth History" section)

Isotopes in Carbonates in Interpretation of Earth History

The heavier isotopes of an element are usually more abundant than the light ones (with the exception of ^{11}B and ^{7}Li among the common elements). Isotope concentrations in different materials are denoted as abundance ratios, $R = {}^{heavy}X/{}^{light}X$, in a sample relative to the ratio in a standard as

$$\delta X = \left(\frac{R_{sample}}{R_{standard}} - 1 \right) \times 1000 \quad (\text{‰})$$

For details of the notation of the isotope abundance, the reader may refer to such textbooks as Faure and Mensing (2004). An equilibrium constant of an isotope exchange reaction between two phases, X_1 and X_2, is usually denoted

$$\alpha_{1-2} = \frac{1 + \delta X_1}{1 + \delta X_2}$$

$$\ln \alpha_{1-2} = \ln \frac{1 + \delta X_1}{1 + \delta X_2} \approx \delta X_1 - \delta X_2$$

and the quantity $1000 \ln\alpha_{1-2}$ is the fractionation factor of the isotope ratio $R = {}^{heavy}X/{}^{light}X$ between phases 1 and 2. Of the main components of (Ca, Mg)CO$_3$, calcium (atomic number $Z = 20$) has seven naturally occurring isotopes, one radioactive cosmogenic ^{41}Ca of half-life

ANTHROPOGENIC 1800 to1994 CO_2 PENETRATION INTO THE OCEAN BASED ON OBSERVATIONS
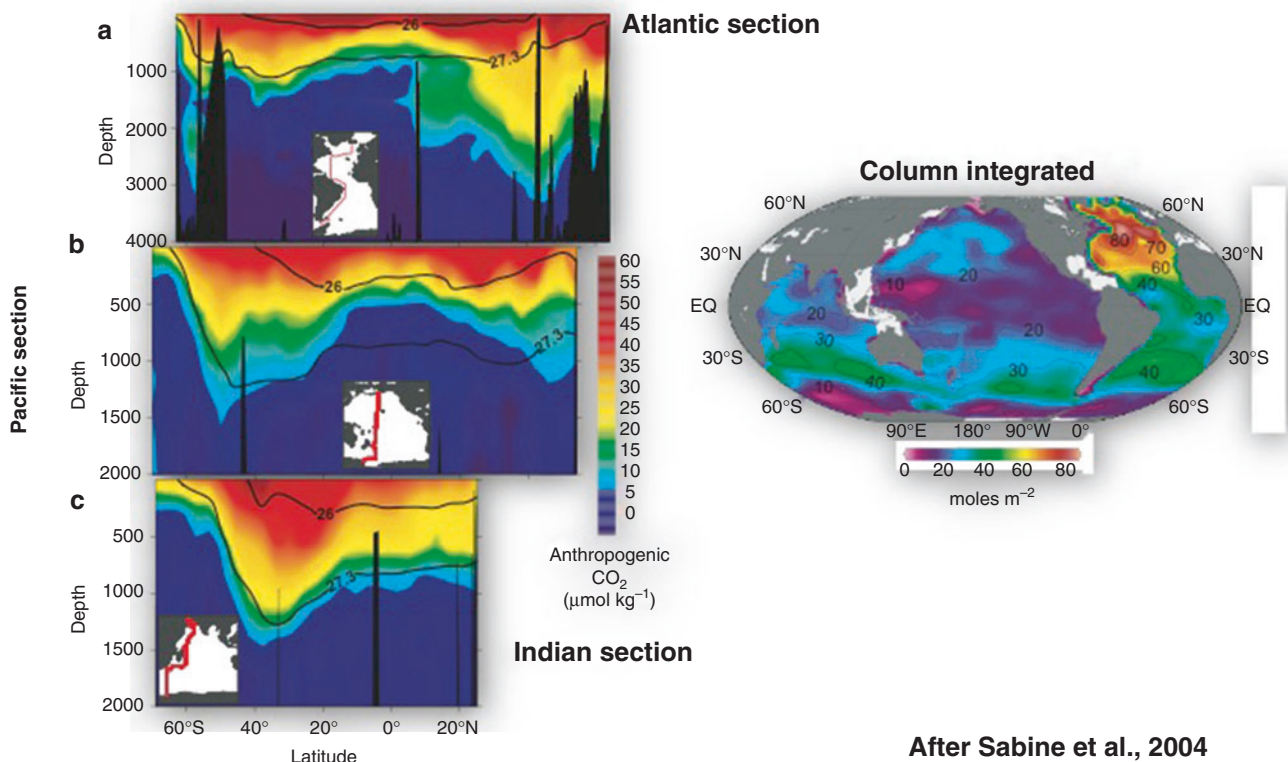
Carbonate Minerals and the CO_2-Carbonic Acid System, Fig. 12 Anthropogenic CO_2 penetration into the world's oceans from 1800 to 1994. Notice in particular the deep penetration and amount of anthropogenic carbon in waters of the region where the North Atlantic deep water forms and sinks (After Sabine et al. (2004))

Carbonate Minerals and the CO_2-Carbonic Acid System, Table 5 Stable isotopes of Ca, C, O, and Mg and their abundances in atomic %

Mass	% atomic abundance	Mass	% atomic abundance	Mass	% atomic abundance	Mass	% atomic abundance
^{40}Ca	96.941	^{12}C	98.93	^{16}O	99.757	^{24}Mg	78.7
^{42}Ca	0.647	^{13}C	1.07	^{17}O	0.038	^{25}Mg	10.13
^{43}Ca	0.135			^{18}O	0.205	^{26}Mg	11.17
^{44}Ca	2.086						
^{46}Ca	0.004						
^{48}Ca	0.187						

102,000 years, and six stable isotopes. Carbon ($Z = 6$) has two stable and one radioactive ^{14}C of half-life 5,730 years. Oxygen ($Z = 8$) and magnesium ($Z = 12$) each has three Table 5:

The most abundant isotope of calcium, ^{40}Ca, is also produced by decay of ^{40}K (Weatherill 1966). Fantle and Tipper (2014) have shown that for average bulk crustal rocks, the rate of ^{40}Ca addition from the decay of ^{40}K is less than 0.3‰ over 1 billion (10^9) years. Translating the addition rate of ^{40}Ca to Ca in the limestone and dolomite masses in Fig. 1, we use the following data: in carbonate rocks (Fig. 1), calcite makes 4.5×10^{20} and dolomite 2.1×10^{20} kg; mean K concentration in Eastern Kansas limestones of 0.22 wt.% K (Runnels and Schleicher 1956); ^{40}K atomic abundance fraction of K 1.17×10^{-4}; decay half-life of ^{40}K to ^{40}Ca 1.47 $\times 10^9$ years; and ^{40}Ca atomic abundance fraction of Ca 0.97. Taking the limestones as pure $CaCO_3$ (40.0 wt.% Ca) and dolomites as $CaMg(CO_3)_2$ (21.7 wt.% Ca), the mass of Ca

Carbonate Minerals and the CO₂-Carbonic Acid System, Table 6 Fractionation factors of isotopic ratios

Isotopes (‰)	$\delta^{13}C/^{12}C$	$\delta^{18}O/^{16}O$	$\delta^{44}Ca/^{40}Ca$	$\delta^{26}Mg/^{24}Mg$
Inorganic precipitation	9.6–13.6[a, b]	37–25[b]	0.9–1.7 tidal dol[d]	−0.7 to −1.3 [d]
	5–17[d]	28–29[c]	0.2–0.7 dol Williston basin[d]	−1.33 to −2.66[e]
Modern seawater	0	0	1[f, i], 1.81[h], 1.7–2.1[j]	+2.8[f]
Biological mineralization	−8 to +2[k]	−6 to +5[k]	0.2–1.2[g] var. taxa	+2[f] coral
			−18 to −2.6[l]	−3 to −1[f] forams
Bioproduction of organic matter	−13 ± 4 C3 plants[n]	27–43[m]	−1.25 to +1.25[j]	
	−27 ± 6 C4 plants[n]			
Standards[o, p]	PDB, VPDB, VSMOW	PDB, VPDB, VSMOW	NIST SRM 915a NIST SRM 915b	DSM3 SRM980

[a]Emrich et al. (1970)
[b]O'Neil et al. (1969)
[c]Gussone et al. (2005)
[d]Farkaš et al. (2012)
[e]Saulnier et el. (2012)
[f]Chang et al. (2004)
[g]Böhm et al. (2006)
[h]Holmden et al. (2012)
[i]Fantle and DePaolo (2007)
[j]Fantle and Tipper (2014)
[k]Henkes et al. (2013)
[l]Zhu and Macdougall (1998)
[m]Tuthorn et al. (2014)
[n]O'Leary (1988), Mackenzie and Lerman (2006)
[o]Coplen (1995)
[p]Hippler et al. (2003)

in sedimentary carbonates is 2.24×10^{20} kg. The mass of ^{40}Ca in the carbonate reservoir is

$$\left(2.24 \times 10^{23} \text{g Ca}/40.078\text{g Ca/mol}\right)$$
$$\times \left(0.969 \text{ mol fraction}^{40}Ca\right) \times \left(39.963 \text{ g}^{40}Ca/\text{mol}\right)$$
$$= 2.17 \times 10^{20}\text{kg}.$$

The result is that 82,000 kg ^{40}Ca/year are added to 2.17×10^{20} kg ^{40}Ca in the carbonate rocks in the sedimentary record. Thus the residence time of ^{40}Ca in carbonate rocks with respect to its production from $^{40}K - 2.17 \times 10^{20}$ kg/8.24×10^{4} kg/year is very long, 2.6×10^{15} years, indicating that a change in the ^{40}Ca isotopic composition of carbonates is insignificant, in the absence of local strong K sources. The fractionation factors of the four isotopic ratios in some natural environments and processes are given in Table 6.

The main goals of studying the isotope fractionation in natural environments is to establish relationships between the fractionation and climate parameters, such as temperature or paleotemperature (Epstein et al. 1951, 1953), partial pressure of atmospheric CO_2, history of seawater, and diagenesis of carbonate sediments (references in Table 6 and others cited therein). The record of $\delta^{13}C$ in Phanerozoic carbonates and Cenozoic carbonates is shown in Fig. 13b. A number of

long-term trends can be distinguished in the Phanerozoic (Lerman and Clauer 2007):

- A secular increase in the $\delta^{13}C$ during the 180 Ma from the Ordovician to the Carboniferous-Permian boundary broadly coincides with the emergence of higher plants and massive storage of organic carbon of lower $\delta^{13}C$ as coal in the Carboniferous.
- The next 100 Ma include glaciations of Gondwana near and above the Carboniferous-Permian boundary and a major extinction at the Permian-Triassic transition. This time represents a slightly declining trend, with much scatter, of the carbonate $\delta^{13}C$. However, some detailed $\delta^{13}C$ profiles across the Permian-Triassic boundary have provided internally consistent trends and information for the modeling of changes in atmospheric CO_2 and O_2 at that time (Berner 2006).
- From the Jurassic to the Miocene, a period from about 200 to 20 Ma, there is a slight increase in the $\delta^{13}C$, although it is smaller than an increase in the Paleozoic over a similar length of time. Within the Jurassic to the Miocene data, there are periods of elevated $\delta^{13}C$ values that lasted about 5–10 Ma and shorter periods of ≤1 Ma that are associated with oceanic anoxic events (Katz et al. 2005).
- The decrease in the $\delta^{13}C$ of carbonates at least during the last 30 Ma to the present represents a trend that may
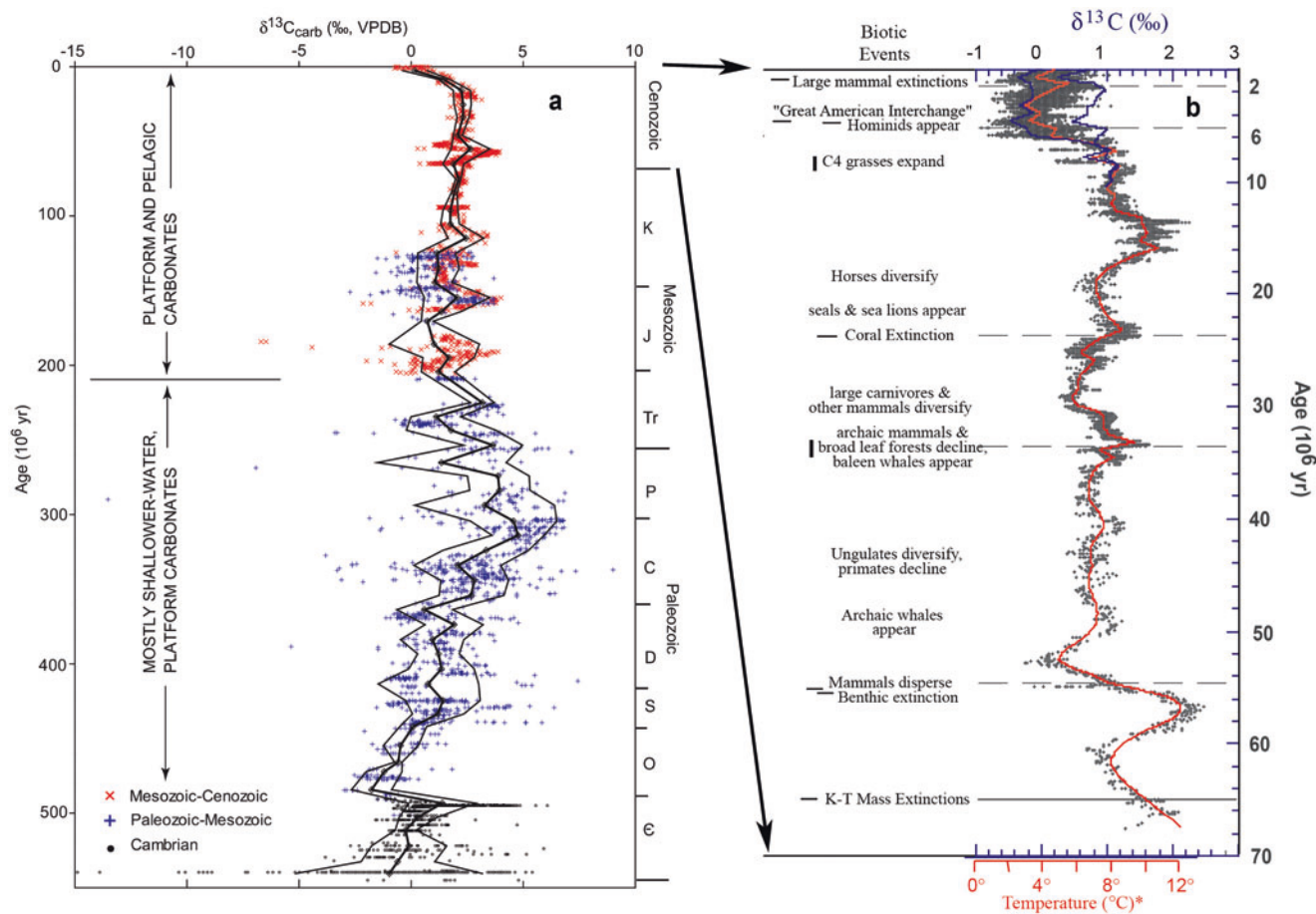
Carbonate Minerals and the CO₂-Carbonic Acid System, Fig. 13 (a) $\delta^{13}C$ values of Phanerozoic carbonates. Cambrian to Jurassic (*black •* and *blue +*) data from Veizer et al. (1999; courtesy of J. Veizer); Jurassic to Recent (*red ×*) from Katz et al. (2005). VPDB scale. Stratigraphic time scale from Gradstein et al. (2004). *Thick line*: consecutive 10-Ma-interval means (5-Ma in the most recent 10-Ma interval); *thin lines* are ±1 standard deviation (From Lerman and Clauer (2007)). (b) $\delta^{13}C$ values of Cenozoic carbonates (Modified from Zachos et al. (2001))

indicate a smaller biological fractionation between the carbonate carbon and organic carbon in the ocean. It has been variably proposed that a greater weathering of old organic matter has increased the delivery of isotopically lighter inorganic carbon forming from the remineralization of ^{13}C-depleted organic matter and it has been, consequently, one cause of the decreasing $\delta^{13}C$ values of marine carbonates. The rise of ^{13}C-enriched terrestrial grasses and the rapid radiation of ^{13}C-enriched diatoms also probably contributed to the depletion of ocean water in ^{13}C and hence to this trend in the carbon isotopes precipitated from the ^{13}C-depleted seawater (Katz et al. 2007). Finally in Fig. 13b, Zachos et al. (2001) relate the changes in $\delta^{13}C$ of the last 65 million years to the important biological, climatic, and orbital changes of the Earth.

Summary

Dissolved CO_2 in aqueous solution in the form of carbonic acid and carbonate ions has played a key role in processes at the Earth's surface over its entire history. Weathering reactions and subsequent precipitation of carbonate sediments together with biological production and burial of organic matter have removed 2.85×10^{20} kg of CO_2 from the atmosphere, leaving there 0.001% of the original mass. Cycling of CO_2 between dissolved forms in the ocean, gaseous form in the atmosphere, and carbonate sediments continues to exert a major control on Earth's climate. Dissolved carbonate exerts a major control on the pH of seawater and other natural waters. Burning of fossil fuels and other anthropogenic activities is increasing the amount of dissolved CO_2 in the ocean and reducing ocean pH,

threatening carbonate-secreting organisms such as corals. Carbonate minerals, primarily calcite and dolomite precipitating from these solutions, constitute the second most abundant class sedimentary rocks.

Cross-References

References

Andersson AJ (2014) The oceanic CaCO$_3$ cycle. In: Holland HD, Turekian KK (eds) Treatise on geochemistry, vol 8. Elsevier, Oxford, pp 519–542

Anthony JW, Bideaux RA, Bladh KW, Nichols MC (2003) Handbook of mineralogy, Borates, Carbonates, Sulphates, vol 5. Mineralogical Society of America, Chantilly. http://www.handbookofmineralogy.org/

Arvidson RS, Mackenzie FT (1997) Tentative kinetic model for dolomite precipitation rate and its application to dolomite distribution. Aquat Geochem 2:273–298

Arvidson RS, Mackenzie FT (1999) The dolomite problem: control of precipitation kinetics by temperature and saturation state. Am J Sci 299:257–288

Bass JD (1995) Elasticity of minerals, glasses, and melts. In: Mineral physics and crystallography: a handbook of physical constants. American Geophysical Union, Washington, DC, pp 45–63

Berner RA (2006) Carbon, sulfur and O$_2$ across the Permian-Triassic boundary. J Geochem Explor 88:416–418

Berner RA, Maasch KA (1996) Chemical weathering and controls on atmospheric O$_2$ and CO$_2$: fundamental principles were enunciated by J. J. Ebelmen in 1845. Geochim Cosmochim Acta 60(9):1633–1637

Bertram MA, Mackenzie FT, Bishop FC, Bischoff WD (1991) Influence of temperature on the stability of magnesian calcites. Am Mineral 76:1889–1896

Bertram MA, Mackenzie FT, Bishop FC, Bischoff WD (1991) Influence of temperature on the stability of magnesian calcites. Am Mineral 76:1889–1896

Birch F (1966) Compressibility; elastic constants. In: Clark SP Jr (ed) Handbook of physical constants, Geological Society of America Memoir, vol 97. Geological Society of America, New York, pp 97–173

Bischoff WD, Mackenzie FT, Bishop FC (1987) Stabilities of synthetic magnesian calcites in aqueous solution: comparison with biogenic materials. Geochim Cosmochim Acta 51:1413–1423

Bischoff WD, Bertram MA, Mackenzie FT, Bishop FC (1993) Diagenetic stabilization pathways of magnesian calcites. Carbonates Evaporites 8:82–89

Böhm F, Gussone N, Eisenhauer A, Reynaud S, Paytan A, Bosellini F, Brachert T, Reitner J, Wörheide G, Dullo W-C (2006) Ca isotope fractionation of inorganic, biologically induced and biologically controlled calcium carbonates. Geophys Res Abstr 8:09686

Broecker WS, Peng T-H (1982) Tracers in the sea. Lamont-Doherty Geological Observatory, Columbia University, Palisades

Busenburg E, Plummer LN (1989) Thermodynamics of magnesian calcite solid-solutions at 25°C and 1 atm pressure. Geochimica et Coscochimica Acta 53:1189–1208

Carlson WD (1980) The calcite-aragonite equilibrium: effects of Sr substitution and anion orientational disorder. Am Mineral 65:1252–1262

Chang VT-C, Williams RJP, Makishima A, Belshawl NS, O'Nion RK (2004) Mg and ca isotope fractionation during CaCO$_3$ biomineralisation. Biochem Biophys Res Commun 323:79–85

Chapman R (2006) A sea water equation of state calculator. The Johns Hopkins Universisty. Applied Physics Laboratory, Laurel. http://fermi.jhuapl.edu/denscalc.html

Chou L, Garrels RM, Wollast R (1989) Comparative study of the kinetics and mechanisms of dissolution of carbonate minerals. Chem Geol 78:269–282

Coplen TB (1995) Discontinuance of SMOW and PDB. Nature 375:285

Emrich K, Ehhalt DH, Vogel JC (1970) Carbon isotope fractionation during the precipitation of calcium carbonate. Earth Planet Sci Lett 8:363–371

Epstein S, Buchsbaum R, Lowenstam HA, Urey HC (1951) Carbonate-water isotopic temperature scale. Geol Soc Am Bull 62:417–426

Epstein S, Buchsbaum R, Lowenstam HA, Urey HC (1953) Revised carbonate-water isotopic temperature scale. Geol Soc Am Bull 64:1315–1326

Fantle MS, DePaolo DJ (2007) Ca isotopes in carbonate sediment and pore fluid from ODP site 807A: the Ca^{2+}(aq)–calcite equilibrium fractionation factor and calcite recrystallization rates in Pleistocene sediments. Geochim Cosmochim Acta 71:2524–2546

Fantle MS, Tipper ET (2014) Calcium isotopes in the global biogeochemical ca cycle: implications for development of a ca isotope proxy. Earth-Sci Rev 129:148–177

Farkaš J, Chackrabati R, Jacobsen SB, Kump LR, Melezhik VA (2012) Chapter 7.10.3: Ca and Mg isotopes in sedimentary carbonates. In: Frontiers in Earth Sciences, vol 8. Springer, New York, pp 1467–1482

Faure G, Mensing TM (2004) Isotopes: principles and applications, 3rd edn. Wiley, Hoboken. xxv+897 pp

Fei Y (1995) Thermal expansion. In: Mineral physics and crystallography: a handbook of physical constants. American Geophysical Union, Washington, DC, pp 29–44

Goldsmith JR, Heard HC (1961) Subsolidus phase relations in the system CaCO$_3$–MgCO$_3$. J Geol 69:45–74

Gradstein FM, Ogg JG, Smith AG (2004) A Geologic Time Scale 2004. Cambridge University Press, New York

Graf DL, Goldsmith JR (1955) Dolomite-magnesian calcite relations at elevated temperatures and CO$_2$ pressures. Geochim Cosmochim Acta 7:109–128

Graf DL, Goldsmith JR (1958) The solid solubility of MgCO$_3$ in CaCO$_3$: a revision. Geochim Cosmochim Acta 13:218–219

Gussone N, Böhm F, Eisenhauer A, Dietzel M, Heuser A, Teichert BMA, Reitner J, Wörheide G, Dullo W-C (2005) Calcium isotope fractionation in calcite and aragonite. Geochim Cosmochim Acta 69(18):4485–4494

Hanks TC, Anderson DL (1969) The early thermal history of the earth. Phys Earth Planet Inter 2:19–29

Hardie LA (1987) Perspectives on dolomitization: a critical review of some current views. J Sediment Petrol 57:166–183

Harker RI, Tuttle OF (1955) Studies in the system CaO-MgO-CO$_2$, part 2. Limits of solid solution along the join CaCO$_3$–MgCO$_3$. Am J Sci 253:274–282

Hay WW, Sloan JL II, Wold CN (1988) Mass/age distribution and composition of sediments on the ocean floor and the global rate of sediment subduction. J Geophys Res 93(B12):14,933–14,940

Henkes GA, Passey BH, Wanamaker AD Jr, Grossman EL, Ambrose WG Jr, Carroll ML (2013) Carbonate clumped isotope compositions of modern marine mollusk and brachiopod shells. Geochim Cosmochim Acta 106:307–325

Hippler D, Schmitt A-D, Gussone N, Heuser A, Stille P, Eisenhauer A, Nägler TF (2003) Calcium isotopic composition of various reference materials and seawater. Geostandards Newslett, Journal of Geostandards and Geoanalytical 27(1):13–19

Holmden C, Papanastassiou DA, Blanchon P, Evans S (2012) $\delta^{44/40}$Ca variability in shallow water carbonates and the impact of submarine groundwater discharge on ca-cycling in marine environments. Geochim Cosmochim Acta 83:179–184

Katz ME, Wright JD, Miller KG, Cramer BS, Fennel K, Falkowski PG (2005) Biological overprint of the geological carbon cycle. Mar Geol 217:323–338. (Falkowsi PG, Knoll AH (eds) Evolution of primary producers in the Sea, Chapter 18. Amsterdam, Elsevier, pp 405–430)

Katz ME, Fennel K, Falkowski PG (2007) Geochemical and biological consequences of phytoplankton evolution. In: Falkowski PG, Knoll A (eds) Evolution of aquatic photoautotrophs. Academic, pp 405–430

Land LS (1985) The origin of massive dolomite. J Geol 33:112–125

Le Quere C, Moriarty R, Andrew RM et al (2015) Carbon budget 2014. Earth Syst Sci Data 7:47–85

Lerman A, Clauer N (2007) Stable isotopes in the sedimentary record. Treatise Geochem 7:1–55

Lerman A, Guidry M, Andersson A, Mackenzie FT (2011) Coastal Ocean last glacial maximum to 2100 CO$_2$-carbonic acid-carbonate system: a modeling approach. Aquat Geochem 17:749–773

Liu L-g, Chen C-c, Lin C-C, Yang Y-j (2005) Elasticity of single-crystal aragonite by Brillouin spectroscopy. Phys Chem Miner 32:97–102

Machel HG, Mountjoy EW (1986) Chemistry and environments of dolomitization – a reappraisal. Earth-Sci Rev 23:175–222

Mackenzie FT, Andersson AJ (2013) The marine carbon system and ocean acidification during Phanerozoic time. Geochem Perspect 2:1–227

Mackenzie FT, Lerman A (2006) Carbon in the geobiosphere – Earth's outer Shell. Springer, Dordrecht. xxi+402 pp

Mackenzie FT, Morse JW (1992) Sedimentary carbonates through Phanerozoic time. Geochim Cosmochim Acta 56:3281–3295

Mackenzie FT, Lerman A, DeCarlo EH (2011) Coupled C, N, P, and O biogeochemical cycling at the land-ocean interface. In: Middleburg J, Laane R (eds) Treatise on coastal and estuarine science, vol 5. Elsevier, New York, pp 317–342

McKenzie JA (1991) The dolomite problem: an outstanding controversy. In: Muller DW, McKenzie JA, Weissert H (eds) Controversies in modern geology: evolution of geological theories in sedimentology, earth history and tectonics. Academic, London, pp 37–54

McKenzie JA, Vasconcelos C (2009) Dolomite Mountains and the origin of the dolomite rock of which they mainly consist: historical developments and new perspectives. Sedimentology 56(1):205–219

Millero F (2013) Chemical oceanography, 4th edn. CRC Press/Taylor & Francis Group, Boca Raton. 547 pp

Mindat (1993–2016) http://www.mindat.org/

Morse JW, Mackenzie FT (1990) Geochemistry of sedimentary carbonates. Elsevier, New York. xvi + 707 pp

NIST (2016) Thermophysical properties of fluid systems. http://webbook.nist.gov/chemistry/fluid/

O'Leary MH (1988) Carbon isotopes in photosynthesis. Bioscience 38:328–335

O'Neil JR, Clayton RN, Mayeda TK (1969) Oxygen isotope fractionation in divalent metal carbonates. J Chem Phys 51(12):5547–5558

Pickett M, Anderrson AJ (2015) Dissolution rates of biogenic carbonates in natural seawater at different pCO2 conditions: a laboratory study. Aquat Geochem 21(6):459–485

Plummer LN, Mackenzie FT (1974) Predicting mineral solubility from rate data: application to the dissolution of magnesian calcites. Am J Sci 274:61–83

Railsback LB (2002) Patterns in the compositions, properties, and geochemistry of carbonate minerals. Department of Geology, University of Georgia, Athens. http://www.gly.uga.edu/railsback/Fundamentals/FundamentalsCarbs.html

Redfern SAT, Wood BJ, Henderson CMB (1993) Static compressibility of magnesite to 20 GPa: implications for MgCO$_3$ in the lower mantle. Geophys Res Lett 20(19):2099–2012

Robie RA, Hemingway BS (1995) Thermodynamic properties of minerals and related substances at 298.15 K and 1 bar (10^{5}Pascals) Pressure and at higher temperatures. USGS Bulletin 2131. iv+461 pp

Ross NA (1997) The equation of state and high-pressure behavior of magnesite. Am Mineral 82:682–688

Runnels RT, Schleicher JA (1956) Chemical composition of Eastern Kansas limestone. Kans Geol Surv Bull 119(3):1–18

Sabine CL, Feely RA, Gruber N, Key RM et al (2004) The oceanic sink for anthropogenic CO$_2$. Science 305(5862):367–371

Saulnier S, Rollion-Bard C, Vigier N, Chaussidon M (2012) Mg isotope fractionation during calcite precipitation: an experimental study. Geochim Cosmochim Acta 91:75–91

Skinner BJ (1966) Thermal expansion. In: Clark SP Jr (ed) Handbook of physical constants, Geological Society of America Memoir, vol 97. Geological Society of America, New York, pp 75–96

Speer JA (1983) Crystal chemistry and phase relations of orthorhombic carbonates. Rev Mineral 11:145–189

Thorstenson DC, Plummer LN (1977) Equilibrium criteria for two component solids reacting with fixed composition in an aqueous phase – example: the magnesian calcites. Am J Sci 277:1203–1223

Tuthorn M, Zech M, Ruppenthal M, Oelmann Y, Kahmen A, del Valle HF, Wilcke W, Glaser B (2014) Oxygen isotope ratios (^{18}O/^{16}O) of hemicellulose-derived sugar biomarkers in plants, soils and

sediments as paleoclimate proxy II: insight from a climate transect study. Geochim Cosmochim Acta 126:624–634

Urey HC (1952) The planets: their origin and development. Yale University Press, New Haven. xvii+245 pp

Veizer J, Ala D, Azmy K, Bruckschen P, Buhl D, Bruhn F, Carden GAF, Diener A, Ebneth S, Goddéris Y, Jasper T, Korte C, Pawellek F, Podlaha OG, Strauss H (1999) $^{87}Sr/^{86}Sr$, $\delta^{13}C$ and $\delta^{18}O$ evolution of Phanerozoic seawater. Chem Geol 161:59–88

Walter LM, Morse JW (1984) Reactive surface area of skeletal carbonate during dissolution: effect of grain size. J Sediment Petrol 54:1081–1090

Walter LM, Morse JW (1985) The dissolution kinetics of shallow marine carbonates in seawater: a laboratory study. Geochim Cosmochim Acta 49:1503–1513

Weatherill GW (1966) Radioactive decay constants and energies. In: Clark SP Jr (ed) Handbook of physical constants, Geological Society of America Memoir, vol 97. Geological Society of America, New York, pp 513–519

Wood BJ, Walter MJ, Wade J (2006) Accretion of the Earth and segregation of its core. Nature 441:825–833

Zachos J, Pagani M, Sloan L, Thomas E, Billups K (2001) Trends, rhythms, and aberrations in global climate 65 Ma to present. Science 292(5517):686–693

Zeebe RE, Wolf-Gladrow D (2001) CO_2 in seawater: equilibrium, kinetics, isotopes. Elsevier, Amsterdam. xiii+346 pp

Zhang J, Reeder RJ (1999) Comparative compressibilities of calcite-structure carbonates: deviations from empirical relations. Am Mineral 84:861–870

Zhong S, Mucci A (1989) Calcite and aragonite precipitation from seawater solutions of various salinities: precipitation rates and overgrowth compositions. Chem Geol 78(3):283–299

Zhu P, Macdougall JD (1998) Calcium isotopes in the marine environment and the oceanic calcium cycle. Geochim Cosmochim Acta 62 (10):1691–1698

Cerium

Catherine Chauvel
ISTerre, University Grenoble Alpes, CNRS, Grenoble, France

Element Data
Atomic Symbol: **Ce**
Atomic Number: **58**
Atomic Weight: 140.115 g/mol
Isotopes and Abundances: ^{136}Ce *0.186%*, ^{138}Ce 0.251%, ^{140}Ce 88.449%, and ^{142}Ce 11.114%
1 Atm Melting Point: 795 °C
1 Atm Boiling Point: 3443 °C
Common Valences: +3 and +4
Ionic Radii: 3+: 101 pm, 4+: 87 pm
Pauling Electronegativity: 1.12

(continued)

Chondritic (CI) Abundance: 0.6379 ppm
Silicate Earth Abundance: 1.675 ppm
Crustal Abundance: 63 ppm
Seawater Abundance: $\approx 1*10^{-6}$ ppm
Core Abundance: ~0

Properties

Cerium is a reactive and gray metal that tarnishes in air and burns when heated. It usually occurs in substitution to major elements in minerals.

History and Use

Cerium was discovered in Bastnäs (Sweden) in 1803 by J. J. Berzelius and W. Hissinger and was named after asteroid Ceres. Cerium is the most abundant of the lanthanide metals (also called rare earth elements), a group of 15 similar elements between lanthanum and lutetium in the periodic table and behaves cosmochemically as a refractory lithophile element.

Cerium has been used for a long time in industry: it is a key constituent of lighter flints; it provides special properties to some stainless steels; it is added to some special glasses and it is a key constituent of polishing powders. It is also used in catalytic converters.

Geochemical Behavior

Cerium is the most abundant rare earth element, but it is still rarely a constituent of mineral phases on Earth. Nevertheless, two common REE minerals exist: monazite $((Ce,La,Nd,Th)PO_4)$ and bastnäsite $((Ce,La,Y)CO_3F)$. During partial melting and fractional crystallization of magmas, it behaves as an incompatible element and is concentrated in melts. It is therefore enriched in basalts relative to their mantle source and enriched in continental crust relative to Earth's mantle. Together with the other REE, it is widely used in geochemistry to trace geological processes.

In contrast to other REE, Ce can have two valences: in the Earth's interior, it is almost exclusively in the +3 as most REE but can be in the +4 in oxidizing environments at the Earth's surface, and consequently, it can be decoupled from other REE in those environments. The decoupling is quantified as the Ce anomaly (Ce_N/Ce_N^*) with $Ce_N^* = 0.5La_N + 0.5Pr_N$ and all concentrations normalized to a reference reservoir that
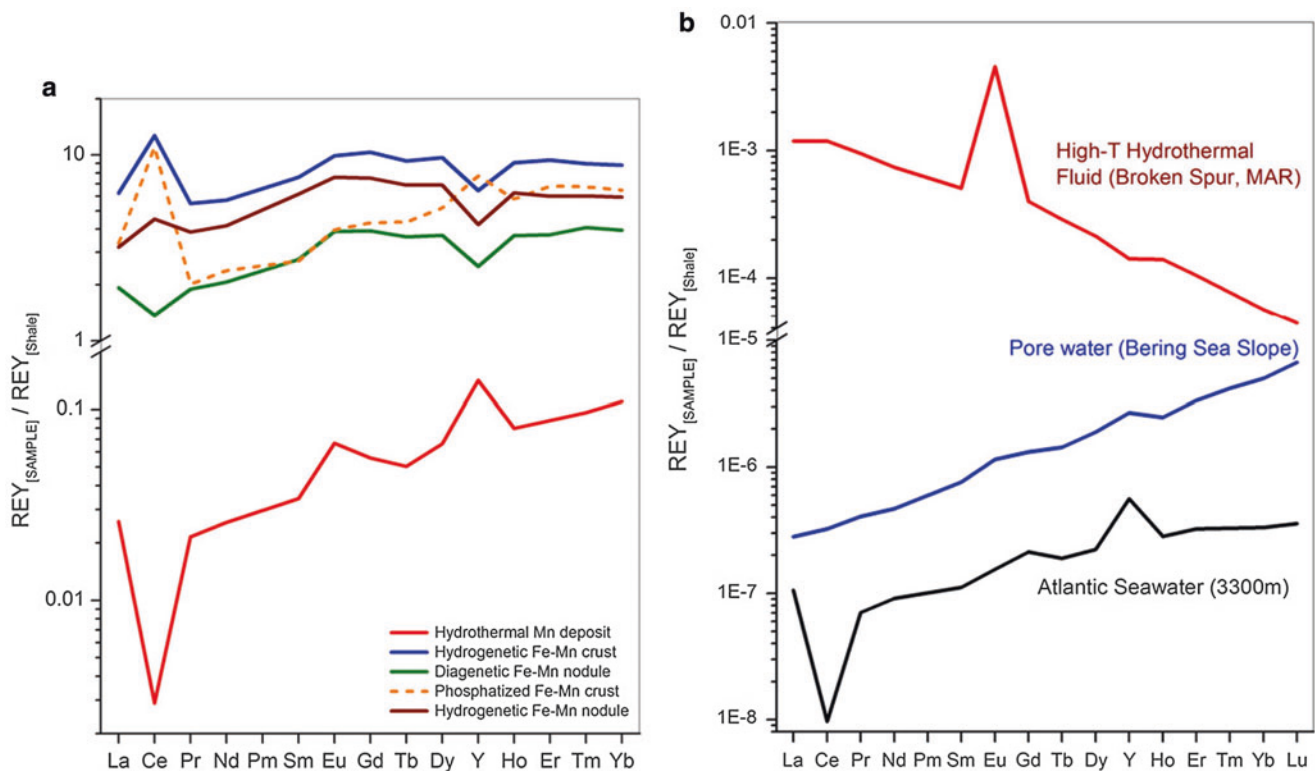
Cerium, Fig. 1 Typical patterns of (**a**) marine hydrothermal Fe–Mn deposits, diagenetic Fe–Mn nodules, hydrogenetic Fe–Mn nodules, hydrogenetic Fe–Mn crusts, and phosphatized hydrogenetic Fe–Mn crusts, and (**b**) high-temperature hydrothermal (black-smoker) fluids, seawater, and marine porewater (From Bau et al. (2014) and references therein)

can be the primitive mantle or another reservoir. During supergene weathering in tropical climates, negative cerium anomalies occur in altered soil materials, and precipitation of cerianite ($(Ce,Th)O_2$) leads to the formation of positive anomalies in other soil layers (Cotten et al. 1995). Similarly, seawater is characterized by a strong negative Ce anomaly, while Fe–Mn nodules have positive Ce anomalies (see Fig. 1) (Bau et al. 2014).

Geochronology and Isotope Geochemistry

Cerium has four isotopes, and one of them, ^{138}Ce (0.251%), is produced by the radioactive decay of ^{138}La with a half-life of ≈292.5 Ga. Because of the very long half-life and the analytical difficulties related to the low abundance of ^{138}Ce, the decay system has hardly been used in geochronology. However, with the arrival on the market of more precise and accurate mass spectrometers, new perspectives are now open.

In the field of isotope geochemistry, it could be an interesting tool to distinguish the type of sedimentary material involved in the source of island arc volcanic rocks. A pioneer study published by Bellot et al. (2015) demonstrates that coupling Ce and Nd isotopes could help distinguish hydrogenetic deposits from hydrothermal or detrital materials. As shown in Fig. 2, different types of sediment evolve on very different evolutionary paths as time goes past; in addition, distinct Ce isotopic compositions can be acquired within a relative short time (less than 200 Ma), an age that corresponds to the oldest subducted oceanic plate in the Pacific.

Coupled Ce and Nd isotopic studies of planetary materials and of early Earth rocks could also be very interesting because of the constraints it could provide on the nature of the material that accreted to form planets and on the nature of the dominant processes during the early stages of Earth evolution.

Biological Utilization and Toxicity

Cerium has no known biological role and has low to moderate level of toxicity.
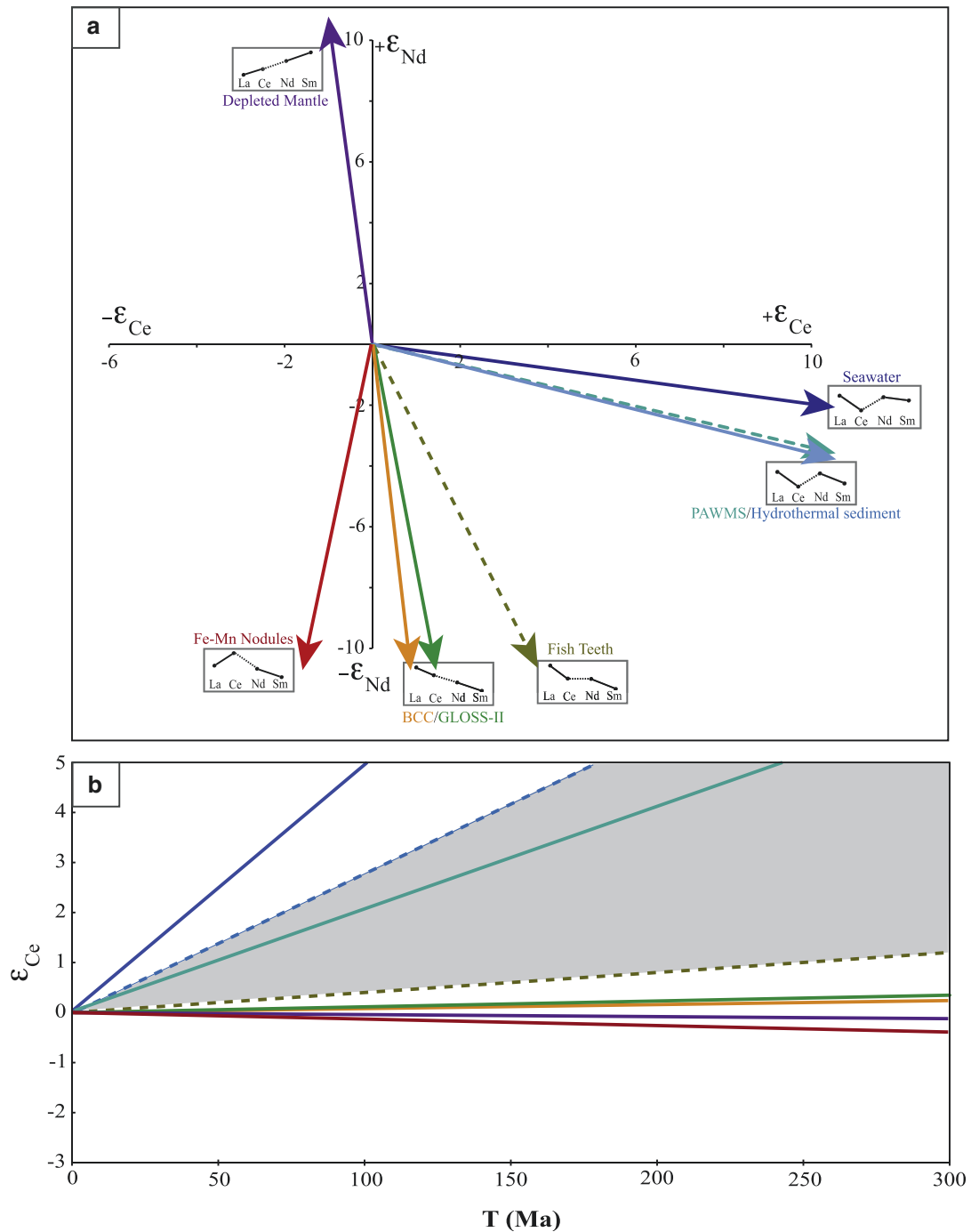
Cerium, Fig. 2 Schematic diagram showing the isotopic trajectories of various Earth reservoirs in Ce–Nd isotopic spaces. ε_{Ce} and ε_{Nd} measure the deviation in 10^4 of Ce and Nd isotopic compositions relative to chondritic references (i.e., $\varepsilon_{Ce} = ([^{138}Ce/^{142}Ce]/[^{138}Ce/^{142}Ce_{CHUR}]$ -1)$*10^4$) (See Bellot et al. (2015) and references therein for further details)

Cross-References

▶ Chemical Weathering
▶ Ferromanganese Crusts and Nodules: Rocks That Grow
▶ Incompatible Elements

▶ Lanthanide Rare Earths
▶ Lanthanum
▶ Lithophile Elements
▶ Marine Sediment
▶ Ocean Biochemical Cycling and Trace Elements

► Oxidation-Reduction Reactions and Eh-pH (Pourbaix) Diagrams

► Supergene

References

Bau M, Schmidt K, Koschinsky A, Hein J, Kuhn T, Usui A (2014) Discriminating between different genetic types of marine ferro-manganese crusts and nodules based on rare earth elements and yttrium. Chem Geol 381:1–9

Bellot N, Boyet M, Doucelance R, Pin C, Chauvel C, Auclair D (2015) Ce isotope systematics of island arc lavas from the Lesser Antilles. Geochim Cosmochim Acta 168:261–279

Cotten J, Le Dez A, Bau M, Caroff M, Maury RC, Dulski P, Fourcade S, Bohn M, Brousse R (1995) Origin of anomalous rare-earth element and yttrium enrichments in subaerially exposed basalts: evidence from French Polynesia. Chem Geol 119:115–138

Chalcophile Elements

Sarah-Jane Barnes
Sciences de la Terre, Université du Québec à Chicoutimi, Chicoutimi, QC, Canada

Definition

The term chalcophile (derived from the Greek for copper-loving) was originally introduced by Goldschmidt (1923) to describe the group of elements that are concentrated in sulfide minerals in meteorites. Traditionally this group is defined as the elements Ag, As, Bi, Cd, Cu, Hg, In, Pb, S, Sb, Se, Te, Tl, and Zn. Goldschmidt classified the other elements in meteorites into two groups: those associated with Fe alloy as siderophile (iron loving) and those concentrated in silicates minerals as lithophile (rock loving). Subsequently Goldschmidt applied his classification to the whole Earth and modified it to include two new groups of elements: atmophile, those concentrated in the atmosphere and biophile elements, those concentrated by organic processes (Goldschmidt 1930).

Distribution in Terrestrial Rocks

Whereas the concepts outlined by Goldschmidt are useful, as is evidenced by the fact the terms, siderophile, chalcophile, and lithophile are in daily use by geochemists, the behavior of an element depends on the composition of the system, oxygen fugacity (fO_2), temperature, and pressure (Li and Audétat 2015); thus, its behavior may vary depending on the context. Lodders (2003) outlined the behavior of the elements during condensation of the elements to form the solar system, and under these low fO_2 conditions, the chalcophile group is restricted to Ag, Cd, Hg, In, Pb, S, Se, Te, and Zn. Low fO_2 conditions would also have prevailed during the segregation of the earth's core and consequently many elements behaved in a siderophile manner. Current estimates of the core composition show enrichment of up to 1000 times primitive mantle (Fig. 2) for elements such as the platinum-group elements (PGE; Ru, Rh, Pd, Os, Ir, Pt). In contrast at the oxygen fugacities found in the Earth's mantle and crust, Fe alloy is very rarely present and many elements that are siderophiles in meteorites and during core segregation partition into sulfide minerals rather than Fe alloy and thus behave as chalcophile elements.

The partition coefficients between sulfide droplets and mid-ocean ridge basalts (MORB) give an indication of how chalcophile each element is under crustal conditions (Fig. 1). Elements with partition coefficients between 1 and 10 may be described as slightly chalcophile (Zn, Mo, As, Sb, Tl, In, and

Chalcophile Elements, Fig. 1 Partition coefficients between mafic magma and sulfide liquid. — indicates partition coefficients between MORB and sulfide droplet; I indicates range of values from experiments conducted at fO_2 between −2 FMQ +2; ↑ indicates minimum partition coefficients; italics indicates the element is volatile; bold indicates that the element is highly siderophile (Data from Barnes and Ripley (2016) and references therein, plus Li and Audétat (2015))
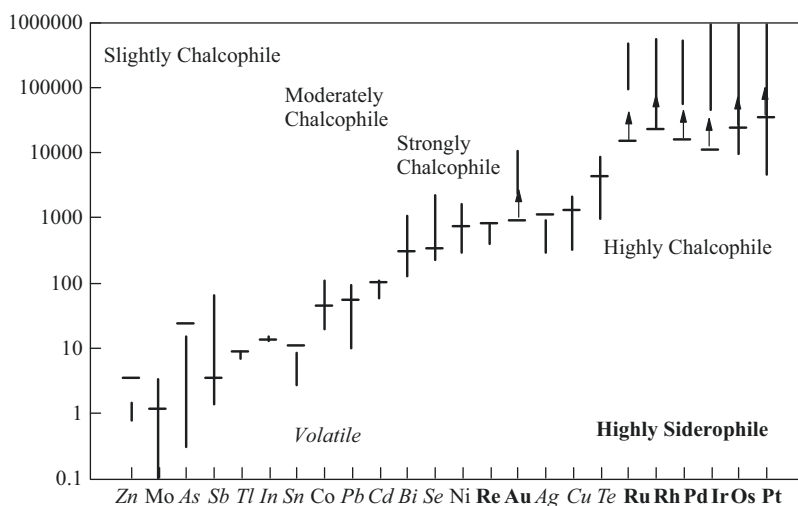
Chalcophile Elements,
Fig. 2 Concentrations of
chalcophile elements in the core,
komatiitic basalt, MORB, and the
continental crust normalized to
primitive mantle and plotted in
order of incompatibility with
komatiitic basalt (Data for the core
from McDonough and Sun
(1995); mantle from Lyubetskaya
and Korenaga (2007); MORB
form Arevalo and McDonough
(2010); continental crust from
Rudnick and Gao (2003);
komatiitic basalt from this work
(median of 52 samples from the
Cape Smith Fold Belt northern
Quebec))
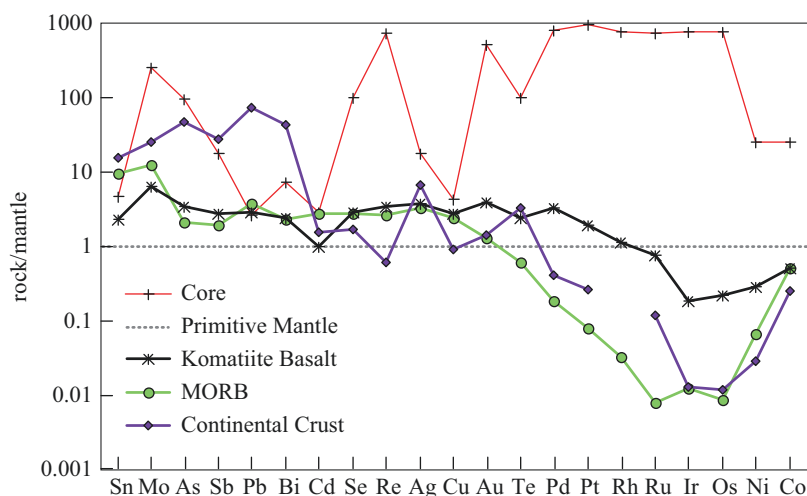
Sn,), those with partition coefficients in the range 20–100 as moderately chalcophile (Pb, Co, Cd), those with a partition coefficient in the 100–1000 range as strongly chalcophile (Bi, Se, Ni, Re), and those with partition coefficients above 1000 as highly chalcophile (Au, Cu, Te, Ru, Rh, Pd, Os, Ir, Pt).

Among the group that behave as highly chalcophile elements under crustal conditions are the PGE which together with Au and Re are commonly referred to as highly siderophile elements because of their very high partition coefficients into Fe alloy (Harvey and Day 2016 and references therein). The highly siderophile elements attract a great deal of interest because of their potential to investigate the early history of planetary formation. In particular the relatively high concentrations of the highly siderophile elements in the Earth's mantle suggest that it is not in equilibrium with the core and that, during late meteorite bombardment, highly siderophile elements were added to the mantle (Dale et al. 2012).

The behavior of the chalcophile elements during mantle melting can be considered by inspection of a mantle-normalized plot of average MORB and komatiitic basalts (Fig. 2). The elements are plotted in approximately decreasing normalized abundance in komatiitic basalt. For komatiitic basalt most of the chalcophile elements from Sn to Pt are present at the two to three times mantle concentrations. Moderately incompatible lithophile elements such as Sm are present in these rocks at similar to slightly higher levels (three to four times mantle); thus most of the chalcophile elements behave as incompatible elements and sulfide phases do not appear to control the behavior of the chalcophile elements at the high degrees of partial melting required to produce komatiitic basalts. In contrast the Ir-platinum-group elements (IPGE, Os, Ir, Ru, and Rh), Ni, and Co are present at less than one times mantle and behave as compatible elements.

The concentrations of the chalcophile elements in MORB show a wider range of values. Tin and Mo are present at close to ten times mantle, most of the chalcophile elements (As to Cu) show a lower degree of enrichment in the range of twice to three times mantle. Tellurium, Au, Ni, and Co are present at 0.1–1 times mantle exhibiting compatible behavior, and the PGE are extremely depleted at 0.01–0.1 times mantle. The variations in the behavior of the chalcophile elements in MORB are generally attributed to the presence of residual sulfides in the MORB source. The PGE exhibit extreme depletion because of their very high partition coefficients into sulfides, whereas the moderately chalcophile elements exhibit a much smaller degree of depletion because the sulfide phases will affect their bulk partition coefficients less (Patten et al. 2013). Tin and Mo at ten times mantle show an enrichment similar to incompatible lithophile elements, suggesting that the presence of sulfide phases has a negligible influence on these elements.

The average continental crust is depleted in most moderately to strongly chalcophile elements and like MORB is particularly depleted in PGE (Fig. 2). However it is enriched at 10–100 times mantle in the slightly to moderately chalcophile elements Sn to Pb and in the strongly chalcophile elements Bi and Ag (Fig. 2).

Naturally all of the chalcophile elements are concentrated into magmatic sulfide liquids when they segregated from mafic magmas, and the Ni and PGE ore deposits that form from the liquids are enriched in all of these elements (Barnes and Ripley 2016). Most of the chalcophile elements are enriched by a factor of 100–1000 relative to mafic magma Fig. 3. The slightly chalcophile elements are less enriched with enrichment factors of approximately 10 reflecting their lower partition coefficients (Figs. 1 and 3).

During crystallization of magma, the silicate liquid may become saturated in a magmatic-hydrothermal fluid.

Chalcophile Elements,
Fig. 3 Mantle-normalized
concentrations of chalcophile
elements from the two largest
magmatic Ni-sulfide deposits,
Sudbury and Noril'sk (Data from
Dare et al. (2011) and Zientek
et al. (1994))
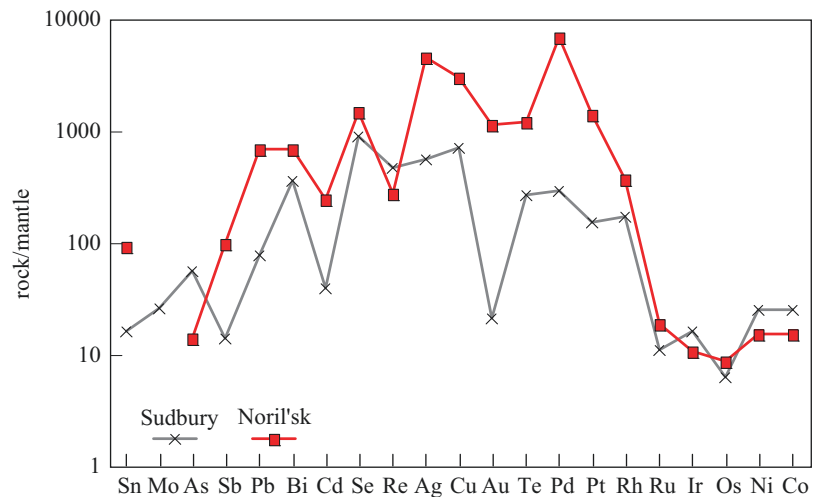
Chalcophile Elements,
Fig. 4 Comparison of mantle-
normalized concentrations of
chalcophile elements in black
shales with the upper continental
crust and MORB (Data from
Ketris and Yudovich (2009), this
work of literature survey, Hu and
Gao (2008), and Arevalo and
McDonough (2010))
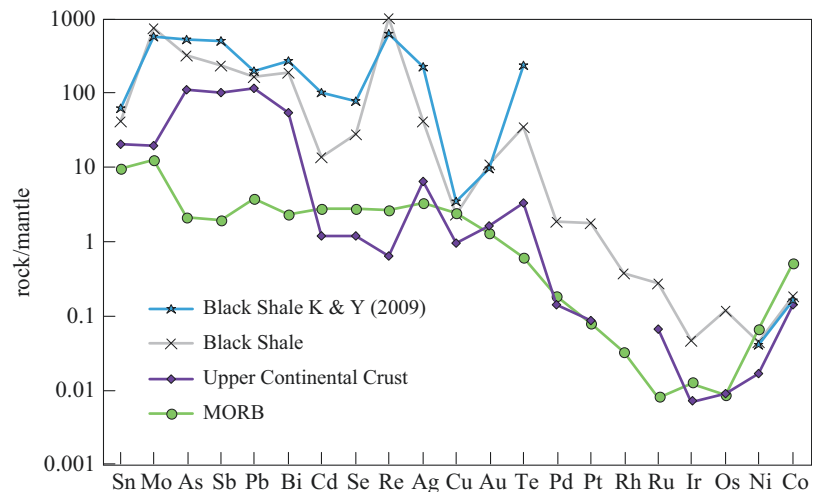
Some chalcophile elements and S partition into these fluids. For example, fluid inclusions from Cu-Mo porphyries are enriched in Cu, Mo, Zn, Ag, Tl Au, Pb, and Bi (John et al. 2010). The fluids then react with country rocks and the chalcophile elements are deposited along with sulfides as a result of the reactions (Keith et al. 1997; John et al. 2010; Richards 2011).

At low pressures the silicate magma or a magmatic-hydrothermal fluid may become saturated with a vapor. Some chalcophile elements preferentially partition into the vapor phase. Based on their condensation temperatures during the formation of the solar system, Lodders (2003) defined Hg, Tl, In, Cd, Se, S. Sn, Te, Pb, Bi, Sb, Ag, Cu, As, and Au as volatile. Volcanic gasses and sublimates have been found to be enriched in these elements (Hinkley et al. 1994; Zelenski et al. 2013). Another effect of the vapor is that magmatic sulfide droplets in the magma may lose S during magma degassing. The loss of S destabilizes the

sulfides and some of the chalcophile elements partition into the vapor.

Black shales are also enriched in many chalcophile elements (Fig. 4). [Some black shales, such as those in southern China, show much greater degree of enrichment than the median (Xu et al. 2013).] Relative to the upper crust (a potential source of the clastic component of the shales), the median black shale is enriched by a factor of 2 to 10 for most of the elements (Ketris and Yudovich 2009). Molybdenum, Cd, Se, Ag, and Te show larger enrichments in the range of 30–100, and Re shows the most extreme degree of enrichment at 1000. Ketris and Yudovich (2009) did not provide estimates for the PGE. But based on a survey of the literature, the PGE are also enriched in black shales at approximately ten times crustal values (Fig. 4). The origin of the enrichment of the metals in black shales has been much debated with one school of thought favoring the precipitation of the metals from seawater in anoxic basins (Xu et al. 2013) and the

other school suggesting that the metals are derived from hydrothermal fluids (Orberger et al. 2003). Recently models involving both processes have become popular (Slack et al. 2015).

Over the past few years, the concentrations of chalcophile elements in pyrites from black shales have become the focus of intense study as a means of exploration for Au deposits (Large et al. 2011). In this model the chalcophile elements are precipitated by organic matter and pyrite and incorporated into the pyrite during diagenesis. During greenschist facies metamorphism, the pyrite recrystallizes and releases many of the chalcophile elements to metamorphic fluids which can migrate to low pressure zones where they precipitate Au and other chalcophile elements.

Summary

The chalcophile elements can be divided into slightly, moderately, strongly, and highly chalcophile based on their partition coefficients between silicate and sulfide melts. Some of the highly and strongly chalcophile elements (PGE, Au, Re) are also highly siderophile, and thus most of the budget of these elements is found in the Earth's core. The slightly chalcophile elements Sn, Mo, As, Sb, and Pb together with Bi are enriched in the continental crust. Black shales are an important reservoir of most chalcophile elements in the Earth's crust. MORB is slightly enriched in most chalcophile elements except the highly chalcophile elements. In the Earth's crust highly chalcophile elements are only found in significant quantities in magmatic sulfide deposits.

Cross-References

- ▶ Antimony
- ▶ Arsenic
- ▶ Bismuth
- ▶ Black Shales and Sapropels
- ▶ Cadmium
- ▶ Copper
- ▶ Earth's Core
- ▶ Geochemical Classification of Elements
- ▶ Indium
- ▶ Lead
- ▶ Mercury
- ▶ Meteorites
- ▶ Mid-Ocean Ridge Basalts (MORB)
- ▶ Ore Deposits
- ▶ Platinum Group Elements
- ▶ Selenium
- ▶ Siderophile Elements
- ▶ Silver
- ▶ Sulfur
- ▶ Tellurium
- ▶ Thallium
- ▶ Zinc

References

Arevalo R Jr, McDonough WF (2010) Chemical variations and regional diversity observed in MORB. Chem Geol 271:70–85

Barnes S-J, Ripley EM (2016) Highly siderophile and strongly chalcophile elements in magmatic ore deposits. Rev Mineral Geochem 81:725–774

Dale CW, Burton KW, Greenwood RC, Gannoun A, Wade J, Wood BJ, Pearson DG (2012) Late accretion on the earliest planetesimals revealed by the highly siderophile elements. Science 336:72–75

Dare SA, Barnes S-J, Prichard HM, Fisher PC (2011) Chalcophile and platinum-group element (PGE) concentrations in the sulphide minerals from the McCreedy East deposit, Sudbury, Canada, and the origin of PGE in pyrite. Mineral Deposita 46:381–407

Goldschmidt VM (1923) Geochemische Verteilungsgesetze der ElementeSkrifter utg. av det Norske Visenskaps-Akademii i Oslo I. Mat-Naturv Klasse 2:1–17

Goldschmidt V (1930) Geochemische Verteilungsgesetze und kosmische Häufigkeit der Elemente. Naturwissenschaften 18:999–1013

Harvey J, Day JM (2016) Highly siderophile and strongly chalcophile elements in high temperature geochemistry and cosmochemistry. Rev Mineral Geochem 81:774

Hinkley TK, Le Cloarec M-F, Lambert G (1994) Fractionation of families of major, minor, and trace metals across the melt-vapor interface in volcanic exhalations. Geochim Cosmochim Acta 58:3255–3263

Hu Z, Gao S (2008) Upper crustal abundances of trace elements: a revision and update. Chem Geol 253(3):205–221

John DA, Ayuso RA, Barton MD, Blakely RJ, Bodnar RJ, Dilles JH, Gray F, Graybeal FT, Mars JC, McPhee DK, Seal RR, Taylor RD, Vikre PG (2010) Porphyry copper deposit model, chap. B of Mineral deposit models for resource assessment: U.S. Geological Survey Scientific Investigations Report 2010-5070–B, p 169

Keith J, Whitney J, Hattori K, Ballantyne G, Christiansen E, Barr D, Cannan T, Hook C (1997) The role of magmatic sulphides and mafic alkaline magmas in the Bingham and Tintic mining districts, Utah. J Petrol 38:1679–1690

Ketris M, Yudovich YE (2009) Estimations of Clarkes for carbonaceous biolithes: world averages for trace element contents in black shales and coals. Int J Coal Geol 78:135–148

Large RR, Bull SW, Maslennikov VV (2011) A carbonaceous sedimentary source-rock model for Carlin-type and orogenic gold deposits. Econ Geol 106:331–358

Li Y, Audétat A (2015) Effects of temperature, silicate melt composition, and oxygen fugacity on the partitioning of V, Mn, Co, Ni, Cu, Zn, As, Mo, Ag, Sn, Sb, W, Au, Pb, and Bi between sulphide phases and silicate melt. Geochim Cosmochim Acta 162:25–45

Lodders K (2003) Solar system abundances and condensation temperatures of the elements. Astrophys J 591:1220–1247

Lyubetskaya T, Korenaga J (2007) Chemical composition of Earth's primitive mantle and its variance: 1. Method and results. J Geophys Res 112:B03211

McDonough WF, Sun S-S (1995) The composition of the Earth. Chem Geol 120:223–253

Orberger B, Pasava J, Gallien JP, Daudin L, Pinti DL (2003) Biogenic and abiogenic hydrothermal sulphides: controls of rare metal distribution in black shales (Yukon Territories, Canada). J Geochem Explor 78:559–563

Patten C, Barnes S-J, Mathez EA, Jenner FE (2013) Partition coefficients of chalcophile elements between sulphide and silicate melts and the early crystallization history of sulphide liquid: LA-ICP-MS analysis of MORB sulphide droplets. Chem Geol 358:170–188

Richards JP (2011) Magmatic to hydrothermal metal fluxes in convergent and collided margins. Ore Geol Rev 40:1–26

Rudnick RL, Gao S (2003) Composition of the continental crust. Treatise Geochem 3:1–64

Slack JF, Selby D, Dumoulin JA (2015) Hydrothermal, biogenic, and seawater components in metalliferous black shales of the Brooks Range, Alaska: synsedimentary metal enrichment in a carbonate ramp setting. Econ Geol 110:653–675

Xu L, Lehmann B, Mao J (2013) Seawater contribution to polymetallic Ni–Mo–PGE–Au mineralization in early Cambrian black shales of South China: evidence from Mo isotope, PGE, trace element, and REE geochemistry. Ore Geol Rev 52:66–84

Zelenski ME, Fischer TP, de Moor JM, Marty B, Zimmermann L, Ayalew D, Nekrasov AN, Karandashev VK (2013) Trace elements in the gas emissions from the Erta Ale volcano, Afar, Ethiopia. Chem Geol 357:95–116

Zientek ML, Likhachev AP, Kunilov VE, Barnes S-J, Meier AL, Carlson RR, Briggs PH, Fries TL, Adrian BM (1994) Cumulus processes and the composition of magmatic ore deposits: examples from the Talnakh District, Russia. In: Lightfoot PC, Naldrett AJ (eds) Proceedings of the Sudbury-Noril'sk symposium, Ontario Geological Survey, Special publication, vol 5, Ontario, pp 373–392

Chelation

Corey D. Pilgrim
Department of Chemistry, University of California, Davis, Davis, CA, USA

Definition

Chelation is the complexation process by which a metal ion is bound to more than one atom in a single ligand. The ligand in question is said to be polydentate and is described by how many bonds are formed to the metal (e.g., a bidentate ligand has two bonds or a tridentate ligand has three bonds). The term chelation uses the Greek root *chela*, which is descriptive of the claws of lobsters and crabs, and is used because the resulting chelate complexes look as if the metal ion is caught between the pincers of the ligand. The favorable process of the replacement of monodentate ligands with polydentate ligands is known as the "chelate effect."

Chelation plays a prominent role in both inorganic chemistry and geologic processes. Water-solvated metal ions do not exist as discrete species in solution; they order the solvent molecules around themselves in different spheres of interaction (Richens 1997). Usually, these water molecules orient such that the negatively charged end of the dipole is attracted to the positively charged metal ion. These solvent molecules are thus coordinating as monodentate ligands around the metal center. Most geochemically important coordination complexes involve the interaction between Lewis acids and Lewis bases, such that the electrons in the coordinating ligand are donating to the electron poor metal center. Chelation occurs when a ligand, with multiple sites that act as Lewis bases, replaces the monodentate ligands around the metal center. This can result in interesting complexes forming – as an example, carbonate is a geologically abundant, bidentate, hard Lewis base which likes to coordinate with metal centers (interestingly, it can even form tricarbonate complexes with the early actinides, Fig. 1a). Another example of a chelating ligand is the molecule ethylenediaminetetraacetate (EDTA). This ligand is a hexadentate ligand that can coordinate a metal center through the lone electron pairs found on the four oxygen and two nitrogen atoms (Fig. 1b). EDTA can fill all octahedral sites around a metal center, effectively surrounding the ion in a cage. EDTA is used medically to trap toxic metals that have been digested by humans. It is also used as a complexometric titrant to determine the metal ion content in mixed solutions. Replacement of lower coordination number ligands by these higher coordination number ligands is known as the chelate effect.

The chelate effect, the process of exchanging lower coordinated ligands for higher coordinated ones, is an entropically favored process. When the higher coordinating ligand displaces the lower coordinating ligand, more species are in solution, where there are then more available translational, vibrational, and rotational modes of freedom. This increases the entropy (ΔS) of the system through the increase in

Chelation, Fig. 1 (a) Triscarbonato uranyl complex, with the axial "–yl" oxygens omitted for clarity. (b) Deprotonated ethylenediaminetetraacetate, chelated around a generic M^{2+} metal center
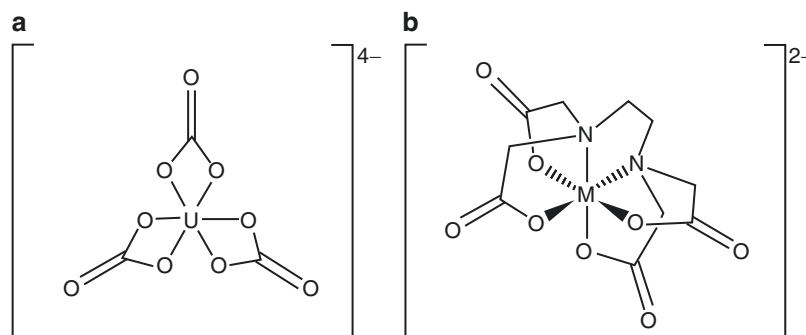
disorder. This process must overcome the enthalpy (ΔH) of the initial complex – the net gain in disorder must be greater than the change in the amount of energy that is stored in the coordinating bond between the Lewis acid–base pairs. When looking at coordination compounds, a few specific donor atoms have prevalence, most notably oxygen and nitrogen. The effects of replacing an oxygen – metal bond from a lower coordinating ligand with another oxygen – metal bond from a higher coordinating ligand are almost negligible, and the entropy of the exchange can be considered as the dominant thermodynamic process involved. However, a careful study of the enthalpy differences must be done if the donor atoms are different.

References

Richens DT (1997) The chemistry of aqua ions, 1st edn. Wiley, Chichester

Chemical Bonds

Barry R. Bickmore and Matthew C. F. Wander
Department of Geological Sciences, Brigham Young University, Provo, UT, USA

Definition

Linus Pauling famously described a chemical bond as "whatever is convenient to the chemist to define as a bond" (Pauling 1960). In the simplest terms, a chemical bond is merely an attraction between atoms in a substance containing an aggregation of two or more atoms. However, while all bonds are based on the attraction between positively charged protons and negatively charged electrons, quantum mechanical effects governing the spatial distribution of electrons give rise to a wide range of bond properties and a continuum of bond types. The standard types include covalent, metallic, ionic, hydrogen, and van der Waals bonds (Gillespie and Popelier 2001).

Traditional Valence Bonds

The strongest chemical bonds (covalent, metallic, and ionic) are sometimes called "valence bonds," due to the fact that they are formed when partially filled *valence atomic orbitals* combine to create molecular orbitals (Albright et al. 2013). The average spatial distribution of electrons (the electron probability density or electron density) around a free atom can be described in terms of atomic orbitals, which form three-dimensional standing wave patterns about the nucleus. As atoms approach one another, their atomic orbitals mix to create molecular orbitals, which form three-dimensional standing wave patterns about multiple nuclei. The resulting redistribution of the bonding electron density causes a net attraction between the atomic centers, but the bond properties depend strongly on the details of the redistribution (Gillespie and Popelier 2001). These details will be discussed here with reference to the *electronegativity* of the participating atoms. (*Electronegativity* is a single-parameter summary of the electron-attracting power of atoms.)

Ionic bonds form between atoms with widely different electronegativity values (metals with nonmetals). In these bonds, molecular orbitals concentrate most of the bonding electron density around the more electronegative atoms, resulting in some atoms with a net negative charge (anions) and others with a net positive charge (cations), which if sufficiently large can behave as separate ions. An ideal ionic bond would involve a cation and anion that can be treated as two point charges, but in real ionic systems, some sharing of valence electrons occurs, the molecular orbitals are not fully spherically symmetrical about the atomic centers, and there is always some orbital overlap, or sharing, of electrons. Therefore, even bonds between atoms with the most disparate electronegativity values are not considered fully ionic (Rohrer 2001).

Covalent bonds form between atoms with similar, high electronegativity values (nonmetals). Here molecular orbitals distribute, or share, the bonding electron density more or less evenly between the atoms involved, with an accumulation of electron density in the overlap region between atomic centers (Popelier 2000). Although fully ionic bonds do not exist, fully covalent bonds do exist between atoms of the same element. Given that covalent bonds involve atoms that tend to hold tightly to their valence electrons, the molecular orbitals form with their associated electron density concentrated very locally, around neighboring atoms. This makes the bonds very localized and directional, i.e., the angles between bonds to a given atom are relatively tightly constrained (Gillespie and Hargittai 1991).

Metallic bonds form between atoms with similar, low electronegativity values (metals). These atoms hold relatively weakly to their valence electrons, and the molecular orbitals formed spread out to encompass a very large number of atoms. Thus, metallically bonded systems are often described as positively charged atoms (nuclei + core electrons) held together by a "sea" of valence electrons shared between all the atoms. When so many atomic orbitals combine, a large number of closely spaced (in terms of energy) molecular orbitals become available, with a relatively small gap (or no

Chemical Bonds, Fig. 1 A van Arkel–Ketelaar triangle, illustrating the continuum of bond types between the ionic, covalent, and metallic limits. The *x*-axis represents the mean electronegativity (χ_{mean}) of the two atoms involved in the bonds in each of the substances plotted. The *y*-axis represents the difference in the two electronegativity values ($\chi_1-\chi_2$)
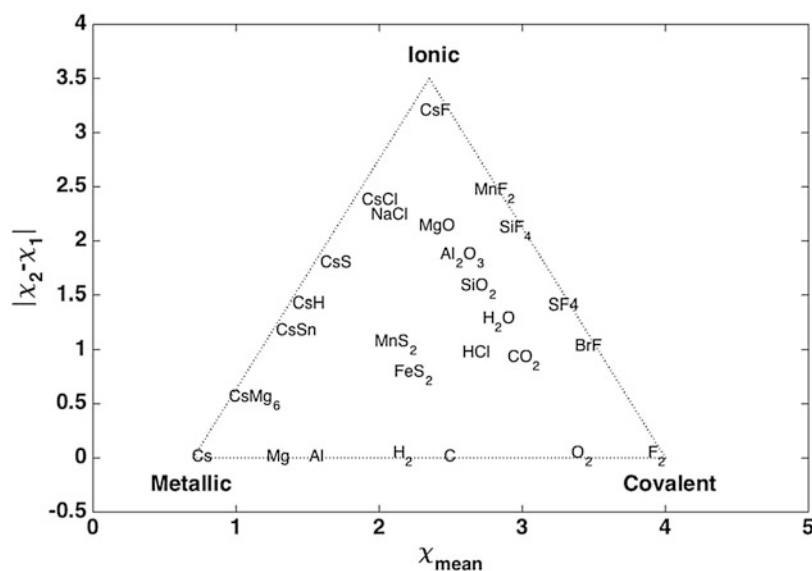
gap) between the filled and unfilled levels. This leads to the high thermal and electrical conductivity of metals, because a relatively small excitation of a bonding electron takes it into molecular orbitals that are comparatively empty and extend throughout the substance. The delocalization of the bonding electrons also results in considerably less directionality and force in the bonds, which explains the malleability of metallic solids (Burdett 1997; Rohrer 2001).

The different types of valence bonds form a continuum, in which the degree of ionicity can be roughly estimated in terms of electronegativity differences between atoms, and covalency/metallicity can be roughly estimated in terms of the average electronegativity of the bonded atoms (Rohrer 2001). Figure 1 shows a van Arkel–Ketelaar triangle, which schematically illustrates this point. However, bonding character can also be affected by factors such as pressure and temperature (Burdett 1997; Batsanov and Batsanov 2012).

One defining attribute of valence bonds is bond order. Bond order refers to the number of valence electron pairs involved in an individual bond, whether shared or transferred (IUPAC 1997; Brown 2002). (In cases where antibonding electron pairs exist, these are subtracted from the bond order.) The bond in an $F_{2(g)}$ molecule, for example, has a bond order of 1, because the electrons from two half-filled atomic orbitals are shared in one bonding molecular orbital. The electrons from three half-filled atomic orbitals are shared in $N_{2(g)}$ molecules, so the bond order is 3. In a $CsF_{(g)}$ molecule, an electron from a half-filled atomic orbital in Cs is transferred to a half-filled orbital on the F, creating an ionic bond with a bond order of 1. The orders of bonds incident to a given atom in a stable substance must sum to the atomic valence of the atom. The atomic valence is equivalent to the

number of H atoms to which it can bond. Given that bond lengths are highly correlated with bond orders (Brown 2002), this creates stringent constraints regarding the combinations of bond lengths that are possible in a stable structure. Although atomic valence values are necessarily integers, bond orders can have non-integer values, especially in condensed phases with extended networks of valence bonds. For example, in corundum (α-Al_2O_3) Al has a valence of 3, while O has a valence of 2. The Al-O bonds have bond orders of ~0.5, so that each Al is bonded to six O atoms, and each O is bonded to four Al atoms. Non-integer orders for individual bonds are possible because molecular orbitals, which must contain an integral number of electrons, can encompass multiple atoms (Brown 2002; Albright et al. 2013).

At least for covalent bonds with integer bond orders, the force constants used to describe bond vibrations are proportional to the bond order (Johnston 1966). This gives rise to another defining attribute of bonds, i.e., the inverse relationship between bond length and strength.

Bonds can also profitably be characterized in terms of bond energy (E_{bond}), which is the average energy per mole of bonds released when molecules are separated into their constituent atoms. A similar quantity can be obtained from dividing the atomization energies of solids by the number of bonds per formula unit (Sanderson 1976). For a bond between two given elements, of a given bond order, E_{bond} values are relatively transferable. Therefore, it is possible to roughly estimate enthalpies of formation by summing bond energies. It is important to note that, for the same bond order, E_{bond} can vary by hundreds of kJ/mol for bonds between different elements. For example, the bond energy for the single bond in $F_{2(g)}$ is 158.67 kJ/mol, whereas that for

$Cs_{2(g)}$ is 43.919 kJ/mol and that for $CsF_{(g)}$ is 517.1 kJ/mol (Luo 2007). However, bond energies are not strictly proportional to bond order, although there is a relationship between the two.

Hydrogen Bonds as Valence Bonds

Hydrogen bonds (H-bonds) are the weaker of conjugate bonds formed between H and two or more highly electronegative atoms such as N, O, or F and are usually designated as X–H...X, where X represents the more electronegative atoms, the solid line represents a strong, polar covalent bond, and the dotted line represents an H-bond. The electron density involved in the strong bond is shifted toward the more electronegative atom, creating a dipole between the two atoms, resulting in a relatively weak electrostatic attraction between the positively charged H and any other electronegative atoms in the vicinity. Thus, the H is bonded strongly to one comparatively electronegative atom and much more weakly to one or more others. Due to the fact that H atoms have only one electron, along with their small size, shifting its electron density toward the anion results in a relatively high positive charge density.

Hydrogen bonds are often treated as simple electrostatic dipole interactions, rather than valence bonds, but in fact, it has been shown that even weak hydrogen bonds have some covalent character, so there is no reason to treat them as anything but weak valence bonds that may be assigned a bond order. In fact, when H-bonds are shorter, the adjacent stronger bonds become longer, as one would expect for a valence bond (Steiner and Saenger 1994; Steiner 2002).

The typical asymmetry of X–H...X bonds is likely to be a product of the small size of H atoms. Symmetric H-bonds, in which the two bonds to H have equal bond orders of 0.5, do exist. However, they are quite rare because bond order falls off exponentially with distance. Therefore, an X–H–X configuration with two 0.5 order bonds draws the X atoms considerably closer to one another than would typically be the case for nonbonded atoms, whereas an asymmetric X–H...X configuration results in a considerably longer X–X distance (Brown 2002). However, symmetric H-bonds become more common at high pressure (Steiner 2002), because X atoms are forced together by compression.

London Dispersion (van der Waals) Forces

London dispersion (van der Waals) forces originate due to oscillations in the instantaneous electron distribution around atoms. The average electron distribution is generally very symmetrically disposed about the nucleus, but at any given instant this may not be the case, creating a small dipole

moment. As atoms approach one another, their oscillations synchronize to maximize attraction. This oscillation is correctly accounted for with electron correlation calculations and is in itself a type of standing wave behavior. A very weak molecular state is created in these cases, which explains why an attraction between filled shells is possible (Housden and Pyper 2007; Krapp and Frenking 2007). This is why noble gases, with filled valence shells, can condense into liquid at very low temperatures.

Bonds and the Distribution of Elements

A number of factors contribute to the distribution of the elements in the Earth, as described by the traditional *Goldschmidt classification* (Faure 1998), but one such factor has to do with bond energies. As noted above, bonds of the same order can vary widely in bond energy with the bond character. Elements with very low electronegativity (e.g., the alkali and alkali earth metals) favor highly ionic bonds with fractional bond orders (i.e., bond order < 1), so they naturally bond easily to O in network solids. Oxygen is the most abundant element in the Earth and the second-most electronegative, and some of the more electronegative elements, such as the halogens, often substitute for O. Therefore, these elements are classified as *lithophile* and are enriched in the crust and mantle. Some of the more electronegative elements, such as C and N, favor covalent bonds with one another, having high bond orders (1 or greater). This results in fewer bonds and discrete molecules rather than network solids. A number of elements with moderately high electronegativity favor covalent bonds with similar elements and low to moderate bond orders, so these tend to congregate in sulfides, and are classified as *chalcophile*. A number of metals with moderately low electronegativity favor metallic bonds with one another, with low bond orders. These tend to form metallic solids and are classified as *siderophile*, because they readily bond with Fe and are enriched in the core.

Summary and Conclusions

Chemical bonds can usefully be characterized in terms of bond order, bond energy, and bond type. Bond orders constrain suitable combinations of bond lengths incident to atoms in stable configurations, and bond energies for bonds of the same order vary widely as a function of bond type. It is impossible to classify a given chemical bond as exclusively one type, however, because van der Waals interactions are present between all neighboring atoms, and even in cases where van der Waals interactions dominate (e.g., noble gas dimers and condensed phases), molecular orbitals play some role. This is why there is a continuum between the

different bond types, based on the affinity for electrons of the bonded atoms. The relationships between bond order and bond energy for different atom pairs are one of the determining factors affecting the distribution of elements in the Earth.

Cross-References

- ▶ Ab Initio Calculations
- ▶ Atmophile Elements
- ▶ Chalcophile Elements
- ▶ Electronegativity
- ▶ Geochemical classification of elements
- ▶ Lithophile Elements
- ▶ Siderophile Elements

References

Albright TA, Burdett JK, Whangbo M-H (2013) Orbital interactions in chemistry. Wiley, Hoboken. 819 p

Batsanov SS, Batsanov AS (2012) Introduction to structural chemistry. Springer, Dordrecht. 542 p

Brown ID (2002) The chemical bond in inorganic chemistry: the bond valence model. Oxford University Press, New York. 278 p

Burdett JK (1997) Chemical bonds: a dialog. Wiley, Chichester. 166 p

Faure G (1998) Principles and applications of geochemistry. Prentice Hall, Upper Saddle River. 600 p

Gillespie RJ, Hargittai I (1991) The VSEPR model of molecular geometry. Allyn and Bacon, Boston. 248 p

Gillespie RJ, Popelier PLA (2001) Chemical bonding and molecular geometry: from Lewis structures to electron densities. Oxford University Press, Oxford. 268 p

Housden MP, Pyper NC (2007) The noble gas dimers as a probe of the energetic contributions of dispersion and short-range electron correlation in weakly-bound systems. Mol Phys 105: 2353–2361

IUPAC (1997) Compendium of chemical terminology. Blackwell Scientific Publications, Oxford

Johnston VHS (1966) Gas phase reaction rate theory. Ronald Press, New York. 372 p

Krapp A, Frenking G (2007) Is this a chemical bond? A theoretical study of $Ng_2@C_{60}$ (Ng = He, Ne, Ar, Kr, Xe). Chem Eur J 13: 8256–8270

Luo Y-R (2007) Comprehensive handbook of chemical bond energies. CRC Press, New York. 1657 p

Pauling L (1960) The nature of the chemical bond. Cornell University Press, Ithaca. 644 p

Popelier PLA (2000) Atoms in molecules: an introduction. Pearson Education, Essex. 164 p

Rohrer GS (2001) Structure and bonding in crystalline materials. Cambridge University Press, Cambridge. 540 p

Sanderson RT (1976) Chemical bonds and bond energy. Academic, New York. 218 p

Steiner T (2002) The hydrogen bond in the solid state. Angew Chem Int Ed 41:48–76

Steiner T, Saenger W (1994) Lengthening of the covalent O–H bond in O–H...O hydrogen bonds re-examined from low-temperature neutron diffraction data of organic compounds. Acta Crystallogr B50:348–357

Chemical Weathering

Jérôme Viers and Priscia Oliva
CNRS/IRD, Paul Sabatier University, Toulouse, France

Definition

Chemical weathering may be defined as the *spontaneous* and *irreversible* thermodynamic process that causes degradation of the mineral phases under the prevailing environmental conditions at the surface of the Earth. If one must differentiate the weathering in the continental and marine environments, chemical weathering is usually considered to be the solid/solution interactive process occurring in contact with the atmosphere. By extension, in the language of the specialists of the critical zone, chemical weathering may be defined as that set of processes which alter a rock into a layer of chemically and physically transformed superficial material (i.e., regolith) which is susceptible to evolve (soil or karst) with time following biogeochemical processes.

Introduction

While this process of chemical modification can be easily formalized by writing on paper, for example, the chemical reaction of dissolving a mineral (1), the reality is much more complex because it actually encompasses a set of chemical, physical, or biological complex interactions:

$$CaAl_2Si_2O_8 s + 4H^+ aq = Ca^{2+} aq + Al_2Si_2O_5(OH)_4 s \quad (1)$$
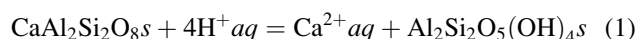
The physical process that causes the dissolution of calcium feldspar (1) is a process of hydrolysis corresponding to the replacement of a cation (Ca^{2+}) on the mineral surface by a proton (H^+). This first step in chemical weathering is the surface protonation of the mineral. The presence of protons in the etching solution is explained by chemical equilibria involving the distribution of CO_2 (atmospheric) between the aqueous and gaseous phases, e.g.:

$$CO_{2(g)} + H_2O = H^+ + HCO_{3(aq)}^- \quad (2)$$
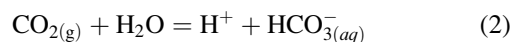
In the conditions at the Earth's surface, chemical weathering processes occur mainly in contact with acidic solutions that result from natural acidification of rainwater in reaction (2) and subsequent acidification of solutions in the soil environment due to microbial activity (decomposition of organic matter) and root respiration (atmospheric CO_2 enrichment of the soil). In certain geological environments

(sulfide-rich volcanic or metamorphic formations), production of acid can be generated by the oxidative dissolution of sulfides such as:

$$FeS_2 s + 15/4 O_2 g + 7/2 H_2O aq$$
$$= 2SO_4^{2-} aq + Fe(OH)_3 s + 4H^+ aq \quad (3)$$
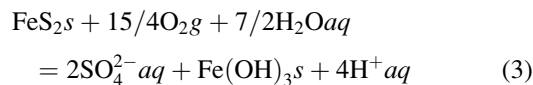
The principal reactions of chemical weathering are hydrolysis (1), oxidation (3), and the dissolution of ionic compounds. Chemical weathering processes in saline or alkaline environment exist but are very minor at the natural environment's surface conditions. The products of these reactions may be both dissolved compounds and secondary solid phases, which may be either well or poorly crystallized. The reaction is said to be incongruent when we have both aqueous and solid phases and congruent when having only dissolved compounds. The principal secondary minerals that form in the conditions at the surface across the critical zone are clay minerals or metal oxyhydroxides which are more stable from a thermodynamic perspective than are the primary minerals. Both secondary phases and residual primary minerals (inherent minerals) constitute soils mineralogical assemblage.

The products of chemical weathering can then be transported by surface water: we speak of transportation for dissolved compounds in solution (Ca^{2+}, HCO_3^-, small organic molecules, etc.) and particulate matter (or sediments) for either mineral or organic solid compounds. Geochemists have conventionally considered that the boundary between the dissolved phase and the particulate phase is defined by membranes filtration of water with the empirical pore diameter being 0.45 or 0.2 micrometers. Data on concentrations (dissolved and particulate) combined with the water discharges of rivers are therefore used to define, respectively, the chemical and physical erosion fluxes. This process of chemical weathering of rocks associated with their physical dismantling and potential material transport by inland waters is responsible for about 15 billion tons of sediment exported from the continents to the oceans annually (Milliman and Farnsworth 2011).

Chemical Weathering: A Major Geological Process

Chemical weathering is a fundamental "geological" process because it plays a major role in the global geodynamic of our planet; this role is complex because it occurs at highly variable scales of time and space.

- At the scale of the weathering front (a zone of transition between the rock and soil) or the soil itself, chemical weathering is accompanied by the release of nutrients (e.g., major elements such as K or Ca, and trace elements such as Fe or Co) essential to the functioning of the continental ecosystems. The soil which is a product of chemical weathering appears here as a fundamental natural resource, nonrenewable on the scale of humanity. It provides numerous economic functions (agricultural production, materials production in quarries, etc.), cultural (recreational, archaeological sites, etc.), or environmental (regulation of water flow, retention of contaminants, etc.). Yet in many parts of the world, soils are subjected to very high stressors (e.g., contamination, salinization, desertification, etc.) and are often irreversibly lost for any use by society.

- On a global scale, chemical weathering plays an important but complex role in regulating the climate of our planet. This role stems from the fact that the chemical weathering of silicate rocks consumes atmospheric CO_2 because the calcium and bicarbonate ions (produced in reactions (1) and (2) above) are carried to the ocean by rivers where they are precipitated (usually biologically) as calcium carbonate (4):

$$Ca^{2+} + HCO_3^- = CaCO_3 + H^+ \quad (4)$$

In the early 1980s, Walker et al. (1981) proposed a negative feedback loop between the climate and the chemical weathering of continental surfaces: an increase in the partial pressure of CO_2 (pCO_2) from the atmosphere induces an increase in air temperature and accelerates the hydrological cycle. This change of physical parameters enhances the chemical weathering of silicate rocks which in turn lowers pCO_2 and therefore regulates the Earth's climate.

However, the links between climate and weathering today appear much more complex than envisioned by Walker et al.; therefore, in recent decades, chemical weathering has undergone numerous studies conducted via different approaches.

The Different Approaches Used to Study Chemical Weathering

The chemical weathering processes can be studied in differing ways:

- They can be studied under controlled laboratory conditions. Many studies have been conducted to examine this process in conditions near to and far from thermodynamic equilibrium. These studies were intended to better understand the reactions occurring on the mineral surface during dissolution and thus gain a better understanding of the parameters controlling the kinetics of dissolution. They allowed the proposal of the empirical laws of chemical weathering (e.g., transition state theory; Berner 1995 and references therein) that revealed the importance of many factors: mineral surfaces, temperature, chemical affinity, proton activity, organic compound).

- Laboratory research on chemical weathering has a long history (about a century), and the nature of these involved processes is still undergoing debate within the scientific community. Most experiments in dissolution yield chemical weathering rates up to four orders of magnitude greater than those estimated from field studies. This discrepancy between the experimental and natural chemical weathering rates is called the "dissolution rate conundrum" (Maher et al. 2006). Under natural conditions, a progressive loss of reactive surface sites for silicate weathering over time is observed. It may be attributed to the inhibitory effect on mineral dissolution due to the presence of Al^{3+} or organic ligands in solution or to surface coating by the secondary phases precipitates in a natural context which are rare in dissolution experiments (Oelkers et al. 1994). Indeed, experimental conditions still remain far from natural circumstances (e.g., duration, fluid / mineral ratios, fluid composition) (White and Brantley 1995). The saturation state of the solution appears to be a key parameter as it controls the effects of microstructures and microtextures on chemical weathering (Chardon et al. 2006 and references therein).

- Chemical weathering processes can be studied in situ by considering the weathering products constituting the regoliths and soils. Mineralogical and/or chemical composition of the regolith represents an integrated view of all the processes that have occurred over time to form this regolith. One approach allows for the establishment of mass balances for chemical elements using references called invariant elements such as zirconium or titanium. This approach has the merit of being able to estimate the flow of chemical elements and, therefore, rates of loss or enrichment of elements throughout the soil profile. However, it often remains impossible to transform these fluxes into chemical erosion rates because the age of a given soil is often very difficult to narrow down.

- A third method is the "watershed" approach. This approach involves studying the fluxes of chemicals leaving the watersheds. These studies involve the hydrological and chemical monitoring of water during the course of continental surface drainage. This approach can be conducted on large river basins (Amazon, Congo, Lena, etc.) or small watersheds. The "large pool" approach offers the advantage of being inclusive of processes over large areas; the "small pool" approach offers the advantage of often working on more homogeneous systems (e.g., as for lithology) rendering the least complex object for study. Over watersheds of varying lithology, chemical erosion rates associated with silicate rocks may be understood by "direct" (Garrels and McKenzie 1967) or 'indirect' methods, the latter by the use of inverse methods of calculation (e.g. Gaillardet et al. 1999). All of these studies allowed highlighting of the roles of certain parameters on the weathering: mineralogy of exposed rocks, surface ages, precipitation/dissolution of clay minerals, presence of easily changeable accessory minerals, movement and time that water resides in the soil, physical erosion, vegetation, anthropogenic disturbance (fertilizer) (Oliva et al. 2003; Perrin et al. 2008).

- More recently, there are several works studying chemical weathering from numerical models (Duffy et al. 2014). These studies seek to examine/simulate chemical weathering occurring today (MacKenzie watershed, Beaulieu et al. 2011) or in the past (Goddéris et al. 2014). This is, for example, the case of the WITCH model based on the law of weathering kinetics (Beaulieu et al. 2011). In recent years, this type of model has been coupled with global dynamic models of vegetation because vegetation plays an important role with regard to the flow of water (in the soil and the soil interface/atmosphere). Vegetation plays a more direct role in the dissolution of minerals because of root activity and the release of organic acids in soil (Drever and Vance 1994). In the future, one challenge will be to model the effects on the evolution of biodiversity on the cycle of elements because vegetation is not only a sink or reservoir for carbon but is this for all of the other chemical elements (Mg, Si, Ca) (Chave 1999; Viers et al. 2005). Recent field and laboratory tests have also shown that the dissolution of phytoliths (siliceous particles produced in the plant and then recovered in the soil) showed faster dissolution kinetics than the secondary minerals (clay) and therefore could play an important role in the silicon cycle on the surface of the Earth (Derry et al. 2005; Fraysse et al. 2009). This is another poorly known effect of the role of vegetation on chemical erosion rates and more generally on the cycle of elements.

Unifying Natural and Experimental Chemical Weathering Rates

During the last decade, one of the major scientific questions circulating about chemical weathering was to understand the existing disparities between the field measurements of natural "chemical weathering rates" and the measurements carried out in the laboratory, the objective being to attempt unification of this dual information. The most significant results were obtained from multidisciplinary approaches in geochemistry and mineralogy (Ferrier et al. 2010) or by focusing on the molecular-level mineral-water interface by means of new observational tools and analyses of mineral surfaces with high resolution [e.g., Raman spectroscopy, high-resolution and energy-filtered TEM, in situ atomic force microscopy (AFM)] as defined in the publications of Hellmann et al. (2012) or Ruiz Agudo et al. (2012). These methods have identified the mechanisms of interface-coupled dissolution-reprecipitation mechanisms during chemical weathering. These results put into question the currently accepted leached-layer model of

chemical weathering (Oelkers et al. 2009; Schott et al. 2012) which involves preferential removal of weakly bonded cations (e.g., Na^+ and K^+) from the surface regions of silicates, which precedes the removal of the more strongly bonded cations (e.g., Al^{3+} and Si^{4+}) at acidic pH values resulting in apparent incongruent dissolution for silicate minerals.

Concurrently, Rasmussen et al. (2011) using a more traditional approach (measurement of the ground flux versus thermodynamic calculations on the basis of Na export) on a set of data very well documented across the Rio Icacos watershed were able to quantify the activation energies (E_a) for the weathering of feldspars comparable to those data given in the literature for the experimental dissolution of albite. These results indicate that to correctly quantify E_a dissolution from field data, certain parameters (i.e., water availability, erosion) rather neglected up to that point, must be considered. It's about the physicochemical and regolith soil data, particularly the availability of water to perform mineral weathering. Rasmussen et al. (2011) calculated an average apparent activation energy of 69 kJ.mol^{-1} Na for positive annual water balance zones and 136 kJ.mol^{-1} Na for water-limited locations, respectively. This suggests that water availability is the dominant factor limiting rate kinetics for albite weathering in the cool climate of the water-limited systems.

The Effect of Water Availability and Time Duration for the Presence of Water

The availability of water is proposed as the factor limiting the rate of chemical weathering in weathering systems by many authors (Maher 2010). Long transit times of water (>1 decade) are consistent with a kinetic control of the weathering by thermodynamics through the precipitation of secondary phases or activity of microorganisms, while the short times that water is present are synonymous with control by the processes of transport and hydrology. Thus, some authors consider that the dependence of chemical weathering on time, which is often considered to be the major parameter in the models of landform contour evolution, is in fact a result of mechanisms controlled by hydrological processes (water availability, time period that water is present, etc.). The concept of a hydrological thermostat ("hydrologic thermostat") was established to describe the role of hydrological processes in the regulation of chemical weathering and associated with the consumption of CO_2 (Maher and Chamberlain 2014). The flow (*runoff*) appears as the most relevant parameter to describe the flux of weathering in comparison with the temperature in many environments. The most important flow of weathering measured at present corresponds to the environments of volcanic islands (Goldsmith et al. 2010; Schopka et al. 2011) in which deeply circulating hydrological systems (table) can play a major role (Schopka and Derry 2012).

Summary and Conclusions

Numerous studies conducted over the past two decades on chemical weathering are related to its ability to remove CO_2 from the atmosphere because that can condition our Earth's climate (West 2012). Understanding the links between the climate and tectonics in the geological history of our planet inevitably involves taking the carbon cycle into account and thus, chemical weathering. Certainly the study of current systems helps to better establish some parametric laws between weathering and climate. However, the relationship between climate, tectonics, erosion, and the sets of potential feedback is still a major subject of study. The study of the role of mountain ranges and flood plains of major rivers in weathering (such as those currently in the Amazon watershed) will remain a preferred subject of study over the coming years (Moquet et al. 2011; Bouchez et al. 2012).

Cross-References

▶ Acid–Base Reactions
▶ Aqueous Solutions
▶ Earth's Atmosphere
▶ Carbon Cycle
▶ Clay Minerals
▶ Critical Zone
▶ Geochemical Thermodynamics
▶ Kinetics of Geochemical Processes
▶ Low-Temperature Geochemistry
▶ Oxidation-Reduction Reactions and Eh-pH (Pourbaix) Diagrams
▶ Oxide Minerals
▶ Silicate Minerals
▶ Soils
▶ Surface Geochemistry

Bibliography

Beaulieu E, Goddéris Y, Labat D, Roelandt C, Calmels D, Gaillardet J (2011) Modeling of water-rock interaction in the MacKenzie basin: competition between sulfuric and carbonic acids. Chem Geol 289:114–123

Berner RA (1995) Chemical weathering and its effect on atmospheric CO_2 and climate. In: White AF, Brantley SL (eds) Chemical weathering rates of silicate minerals, Reviews in mineralogy, vol 31. Mineralogical Society of America, Washington, DC, pp 565–583

Bouchez J, Gaillardet J, Lupker M, Louvat P, France-Lanord C, Maurice L, Armijos E, Moquet J-S (2012) Floodplains of large rivers: weathering reactors or simple solos? Chem Geol 332(333):166–184

Chardon D, Chevilotte V, Beauvais A, Grandin G, Boulangé B (2006) Planation, bauxites and epeirogeny: one or two paleosurfaces on the West African margin? Geomoph 82:273–282

Chave J (1999) Study of structural, successional and spatial patterns in tropical rain forests using TROLL, a spatially explicit forest model. Ecol Model 124:233–254

Derry LA, Kurtz AC, Ziegler K, Chadwick OA (2005) Biological control of terrestrial silica cycling and export fluxes to watersheds. Nature 433:728–731

Drever JI Vance GF (1994) Role of soil organic acids in mineral weathering process. In: Pittman ED, Lewan MD (eds) Organic acids in geological processes, Springer-Verlag, Berlin, 482pp

Duffy C, Shi Y, Davis K, Slingerland R, Li L, Sullivan PL, Goddéris Y, Brantley SL (2014) Designing a suite of models to explore critical zone function. Proc Earth Planet Sci 10:7–15

Ferrier KL, Kirchner JW, Riebe CS, Finkel RC (2010) Mineral-specific chemical weathering rates over millennial timescales: measurements at Rio Icacos, Puerto Rico. Chem Geol 277:101–114

Fraysse F, Pokrovsky O, Schott J, Meunier JD (2009) Surface chemistry and reactivity of plant phytoliths in aqueous solutions. Chem Geol 258:197–206

Gaillardet J, Dupré B, Louvat P, Allègre CJ (1999) Global silicate weathering and CO_2 consumption rates deduced from the chemistry of large rivers. Chem Geol 159:3–30

Garrels RM, Mackenzie FT (1967) Origin of the chemical compositions of some springs and lakes. Am Chem Soc Adv Chem Ser 67:222–242

Goddéris Y, Donnadieu Y, Le Hir G, Lefebvre V, Nardin E (2014) The role of paleogeography in the Phanerozoic history of atmospheric CO_2 and climate. Earth Sci Rev 128:122–138

Goldsmith ST, Carey AE, Johnson BM, Welch SA, Berry Lyons W, McDowell WH, Pigott JS (2010) Stream geochemistry, chemical weathering and CO_2 consumption potential of andesitic terrains, Dominica, lesser Antilles. Geochim Cosmochim Acta 74:85–103

Hellmann R, Wirth R, Daval D, Barnes JP, Penisson JM, Tisserand D, Epicier T, Florin B, Hervig RL (2012) Unifying natural and laboratory chemical weathering with interfacial dissolution-reprecipitation: a study based on the nanometer-scale chemistry of fluid-silicate interfaces. Chem Geol 294:203–216

Maher K (2010) The dependence of chemical weathering rates on fluid residence time. Earth Plan Sci Lett 294:101–110

Maher K, Chamberlain CP (2014) Hydrologic regulation of chemical weathering and the geologic carbon cycle. Science 342:1502–1504

Maher K, Steefel CI, DePaolo DJ, Viani BE (2006) The mineral dissolution rate conundrum: insights from reactive transport modelling of U isotopes and pore fluid chemistry in marine sediments. Geochim Cosmochim Acta 70:337–363

Milliman JD, Farnsworth KL (2011) River discharge to the coastal ocean: a global synthesis. Cambridge, Cambridge University Press, 392pp

Moquet J-S, Crave A, Viers J, Seyler P, Armijos E, Bourrel L, Chavarri E, Lagane C, Casimiro WSL, Pombosa R, Noriega L, Vera A, Guyot J-L (2011) Chemical weathering and atmospheric soil/CO_2 uptake in the Andean and foreland Amazon basins. Chem Geol 287:1–26

Oelkers EH, Schott J, Devidal JL (1994) The effect of aluminum, pH, and chemical affinity on the rates of aluminosilicate dissolution reactions. Geochim Cosmochim Acta 58:2011–2024

Oelkers EH, Golubev SV, Chairat C, Pokrovsky OS, Schott J (2009) The surface chemistry of multi-oxide silicates. Geochim Cosmochim Acta 73:4617–4634

Oliva P, Viers J, Dupré B (2003) Chemical weathering in granitic environments. Chem Geol 202:225–256

Perrin A-S, Probst A, Probst J-L (2008) Impact of nitrogenous fertilizers on carbonate dissolution in small agricultural catchments: implications for weathering CO_2 uptake at regional and global scales. Geochim Cosmochim Acta 72:3105–3123

Rasmussen C, Brantley S, deB Richter D, Blum A, Dixon J, White AF (2011) Strong climate and tectonic control on plagioclase weathering in granitic terrain. Earth Plan Sci Lett 301:521–530

Ruiz-Agudo E, Putnis CV, Rodriguez-Navarro C, Putnis A (2012) Mechanism of leached layer formation during chemical weathering of silicate minerals. Geology 40:947–950

Schopka HH, Derry LA (2012) Chemical weathering fluxes from volcanic islands and the importance of groundwater: the Hawaiian example. Earth Plan Sci Lett 339/340:67–78

Schopka HH, Derry LA, Arcilla CA (2011) Chemical weathering, river geochemistry and atmospheric carbon fluxes from volcanic and ultramafic regions on Luzon Island, the Philippines. Geochim Cosmochim Acta 75:978–1002

Schott J, Pokrovsky O, Spalla O, Devreux F, Gloter A, Mielczarski A (2012) Formation, growth and transformation of leached layers during silicate minerals dissolution: the example of wollastonite. Geochim Cosmochim Acta 98:259–281

Viers J, Barroux G, Pinelli M, Seyler P, Oliva P, Dupré B, Boaventura G (2005) The influence of the Amazonian floodplain ecosystems on the trace element dynamics of the Amazon River mainstem (Brazil). Sci Total Environ 339:219–232

Walker JCG, Hays PB, Kasting JF (1981) A negative feedback mechanism for the long-term stabilization of Earth's surface temperature. J Geophys Res 86:9776–9782

West AJ (2012) Thickness of the chemical weathering zone and implications for erosional and climatic drivers of weathering and for carbon-cycle feedbacks. Geology 40:811–814

White AF, Brantley SL (1995) Chemical weathering rates of silicate minerals: an overview. In: White AF, Brantley SL (eds) Chemical weathering rates of silicate minerals, Reviews in mineralogy, vol 31. Mineralogical Society of America, Washington, DC, pp 1–22

Chlorine

Mark A. Kendrick

Research School of Earth Sciences, Australian National University, Canberra, ACT, Australia

Element Data

Atomic Symbol: Cl

Atomic Number: 17

Atomic Weight: 35.453

Isotopes and Abundances: stable ^{35}Cl (75.76%) and ^{37}Cl (24.24%) and radioactive ^{36}Cl ($t_{1/2} = 301.3$ ka)

1 Atm Melting Point: 171.65 K

1 Atm Boiling Point: 239.11 K

Common Valences: $-1, 1, 3, 5, 7$

Ionic Radii: 1.8 Å

Pauling Electronegativity: 3.16

First Ionization Potential: 1256.2 kJ mol^{-1}

Chondritic (CI) Abundance: 680 ppm

Silicate Earth Abundance: 15–30 ppm

Crustal Abundance: 140–470 ppm

Seawater Abundance: 19,300 ppm

Core Abundance: <20 ppb?

Properties

Chlorine is a diatomic toxic green-yellow gas at room temperature with a bleach-like smell. However, Cl is characterized by an S^2P^5 outer electron shell configuration and is highly electronegative, meaning it rarely exists in its elemental form in nature. Chlorine most commonly forms the chloride ion with a valence of -1, but it can exist in a number of different valence states. Chloride forms strong ionic bonds in salts and substitutes for the OH group in many hydrous minerals. Hydrogen chloride [$HCl_{(g)}$] is a diatomic gas at room temperature and forms hydrochloric acid $HCl_{(aq)}$ when dissolved in water.

History and Use

Elemental $Cl_{2(g)}$ was first produced by the Swedish scientist Carl Wilhelm Scheele in 1774. Scheele isolated $Cl_2(g)$ by heating hydrochloric acid with the mineral pyrolusite (MnO_2) but believed the resulting gas was an oxide he named "dephlogisticated muriatic acid air." Later experiments showed that this gas would not decompose during reaction with charcoal, phosphorus, or ammonia, and by 1810 Sir Humphrey Davy concluded the gas was an element (Davy 1811). The name chlorine is derived from the Greek word chloros meaning green-yellow (Davy 1811).

Chloride in common salt has been used in cooking and food preservation since prehistoric times. Salt is produced commercially by the evaporation of seawater or mining. Chlorine gas is produced for industrial purposes by electrolysis of salt solutions or molten sodium or magnesium chloride. Chlorine is used to kill bacteria in drinking water and swimming pools and in the manufacture of a wide range of products including paper, paints, textiles, and plastics. PVC (polyvinyl chloride) alone is used extensively in the building and automotive industries. The high electronegativity of Cl means Cl or Cl compounds are used as oxidizing agents or in substitution reactions involved in the manufacture of many pharmaceuticals and some insecticides. In the past Cl was used to make chloroform ($CHCl_3$) which is a toxic but powerful anesthetic, chlorofluorocarbons (CFCs) were used as refrigerants and aerosol propellants before being linked to destruction of stratospheric ozone, and Cl gas was used as a highly toxic chemical weapon in World War 1.

Distribution in the Cosmos and on Earth

The solar photosphere contains 4.8 ppm Cl, making it the eighteenth most abundant element in the solar system (Lodders 2003). Chlorine is moderately volatile with a 50% condensation temperature of 954 K at 10^{-4} bar (Lodders 2003). Chlorine has a concentration of ~680 ppm in CI chondrites compared to an estimated concentration of ~15–30 ppm in the Earth's theoretical primitive mantle (McDonough and Sun 1995). Chlorine is depleted on Earth relative to other elements of similar volatility, and because Cl has a low compatibility in Fe-Ni alloys and is therefore expected to have a low concentration in the Earth's core, it is suggested that Cl was probably lost during Earth's accretion either with the early atmosphere or with crustal components removed by collisional erosion (Sharp and Draper 2013).

Chlorine is a strongly incompatible element and is concentrated in the Earth's surface reservoirs. Seawater with 1.9 wt. % Cl (~3.5 wt % salt) contains a bit less than half, and evaporites with up to 60 wt. % Cl contain about a quarter of the total Cl in the Earth's surface reservoirs (Schilling et al. 1978).

Chlorine has a residence time of 100s of Myr in seawater, suggesting a constant concentration; however, depending on the amount of Cl stored in evaporites, seawater salinities could have been very different (more saline) in the distant geological past (Hay et al. 2006). Sedimentary formation waters have salinities that commonly range from ~1 up to ~30 wt. % salt, but can include even higher salinities (Hanor 1994). Average continental crust has been variably estimated to contain 130–470 ppm Cl compared to ~1–5 ppm Cl in the depleted mantle (Rudnick and Gao 2003; Shimizu et al. 2016). Primitive mid-ocean ridge and ocean island basalt glasses contain ~30–2000 ppm Cl (Schilling et al. 1978; Michael and Cornell 1998; Kendrick et al. 2015). The average Cl content of altered ocean crust is not well constrained but could be as high as 100–500 ppm (Sano et al. 2008). High concentrations of Cl are common in metamorphic environments characterized by low fluid-rock ratios, and parts of the oceanic crust and lithosphere contain amphibole and serpentine with wt. % levels of Cl (Sharp and Barnes 2004; Kendrick et al. 2013; Kendrick 2017). The long-term exchange of Cl between the Earth's mantle and surface reservoir over time is an area of active research.

Significance in Geochemistry

Chlorine is undersaturated in typical submarine basaltic lavas and behaves as a lithophile element in the mantle. However, $HCl_{(g)}$ is degassed from subaerial volcanoes and has a significant influence on climate and ozone depletion (Kutterolf et al. 2013). Chloride is the dominant anion in geofluids, including magmatic fluids exsolved in the crust. Chloride acts as an important ligand enabling the transport of metals in hydrothermal solution (Yardley, 2005).

In sedimentary environments with a high water-rock ratio, fluid chlorinity is often considered to be conservative and can be used to infer a fluid source or migration pathway. In some cases the movement of saline formation waters (oil field brines) is linked with hydrocarbon migration. In higher-temperature metamorphic environments with lower fluid-rock ratios, the concentration of Cl in a geofluid is not conservative. Fluid salinity provides important evidence for hydrothermal phase separation and the Cl content of metamorphic minerals track the involvement of saline fluids in metamorphic processes (Kendrick 2017).

Chlorine Isotopes

Chlorine stable isotope ratios reported relative to standard mean ocean chloride vary by ~10 ‰ on Earth. Chondrites and samples from the terrestrial mantle typically have $\delta^{37}Cl$ of slightly less than seawater (0 ‰), suggesting that Cl was isotopically uniform in the inner solar nebular (Sharp et al. 2013). Minor variations in mantle $\delta^{37}Cl$, including maximum $\delta^{37}Cl$ of up to +3 ‰, have been attributed to the subduction of sediments (John et al. 2010). However, the majority of materials from the Earth's surface including sediments have $\delta^{37}Cl$ of less than seawater, and the mechanisms for isotope fractionation are not well understood (Barnes and Straub 2010). The Moon exhibits much greater variation in $\delta^{37}Cl$ with maximum values of +25 ‰ attributed to fractionation during lunar degassing of metal-halides from anhydrous magmas at low atmospheric pressures (Sharp et al. 2010). The short-lived ^{36}Cl isotope ($t_{1/2}$ = 301.3 ka) is used in dating groundwater and cosmogenic exposure dating of landforms formed by lava flows or glacial erosion surfaces ranging from tens of thousands of years to about 1 Ma (Ivy-Ochs and Kober 2008).

Biological Utilization and Toxicity

Chlorine gas is a respiratory irritant, and it can be detected by a bleach-like odor at concentrations of less than 1 ppm; it causes immediate chest pain, vomiting, and shortness of breath at concentrations of ~30 ppm; and is fatal within minutes at concentrations of more than ~1000 ppm (About Chlorine 2016). In contrast, chloride is the dominant anion enabling cellular level electrochemistry, meaning that Cl is an essential element for life.

Cross-References

References

About Chlorine. Retrieved May 2016, The Chlorine Institute. Available at: http://chlorineinstitute.org/stewardship/about-chlorine

Barnes JD, Straub SM (2010) Chorine stable isotope variations in Izu Bonin tephra: implications for serpentinite subduction. Chem Geol 272(1–4):62–74

Davy H (1811) On a combination of oxymuriatic gas and oxygene gas. Philos Trans R Soc Lond 101:155–162

Hanor JS (1994) Origin of saline fluids in sedimentary basins. In: Parnell J (ed) Geofluids: origin, migration and evolution of fluids in sedimentary basins, Geological society special publication. Geological Society, London, pp 151–174

Hay WW, Migdisov A, Balukhovsky AN, Wold CN, Flögel S, Söding E (2006) Evaporites and the salinity of the ocean during the Phanerozoic: implications for climate, ocean circulation and life. Palaeogeogr Palaeoclimatol Palaeoecol 240(1–2):3–46

Ivy-Ochs S, Kober F (2008) Surface exposure dating with cosmogenic nuclides. Quat Sci J 57(1–2):179–209

John T, Layne GD, Haase KM, Barnes JD (2010) Chlorine isotope evidence for crustal recycling into the Earth's mantle. Earth Planet Sci Lett 298(1–2):175–182

Kendrick MA (2017) Halogens in seawater, marine sediments and the altered oceanic lithosphere. In: Harlov DE, Aranovich LY (eds) The role of halogens in terrestrial and extraterrestrial processes. Springer, Berlin. In press

Kendrick MA, Honda M, Pettke T, Scambelluri M, Phillips D, Giuliani A (2013) Subduction zone fluxes of halogens and noble gases in seafloor and forearc serpentinites. Earth Planet Sci Lett 365:86–96

Kendrick MA, Jackson MG, Hauri E, Phillips D (2015) The halogen (F, Cl, Br, I) and H_2O systematics of Samoan lavas: assimilated seawater, EM2 and high 3He/4He components. Earth Planet Sci Lett 410:197–209

Kutterolf S, Hansteen TH, Appel K, Freundt A, Krüger K, Pérez W, Wehrmann H (2013) Combined bromine and chlorine release from large explosive volcanic eruptions: a threat to stratospheric ozone? Geology 41(6):707–710

Lodders K (2003) Solar system abundances and condensation temperatures of the elements. Astrophys J 591:1220–1247

McDonough WF, Sun S-s (1995) The composition of the earth. Chem Geol 120:223–253

Michael PJ, Cornell WC (1998) Influence of spreading rate and magma supply on crystallization and assimilation beneath mid-ocean ridges: evidence from chlorine and major element chemistry of mid-ocean ridge basalts. J Geophys Res Solid Earth 103(B8):18325–18356

Rudnick RL, Gao S (2003) Composition of the continental crust. In: Treatise of geochemistry. Elsevier, Amsterdam, pp 1–64

C

Sano T, Miyoshi M, Ingle S, Banerjee NR, Ishimoto M, Fukuoka T (2008) Boron and chlorine contents of upper oceanic crust: basement samples from IODP Hole 1256D. Geochem Geophys Geosyst 9(12): Q12O15

Schilling JG, Unni CK, Bender ML (1978) Origin of chlorine and bromine in the oceans. Nature 273:631–636

Sharp ZD, Barnes JD (2004) Water-soluble chlorides in massive seafloor serpentinites: a source of chloride in subduction zones. Earth Planet Sci Lett 226(1–2):243–254

Sharp ZD, Draper DS (2013) The chlorine abundance of earth: implications for a habitable planet. Earth Planet Sci Lett 369–370:71–77

Sharp ZD, Shearer CK, McKeegan KD, Barnes JD, Wang YQ (2010) The chlorine isotope composition of the moon and implications for an anhydrous mantle. Science 329(5995):1050–1053

Sharp ZD, Mercer JA, Jones RH, Brearley AJ, Selverstone J, Bekker A, Stachel T (2013) The chlorine isotope composition of chondrites and earth. Geochim Cosmochim Acta 107:189–204

Shimizu K, Saal AE, Myers CE, Nagle AN, Hauri EH, Forsyth DW, Kamenetsky VS, Niu Y (2016) Two-component mantle melting-mixing model for the generation of mid-ocean ridge basalts: implications for the volatile content of the Pacific upper mantle. Geochim Cosmochim Acta 176:44–80

Yardley BWD (2005) 100th anniversary special paper: metal concentrations in crustal fluids and their relationship to ore formation. Econ Geol 100(4):613–632

Chlorine Isotopes

Magali Bonifacie
Institut de Physique du Globe de Paris, Sorbonne Paris Cité, Université Paris Diderot, Paris, France

Introduction

Chlorine has 24 isotopes with mass numbers ranging from ^{28}Cl to ^{51}Cl. There are only two stable isotopes: ^{35}Cl and ^{37}Cl with respective proportions of 75.76% and 24.24% (Berglund and Wieser 2011). The longest-lived radioactive isotope is ^{36}Cl (half-life of 301,000 years); all other isotopes having half-lives of less than 1 h. Variations of the chlorine isotope ratio ($R = {}^{37}$Cl/^{35}Cl) are expressed in the δ-notation with δ^{37}Cl $= \left(R_{sample} / R_{standard} - 1 \right) * 1000$. The international reference standard for chlorine is the terrestrial ocean Standard Mean Ocean Chloride (SMOC), with δ^{37}Cl $= 0$ ‰ (Godon et al. 2004a; Kaufmann et al. 1984).

History and Overview

Chlorine undergoes volatile and incompatible behavior during silicate melting and is water soluble. For these reasons, geological processes (including partial melting, magma degassing, hydrothermal activity, and weathering) have mostly concentrated Cl at the Earth's surface, particularly in the ocean, evaporites, and crustal brines. The most common and stable oxidation state of chlorine is -I, with chloride (Cl$^-$) being the main anion of most geological fluids.

Chlorine stable isotopic variations in geological samples were first reported in formation waters from the Gulf of Mexico (Kaufmann et al. 1984). Since then, chlorine stable isotopes have been used as a tool for tracing the origin and fate of fluids and rocks from the Earth's surface and interior (e.g., fluid movement in sedimentary basins, magma degassing, cycling of the subducted lithosphere into the mantle). Excluding volcanic fumaroles, the large majority of terrestrial samples analyzed to date have δ^{37}Cl between -2 and $+2$ ‰ (Fig. 1) requiring precise analytical methods to be able to identify and interpret small variations.

Stable Chlorine Isotope Measurements

Though chlorine isotopic compositions were, in the 1990s, measured via thermal ionization mass spectrometry (TIMS), δ^{37}Cl measurements are now mostly performed via gas source isotope ratio mass spectrometry (GS-IRMS) on gaseous methyl chloride. This requires prior precipitation of soluble chlorides Cl$^-$ into AgCl$_{(s)}$, followed by the formation of CH$_3$Cl$_{(g)}$, via AgCl reaction with excess CH$_3$I$_{(g)}$ (Eggenkamp 1994). This method allows to reach the best precision on δ^{37}Cl measurements that are typically about ± 0.04 ‰ and ± 0.3 ‰ (1σ) when using either dual-inlet (Godon et al. 2004a; Bonifacie et al. 2005) or continuous-flow (Sharp et al. 2007) introduction modes. The determination of δ^{37}Cl of silicate bulk rocks and minerals requires an additional step of Cl extraction from the silicate network, usually made via pyrohydrolysis (Bonifacie et al. 2007a), before AgCl precipitation. Only recently, δ^{37}Cl values of rocks and minerals have been determined in situ with secondary ion mass spectrometry (SIMS) in Cl-rich terrestrial basaltic to andesitic glasses (Godon et al. 2004c; John et al. 2010; Layne et al. 2009) or melt inclusions (Manzini et al. 2017) but also in some extraterrestrial samples as chondritic sodalites (Sharp et al. 2007) or Cl-rich apatites from the Moon or Martian meteorites (Boyce et al. 2015; Sharp et al. 2010b; Williams et al. 2016). However, the uncertainty associated with δ^{37}Cl measurements by SIMS is still relatively large ± 0.5 ‰ (1σ) for samples with percent-level Cl (Williams et al. 2016) and larger for lower Cl-content samples.

Chlorine Isotope Fractionations

Many physical and chemical processes are likely to segregate isotopes of a single element according to their mass and following either thermodynamic equilibrium laws or kinetic processes. Theoretical studies based on ab initio calculations
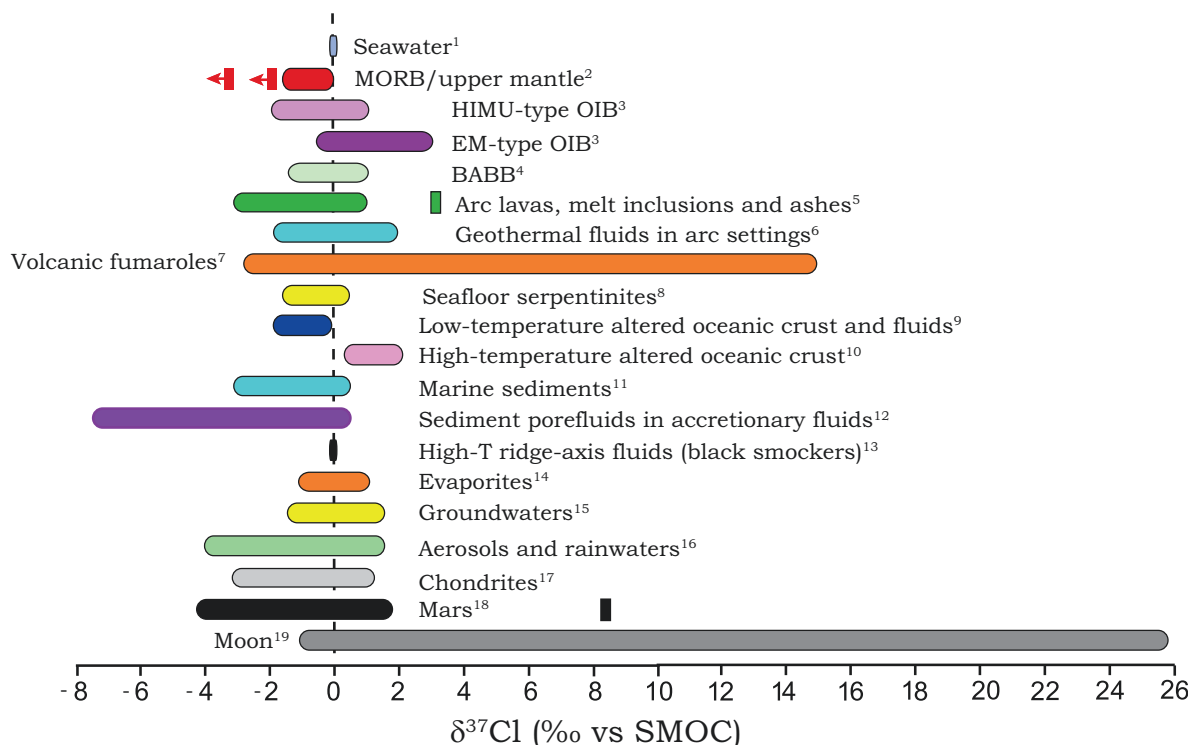
Chlorine Isotopes, Fig. 1 Chlorine isotope variations in terrestrial and extraterrestrial reservoirs. (1) Kaufman et al. (1984), Godon et al. (2004a). (2) Bonifacie et al. (2007a, 2008a), Sharp et al. (2007), Layne et al. (2009). (3) John et al. (2010). (4) Layne et al. (2009). (5) Barnes et al. (2009), Barnes and Straub (2010), Manzini et al. (2017). (6) Li et al. (2015), Chiaradia et al. (2014), Rodriguez et al. (2016). (7) Sharp et al. (2010a), Rizzo et al. (2013), Rodriguez et al. (2016). (8) Bonifacie et al. (2008b), Barnes and Sharp (2006). (9 and 10) Bonifacie et al. (2007a, 2007b), Barnes and Cisneros (2012). (11) Barnes and Straub (2010). (12) Godon et al. (2004b). (13) Bonifacie et al. (2005). (14) Eastoe et al. (2007). (15) Eastoe et al. (2001), Kaufmann et al. (1993), Stotler et al. (2010). (16) Koehler and Wassenaar (2010). (17) Bonifacie et al. (2007a), Sharp et al. (2007, 2013). (18) Williams et al. (2016). (19) Sharp et al. (2010b), Boyce et al. (2015)

have reported equilibrium fractionations between different Cl-bearing molecules of geochemical or environmental importance including chloride salts (e.g., NaCl, KCl, RbCl), gas-phase molecules (such as HCl and Cl_2 or molecule of interest in atmosphere as ClO, $ClONO_2$), dissolved species, and $FeCl_2$ and $MnCl_2$ as analogs for Cl-bearing silicates (Czarnacki and Hałas 2012; Richet et al. 1977; Schauble et al. 2003). Their main conclusions are (i) Cl isotope equilibrium fractionations are limited to only a few per mil when Cl is under $-I$ oxidation state (the majority of geological samples) with fractionation decreasing with increasing temperature, (ii) the magnitude of fractionation is predicted to increase with the increasing oxidation state of Cl (e.g., ClO_4 is 75 ‰ enriched relative to chloride at 25 °C), and (iii) silicates are predicted to be enriched compared to coexisting brines (from about 2 ‰ to 3 ‰ at 25 °C). Experimental work to constrain equilibrium fractionations have been limited to chloride salt precipitation (Eggenkamp et al. 2016; confirming the theoretical predictions of less than 0.5 ‰ fractionations at 22 °C) or gaseous HCl in equilibrium with aqueous chloride (Sharp et al. 2010a; confirming the predicted ~1.5 ‰ gas enrichment at 50 °C). On the other hand,

kinetic fractionations are suggested to occur at low temperature during processes such as (i) diffusion (^{35}Cl diffusing faster than ^{37}Cl; Desaulniers et al. 1986; Eggenkamp and Coleman 2009; Richter et al. 2006), (ii) ion filtration (this process results from a fluid flow forcing solute ions such as Cl^- through a negatively charged low-permeability medium/membrane such as clays – ^{35}Cl being more efficiently repelled than ^{37}Cl, the solution passing through the membrane is enriched in ^{37}Cl, and the solution on the inflow side is Cl-enriched but ^{37}Cl depleted; (Campbell 1985; Phillips and Bentley 1987)), or (iii) HCl dynamically escaping from an acid solution (Sharp et al. 2010a). Eggenkamp (2014) presents a detailed and up-to-date review of the aforementioned and other known Cl isotope fractionations.

Key Research Findings and Applications as a Geochemical Tracer

Multiple studies have used $\delta^{37}Cl$ values to trace the origin of salinity and the hydrodynamic history of saline fluids found in the continental crust, brines in sedimentary basins (e.g.,

Eastoe et al. 2001; Kaufmann et al. 1993), or crystalline waters from old cratons (e.g., Shouakar-Stash et al. 2007; Stotler et al. 2010). In contrast to most chemical tracers that are prone to changes upon water-rock interactions, chlorine is mainly conservative, therefore Cl isotopes are used to identify fluid circulation in sedimentary basins and quantify diffusion in aquifers (e.g., Eggenkamp 1994; Giunta 2015; Lavastre et al. 2005).

Over the last decade, $\delta^{37}Cl$ values have been increasingly used to constrain the source and/or degassing of terrestrial and extraterrestrial rocks and magmas. Notably, since chlorine isotopes are thought to not fractionate during high-temperature dehydration of the subducting slab (Bonifacie et al. 2008b; Selverstone and Sharp 2013), $\delta^{37}Cl$ is used to better constrain the deep-Earth cycling of halogens and the origin of mantle chemical heterogeneity. Since the work constraining the Cl composition of the depleted mantle (Bonifacie et al. 2008a; Sharp et al. 2007), several studies have used $\delta^{37}Cl$ values for tracing the source of ocean island basalts (Halldórsson et al. 2016; John et al. 2010), back-arc basalts (Layne et al. 2009; Barnes et al. 2009), or arc magmas (e.g., Barnes and Straub 2010; Barnes et al. 2009).

Chlorine shows a unique combination of geochemical properties that can inimitably trace the history of magmas from their origin through their differentiation, degassing, and interactions with meteoric or hydrothermal fluids. Notably, chlorine is among the last volatiles degassed (mainly as HCl) from magmas, is chemically nonreactive (unlike most other main volatile elements), and is highly hydrophilic. Fumaroles, geothermal waters, and rocks of various arc volcanoes have been investigated in order to trace the source of magmas [for instance, the Poas volcano (Rodríguez et al. 2016; Sharp et al. 2010a), the Soufrière de Guadeloupe (Li et al. 2015), or the Mount Etna (Rizzo et al. 2013) or along an active arc setting (e.g., Barnes et al. 2009; Chiaradia et al. 2014; Li et al. 2015)]. Some studies also presented a time-related evolution of $\delta^{37}Cl$ in springwaters and fumaroles to test their relevance for volcanic surveillance (Li et al. 2015; Rodríguez et al. 2016). In parallel, the highly ^{37}Cl-enriched apatites of lunar basalts (with $\delta^{37}Cl$ up to +25 ‰) have been explained as resulting from the degassing of metal halides from an anhydrous mantle (Sharp et al. 2010a) or alternatively from the degassing of a lunar magma ocean early in the Moon's history (Boyce et al. 2015).

Summary and Future Directions

Because of the unique characteristics of chlorine when compared to most other abundant and geochemically important volatiles or mobile elements on Earth, $\delta^{37}Cl$ are increasingly used to reveal the origin and fate of terrestrial and extraterrestrial reservoirs. However, before reaching their full potential as a geochemical tracer, there is still a need of strengthening our fundamental knowledge on Cl isotope systematics (mainly further determination of isotopic fractionations between Cl species in various conditions and improvements of analytical methods in order to determine precise $\delta^{37}Cl$ on Cl-poor samples). Another promising aspect is the recent advance in measuring bromine stable isotope compositions in low Br-content geological samples (Louvat et al. 2016). Because Br shares most chemical characteristics with Cl (although slightly more reactive), the coupled used of Cl and Br stable isotopes should undoubtedly unravel important features of the halogen geodynamics.

Cross-References

▶ Ab Initio Calculations
▶ Bromine
▶ Chlorine
▶ Gas Source Mass Spectrometry (GS-MS)
▶ Halogens
▶ Hydrothermal Solutions
▶ Mantle Geochemistry
▶ Ocean Biochemical Cycling and Trace Elements
▶ Stable Isotope Geochemistry

References

Barnes JD, Cisneros M (2012) Mineralogical control on the chlorine isotope composition of altered oceanic crust. Chem Geol 326–327:51–60. https://doi.org/10.1016/j.chemgeo.2012.07.022

Barnes JD, Sharp ZD (2006) A chlorine isotope study of DSDP/ODP serpentinized ultramafic rocks: insights into the serpentinization process. Chem Geol 228:246–265. https://doi.org/10.1016/j.chemgeo.2005.10.011

Barnes JD, Straub SM (2010) Chorine stable isotope variations in Izu Bonin tephra: implications for serpentinite subduction. Chem Geol 272:62–74. https://doi.org/10.1016/j.chemgeo.2010.02.005

Barnes JD, Sharp ZD, Fischer TP, Hilton DR, Carr MJ (2009) Chlorine isotope variations along the Central American volcanic front and back arc. Geochem Geophys Geosyst 10. https://doi.org/10.1029/2009GC002587

Berglund M, Wieser M (2011) Isotopic compositions of the elements 2009 (IUPAC technical report). Pure Appl Chem. 397–410. https://doi.org/10.1351/PAC-REP-10-06-02

Bonifacie M, Charlou JL, Jendrzejewski N, Agrinier P, Donval JP (2005) Chlorine isotopic compositions of high temperature hydrothermal vent fluids over ridge axes. Chem Geol 221:279–288. https://doi.org/10.1016/j.chemgeo.2005.06.008

Bonifacie M, Jendrzejewski N, Agrinier P, Coleman M, Pineau F, Javoy M (2007a) Pyrohydrolysis-IRMS determination of silicate chlorine stable isotope compositions. Application to oceanic crust and meteorite samples. Chem Geol 242:187–201. https://doi.org/10.1016/j.chemgeo.2007.03.012

Bonifacie M, Monnin C, Jendrzejewski N, Agrinier P, Javoy M (2007b) Chlorine stable isotopic composition of basement fluids of the eastern flank of the Juan de Fuca Ridge (ODP Leg 168). Earth Planet Sci Lett 260:10–22. https://doi.org/10.1016/j.epsl.2007.05.011

Bonifacie M, Jendrzejewski N, Agrinier P, Humler E, Coleman M, Javoy M (2008a) The chlorine isotope composition of Earth's mantle. Science 319:1518–1520. https://doi.org/10.1126/science.1150988

Bonifacie M, Busigny V, Mével C, Philippot P, Agrinier P, Jendrzejewski N, Scambelluri M, Javoy M (2008b) Chlorine isotopic composition in seafloor serpentinites and high-pressure metaperidotites. Insights into oceanic serpentinization and subduction processes. Geochim Cosmochim Acta 72:126–139. https://doi.org/10.1016/j.gca.2007.10.010

Boyce JW, Treiman AH, Guan Y, Ma C, Eiler JM, Gross J, Greenwood JP, Stolper EM (2015) The chlorine isotope fingerprint of the lunar magma ocean. Sci Adv 1:e1500380–e1500380. https://doi.org/10.1126/sciadv.1500380

Campbell D (1985) Fractionation of stable chlorine isotopes during transport through semipermeable membranes. The University of Arizona, Vasa

Chiaradia M, Barnes JD, Cadet-Voisin S (2014) Chlorine stable isotope variations across the quaternary volcanic arc of Ecuador. Earth Planet Sci Lett 396:22–33. https://doi.org/10.1016/j.epsl.2014.03.062

Czarnacki M, Hałas S (2012) Isotope fractionation in aqua -gas systems: Cl 2 -HCl-Cl −, Br 2 -HBr-Br − and H 2 S-S 2−. Isot Environ Health Stud 48:55–64. https://doi.org/10.1080/10256016.2011.616269

Desaulniers DE, Kaufmann RS, Cherry JA, Bentley HW (1986) 37Cl-35Cl variations in a diffusion-controlled groundwater system. Geochim Cosmochim Acta 50:1757–1764. https://doi.org/10.1016/0016-7037(86)90137-7

Eastoe CJ, Long A, Land LS, Kyle JR (2001) Stable chlorine isotopes in halite and brine from the gulf coast basin: brine genesis and evolution. Chem Geol 176:343–360. https://doi.org/10.1016/S0009-2541(00)00374-0

Eastoe CJ, Peryt TM, Petrychenko OY, Geisler-Cussey D (2007) Stable chlorine isotopes in Phanerozoic evaporites. Appl Geochem 22:575–588. https://doi.org/10.1016/j.apgeochem.2006.12.012

Eggenkamp HGM (1994) The geochemistry of chlorine isotopes. Thesis. Utrecht University

Eggenkamp HGM (2014) The geochemistry of stable chlorine and bromine isotopes, Advance in isotope geochemistry. Edited by Springer, p 172

Eggenkamp HGM, Coleman ML (2009) The effect of aqueous diffusion on the fractionation of chlorine and bromine stable isotopes. Geochim Cosmochim Acta 73:3539–3548. https://doi.org/10.1016/j.gca.2009.03.036

Eggenkamp HGM, Bonifacie M, Ader M, Agrinier P (2016) Experimental determination of stable chlorine and bromine isotope fractionation during precipitation of salt from a saturated solution. Chem Geol 433:46–56. https://doi.org/10.1016/j.chemgeo.2016.04.009

Giunta T (2015) Contraintes sur la géochimie isotopique du Chlore et du Brome dans les eaux de sub-surface. Thesis. Paris Diderot – Institut de Physique du Globe

Godon A, Jendrzejewski N, Eggenkamp HGM, Banks DA, Ader M, Coleman ML, Pineau F (2004a) A cross-calibration of chlorine isotopic measurements and suitability of seawater as the international reference material. Chem Geol 207:1–12. https://doi.org/10.1016/j.chemgeo.2003.11.019

Godon A, Jendrzejewski N, Castrec-Rouelle M, Dia A, Pineau F, Boulégue J, Javoy M (2004b) Origin and evolution of fluids from mud volcanoes in the Barbados accretionary complex. Geochim Cosmochim Acta 68:2153–2165. https://doi.org/10.1016/j.gca.2003.08.021

Godon A, Webster JD, Layne GD, Pineau F (2004c) Secondary ion mass spectrometry for the determination of δ37Cl Part II. Intercalibration of SIMS and IRMS for aluminosilicate glasses. Chem Geol 207:291–303. https://doi.org/10.1016/j.chemgeo.2004.04.003

Halldórsson SA, Barnes JD, Stefánsson A, Hilton DR, Hauri EH, Marshall EW (2016) Subducted lithosphere controls halogen enrichments in the Iceland mantle plume source. Geology 44:679–682. https://doi.org/10.1130/G37924.1

John T, Layne GD, Haase KM, Barnes JD (2010) Chlorine isotope evidence for crustal recycling into the Earth's mantle. Earth Planet Sci Lett 298:175–182. https://doi.org/10.1016/j.epsl.2010.07.039

Kaufmann RS, Long A, Bentley H, Davis S (1984) Natural chlorine isotope variations. Nature 309:338–340

Kaufmann RS, Frape S, McNutt R, Eastoe CJ (1993) Chlorine stable isotope distribution of Michigan basin formation waters. Appl Geochem 8:403–407

Koehler G, Wassenaar LI (2010) The stable isotopic composition (37Cl/35Cl) of dissolved chloride in rainwater. Appl Geochem 25:91–96. https://doi.org/10.1016/j.apgeochem.2009.10.004

Lavastre V, Jendrzejewski N, Agrinier P, Javoy M, Evrard M (2005) Chlorine transfer out of a very low permeability clay sequence (Paris Basin, France): 35Cl and 37Cl evidence. Geochim Cosmochim Acta 69:4949–4961. https://doi.org/10.1016/j.gca.2005.04.025

Layne GD, Kent AJR, Bach W (2009) δ37Cl systematics of a backarc spreading system: the Lau basin. Geology 37:427–430. https://doi.org/10.1130/G25520A.1

Li L, Bonifacie M, Aubaud C, Crispi O, Dessert C, Agrinier P (2015) Chlorine isotopes of thermal springs in arc volcanoes for tracing shallow magmatic activity. Earth Planet Sci Lett 413:101–110. https://doi.org/10.1016/j.epsl.2014.12.044

Louvat P, Bonifacie M, Giunta T, Michel A, Coleman M (2016) Determination of bromine stable isotope ratios from saline solutions by "wet plasma" MC-ICPMS including a comparison between high- and low-resolution modes, and three introduction systems. Anal Chem 88:3891–3898. https://doi.org/10.1021/acs.analchem.6b00062

Manzini M, Bouvier A-S, Barnes JD, Bonifacie M, Rose-Koga EF, Ulmer P, Métrich N, Bardoux G, Williams J, Layne GD, Straub S, Baumgartner LP, John T (2017) SIMS chlorine isotope analyses in melt inclusions from arc settings. Chem Geol. https://doi.org/10.1016/j.chemgeo.2016.12.002

Phillips FM, Bentley HW (1987) Isotopic fractionation during ion filtration. Geochim Cosmochim Acta 51:683–695

Richet P, Bottinga Y, Javoy M (1977) A review of hydrogen, carbon, nitrogen, and chlorine stable isotope fractionation among gaseous molecules. Annu Rev Earth Planet Sci 5:65–110

Richter FM, Mendybaev RA, Christensen JN, Hutcheon ID, Williams RW, Sturchio NC, Beloso AD (2006) Kinetic isotopic fractionation during diffusion of ionic species in water. Geochim Cosmochim Acta 70:277–289. https://doi.org/10.1016/j.gca.2005.09.016

Rizzo AL, Caracausi A, Liotta M, Paonita A, Barnes JD, Corsaro RA, Martelli M (2013) Chlorine isotope composition of volcanic gases and rocks at Mount Etna (Italy) and inferences on the local mantle source. Earth Planet Sci Lett 371:134–142. https://doi.org/10.1016/j.epsl.2013.04.004

Rodríguez A, Eggenkamp HGM, Cruz MM, van Bergen MJ (2016) Chlorine isotope and Cl–Br fractionation in fluids of Poás volcano (Costa Rica): insight into an active volcanic–hydrothermal system. J Volcanol Geotherm Res 325:70–85. https://doi.org/10.1016/j.jvolgeores.2016.05.020

Schauble EA, Rossman GR, Taylor HPJ (2003) Theoretical estimates of equilibrium chlorine-isotope fractionations. Geochim Cosmochim Acta 67:3267–3281. https://doi.org/10.1016/S0016-7037(00)01375-3

Selverstone J, Sharp ZD (2013) Chlorine isotope constraints on fluid-rock interactions during subduction and exhumation of the Zermatt-Saas ophiolite. Geochem Geophys Geosyst 14:4370–4391. https://doi.org/10.1002/ggge.20269

Sharp ZD, Barnes JD, Brearley AJ, Chaussidon M, Fischer TP, Kamenetsky VS (2007) Chlorine isotope homogeneity of the mantle, crust and carbonaceous chondrites. Nature 446:1062–1065. https://doi.org/10.1038/nature05748

Sharp ZD, Barnes JD, Fischer TP, Halick M (2010a) An experimental determination of chlorine isotope fractionation in acid systems and applications to volcanic fumaroles. Geochim Cosmochim Acta 74:264–273. https://doi.org/10.1016/j.gca.2009.09.032

Sharp ZD, Shearer CK, McKeegan KD, Barnes JD, Wang YQ (2010b) The chlorine isotope composition of the moon and implications for an anhydrous mantle. Science 329:1050–1053. https://doi.org/10.1126/science.1192606

Sharp ZD, Mercer JA, Jones RH, Brearley AJ, Selverstone J, Bekker A, Stachel T (2013) The chlorine isotope composition of chondrites and Earth. Geochim Cosmochim Acta 107:189–204

Shouakar-Stash O, Alexeev SV, Frape SK, Alexeeva LP, Drimmie RJ (2007) Geochemistry and stable isotopic signatures, including chlorine and bromine isotopes, of the deep groundwaters of the Siberian platform, Russia. Appl Geochem 22:589–605. https://doi.org/10.1016/j.apgeochem.2006.12.005

Stotler RL, Frape SK, Shouakar-Stash O (2010) An isotopic survey of $\delta^{81}Br$ and $\delta^{37}Cl$ of dissolved halides in the Canadian and Fennoscandian shields. Chem Geol 274:38–55. https://doi.org/10.1016/j.chemgeo.2010.03.014

Williams JT, Shearer CK, Sharp ZD, Burger PV, Cubbin FMMC, Santos AR, Agee CB, Keegan KDMC (2016) The chlorine isotopic composition of Martian meteorites 1: chlorine isotope composition of Martian mantle and crustal reservoirs and their interactions. 19:1–19. https://doi.org/10.1111/maps.12647

Chondrites

Sara Russell
Department of Earth Sciences, The Natural History Museum, London, UK

Definition

Chondrites are the most common type of *meteorites*, making up around 80% of all known meteorite falls. Chondrites are stony meteorites and most are dark brown, gray, and/or black in color. Chondrites are accreted material from nebular components formed within the dusty cloud that circulated around the young Sun. They avoided igneous differentiation and so contain approximately solar proportions of the elements. Therefore, they likely originated on minor planets (mainly asteroids) which were not large enough to generate heat to melt. Most chondrites preserve an original texture from the time of their accretion. This texture consists of ~mm sized spherical silicate balls called chondrules surrounded by a submicron sized material called matrix (Fig. 1). In some chondrites, metal and/or sulfides are common and in some can be found refractory inclusions, including calcium-aluminum-rich inclusions (CAIs). Less heated chondrites typically contain primordial organic material and presolar grains that formed around ancient ancestral stars.Organic material can be complex and includes polyaromatic hydrocarbons. More details about chondrites and their classification can be found in Krot et al. (2013); Scott and Krot (2013); and Grady et al. (2014).

Alteration of Chondrites

As well as classifications of chemical class, chondrites are classified according to the degree of alteration (aqueous interaction and/or heating) they experienced on their parent asteroid. This is called the petrological scale and chondrites are numbered from 1 to 6 (Van Schmus and Wood 1967). According to this classification scheme, petrological types 2 and 1 show increasing amounts of aqueous alteration from 2 to 1, and types 3 to 6 show increasing amounts of changes due to heating. Type 1 chondrites only rarely contain anhydrous minerals; typically silicates have been entirely transformed to clays. Type 2 chondrites contain visible chondrules but also abundant phyllosilicate minerals. Type 3 chondrites are petrologically pristine, with clearly defined chondrules composed of anhydrous olivine, pyroxene, metal, and minor minerals, and containing glass in chondrule mesostasis. A continuum exists from type 3 to type 6 chondrites that have lost almost all their petrological texture and chondrules are barely visible. Meteorites that have been completely melted but retain a chondritic bulk composition are occasionally termed "Type 7 chondrites."

Chondrites are often affected by shock processing, most commonly while on their parent body. This can result in the formation of veins and mineralogical effects such as planar deformation features. A classification system for shock in ordinary chondrites was devised by Stöffler et al. (1991).

Another process that can affect chondrites, especially finds rather than falls, is terrestrial *weathering*. The most obvious effects of terrestrial weathering are oxidation of native iron to form oxides. Weathering also affects bulk chemistry and the silicate mineralogy of the sample, with CCs most easily affected (Bland et al. 2006).

Classification

Chondrites are cateogorized according to their chemical and isotopic properties, with the three main types or *classes* being ordinary chondrites, carbonaceous chondrites, and enstatite chondrites (Fig. 1).There are rare chondrites that do not fit into these classes: the Rumuruti type chondrites (R chondrites) and the Kakangari type chondrites (K chondrites). Additionally, a few chondrites do not fall into any of these types and are classified as ungrouped. These classes are further subdivided into *groups*, as outlined below. In addition, the chondrite is assigned a *petrologic type*, which is an indication of the type of asteroidal processing it has experienced.

Ordinary Chondrites (OC): Ordinary chondrites are the most common type of meteorite and around 95% of all chondrite falls are OCs. OCs are composed of chondrules rich in olivine and pyroxene, with minor silicates, oxides, sulfides,

and metal, surrounded by fine grained matrix that is composed of chondrule-like fragments and sometimes amorphous material. Ordinary chondrites are typically petrological types 3–6. They contain metal in the form of Fe-Ni in varying proportions. Ordinary chondrites are further subdivided into three groups, H, L, and LL, according to their metal content and composition of silicates. H chondrites contain 15–20% free metal (a Fe-Ni alloy) and the olivine composition is $Fa_{16–20}$; L chondrites contain 7–11% free metal and their olivine composition is $Fa_{21–25}$; LL chondrites contain 3–5% free metal and olivine of $Fa_{26–32}$. Ordinary chondrites have oxygen isotope compositions distinct from terrestrial samples (Fig. 2). The JAXA Hayabusa mission returned material from an S type asteroid, which is remarkably similar to LL chondrite material (Nakamura et al. 2011). Therefore, S type asteroids are likely to be the source of most ordinary chondrites.

Carbonaceous Chondrites (CC): Although a minor contribution to known meteorites, carbonaceous chondrites have been extensively studied as they have suffered on minimal heating while on their parent bodies, and their petrological types are usually 1–3. The term carbonaceous is misleading; they typically contain no more than a few percent carbon and often much less. Carbonaceous chondrites are exceptionally diverse in texture and chemistry. The CCs are divided into classes, represented by a letter that usually refers to the type specimen of that class.

CV meteorites, which contain large chondrules of up to several mm in size and rather abundant white CAIs (around 5 vol%) which are irregular or rounded in shape and can be up to cm in size.

CK meteorites contain textural and oxygen isotope similarities to the CV meteorites, but they are more oxidized. CK are the only carbonaceous chondrites that are mostly typically metamorphosed, with petrological types 4–6 most common. Some researchers believe CV and CK are the same or related group (e.g., Greenwood et al. 2010).

Chondrites, Fig. 1 The Parnallee meteorite that fell in India in 1857. This type 3 ordinary chondrite (LL) contains distinct rounded chondrules surrounded by a fine grained matrix. Natural History Museum specimen number BM 34792. The specimen is approximately 16 cm across

Chondrites, Fig. 2 Oxygen isotope composition of chondrites. On a three-isotope oxygen diagram, $^{17}O/^{16}O$ ratio vs. $^{18}O/^{16}O$ ratio, both normalized to the Standard Mean Ocean Water value, chondrite groups occupy distinct regions. CCs typically plot below the terrestrial fractionation line; most non-CCs above it. $\delta^{17,18}O = [(^{17,18}O/^{16}O)$ sample$/(^{17,18}O/^{16}O)_{SMOW}-1] \times 1,000$ (From Scott and Krot 2013)

CO chondrites have a similar bulk chemistry to CVs and a similar abundance of CAIs, but both chondrules and CAIs in these meteorites are much smaller, around ~100 μm typically.

CM chondrites contain small chondrules and abundant matrix (around 50%). They are nearly always petrological type 2 and have experienced significant aqueous alteration.

CI chondrites have been extensively aqueously altered, which has destroyed much of their original texture and mineralogy. These chondrites have no (or very rare) chondrules and consist almost entirely of water-formed minerals such as phyllosilicates, sulfides, carbonates, and oxides. CIs are the most chemically primitive chondrites, and their bulk composition resembles that of the Sun, apart from volatile species such as H and He (e.g., Lodders 2003).

CR chondrites contain large chondrules similar in size to those in CV chondrites, but they only rarely contain CAIs. Iron nickel metal is abundant. Matrix makes up around 50% of the rock.

CH chondrites are very enriched in metal, have very small chondrules (~20 microns), and also contain CAIs. CH chondrites are exceptional among meteorite groups in that they do not contain true matrix, but instead the chondrules are closely packed. They are highly depleted in volatile elements.

CB chondrites contain large amounts of metal and are subdivided into two chemically similar textural types. CBa meteorites have extremely large chondrules (>cm in size), large metal grains, and are depleted in CAIs. CBb meteorites contain smaller chondrules (mm in size) and contain CAIs.

The CR, CB, and CH chondrites contain geochemical similarities to each other (e.g., they all have elevated $^{15}N/^{14}N$ compared to other chondrite groups) and are referred to as a clan.

Carbonaceous chondrites are darker in color than most other meteorites, and spectroscopically they resemble some C type or related asteroids such as G, B, or D. These asteroids are therefore the likely source for carbonaceous chondrites. Carbonaceous chondrites may preferentially originate in the outer regions of the main asteroid belt. There have been suggestions in the literature that CI chondrites may have a cometary source (e.g., Gounelle et al. 2010).

Enstatite chondrites (EC): Enstatite chondrites are highly reduced rocks that are rich in Fe, Ni-metal, and sulfides. Enstatite ($MgSiO_3$) is common, and Fe is almost absent in silicates. ECs are divided into two groups: the EH meteorites that contain chondrules around 0.2 mm in diameter and high abundance of metal and EL meteorites that contain larger chondrules (~0.5 mm) and less free metal. Enstatite chondrites have similar isotopic compositions to the Earth (Fig. 2). They are spectrally similar to many E-type asteroids.

Kakangari type chondrites (K): These are matrix-rich chondrites that are highly reduced.

Rumuruti type chondrites (R): Rumurutiite meteorites are enriched in matrix and are very oxidized with essentially no free metal.

Oxygen Isotopes

Measurements of the ratios of the three stable isotopes of oxygen (^{16}O, ^{17}O, and ^{18}O) are an essential tool in understanding the relationships between meteorite classes and groups (Fig. 2). On a graph of $^{17}O/^{18}O$ as a function of $^{18}O/^{16}O$, most terrestrial objects fall on a mass-related fractionation line of slope ~0.5, whereas meteorites fall off this line, with each group occupying a distinct oxygen isotope field. Meteorites with similar oxygen isotopic composition may have formed on the same or related asteroids, whereas differences may indicate an origin on separate parent bodies (e.g., Clayton 1993).

Ages of Chondrites

While the exact timing of accretion of chondrites has not been measured, age dates for many chondritic components have been reported, with Pb-Pb data giving the most accurate absolute ages. CAIs have ages of around 4567 Myr while chondrules tend to give similar or younger ages by a few Myr (e.g., Connelly et al. 2012). A minimum age of the accreted parent body can be determined from the age of alteration products that formed on the asteroid; for example, Mn-Cr isotopic data suggests that chondrites accreted and carbonates formed ~3Myr after the formation of the constituents of chondrites (e.g., Fujiya et al. 2011).

Summary and Conclusions

Chondrites are an invaluable tool for the geochemist, as they provide information about the original material from which terrestrial planets accreted. There is a great diversity in geochemistry, isotope compositions, and texture among chondrites, which likely reflects a diversity among the asteroids that are the source of most chondrites. Increased astronomical observations along with recent and upcoming sample return missions are helping us to refine our understanding of the sources of chondrites.

Cross-References

▶ Chemical Weathering
▶ Chondrules
▶ Meteorites
▶ Oxygen Isotopes
▶ Refractory Inclusions in Chondritic Meteorites

References

Bland PA, Zolensky M, Benedix G, Sephton M (2006) Weathering of chondritic meteorites. In: Lauretta D, McSween HP (eds) Meteorites and the early solar system II. University of Arizona Press, Tucson

Clayton RN (1993) Oxygen isotopes in meteorites. Annu Rev Earth Planet Sci 21:115–149

Connelly JN, Bizzarro M, Krot AN, Nordlund A, Wielandt D, Ivanova MA (2012) The absolute chronology and thermal processing of solids in the solar protoplanetary disk. Science 297:1678–1683

Fujiya W, Sugiura N, Hotta H, Ichimura K, Sano Y (2011) Evidence for the late formation of hydrous asteroids from young meteoritic carbonates. Nat Commun 3:627

Gounelle M, Spurny P, Bland PA (2010) The orbit and atmospheric trajectory of the Orgueil meteorite from historical records. Meteorit Planet Sci 41:135–150

Grady MM, Pratesi G, Cecchi VM (2014) Atlas of meteorites. Cambridge University Press, New York

Greenwood RC, Franchi IA, Kearsley AT, Alard O (2010) The relationship between CK and CV chondrites. Geochim Cosmochim Acta 74:1684–1705

Krot AN, Keil K, Goodrich C, Weisberg MK, Scott ERD (2013) Classification of meteorites. In: Davis AM, Holland HD, Turekian KK (eds) Meteorites and cosmochemical processes, Treatise on geochemistry, vol 1. Elsevier, Oxford, pp 1–63

Lodders K (2003) Solar system abundances and condensation temperatures of the elements. Astron J 591:1220–1247

Nakamura T, Noguchi T, Tanaka M et al (2011) Itokawa dust particles: a direct link between S-type asteroids and ordinary chondrites. Science 333:1113–1116

Scott ERD, Krot AN (2013) Chondrites and their components. In: Davis AM, Holland HD, Turekian KK (eds) Meteorites and cosmochemical processes, Treatise on geochemistry, vol 1. Elsevier, Oxford, pp 65–137

Stoffler D, Keil K, Scott ERD (1991) Shock metamorphism of ordinary chondrites. Geochim Cosmochim Acta 55:3845–3867

Van Schmus WR, Wood JA (1967) A chemical-petrologic classification for the chondritic meteorites. Geochim Cosmochim Acta 31:747–765

Chondrules

Rhian Jones

School of Earth and Environmental Sciences, The University of Manchester, Manchester, UK

Definition

Chondrules are the most abundant component of chondrite meteorites. The term chondrule comes from the ancient Greek word for the kernel of a grain of wheat, χονδρος (chondros), which chondrules roughly resemble in size and shape. Chondrules are rounded, millimeter, or submillimeter stone particles. They are among the oldest solid materials in the solar system. Shapes and textures of chondrules indicate that they formed from molten droplets which were floating freely in the gas of the protoplanetary disk at the time of cooling and solidification. After formation, chondrules accreted with other materials to form asteroids, from which chondrite meteorites are derived. There is debate about the heating process that melted chondrules and the environment in which they formed. Properties of chondrules can be used to infer physical and chemical conditions within the protoplanetary disk in the first few million years of solar system history.

Chemistry and Mineralogy of Chondrules

Chondrules constitute up to 80% by volume of ordinary (O) and enstatite (E) chondrites and approximately 50% of carbonaceous (C) chondrites (Scott and Krot 2014, Zanda 2004). This high abundance has been used to estimate that chondrules made up about 10^{24} g of material in the early solar system (Desch et al. 2012), and thus they provide an important record of materials that remain from the protoplanetary disk environment. The description of chondrules presented here considers only the primary properties of chondrules, i.e., properties that pertain to their formation and history prior to incorporation into the asteroid parent bodies of their host chondrites. Most chondrites have undergone secondary processing after accretion to their parent asteroids, to varying degrees, including aqueous alteration, heating that resulted in metamorphism, and/or shock resulting from impacts. Primary properties of chondrules must often be deduced by considering the nature of any alteration and disentangling effects that may have altered or erased primary signatures. Chondrules occur in all chondrite groups except for the CI chondrites, which have undergone complete aqueous alteration of the initially anhydrous assemblage, to the extent that any chondrules that were originally present have been obliterated.

The basic chemical and mineralogical properties of individual chondrules are similar, but they differ in detail. Chondrule chemistry varies widely both within and among chondrite groups and classes (Jones et al. 2005; Jones 2012). Average major element contents for bulk chondrules (Fe, Mg, Si, Ca, Al) are similar to solar or CI chondrite abundances, and there is little fractionation among refractory elements (e.g., Ca, Al, Ti, Mg, rare earth elements). However, bulk compositions of individual chondrules are variable, for example, within a single chondrite the ratio of refractory elements to Si can vary by about a factor of 3, and the Fe/Si ratio can vary by more than an order of magnitude. Abundances of moderately volatile elements (e.g., Mn, Na, K, S) are also highly variable among individual chondrules.

In all chondrite groups, there is a range of chondrule textures (Connolly and Desch 2004; Lauretta et al. 2006; Jones 2012; Scott and Krot 2014) (Fig. 1). The dominant silicate minerals are olivine ($(Mg,Fe)_2SiO_4$) and pyroxene
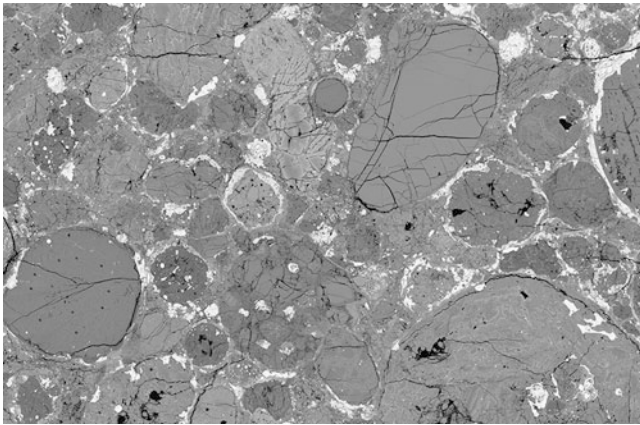
Chondrules, Fig. 1 The Semarkona ordinary chondrite: back-scattered electron image, ~9 mm across. Chondrules are round or have rounded outlines. Individual chondrules have different textures, as well as different chemical compositions. The most abundant minerals are olivine and pyroxene, for which darker shades of *gray* correspond to higher $Mg/(Mg + Fe)$ ratio. *White* grains are metal and/or sulfide (Image by J. Lewis)

$((Mg,Fe,Ca)_2Si_2O_6)$: individual chondrules have varying ratios of olivine/pyroxene, from 100% olivine to 100% pyroxene, and an interstitial feldspathic phase that may be crystalline feldspar $(CaAl_2Si_2O_8\text{-}NaAlSi_3O_8)$ or glass. Chondrules also contain varying amounts of Fe-Ni metal and/or sulfide minerals. In most chondrules, olivine and pyroxene grains have regular crystal forms: these chondrules are described as having porphyritic textures. Olivine and pyroxene can also show a range of morphologies that are a function of growth rate including hopper morphologies, elongate barred grains (usually bars of olivine), radiating needles, and cryptocrystalline textures. Two common types of chondrules are defined based on their textures and chemical characteristics (Brearley and Jones 1998). Type I chondrules are chemically reduced: olivine and pyroxene have a high atomic $Mg/(Mg + Fe)$ ratio, commonly around 0.99, and they contain abundant metallic iron, commonly kamacite $(Fe_{\sim0.95}Ni_{\sim0.05})$. Type II chondrules are more oxidized: olivine and pyroxene have lower atomic $Mg/(Mg + Fe)$ ratios than type I chondrules, and olivine and pyroxene grains usually show strong growth zoning (igneous zoning), e.g., $Mg/(Mg + Fe)$ ratios from around 0.8 to 0.7 in ordinary chondrites. Compared with type I chondrules, type II chondrules contain less metallic iron but more iron sulfide (typically troilite, FeS), and they have higher abundances of moderately volatile elements than type I chondrules (Na, Mn, P, S).

The majority of olivine and pyroxene grains in chondrules crystallized from melt as the droplet cooled. There is also a population of identifiable grains called relict grains which were inherited from previous generations of chondrules and did not melt during the heating event (Jones 2012). These include MgO-rich olivine (forsterite) in type II chondrules and relict grains of MgO-rich olivine in type I chondrules. Relict grains termed dusty olivine are grains of FeO-rich olivine that were incorporated into type I chondrules. During the heating event that melted the type I chondrule, the FeO-rich olivine grain underwent reduction, and small blebs of Fe metal precipitated which give the grain a dusty appearance in transmitted or reflected light. Chemical compositions and oxygen isotope compositions of relict grains are consistent with formation in previous generations of chondrules and provide evidence that there were multiple heating episodes in the chondrule-formation region. Further evidence for repeated heating is found in igneous rims on chondrules: these represent a second episode of heating that melted a dusty rim that was deposited after the host chondrule solidified.

There are significant differences in the chondrule populations among the different chondrite classes and groups (Jones 2012). These include properties such as mean chondrule sizes and the distribution of different textural types of chondrules. There are chemical differences between chondrules of similar textural type that occur in different chondrite groups, and abundances of relict grains in chondrules of the same textural type vary among chondrite groups. Also, chondrules from O, C, and E chondrites have different oxygen isotope compositions. Differences in chondrule properties specific to individual chondrite groups indicate that the disk was chemically heterogeneous and that chondritic asteroids accreted from localized batches of materials.

Oxygen Isotope Compositions of Chondrules

Oxygen isotope compositions of early solar system materials are an important record of relationships among different components of chondrites, as well as among different chondrite groups. In an oxygen three-isotope diagram ($\delta^{17}O$ vs. $\delta^{18}O$, where $\delta^nO = [(^nO/^{16}O)_{sample}/(^nO/^{16}O)_{SMOW} - 1]^*10^3$ and SMOW = standard mean ocean water), mass-dependent isotopic fractionation results in a distribution of compositions along a line of slope 0.52, an example of which is the terrestrial fractionation line, TFL. Oxygen isotope compositions of chondrules in O, E, and C chondrites lie above, along, and below TFL, respectively (Clayton 2003; Krot et al. 2006; Yurimoto et al. 2008; Scott and Krot 2014). Chondrules have significantly higher values of $\delta^{17}O$ and $\delta^{18}O$ than calcium-aluminum inclusions (CAIs), which have $\delta^{18}O$ values around −40‰, close to values inferred for the sun. For bulk chondrules, $\delta^{18}O$ values are typically in the range −10 to +7‰. Oxygen isotope compositions of chondrules in C chondrites lie on arrays that have a slope close to one on the oxygen three-isotope diagram, which indicates mixing of

isotopic reservoirs that were related by non-mass-dependent processes. Isotopic self-shielding, possibly within the protoplanetary disk or in its precursor molecular cloud, could have led to an isotopically heavy ice component that evaporated in the region of chondrule formation and became incorporated into chondrule materials (Clayton 2003; Krot et al. 2006; Yurimoto et al. 2008).

Chondrule Precursor Material

Since chondrules are solidified melt droplets, the precursor material from which they formed has largely been erased during melting. Relict grains are a direct record of precursor material that would have been present as grains tens of micrometers across in the precursor assemblage. The remainder of the precursor material was probably a fine-grained mixture of silicates, metal, and sulfide grains (e.g., Jones et al. 2005), although in chondrule-formation models that involve collisions between molten planetesimals, the predominant precursor material would have been molten. Matrix in chondritic meteorites consists of a fine-grained assemblage of silicate, oxide, metal, and sulfide materials (Scott and Krot 2014), but it is not chemically equivalent to material needed for chondrule precursors. Chondrules and matrix show chemical complementarity in that their combined chemistry is similar to solar abundances, suggesting that each chondrite group formed in a chemical reservoir of broadly solar composition, after condensation of refractory, common, and moderately volatile elements.

A group of chondrules described as aluminum-rich chondrules spans the compositional gap between CAIs and the common ferromagnesian chondrules (Connolly and Desch 2004). Relict fragments of CAIs are observed in these chondrules (Krot et al. 2009). Oxygen isotope compositions of chondrules from C chondrites also show clear relationships to CAIs and other types of refractory inclusions. Hence, fragments of CAIs are plausible components of chondrule precursor material.

Thermal Histories of Chondrules

Thermal histories of chondrules have been deduced from their textures and mineralogy, as well as from analogue experiments (Desch and Connolly 2004; Hewins et al. 2005; Lauretta et al. 2005; Jones et al. 2005; Desch et al. 2012). The ambient temperature prior to heating was below the temperature at which sulfur condensed from the solar nebula gas, <400 °C. Peak temperatures for chondrule formation were close to the temperature of complete melting of the chondrule material, around 1500–1600 °C. The duration of

heating at the peak temperature was short, seconds to minutes, in order to retain moderately volatile elements such as Na and S that would evaporate during an extended period of melting. Retention of Na also requires a high gas density. After melting, chondrules cooled at rates that range from around five to several hundreds of degrees per hour. These cooling rates are constrained by laboratory experiments that reproduce chondrule textures, as well as considerations such as the development of igneous growth zoning in olivine and dissolution rates of relict grains. The wide range of cooling rates is responsible for production of different chondrule textures because morphologies of olivine and pyroxene grains are a function of growth rate, which is a function of undercooling. Chondrule cooling rates are significantly slower than cooling rates that would result from black-body radiation of isolated molten droplets into free space, indicating that they formed in a gas of higher density (Alexander and Ebel 2012).

Ages of Chondrules

Chondrules formed within the first few million years of solar system history. Absolute ages of chondrules determined by high-precision Pb-Pb radiometric dating range from 4567 to 4565 Ma (see Krot et al. 2009; Wadhwa 2014). Ages are also measured based on chronometers that use extinct short-lived radioisotopes that were present in the early solar system, such as ^{26}Al which decays to ^{26}Mg with a half-life of 0.75 My. Most ^{26}Al ages for chondrules are within 1–3 million years after the CAI formation age (4567 Ma) (Krot et al. 2009; Desch et al. 2012; Kita and Ushikubo 2012). Hence, chondrule formation appears to have begun contemporaneously with CAI formation and persisted throughout the time period when planetesimals were accreting. Most measured chondrule ages are younger than the time scales of differentiation on the earliest planetesimals (Wadhwa 2014). It is possible that chondrule formation occurred prior to formation of those bodies and that earlier generations of chondrules no longer exist because the bodies in which they were incorporated have been melted.

Chondrules in the metal-rich CB and CH chondrite groups differ from other O, C, and E groups. Chondrules in the CB_a chondrites are unusually large (up to cm sized), whereas those in the CB_b and CH chondrites are small (mean diameters 0.5 and <0.1 mm, respectively). These meteorites have a high proportion of non-porphyritic chondrules (Scott and Krot 2014). They likely formed in a large impact plume that resulted from a collision involving a metal-rich body. Ages of chondrules in CB chondrites are significantly younger than typical chondrules in most chondrite groups, 4563 Ma, so they probably formed after the nebular gas had dissipated (Desch et al. 2014; Wadhwa 2014).

Chondrule-Formation Models

Chondrule-formation models must take into account the chemical, isotopic, and physical properties of chondrules and the constraints those properties impose. A variety of models has been proposed to account for the rapid heating and cooling events that chondrules experienced, but no single model is clearly preferred. Models include heating in a shock front as a result of gas drag combined with radiant heat, heating in the X-wind that lofted chondrules above the nebular midplane in the magnetocentrifugal outflow, lightning within the disk, collisions involving partially or completely molten planetesimals, and collisions involving solid planetesimals (e.g., Connolly and Desch 2004; Desch et al. 2012; Johnson et al. 2015). For the shock model, chondrule formation could have occurred in the bow shock of a planetesimal moving through the disk in an eccentric orbit or in the shock front associated with gravitational instabilities in the disk. A chondrule-formation process has not been detected directly in astronomical observations of protoplanetary disks around young stellar objects.

Summary

Chondrules formed from partially to fully molten liquid droplets that solidified into approximately spherical, (sub) millimeter-sized beads. They formed within one to three million years of the formation of the first solids in the solar system. Chondrules have approximately chondritic chemical compositions and consist predominantly of olivine, pyroxene, a feldspathic phase, metal, and sulfide. Chemical, isotopic, and physical properties of chondrules vary among the different chondrite groups. Chondrule cooling rates inferred from their textures and mineralogy are between a few to several hundred degrees per hour. Models for the mechanism that resulted in chondrule formation include heating within shock fronts and collisions between either solid or partially molten planetesimals during the early stages of formation of the solar system.

Cross-References

▶ Aluminum
▶ Chondrites
▶ Experimental Mineralogy and Petrology
▶ Geochronology and Radiogenic Isotopes
▶ Iron
▶ Meteorites
▶ Mineralogy
▶ Refractory Inclusions in Chondritic Meteorites
▶ Silicate Melts
▶ Silicate Minerals

References

Alexander CMO'D, Ebel DS (2012) Questions, questions: can the contradictions between the petrologic, isotopic, thermodynamic, and astrophysical constraints on chondrule formation be resolved? Meteorit Planet Sci 47:1157–1175

Brearley AJ, Jones RH (1998) Chondritic meteorites. In: Papike JJ (ed) Planetary materials. Reviews in mineralogy, vol 36. Mineralogical Society of America, Chantilly, pp 3-1–3-398

Clayton RN (2003) Oxygen isotopes in meteorites. In Davis AM (ed) Meteorites, comets and planets. Treatise on geochemistry, vol 1. Elsevier, Oxford, pp 129–142

Connolly HC Jr, Desch SJ (2004) On the origin of the "kleine Kügelchen" called chondrules. Chem Erde 64:95–125

Desch SJ, Morris MA, Connolly HC, Boss AP (2012) The importance of experiments: constraints on chondrule formation models. Meteorit Planet Sci 47:1139–1156

Hewins RH, Connolly HC Jr, Lofgren GE, Libourel G (2005) Experimental constraints on chondrule formation. In Krot AN, Scott ERD, Reipurth B (eds) Chondrites and the protoplanetary disk. Astronomical Society of the Pacific conference series, 341. Astronomical Society of the Pacific, San Francisco, pp 286–316

Johnson BC, Minton DA, Melosh HJ, Zuber MT (2015) Impact jetting as the origin of chondrules. Nature 517:339–341

Jones RH (2012) Petrographic constraints on the diversity of chondrule reservoirs in the protoplanetary disk. Meteorit Planet Sci 47:1176–1190

Jones RH, Grossman JN, Rubin AE (2005) Chemical, mineralogical and isotopic properties of chondrules: clues to their origins. In Krot AN, Scott ERD, Reipurth B (eds) Chondrites and the protoplanetary disk. Astronomical Society of the Pacific conference series, 341. Astronomical Society of the Pacific, San Francisco, pp 251–285

Kita NT, Ushikubo T (2012) Evolution of protoplanetary disk inferred from ^{26}Al chronology of individual chondrules. Meteorit Planet Sci 47:1108–1119

Krot AN, Yurimoto H, McKeegan KD, Leshin L, Chaussidon M, Libourel G, Yoshitake M, Huss GR, Guan Y, Zanda B (2006) Oxygen isotopic compositions of chondrules: implications for evolution of oxygen isotopic reservoirs in the inner solar nebula. Chem Erde 66:249–276

Krot AN, Amelin Y, Bland P, Ciesla FJ, Connelly J, Davis AM, Huss GR, Hutcheon ID, Makide K, Nagashima K, Nyquist LE, Russell SS, Scott ERD, Thrane K, Yurimoto H, Yin Q-Z (2009) Origin and chronology of chondritic components: a review. Geochim Cosmochim Acta 73:4963–4997

Lauretta DS, Nagahara H, Alexander CMO'D (2006) Petrology and origin of ferromagnesian silicate chondrules. In: Lauretta DS, McSween HY (eds) Meteorites and the early solar system II. University of Arizona Press, Tucson, pp 431–459

Scott ERD, Krot AN (2014) Chondrites and their components. In Davis AM (ed) Meteorites and cosmochemical processes, 2nd edn. Treatise on geochemistry, vol 1. Elsevier, Oxford, pp 65–137

Wadhwa M (2014) Solar system time scales from long-lived radioisotopes in meteorites and planetary materials. In Davis AM (ed) Meteorites and cosmochemical processes, 2nd edn. Treatise on geochemistry, vol 1. Elsevier, Oxford, pp 397–418

Yurimoto H, Krot AN, Choi BG, Aléon J, Kunihiro T, Brearley AJ (2008) Oxygen isotopes of chondritic components. In: MacPherson GJ (ed) Oxygen in the solar system. Reviews in mineralogy, vol 68. Mineralogical Society of America, Chantilly, pp 141–186

Zanda B (2004) Chondrules. Earth Planet Sci Lett 224:1–17

Chromium

Monica Vasiliu and David A. Dixon
Department of Chemistry, University of Alabama,
Tuscaloosa, AL, USA

Element Data
Atomic Symbol: Cr.
Atomic Number: 24.
Atomic Weight: 51.9961.
Isotopes and Abundances: ^{50}Cr 4.35%, ^{52}Cr 83.79%, ^{53}Cr 9.50%, ^{54}Cr 2.36%.
1 Atm Melting Point: 2130 ± 20 K.
1 Atm Boiling Point: 2945.
Common Valences: 2, 3, 4, 6.
Ionic Radii: (+II) 84, (+III) 64, (+IV) 56, (+VI) 44 ppm.
Pauling Electronegativity: 1.66.
First Ionization Potential: 6.76 eV.
Chondritic (CI) Abundance: 2660 ppm.
Silicate Earth Abundance: 2625 ppm.
Crustal Abundance: ~100 ppm.
Seawater Abundance: 0.2 ppb.
Core Abundance: 0.90%.

Properties

Chromium (Emsley 1991, 2001; Anthoni 2006; Anders and Grevesse 1989; McDonough 2005) is a lustrous, brittle, hard, and very corrosion-resistant metal. It has a silver-gray color with a blue tinge and it can be highly polished. It does not tarnish in air, but when heated it burns forming the green chromic oxide. Chromium is unstable in oxygen as it immediately reacts to form a thin oxide layer that is impermeable to oxygen and protects the metal below. Chromium dissolves in HCl and H_2SO_4 but not in H_3PO_4. None of the naturally occurring chromium isotopes are radioactive.

History and Use

Chromium was discovered in 1797 by Louis Nicolas Vauquelin while experimenting with a material known as Siberian red lead, the mineral crocoite ($PbCrO_4$). He produced chromium oxide by mixing crocoite with hydrochloric acid. Although he believed a method for isolating chromium didn't yet exist, Vauquelin showed in 1798 that he was able to obtain metallic chromium by simply heating chromium oxide in a charcoal oven.

Chromium can be polished to form a very shiny surface and is often plated to other metals to form a protective and attractive covering. Chromium is added to steel to harden it and to form stainless steel, an iron-based alloy that contains at least 10% chromium. Other chromium-steel alloys are used to make armor plate, safes, ball bearings, and cutting tools. Chromium compounds are also used to anodize aluminum, a process which coats aluminum with a thick, protective layer of oxide. Chromite, chromium's primary ore, is used to make molds for the firing of bricks because of its high melting point, moderate thermal expansion, and stable crystal structure.

Crocoite or lead chromate is also known as chrome yellow and has been used as a yellow pigment in paints. Chromic oxide (Cr_2O_3), also known as chrome green, is the ninth most abundant compound in the Earth's crust and is a widely used green pigment. Ruby (variety of corundum, Al_2O_3) and emerald (variety of beryl, $Be_3Al_2(SiO_3)_6$) owe their colors to chromium compounds. Potassium dichromate ($K_2Cr_2O_7$) is used in the tanning of leather, while other chromium compounds are used as mordants (materials which permanently fix dyes to fabrics). Chromium(IV) oxide (CrO_2) is used to manufacture magnetic tape.

Geochemical Behavior

Chromium is not found free in nature and is found mainly as chromite. This ore is found in many places including South Africa, India, Kazakhstan, and Turkey. Chromium metal is usually produced by reducing chromite with carbon in an electric-arc furnace or reducing chromium(III) oxide with aluminum or silicon.

Chromium enters the air, water, and soil in the chromium (III) and chromium(VI) oxidation states through natural processes and human activities. Most of the chromium in air will eventually settle and end up in waters or soils. Chromium in soils strongly attaches to soil particles and as a result it will not move toward groundwater. In water, chromium will absorb on sediment and become immobile. Only a small part of the chromium that ends up in water will eventually dissolve.

The main human activities that increase the concentrations of chromium(III) are steel, leather, and textile manufacturing. The main human activities that increase chromium(VI) concentrations are chemical, leather, and textile manufacturing and electro painting, as industrial examples. These applications will mainly increase concentrations of chromium in water. Through coal combustion, chromium will also end up in air, and through waste disposal, chromium will end up in soils.

Sodium dichromate is a corrosion inhibitor and was added to the Columbia River water used to cool the nuclear reactors, which produced plutonium for nuclear weapons at the

Hanford site in Washington, USA. Some of this material spilled or leaked from pipes leading to soil contamination. Large holes of at least 26 m deep and more than 5000 m² at the top were dug down to the groundwater. Approximately two million tons of contaminated soil containing an estimated 129 tons of concentrated chromium was removed and transported to a lined landfill at Hanford. The most contaminated soil is mixed with cement to prevent additional leaching. This led to the reduction of risk to a key salmon spawning region in the Columbia River.

Biological Utilization and Toxicity

Chromium(III) is an essential trace element for organisms including humans, who consume approximately 1 mg a day, because it can disrupt the sugar metabolism pathway, for example, leading to heart conditions, when the daily dose is too low (Vincent 2013). Like other metals that organisms require in trace amounts, chromium can be quite toxic, especially chromium(VI) (chromates (CrO_4^{2-})), which can alter genes, for example, causing cancer. Humans can be exposed to chromium through breathing, eating, or drinking and skin contact with chromium or chromium-containing compounds. The level of chromium in air and water is generally low; however, conytaminated well water may contain the dangerous hexavalent chromium(VI). Food consumption is the main route of chromium(III) uptake, as chromium(III) occurs naturally in many vegetables, fruits, meats (kidneys), yeasts, and grains (brewer's yeast, wheat germ). Various methods of food preparation and storage may alter the chromium content of food; for example, food stored in steel tanks or cans can absorb chromium.

Crops contain biological control systems that arrange the chromium uptake to be low enough not to cause any harm, but when the amount of chromium in the soil rises, this can lead to higher concentrations in crops. Acidification of soil can also influence chromium uptake by crops. Plants usually absorb only chromium(III). This may be the essential kind of chromium, but when concentrations exceed a certain value, negative impacts on animal health can still occur.

Chromium is not known to accumulate in the bodies of fish, but high concentrations of chromium, due to the disposal of metal products in surface waters, can damage the gills of fish that swim near the point of disposal. In animals, chromium can cause respiratory problems, a lower ability to fight disease, birth defects, infertility, and tumor formation.

Cross-References

► Chromium Isotopes
► Transition Elements

References

Anders E, Grevesse N (1989) Abundances of the elements: Meteoritic and solar. Geochimica et Cosmochimica Acta 53:197–214. http://meteorites.wustl.edu/goodstuff/chondritic_abundances.htm

Anthoni JF (2006) The chemical composition of seawater in. http://www.seafriends.org.nz/oceano/seawater.htm

Emsley J (1991) The elements, 2nd edn. Clarendon Press, Oxford

Emsley J (2001) Nature's building blocks an A-Z guide to the elements. Oxford University Press, Oxford

McDonough WF (2005) Compositional model for the Earth's core. In: Carlson RW (ed) The Mantle and Core. Elsevier, Oxford, pp. 547–568. http://www.knowledgedoor.com/2/elements_handbook/element_abundances_in_the_earth_s_core.html

Vincent JB (2013) The bioinorganic chemistry of chromium. Wiley, Chichester, p 1213

Chromium Isotopes

Devon B. Cole[1], Xiangli Wang[1], Liping Qin[2],
Noah J. Planavsky[1] and Christopher T. Reinhard[3]
[1]Department of Geology and Geophysics, Yale University, New Haven, CT, USA
[2]Department of Earth and Space Science, China University of Science and Technology, Hefei, Hubei, China
[3]School of Earth and Atmospheric Science, Georgia Institute of Technology, Atlanta, GA, USA

Definition

Chromium has four naturally occurring stable isotopes (^{50}Cr, ^{52}Cr, ^{53}Cr, and ^{54}Cr) with natural abundances of 4.35%, 83.79%, 9.50%, and 2.36%, respectively. Among these, ^{50}Cr, ^{52}Cr, and ^{54}Cr are nonradiogenic, while ^{53}Cr is the radiogenic product of ^{53}Mn, an extinct nuclide with a half-life of 3.7 Myr. Chromium isotope variations in terrestrial samples are reported using the ratio $^{53}Cr/^{52}Cr$, expressed in conventional delta notation ($\delta^{53}Cr$) relative to NIST SRM 979, a metallic Cr standard from the National Institute of Standards and Technology. In meteorite samples, the ratio $^{54}Cr/^{52}Cr$ is sometimes used to report nuclear synthetic anomalies (conventionally reported in epsilon notation). Chromium isotopes have a wide range of applications in cosmochemistry, geochemistry, and environmental remediation efforts.

Introduction

The earliest work on Cr isotopes was largely focused on cosmochemical processes, namely the application of the short-lived ^{53}Mn-^{53}Cr radiochronometer to date early solar system events (e.g., Birck and Allègre 1984). Other early

work was been driven by the need to monitor hexavalent Cr as an environmental contaminant, which has resulted in a well-developed framework for understanding low-temperature mass-dependent Cr isotope systematics. Building on this foundation, there has been a surge of recent work focused on using Cr isotopes as a paleoredox proxy. Most recently, work has also focused on improving our understanding of Cr cycling on the modern Earth surface and on developing a global isotope mass balance for the Cr system. Given the broad scope of Cr isotope work, we will touch only briefly on each of the primary applications for the system and then highlight aspects of the Cr system that have drawn recent attention.

Methods

Chromium isotopes can be measured either by thermal ionization mass spectrometry (TIMS) or by multicollector inductively coupled plasma source mass spectrometry (MC-ICP-MS). Typically a tracer containing known concentrations of two isotopes (most commonly ^{50}Cr and ^{54}Cr) is added to samples prior to sample preparation. This method, known as the "double-spike" method, can be used to correct for any fractionation during sample preparation or analysis based on the known and measured ^{50}Cr/^{54}Cr ratio. Due to isobaric interferences with ^{51}V, ^{49}Ti, and ^{56}Fe, and the relatively small range of Cr isotopic variation seen in nature, chemical purification of samples is required prior to analysis. This is typically accomplished via column chromatography using cation or anion exchange methods (e.g., Schoenberg et al. 2008; Yamakawa et al. 2009), followed by additional column purification to remove remaining Fe, Ti, and V. Analysis on TIMS is relatively straightforward – Cr is ionized at ~1200–1400 °C, which is below the temperatures required to efficiently ionize Fe. Interferences during MC-ICP-MS analysis can be much more problematic, in particular polyatomic interferences associated with the use of Ar as a plasma gas. These require the measurement of Cr on the "shoulder," instead of in the center of a flat peak as is typical of most systems. Additionally, these analyses typically must be conducted with a high mass resolution instrument in order to distinguish Cr and Fe peaks (Weyer and Schwieters 2003).

Cosmochemistry

Early work on chromium isotope systematics in natural materials focused on mass-independent effects, i.e., radiogenic effects on ^{53}Cr, and nucleosynthetic effects on ^{54}Cr. Mass-independent Cr isotopic composition are typically expressed in ε notation (deviation of the isotopic ratio of the sample

from the standard multiplied by 10,000). In contrast to mass-dependent measurements, measured isotope ratios are corrected for the mass-dependent fractionations that occur naturally and during sample preparation and instrumental analysis by assuming a natural ratio for two isotopes (often least affected by mass-independent effects) of the same element. In the case of Cr, ^{50}Cr and ^{52}Cr are usually used for normalization.

The decay product of short-lived nuclide ^{53}Mn (half-life 3.7 Myr) is ^{53}Cr (Kaye and Cressy 1965). Due to the relatively short half-life, the change in parent/daughter ratio was extremely large during the early evolution of the solar system, and thus short-lived nuclide systems are sensitive to tracking events during this period. Further, because the parent isotope is extinct, examination of the change in daughter isotopes (differentiation between Mn and Cr leads to varying Mn/Cr ratio and thus different ^{53}Cr ingrowth) can further provide age information. ^{53}Mn-^{53}Cr is one of the few short-lived chronometers that have achieved prominence (Birck and Allègre 1985, 1988; Rotaru et al. 1992; Lugmair and Shukolyukov 1998), which is partially due to the relatively high abundances of both Mn and Cr in many solar system objects. These applications are explored further by McKeegan and Davis (2014) and Qin and Wang (2017).

In a second application of mass-independent fractionation, anomalies in ^{54}Cr/^{52}Cr relative to terrestrial rocks have been reported for both bulk meteorites and individual meteorite components (Birck and Allègre 1984; Papanastassiou 1986; Rotaru et al. 1992; Podosek et al. 1997; Trinquier et al. 2008; Qin et al. 2011). These are thought to be the result of incomplete mixing of nuclides synthesized in different nucleosynthetic sources with distinct isotopic signatures. Such isotope anomalies have been found for a range of other elements in addition to Cr (further discussed by Qin and Carlson (2016)). These isotope anomalies have been very useful for identifying the sources of materials accreted into the early solar nebula. Anomalies at the whole meteorite scale are especially useful for understanding heterogeneity in the solar nebula, can act as fingerprints of specific meteorites, and can be used to probe the genetic relationship between different meteorite groups.

High-Temperature Terrestrial Settings

Mass-dependent fractionation of Cr under high-T settings is much less constrained compared to that under low-T settings. This limits the application of Cr isotopes to trace geological and planetary processes. Such studies are also important for constraining the Cr isotope inventories of major terrestrial reservoirs, which often serve as the basis for the application of Cr isotopes in low-T settings. An early study by Schoenberg et al. (2008) found a limited variation in the Cr isotopic

composition of different types of igneous rocks and marine sediments, and the bulk silicate earth (BSE) value of $\delta^{53}Cr$ was therein estimated to be $-0.124 \pm 0.101‰$. These authors argued for a homogeneous mantle source and limited Cr isotopic fractionation during partial melting and magma differentiation (Schoenberg et al. 2008). Chondrites show a similarly limited range of variations (Qin and Carlson 2016; Bonnand et al. 2016b; Schoenberg et al. 2016). A recent Cr isotopic study by Xia et al. (2017) on mantle xenoliths from various locations showed much larger variation ($\delta^{53}Cr$ ranging from $-1.36‰$ to $0.75‰$), than found by Schoenberg et al. (2008). Although some of the variations are likely due to secondary processes such as metasomatism and these results suggest some mantle heterogeneity, the variation is mainly caused by interaction of mantle peridotites with silicate melts long before they were brought to the surface. This study also confirmed that partial melting does not lead to significant Cr isotopic fractionation. The most recent estimate of the BSE value is $-0.14 \pm 0.12‰$ (Xia et al. 2017), in concert with the previously determined value (Schoenberg et al. 2008). Studies on subducted continental and oceanic crusts showed that dehydration does not fractionation Cr isotopes, probably due to limited dissolution of Cr(III) in the fluids or limited amounts of fluid generated (Shen et al. 2015; Wang et al. 2016a). However, serpentinized oceanic crusts have been shown to be significantly isotopically heavier than BSE (Wang et al. 2016a; Xia et al. 2017) and the missing isotopically light source warrants future studies.

Further insights on high-T Cr isotopic behavior can be gained from the study of intermineral isotopic fractionation of mantle minerals. Based on first-principle calculations, Moynier et al. (2011) made theoretical estimations of Cr isotopic fractionation between co-existing minerals under conditions of planetary core-mantle segregation. The differences between most Cr(II) and Cr(0)-bearing minerals are minor at high temperatures, but the difference between those with Cr(III) and Cr(0) can be much larger. Farkaš et al. (2013) observed that chromites of different origins all have slightly heavier Cr isotopic compositions (with an average $\delta^{53}Cr$ value of $-0.079 \pm 0.129‰$) than the BSE value. This finding was confirmed in a later study by Shen et al. (2015). Lunar mare basalts show Cr isotopic variation correlated with MgO content, likely due to spinel crystallization (Bonnand et al. 2016a). More modeling and laboratory observations are needed to further characterize mineral-scale Cr isotope heterogeneity.

Environmental Applications

Chromium has two major species in the natural surface environment – trivalent and hexavalent – denoted as Cr(III)

and Cr(VI), respectively. Cr(VI) is carcinogenic and soluble in aquatic solution, while Cr(III) is sparingly soluble and can act as a micronutrient (Bartlett and Kimble 1976, 1979; Rai et al. 1987, 1989; Fendorf 1995). The major source of Cr (VI) to the environment is from industrial activities such as electrical plating and leather tanning (e.g., Megharaj et al. 2003), although geogenic pollution can also occur in areas covered with Cr-rich ultramafic bedrocks (e.g., Bartlett and James 1979; Oze et al. 2007).

The reduction of Cr(VI) to insoluble Cr(III) can remove Cr(VI) from groundwater (e.g., Cheung and Gu 2007; Dhal et al. 2013). Natural attenuation (Palmer and Puls 1994), active remediation (e.g., the use of permeable reactive barriers (Blowes et al. 1997, 2000; Puls et al. 1999; Wilkin et al. 2005) and biostimulation (Oliver et al. 2003; Cheung and Gu 2007; Dhal et al. 2013)) has been used to remove potentially dangerous levels of Cr(VI) from groundwater. Cr isotopes are a key tool used to monitor the effectiveness of these techniques. Light isotopes are preferentially reduced (and removed from groundwater) relative to heavy ones, leading to systematically increasing $\delta^{53}Cr$ in the remaining Cr(VI) thereby creating a means to track the extent of reduction and removal of Cr from this soluble pool (e.g., Ellis et al. 2002; Basu and Johnson 2012). The preferential reduction of light isotopes is linked to weaker chemical bonds in lower mass isotopes (Urey 1947; Bigeleisen 1965).

Numerous laboratory and field studies have been conducted to determine the fractionation factor during reduction (α). The α values determined in the lab range from as high as 0.9996 ($-0.04‰$) to as low as 0.9920 ($-8‰$) (see Qin and Wang 2017 for a more detailed review), in contrast to the narrower range observed in the field, which range from ca. 0.3‰ to ca. $-2‰$ (Berna et al. 2010; Izbicki et al. 2012). Lower fractionations derived from field studies likely result from a diffusion-reaction process, where Cr(VI) must diffuse into isolated reduction zones and the isotopically fractionated Cr(VI) can then diffuse back into solution (e.g., Clark and Johnson 2008). This systematic change in $\delta^{53}Cr$ during reduction can be described by a Rayleigh distillation model whereby groundwater $\delta^{53}Cr$ will become increasingly heavy as mobile Cr (VI) is reduced (e.g., Ellis et al. 2002; Scott et al. 2004; Abe and Hunkeler 2006).

Interpretation of Cr isotope data from field samples requires a clear understanding of several nonredox-dependent processes. Significantly, adsorption of Cr(VI) to mineral surfaces does not induce Cr isotope fractionation (Ellis et al. 2004) and therefore does not interfere with the use of Cr isotopes in tracking reduction. However, isotope exchange between remaining Cr(VI) and previously formed Cr(III) (Altman and King 1961) can lead to large isotope fractionations (Schauble et al. 2004; Wang et al. 2015). The
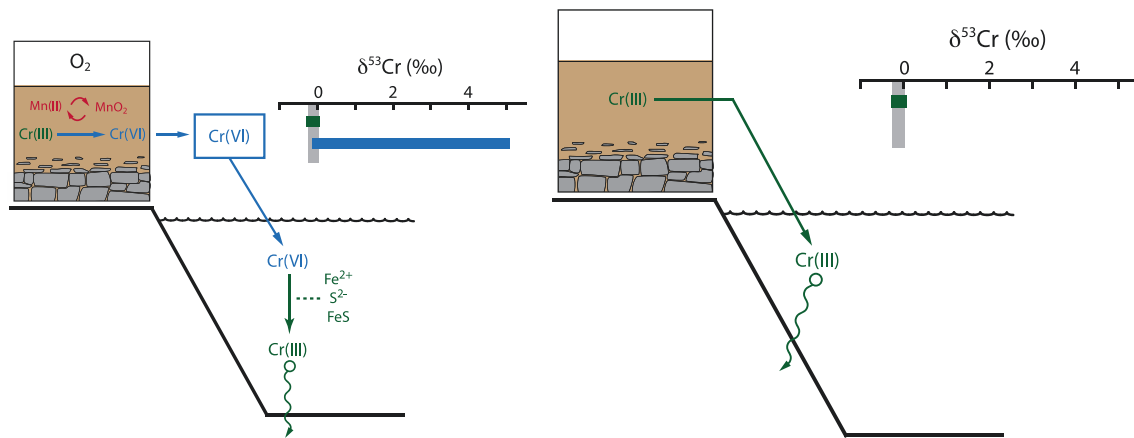
Chromium Isotopes, Fig. 1 Schematic of Cr cycle as a paleobarometer for atmospheric oxygen level. Large Cr isotope fractionations are expected in an oxic world (left hand side), while limited fractionations are expected in an anoxic world

timescale and impact of isotope exchange depends on the Cr concentrations and the relative masses of dissolved Cr (VI) and exposed Cr(III). Therefore, field conditions must be taken into account to assess uncertainties related to isotope exchange when using groundwater $\delta^{53}Cr$ to detect and quantify the extent of Cr(VI) reduction. Furthermore, additional complications can arise from solubilization of Cr(III) by organic ligands and reoxidation of previously formed Cr (III) (e.g., Bartlett and James 1979; Buerge and Hug 1998), which are still poorly understood. In sum, the Cr isotope system is useful redox proxy that can move forward our understanding of hexavalent Cr contamination. However, potential complications regarding isotope exchange, ligand mobilization, and oxidation continue to pose challenges and offer future research opportunities.

Cr Isotopes as a Paleoredox Proxy

More recently, Cr isotopes have emerged as a tracer of Earth's atmospheric oxygenation (e.g., Frei et al. 2009, 2013; Crowe et al. 2013; Planavsky et al. 2014; Cole et al. 2016; Gilleaudeau et al. 2016). The simplest application of Cr isotopes as a paleoredox proxy relies on the basic idea that variability of $\delta^{53}Cr$ in sedimentary rocks requires mobile Cr (VI) on Earth's surface and that the oxidation of Cr(III) to Cr (VI), via Mn oxides, requires free oxygen. The isotopic variability of this mobile pool has been demonstrated in modern riverine and marine systems (e.g., Bonnand et al. 2013; Frei et al. 2014; Scheiderich et al. 2015; Wu et al. 2017; D'Arcy et al. 2016; Farkaš et al. 2013; Novak et al. 2014), while the potential to record these signals in sedimentary archives has also been demonstrated in modern systems (e.g., Reinhard et al. 2014; Gueguen et al. 2016; Pereira et al. 2016; Wang et al. 2016b). Oxidized and mobile Cr(VI) is isotopically

enriched, while residual soils are isotopically depleted. Using this framework, a lack of variability in the $\delta^{53}Cr$ sedimentary record should be indicative of very low surface oxygen levels, not capable of inducing oxidative Cr cycling, while the onset of variability in the $\delta^{53}Cr$ record should mark a shift to oxidative terrestrial weathering of Cr and an oxidized surface environment (Fig. 1).

Initial paleoredox Cr isotope studies have focused on reconstructing this record of Earth's oxygenation using banded iron formations (BIFs) and ironstones as an archive for Cr (Frei et al. 2009; Planavsky et al. 2014). These sediments can provide an ideal sedimentary archive as they are likely to develop large authigenic (seawater-derived) Cr enrichments with little detrital input and should be well rock-buffered and therefore resistant to later diagenetic influence. Unfortunately, these formations are not common throughout the rock record, and while they indicate a shift to an oxidizing Earth surface by the early Neoproterozoic, these records lack necessary temporal resolution. Significantly however, the oxygen level at which surface Cr oxidation can proceed has been suggested as ~0.1% and 1% present atmospheric levels (PAL), based on kinetics of Mn oxidation and the lack of available Fe(II) in order to prevent reduction, respectively (Crowe et al. 2013; Planavsky et al. 2014). These estimates are below theoretical and experimental estimates for the minimum oxygen needs of the earliest complex animals (Sperling et al. 2013; Mills et al. 2014). As such, understanding the timing of this shift to and Earth system capable of the terrestrial oxidative weathering of Cr has major implications for understanding the rise of complex life and the relationship between biologic innovation and environmental factors.

A number of other sedimentary archives also have the potential to record shifts in the $\delta^{53}Cr$ record, including organic-rich black shales and carbonates, which are both

ubiquitous throughout the rock record. Work on shales has demonstrated that these sediments are capable of recording modern marine variability in δ^{53}Cr values in the recent sedimentary record (e.g., Reinhard et al. 2014; Gueguen et al. 2016), and this archive has been expanded into deep time, providing increased resolution in understanding the transition to an oxidizing Earth surface, just prior to the earliest evidence of complex life (Cole et al. 2016). Additional work on shales from the Cretaceous shows a negative δ^{53}Cr excursion, coincident with Ocean Anoxic Event II, suggesting that with new developments in our understanding of the Cr mass balance there is also potential to track marine redox changes in the sedimentary record (Wang et al. 2016c).

Others have focused on investigating δ^{53}Cr isotopes in carbonates, both in laboratory experiments and in modern settings, as well as in deep time records. Laboratory work has suggested that moderate fractions are possible during carbonate precipitation when Cr(VI) is incorporated in to the crystal lattice (Tang et al. 2007; Rodler et al. 2015). These abiogenic fractionations were observed to be ~0.3‰, while biogenic uptake can vary much more significantly, ranging from −0.5 to 0.3‰ in corals, and showing species-dependent variations in foraminiferal calcification (Rodler et al. 2015; Pereira et al. 2016; Wang et al. 2016b). Further, there has not yet been an investigation of Cr(III) incorporation into carbonates and the fractionations that could be associated with this process. Despite these complexities, the currently observed abiogenic fractionations are small enough that abiogenic carbonates could potentially record a shift in Earth's redox state (e.g., Frei et al. 2011; Gilleaudeau et al. 2016). Gilleaudeau et al. (2016) reported both unfractionated and some fractionated δ^{53}Cr values from bulk carbonate analyses as ~1.1 Ga, which if primary, would suggest oxygen levels above ~0.1–1% PAL by the late Mesoproterozoic. However, carbonate rocks can be susceptible to later diagenetic alteration, and trace metal signatures are frequently diagenetic in origin as these lithologies are somewhat poorly rock-buffered (e.g., Brand and Veizer 1980; Jahn and Cuvellier 1994).

In sum, the Cr isotope system, even in its relatively nascent state as a paleoredox proxy, has proven a sensitive and useful tool in shaping our understanding of Earth's redox evolution. With further developments in our understanding of modern systems, the Cr mass balance, and sedimentary archives, this system is poised to provide many new high-resolution insights into the redox story of Earth's oceans and atmosphere through time.

Summary and Conclusions

Chromium isotopes are now an established system being routinely measured in a wide range of applications. Work in this system has revealed important new insights in the fields of cosmochemistry, environmental remediation and monitoring procedures, and most recently in reconstructing Earth's redox evolution, which has been a major contribution to the ongoing debate about the relationship between environmental factors and the evolution of life on this planet.

Cross-References

▶ Chromium
▶ Paleoenvironments

References

Abe Y, Hunkeler D (2006) Does the Rayleigh equation apply to evaluate field isotope data in contaminant hydrogeology? Environ Sci Technol 40:1588–1596

Altman C, King EL (1961) The mechanism of the exchange of chromium (III) and chromium(VI) in acidic solutions. J Am Chem Soc 83:2825–2830

Bartlett R, James B (1979) Behavior of chromium in soils: III. Oxidation. J Environ Qual 8:31–35

Bartlett R, Kimble J (1976) Behavior of chromium in soils: II. Hexavalent forms. J Environ Qual 5:383–386

Basu A, Johnson TM (2012) Determination of hexavalent chromium reduction using Cr stable isotopes: isotopic fractionation factors for permeable reactive barrier materials. Environ Sci Technol 46:5353–5360

Berna EC, Johnson TM, Makdisi RS, Basu A (2010) Cr stable isotopes as indicators of Cr (VI) reduction in groundwater: a detailed time-series study of a point-source plume. Environ Sci Technol 44:1043–1048

Bigeleisen J (1965) Chemistry of isotopes. Science 147:463

Birck J-L, Allègre CJ (1984) Chromium isotopic anomalies in Allende refractory inclusions. Geophys Res Lett 11:943–946

Birck J-L, Allègre CJ (1985) Evidence for the presence of 53Mn in the early solar system. Geophys Res Lett 12:745

Birck J-L, Allègre CJ (1988) Manganese chromium isotope systematics and development of the early solar system. Nature 331:579–584

Blowes DW, Ptacek CJ, Jambor JL (1997) In-situ remediation of Cr (VI)-contaminated groundwater using permeable reactive walls: laboratory studies. Environ Sci Technol 31:3348–3357

Blowes DW, Ptacek CJ, Benner SG, McRae CW, Bennett TA, Puls RW (2000) Treatment of inorganic contaminants using permeable reactive barriers. J Contam Hydrol 45:123–137

Bonnand P, James RH, Parkinson IJ, Connelly DP, Fairchild IJ (2013) The chromium isotopic composition of seawater and marine carbonates. Earth Planet Sci Lett 382:10–20

Bonnand P, Parkinson IJ, Anand M (2016a) Mass dependent fractionation of stable chromium isotopes in mare basalts: implications for the formation and the differentiation of the Moon. Geochim Cosmochim Acta 175:208–221

Bonnand P, Williams H, Parkinson I, Wood B, Halliday A (2016b) Stable chromium isotopic composition of meteorites and metal–silicate experiments: implications for fractionation during core formation. Earth Planet Sci Lett 435:14–21

Brand U, Veizer J (1980) Chemical diagenesis of a multicomponent carbonate system – 1: trace elements. J Sediment Res 50:1219–1236

Buerge IJ, Hug SJ (1998) Influence of organic ligands on chromium (VI) reduction by iron(II). Environ Sci Technol 32:2092–2099

Cheung K, Gu J-D (2007) Mechanism of hexavalent chromium detoxification by microorganisms and bioremediation application potential: a review. Int Biodeterior Biodegrad 59:8–15

Clark SK, Johnson TM (2008) Effective isotopic fractionation factors for solute removal by reactive sediments: a laboratory microcosm and slurry study. Environ Sci Technol 42:7850–7855

Cole DB, Reinhard CT, Wang X, Gueguen B, Halverson GP, Gibson T, Hodgskiss MSW, McKenzie NR, Lyons TW, Planavsky NJ (2016) A shale-hosted Cr isotope record of low atmospheric oxygen during the Proterozoic. Geology 44:555

Crowe SA, Dossing LN, Beukes NJ, Bau M, Kruger SJ, Frei R, Canfield DE (2013) Atmospheric oxygenation three billion years ago. Nature 501:535–538

D'Arcy J, Babechuk MG, Døssing LN, Gaucher C, Frei R (2016) Processes controlling the chromium isotopic composition of river water: constraints from basaltic river catchments. Geochim Cosmochim Acta 186:296–315

Dhal B, Thatoi H, Das N, Pandey B (2013) Chemical and microbial remediation of hexavalent chromium from contaminated soil and mining/metallurgical solid waste: a review. J Hazard Mater 250:272–291

Ellis AS, Johnson TM, Bullen TD (2002) Chromium isotopes and the fate of hexavalent chromium in the environment. Science 295:2060

Ellis AS, Johnson TM, Bullen TD (2004) Using chromium stable isotope ratios to quantify Cr (VI) reduction: lack of sorption effects. Environ Sci Technol 38:3604–3607

Farkaš J, Chrastny V, Novak M, Cadkova E, Pasava J, Chakrabarti R, Jacobsen SB, Ackerman L, Bullen TD (2013) Chromium isotope variations ($\delta^{53/52}$Cr) in mantle-derived sources and their weathering products: implications for environmental studies and the evolution of $\delta^{53/52}$Cr in the Earth's mantle over geologic time. Geochim Cosmochim Acta 123:74–92

Fendorf SE (1995) Surface reactions of chromium in soils and waters. Geoderma 67:55–71

Frei R, Gaucher C, Poulton SW, Canfield DE (2009) Fluctuations in Precambrian atmospheric oxygenation recorded by chromium isotopes. Nature 461:250–253

Frei R, Gaucher C, Døssing LN, Sial AN (2011) Chromium isotopes in carbonates – a tracer for climate change and for reconstructing the redox state of ancient seawater. Earth Planet Sci Lett 312:114–125

Frei R, Gaucher C, Stolper D, Canfield DE (2013) Fluctuations in late Neoproterozoic atmospheric oxidation – Cr isotope chemostratigraphy and iron speciation of the late Ediacaran lower Arroyo del Soldado Group (Uruguay). Gondwana Res 23:797–811

Frei R, Poiré D, Frei KM (2014) Weathering on land and transport of chromium to the ocean in a subtropical region (Misiones, NW Argentina): a chromium stable isotope perspective. Chem Geol 381:110–124

Gilleaudeau G, Frei R, Kaufman A, Kah L, Azmy K, Bartley J, Chernyavskiy P, Knoll A (2016) Oxygenation of the mid-Proterozoic atmosphere: clues from chromium isotopes in carbonates. Geochem Perspect Lett 2:178–187

Gueguen B, Reinhard CT, Algeo TJ, Peterson LC, Nielsen SG, Wang X, Rowe H, Planavsky NJ (2016) The chromium isotope composition of reducing and oxic marine sediments. Geochim Cosmochim Acta 184:1–19

Izbicki JA, Bullen TD, Martin P, Schroth B (2012) Delta Chromium-53/52 isotopic composition of native and contaminated groundwater, Mojave Desert, USA. Appl Geochem 27:841–853

Jahn B-M, Cuvellier H (1994) Pb–Pb and U–Pb geochronology of carbonate rocks: an assessment. Chem Geol 115:125–151

Kaye J, Cressy P (1965) Half-life of manganese-53 from meteorite observations. J Inorg Nucl Chem 27:1889–1892

Lugmair GW, Shukolyukov A (1998) Early solar system timescales according to ^{53}Mn-^{53}Cr systematics. Geochim Cosmochim Acta 62:2863–2886

McKeegan KD, Davis AM (2014) Early solar system chronology. In: Turekian KK, Holland HD (eds) Treatise on geochemistry, 2nd edn. Elsevier, Oxford/San Diego, pp 431–460

Megharaj M, Avudainayagam S, Naidu R (2003) Toxicity of hexavalent chromium and its reduction by bacteria isolated from soil contaminated with tannery waste. Curr Microbiol 47:0051–0054

Mills DB, Ward LM, Jones C, Sweeten B, Forth M, Treusch AH, Canfield DE (2014) Oxygen requirements of the earliest animals. Proc Natl Acad Sci U S A 111:4168–4172

Moynier F, Yin Q-Z, Schauble E (2011) Isotopic evidence of Cr partitioning into Earth's core. Science 331:1417–1420

Novak M, Chrastny V, Čadková E, Farkas J, Bullen T, Tylcer J, Szurmanova Z, Cron M, Prechova E, Curik J (2014) Common occurrence of a positive δ^{53}Cr shift in Central European waters contaminated by geogenic/industrial chromium relative to source values. Environ Sci Technol 48:6089–6096

Oliver DS, Brockman FJ, Bowman RS, Kieft TL (2003) Microbial reduction of hexavalent chromium under vadose zone conditions. J Environ Qual 32:317–324

Oze C, Bird DK, Fendorf S (2007) Genesis of hexavalent chromium from natural sources in soil and groundwater. Proc Natl Acad Sci U S A 104:6544–6549

Palmer CD, Puls RW (1994) Natural attenuation of hexavalent chromium in ground water and soils. U.S. Environmental Protection Agency Ground Water Issue. EPA/540/5-94/505, Washington DC, pp 1–12

Papanastassiou DA (1986) Chromium isotopic anomalies in the Allende meteorite. Astrophys J 308:L27–L30

Pereira NS, Voegelin AR, Paulukat C, Sial AN, Ferreira VP, Frei R (2016) Chromium-isotope signatures in scleractinian corals from the Rocas Atoll, Tropical South Atlantic. Geobiology 14:54–67

Planavsky NJ, Reinhard CT, Wang X, Thomson D, McGoldrick P, Rainbird RH, Johnson T, Fischer WW, Lyons TW (2014) Low mid-Proterozoic atmospheric oxygen levels and the delayed rise of animals. Science 346:635–638

Podosek FA, Ott U, Brannon JC, Neal CR, Bernatowicz TJ (1997) Thoroughly anomalous chromium in Orgueil. Meteorit Planet Sci 32:617–627

Puls RW, Paul CJ, Powell RM (1999) The application of in situ permeable reactive (zero-valent iron) barrier technology for the remediation of chromate-contaminated groundwater: a field test. Appl Geochem 14:989–1000

Qin L, Carlson RW (2016) Nucleosynthetic isotope anomalies and their cosmochemical significance. Geochem J 50:43–65

Qin L, Wang X (2017) Chromium isotope geochemistry. Rev Mineral Geochem 82:379–414

Qin L, Carlson RW, Alexander CMOD (2011) Correlated nucleosynthetic isotopic variability in Cr, Sr, Ba, Sm, Nd and Hf in Murchison and QUE 97008. Geochim Cosmochim Acta 75:7806–7828

Rai D, Sass BM, Moore DA (1987) Chromium(III) hydrolysis constants and solubility of chromium(III) hydroxide. Inorg Chem 26:345–349

Rai D, Eary L, Zachara J (1989) Environmental chemistry of chromium. Sci Total Environ 86:15–23

Reinhard CT, Planavsky NJ, Wang X, Fischer WW, Johnson TM, Lyons TW (2014) The isotopic composition of authigenic chromium in anoxic marine sediments: a case study from the Cariaco Basin. Earth Planet Sci Lett 407:9–18

Rodler A, Sánchez-Pastor N, Fernández-Díaz L, Frei R (2015) Fractionation behavior of chromium isotopes during coprecipitation with

calcium carbonate: implications for their use as paleoclimatic proxy. Geochim Cosmochim Acta 164:221–235

Rotaru M, Birck J-L, Allègre CJ (1992) Clues to early solar system history from chromium isotopes in carbonaceous chondrites. Nature 358:465–470

Schauble E, Rossman GR, Taylor HP Jr (2004) Theoretical estimates of equilibrium chromium-isotope fractionations. Chem Geol 205:99–114

Scheiderich K, Amini M, Holmden C, Francois R (2015) Global variability of chromium isotopes in seawater demonstrated by Pacific, Atlantic, and Arctic Ocean samples. Earth Planet Sci Lett 423:87–97

Schoenberg R, Zink S, Staubwasser M, Von Blanckenburg F (2008) The stable Cr isotope inventory of solid Earth reservoirs determined by double spike MC-ICP-MS. Chem Geol 249:294–306

Schoenberg R, Merdian A, Holmden C, Kleinhanns IC, Haßler K, Wille M, Reitter E (2016) The stable Cr isotopic compositions of chondrites and silicate planetary reservoirs. Geochim Cosmochim Acta 183:14–30

Scott K, Lu X, Cavanaugh C, Liu J (2004) Optimal methods for estimating kinetic isotope effects from different forms of the Rayleigh distillation equation. Geochim Cosmochim Acta 68:433–442

Shen J, Liu J, Qin L, Wang SJ, Li S, Xia J, Ke S, Yang J (2015) Chromium isotope signature during continental crust subduction recorded in metamorphic rocks. Geochem Geophys Geosyst 16:3840–3854

Sperling EA, Halverson GP, Knoll AH, Macdonald FA, Johnston DT (2013) A basin redox transect at the dawn of animal life. Earth Planet Sci Lett 371–372:143–155

Tang Y, Elzinga EJ, Jae Lee Y, Reeder RJ (2007) Coprecipitation of chromate with calcite: batch experiments and X-ray absorption spectroscopy. Geochim Cosmochim Acta 71:1480–1493

Trinquier A, Birck J-L, Allègre CJ, Göpel C, Ulfbeck D (2008) ^{53}Mn-^{53}Cr systematics of the early solar system revisited. Geochim Cosmochim Acta 72:5146–5163

Truex M, Vermeul V, Fruchter J (2009) Treatability testing of an in situ bio-stimulation barrier for nitrate and chromium treatment. 2009 Waste Management Symposium - WM2009/WM'09: HLW, TRU, LLW/ILW, Mixed, Hazardous Wastes and Environmental Management - Waste Management for the Nuclear Renaissance, United States

Urey HC (1947) The thermodynamic properties of isotopic substances. J Chem Soc (Resumed) 562–581

Wang X, Johnson TM, Ellis AS (2015) Equilibrium isotopic fractionation and isotopic exchange kinetics between Cr (III) and Cr (VI). Geochim Cosmochim Acta 153:72–90

Wang X, Planavsky NJ, Reinhard CT, Zou H, Ague JJ, Wu Y, Gill BC, Schwarzenbach EM, Peucker-Ehrenbrink B (2016a) Chromium isotope fractionation during subduction-related metamorphism, black shale weathering, and hydrothermal alteration. Chem Geol 423:19

Wang X, Planavsky NJ, Hull PM, Tripati AE, Zou HJ, Elder L, Henehan M (2016b) Chromium isotopic composition of core-top planktonic foraminifera. Geobiology 15:51–64

Wang X, Reinhard CT, Planavsky NJ, Owens JD, Lyons TW, Johnson TM (2016c) Sedimentary chromium isotopic compositions across the Cretaceous OSE2 at Demerara Rise Site 1258. Chem Geol 429:85–92

Weyer S, Schwieters J (2003) High precision Fe isotope measurements with high mass resolution MC-ICPMS. Int J Mass Spectrom Ion Process 226:355–368

Wilkin RT, Su C, Ford RG, Paul CJ (2005) Chromium-removal processes during groundwater remediation by a zerovalent iron permeable reactive barrier. Environ Sci Technol 39:4599–4605

Wu W, Wang X, Reinhard CT, Planavsky NJ (2017) Chromium isotope systematics in the Connecticut River. Chem Geol 456:98

Xia J, Qin L, Shen J, Carlson RW, Ionov DA, Mock TD (2017) Chromium isotope heterogeneity in the mantle. Earth Planet Sci Lett. https://doi.org/10.1016/j.epsl.2017.1001.1045

Yamakawa A, Yamashita K, Makishima A, Nakamura E (2009) Chemical separation and mass spectrometry of Cr, Fe, Ni, Zn, and Cu in terrestrial and extraterrestrial materials using thermal ionization mass spectrometry. Anal Chem 81:9787–9794

Clapeyron's Equation

Masaki Akaogi
Department of Chemistry, Gakushuin University, Tokyo, Japan

Definition

We consider here that a substance changes from a reactant phase to a product phase and that both the phases are in equilibrium at pressure (P) and temperature (T). Clapeyron's equation expresses the stability relation between the reactant and product phases and gives a dP/dT slope of equilibrium phase boundary between the reactant and the product as a function of P and T. This equation is one of the most important equations for understanding thermodynamic stability relations in geochemical, petrological, and mineralogical processes. For example, when α-quartz SiO_2 is in equilibrium with coesite at certain P, T conditions, Clapeyron's equation gives the slope of the equilibrium quartz-coesite transition boundary in a P-T space where quartz is stable at relatively lower P and higher T and coesite at relatively higher P and lower T.

Clapeyron's Equation

When reactant and product phases are in equilibrium at P and T, and changes of entropy (ΔS) and volume (ΔV) accompany with the reaction at P and T, Clapeyron's equation is given as:

$$dP/dT = \Delta S/\Delta V \qquad (1)$$

If the reaction reaches equilibrium state, $\Delta H = T\Delta S$, where ΔH is enthalpy of reaction. Therefore, Eq. 1 is rewritten as:

$$dP/dT = \Delta H/T\Delta V \qquad (2)$$

Note that ΔS, ΔV, and ΔH are entropy, volume, and enthalpy changes at the P, T conditions considered. In principle, the values of ΔS, ΔV, and ΔH cannot be assumed as constants along the equilibrium phase boundary, and

therefore the slope is not constant. However, in solid-solid phase transitions in limited P, T ranges, ΔS, ΔV, and ΔH may generally be approximated as constants, resulting in a constant slope. In reactions involving vapor or liquid phase, the boundary is generally curved, because the vapor or liquid phase has higher entropy and is more compressible than the solid phase. Several textbooks on thermodynamics show a simple derivation of Clapeyron's equation from thermodynamic principles (e.g., Richet 2001).

It should be noted that Clapeyron's equation is applicable to the first-order phase transitions but cannot be applied to the second-order transitions in which both ΔS and ΔV are zero. Clapeyron's equation is useful for understanding stability relations of a substance and for constructing phase diagrams by combining with Schreinemaker's rule.

Summary

Clapeyron's equation is widely used in thermodynamics for materials of geochemical, petrological, and mineralogical interests. One of important applications of Clapeyron's equation in the fields is to evaluate dP/dT slopes of phase transition boundaries in silicates at high pressure and high temperature. In particular, dissociation reaction of spinel-type $(Mg,Fe)_2SiO_4$ to perovskite-type $(Mg,Fe)SiO_3$ and $(Mg,Fe)O$, called the post-spinel transition, which occurs at 660 km depth in the Earth's mantle, has a phase boundary with a negative dP/dT slope. The transition with the negative Clapeyron slope provides substantial resistance for subduction of slabs, resulting in significant effects on mantle dynamics and geochemical evolution of the mantle (e.g., Christensen 1995).

Cross-References

- ▶ Enthalpy
- ▶ Entropy
- ▶ Equilibrium
- ▶ Experimental Mineralogy and Petrology
- ▶ Free Energy
- ▶ Geochemical Thermodynamics
- ▶ Geothermometry and Geobarometry
- ▶ Mantle Geochemistry
- ▶ Phase Equilibria

References

Christensen U (1995) Effects of phase transitions on mantle convection. Annu Rev Earth Planet Sci 23:65–87
Richet P (2001) The physical basis of thermodynamics. Kluwer/Plenum Publishers, New York, 442 pp

Clay Membranes

Ian C. Bourg
Department of Civil and Environmental Engineering and Princeton Environmental Institute, Princeton University, Princeton, NJ, USA

Definition

Clay membranes are clay-rich media (soils, sediments, or sedimentary rocks) that exhibit partial restriction of solute migration relative to that of water, i.e., semipermeable membrane properties.

Geochemical Importance

Clay membrane properties have the potential to significantly modulate the groundwater hydrology of clay-rich media, at least in some cases. They have been studied as a potential cause of erratic fluid pressures in sedimentary formations and, also, because of their potential impacts on well-bore stability, chemico-osmotic consolidation, water and nutrient fluxes in soils, and waste isolation using natural and engineered clay barriers (Takeda et al. 2014).

Phenomenology

Clay membranes give rise to two geochemical phenomena: hyperfiltration and osmosis. Hyperfiltration occurs when a hydraulic pressure gradient drives water flow across a clay membrane. For solutes that exhibit restricted migration through the membrane, the solute concentration of the permeate is depleted by a dimensionless factor σ known as the osmotic efficiency or solute reflection coefficient.

Osmosis occurs when a clay membrane separates two aqueous reservoirs with different concentrations of a solute. The associated gradients in chemical potential give rise to a diffusive flux of solute toward the dilute reservoir and of water toward the concentrated reservoir. If the porous medium separating the two reservoirs partially restricts solute migration relative to that of water, a net flux of solution (the osmotic flux) occurs toward the concentrated reservoir.

Reported values of σ in fine-grained sedimentary rocks range from 0 to 0.5, with a tendency of σ to increase with decreasing permeability and salinity (Takeda et al. 2014). Values of σ up to ~1.0 have been reported in compacted smectite or bentonite samples, with a strong dependence on salt concentration, counterion valence, and compaction (Kemper and Rollins 1966; Malusis et al. 2012).

Fundamental Basis

Porous media exhibit semipermeable membrane properties if their pores are sufficiently narrow that steric or electrostatic effects significantly hinder solute migration. In clay membranes, the predominant mechanism is the partial exclusion of anions from the electrical double layer (EDL), the region of interfacial water where electrolyte ions screen the negative surface charge of the clay particles. Anion exclusion restricts the migration of anions through the clay membrane and, therefore, that of cations because of the electroneutrality requirement.

   Theories of the structure of the electrical double layer, such as the Gouy-Chapman model, predict that anion exclusion has a characteristic length scale d_a equal to twice the Debye length (Tournassat and Appelo 2011). At room temperature in a 0.1 M NaCl electrolyte, d_a equals ~2 nm on each pore wall, suggesting that anions are almost completely excluded from pores narrower than ~4 nm. The anion exclusion thickness d_a varies with the inverse square root of ionic strength and decreases significantly in the presence of multivalent cations.

   In clay-rich sedimentary rocks, the largest pore-width mode observed by nitrogen adsorption or mercury intrusion porosimetry is often on the order of ~10 nm. This value is consistent with the observation that the anion-accessible pore space equals roughly half of the total pore space in many clay-rich rocks. Together, these observations suggest that most fine-grained sedimentary rocks have the potential to behave as clay membranes, particularly in aqueous chemistry conditions where the Debye length is large (low salinity, Na^+ as the predominant exchangeable cation) and where pores are small (low porosity, high content of smectite clay).

Mathematical Formulation

At the macroscopic scale, solution volumetric flux $\mathbf{J}_v$ (m s^{-1}) and solute molar flux relative to solution $\mathbf{J}^d_s$ (mol m^{-2} s^{-1}) in clay membranes are commonly described using the following pair of equations derived from non-equilibrium thermodynamics:

$$\mathbf{J}_v = L_{11}\nabla P + L_{12}\nabla\mu_s \qquad (1)$$

$$\mathbf{J}^d_s = L_{21}\nabla P + L_{22}\nabla\mu_s \qquad (2)$$

where $L_{12} = L_{21}$ based on Onsager's reciprocity rule. The most appropriate formulation of the L_{ij} parameters is not entirely settled, however, as noted below. One possible formulation yields the following expressions for $\mathbf{J}_v$ and for the

net solute flux $\mathbf{J}_s = c_s\mathbf{J}_v + \mathbf{J}^d_s$ (Malusis et al. 2012; Takeda et al. 2014):

$$\mathbf{J}_v = -(k/\mu)\Big(\Delta P - \sigma\nabla\prod\Big) \qquad (3)$$

$$\mathbf{J}_s = (1 - \sigma)c_s\mathbf{J_v} - D_e\nabla c_s \qquad (4)$$

where k is the intrinsic permeability of the porous medium (m^2), μ is the dynamic viscosity of the solution (Pa s), P is pressure (Pa), Π is osmotic pressure (Pa), D_e is the effective diffusion coefficient of the solute in the porous medium (m^2 s^{-1}), and c_s is solute concentration (mol m^{-3}). The osmotic pressure gradient ideally is given by Van't Hoff's relation: $\Pi = \nu RTc_s$, where R is the ideal gas constant (Pa m^3 mol^{-1} K^{-1}), T is absolute temperature (K), and ν is the number of constituents in the solute (e.g., $\nu = 2$ for NaCl).

Unresolved Issues

Several incompletely resolved issues exist in the study of clay membrane properties, particularly with regard to the choice of formulation for the L_{ij} parameters in Eqs. 1 and 2 (Bader and Kooi 2005; Malusis et al. 2012). For example, the common assumption that $\mathbf{J}_v$ is accurately described by Darcy's law if $\nabla\mu_s = 0$ yields an advective coefficient $L_{11} = k/\mu$. The definition of the reflection coefficient can then be used to write $\sigma = -L_{12}/c_sL_{11}$, which yields $L_{12} = -\sigma (k/\mu) c_s$. This formulation (used in Eq. 3) describes the osmotic flux of solution as an advective phenomenon (dependent on k) even though its fundamental origin is a difference in the diffusive fluxes of water and solute.

   A second unresolved issue is whether a full characterization of clay membrane behavior requires two parameters: the reflection coefficient σ describing the tendency of the solute to resist *advection* through the membrane and an additional coefficient σ_d describing the tendency of the solute to resist *diffusion* through the membrane (Katchalsky and Curran 1965). Geochemical studies have often used the simplifying assumption $\sigma_d = \sigma$ while noting that the validity of this assumption is not entirely settled (Bader and Kooi 2005; Malusis et al. 2012).

   A third important conceptual question is the manner in which Eqs. 1 and 2 should be solved in clay membranes of non-negligible thickness, where $\mathbf{J}_v$ and $\mathbf{J}^d_s$ are not inherently at steady state. Existing schemes rely on treating σ as invariant with time (Takeda et al. 2014), despite strong evidence that σ can vary significantly with time if salt diffusion and cation exchange occur in the membrane (Shackelford and Lee 2003).

A fourth important question is whether membrane efficiency (σ) can be correlated with other properties of the porous medium (Malusis et al. 2012). Experimental results suggest possible correlations with salinity, in agreement with the strong salinity dependence of EDL thickness, and permeability, in agreement with the expected sensitivity of both permeability and membrane efficiency to the width and connectivity of the largest pores (Takeda et al. 2014). Relatively little progress has been made on relating these results to the microstructure of clayey media, because of the difficulty of precisely characterizing the pore networks that control σ in these media and because the microstructure itself, in some cases, is sensitive to salinity (Tournassat and Appelo 2011).

Summary

Clay membrane behavior is relatively widely observed in sedimentary rocks and compacted clay barriers. Observations of this behavior reflect conditions where flow in a clay-rich medium is controlled by pores with a pore width on the order of ~10 nm or less. The osmotic efficiency of clay membranes decreases significantly with increasing salinity, pore width, and counterion valence. Significant conceptual questions remain unanswered with regard to the geochemical modeling of clay membranes.

Cross-References

▶ Clay Minerals
▶ Diffusion
▶ Soils

References

Bader S, Kooi H (2005) Modelling of solute and water transport in semipermeable clay membranes: comparison with experiments. Adv Water Resour 28:203–214

Katchalsky A, Curran PF (1965) Biophysics. Harvard University Press, Cambridge, MA, 248 pp

Kemper WD, Rollins JB (1966) Osmotic efficiency coefficients across compacted clays. Soil Sci Soc Am Proc 30:529–534

Malusis MA, Shackelford CD, Maneval JE (2012) Critical review of coupled flux formations for clay membranes based on nonequilibrium thermodynamics. J Contam Hydrol 138–139:40–59

Shackelford CD, Lee J-M (2003) The destructive role of diffusion on clay membrane behavior. Clay Clay Miner 51:186–196

Takeda M, Hiratsuka T, Manaka M, Finsterle S, Ito K (2014) Experimental examination of the relationships among chemico-osmotic, hydraulic, and diffusion parameters of Wakkanai mudstones. J Geophys Res Solid Earth 119

Tournassat C, Appelo CAJ (2011) Modelling approaches for anion-exclusion in compacted Na-bentonite. Geochim Cosmochim Acta 75:3698–3710

Clay Minerals

Josh Wimpenny
Nuclear and Chemical Sciences Division, Lawrence Livermore National Laboratory, Livermore, CA, USA

C

Definition

Clay minerals are a diverse group of minerals that are fine grained and crystalline and ultimately form from the aqueous alteration of primary igneous minerals at or near the surface of the Earth. They have a layered structure, commonly consisting of repeating sheets of Si tetrahedra and Al octahedra. The wide diversity of clay minerals stems from the way that these sheets stack together and the identity of ions that commonly substitute into the clay mineral structure. Due to their unique layered structure and their effectiveness as ion exchangers, the formation of clay minerals can have a significant impact over the chemical and isotopic compositions of solid and fluid phases during weathering.

Introduction

Clay minerals are a highly diverse and abundant group of minerals that derive from the interaction of water with rock in the Earth's crust. Because clay minerals are often found in the clay-size fraction of sediments and soils (i.e., below 2 µm), the terms "clay" and "clay minerals" are often used interchangeably. However, the term clay minerals refers to a distinct group of minerals with a layered structure, rather than having grain-size significance.

Clay minerals are comprised of repeating aluminosilicate layers (or sheets), and the way that these sheets stack together helps to control their physical properties and chemical composition. Clay minerals form in a range of conditions (pH, temperature, pressure), and clay-rich sediments result from a range of different formation mechanisms, from solid-state alteration to dissolution and neoformation, to detrital inheritance (Singer 1980). Due to their layered structures, large surface area, and prevalence in the Earth's crust, the formation of clay minerals can have a significant impact over the chemical and isotopic composition of crustal rocks, sediments, and soils, and understanding how and when clay minerals have formed can shape our understanding of past weathering regimes and changes in the Earth's climate. Furthermore, the alteration of primary silicate minerals and formation of clay minerals have a significant impact on the chemical and isotopic composition of crustal fluids, including rivers, lakes,

and groundwaters, and, ultimately, help to control the past chemical composition of the Earth's oceans.

The unique physical and chemical properties of clay minerals mean that understanding how and why they form is critical in our understanding of natural processes, such as changes in past climate and crustal cycling, as well as facilitating our development of natural resources such as aquifers and oil and gas fields. Our utilization of clay minerals goes further still. Clay minerals are currently directly involved in many industrial applications and find their way into our homes where they are used on a daily basis, from ceramics to building materials to the production of paper, as well as in major engineering projects such as dams and landfill sites. Clay minerals are found in a wide range of environments, from soils and weathering profiles, to hydrothermal systems, to lake and estuaries and deep sea sediments. The ubiquitous occurrence of clay minerals on Earth has even helped to guide our ongoing exploration of the solar system. Recently, the Mars rover Curiosity was sent to a clay-rich region of the red planet because of the link between formations of clay minerals with liquid water. The finding of clay minerals on Mars suggests a distant past with a once water-rich environment that could have harbored life.

In this summary of clay mineralogy, we will discuss (i) the basics of clay mineralogy, (ii) the most common types of clay minerals and their uses, (iii) the ion exchange processes and their significance in influencing the chemical composition of rivers and the oceans, and (iv) the human uses for clay minerals.

Clay Mineral Structure and Ion Exchange

The basic structure of clay minerals consists of repeating sequences of Si-O tetrahedra (T) and Al-O octahedra (O) that form layers or sheets that bind together by sharing oxygens (Merkel et al. 2005). In tetrahedral coordination, the central cation is surrounded by four oxygen atoms, while in octahedral coordination, the central cation is surrounded by six oxygen atoms. The distinctive clay mineralogies and their chemical and physical properties are, to a first order, controlled by how these sheets of Si tetrahedra and Al octahedra stack together. For this reason, clay minerals are often described by the ratio of T:O layers in their structure. For example, the kaolin group of clay minerals is comprised of tightly packed alternating T-O units and so is called 1:1 clay minerals. Another common group of clay minerals, the mica group, consists of repeating T-O-T units and so is referred to as 2:1 clay minerals. The 2:1 clay minerals are some of the most common in the crust and include the highly abundant mineral smectite, vermiculite, and illite. The layer of oxygen atoms that bound the basal tetrahedral layer in a 2:1 clay mineral is often referred to as the siloxane layer (e.g., Sposito

et al. 1999), and the characteristic spacing between adjacent tetrahedral layers is called the interlayer (Drever 1988).

While the basic structure of clay minerals is dominated by Si and Al, clay minerals can contain significant quantities of other cations due to structural substitution reactions. The most common is the replacement of Si^{4+} in the tetrahedral sheet by Al^{3+}, with a limit to ~15% substitution (Krauskopf and Bird 1967), and replacement of Al^{3+} in the octahedral sheet, in which both the identity of the exchanging cation and the amount of substitution can vary. The most common cations that exchange into the octahedral sheet are Mg^{2+}, Fe^{2+}, and Ca^{2+}. In these isomorphic substitutions, the charge of the replacing cation is less important than the length of the cation-oxygen bond. For this reason, these substitutions often result in a charge imbalance, which is typically negative and is considered to be permanent (Odom 1984; Drever 1988; Appelo and Postma 2005; Merkel et al. 2005). An example is the substitution of Mg^{2+} for Al^{3+} in the octahedral layer of pyrophyllite, resulting in the formation of the common smectite group mineral montmorillonite. This isomorphic substitution of cations into structural layers can be significant; in the case of montmorillonite, the clay can contain upward of 3 Wt % Mg (Mermut and Cano 2001). Isomorphic substitutions are not common in all clay minerals; they do not occur to any significance in the kaolin group minerals, and as a consequence, these minerals do not develop a significant charge imbalance.

Where isomorphic substitutions do occur, the resulting negative structural charge is balanced by adsorption of freely exchangeable positively charged cations from solution (e.g., Mg^{2+}, Ca^{2+}, Na^+, and H^+). Adsorption of cations onto clay minerals is typically described as occurring in one of two ways: inner-sphere or outer-sphere adsorption (e.g., Sposito et al. 1999; Strawn and Sparks 1999). Outer-sphere complexes contain a water molecule in between constituent ions of the complex, which are solvated (Sposito et al. 1999; Appelo and Postma 2005). Outer-sphere complexation usually occurs on the basal planes, or interlayer, of the clay mineral (Strawn and Sparks 1999). Inner-sphere complexation occurs when the water molecule is expelled and covalent bonding can occur (Appelo and Postma 2005).

There is a general order of chemical affinity for adsorption of cations from solution. Typically the divalent cations (e.g., Mg^{2+}, Ca^{2+}) have a stronger affinity for adsorption than the monovalent cations (e.g., Na^+, K^+). However, within cations of the same charge, those that have the smallest hydrated ionic radii typically have the strongest adsorption affinity. Adsorbed ions are commonly incorporated into the clay interlayer region where they electrostatically bond to the siloxane layers on the basal plane of Si-tetrahedral layers (Odom 1984; Drever 1988; Strawn et al. 2004; Merkel et al. 2005). This ensures net charge neutrality across the clay mineral structure. The uptake of exchangeable cations is

usually more important where there is the greatest charge imbalance, i.e., where isomorphic substitution has occurred, and the capacity for electrostatic uptake is greatest. The capacity of clay minerals for ion exchange or adsorption (the cation exchange capacity or CEC) is dependent on pH and the type of ions that already occupy exchange sites. In general, the expandable clay minerals such as smectite and vermiculite have higher CEC values than non-expandable minerals such as kaolinite and illite (Ma and Eggleton 1999).

Minerals in which substitution reactions do not occur and interlayer expansion is not important (e.g., kaolinite) can still be important adsorbing agents. Other important adsorption sites include surface hydroxyl sites that form at edge sites where the clay structure has been interrupted (Papelis and Hayes 1996) or silanol sites which can be amphoteric (Peacock and Sherman 2005).

Common Clay Minerals

As described, there is a diverse range of clay minerals, but they have, in general, similar structural components. In the following the main groups of clay minerals will be described, from the simple phases similar to layered double hydroxides to expandable clay minerals such as the smectite group. Basic physical properties of the main clay groups are given in Table 1, while chemical formulas of clay minerals from each group are given in Table 2. Illustrations of the structure of kaolin, smectite, and mica group minerals are shown in Fig. 1.

Gibbsite, Brucite, and Layered Double Hydroxides (LDH)

These minerals differ from what are typically thought of as phyllosilicates, because they do not consist of layers of both Si tetrahedra and Al octahedra, instead being more analogous to the octahedral sheet itself. The structure of these minerals is two closely packed layers of hydroxyl ions (hence layered double hydroxides) with cations in octahedral coordination between the two sheets (Drever 1988). In the case of brucite, this octahedral cation is Mg^{2+}, and each Mg^{2+} is coordinated by 6 OH^- ions, while each OH- ions is coordinated to 3 Mg^{2+} ions. In this way the charges balance with the formula $Mg(OH)_2$, and all of the octahedral sites are filled. In the case of gibbsite, the octahedral cations are Al^{3+}. Because Al is trivalent, it cannot be coordinated in the same way as Mg^{2+} without resulting in a charge imbalance. Hence in gibbsite every third octahedral site is left empty so it has a formula $Al(OH)_3$. Clay minerals in which the octahedral vacancies are all filled (e.g., brucite) are called trioctahedral, while those in which only two out of three octahedral sites are occupied are called dioctahedral.

The dioctahedral mineral gibbsite is particularly relevant to further discussion, not only because of its analogous structure to the octahedral sheet in most phyllosilicates but because of its capacity for swelling and uptake of cations and anions into structural sites and the interlayer. By definition the dioctahedral clay minerals have one void in the octahedral layer that has potential to be filled, albeit the radius of the void limits the cation size. In simple minerals such as gibbsite, the voids have easy access for small cations including Li^+ and Mg^{2+}. The uptake of Li^+ into the octahedral vacancy in gibbsite would result in a charge imbalance; hence Li also takes its accompanying counterion such as Cl^-. Experiments have shown that reaction of LiCl solutions with gibbsite results in appreciable uptake of Li, and large swelling of the clay layers, as significant anions are required to maintain charge balance (e.g., Fogg and O'Hare 1999; Wimpenny et al. 2015). This interlayer expansion is an important quality

Clay Minerals, Table 1 Physical characteristics of clay mineral groups (Data taken from Drever 1988 and Appelo and Postma 2005)

	Kaolin group	Smectite group	Mica group	Chlorite
Structure	T-O (1:1)	T-O-T (2:1)	T-O-T (2:1)	T-O-T-(O) (2:2)
Layer charge	<0.01	0.5–1.2	1.4–2	variable
Unit layer	7A	Ranges depending on interlayer: 14A to 17A	10A	14A
Cation exchange capacity (CEC) meq/100 g	1–10	80–150	10–40	<10

Clay Minerals, Table 2 Examples and formulas of common clay minerals based on mineral group

Group	Mineral	Formula
Kaolin/ serpentine group	Kaolinite	$Al_2Si_2O_5(OH)_4$
	Serpentine	$Mg_3Si_2O_5(OH)_4$
Smectite	Pyrophyllite	$Al_2Si_4O_{10}(OH)_2$
	Talc	$Mg_3Si_4O_{10}(OH)_2$
	Montmorillonite	$(Na,Ca)_{0.33}(Mg,Al)_2(Si_4O_{10})(OH)_2.nH2O$
	Saponite	$Ca_{0.25}(Mg,Fe)_3((AlSi)_4O_{10})(OH)_2.nH2O$
	Hectorite	$Na_{0.3}(Mg,Li)_3(Si_4O_{10})(F,OH)_2$
	Beidellite	$(Na,Ca_{0.5})_{0.3}Al_2((Si,Al)_4O_{10})(OH)_2.nH2O$
Mica	Muscovite	$KAl_2(AlSi_3O_{10})(OH)_2$
	Phlogopite	$KMg_3(AlSi_3O_{10})(OH)_2$
	Paragonite	$NaAl_2(AlSi_3O_{10})(OH)_2$
Chlorite	Clinochlore	$Mg_5Al(AlSi_3O_{10})(OH)_8$
	Chamosite	$(Fe^{2+},Mg,Al,Fe^{3+})_6((Al,Si)_4O_{10})(OH,O)_8$

a

Kaolin group e.g. kaolinite $Al_2Si_2O_5(OH)_4$

Si tetrahedral layer

Al octahedral layer

No interlayer ions

Uni layer ~7A thick

b

Smectite e.g. montmorillonite $(Na,Ca)_{0.33}(Mg,Al)_2(Si_4O_{10})(OH)_2 \cdot nH_2O$

Si tetrahedral layer

Al, Mg octahedral layer

Exchangeable cations in interlayer

Unit layer ~14A thick

c   **Mica group** e.g. muscovite $KAl_2(AlSi_3O_{10})(OH)_2$

Si tetrahedral layer

Al octahedral layer

Fixed potassium in interlayer

Unit layer ~10A thick

Clay Minerals, Fig. 1 Structure of the three major clay mineral groups: (**a**) kaolin, (**b**) smectite, and (**c**) mica. Figures show the stacking of Si tetrahedra and Al octahedra and characteristic basic spacing

of clay minerals that can have implications not only for the bulk clay chemical composition but also on the chemical composition of the fluid phase in which the clay is reacting (e.g., rivers and seawater).

Kaolin Group

Kaolin group minerals are one of the most common clay minerals during weathering and are particularly prone to formation in warm, humid climates (Dixon 1989). Kaolin minerals are all 1:1 phyllosilicates, with a unit structure comprising a single Si-tetrahedral sheet bonded to a single Al-octahedral sheet (analogous to gibbsite) by sharing oxygen atoms between adjacent Si and Al atoms (Murray 1991; Angove et al. 1997). These 1:1 layers stack together by hydrogen bonding and van der Waals forces. The way that these aluminosilicate layers stack together determines the distinct kaolin group minerals. For example, halloysite differs from kaolinite by having a layer of water molecules between the T-O unit layers. These minor differences can affect the

dominant clay form; while kaolinite typically forms plates, halloysite forms characteristic nanotubes (Tan et al. 2015). Isomorphic exchange can occur in kaolin group minerals, but these reactions are not common, and minimal charge deficit is associated with the structure. One of the most common ions to be incorporated into structural sites in kaolinite is iron, although levels are still typically low (less than a Wt %), and it is difficult to tell whether the Fe is actually structurally incorporated into the clay, or is an artifact of a mixed kaolinite-smectite (Dixon 1989). In addition to isomorphic exchange being relatively unimportant, the bonding between the 1:1 layers in kaolin minerals is relatively strong, so that interlayer exchange cannot occur (Angove et al. 1997). The low-layer charge and no interlayer mean that the cation exchange capacity of kaolinite is much lower than expandable clays such as smectites (see later), typically ~1–10 $cmol_c/kg$ (Drever 1988). Any limited sorption capacity of kaolinites is usually caused by broken bonds at the layer edge (Bolland et al. 1976; Ma and Eggleton 1999) and the presence of

pH-dependent functional groups on the clay surface and edge sites (Papelis and Hayes 1996; Strawn et al. 2004; Merkel et al. 2005).

Smectite Group

The smectite group clay minerals are 2:1, or T-O-T, phyllosilicates. As described this means that they have two octahedral sheets bounding a single tetrahedral layer. Other common 2:1 phyllosilicates will be described later on and include micas and chlorite, although there are important structural differences between these minerals and smectite.

Due to the common occurrence of isomorphic substitution into the phyllosilicate structural layers in 2:1 clay minerals, there are a wide range of smectite group clays found in nature. For this reason, we will start with the simplest case, in which the tetrahedral and octahedral sheets are pure. If the octahedral sheet is similar to gibbsite ($Al(OH)_3$), the resulting clay mineral is called pyrophyllite and has the formula $Al_2Si_4O_{10}(OH)_2$. If the octahedral sheet is similar to brucite ($Mg(OH)_2$), the resulting clay mineral is called talc and has the formula $Mg_3Si_4O_{10}(OH)_2$ (Drever 1988). Common smectite group clay minerals and their chemical formula are shown in Table 2. Changes in their chemical composition relative to these end-member compositions result directly from isomorphic exchange, i.e., exchange of trivalent cations for Si^{4+}, divalent cations for Al^{3+}, and/or monovalent cations for Mg^{2+}.

A key property of smectite clay minerals that differentiate them from kaolin and other 2:1 group clay minerals is the relative expandability of the interlayer and the fact that the interlayer can be hydrated. The uptake of exchangeable cations results from the relative charge imbalance caused by isomorphic exchange into structural layers. The most common exchangeable cations in smectite minerals are Mg^{2+}, Ca^{2+}, Fe^{2+}, Na^+, and H^+, although other cations will also exchange (Odom 1984). Although many smectites contain abundant amounts of Mg^{2+}, the amount of Mg and Ca in the interlayer is usually very similar, and smectite minerals with both Mg and Ca are usually very common. The amount of water that can be incorporated into the smectite will depend on the identity of the interlayer species, for example, where Mg or Ca^{2+} is present, two layers of water molecules can be incorporated and the smectite will expand to ~14A (Drever 1988). In contrast, a smectite in which Na is the dominant cation in the interlayer can expand by up to 10 times its original size. In fact the swelling of Na-rich smectites can cause complete dissociation of individual smectite crystals, resulting in dispersion and the formation of a colloidal-like solution with an increased viscosity. For this reason, Na montmorillonites are in high demand in the oil industry as drilling muds (Murray 1991). Ultimately, the cation exchange capacity (CEC) of a smectite mineral will of course depend on its chemical composition, but is usually in the range of 70–130 meq/100 g (Odom 1984; Murray 1991). Most of this CEC is caused by charge deficiency resulting from structural substitution reactions (Odom 1984).

Vermiculites

Vermiculite is a mineral similar in structure to the smectite group minerals but has a greater charge across the interlayer. As a result, the interlayer is less readily expandable than in smectite minerals, and the amount of cation exchange is lower, although because of the higher charge, the CEC of vermiculite is greater than in most smectites.

Mica Group

Mica group clay minerals are also 2:1 clay mineral similar to smectites. However, the isomorphic substitution in mica group clay minerals typically occurs in the tetrahedral layer, where Si^{4+} is replaced by Al^{3+}. The resulting charge deficit is accounted for by incorporation of K+ into the interlayer. Because the charge deficit is derived from the tetrahedral layers, the K is held very tightly in the interlayer (Krauskopf and Bird 1967) and is generally not exchangeable. Common mica group minerals include muscovite, phlogopite, and biotite (see Table 2). Mica group minerals are also commonly referred to as illite. Most natural illites are actually mixed layers of muscovite-like minerals and smectite-like minerals (Drever 1988). Illites make up the bulk of ancient shales, and illitization reactions are common during late diagenesis of siliciclastic materials (Drever 1988; Milliken 2003).

Chlorite Group

Chlorite consists of a 2:1-layered structure similar to the structure of smectite and illite. However, a major difference in the structure of chlorite is that a structural charge imbalance remains even after uptake of exchangeable cations. In chlorites the negative charge is compensated for by the formation of a brucite-like layer within the interlayer region (Velde and Meunier 2008). This brucite-like layer is bonded to the basal tetrahedral layers by coulomb attraction and can be rich in Mg, Al, or Fe (Bailey 1972). Hence the structure of chlorite is essentially 2:1:1 or 2:2 (Drever 1988). Most chlorites are trioctahedral, containing Mg in both the structural octahedral layer and in the interlayer sheet. However, Fe-rich chlorites also exist and occur commonly in iron-ore deposits. Chlorites form in nature via diagenesis of mafic and ultramafic rocks at low- to medium-grade metamorphic conditions, or from the alteration of volcanic rocks. Chlorites have also been synthesized in the laboratory from hydrothermal alteration of montmorillonite and Al or Mg hydroxides (Slaughter and Milne 2013).

Clay Mineral Formation

Clay minerals ultimately form from the alteration of primary silicate minerals. These primary phases form from the crystallization of magma at high temperature and a range of pressures in the Earth's crust. After crystallization and cooling, these primary minerals may be exposed to surface conditions through uplift and erosion. In the low-temperature and low-pressure environment of the Earth's surface, minerals derived from igneous processes are unstable, with those minerals forming at highest temperature, such as olivine, being the least stable at surface conditions. Clay minerals are either direct or indirect alteration products of these unstable primary phases, forming through incomplete (or incongruent) weathering. The relative insolubility of aluminum compounds such as Al oxide (Appelo and Postma 2005) is a major reason that clay minerals are so ubiquitous throughout the crust.

The type of clay mineral that forms during weathering will be dependent on many factors including the type of primary mineral or rock that is being weathered, the fluid composition, the pH and temperature of that fluid, the water-rock contact time, and the influence of biological agents (Galan and Ferrell 2013). While clay minerals are more stable than primary igneous minerals at the Earth's surface, clay minerals themselves can continue to alter during weathering. With increasing intensity of alteration (i.e., temperature and water-rock contact time), clay minerals will tend to change from containing higher amounts of structural Si and other cations to containing higher concentrations of Al, for example, the transition from montmorillonite to kaolinite to gibbsite (Appelo and Postma 2005). Thus aluminum oxide minerals such as gibbsite are typically a product of the more extreme weathering environments.

Continuing alteration of clay minerals can often be associated with a change in the environment (e.g., solution composition, temperature and runoff, pH) such as that associated with a change in climate or progressive burial. This is most easily observed in weathering profiles such as in the study of laterites, which contain distinct layers with different clay mineralogies, caused by abrupt change in climate and subsurface processes such as a fluctuating water table. The formation processes of clay minerals are diverse, ranging from newly formed clays by direct precipitation from solution to solid-state alteration in which the previous clay mineral structure is retained in the new form (e.g., transformation by ion exchange) or in which structural reorganization takes place (e.g., during diagenesis). This diversity in formation mechanism is intuitive if we consider that clay minerals are found in a wide range of environments within the Earth's crust and subjected to changing chemical and physical conditions. A more detailed consideration of clay mineral formation mechanisms follows:

Direct Precipitation or Neoformation

The classic way to envisage the formation of a new mineral is via direct crystallization from a solution, which can also be termed direct precipitation or neoformation. This mechanism requires that a solution has a pH, temperature, and dissolved solid content that promotes precipitation of a new mineral. Based on knowledge of these parameters, it is possible to calculate how stable a mineral phase is in a solution by calculation of its saturation state. Such calculations can provide information about whether a mineral is more likely to dissolve or precipitate in a solution, i.e., whether it is undersaturated or oversaturated. It is important to realize that simply because a certain mineral is oversaturated in solution, it will not necessarily precipitate. The type of clay mineral that forms via neoformation will be dependent on many factors including precursor mineralogy, climate, drainage, and weathering time (Eberl et al. 1984). For example, a classic study in Hawaii, where the bedrock is all basalt, shows that different clay minerals predominantly form in different microclimates (Eberl et al. 1984 and references within). In this case, smectite formed on the drier part of the island, while gibbsite formed where rainfall was much higher. Thus clay minerals that are comprised of soluble cations such as Mg and Ca will only form where these cations can accumulate, such as in dry climates or regions where drainage is poor. In contrast, clay minerals that comprise mostly insoluble elements such as gibbsite will form where rainfall is high and drainage is good so Al will accumulate (Eberl et al. 1984).

At the extreme high-temperature end of the scale, clay minerals can form directly from magma-derived fluids. These fluids originate from deeper in the crust (e.g., a cooling magma chamber) and interact with crustal rocks, stripping out silica and aluminum and forming clay minerals at temperatures up to 450 °C (Kerr 1955). Hydrothermal alteration will typically cause clay formation on a limited scale, restricted to contact metamorphic zones in which temperature is elevated (>50 °C). The clay minerals that form will be controlled not only by temperature but also on the environment of formation, for example, a hydrothermal vent on the seafloor versus a continental extensional setting such as the Basin and Range in western United States.

Diagenesis and Solid-State Alteration

Solid-state alteration can take place either by ion exchange or by alteration of the structural layers in a clay mineral (Eberl et al. 1984). For example, the interlayer leaching of potassium from the interlayer of an illite will result in vermiculite formation (Wilson 1999); this is a common process in soils where the alteration of micas and chlorite can progress in sequence through vermiculite, smectitic mixed layers, degraded smectite, and finally amorphous compounds such as allophane (Chamley 2013). Such a progression is usually observed as one moves from the base to the top of a soil

profile. Other common solid-state alteration phases include products of igneous rock weathering such as that experienced by basaltic lavas or large-scale granitic intrusions. Typically the type of clay mineral formed will depend on the precursor igneous mineralogy and fluid composition and residence time. For example, plagioclase feldspar is typically replaced by kaolinite (e.g., Nesbitt et al. 1997), particularly in more intense weathering regimes where more mobile cations like Mg, Ca, and Na are removed from the rock. In humid tropical environments, highly altered weathering profiles called laterites develop on crustal rocks, for example, the Deccan traps flood basalts in India. Here clay minerals such as kaolinite replace the primary mineralogy, and as weathering progresses, all primary igneous textures are lost, suggesting that both transformation and neoformation of clay minerals occur.

As clay minerals are buried within the Earth's crust, they undergo transformation induced by changes in the pressure and temperature. Notably these changes in PT conditions will progressively expel water from a clay mineral structure and cause a decrease in porosity. In summarizing diagenetic alteration of clay minerals, authors have typically invoke a number of stages of alteration that will ultimately depend on the type of clay protolith. With progressive burial (i.e., increasing PT conditions), there is initial compaction, loss of interlayer cations and water, and a decrease in porosity (Segonzac 1970; Aoyagi and Kazama 1980), although recirculation of water can still occur and can cause retrograde or reverse weathering reactions to occur. In alkaline environments rich in K and Na, the diagenesis of dioctahedral smectite can result in the formation of mixed layer illite-smectite minerals. This reaction usually proceeds at ~60 °C (Perry and Hower 1970), and while the initial distribution of illite and smectite layers is random but with increasing temperature and pressure and increased illite proportion, the distribution of the illite-smectite layers becomes ordered. The reaction is thought to occur as increasing amounts of Al^{3+} substitute into the Si-tetrahedral layer of smectite. This results in an increasing charge across the interlayer, and interlayer K^+ becomes dehydrated, i.e., resulting in the formation of illite (or mica). The identity of the clay mineral that forms from diagenetic reaction will depend on the chemical composition of the precursor mineral and fluid phases. For example, the burial of trioctahedral smectite (i.e., Mg^{2+}-rich montmorillonite) usually results in the formation of chlorite minerals (Galan and Ferrell 2013), while the diagenesis of kaolinite can result in transformation to a more ordered form called dickite, although dickite can also form from K feldspar and other Al-rich silicate minerals.

Further burial and compaction results in complete dehydration with the mixed layer smectite-illites converted to illite and chlorite. These reactions are not usually reversible. At even higher metamorphic grade, the chlorite and illite become ordered, and particle sizes increase to above what is typically considered to be clay sized (<2 μm).

Detrital Inheritance

While neoformation and solid-state alteration are the two main mechanisms by which clay minerals form, a third mechanism can account for large-scale clay deposits; this accumulation of clay minerals from disparate sources is often termed detrital inheritance. Inheritance is an important mechanism because of the stability of the clay mineral group at the Earth's surface, meaning reaction rates are slow and clay minerals can survive physical and/or chemical weathering in their original location and transport to a new accumulation zone. An obvious location for detrital inheritance is in soil profiles that have directly formed from weathering of a sedimentary sequence.

An important region of clay mineral inheritance is on the seafloor, where continental sediments are deposited via outflow from rivers and from aerial deposition. Riverine transport is one of the most important mechanisms, and accumulation of continental detritus, including abundant clay minerals, is common at the continental margin. As one would expect, the clay mineralogy of oceanic sediments usually corresponds to the dominant mineralogy and climate of the adjacent continental region (Eberl et al. 1984; Thiry 2000). Thus kaolin minerals are more common in the tropics, while illite and chlorite are more common at high latitudes, possibly due to their production during glacial weathering (Thiry 2000). As one moves further from the continent, the dominant clay mineralogy changes depending on clay settling time, which is related to the ease with which a clay mineral flocculates. Far out from the continental margin on the abyssal plain, the rate of clay mineral sedimentation is incredibly slow (cm per 1000 years). Here the sediment accumulation is comprised of mixed calcareous ooze and detrital clay minerals that are fine-grained Aeolian sediments and volcanic ash.

While all three mechanisms are important in the formation of clay mineral-rich sediments, they are not mutually exclusive processes; often they work in tandem, and it can be difficult to discern one process from another, i.e., at what point does transformation become neoformation? For example, detrital clay minerals often undergo ion exchange processes in the oceans; the exchange of Ca^{2+} in clay minerals for Mg^{2+} in seawater is such an effective process that it has implications for long-term CO2 drawdown, carbon storage, and climate change (Gislason et al. 1996).

Clay Mineral Isotope Geochemistry

Investigating the isotopic fractionation of stable isotope systems is an established technique within geochemistry that can provide a wide range of useful information about the

formation and chemical evolution of clay minerals. The fractionation of stable isotope systems is mass dependent and is also controlled by temperature (Urey 1947) and the bonding environment (Bigleisen and Mayer 1947). The isotopic composition of a clay mineral will depend on the isotopic composition of the precursor mineral and the fluid phase from which the clay forms. It will also be dependent on the temperature of the system (less fractionation at higher T) and whether the clay mineral forms in a system at equilibrium, or through a unidirectional or kinetic process. Furthermore, isotopic compositions can be altered post-formation in environments where the chemical properties of an element might change (e.g., change in redox conditions between Fe^{2+} and Fe^{3+}), or during re-equilibration at higher temperatures. For example, studies of O and H isotopes in clay minerals provide useful information about the conditions of clay formation and subsequent post-formation processes, because many clay minerals tend to retain their initial O and H isotopic compositions unless subjected to diagenetic or metamorphic conditions (Sheppard and Gilg 1996). For example, detrital clay minerals in the oceans often retain their continental H and O isotope signatures (Sheppard and Gilg 1996). The unique layered structure of clay minerals and importance of ion exchange and adsorption mean that careful isotopic analyses of clay minerals can also shed light on recent fluid interactions by isolating and examining the isotopic composition of interlayer ions in minerals such as smectite. Isotopic analyses have shown that interlayer cations and water rapidly exchange with fluid phases, meaning the interlayer reservoir can be isotopically distinct to the composition of the structural sheets (e.g., Savin and Epstein 1970; Wimpenny et al. 2015).

While the stable isotope systems of H, C, N, and O have been well established for many decades, advancing technology means a wide range of stable isotopic systems from Li all the way up to U can now be studied, many of which are influenced by clay mineral formation. The utility of these isotope systems varies, from understanding global weathering processes (e.g., Li, Mg), to tracing nutrient use (e.g., Fe isotopes), to understanding the transport and distribution of potentially toxic heavy metals (e.g., Cr, Cd, Hg). In all cases, to understand the geochemistry and isotopic composition of these elements in waters and sediments from the Earth's crust requires understanding of the way clay minerals influence their mass budget during weathering and, because their uptake and incorporation into clays usually occurs with an isotopic preference, how the formation of phyllosilicates influences their isotopic composition. Through a combination of field studies and experimental work, an increasing understanding of isotopic behavior has been gained detailing the sense and isotopic fractionation factor associated with elemental uptake or sorption into clay minerals.

While stable isotope systems can provide useful information about general clay mineral formation processes, radiogenic isotope systems can potentially provide information about when and from what parent material the clay mineral formed or originated. A problem with utilizing clay minerals as a dating tool is that they have often undergone burial and diagenesis which could influence the meaning of any obtained age (i.e., what event are we dating?). However certain chronometers such as the Ar-Ar and Rb-Sr systems have proved successful in dating clay mineral formation, particularly in the study of illite formation (e.g., Kelley 2002). For example, Clauer et al. (1997) used both Ar-Ar and Rb-Sr dating techniques to assess the timing of diagenetic illite formation in a sandstone reservoir rock from the North Sea.

Regardless of whether age dating results in reliable age determination, radiogenic isotope systems can also provide useful information about clay provenance. This is because different rock types often have different radiogenic isotopic compositions due to differences in age and/or the way elements partition into different minerals. Thus two different potential source terrains for an inherited clay sediment can be distinguished based upon their radiogenic isotopic composition. It is also important to understand the radiogenic isotopic characteristics of clay minerals when interpreting water-rock interactions. For example, the rubidium ion (Rb^+) commonly substitutes for K^+ in micaceous minerals due to similarity in ionic radius and charge. The relatively high concentration of Rb in micas means that their Rb/Sr ratio is also elevated, and because ^{87}Rb decays to ^{87}Sr over time, these minerals can develop highly radiogenic $^{87}Sr/^{86}Sr$ ratios. In glacial rivers where interlayer leaching of biotite is an important process, the Sr isotopic signal delivered to rivers is often far more radiogenic than the bedrock. This has important consequences for the evolution of Sr isotopes in the ocean during the Cenozoic.

Clay Minerals in the Solar System

The search for life outside of own planet has important implications for how we understand our own origin and the origin of life throughout the universe. Though we do not understand exactly how life on Earth started, we know that liquid water is a key prerequisite for life to begin, develop, and ultimately thrive over geological time. Thus the search for life, or past signs that life was once present, hinges on the ability to identify regions that have once known liquid water. As has already been discussed, clay minerals form due to the interaction of primary igneous minerals with water and are the most ubiquitous alteration minerals on Earth. Of the many planets and moons in our solar system, one of the most

promising places to look for the presence of clay minerals is on our neighbor, Mars. This comes from two lines of evidence: orbital observations from probes and satellites and pieces of Martian crust in the meteorite record.

Orbital observations (e.g. Ehlmann et al. 2008, 2011) have identified a diverse range of clay minerals on Mars surface with the most common clay minerals being Fe-Mg smectites and chlorite. The abundance of chlorite suggests the clays formed in closed system environments at temperatures ranging from ambient to hydrothermal (~400 °C). From these observations and stratigraphic relationships upon Mars, some estimates of the relative timing of clay formation have been made, with the most important period of clay mineral formation occurring between 4.1 and 3.1 billion years ago. These observations suggest that earlier in this period (4.1–3.7By), there was widespread hydrothermal alteration in the subsurface of Mars and, due to the presence of sedimentary structures, the presence of liquid water at the surface, if only as a short-lived phenomenon. As time progressed (3.7–3.1By), the formation of clay minerals is hypothesized to have declined, perhaps because heat sources for hydrothermal alteration (e.g., impacts, volcanism) also declined at this time. Younger terrains (<3.1By) are dominated by crystalline materials. These observations are indicative of Mars being water rich early in its history and transitioning to being increasingly arid.

Unfortunately, we cannot study the Martian crust here on Earth because a sample return mission from Mars is, as yet, not possible due to its extreme technical difficulty and prohibitive cost. Further investigation of Mars surface, the presence of clay minerals, and the possibility of discovering life can be addressed in one of two ways: the study of the Martian meteorite record and sending a remote controlled lander onto Mars surface. While a growing number of Martian meteorites have been identified, they are not ideal rocks in which to look for these chemical signatures. They are derived from impact so have been altered both during impact and ejection from Mars and on entry to the Earth's atmosphere. But perhaps more fundamentally, we have no control over where they came from; from remote observations, it is clear that some locations on Mars are more promising as once having known the presence of water.

These problems can be avoided by sending a rover to make remote measurements on Mars surface, with the caveat that instruments on a rover are far less sophisticated than instruments found in laboratories on Earth. In NASA's recent Mars Science Laboratory (MSL) mission, the rover Curiosity was sent to Gale Crater, an area where hydrated clay minerals and sulfates had been identified from orbit (Ehlmann et al. 2008; Ehlmann et al. 2011; Grotzinger et al. 2014). Recently, Curiosity traversed an area of Gale Crater, encountering sandstones and mudstones interpreted to have a fluvial origin

(Grotzinger et al. 2015). Detailed analysis of a mudstone layer identified around 20% saponitic smectite, probably formed by aqueous alteration of primary olivine in a lacustrine environment. These initial analyses by Curiosity point to an environment that could conceivably have been habitable to basic life once in Mars history.

Clay Mineral Uses

There are a wide range of uses for clay minerals based on their unique mineralogical properties including grain size, surface area, adsorption, color, plasticity, and fire strength (Murray 1991). A brief summary of clay mineral uses is given in the following:

Kaolinites

They are relatively soft (1.5 on Mohs scale) so it is not abrasive and can be used in many industrial applications without causing degradation of machines. They are used in ceramics because they fire to a white color and don't shrink after firing (Murray 2000). The fact that kaolinite is highly dispersible and particles form micron-sized platelets that orient on coated surfaces means they are used to provide a sheened or glossy finish for paper. Calcining kaolinite drives off the hydroxyl groups from the structure. This meta-kaolin has dielectric properties and so has been used as a filler in electric wiring. Kaolinites have a diverse range of applications although their exact use will differ depending on specific properties of the deposit. For example, only kaolinites with the correct color can be used for ceramics. Kaolinites are used as the raw material for the production of fiberglass (Murray 1991) due to the health risks of asbestos.

Smectites

The high-charge, surface area, and cation exchange capacity mean smectites are highly absorbent. When mixed with water, the swelling properties of the clay give the fluid a high viscosity. The largest swelling properties are exhibited by Na montmorillonites. These can expand by up to ten times their original size when immersed in water (Murray 1991). These smectites can yield large volumes of drilling mud. While other smectite minerals such as Ca montmorillonite can be treated to exchange Ca for Na in the interlayer and increase the cation exchange properties and swelling volume, these clays are less useful than naturally occurring Na bentonite. High-swelling clays such as Na bentonites are also commonly used where water barriers are necessary, e.g., in the construction of dams, containment of chemicals in toxic waste dumps, landfill, and nuclear waste disposal sites. Blends of Ca and Na smectites are also typically used as absorbents in animal waste products such as cat litter.

Micas

The most commercially useful micas are muscovite and phlogopite. Both phlogopite and muscovite mica are used as electrical insulators. Dry ground mica has a wide variety of uses from dry wall filler, to an additive to paint, to a reinforcement material in plastics. Ground mica is also used in drilling mud for oil and gas wells where it prevents loss of circulation by filling cracks and reducing porosity in the well. Wet ground mica is used in pearlescent paints and the cosmetic industry where it is incorporated into a range of products from lipstick and nail polish to moisturizing lotion.

Mixtures of shale and chlorite are commonly used in construction, particularly in the production of bricks and cement (Virta 2013, USGS).

Summary

Clay minerals are ubiquitous in the weathering environment. Their diversity in chemical composition and unique physical and chemical properties stems from their layered structure and the ability to take up exchangeable ions from solution. Because clay minerals form from alteration of primary rocks and minerals near the surface of the Earth, they have a direct influence over the chemical evolution of the crust and provide a critical control over the chemical and isotopic composition of river and groundwaters that ultimately feed the oceans. For this reason, characterizing how elements and isotopic systems behave during incorporation into clay minerals will ultimately help us understand large-scale processes such as the impact of climate change, or tectonic shifts on past ocean chemistry. The association between clay minerals and water means that the presence of clay minerals can also guide our exploration of the solar system and the search for life on other worlds. Finally, understanding the physical and chemical properties of clay minerals has practical benefits to society; clay minerals are used widely in industry from drilling mud in oil field exploration to building supplies and plastics to uses around our homes such as in paints and coatings on paper. The utility of clay minerals stems from their unique physical and chemical properties; furthering our understanding of these minerals will both enhance future scientific studies and have important industrial implications.

Cross-References

- ▶ Chemical Weathering
- ▶ Clay Membranes
- ▶ Diagenesis
- ▶ Fluid–Rock Interaction
- ▶ Silicate Minerals

References

Angove MJ, Johnson BB, Wells JD (1997) Adsorption of cadmium (II) on kaolinite. Colloids Surf A Physicochem Eng Asp 126(2):137–147

Aoyagi K, Kazama T (1980) Transformational changes of clay minerals, zeolites and silica minerals during diagenesis. Sedimentology 27(2):179–188

Appelo CAJ, Postma D (2005) Geochemistry, groundwater and pollution. CRC Press, Leiden

Bailey SW (1972) Determination of chlorite compositions by X-ray spacings and intensities. Clay Clay Miner 20(6):381–388

Bigeleisen J, Mayer MG (1947) Calculation of equilibrium constants for isotopic exchange reactions. J Chem Phys 15(5):261–267

Bolland MDA, Posner AM, Quirk JP (1976) Surface charge on kaolinites in aqueous suspension. Soil Res 14(2):197–216

Chamley H (2013) Clay sedimentology. Springer Science & Business Media, Berlin

Clauer N, Srodon J, Francu J, Sucha V (1997) K-Ar dating of illite fundamental particles separated from illite-smectite. Clay Miner 32(2):181–196

Dixon JB (1989) Kaolin and serpentine group minerals. In: Minerals in soil environments, SSSA Book series, vol 1. SSSA, Madison. 2:467–526

Drever JI (1988) The geochemistry of natural waters, vol 437. Prentice Hall, Englewood Cliffs

Eberl DD, Farmer VC, Barrer RM (1984) Clay mineral formation and transformation in rocks and soils [and discussion]. Philos Trans R Soc Lond A 311(1517):241–257

Ehlmann BL, Mustard JF, Fassett CI, Schon SC, Head JW III, Des Marais DJ, . . . Murchie SL (2008) Clay minerals in delta deposits and organic preservation potential on Mars. Nat Geosci, 1(6):355–358

Ehlmann BL, Mustard JF, Murchie SL, Bibring JP, Meunier A, Fraeman AA, Langevin Y (2011) Subsurface water and clay mineral formation during the early history of Mars. Nature 479(7371):53–60

Fogg AM, O'Hare D (1999) Study of the intercalation of lithium salt in gibbsite using time-resolved in situ X-ray diffraction. Chem Mater 11(7):1771–1775

Galan E, Ferrell RE (2013) Genesis of clay minerals. In: Handbook of clay science, vol 5. Elsevier, Amsterdam, p 83

Gislason SR, Arnorsson S, Armannsson H (1996) Chemical weathering of basalt in Southwest Iceland; effects of runoff, age of rocks and vegetative/glacial cover. Am J Sci 296(8):837–907

Grotzinger JP, Sumner DY, Kah LC, Stack K, Gupta S, Edgar L, . . . Milliken R (2014) A habitable fluvio-lacustrine environment at Yellowknife Bay, Gale Crater, Mars. Science 343(6169):1242777

Grotzinger JP, Gupta S, Malin MC, Rubin DM, Schieber J, Siebach K, . . . Calef F (2015) Deposition, exhumation, and paleoclimate of an ancient lake deposit, Gale crater, Mars. Science 350(6257):aac7575

Kelley S (2002) K-Ar and Ar-Ar dating. Rev Mineral Geochem 47(1):785–818

Kerr PF (1955) Hydrothermal alteration and weathering. Geol Soc Am Spec Pap 62:525–546

Krauskopf KB, Bird DK (1967) Introduction to geochemistry, vol 721. McGraw-Hill, New York

Ma C, Eggleton RA (1999) Cation exchange capacity of kaolinite. Clay Clay Miner 47(2):174–180

Merkel BJ, Planer-Friedrich B, Nordstrom D (2005) Groundwater geochemistry. In: A practical guide to Modeling of natural and contaminated aquatic systems, vol 2. Springer, Berlin

Mermut AR, Cano AF (2001) Baseline studies of the clay minerals society source clays: chemical analyses of major elements. Clay Clay Miner 49(5):381–386

Milliken KL (2003) Late diagenesis and mass transfer in sandstone shale sequences. In: Treatise on geochemistry, vol 7. Elsevier, Amsterdam, pp 159–190

Murray HH (1991) Overview – clay mineral applications. Appl Clay Sci 5(5):379–395

Murray HH (2000) Traditional and new applications for kaolin, smectite, and palygorskite: a general overview. Appl Clay Sci 17(5):207–221

Nesbitt HW, Fedo CM, Young GM (1997) Quartz and feldspar stability, steady and non-steady-state weathering, and petrogenesis of siliciclastic sands and muds. J Geol 105(2):173–192

Odom IE (1984) Smectite clay minerals: properties and uses. Philos Trans R Soc Lond A 311(1517):391–409

Papelis C, Hayes KF (1996) Distinguishing between interlayer and external sorption sites of clay minerals using X-ray absorption spectroscopy. Colloids Surf A Physicochem Eng Asp 107:89–96

Peacock CL, Sherman DM (2005) Surface complexation model for multisite adsorption of copper (II) onto kaolinite. Geochim Cosmochim Acta 69(15):3733–3745

Perry E, Hower J (1970) Burial diagenesis in Gulf Coast pelitic sediments. Clay Clay Miner 18(3):165–177

Savin SM, Epstein S (1970) The oxygen and hydrogen isotope geochemistry of clay minerals. Geochim Cosmochim Acta 34(1):25–42

Segonzac GD (1970) The transformation of clay minerals during diagenesis and low-grade metamorphism: a review. Sedimentology 15(3–4):281–346

Sheppard SMF, Gilg HA (1996) Stable isotope geochemistry of clay minerals. Clay Miner 31(1):1–24

Singer A (1980) The paleoclimatic interpretation of clay minerals in soils and weathering profiles. Earth Sci Rev 15(4):303–326

Slaughter M, Milne I (2013) The formation of chlorite-like structures from montmorillonite. Clay Clay Miner 1960:114–124

Sposito G, Skipper NT, Sutton R, Park SH, Soper AK, Greathouse JA (1999) Surface geochemistry of the clay minerals. Proc Natl Acad Sci 96(7):3358–3364

Strawn DG, Sparks DL (1999) The use of XAFS to distinguish between inner-and outer-sphere lead adsorption complexes on montmorillonite. J Colloid Interface Sci 216(2):257–269

Strawn DG, Palmer NE, Furnare LJ, Goodell C, Amonette JE, Kukkadapu RK (2004) Copper sorption mechanisms on smectites. Clay Clay Miner 52(3):321–333

Tan D, Yuan P, Annabi-Bergaya F, Dong F, Liu D, He H (2015) A comparative study of tubular halloysite and platy kaolinite as carriers for the loading and release of the herbicide amitrole. Appl Clay Sci 114:190–196

Thiry M (2000) Palaeoclimatic interpretation of clay minerals in marine deposits: an outlook from the continental origin. Earth Sci Rev 49(1):201–221

Urey HC (1947) The thermodynamic properties of isotopic substances. J Chem Soc (Resumed). 562–581

Velde BB, Meunier A (2008) The origin of clay minerals in soils and weathered rocks: with 23 tables. Springer Science & Business Media, Berlin

Virta RL (2013) Common clay and shale. Min Eng 2013(July):36–37

Wilson MJ (1999) The origin and formation of clay minerals in soils: past, present and future perspectives. Clay Miner 34(1):7

Wimpenny J, Colla CA, Yu P, Yin QZ, Rustad JR, Casey WH (2015) Lithium isotope fractionation during uptake by gibbsite. Geochim Cosmochim Acta 168:133–150

Coal

Stephen F. Greb[1], Cortland F. Eble[1] and James C. Hower[2]
[1]Kentucky Geological Survey, University of Kentucky, Lexington, KY, USA
[2]Center for Applied Energy Research, University of Kentucky, Lexington, KY, USA

Definition

Coal is a naturally occurring sedimentary carbonaceous rock composed of at least 50% organic matter by weight, and 70% carbonaceous material by volume, mostly from the diagenesis (chemical and physical alteration) of plant material in buried peat (Schopf 1956, 1966; Alpern and DeSousa 2002). Coal is a solid hydrocarbon. It is a rock that can burn. Coal does not have a distinct chemical formula, although it is dominated by complexly bound C, H, O, N, and S. Coal has an organic matrix but also contains inorganic (mineral) and fluid components. The chemical variability in coal is a result of (1) variability in the soils and weathered surfaces upon which the peat accumulated, (2) different types of plants and plant remains in peat, different types of peat mires, (3) the depositional history of the peat mire, (4) the syndepositional environments lateral to the peat which contributed inorganic sediment to the mire, (5) burial environments and history, (6) the long diagenetic history in which the peat was altered to coal, and (7) the exhumation history in which the coal was brought back to the surface or near-surface.

Coal Origins

Coal is physically, chemically, and thermally altered peat. *Peat* is partially decayed plant material, mineral matter, and water, which accumulates in anoxic swamps or mires (peat-forming wetlands). Peats generally have organic contents greater than 75%, inorganic mineral contents less than 25%, and water contents of 75–90% (Schopf 1966; Jarrett 1983; Clymo 1987; Alpern and deSousa 2002). Because they represent buried organic material, peats are natural carbon sinks and are an important component of the global carbon cycle (Gorham 1991; Yu et al. 2011). The plant material in peat varies, but in general, consists of organic compounds and plant tissues (wood, cortical tissues, roots, leaf cuticles, spores, pollens, etc.) which are composed of carbohydrates (mainly cellulose), lignins, proteins, lipids, waxes, and resins. Summaries of the chemistry of these tissues can be found in Bouška (1981), Given (1984), de Leeuw and Largeau (1993), and Krevelen (1993). The plants also contain inorganic

constituents, which are the precursors of some of the mineral matter in coal (see "Mineral Content").

The breakdown of plant parts through microbial and chemical activity while the peat is accumulating is termed *peatification*. Peatification involves oxidation, fermentation, gelification, methanogenesis, and humification, among other processes. Anaerobic transformation of carbon occurs through fermentation, which results in formation of low-molecular weight, acids, alcohols, and carbon dioxide (CO_2). In methanogenesis, bacteria convert cellulose (and other carbohydrates) into biogenic methane (CH_4). *Humification* is the physical and biochemical breakdown of plant tissues into humic substances (Stach et al. 1982; Krevelen 1993; Mitsch and Gosselink 2000). Most of the cellulose in plant debris is broken down by fungi and bacteria during peatification and only small amounts survive into low-rank coalification. Lignins, sporopollenins, cutans, suberans (periderm), resins, and algaenans are also degraded but can survive peatification and humification into coalification as different types of macerals (Stach et al. 1982; Given 1984; Teichmüller 1989; de Leeuw and Largeau 1993; Krevelen 1993; Hatcher and Clifford 1997). Biomarkers from organic compounds of these plant tissues have also been detected from organic geochemistry of the hydrocarbon fractions of the soluble organic matter of coals (Hatcher et al. 1982; Tissot and Welte 1984; Bustin et al. 1985).

Peat Mires

Not all peats form coal. Those peats which have a chance to become coal beds generally must be widespread, thick, and accumulate for thousands of years (or more). For thick peats to accumulate, plant production and plant-part accumulation must be greater than the rate of organic decay. Organic decay is slowed in most peats by maintaining waterlogged, anaerobic, acidic conditions. Maintenance of high water tables requires precipitation or groundwater contributions in excess of evaporation. Hence, climate plays a significant role in peat accumulation. Additionally, for thick peats to accumulate they must be protected from significant clastic sediment input or oxygenation (Moore and Shearer 2003; Clymo 1987; Stach et al. 1982).

Peat accumulates in a variety of different types of wetlands including bogs, fens, mires, and swamps. Two broad divisions based on chemistry and hydrology are (1) rheotrophic (minerotrophic) and (2) ombrotrophic (Mitsch and Gosselink 2000; Moore 1989; Clymo 1987). Rheotrophic peat-forming wetlands are groundwater sourced and tend to fill depressions in the landscape, while ombrotrophic mires are rainwater sourced and build up above the landscape (Fig. 1). These basic distinctions have profound influence on the resulting precursor peat chemistry, because topography-filling rheotrophic peats can be intermittently inundated by flood waters containing dissolved and suspended inorganic
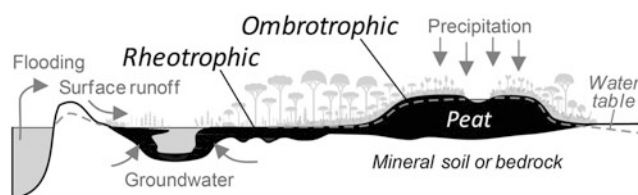
Coal, Fig. 1 Two broad subdivisions of peat, the precursors of coal

sediment, the precursors of mineral matter and much of the ash in coals. In contrast, ombrotrophic peats which build up above the level of bounding lakes or rivers are more sheltered from water-born sediment influx and receive only wind-born detrital minerals. Such peats will produce coals with low ash yields (Eble and Grady 1993; Neuzil et al. 1993; Staub 1991; Cecil et al. 1985). Different types of peat may grade into each other and succeed each other through time.

Peat Accumulation and Preservation

In order for thick peats to accumulate and be preserved, space must be generated for preservation. Relative to the accumulation and burial of peat, accommodation space can be generated (1) below the peat through compaction of underlying sediments or tectonic subsidence; (2) within the peat through biochemical processes resulting in auto-compaction; and (3) above the peat through base-level or sea-level rise. Optimal conditions for thick peat accumulation are when the rates of peat accumulation keep pace with the net rate of subsidence, sea-level change, and sedimentation (McCabe 1984; Butler et al. 1988; Diessel 1992; Bohacs and Suter 1997; Holz et al. 2002).

Peats Through Geologic Time

Time is another variable relative to coal. The oldest mires, and therefore oldest true peats, were in the Late Devonian, following the evolution of vascular plants on land. Although coals occur in rock strata from the Devonian Period through the Neogene Period, they are more common at certain times than others, because of changing global climatic and tectonic conditions. Also, plants have evolved through time, resulting in changes to the vegetative components of peats and the coals they form (Collinson and Scott 1987; Cross and Phillips 1990; Greb et al. 2006a). Different plants have different rates of decomposition and provide different chemical constituents (lignins, resins, etc.) to peat. Most plants contain inorganic elements which contribute to mineral matter in the peat and ultimately the coal formed from the peat. For example, Permian-age coals from southern continents (Australia, India) have higher inertinite (see "Coal Macerals") contents than Carboniferous-age coals from Europe and North America, because the precursor peats had different flora accumulating under different climates (Hunt and Smyth 1989; Taylor et al. 1989).

Peat	Low-rank coal					Medium-rank coal					High-rank coal			Coal Rank (U.S. ASTM)
	Lignite		Sub-bituminous			Bituminous					Anthracitic			
						high volatile C	high volatile B	high volatile A	medium volatile	low volatile	Semi-anthracite	Anthracite	Meta-anthracite	
	B	A	C	B	A									
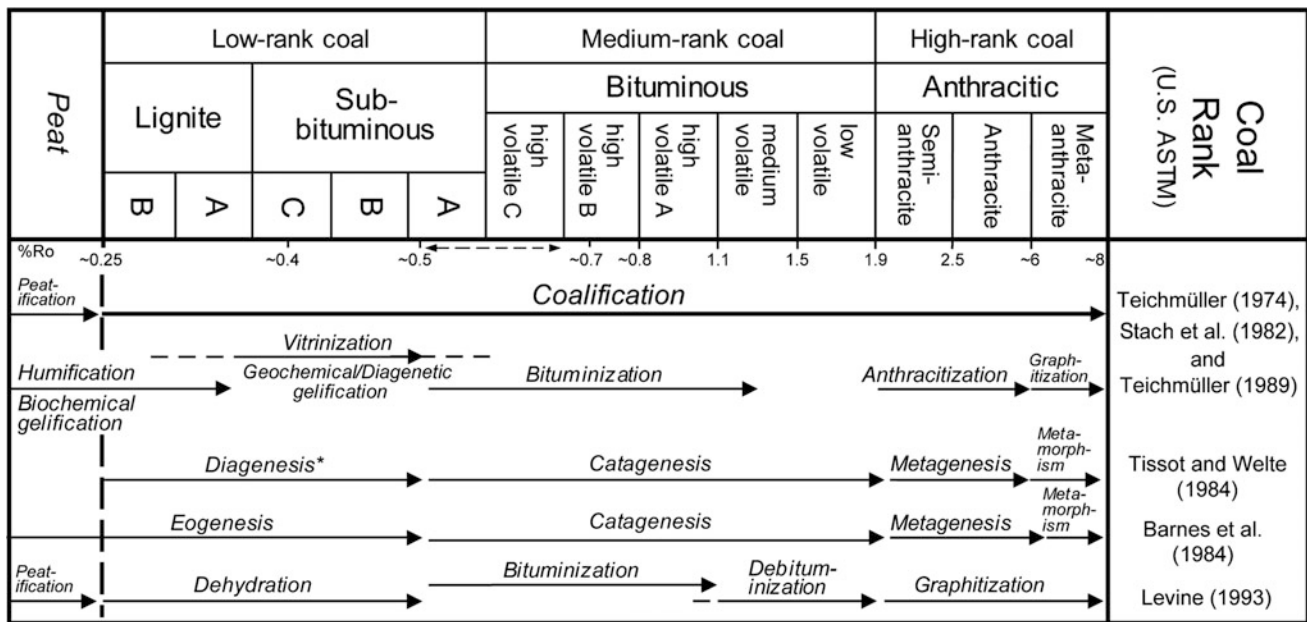
Coal, Fig. 2 Diagram showing stages of coalification cited in different reports relative to their approximate US coal rank (Note the term *diagenesis* was used by Tissot and Welte (1984) for the initial stages of coalification but in many reports it is used synonymously with the entire coalification process. %Ro vitrinite reflectance in oil. %Ro data from Teichmüller and Teichmüller (1982). In the US classification system, vitrinite reflectance values overlap between subbituminous A and high volatile bituminous C ranks, which is shown here as a *dashed line*)

Coalification

Coalification is the process by which peat is transformed into coal. The increasing alteration of coal is classified by rank (see next section). Coalification involves the breakdown of the original plant components in peat and the preservation of other more resistant plant components followed by reorganization of the biopolymers and geopolymers that survive (Hatcher and Clifford 1997). Historically, several processes were used to describe the transformation of peat and its constituent plant parts into coal and its components (Stach et al. 1982; Teichmüller 1974, 1989 in Fig. 2). More recent explanations have subdivided coalification into a series of stages relative to thermal maturation of source rocks (Tissot and Welte 1984; Barnes et al. 1984; Levine 1993; in Fig. 2). These stages approximate different processes which dominate coalification at different temperatures, although in some cases, they are overlapping. These processes are discussed further under *coal rank.*

Not included in Fig. 2, are alterations to coal chemistry which may accompany igneous intrusions, hydrothermal fluids, and natural exhumation of deeply buried coal to the surface where it can be introduced (again) to near-surface and surface processes. A *telogenesis* stage is sometimes added to the coalification tract to include these processes (Barnes et al. 1984; Bustin et al. 1985). The diagenesis of coal is irreversible. Once a coal reaches its highest rank, it remains at that rank; however, minerals and elements within the coal may be oxygenated or react with minerals in groundwater during exhumation and telogenesis.

Coal Classification: Rank, Grade, and Types

Different countries and, in some cases, industries classify coal in different ways. Three general means of classification are based around parameters of (1) rank, (2) grade or quality, and (3) type or macroscopic and microscopic characterization.

Coal Rank

Coal rank is the terminology used to classify coal based on its relative coalification. In general, increasing coalification results in the loss of moisture and compounds rich in hydrogen and oxygen and the relative enrichment of carbon. Krevelen (1993) provides a good summary of different global classification schemes and the parameters upon which they are based. In the US classification scheme, calorific value is used to subdivide low-rank through medium-rank coals, and volatile matter or fixed carbon content is used for higher medium rank and high-rank coals (Fig. 3, ASTM 2014). Calorific value is a measure of the amount of energy produced from coal when it is combusted. Volatile matter is a measure of the nonwater gases formed from a coal sample during heating under oxygen-free conditions. Fixed carbon is a calculated value of the amount of nonvolatile carbon remaining

U.S. Rank (ASTM)			Calorific Value (dmmf) (Btu/lb.)	Volatile Matter (dmmf) (%)	Fixed Carbon (dmmf) (%)	Vitrinite reflectance in oil (%Ro)	Moisture Content (af) (%)	International Rank (ISO)		
High rank	Anthracitic	Meta-anthracite		2	98	~8.0 ~6.0 4.0		A	High rank	Anthracite
		Anthracite				3.0 2.5		B		
		Semi-anthracite		8	92	2.0 1.9		C		
Medium rank	Bituminous	low volatile		14	86	1.5 1.4		A	Medium rank	Bituminous
		medium volatile		22	78	1.1 1.0		B		
		high volatile A	14,000	31	69	0.8		C		
		high volatile B	13,000			~0.66				
		high volatile C	11,500			0.6		D		
Low rank	Sub-bituminous	A	10,500			0.5 ~0.49		A	Low rank	Sub-bituminous
		B	9,500			~0.42 0.4		B		Lignite
		C	8,300			~0.37	35	C		
	Lignite	A	6,300							
		B	5,000	> 60	25	~0.25	75			
Peat								Peat		

Coal, Fig. 3 Comparison of US and international rank subdivisions of coal. Critical values of defining parameters (calorific value, volatile matter, fixed carbon) for the US system (ASTM 2014) and defining parameters (vitrinite reflectance, moisture content) for the international system (ISO 2005) are shown in *bold*. Typical vitrinite reflectance values for US coal ranks and for the peat-lignite subdivision also shown for comparison (Data from Teichmüller and Teichmüller 1982). In the US classification system, vitrinite reflectance values overlap between subbituminous A and high volatile bituminous C ranks (Data from ASTM 2014; Schweinfurth and Finkelman 2003; ISO 2005; Diessel 1992; Given 1984; Stach et al. 1982). *dmmf* dry, mineral-matter-free basis, *af* ash-free basis)

in a coal sample after combustion of the sample. In the international system, moisture content is used to subdivide low-rank coals, while the reflective properties of vitrinite (a coal maceral discussed in a following section) are used to subdivide medium- and high-rank coals (Fig. 3, ISO 2005).

Ash yield and the percentage of vitrinite reflectance are used for further subdivisions and modifiers. Vitrinite reflectance can be used to compare the two classifications (Fig. 3).

Lignites are the lowest rank of coals. They are brown in color and have an earthy, crumbly texture. The boundary between what is termed peat and what is termed lignite is transitional, but having 75% or less moisture content (weight %) is a common parameter for lignite (UNECE 1998; Alpern and DeSousa 2002; ISO 2005). The dominant processes during the lignite stage of coalification are physical compaction, dewatering (dehydration stage in Fig. 2), and biogeochemical gelification (Fig. 2). Moisture content decreases dramatically from peat to lignite and subbituminous ranks as the coal is compacted by increasing burial. Additional moisture is lost through the loss of methoxyl ($-OCH_3$), hydroxyl ($-OH$), carboxyl (COOH–), and carbonyl (C=O) functional groups. Compaction from moisture loss is also associated with increasing hardness and development of

fracture or joint sets in the coal called cleats (Taylor et al. 1998; Mukhopadhyay and Hatcher 1993; Krevelen 1993; Levine 1993; Teichmüller 1989; Given 1984; Hatcher et al. 1982; Stach et al. 1982). The carbon structure of lignites is dominated by catechol-like carbon rings (Hatcher and Clifford 1997). Catechols have two hydroxyl groups linked to an aromatic carbon (benzene-like) ring.

Subbituminous coals are the second division of low-rank coals (Figs. 2 and 3). In appearance and physical properties they are transitional between lignites and bituminous coals. Subbituminous C coals in the US rank system are brown and earthy like lignites, whereas subbituminous A coals are gray to black and shiny like bituminous coals. During coalification of subbituminous coals, moisture loss continues, but biochemical gelification is replaced by geochemical gelification, also termed vitrinization (Fig. 2). Vitrinization involves homogenization, compression, decarboxylation (loss of –COOH), and dewatering (dehydration) of low-rank huminite macerals to form vitrinite macerals (Mukhopadhyay and Hatcher 1993; Krevelen 1993; Teichmüller 1989; Given 1984; Stach et al. 1982; Schopf 1948). Continued loss of oxygen-bearing functional groups transforms the carbon structure of subbituminous coals from catechol-like structures

to phenols and alkylated phenols (Hatcher and Clifford 1997). Phenols have one hydroxyl group linked to a carbon ring.

In the transition from subbituminous B to A and bituminous C rank (US rank system), the color of coal changes, from brown to black. This color change is caused by chemical (diagenetic) gelification of humic substances and marks the beginning of the bituminization or catagenesis stage of coalification (Fig. 2). Bituminization involves the generation and entrapment of hydrocarbons from thermal processes, depolymerization of the coal matrix, and increased hydrogen bonding (Teichmüller 1974, 1989; Stach et al. 1982; Bustin et al. 1985; Levine 1993).

Bituminous coals are black, shiny, and generally hard. Bituminous coals begin with abundant volatile matter (high volatile bituminous coals) but with increased rank, volatile matter is lost (medium volatile and low volatile bituminous coals). In the high volatile bituminous rank, bituminization continues and transforms the molecular phase of the coal from a water-based to bitumen-based system (Teichmüller 1989; Levine 1993). The high volatile bituminous rank is approximately equivalent to the oil-forming window of hydrocarbon generation in source rocks (Teichmüller 1974, 1989; Hunt 1979; Levine 1993; Mukhopadhyay and Hatcher 1993). Coalification from the uppermost high volatile A through low volatile ranks is dominated by thermal degradation and repolymerization (cracking) of the molecular components of the coal and expulsion of low-molecular weight hydrocarbons, especially thermogenic methane. This is the thermogenic gas window in coals (Teichmüller 1974, 1989; Tissot and Welte 1984; Barnes et al. 1984; Bustin et al. 1985; Levine 1993; Mukhopadhyay and Hatcher 1993). Thermogenic gas is generated at burial temperatures of 150–220 °C (Hood et al. 1975; Quigley and Mackenzie 1988; Stolper et al. 2014).

At the bituminous stage of coalification, aromaticity increases through the condensation of phenols to heterocyclic aromatic compounds and benzene-like structures (Hatcher and Clifford 1997).

High volatile bituminous coals (high volatile B and C) are classified using gross calorific value in the US system. Calorific value, however, does not systematically change above the high volatile A bituminous rank, so other parameters are used to classify higher rank coals. Medium volatile and low volatile bituminous ranks in the US system are defined based on volatile matter or fixed carbon (Fig. 3, ASTM 2014). The international system uses vitrinite reflectance to subdivide bituminous coals (Fig. 3, ISO 2005).

Anthracitic coals are high rank coals (Figs. 2 and 3). They are shiny (glassy) and break with a conchoidal fracture. The anthracitic rank is characterized by a sharp decrease in hydrogen content and the H/C ratio. From the semianthracite to anthracite rank, coalification involves condensation of small aromatic ring to larger ordered structures (Stach et al. 1982; Krevelen 1993; Levine 1993). Most coals do not reach anthracitic rank, which requires high heat, generally considered to be greater than 200–250 °C (Bostick 1979; Hunt 1979; Price 1983), from very deep burial, tectonic metamorphism, or contact metamorphism. It is commonly thought that further heating would transform meta-anthracite coal to graphite, a crystalline form of carbon. However, the activation energy for the formation of graphite may be too high to be formed in nature by heating alone, and significant strain energy appears to be required to produce natural graphite from anthracitic coals (Wilks et al. 1993; Bustin et al. 1995; Bustin 1999).

Heat related to burial depth and geothermal fluids is considered the leading cause for coal rank changes (Teichmüller 1989; Daniels et al. 1990; Hower and Gayer 2002; Ruppert et al. 2010). The maximum heat achieved and the duration of that heating event are important factors in maturation and rank changes (Lopatin 1971; Bostick 1979; Teichmüller 1989).

Coal Grade

Coal grade is generally an economic or technological classification reflecting the relative quality of a coal for a particular use. For example, the grade of coals used to generate steam in electric power utilities (called *steam coals*) usually is a reference to a coal's ability to combust with minimal leftover material and minimal emitted pollutants, based on government regulation. Likewise, coal used to produce steel, referred to as metallurgical coal, or *met-coal*, has very specific grade requirements. The coal must be very low in ash (generally <10%) and sulfur (<1%), have volatile matter contents between about 20% and 30%, and have a favorable balance of volatile and inert components. Element concentrations are important as well, as certain elements (e.g., phosphorous) are deleterious (e.g., Zimmerman 1979; Stach et al. 1982). In many cases, different coals are blended to achieve the grade and quality needed for a specific use.

Coal Types

The term "type" relative to coal description and classification unfortunately has many different uses (e.g., O'Keefe et al. 2013), but in coal science, type refers to the general appearance of a coal, which is based on the manner in which the coal (or parts of the coal) was deposited. Shearer and Moore (1999) provide a brief summary of maceral-based and botanical-based type classifications. Stach et al.'s (1982) classification (based in part on Stopes 1919; Schopf 1960) has two types: humic and sapropelic. *Humic* coals are banded coals and are most abundant. The humic type is divided into four lithotypes (vitrain, clarain, durain, and fusain) based on appearance (Table 1). A single humic coal bed may contain all four lithotypes. *Sapropelic* coals are nonbanded coals that form in standing water (ponds, lakes) within peatlands. Sapropelic coals are subdivided into cannel and boghead coals, based on whether the dominant organic material is pollen and spores (cannel), or algae (boghead) (Table 1).

Coal, Table 1 Coal types and their dominant microlithotypes and maceral content. Many different types of macerals can be found in microlithotypes, and many microlithotypes can be found in lithotypes

Coal type	Lithotype (macroscopic)	Appearance	Dominant microscopic components	
			Microlithotype	Macerals
Humic (banded)	Vitrain	Bright, black, shiny and brittle bands, usually with fissures. Tends to break into small cubes	Vitrite	Vitrinite/huminite
	Clarain	Semi-bright (between vitrain and clarain), black, and very finely (mm-scale) interlayered bands of vitrain, durain, and sometimes fusain	Clarite, clarodurite	Vitrinite/ huminite, inertinite
	Durain	Dull, black to gray-black bands with rough surface. Bands have less fissures than vitrain. Tends to break into lumps	Durite, durolaclarite	Inertinite, vitrinite/huminite
	Fusain	Silky lustre, black to gray-black, fibrous bands. Soft and friable, sometimes like charcoal	Inertite, vitrinertite	Inertinite, vitrinite/huminite
Sapropelic (nonbanded)	Cannel	Dull to greasy lustre, black, very hard nonbanded coal. Breaks with conchoidal fracture	Liptite	Sporinite (a liptinite group maceral)
	Boghead	Similar to cannel but brownish	Liptite	Alginite (a liptinite group maceral)

Data from Stach et al. (1982)

Sapropelic coals are far less common than humic coals and may occur as layers or benches, within an otherwise humic coal. Further subdivisions of sapropelic coals are shown in Hutton and Hower (1999).

Relative to geochemistry, different coal types begin with different weight percentages of carbon (C), hydrogen (H), and oxygen (O). For example, humic coals are initially rich in oxygen and poor in hydrogen, whereas sapropelic boghead coals are rich in hydrogen and poor in oxygen. Ratios of H/C to O/C change along different paths for sapropelic and humic coals through medium volatile bituminous rank (Krevelen 1952, 1993; Tissot and Welte 1984; Levine 1993).

Different countries and industries may have their own "type" classification and in some cases, existing classifications are added, or subdivided further, based on local or regional needs. For example, Hagemann and Hollerbach (1980) subdivided German lignite classes into four lithotypes based on texture and the ratio between ground mass and identifiable plant remains, and varieties of lithotypes based on color and hue, evidence of gelification, the presence of organic inclusions, and surface texture.

Coal Microlithotypes

Each coal type is composed of microlithotypes (Table 1). *Microlithotypes* are microscopic associations of macerals (see next section) with a minimum band width of 50 microns (ICCP 1963). Microlithotypes can be mono-, bi-, or tri-maceralic depending whether they contain one, two, or three of the maceral groups. A fourth microlithotype group, termed carbominerite, can also be identified for microlithotypes which contain more than 25% mineral

matter. Humic coal lithotypes commonly consist of vitrite, clarite, vitrinertite, duroclarite, or inertite microlithotypes. Sapropelic coal lithotypes tend to consist of liptite, vitrinertoliptite, and durite microlithotypes (ICCP 1963; Stach et al. 1982; O'Keefe et al. 2013). End-member microlithotypes (vitrite, liptite, and inertite) represent coal that is dominantly (>95%) composed of vitrinite, liptinite, and inertinite, respectively. Coal with varying proportions of different macerals is classified accordingly to their composition. For example, the bimacerite clarite is composed of >95% vitrinite and liptinite, while durite is composed of >95% inertinite and liptinite.

The chemistry of micolithotypes can influence the physical behavior of coals (e.g., Suárez-Ruiz and Crelling 2008). For example, the relative composition of inertinites from microlithotypes can be used as an indicator of coke strength in coking coals (Brown et al. 1964). It also influences the ability to grind (Hower et al. 1987; Moore and Shearer 1999) and break (Esterle et al. 2002), which influence coal processing for electrical and commercial uses.

Coal Macerals

Macerals are microscopic components of coal that are distinguished and classified based on petrographic properties, observed in reflected light on polished surfaces. They are the building blocks of microlithotypes. Macerals represent the altered remains and byproducts of the original plant material and are analogous to the sediment grains and cements that compose a clastic sedimentary rock. The current maceral classification and the plant parts from which they originate are shown in Fig. 4.

Low-rank Macerals			Higher-rank Macerals			Origin
Group	Subgroup	Maceral	Group	Subgroup	Maceral	
Huminite	Humotelinite	Texinite →	Vitrinite	Telovitrinite	Telinite	Plant cell walls (with visible structure)
		Ulminite →			Collotelinite	Plant cell walls (gelified, structureless)
	Humotelinite	Attrinite →		Detrovitrinite	Vitrodetrinite	Small particles of attritus (huminitic particles)
		Densinite →			Collodetrinite	Mottled groundmass (originally attritus)
	Humocollinite	Corpohuminite →		Gelovitrinite	Corpogelinite	Primary and secondary cell infillings from humic gels
		Gelinite			Gelinite	Crack infillings of amorphous humic matter
Liptinite		Sporinite			Sporinite	Outer membranes of plant spores and pollen
		Cutinite			Cutinite	Outer coatings (cuticles) of leaves, roots, stems
		Suberinite			Suberinite	Suberinized cell walls of cork in bark and roots
		Resinite			Resinite	Plant resins, balsams, latexes, fats, and waxes
		Alginite			Alginite	Algae (mostly planktonic)
		Bituminite			Bituminite	Amorphous degraded material of algal or bacterial origin
		Exsudatinite*			Exsudatinite	Secondary crack-filling material after oil generation
		Liptodetrinite			Liptodetrinite	Mechanically degraded particles and residues of liptinites
		Chlorophyllinite			X	Chlorophyll-derived material in peat through lignite rank
Inertinite		Fusinite			Fusinite	Fusinization of plant cell walls (fires, decarboxylation, etc.)
		Semifusinite			Semifusinite	Weakly humified and dehydrated plant tissues
		Funginite			Funginite	Fungal spores, sclerotia, and other fungal tissues
		Secretinite			Secretinite	Oxidation of resin and possibly humic gels
		Macrinite			Macrinite	Dehydrated flocculated humic matrix substances
		Inertodetrinite			Inertodetrinite	Fusinization of tiny varied inertinite precursors
		X			Micrinite	Secondary coalification residues of liptinitic substances

Coal, Fig. 4 Terminology of macerals and their suspected origins. *Arrows* show direct relationship between low rank maceral and higher rank macerals (Data from ICCP 1971, 1998, 2001; Stach et al. 1982; Scott 2002; Sýkorová et al. 2005; Pickel et al. 2017)

Macerals were originally defined based on their relative reflectance in incident light (Stopes 1935). They are classified intro three broad groups: liptinites, vitrinites, and inertinites. For low-rank coals, the precursor of vitrinite is referred to as huminite. Different macerals have different coalification tracks, or different rates at which hydrogen, carbon, and oxygen contents change in the macerals with rank, although in general, macerals increase in aromaticity from liptinite to vitrinite to inertinite, and aromaticity increases within each maceral group with rank. Different macerals also have different volatility. Vitrinite, liptinite, and a portion of semifusinite tend to be volatile, while inertinite macerals tend to be inert. Also, some macerals may be more likely to be associated with mineral matter. For example, fusain contains many pores, which are often filled with mineral matter (Masterlerz and Bustin 1993; Krevelen 1993; Given 1984; Stach et al. 1982).

Huminite-Vitrinite
Huminite and vitrinite group macerals are largely derived from woody and structurally resistant plant tissues (Fig. 4). Huminite group macerals in low-rank coals are the precursors of vitrinite macerals in higher-rank coals and vitrinite group macerals are the dominant macerals in most humic medium- and high-rank coal beds. These macerals are defined by structural features representing the degree of gelification of the precursor plant material. They have high oxygen contents and low carbon contents relative to the other maceral groups, but carbon content increases with rank (Sýkorová et al. 2005; ICCP 1998; Stach et al. 1982).

Huminite and vitrinite macerals increase in aromaticity through coalification, which influences their reflectivity. Vitrinite macerals are gray in reflected light, but their reflectance increases uniformly through coalification, providing a parameter that can be used to measure rank in coal (Fig. 2), and thermomaturity in organic-rich shales containing particles of vitrinite and bitumen. Bitumen is a thermomaturation product of kerogen in organic-rich petroleum source rocks (Hunt 1979; Tissot and Welte 1984; Teichmüller 1989; Littke 1999).

Inertinite
Inertinite group macerals are the oxidized remains of woody and other plant tissues, as well as humic gels and coprolites (Fig. 4). Different macerals in the inertinite group are defined based on the presence or absence of original plant structure. The term implies that these macerals are chemically more inert than other macerals, particularly in carbonization (making coke for steel) processes. They tend to be carbon-rich and hydrogen-poor. The carbon content depends on the origin of the maceral and extent of desiccation or redox processes it underwent during peatification. Inertinite macerals are highly reflective and appear white in reflected light, but they become difficult to distinguish petrographically at anthracite rank because all macerals have the same high reflectance by that stage of coalification (Stach et al. 1982; Teichmuller 1989; ICCP 2001).

Liptinite
Liptinite group macerals are black or brown in reflected white light and fluoresce under blue or ultraviolet light. They are

derived from cutans (waxes), resins, spores, and pollens in plants (Fig. 4) and as such, they tend to be hydrogen rich. Liptinites are involved in two coalification jumps. The first occurs in high volatile bituminous B and C coals when they begin to expulse liquids. The second occurs at or near the boundary of high volatile and medium volatile coals, where they lose their fluorescent properties, and their reflectance becomes similar to vitrinite (Stach et al. 1982; Teichmüller 1974, 1989; Pickel et al. 2017).

Coal Molecular Structure

There is no singular molecular chemical model for coal because coals are chemically and physically micro-heterogenous, both between different coals and within individual coals. Coals are aromatic (consist chiefly of aromatic [pentagonal rings] of carbon) compounds, and more than 100 molecular models have been proposed for the "basic" coal molecule. Mathews and Chaffie (2012), Mathews et al. (2011), and Marzec (2002) provide summaries of these models. Most modern models illustrate coal as a complex macromolecular network, which changes with rank. Levine (1993) summarized the macromolecular coal model as a (1) three-dimensional macromolecular matrix fraction composed mostly of single or polycyclic aromatic carbon structures fringed by H- and O-bearing functional groups and cross-linked by H- and O- bridge structures; and a (2) molecular fraction formed by tightly bound oils and asphaltenes of medium- to high-molecular weight and lower molecular weight compounds either physically entrapped or loosely bound to the matrix. The lower molecular weight fraction includes H_2O, CH_4, and CO_2, which change with rank.

Mineral Content

Coal is also comprised of minerals, separate or entrapped within the organic coal matrix. Mineral matter occurs as nonmineral inorganics and discrete inorganic crystalline and noncrystalline particles or masses. The minerals in a coal may have originated in the original peat (detrital, authigenic, biogenic) or may have been introduced, remobilized, or transformed within the coal at any time during post-peat coalification (Table 2). More than 120 minerals and inorganic compounds have been documented in coals worldwide (Schweinfurth and Finkelman 2003; Ward 2002; Vassilev and Vassileva 1996; Finkelman 1981). Table 3 shows some of the minerals which have been reported from coal.

Minerals in coal commonly occur as single crystals or concentrations of crystals within the coal matrix or in voids (fractures, cleats, rotted roots, etc.) within the coal.

Authigenic minerals (Table 2) tend to be very fine grained (microns) and embedded in the coal matrix, often occurring within cell-sized voids of individual macerals. In contrast, diagenetic minerals (Table 2) tend to be coarser crystalline, macroscopic concentrations in cleat and fracture fills. This distinction is significant as cleat-filling minerals are generally easier to remove from coal prior to utilization than authigenic minerals (Rao and Gluskoter 1973; Mackowsky 1982; Renton 1982; Ward 1989; Krevelen 1993). The amount, particle size, and type of mineral matter in coal influence a wide variety of uses, including combustion for steam for electrical energy production and the production of metallurgical coke to make steal. Understanding mineral components is not only important for the practical processes and maintenance of combustion equipment but also chemical reactions during combustion, and the resultant composition of emissions and solid residues, especially in countries where the chemical composition of the emissions or residues is regulated.

Silicate Minerals

The most common minerals in coal are silicates, especially quartz and assorted clays (Table 3). Quartz is a common detrital mineral in flood waters and can also be deposited in peats from wind-blown sediment and volcanic ash falls (e.g., Neuzil et al. 1993; Ruppert et al. 1993). Biogenic opaline quartz accumulates from plant phytoliths and in sponge spicules in peat (Andrejko et al. 1983; Davis et al. 1984; Ruppert et al. 1993). Although most quartz in coal is syngenetic, diagenetic quartz-filling cleats are also reported in high-rank coals (Ward 2002; Spears 1987; Renton 1982).

Feldspars are minor mineral constituents in coals. Most feldspars are detrital in origin. Micas are rare, but detrital micas, which were weathered by acidic peat waters, may be the source for many clays, especially chlorite, in coal beds (Staub and Cohen 1978; Davis et al. 1984; Vassilev and Vassileva 1996).

Clay minerals are the most common silicate minerals in coal, and total clays often constitute the majority of mineral matter in coal. Kaolinite and illite are two of the most common clays in coals, but different types of clays are common in different coals in different basins (Table 3). Clays are common constituents of flood waters, so are common detrital additions to peats. Authigenic clays in peat can be sourced from (1) inorganic constituents in the original plant material, which become amorphous inorganics in the peat, which in turn, are altered to clays (Renton et al. 1979); (2) weathering of volcanic ash (Stach et al. 1982; Ward 2002); (3) from altered detrital muscovite (Staub and Cohen 1978; Davis et al. 1984); and from leaching and alteration of bedrock and underlying soil materials (Spears 1987). Kaolinite is favored in acidic peats, whereas smectite-dominated mixed layer clays dominate in neutral pH conditions. Smectite can

Coal, Table 2 Terminology used to describe the relative timing of mineral formation, deposition, or emplacement in peat and coal, and some of the sources and processes involved

Timing of mineral emplacement				Source/Origin		Dominant processes and products
Non-mineral inorganics	Higher Rank Coals ← Lignite ← Peat	Syngenetic (Primary)	Early (During peat accumulation)	Authigenic	Peat pore fluids	Dissolved salts and other inorganics in peat pore waters
Inorganic mineral particles (Crystalline and non-crystalline)					Biogenic	Inorganic elements in organic compounds in peat
				Allogenic Detrital	Clastic Epiclastic	Aqueous: Sediment deposited in peat from adjacent waters
						Aeolian: Air-born dust and sediment in peat
					Ash falls	Deposition of volcanic ash in peat
			Both Early and Late	Authigenic	Biogenic	Inorganic components of plants (e.g. pytholiths) and animals (e.g. spicules) produced through biologic/metabolic activity
					Chemical precipitates (pore filling)	Alteration of detrital and biogenic minerals in peat
						Bacterial reduction of sulfates sourced from peat processes and from marine flood waters
			Late (after burial)			Pre-compactional minerals formed from soluble ions during biochemical gelification at low temperatures
		Diagenetic (Secondary)		Epigenic	Chemical precipitates and transformations (cleat filling)	Transformation of minerals in coal through interactions with fluids and gases produced by coalification processes or from geothermal fluids at increasing burial temperatures and pressures
						Remobilization of minerals and ions in coal and fluids with increasing heat, pressure, and fluid chemical evolution, resulting in mineral deposition in cleats and fractures
						Metamorphism from igneous intrusions or geologic metamorphism at higher anthracitic ranks
		Telogenetic (Tertiary)			Chemical precipitates	Oxidation of minerals in coal at the surface after exhumation
						Mineralogical reactions associated with burning coal at the surface after exhumation

From data in Mackowsky (1982), Ward (2002). A telogenesis stage is added here to show processes at the surface which can precipitate minerals in coal

later be transformed to illite during diagenesis. Kaolinite and illite can also be formed by diagenetic transformations and are common in cleat and fracture fills in coal beds (Rao and Gluskoter 1973; Renton et al. 1979; Renton 1982; Spears 1987; Vassilev and Vassileva 1996).

Carbonate Minerals

Siderite, calcite, dolomite, and ankerite are common, and sometimes abundant constituents of the mineral fraction of coals (Table 3). In anaerobic, alkaline peat sediments, iron can accumulate as siderite (Postma 1977, 1982; Shotyk et al. 1992), possibly from CO_2 released by organic decay (Gould and Smith 1979; Ward 1989). Concretionary masses of calcite in coal beds, called coal balls, are found in some coal basins. Many coal balls preserve the cellular structure of plants in the peats in which they formed so are early syngenetic (e.g., Stopes and Watson 1909; Phillips 1980; Scott et al. 1996). Syngenetic dolomite may be introduced to peats if peats are

buried by marine waters (Stach et al. 1982). Carbonates can also be diagenetic. Calcite, and to a lesser extent, dolomite and ankerite are common fracture- and cleat-filling minerals formed in medium- and high-rank coals (Rao and Gluskoter 1973; Mackowsky 1982; Ward 1989, 2002). Some cleat-filling calcite cements may also result from telogenesis and precipitation from meteoric groundwater during exhumation (e.g., Kolker and Chou 1994).

Sulfide and Sulfate Minerals

Sulfur occurs in three forms in coal: (a) organic sulfur from the organic compounds in the coal; (b) sulfide minerals; and (c) sulfate minerals (usually hydrous iron and calcium sulfates) produced by oxidation of pyritic sulfides. At least 24 sulfate minerals and 19 sulfide minerals have been identified in coals (Ward 1989, 2002; Casagrande 1987; Davis 1982; Finkelman 1981). Pyrite and marcasite are the most

Coal, Table 3 Some of the minerals found in coals. Occurrence and abundance varies within and between coal beds. Not all minerals are found in all coals

Silicates		Carbonates	Sulfides
Amphibole $(Ca,Na)_{2-3}(Mg,Fe,Al)_5(Al,Si)_8O_{22}(OH)_2$ Epidote $Ca_2Al_2(Fe^{3+},Al)(SiO_4)(Si_2O_7)O(OH)$ Homeblende $Ca_2(Mg,Fe,Al)_5(Al,Si)_8O_{22}(OH)_2$ Kyanite Al_2SiO_5 ▶ **Quartz-Chalcedony SiO_2** Pyroxene-Enstatite $MgSiO_3$ Pyroxene-Augite $(Ca,Na)(Mg,Fe^{2+},Al,Fe^{3+},Ti)(Si,Al)_2O_6$ Staurolite $Fe^{2+}_2Al_9O_8(SiO_4)_4(O,OH)_2$ Tourmaline $(Na,Ca)(Mg,La,Fe,Mn)_3Al_6(BO_3)_3Si_6O_{18}(OH)_4$ ○ Zircon $ZrSiO_4$		Alstonite $BaCa(CO_3)_2$ Ankerite $Ca(Fe^{2+},Mg,Mn)CO_3$ Aragonite $CaCO_3$ ▶ **Calcite $CaCO_3$** Dawsonite $NaAlCO_3(OH)_2$ ○ Dolomite $CaMg(CO_3)_2$ ▶ **Siderite $FeCO_3$** Strontianite $SrCO_3$ Witherite $BaCO_3$	○ Chalcopyrite $CuFeS_2$ ○ Galena PbS Greigite $Fe^{2+}Fe^{3+}_2S_4$ ○ Marcasite FeS_2 Millerite NiS ▶ **Pyrite FeS_2** Pyrrhotite $Fe_{(1-x)}S$ ○ Sphalerite $(Zn,Fe)S_2$ Stibnite SbS
Clay Minerals		Oxidesand Hydroxides	Sulfates
▶ **Chlorite $(Mg_5Al)(AlSi_3)O_{10}(OH)_8$** ▶ **Kaolinite $Al_2Si_2O_5(OH)_4$** ▶ **Illite $KAl_2(AlSi_7)O_{20}(OH)_4$** ▶ **Interstratified (mixed-layer) clays** ▶ **Smectite (Montmorillonlite) $(1/2Ca, NA)_{0.7}(Al, Mg, Fe)_4[(Si, Al)_4O_{10}]_2(OH)_2 \cdot n H_2O$**		○ Anatase-Rutile TiO_2 Boehmite $Al \cdot O \cdot H$ Brucite $Mg(OH)_2$ Corundum Al_2O_3 Diaspore $AlO(OH)$ Gibbsite $Al(OH)_3$ Goethite-Limonite $Fe(OH)_3$ Hematite Fe_2O_3 Magnetite $Fe^{2+}Fe^{3+}O_4$ Portlandite $Ca(OH)_2$ Spinel $MgAl_2O_4$	Alunite $KAl_3(SO_4)_2(OH)_6$ Anhydrite $CaSO_4$ ○ **Barite $BaSO_4$** Bassanite $CaSO_4 \cdot 1/2 H_2O$ Bloedite $Na_2Mg(SO_4)_2$ Celestite $SrSO_4$ Coquimbite $Fe_2(SO_4)_3 \cdot 9H_2O$ Glauberite $Na_2Ca(SO_4)_2$ Gypsum $CaSO_4 \cdot 2H_2O$ Hexahydrite $MgSO_4 \cdot 6H_2O$ Jarosite $(Na,K)Fe_3(SO_4)_2(OH)_6$ Melanterite $FeSO_4 \cdot 7H_2O$ Natrojarosite
Feldspars			
○ Plagioclase-Albite $NaAlSi_3O_8$ ○ Plagioclase-Anorthite $CaAl_2Si_2O_8$ ○ Orthoclase-Microcline $KAlSi_3O_8$ ○ o Sanidine $(K,Na)AlSi_3O_8$	**Legend** ▶ **Major minerals** ○ Minor minerals Rare minerals		
Zeolites		Phosphates	
○ **Analcime $NaAlSi_2O_6 \cdot H_2O$** Clinoptilolite-Heulandite $(Na,K,Ca)_{2-3}Al_3(Al,Si)_2Si_{13}O_{36} \cdot 12H_2O$		○ Apatite $Ca_5F(PO_4)_3(OH,F,Cl)$ ○ Crandallite	

Coal, Table 3 (continued)

	Other	Phosphates	Halides
Laumontite $Ca(AlSi_2O_6)_2•4H_2O$ Mordenite $(Ca,Na_2,K_2)Al_2Si_{10}O_{24}•7H_2O$		$(Y)CaAl_3(PO_4)_2(OH)_5·H_2O$ o Florencite $(Ce)Al_3(PO_4)_2(OH)_6$ o Gorceixite $BaAl_3(PO_4)_2(OH)_5•H_2O$ o Goyazite $SrAl_3(PO_4)_2(OH)_5•H_2O$ o Monazite $(Ce,La,Y,Th,Nd)PO_4$ o Xenotime $(Y,Er)PO_4$	$NaFe_3(SO_4)_2(OH)_6$ Rozenite $FeSO_4•4H_2O$ Szomolnokite $FeSO_4•H_2O$ Thenardite Na_2SO_4 Tschermigite $NH_4Al(SO_4)_2•12H_2O$
	Chromite $FeCr_2O_4$ o **Clausthalite PbSe** Corundum Al_2O_3 Crocoite $PbCrO_4$	o Apatite $Ca_5F(PO_4)_3(OH,F,Cl)$ o Crandallite $(Y)CaAl_3(PO_4)_2(OH)_5·H_2O$ o Florencite $(Ce)Al_3(PO_4)_2(OH)_6$ o Gorceixite $BaAl_3(PO_4)_2(OH)_5•H_2O$ o Goyazite $SrAl_3(PO_4)_2(OH)_5•H_2O$ o Monazite $(Ce,La,Y,Th,Nd)PO_4$ o **o** Xenotime $(Y,Er)PO_4$	Chlorine-Halite NaCl Sylvite KCl

From data in Rao and Gluskoter (1973), Finkelman (1981), Mackowsky (1982), Renton (1982), Vassilev and Vassileva (1996, 2000), Hower et al. (1999), Ward (2002), Schweinfurth and Finkelman (2003)

common sulfide minerals in coal (Table 3). These may be authigenic or diagenetic. Authigenic pyrite can form in peat while the peat is accumulating, or in peats buried by marine waters (e.g., Casagrande 1987). Authigenic pyrite may occur as single crystals or clusters of crystals in individual macerals of coal. Diagenetic (epigenetic) pyrite tends to fill veins and cleats in coal and be more coarsely crystalline (Rao and Gluskoter 1973; Mackowsky 1982; Vassilev and Vassileva 1996). Additional diagenetic sulfide minerals include sphalerite, galena, and chalcopyrite, especially from coals which have encountered hydrothermal fluids (Mackowsky 1982; Finkelman 1981, 1985). Many of the sulfate minerals found in coal (e.g., coquimbite, jarosite, melanterite, rozenite, szomolmokite) result from exposure of sulfide minerals in coal at the surface (e.g., Rao and Gluskoter 1973).

Pyrite (FeS_2) breaks down with potentially deleterious consequences in many parts of the coal mining and utilization cycle. Weathering of mined exposures of coal and high-sulfur stratum, or abandoned spoil piles with significant pyrite concentrations, can result in acid-mine drainage (ARC 1969; NRC 1990; Brady et al. 1998; Greb et al. 2006b; Finkelman and Greb 2008). In boilers and furnaces, pyrite breaks down into elemental iron and sulfur, which can lead to corrosion and fouling. Each element combines with oxygen to form oxides. Iron oxide becomes part of the bottom or fly ash. Sulfur dioxide (SO_2) is emitted in the gas stream, which can react with water vapor to form sulfurous acid (H_2SO_3), which oxidizes to sulfuric acid (H_2SO_4), a major component of acid rain (EIA 1997, 2001; U.S. EPA 2004; Greb et al. 2006b). Many different types of mitigation are employed to

Coal, Fig. 5 Periodic table of naturally occurring elements, showing the elements reported from coal. Not all elements are found in all coals (After Schweinfurth and Finkelman 2003, Fig. 9)

remove or reduce pyrite from mined coal and to reduce or limit sulfurous emissions during and following combustion. Many techniques are also available for limiting acid-mine drainage from mine sites, and from mitigating drainage from mine sites which were abandoned before modern regulations in developed countries.

Major, Minor, and Trace Elements

Figure 5 shows the elements that have been reported in coal. Although coal does not have a unique chemical structure, the major elements (more than 1%) in the coal matrix are carbon (C), hydrogen (H), oxygen (O), nitrogen (N), and sulfur (S) (Fig. 5). The relative percentage of carbon increases with rank, while oxygen and hydrogen decrease with rank. Major elements are mostly organically associated, although they are found in inorganic (mineral) associations as well. Minor elements (1.0–0.01%) in coal are Na, Mg, Al, Si, P, K, Ca, Ti, Mn, and Fe (Fig. 5). Most of the minor elements are associated with the mineral constituents in coal, although phosphorus (P) is also organically associated. Minor elements are relatively common in coal but do not occur in all coal seams and occur in different concentrations in different seams (Finkelman 1981, 1985; Schweinfurth and Finkelman 2003; Swain 2013).

Trace elements (Fig. 5) are elements which occur in concentrations of 100 parts per million or smaller. Not all coals contain these elements, and concentrations of these elements vary greatly among and within coal beds. Similar to mineral matter, trace elements may be introduced during peatification or at any stage of coalification. Most appear to be syngenetic. From the peat through lignite stage of coalification, fresh cations may be introduced from groundwater and by ion exchange with carboxyl acids or their salts. Organic acids in peat and low-rank coals provide a large capacity for ion-exchange and complexation of metal ions into organometallic compounds (Rashid 1974; Nissenbaum and Swain 1976; Miller and Given 1986; Given and Miller 1987; Mitsch and Gosselink 2000; Li et al. 2010). Some trace elements are also epigenetic and are introduced with epigenetic minerals.

An important aspect of trace elements is their chemical association. Trace elements can be organically bound to the coal matrix or associated with mineral matter. The elements B, Be, Ga, Ge, and Sb are usually organically bound. The elements As, Cr, Ni, Se, Ti, U, and V, among others, may be either organically bound or occur in mineral matter, depending on the coal. Most of the other trace elements in coal shown in Fig. 5 are associated with mineral matter (Gluskoter et al. 1977; Miller and Given 1986; Given and Miller 1987; Goodarzi 1988; Finkelman 1995; Swaine

2013). In fact, some elements tend to have associations with certain minerals. For example, Cr, Hf, Rb, Ti, and Zr are commonly associated with aluminosilicate minerals like micas, feldspars, and clays (e.g., Suárez-Ruiz and Crelling 2008). Be, Cr, Mn, and Ni are commonly associated with the clay mineral chlorite. As, Cd, Co, Hg, Ni, Sb, and Se are commonly associated with the sulfide minerals pyrite and marcasite (e.g., Schweinfurth and Finkelman 2003). Understanding the chemical association of trace elements in a coal can aid in (1) determining if the elements can be or need to be removed or diminished from the coal prior to utilization, (2) where the elements will end up (emissions, solid residues) during and following coal utilization, and (3) determining the best mechanisms for mitigating any potential technological or environmental issues an element may have in the utilization process based on best practices and regulations.

Of the trace elements which can occur in coal, there are 15 which are listed as hazardous air pollutants (HAPS) by the US EPA (Fig. 5) although currently, mercury (Hg) is the only element of the 15 regulated and monitored from coal-fired power plant emissions in the United States (U.S. EPA 1998, 2016a). Many of the other HAPS (As, Cd, Co, Hg, Pb, some Se, and Sb) are commonly associated with sulfide minerals (see previous section), so removal of (or at least reducing) sulfide minerals from the coal prior to combustion in preparation plants aids in mitigation.

Coal Utilization

The majority of chemical testing of coal beds is conducted to (1) determine how a particular bed will react during its prospective use; (2) what and how much solid, particulate, and gaseous products may be produced from its use; and (3) address any technological or environmental issues resulting from coal utilization. Globally, coal is mostly combusted to generate steam to provide electrical power. Hence, much of the geochemical analysis of coal is aimed at understanding combustion characteristics and potential environmental issues of coal combustion. Environmental issues depend on the coal, the local environment (climate, pH, moisture, etc.), combustion technology, and the type of pollution control systems used in the process. A variety of coal-combustion emissions (SO_2, NO_x, etc.) are regulated in developed countries (e.g., U.S. EPA 1998). Concerns about CO_2 emissions and global climate change have also sparked limits on carbon emissions in some countries (Houghton et al. 1990; UN 1998; Stocker et al. 2013; U.S. EPA 2016b; EU 2016). Other than emissions, the chemistry of solid combustion residues and by-products is also important for determining potential by-product uses or for mitigating potential groundwater issues related to disposal of combustion residues in

landfills (Adriano et al. 1980; U.S. EPA 1999, 2015; Izquierdo and Querol 2012). More information and references concerning environmental chemistry and issues of coal utilization, including various emissions, and solid residues, can be found at government agencies charged with their regulation and in Greb (2006).

Coal also has *nonfuel* uses. The principle nonfuel use of coal is to make metallurgical coke, which is used to make steel. A by-product of metallurgical coke are coal tars, which can be used to produce a wide array of aromatic chemicals. The pitch fraction of the tar can also be used to make an array of specialty carbon materials such as graphite and carbon fibers. Coal can also be gasified to make synthesis gases and other chemicals and can be liquefied to make synthetic fuels (Miura 2000; Schobert and Song 2002). More information about the commercial chemistry of coal and coal by-products can be found in Bouška (1981), Given (1984), Berkowitz (1985), and Krevelen (1993).

Conclusions

Coal is a complex material composed of an organic matrix, as well as inorganic and fluid constituents. Coal is diagenetically altered peat. Much of the chemistry of a particular coal is inherited from its peat precursor, but overprinted by its diagenetic history. This results in variability between and within coal beds. Coal chemistry changes with rank, which is largely a function of burial and thermal diagenesis. Variability in coal composition can generally be seen and analyzed at different scales, from the whole seam or benches of a seam, to bands in the seam (type), to microscopic bands and associations (microlithotype), to macerals (microscopic particles), to sub-maceral elemental composition. Understanding a coal's composition requires an understanding of a particular coal from its genesis as peat, through its geologic history to exhumation and exposure. How detailed the analysis of a particular coal is, generally depends on the coal's end use. Most chemical analyses on coals are done to determine parameters which influence the technological utilization of the coal, and to plan for any environmental or regulatory considerations of that particular use. Such considerations involve more than the coal itself, but also the equipment used and regulations, which vary considerably around the globe.

Cross-References

▶ Acid–Base Reactions
▶ Authigenesis
▶ Biogenic Methane

References

Adriano DC, Page AL, Elsewi AA, Chang AC, Staughan I (1980) Utilization and disposal of fly ash and other coal residues in terrestrial ecosystems: a review. J Environ Qual 9:333–334

Alpern B, de Sousa ML (2002) Documented international enquiry on solid sedimentary fossil fuels; coal: definitions, classifications, reserves-resources, and energy potential. Int J Coal Geol 50(1):3–41

Andrejko MJ, Cohen AD, Raymond R (1983) Origin of mineral matter in peat. In: Raymond R, Andrejko MJ (eds) Mineral matter in peat, its occurrence, form, and distribution. Los Alamos National Laboratory, Los Alamos, pp 3–24

Appalachian Regional Commission (1969) Acid mine drainage in Appalachia: Congressional house document no. 91-180, v. I, II, and III, Washington, DC

ASTM (2014) D388-12 Standard classification of coal by rank. ASTM International, West Conshohocken, v. 5.06–Gaseous fuels; Coal and coke; Bioenergy and industrial chemicals from biomass: 396–402

Barnes MA, Barnes WC, Bustin RM (1984) Diagenesis 8. Chemistry and evolution of organic matter. Geosci Can 11(3):102–114

Berkowitz N (1985) The chemistry of coal. Coals science and technology, vol 7. Elsevier, New York

Bohacs K, Suter J (1997) Sequence stratigraphic distribution of coaly rocks: fundamental controls and paralic examples. Am Assoc Pet Geol Bull 81(10):1612–1639

Bostick NH (1979) Microscopic measurement of the level of catagenesis of solid organic matter in sedimentary rocks to aid exploration for petroleum and to determine former burial temperatures a review. SEPM Spec Publ 26:17–43

Bouška V (1981) Geochemistry of coal. Coal science and technology, vol 1. Elsevier, New York

Brady BC, Kania T, Smith WM, Hornberger RJ (eds) (1998) Coal mine drainage prediction and pollution prevention in Pennsylvania. Pennsylvania Department of Environmental Protection, Harrisburg

Brown HR, Taylor GH, Cook AC (1964) Prediction of coke strength from the rank and petrographic composition of Australian coals. Fuel 43:43–54

Bustin RM (1999) Coal origins and diagenesis. In: Marshall CP, Rhodes WF (eds) Encyclopedia of geochemistry. Kluwer, Boston, pp 90–92

Bustin RM, Barnes MA, Barnes WC (1985) Diagenesis 10. Quantification and modelling of organic diagenesis. Geosci Can 12(1):4–21

Bustin RM, Ross JV, Rouzaud JN (1995) Mechanisms of graphite formation from kerogen: experimental evidence. Int J Coal Geol 28(1):1–36

Butler J, Marsh H, Goodarzi F (1988) World coals: genesis of the world's major coalfields in relation to plate tectonics. Fuel 67(2):269–274

Casagrande DJ (1987) Sulphur in peat and coal. In: Scott AC (ed) Coal and coal-bearing strata–recent advances. Geological Society, London, Special Publications 32(1):87–105

Cecil CB, Stanton RW, Neuzil SG, Dulong FT, Ruppert LF, Pierce BS (1985) Paleoclimate controls on late Paleozoic sedimentation and peat formation in the central Appalachian Basin (USA). Int J Coal Geol 5(1):195–230

Clymo RS (1987) Rainwater-fed peat as a precursor of coal. In Scott AC (ed) Coal and coal-bearing strata–recent advances. Geological Society, London, Special Publications 32(1):17–23

Collinson ME, Scott AC (1987) Implications of vegetational change through the geological record on models for coal-forming environments. In Scott AC (ed) Coal and coal-bearing strata–recent advances. Geological Society, London, Special Publications 32(1):67–85

Cross AT, Phillips TL (1990) Coal-forming through time in North America. Int J Coal Geol 16(1):1–46

Daniels EJ, Altaner SP, Marshak S, Eggleston JR (1990) Hydrothermal alteration in anthracite from eastern Pennsylvania: implications for mechanisms of anthracite formation. Geology 18(3):247–250

Davis A (1982) Sulfur in coal. Earth and Mineral Science Letters 51:1–18

Davis A, Russell SJ, Rimmer SM, Yeakel JD (1984) Some genetic implications of silica and aluminosilicates in peat and coal. Int J Coal Geol 3(4):293–314

De Leeuw JW, Largeau C (1993) A review of macromolecular organic compounds that comprise living organisms and their role in kerogen, coal, and petroleum formation. In: Engel M, Macko SA (eds) Organic geochemistry. Springer, New York, pp 23–72

Diessel CFK (1992) Coal formation and sequence stratigraphy. Springer, Berlin

Eble CF, Grady WC (1993) Palynologic and petrographic characteristics of two middle Pennsylvanian coal beds and a probable modern analogue. In: Cobb JC, Cecil CB (eds) Modern and ancient coal-forming environments. Geological Society of America, Special Paper 286:119–138

Energy Information Administration (1997) Effects of title IV of the Clean Air Act Amendments of 1990 on utilities: an update: U.S. Department of Energy, Washington, DC, EIA-0582

Energy Information Administration (2001) Reducing emissions of sulfur dioxide, nitrogen oxides, and mercury from electric power plants: U.S. Department of Energy, Office of Integrated Analysis and Forecasting, Washington, DC

Esterle JS, Kolatschek Y, O'Brien G (2002) Relationship between in situ coal stratigraphy and particle size and composition after breakage in bituminous coals. Int J Coal Geol 49(2):195–214

European Union (EU) (2016) Climate action. Website, http://ec.europa.eu/clima/index_en.htm. Accessed Jan 2016

Finkelman RB (1981) Modes of occurrence of trace elements in coal. U.S. Geological Survey Open-File Report, OFR-81-99

Finkelman R B (1985) Mode of occurrence of accessory sulfide and selenide minerals in coal. In: Cross AT (ed) Neuviene Congress

International de Stratigraphic et de Geologic du Carbonifere. Compte Rendu. 4:407–412

Finkelman RB (1995) Mode of occurrence of environmentally-sensitive trace elements in coal. In: Swaine DJ, Goodarzi F (eds) Environmental aspects of trace elements in coal. Springer, New York, Energy and the Environment 2:24–50

Finkelman R, Greb S (2008) Environmental and health impacts [of coal], Chapter 10. In: Suárez-Ruiz I, Crelling JC (eds) Applied coal petrology-the role of petrology in coal utilization. Elsevier Publications, Amsterdam, pp 263–287

Given PH (1984) An essay on the organic geochemistry of coal. In: Gorbaty ML, Larsen JW, Wender I (eds) Coal science, v.3. Academic, New York: 63–252

Given PH, Miller RN (1987) The association of major, minor and trace inorganic elements with lignites. III. Trace elements in four lignites and general discussion of all data from this study. Geochim Cosmochim Acta 51(7):1843–1853

Gluskoter HJ, Ruch RR, Miller WG, Cahill RA, Dreher GB (1977) Trace elements in coal: occurrence and distribution. Illinois State Geological Survey, Circular, Urbana 499

Goodarzi F (1988) Elemental distribution in coal seams at the Fording coal mine, British Columbia, Canada. Chem Geol 68:129–154

Gorham E (1991) Northern peatlands: role in the carbon cycle and probable responses to climatic warming. Ecol Appl 1(2):182–195

Gould KW, Smith JW (1979) The genesis and isotopic composition of carbonates associated with some Permian Australian coals. Chem Geol 24:137–150

Greb SF (2006) Coal and the environments references: Kentucky Geological Survey, University of Kentucky. Website, http://www.uky.edu/KGS/coal/coal_reference.htm. Accessed Jan 2016

Greb SF, DiMichele WA, Gastaldo RA (2006a) Evolution and importance of wetlands in earth history. In: Greb SF, DiMichele WA (eds) Wetlands through time. Geological Society of America Special Paper 399:1–40

Greb SF, Eble CF, Peters DC, Papp AR (2006b) Coal and the environment. American Geological Institute, Environmental Education Series, Alexandria

Hagemann HW, Hollerbach A (1980) Relationship between the macropetrographic and organic geochemical composition of lignites. Phys Chem Earth 12:631–638

Hatcher PG, Clifford DJ (1997) The organic geochemistry of coal: from plant materials to coal. Org Geochem 27(5):251–274

Hatcher PG, Breger IA, Szeverenyi N, Maciel GE (1982) Nuclear magnetic resonance studies of ancient buried wood–II. Observations on the origin of coal from lignite to bituminous coal. Org Geochem 4(1):9–18

Holz M, Kalkreuth W, Banerjee I (2002) Sequence stratigraphy of paralic coal-bearing strata: an overview. Int J Coal Geol 48(3):147–179

Hood ACCM, Gutjahr CCM, Heacock RL (1975) Organic metamorphism and the generation of petroleum. Am Assoc Pet Geol Bull 59(6):986–996

Houghton JT, Jenkins GJ, Ephraums JJ (eds) (1990) Report prepared for intergovernmental panel on climate change by working group I. Cambridge University Press, Cambridge

Hower JC, Gayer RA (2002) Mechanisms of coal metamorphism: case studies from Paleozoic coalfields. Int J Coal Geol 50(1):215–245

Hower JC, Graese AM, Klapheke J (1987) Influence of microlithotype composition on Hardgrove grindability for selected eastern Kentucky coals. Int J Coal Geol 7:227–244

Hower JC, Ruppert LF, Eble CF (1999) Lanthanide, yttrium, and zirconium anomalies in the Fire Clay coal bed, Eastern Kentucky. Int J Coal Geol 39:141–153

Hunt JM (1979) Petroleum geochemistry and geology. W.H. Freeman and Co, San Francisco, 617p

Hunt JW, Smyth M (1989) Origin of inertinite-rich coals of Australian cratonic basins. Int J Coal Geol 11(1):23–46

Hutton AC, Hower JC (1999) Cannel coals: implications for classification and terminology. Int J Coal Geol 41(1):157–188

International Committee for Coal and Organic Petrology (ICCP) (1998) The new vitrinite classification (ICCP system 1994). Fuel 77:349–358

International Committee for Coal and Organic Petrology (ICCP) (2001) The new inertinite classification (ICCP system 1994). Fuel 80:459–471

International Committee for Coal Petrology (ICCP) (1963) International handbook of coal petrography, 2nd edn. Centre National de la Recherche Scientifique, Academy of Sciences of the USSR, Paris, Moscow

International Committee for Coal Petrology (ICCP) (1971) International handbook of coal petrology, first supplement to, 2nd edn. Centre National de la Recherche Scientifique, Paris

ISO (International Organization for Standardization) (2005) Classification of coal. ISO (International Organization for Standardization), 11760. 1st edition, Geneva

Izquierdo M, Querol X (2012) Leaching behaviour of elements from coal combustion fly ash: an overview. Int J Coal Geol 94:54–66

Jarrett PM (ed) (1983) Testing of peats and organic soils. Symposium Proceedings, Toronto, Canada, June 23, 1982, ASTM Committee D-18 on Soil and Rock, ASTM Special Technical Publication 820

Kolker A, Chou CL (1994) Cleat-filling calcite in Illinois Basin coals: trace-element evidence for meteoric fluid migration in a coal basin. J Geol 102(1):111–116

Krevelen DW van (1952) Some chemical aspects of coal genesis and coal structure. In: Troisième Congres pour l'avancement des études de stratigraphie et de géologie du Carbonifère, Heelen, Compte Rendu 1:359–363

Krevelen DW van (1993) Coal: typology, physics, chemistry, constitution, 3rd edn. Elsevier, New York

Levine JR (1993) Coalification: the evolution of coal as source rock and reservoir rock for oil and gas. In: Law BE, Rice, DD (eds) Hydrocarbons from coal. American Association of Petroleum Geologists, Studies in Geology, 38:39–77

Li Z, Ward CR, Gurba LW (2010) Occurrence of non-mineral inorganic elements in macerals of low-rank coals. Int J Coal Geol 81(4):242–250

Littke R (1999) Coal: Vitrinite reflectance and maturity. In: Marshall CP, Rhodes WF (eds) Encyclopedia of geochemistry. Kluwer, Boston, p 96

Lopatin NV (1971) Temperature and geologic time as factors in coalification (in Russian). Akad Nauk SSSR Izv Ser Geol 3:95–106

Mackowsky M-T (1982) Minerals and trace elements occurring in coal. In: Stach E, Mackowsky M-T, Teichmüller M, Taylor GH, Chandra D, Teichmüller R (eds) Stach's textbook of coal petrology, 3rd edn. Gebrüder Borntraeger, Berlin, pp 153–171

Marzec A (2002) Towards an understanding of the coal structure: a review. Fuel Process Technol 77:25–32

Mastalerz M, Bustin RM (1993) Variation in maceral chemistry within and between coals of varying rank: an electron microprobe and micro-FTIR investigation. J Microsc 171(2):153–166

Mathews JP, Chaffee AL (2012) The molecular representations of coal–a review. Fuel 96:1–14

Mathews JP, Van Duin AC, Chaffee AL (2011) The utility of coal molecular models. Fuel Process Technol 92(4):718–728

McCabe PJ (1984) Depositional environments of coal and coal-bearing strata. In: Rahmani RA, Flores, RM (eds) Sedimentology of coal and coal-bearing sequences. International Association of Sedimentologists, Special Publication 7:13–42

Miller RN, Given PH (1986) The association of major, minor and trace inorganic elements with lignites. I. Experimental approach and study of a North Dakota lignite. Geochim Cosmochim Acta 50(9):2033–2043

Mitsch WJ, Gosselink JG (2000) Wetlands, 3rd edn. Wiley, New York

Miura K (2000) Mild conversion of coal for producing valuable chemicals. Fuel Process Technol 62(2):119–135

Moore PD (1989) The ecology of peat-forming processes: a review. Int J Coal Geol 12(1):89–103

Moore TA, Shearer JC (1999) Coal: types and characteristics. In: Marshall CP, Rhodes WF (eds) Encyclopedia of geochemistry. Kluwer, Boston, pp 92–96

Moore TA, Shearer JC (2003) Peat/coal type and depositional environment – are they related? Int J Coal Geol 56(3):233–252

Mukhopadhyay PK, Hatcher PG (1993) Composition of coal. In: Law BE, Rice DD (eds) Hydrocarbons from coal. American Association of Petroleum Geologists, Studies in Geology 38:79–118

National Research Council (1990) Surface mining effects: committee on ground water recharge in surface-mined areas. Water Science and Technology Board, National Research Council, National Academy Press, Washington, DC

Neuzil SG, Supardi SG, Cecil CB, Kane JS, Soedjono K (1993) Inorganic geochemistry of domed peat in Indonesia and its implication for the origin of mineral matter in coal. In: Cobb JC, Cecil CB (eds) Modern and ancient coal-forming environments. Geological Society of America, Special Paper 286:23–44

Nissenbaum A, Swaine DJ (1976) Organic matter-metal interactions in recent sediments: the role of humic substances. Geochim Cosmochim Acta 40(7):809–816

O'Keefe JM, Bechtel A, Christanis K, Dai S, DiMichele WA, Eble CF, Esterle JS, Mastalerz M, Raymond AL, Valentim BV, Wagner NJ, Ward CR, Hower JC (2013) On the fundamental difference between coal rank and coal type. Int J Coal Geol 118:58–87

Pickel W, Kus J, Flores D, Kalaizidis S, Christanis K, Cardott BJ, Misz-Kennan M, Rodrigues S, Hentschel A, Hamor-Vido M, Crosdale P, Wagner N, ICCP (2017) Classification of liptinite – ICCP system 1994. Int J Coal Geol 169:40–61

Phillips TL (1980) Stratigraphic and geographic occurrences of permineralized coal-swamp plants-Upper Carboniferous of North America and Europe. Biostratigraphy of fossil plants: 25–92

Postma D (1982) Pyrite and siderite formation in brackish and freshwater swamp sediments. Am J Sci 282(8):1151–1183

Postma D (1977) The occurrence and chemical composition of recent Fe-rich mixed carbonates in a river bog. J Sediment Petrol 47:1089–1098

Price LC (1983) Geologic time as a parameter in organic metamorphism and vitrinite reflectance as an absolute paleogeothermometer. J Pet Geol 6(1):5–37

Quigley TM, Mackenzie AS (1988) The temperatures of oil and gas formation in the sub-surface. Nature 333(6173):549–552

Rao CP, Gluskoter HJ (1973) Occurrence and distribution of minerals in Illinois coals. Circular, 476. Illinois State Geological Survey, Urbana

Rashid MA (1974) Absorption of metals on sedimentary and peat humic acids. Chem Geol 13(2):115–123

Renton JJ (1982) Mineral matter in coal. In: Meyers RA (ed) Coal structures. Academic, New York, pp 283–326

Renton JJ, Cecil CB, Stanton R, Dulong F (1979) Compositional relationships of plants and peats from modern peat swamps in support of a chemical coal model. In: Donaldson AC, Presley MW, Renton JJ (eds) Carboniferous coal short course and guidebook, vol 3. West Virginia Geologic and Economic Survey, Morgantown, pp 43–56

Ruppert LF, Neuzil, SG, Cecil CB, Kane JS (1993) Inorganic constituents from samples of domed and lacustrine peat, Sumatra, Indonesia. In: Cobb JC, Cecil CB (eds) Modern and ancient coal-forming environments. Geological Society of America Special Paper 286:83–96

Ruppert LF, Hower JC, Ryder RT, Levine JR, Trippi MH, Grady WC (2010) Geologic controls on thermal maturity patterns in Pennsylvanian coal-bearing rocks in the Appalachian basin. Int J Coal Geol 81:169–181

Schobert HH, Song C (2002) Chemicals and materials from coal in the 21st century. Fuel 81:15–32

Schopf JM (1948) Variable coalification; the processes involved in coal formation. Econ Geol 43(3):207–225

Schopf JM (1956) A definition of coal. Econ Geol 51(6):521–527

Schopf JM (1960) Field description and sampling of coal beds. U.S. Geological Survey, Bulletin 1111-B, 70 p

Schopf JM (1966) Definitions of peat and coal and of graphite that terminates the coal series (graphocite). J Geol 74(5):584–592

Schweinfurth SP, Finkelman RB (2003) Coal–a complex natural resource: an overview of factors affecting coal quality and use in the United States. Circular, 1143. U.S. Geological Survey, Urbana

Scott AC (2002) Coal petrology and the origin of coal macerals: a way ahead? Int J Coal Geol 50(1):119–134

Scott AC (1989) Observations on the nature and origin of fusain. Int J Coal Geol 12(1):443–475

Scott AC, Mattey DP, Howard R (1996) New data on the formation of Carboniferous coal balls. Rev Palaeobot Palynol 93:317–331

Shearer JC, Moore TA (1999) Coal: organic petrography. In: Marshall CP, Rhodes WF (eds) Encyclopedia of geochemistry. Kluwer, Boston, pp 87–90

Shotyk WH, Nesbitt W, Fyfe WS (1992) Natural and antropogenic enrichments of trace metals in peat profiles. Int J Coal Geol 20:49–84

Spears DA (1987) Mineral matter in coals, with special reference to the Pennine Coalfields. In: Scottt AC (ed) Coal and coal-bearing strata–recent advances. Geological Society, London, Special Publications 32:171–185

Stach E, Mackowsky M-T, Teichmüller M, Taylor GH, Chandra D, Teichmüller R (1982) Stach's textbook of coal petrology. Gebrüder Borntraeger, Stuttgart

Staub JR (1991) Comparisons of central Appalachian carboniferous coal beds by benches and a raised Holocene peat deposit. Int J Coal Geol 18(1):45–69

Staub JR, Cohen AD (1978) Kaolinite enrichment beneath coals; a modern analog, Snuggedy swamp, South Carolina. J Sediment Petrol 48:203–210

Stocker TF, Qin D, Plattner G-K, Tignor M, Allen SK, Boschung J, Nauels A, Xia Y, Bex V, Midgley PM, IPCC (eds) (2013) Climate change 2013: the physical science basis. Cambridge University Press, Cambridge

Stolper DA, Lawson M, Davis CL, Ferreira AA, Neto ES, Ellis GS, Lewan MD, Martini AM, Tang Y, Schoell M, Sessions AL (2014) Formation temperatures of thermogenic and biogenic methane. Science 344(6191):1500–1503

Stopes M (1919) On the four visible ingredients in banded bituminous coal. Proc R Soc Lond B9:470–487

Stopes MC (1935) On the petrology of banded bituminous coals. Fuel 14:4–13

Stopes MC, Watson DMS (1909) On the present distribution and origin of the calcareous concretions in coal seams, known as "coal balls". Phil Trans R Soc Lond B 200:167–218

Suárez-Ruiz I, Crelling JC (eds) (2008) Applied coal petrology–the role of petrology in coal utilization. Elsevier Publications, New York

Swaine DJ (2013) Trace elements in coal. Butterworth-Heinemann, Boston

Sýkorová I, Pickel W, Christanis K, Wolf M, Taylor GH, Flores D (2005) Classification of huminite–ICCP system 1994. Int J Coal Geol 62:85–106

Taylor GH, Liu SY, Diessel CFK (1989) The cold-climate origin of inertinite-rich Gondwana coals. Int J Coal Geol 11(1):1–22

Taylor GH, Teichmüller M, Davis A, Diessel CFK, Littke R, Robert P (1998) Organic petrology. Gebrüder Borntraeger, Berlin/Stuttgart

Teichmüller M (1974) Generation of petroleum-like substances in coal seams as seen under the microscope. In: Tissot BP, Bienner F (eds) Advances in geochemistry. Éditions Technip, Paris. Proceedings of the 6th international meeting on organic geochemistry, Rueil-Malmaison, 18–21 Sept, pp 379–408

Teichmüller M (1989) The genesis of coal from the viewpoint of coal petrology. Int J Coal Geol 12:1–87

Teichmüller M, Teichmüller R (1982) Fundamentals of coal petrology. In: Stach E, Mackowsky M-T, Teichmüller M, Taylor GH, Chandra D, Teichmüller R (eds) Stach's textbook of coal petrology. Gebrüder Borntraeger, Stuttgart: 5–108

Tissot B, Welte DH (1984) Petroleum formation and occurrence, 2nd edn. Springer, Berlin

U.S. Environmental Protection Agency (1997) Mercury study report to Congress-, v. 1, Executive summary: Office of Air Quality, Planning, and Standards, and Office of Research and Development, Washington, DC, EPA-452/R-97-003

U.S. Environmental Protection Agency (1999) Report to Congress–wastes from the combustion of fossil fuels. Office of Solid Waste and Emergency Response, Washington, DC, EPA 530-S-99-010, Executive Summary, 1 and 2

U.S. Environmental Protection Agency (2004) Acid rain program, 2003 progress report: Washington, D.C., EPA 430-R-04-009, 17 p.

U.S. Environmental Protection Agency (2015) Final rule: disposal of coal combustion residuals from electric utilities. http://www.epa.gov/coalash/coal-ash-rule. Accessed Jan 2016

U.S. Environmental Protection Agency (EPA) (2016a) Mercury and air toxics standards. http://www3.epa.gov/mats/. Accessed Jan 2016

U.S. Environmental Protection Agency (EPA) (2016b) Climate change. http://www3.epa.gov/climatechange/. Accessed Jan 2016

U.S. Environmental Protection Agency (US EPA) (1998) Study of hazardous air pollutant emissions from electric utility steam generating units–Final report. U. S. Environmental Protection Agency, Office of Air Quality, Research Triangle Park, North Carolina, EPA-453/R-98-004a, volumes 1 and 2, varied pagination

United Nations (1998) Kyoto protocol to the United Nations framework convention on climate change, Dec. 10, 1997, U.N. Doc FCCC/CP/1997/7/Add.1, 37 I.L.M. 22. UN, Geneva

United Nations Economic Commission for Europe (UN-ECE) (1998) International classification of in-seam coals. UN Economic Commission for Europe, Committee on Sustainable Energy, Geneva

Vassilev SV, Vassileva CG (1996) Occurrence, abundance and origin of minerals in coals and coal ashes. Fuel Process Technol 48(2):85–106

Vassilev SV, Eskenazy GM, Vassileva CG (2000) Contents, modes of occurrence and origin of chlorine and bromine in coal. Fuel 79(8):903–921

Ward CR (1989) Minerals in bituminous coals of the Sydney basin (Australia) and the Illinois basin (U.S.A.) Int J Coal Geol 13:455–479

Ward CR (2002) Analysis and significance of mineral matter in coal seams. Int J Coal Geol 50(1):135–168

Wilks KR, Mastalerz M, Bustin RM, Ross JV (1993) The role of shear strain in the graphitization of a high-volatile bituminous and an anthracitic coal. Int J Coal Geol 22:247–277

Yu Z, Beilman DW, Frolking S, MacDonald GM, Roulet NT, Camill P, Charman DJ (2011) Peatlands and their role in the global carbon cycle. EOS Trans Am Geophys Union 92(12):97–98

Zimmerman RE (1979) Evaluation and testing of the coking properties of coal. Miller Freeman Publications, San Francisco

Cobalt

Olivier Pourret and Michel-Pierre Faucon
UniLaSalle, Beauvais Cedex, France

C

Element Data

Atomic Symbol: **Co**

Atomic Number: **27**

Atomic Weight: 58.933195 g/mol

Isotopes and Abundances: ^{59}Co 100%

1 Atm Melting Point: 1495 °C

1 Atm Boiling Point: 2927 °C

Common Valences: 2+, 3+

Ionic Radii: 65 pm (2+, 6-fold coordination)

Pauling Electronegativity: 1.88

First Ionization Energy: 7.88 eV

Chondritic (CI) Abundance: 513 ppm[a]

Silicate Earth Abundance: 102 ppm[a]

Crustal Abundance: 26.6 ppm[b]

Seawater Abundance: ~3–300 pmol/kg[c]

Core Abundance: 0.25%[d]

[a]Palme et al. (2014)

[b]Rudnick and Gao (2014)

[c]Bruland et al. (2014)

[d]McDonough (2014)

Properties

Cobalt (chemical symbol, Co) is a d-block transition metal, bluish white. It appears in the first long period of the periodic table between iron and nickel. Cobalt shares many chemical and physical properties with these two elements. Naturally occurring Co consists of a single stable isotope: ^{59}Co, whereas ^{60}Co is an artificial isotope that is an important γ-ray source. Cobalt has two main oxidation states (2+ and 3+). The common oxidation state for simple compounds is Co^{2+}. Depending upon geometry and environment, Co ionic radii vary between 56 pm and 90 pm. Cobalt is a transitional, compatible, and siderophile (chalcophile and lithophile in the Earth's crust) element, has a high melting point of 1495 °C, and is ferromagnetic. Cobalt has an electronegativity of 1.88 on the Pauling scale and displays a first ionization potential of 7.88 eV. More details can be found in Blackman (2006), Raveau and Seikh (2012), and Haynes (2015).

History and Use

Cobalt has been utilized by the society since the Bronze Age, mainly to impart a rich blue color to glass and ceramics. Its name derives from the German word kobald (goblin or evil spirit) and Greek word cobalos (mine), because Co minerals fooled miners with their bright colors. However, it was only isolated as a pure metal by Swedish chemist Brandt in 1735. Demand for Co remained subdued until the turn of the twentieth century and the development of cobalt-chromium alloys. Indeed, the demand for Co increased considerably after the Second World War, driven by the use of high-purity Co in jet engines and gas turbines. Cobalt demand has further accelerated in the past 30 years. Indeed, it reflects the increased use of Co as an essential constituent of materials used in high-technology industries including rechargeable batteries, super-alloys, and catalysts. Cobalt, like Fe, can be magnetized and so is used to make magnets. It is alloyed with Al and Ni to make particularly powerful magnets. Other alloys of Co are used in jet turbines and gas turbine generators, where high-temperature strength is important. Cobalt metal is sometimes used in electroplating because of its attractive appearance, hardness and resistance to oxidation, and thus corrosion. Cobalt salts have been used for centuries to produce brilliant blue colors in paint, porcelain, glass, and pottery. Cobalt is one of the elements defined as a critical metal to clean energy over the next 5–15 years, because of its use in lithium ion batteries: each electric-powered vehicle will demand 9.4 kg of Co (Crundwell et al. 2011). Although Co does not get a ton of press, it is a pretty important metal in this day and age. The artificial radionuclide ^{60}Co is widely used in cancer treatment, as a tracer, and for radiotherapy.

Geochemical Behavior

Cobalt is often associated with Ni, Ag, Pb, Cu, and Fe-Mn ores, from which it is most frequently obtained as a by-product (Gunn 2014). The main known ore deposits are found in Katanga (Democratic Republic of Congo) (Decrée et al. 2015), whereas some recent discoveries evidenced that central Pacific Ocean may have Co-rich deposits (i.e., manganese nodules and Co-rich ferromanganese crusts) (Josso et al. 2017) at relatively shallow depths. Almost 50% of the world's cobalt supply in 2014 was mined in the Democratic Republic of Congo. Mining and smelter activities in Katanga have contaminated soil, water, and urban environments (Pourret et al. 2016).

Cobalt forms a number of minerals: cobaltite [CoAsS], skutterudite [CoAs$_{3-x}$], erythrite [Co$_3$(AsO$_4$)$_2$.8H$_2$O], spherocobaltite [CoCO$_3$], and heterogenite [CoO(OH)]. It is widely distributed in igneous and sedimentary rocks and minerals. Cobalt is also present in meteorites (i.e., iron-nickel

metal contains a few tenths of a percent cobalt). Its average content in the Earth's crust is approximately 25–30 ppm, though widely distributed, stands only 33rd in order of abundance, and is less common than all other transition metals except scandium. It is, however, more dispersed in the crust than either of those elements, and concentrated mineral deposits are consequently rare. The average Co contents of CI chondrites estimated in a few studies are quite consistent, ranging from 500 ppm to 513 ppm. The bulk Earth has a Co content of 880 ppm, lower than that in the metallic core (0.25%). Cobalt contents in the bulk continental crust vary significantly from 15 ppm to 30 ppm. In particular, Co is most abundant in ultramafic rocks with an average concentration of 110 ppm. During differentiation of a basaltic magma, most of Co enters the ferromagnesian minerals. Cobalt content of these minerals depends on the total number of Fe-Mg lattice sites and is independent of the Fe/Mg ratio. Cobalt is strongly coherent with Mg in granitic rocks and behaves like Mg in its partition relations between metamorphic minerals. The acceptance of both Co and Mg is more selective at lower grades of metamorphism. These aspects have been further reviewed by Gunn (2014), McDonough (2014), Palme et al. (2014), and Rudnick and Gao (2014).

Cobalt is also a naturally occurring element in air, soil, plants, and water. The mean concentration of Co in the open ocean is very low (~40 pmol/kg) which in part reflects its short residence time. Co^{2+} is the principal aquatic species in seawater (Bruland et al. 2014). There has been considerable speculation on its mode of uptake in deep-sea manganese nodules and crusts. Cobalt tends to be associated with either Mn or Fe oxyhydroxides (Brown and Calas 2012). Cobalt may substitute as exchangeable Co^{2+} in marine manganates and then be oxidized to Co^{3+} by Mn^{4+}, whereas Co^{3+} may substitute for Fe^{3+} in Fe oxyhydroxide minerals. Cobalt may also be incorporated in birnessite as Co(II) at pH 7 and Co(III) above pH 8. The aqueous speciation and chemistry of Co in terrestrial environments is now an important focus of research, as the solution speciation of Co has a critical influence on its biological activity in the environment. Although there is a lack of comprehensive data on aqueous Co concentrations in soil porewaters, groundwater, and surface waters, natural Co concentrations vary mostly from 0.006 µg/L to 0.43 µg/L (Gaillardet et al. 2014). Cobalt is considered as moderately mobile with a mobility 10 times less than that of Na. Cobalt chemistry is dominated by the Co(II) oxidation state in the aqueous phase of terrestrial environments primarily due to the extremely low solubility of Co(III). There is no universal agreement on the importance of Co (II) complexation in the solution phase of terrestrial environments and, furthermore, on the nature of the major binding inorganic and organic ligands. The kinetics of Co (II) complexation to, and dissociation from, natural organic

complexing ligands are such that the speciation of Co is likely to significantly diverge from estimates based on thermodynamic equilibrium calculations. As a result, an accurate understanding of Co bioavailability, toxicity, and transport in terrestrial aquatic environments will only be achieved when thermodynamics can be reconciled with reaction kinetics.

Biological Utilization and Toxicity

Cobalt is an essential trace element in life and plays an important role in biochemical reactions essential for life, notably in the coenzyme cobalamin (Co chelated to four N atoms at the center of a porphyrin-like structure, Chivers 2014). Cobalamin has a complex biochemistry, and there is a number of cobalamin-dependent enzymes. Cobalamin-dependent enzymes influence nodulation and N_2 fixation in legume plants that can be used to supply nitrogen in crops (Underwood 1977). Cobalt deficiency affects nodule development, function, and nitrogen fixation. Cobalamin, also called vitamin B-12, is essential for human and animal health, nutrition, and growth. The amount needed is very small. Dietary Co intake is estimated to range 5–40 μg/day in the general human population (Simonsen et al. 2012).

Understanding the factors which affect Co uptake by plants across a range of soil types is essential for food quality as well as for possible remediation of contaminated sites. The relevant pedogenic processes contributing to Co uptake from soils by plants includes total, extractable, and exchangeable soil Co concentrations, pH and other soil chemical parameters, microbial variations, as well as anthropogenic inputs. In soils, Co is fixed by Mn-oxides in a non-extractable form, and its bioavailability is inversely proportional to the Mn content of the soil (Collins and Kinsela 2010).

High and frequent Co exposures can affect nervous system and cause an *axonopathy* (Flora 2014). Chronic inhalational intake of cobalt dust can lead to diffuse-inflammatory reactions of the bronchial mucosa and chronic respiratory tract disorders (Banza et al. 2009; Cheyns et al. 2014). In large doses, some Co forms are carcinogenic. Some plant species, also called metallophytes, have adapted to natural and contaminated Co-rich soils (Faucon et al. 2007). Among these metallophytes, some are able to hyperaccumulate Co in plant shoots (>300 ppm, without toxicity symptoms and growth inhibition) (Lange et al. 2017).

Summary

Cobalt production hugely increases in the last decade as the global demand for Co increases. However, its exploitation becomes a new urgent environmental issue, especially in region such as Democratic Republic of Congo. Cobalt has been suggested to be a potentially dangerous pollutant, and the United States Environmental Protection Agency classifies Co in the priority list of environmental risk elements. A better understanding of Co biogeochemical behavior may support to assess the risk to the environment and to human health and to assist in developing new remediation tools.

Cross-References

▶ Complexes
▶ Copper
▶ Ferromanganese Crusts and Nodules: Rocks That Grow
▶ Manganese
▶ Ore Deposits
▶ Siderophile Elements
▶ Trace Elements
▶ Transition Elements

References

Banza CLN, Nawrot TS, Haufroid V, Decrée S, De Putter T, Smolders E, Kabyla BI, Luboya OS, Ilunga AN, Mutombo AM, Nemery B (2009) High human exposure to cobalt and other metals in Katanga, a mining area of the Democratic Republic of Congo. Environ Res 109:745–752

Blackman AG (2006) Cobalt: inorganic & coordination chemistry. In: Encyclopedia of inorganic chemistry. Wiley, Chichester

Brown GE, Calas G (2012) Section 18. Mineral-water interfaces as driving forces for metal concentration: the example of cobalt trapping by Mn-Oxides. Geochem Perspect 1:667–669

Bruland KW, Middag R, Lohan MC (2014) 8.2 – controls of trace metals in seawater. In: Holland HD, Turekian KK (eds) Treatise on geochemistry, 2nd edn. Elsevier, Oxford, pp 19–51

Cheyns K, Banza Lubaba Nkulu C, Ngombe LK, Asosa JN, Haufroid V, De Putter T, Nawrot T, Kimpanga CM, Numbi OL, Ilunga BK et al (2014) Pathways of human exposure to cobalt in Katanga, a mining area of the D.R. Congo. Sci Total Environ 490:313–321

Chivers PT (2014) Chapter 14 Cobalt and nickel. In: Maret W, Wedd A (eds) Binding, transport and storage of metal ions in biological cells. The Royal Society of Chemistry, Cambridge, UK, pp 381–428

Collins RN, Kinsela AS (2010) The aqueous phase speciation and chemistry of cobalt in terrestrial environments. Chemosphere 79:763–771

Crundwell FK, Moats MS, Ramachandran V, Robinson TG, Davenport WG (2011) Extractive metallurgy of nickel, cobalt and platinum group metals. Elsevier, Amsterdam

Decrée S, Pourret O, Baele J-M (2015) Rare earth element fractionation in heterogenite (CoOOH): implication for cobalt oxidized ore in the Katanga Copperbelt (Democratic Republic of Congo). J Geochem Explor 159:290–301

Faucon MP, Shutcha MN, Meerts P (2007) Revisiting copper and cobalt concentrations in supposed hyperaccumulators from SC Africa: influence of washing and metal concentrations in soil. Plant Soil 301:29–36

Flora SJS (2014) Chapter 22 – Metals. In: Aronson JK (ed) Side effects of drugs annual. Elsevier, Amsterdam, pp 297–322

Gaillardet J, Viers J, Dupré B (2014) 7.7 – trace elements in river waters. In: Holland HD, Turekian KK (eds) Treatise on geochemistry, 2nd edn. Elsevier, Oxford, pp 195–235

Gunn G (2014) Critical metal handbook. Wiley, Chichester

Haynes WM (2015) CRC handbook of chemistry and physics, 96th edn. CRC Press, Boca Raton

Josso P, Pelleter E, Pourret O, Fouquet Y, Etoubleau J, Cheron S, Bollinger C (2017) A new discrimination scheme for oceanic ferromanganese deposits using high field strength and rare earth elements. Ore Geol Rev 87:3–15

Lange B, van der Ent A, Baker AJM, Echevarria G, Mahy G, Malaisse F, Meerts P, Pourret O, Verbruggen N, Faucon M-P (2017) Copper and cobalt accumulation in plants: a critical assessment of the current state of knowledge. New Phytol 213:537–551

McDonough WF (2014) 3.16 – compositional model for the Earth's core. In: Holland HD, Turekian KK (eds) Treatise on geochemistry, 2nd edn. Elsevier, Oxford, pp 559–577

Palme H, Lodders K, Jones A (2014) 2.2 – solar system abundances of the elements. In: Holland HD, Turekian KK (eds) Treatise on geochemistry, 2nd edn. Elsevier, Oxford, pp 15–36

Pourret O, Lange B, Bonhoure J, Colinet G, Decrée S, Mahy G, Séleck M, Shutcha M, Faucon M-P (2016) Assessment of soil metal distribution and environmental impact of mining in Katanga (Democratic Republic of Congo). Appl Geochem 64:43–55

Raveau B, Seikh MM (2012) Cobalt oxides: from crystal chemistry to physics. Wiley, Weinheim

Rudnick RL, Gao S (2014) 4.1 – composition of the continental crust. In: Turekian HD, Holland KK (eds) Treatise on geochemistry, 2nd edn. Elsevier, Oxford, pp 1–51

Simonsen LO, Harbak H, Bennekou P (2012) Cobalt metabolism and toxicology – a brief update. Sci Total Environ 432:210–215

Underwood EJ (1977) 5 – cobalt. In: Underwood EJ (ed) Trace elements in human and animal nutrition, 4th edn. Academic, New York, pp 132–158

Colloids

Jean-François Boily
Department of Chemistry, Umeå University, Umeå, SE, Sweden

Definition

Colloids are (in)organic (poly)molecular particles in which at least one dimension is of the order ~1–1000 nm in length. They may occur as individually dispersed and/or aggregated particles of a given substance suspended in another substance. They cannot be separated by conventional forms of filtration or centrifugation.

Introduction

Colloidal suspensions consist of particles of one phase (solid, liquid, gas) in a second continuous phase. Particles are ~1–1000 nm (or even ~10 μm) wide in at least one direction,

Colloids, Table 1 Colloidal systems according to states of matter[a]

Dispersed phase	Dispersing medium	Colloidal system	Examples
Gas	Liquid	Foam	Gas bubbles in water and magmas
	Solid	Solid foam	Pumice
Liquid	Gas	Liquid aerosol	Fog
	Liquid	Emulsion	Water-in-oil emulsions
	Solid	Gel	Fluid inclusions
Solid	Gas	Solid aerosol	Atmospheric mineral "dust"
	Liquid	Sol, suspensions	Mineral particles in aquatic environments
	Solid	Solid sol	Opals

[a]After Yariv and Cross (1979)

can be amorphous or crystalline, and be composed of inorganic, organic, or biological materials. Colloids of interest to Earth Sciences can be dispersed in solids, liquids, and gases, with representative examples shown in Table 1. Notable examples of colloids of biogeochemical importance include clays, fine silt, condensed Al(III) and Fe(III) (oxyhydr)oxides, as well as humic substances. Biocolloids are of organic nature and can include bacteria, viruses, protozoae, including macromolecular breakdown products and exudates.

In contrast to dissolved substances in homogeneous solutions, colloids can undergo Brownian motion due to collisions with molecules of the host medium. Many can also scatter light (Tyndall effect) when suspended in light-transparent media. Stable colloidal suspensions, namely those that do no settle effectively, are stabilized by strong solvation forces from the dispersing medium, thus effectively overcoming gravitational forces. Destabilized colloids can however agglomerate and settle if this fine balance of forces is compromised. Note that "flocculation," "agglomeration," and "coagulation" are terms that are often used interchangeably in the literature. Still, "coagulation" can be more specifically used to refer to the near irreversible aggregation of tightly packed colloids into a "coagulum," while "flocculation" can pertain to loose and open colloidal aggregates that can be readily dispersed by external forces.

Because colloids can expose reactive functional groups capable of removing molecules from the host medium, they can play key roles in the (bio)geochemical cycling of elements and mass transport in nature. For instance, the biogeochemical cycling of elements can be strongly coupled to the occurrence and reactivity of high specific surface area iron (oxyhydr)oxide colloids (Raiswell and Canfield 2012). Colloidal transport through waterways of Earth's surface or through porous/fissured media of Earth's upper crust represents an additional important vector affecting mass transport.

In this article an overview of representative colloids and colloidal processes of central interest to Earth Sciences is presented. It briefly highlights settings from Earth's atmosphere and low-temperature environments to those relevant to magmatic settings.

Colloidal Suspension Properties

Colloids form (i) chemically by *condensation* of new phases from molecular units (e.g., hydrolysis and precipitation of Al(III)), or (ii) by physical or chemical *comminution* (dispersion) of host materials into smaller fragments. As these are materials with high surface area to bulk mass ratios, surfaces play a determining role on the behavior of colloids. These particles can then be subjected several forces that can even overcome gravitational forces and suspend particles temporarily or indefinitely, namely with suspension times from seconds to years. The concept of colloidal stability ratio (W) accounts suspension stability in terms of the the ratio of the rates of diffusion-controlled to interaction force-controlled interparticle collision (*cf.* Hunter 1981). In thermodynamic parlance, the total Gibbs free energy of colloidal suspensions can be given by a balance of attractive and repulsive contribution (Fig. 1; Moore et al. 2015):

$$\Delta G_{total} = \Delta G_{repulsive} + \Delta G_{attractive} \quad (1)$$

Each of these latter terms can be broken into components referring to distinct physicochemical phenomena including solvation, electrostatic (electric double layers), steric, polymer flocculation, and hydrophobic contributions.

In vacuum or inert air, van der Waals attractive force can drive aggregation as a means to minimize surface energies of colloidal particles. These energies can however also be decreased via adsorption of solvents, such as water, which in turn form *excluded volumes* that hinder particle-particle collisions. Adsorption reactions involving potential-determining ions and counterions (e.g., Na^+ and Cl^-) can also generate an electric double layer (EDL) repelling charged particles from one another. The magnitude and sign of the EDL potential as well as its thickness affect colloidal stability. This is classically expressed by DLVO theory (Derjaguin, Landau, Verway and Overbeek (Verwey and Overbeek 1948) by accounting for the interplay of electrostatic repulsion of the EDL and of van der Waals attraction between particles. Stable colloidal suspensions thus result from dominant electrostatic repulsion between particles. Stability may however be compromised by changes in salinity because weakly- to non-binding ions (e.g., Na^+, Cl^-) can effectively contract EDL thickness. This can be accounted by the Debye screening length (Hunter 1981), which can range from
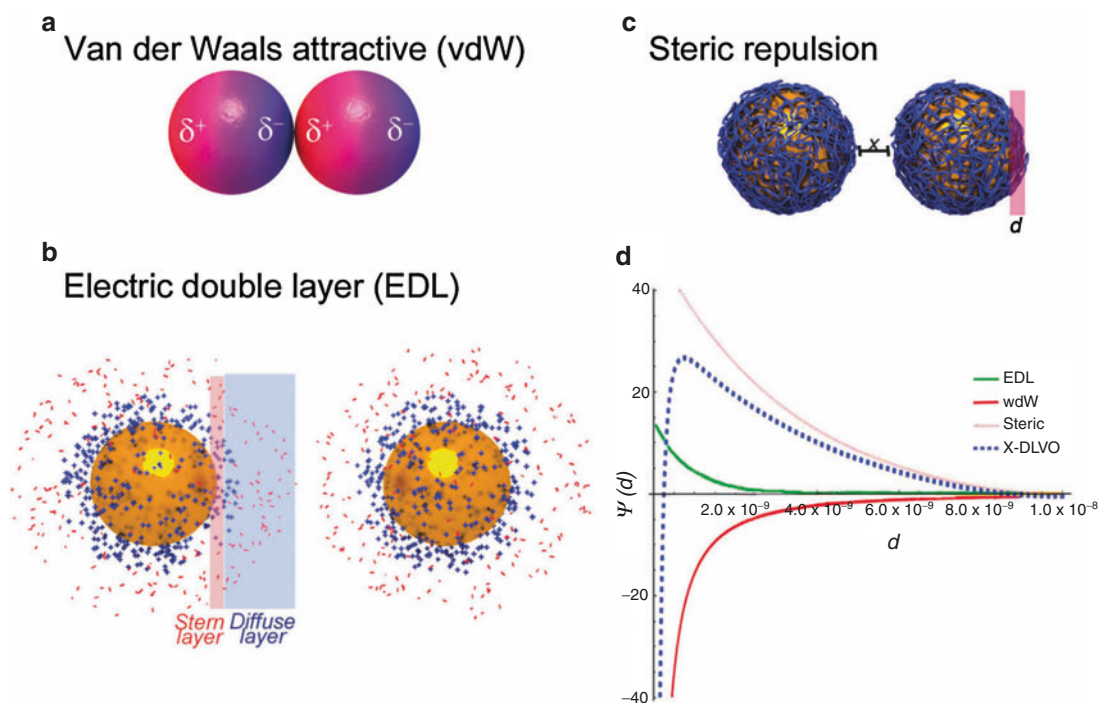
Colloids, Fig. 1 Colloidal interactions. (**a**) Van der Waals attractive forces. (**b**) Electric double layer formed at charged particle surfaces. (**c**) Steric repulsion caused by sorbed macromolecules. (**d**) Potential energy distance curve (DLVO, *blue dashed*) broken down for contributions from van der Waals (*red*), electric double layer (*green*), and steric (*pink*). (Taken from Moore et al. (2015)

~300 nm at 0.001 M to ~11 nm at 0.7 M, the latter being close to seawater. Thus, when fluvial colloids are discharged into estuarine environments, or when water evaporates from a colloidal suspension, the contraction of the EDL enables attractive to van der Waals forces to drive particle flocculation and sedimentation. At the same time, colloidal stability can be compromised by changes in pH or binding of foreign species (e.g., metal ions, natural organic matter) affecting the magnitude and sign of EDL potentials, and therefore electrostatic contributions to colloidal stability.

Additionally, adsorption of polymeric-like molecules, such as possibly natural organic matter, can present possibilities for *steric stabilization*. Particle-particle interactions can be inhibited by an an osmotic pressure effect driving water molecules between interpenetrating polymeric units of approaching particles. Loss of degrees of freedom of polymers between particles also result in a lost of entropy, and thus induce a thermodynamically unfavorable condition for colloidal stability.

Examples of Colloids on Earth

Colloids are of widespread occurrence in terrestrial environments. Predominant forms of sedimentary rocks (shales, sandstones and limestones) in fact cover ~73% of modern-day continents and can be made up of considerable portions of colloidal particles. In soils, they can be generated by the physicochemical breakdown of host rock, or by precipitation from aqueous solution (e.g., via hydrolysis of Al(III) and Fe(III)). Gravitation of colloids from upper soil horizons to accumulative horizons in the lower portion of soils is an additional process contributing to mass transfer across soil profiles. Likewise, the transport of colloids in porous or fissured environments of Earth's upper crust is key to the understanding on nutrient, metal, radionuclide and contaminant transport.

Sedimentation of colloidal suspensions in open waterways can be strongly affected by particle density, size, and water movement. For instance, while an important quantity of matter collected by rivers is deposited as sediments at estuaries, fines such as clays, silt, and organic matter are transported further to oceans. Additionally, particles may remain in suspension or be resuspended by wave, tidal, and flood activities in spite of favorable physicochemical conditions for flocculation.

Opals are another example of sedimentary deposits consisting of colloidal particles. These mineraloids can be refered as *colloidal crystals* and consist of (hexagonal, cubic) close-packed colloidal particles of hydrated SiO_2 spheres of ~150–300 nm in size. They can form from evaporated silica-rich solutions that have leached through sandstones. Subsequent compaction and partial dehydration of the silica spheres produce opals with various degrees of organisation, with gemstone-like attributes.

Gas bubbles represent another form of colloidal entity strongly relevant to Earth sciences. Bubbles expelled by biotic, diagenetic, and igneous processes can be dispersed in the form of a foam. Water-based foams can, for instance, reduce the permeability of porous media, such as soils and sediments. Air bubbles can also be captured in freezing soils or (sea) water (Deville 2017), which are in turn used for tracking paleoclimates. Nucleation and growth of bubbles in magmas are also key to understand explosive in relation to effusive volcanic eruptions. Gas bubbles in pumice, a vecicular volcanic glass, are also viewed as colloids (Table 1).

Finally, the atmosphere can also be considered as a colloidal system. Colloids in these systems are more often refered to as solid or liquid aerosols. A notable example is water droplet formation from the condensation of atmospheric water vapor (*e.g.*, fog, cloud, mist, droplets), and with droplet sizes in the ~1–100 100 μm range. Atmospheric mineral dust particles ejected from volcanoes, blown from deserts, and, more recently, produced by industry play integral parts to atmospheric processes, and most notably in ice nucleation (Hoose and Möhler 2012). Deposition of iron-bearing particles to the oceans is, moreover, a key input to ocean productivity and biogeochemistry (Tagliabue et al. 2017).

Summary

Colloids are inorganic and organic fines of diverse compositions and sources. They are of widespread occurrence in continental, oceanic, and atmospheric environments. The high surface-to-bulk mass ratio of these particles is especially responsible for their large chemical reactivity and for their important roles in the biogeochemical cycling of elements in nature and even in atmospheric processes.

Cross-References

▶ Aqueous Solutions
▶ Chemical Weathering
▶ Earth's Atmosphere
▶ Entropy
▶ Equilibrium
▶ Fluid–Rock Interaction
▶ Geochemical Thermodynamics
▶ Laboratory Simulations of Organic Geochemical Processes at Elevated Temperatures
▶ Low-Temperature Geochemistry
▶ Marine Sediment
▶ Surface Geochemistry
▶ Volcanic Gases
▶ Water

References

Deville S (2017) Freezing colloids: observations, principles, control, and use. Springer, Switzerland

Hoose C, Möhler O (2012) Heterogeneous ice nucleation on atmospheric aerosols: a review of results from laboratory experiments. Atmos Chem Phys 12:9817–9854

Hunter RJ (1981) Zeta potential in colloid science: principles and applictions. Academic Press, New York

Moore TL et al (2015) Nanoparticle colloidal stability in cell culture media and impact on cellular interactions. Chem Soc Rev 44:6287–6305. https://doi.org/10.1039/C4CS00487F

Raiswell R, Canfeild DE (2012) The iron biogeochemical cycle past and present. Geochem Perspect 1:1–217

Tagliabue A, Bowie AR, Boyd PW, Buck KN, Johnson KS, Saito MA (2017) The integral role of iron in ocean biogeochemistry. Nature 543:51–59. https://doi.org/10.1038/nature21058

Verwey EJW, Overbeek JTG (1948) Colloidal dispersions. Cambridge University Press, New York

Yariv S, Cross H (1979) Geochemistry of colloid systems: for earth scientists. Springer-Verlag, Berlin, Heidelberg

Complexes

Jay R. Black
School of Earth Sciences, The University of Melbourne, Melbourne, VIC, Australia

Synonyms

Aqueous species; Coordination complex; Ion pair

Definition

Complexes are compounds that form in solutions due to interactions between ions or neutral molecules forming coordinating bonds between them. Coordination complexes commonly form between positively charged cations (e.g., Ca^{2+}, Mg^{2+}, Na^+ and Cu^{2+}), which act as a central atom and are bound to negatively charged anion species (e.g., Cl^-, SO_4^{2-}, HCO_3^- and F^-) or neutral species (e.g., H_2O and NH_3), also referred to as ligands. The types of bonds that form may be ionic due to Coulombic forces or covalent due to sharing of electrons between atoms or other types of interactions such as dipole-dipole interactions (See entries ▶ "Chemical Bonds" and ▶ "Van der Waals Force"). Ligands that form more than one bond with a central metal atom, thus occupying more than one coordination site, are called chelates (See entry ▶ "Chelation"). Many organic ligands act as chelates forming multiple bonds with a metal, such as porphyrin a ring shaped tetradendate ligand which binds metals in the center via 4 bonds (See entry ▶ "Porphyrins"). Complexes that form

with more than one metal center are referred to as multi- or polynuclear complexes (Stumm and Morgan 1996).

Complex Formation and Coordination Chemistry

A general chemical reaction for complex formation can be written with an acidic electron accepting group (the metal) and a basic electron donating group (the ligand), much in the same sense as that of acid–base chemistry (See entry ▶ "Acid–Base Reactions") but defined as:

$$mM^{i+} + nL^{j-} = (M_mL_n)^{(mi+nj)} \qquad (1)$$
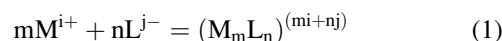
where, M is a metal of charge i + and L is a ligand of charge j-, m and n being stoichiometric constants.

In aqueous solutions metals will form a coordination complex with water molecules, which form an inner sphere of hydration of varying coordination depending upon the metals type (See entry ▶ "Aqueous solutions"). For instance, at most ionic strengths Mg^{2+} forms an octahedrally coordinated inner sphere complex with 6 molecules of H_2O ($Mg(H_2O)_6^{2+}$, see Bock et al. 1994), whereas, Li^+ forms a tetrahedrally coordinated inner sphere complex with 4 molecules of H_2O ($Li(H_2O)_4^+$, see Rudolph et al. 1995) (Fig. 1). The water molecules bound to the inner sphere of a complex are often omitted, for instance, $Mg^{2+}_{(aq)}$ would refer to the $Mg(H_2O)_6^{2+}$ complex and the subscript (aq) is commonly used to designate an aqueous complex. Thus, a knowledge of coordination chemistry is needed to understand the chemical environment of an aqueous complex.

Inner-Sphere and Outer-Sphere Complex Formation

The inner sphere constitutes ligands that are directly bonded to the metal center in the inner coordination environment. Beyond the coordination environment of the inner sphere of a complex the solvent or solutes may also be ordered around a complex forming an outer sphere coordination environment due to electrostatic interaction between the central cation and solvated anions or dipole-dipole interactions with water. As the types of interactions leading to the formation of an outer sphere complex are often weaker than inner sphere interactions, the structure of the outer sphere is often not considered until higher ionic strengths are reached where ion pairing becomes more important (See entry ▶ "Debye-Hückel Equation"). However, considering the second solvation sphere of an aqueous complex is often important in order to accurately predict the vibrational spectra of the complex (e.g., $Li(H_2O)_4^+ \cdot 4H_2O$, Fig. 1; Pye et al. 1996). Inner and outer

Complexes, Fig. 1 Molecular
models of aqueous complexes of
octahedral $Mg(H_2O)_6^{2+}$ (on the
left) and tetrahedral Li
$(H_2O)_4^+$.$4H_2O$ (on the *right*)
showing both the inner sphere and
outer sphere solvation of the
lithium ion
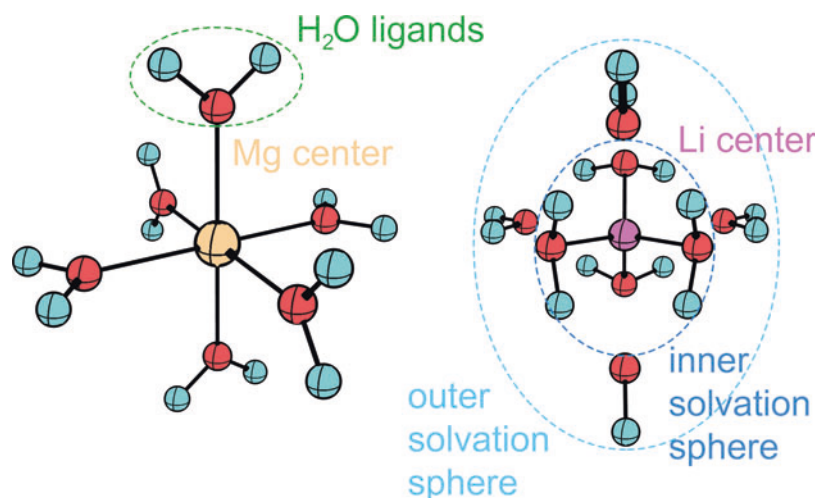
sphere complexes are also important to the complex structure that forms at mineral surfaces at the water-mineral interface where a minerals surface charge affects the adsorption of aqueous metals and ligands forming surface complexes (See entries ▶ "Surface Geochemistry" and ▶ "Gouy-Chapman Theory").

For example, sulphate may form an outer-sphere complex with magnesium or ion pair (Eq. 2). As the concentration of sulphate in solution increases it may exchange with a water bound to the inner sphere of the hexaaquomagnesium complex, thus going from being bound as an outer-sphere complex to a inner-sphere complex or contact ion pair (Eq. 3):

$$\left[Mg(H_2O)_6\right]^{2+} + SO_4^{2-} = \left[Mg(H_2O)_6\right].SO_4 \quad (2)$$

$$\left[Mg(H_2O)_6\right].SO_4 = \left[MgSO_4(H_2O)_5\right] + H_2O \quad (3)$$
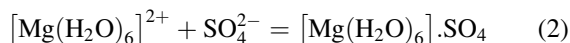
The ligand-exchange reactions shown in Eqs. 2 and 3 simplify the solvation structure, as the sulfate ligand may also be solvated and bound as an outer-sphere complex via it's solvation sphere. Rates of ligand exchange between the inner and outer spheres are often quite rapid in aqueous solution (See entry ▶ "Kinetics of Geochemical Processes").

Complex Speciation and Stability

The addition of many solutes and ligand types to an aqueous solution may lead to various metal complexes forming in solution, the distribution of these complexes or aqueous species is known as the aqueous or complex speciation of the solution. Simply varying the pH of an aqueous solution may lead to the formation of various metal hydrolysis products (i.e., the formation of soluble metal hydroxides and oxide

complexes). The hydrolysis of cations has been reviewed in detail by Baes and Mesmer (1976). Complex speciation affects many environmental processes from the solubility of minerals (See entry ▶ "Solubility"), to the transport of metals in hydrothermal fluids and their eventual deposition as an ore deposit (See entries ▶ "Hydrothermal Solutions" and ▶ "Ore Deposits").

The thermodynamic stability of aqueous complexes can be measured and is defined by an equilibrium constant for reactions such as those represented by Eq. 1 (See entry ▶ "Equilibrium constant"). Ligand substitution reactions can be written in a stepwise or cumulative manner and formation constants defined as K (Eqs. 4, 5, and 6) or β (Eq. 7), respectively:

Stepwise complex formation and constants:

$$M^+ + L^- \overset{K_1}{=} ML^0 \text{ where } K_1 = \frac{\left[ML^0\right]}{\left[M^+\right]\left[L^-\right]} \quad (4)$$

$$ML^0 + L^- \overset{K_2}{=} ML_2^- \text{ where } K_2 = \frac{\left[ML_2^-\right]}{\left[ML^0\right]\left[L^-\right]} \quad (5)$$

$$ML_{(n-1)}^{(2-n)} + L^- \overset{K_n}{=} ML_n^{(1-n)} \text{ where } K_n = \frac{\left[ML_n^{(1-n)}\right]}{\left[ML_{(n-1)}^{(2-n)}\right]\left[L^-\right]} \quad (6)$$
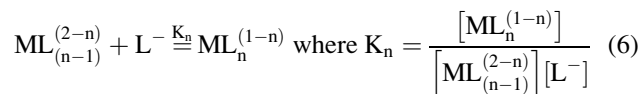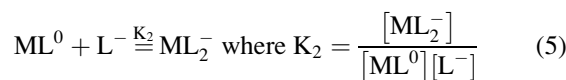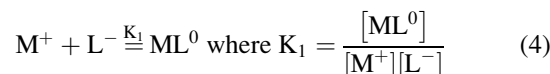
Cumulative complex formation and constant:

$$M^+ + nL^- \overset{\beta_n}{=} ML_n^{(1-n)} \text{ where } \beta_n = \frac{\left[ML_n^{(1-n)}\right]}{\left[M^+\right]\left[L^-\right]^n} \quad (7)$$
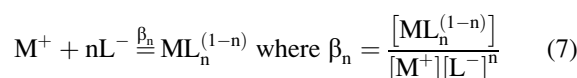
The cumulative formation constant is related to the stepwise formation constant by the expression:

$$\beta_n = K_1 \cdot K_2 \ldots \cdot K_n \quad (8)$$

The concentration of aqueous complexes as defined by the formation constants above (Eqs. 4, 5, 6, and 7) does not account for species activity, which is affected by the ionic strength of a solution where ion pairing increases with increasing ionic strength (See entries ▶ "Activity and Activity Coefficients" and ▶ "Debye-Hückel Equation").

Complex stability is affected by the strength of bonds which form, and as metals can be treated as hard or soft Lewis acids and ligands as hard or soft Lewis bases, the stability and reactions between complexes can be treated similarly to Lewis acid–base chemistry (Pearson 1963; Stumm and Morgan 1996) (See entry ▶ "Acid–Base Reactions"). Pearson's HSAB (Hard Soft Acid Base) principles can be used to determine the relative strength of bonds that form between metals and ligands (Liu et al. 2014; Pearson 1963).

Temperature and pressure of a system also affect complex stability. With increasing temperature the dielectric constant of water decreases making it less polarizable, which leads to a decrease in the coordination number of waters solvating an ion (Seward and Driesner 2004). Increasing pressure in a system may also lead to change in coordination environment of a complex due to changes in the solvent structure again leading to a dehydration of an ion (Seward and Driesner 2004). These changes in ion hydration and solvent structure inherently lead to a change in water activity affecting the water-rock interactions and complex formation and stability at higher temperatures and pressures.

Complex Speciation in the Environment

The formation of aqueous complexes affects many natural processes, from mineral solubility to metal transport in hydrothermal solutions. Formation waters occurring deep within the aquifers of sedimentary basins range in composition from fresh to extremely saline, and their composition can affect the diagenesis of minerals within the basin (See entry ▶ "Diagenesis"). Hydrothermal fluids found much deeper in the Earth's crust and potentially originating from the mantle or other sources can vary in composition significantly (See entry ▶ "Hydrothermal Solutions"). Hydrothermal fluids can transport high concentrations of various metals through complexation with ligands such as Cl^-, HS^- and OH^-. For example, the formation of gold complexes in hydrothermal solutions containing Cl^-, Br^-, HS^- and $NH_{3(aq)}$ ligands (Liu et al. 2014), where Au^+ preferentially binds with HS^- ligands to form a $Au(HS)_2^-$ complex.

The chemistry of Earth's oceans is affected by the complex speciation between a number of dissolved metals and ligands found in seawater. For instance, the ionic strength (I) of seawater (I = c. 0.69 m) leads to significant ion pairing and formation of complexes of $MgHCO_3^+$, $MgCO_3^0$, $MgSO_4^0$, $NaHCO_3^0$, $NaCO_3^-$, $NaSO_4^-$, $CaHCO_3^+$, $CaCO_3$, $CaSO_4^0$ and KSO_4^- in excess of 0.01 millimolal in solution. The pH of seawater is influenced by this complex speciation and in particular the equilibrium established between the bicarbonate (HCO_3^-) and carbonate (CO_3^{2-}) ligands, dissolved CO_2 and various metals (See entry ▶ "Carbon Cycle").

Understanding complex speciation is important to contaminant transport in shallow groundwater environments where toxic or radioactive metals have been mobilized in surface and groundwaters. For example, the persistence of methylmercury complexes (e.g., CH_3Hg^+, CH_3HgS^-, $(CH_3)_2Hg^0$, CH_3HgOH^0 and CH_3HgCl^0) in the environment, of which the neutral complexes are highly mobile increasing their bioavailability (Stumm and Morgan 1996).

Summary and Conclusions

Complex formation and speciation is important to understanding the distribution and transport of metals in the environment. The formation of aqueous complexes affects the solubility of minerals and transport of dissolved solutes in the environment from the Earth's oceans to formation waters in sedimentary basins and hydrothermal fluids. Complex stability is affected by the concentration and type of ligands available to bond with metals, as well as the temperature and pressure of a system. Further information about complex formation, structure and bonding can be found in most inorganic chemistry text books discussing crystal field theory and ligand field theory (e.g., Shriver and Atkins 1999).

Cross-References

▶ Acid–Base Reactions
▶ Activity and Activity Coefficients
▶ Aqueous Solutions
▶ Chelation
▶ Chemical Bonds
▶ Debye-Hückel Equation
▶ Diagenesis
▶ Equilibrium Constant
▶ Gouy-Chapman Theory
▶ Hydrothermal Solutions
▶ Kinetics of Geochemical Processes
▶ Ore Deposits
▶ Porphyrins
▶ Surface Geochemistry
▶ Van der Waals Force

References

Baes CF, Mesmer RE (1976) The Hydrolysis of Cations. Wiley, New York, 489 pp

Bock CW, Kaufman A, Glusker JP (1994) Coordination of water to magnesium cation. Inorganic Chemistry 33:419–427

Liu W, Etschmann B, Testemale D, Hazemann J-L, Rempel K, Müller H, Brugger J (2014) Gold transport in hydrothermal fluids: competition among the Cl⁻, Br⁻, HS⁻ and NH$_{3(aq)}$ ligands. Chemical Geology 376:11–19

Pearson RG (1963) Hard and soft acids and bases. Journal of the American Chemical Society 85:3533–3540

Pye CC, Rudolph W, Poirier RA (1996) An ab Initio investigation of lithium ion hydration. The Journal of Physical Chemistry 100:601–605

Rudolph W, Brooker MH, Pye CC (1995) Hydration of lithium ion in aqueous solution. The Journal of Physical Chemistry 99:3793–3797

Seward TM, Driesner T (2004) Chapter 5, Hydrothermal solution structure: experiments and computer simulations. In: Palmer DA, Fernández-Prini RJ, Harvey AH (eds) Aqueous Systems at Elevated Temperatures and Pressures: Physical Chemistry in Water, Steam and Hydrothermal Solutions. Elsevier, Amsterdam, pp 149–182

Shriver DF, Atkins PW (1999) Inorganic Chemistry, 3rd edn. Oxford University Press, Oxford, 763 pp

Stumm W, Morgan JJ (1996) Aquatic Chemistry: Chemical Equilibria and Rates in Natural Waters, 3rd edn. Wiley, New York, 1022 pp

Compound-Specific Isotope Analysis

Yi Ge Zhang
Department of Oceanography, Texas A&M University, College Station, TX, USA

Definition

Compound-specific isotope analysis (CSIA), as opposed to bulk analysis, determines the isotopic signatures (for example, $^{13}C/^{12}C$, D/H, $^{15}N/^{14}N$, $^{18}O/^{16}O$) at the molecular level. The separation and purification of organic compounds can be achieved by gas chromatography (GC) or liquid chromatography (LC). The analysis of stable isotopes requires an isotope ratio mass spectrometry (IRMS).

Analytical Methods: GC-IRMS

Traditionally, CSIA refers only to the stable isotope measurements of the molecules separated by GC. The system usually consists of a GC, a chemical reaction interface, and an IRMS (Sessions 2006; Summons 2000). Individual compounds are separated by the GC, followed by quantitative conversion at the interface, and continuous-flow isotopic analysis using the IRMS. The interface either diverts or removes the interfering compounds such as the solvents and H_2O.

Early CSIA focused on stable carbon isotopes (Hayes et al. 1989; Matthews and Hayes 1978). Organic molecules can be rapidly and quantitatively combusted to CO_2, done by metal oxides (e.g., CuO, NiO) with the presence of catalysts (e.g., Pt) at high temperature (900–1200 °C). The oxidizing reagents are regenerated by flushing the combustion reactor with O_2 after analysis (Merritt et al. 1995). The solvent peak is usually diverted by backflushing the reactor with a He flow. And the impurities in the CO_2 stream (H_2O, S, and N oxides) are removed by Nafion™, a selectively permeable membrane of the sulfonated fluoropolymer (Leckrone and Hayes 1997), and by passing the combusted gas through the elemental copper at a lower temperature. CO_2 is then analyzed in a gas source IRMS, which usually consists of an electron-impact ionization source, a magnetic-sector analyzer, and several Faraday cup detectors which receive analog signals of the ion currents.

Compound-specific nitrogen isotope measurement is also based on combustion/reduction, which produces NO_x then reduced to N_2 (Merritt and Hayes 1994). Notably, a bacterial method which could be used to convert organic N to N_2O significantly reduces the amount of N required for accurate measurements (Sigman et al. 2001). Hydrogen isotope analysis is usually achieved by pyrolysis using carbon-lined reactors heated to > 1440 °C (Burgoyne and Hayes 1998). In the IRMS ion source, H_2 reacts to form H_3^+ and therefore the "H_3-factor" must be determined and corrected for (Sessions et al. 2001). Oxygen isotope measurements also rely on pyrolysis and reduction, which transfers O from organic material to CO.

Recent Developments

GC-IRMS has greatly expanded our ability to analyze compound-specific isotopes on GC-amenable molecules. However, many higher molecular weight, more complex compounds cannot be directly vaporized in the traditional GC. Further, the process of combustion/pyrolysis destroys the position-specific isotope signatures. Nonetheless, recent efforts have made interesting developments to tackle these issues.

Compound Separations Without a GC

A large number of nonvolatile biochemical such as nucleic acids, proteins, polar lipids, and carbohydrates cannot be separated by the traditional GC. To tackle this problem, a variety of offline preparative procedures (e.g., prep LC) were developed to fraction-collect and purify the compounds of interest, for further "bulk" analysis. The stable isotope

measurements can be achieved on the conventional elemental analyzer (EA)-IRMS or the spooling wire microcombustion (SWiM-IRMS)(Sessions et al. 2005) and nano-EA-IRMS (Polissar et al. 2009), both of which significantly reduce the quantities needed for isotope ratio monitoring. For example, the precision on the SWiM-IRMS is about 0.4‰ for ~2 μg C (Pearson et al. 2016).

High-Temperature GC-IRMS

An alternative approach to volatize the larger compounds is to increase the temperature of the GC oven, from ~320 °C to a maximum of ~450 °C. Studies have shown that if connections are all air-tight by using metal ferrules, high-temperature resistant components as well as sensitive systems that discriminates the analytes from high column bleeding, the GC-MS system can detect *n*-alkanes with more than 100 carbon atoms (Sutton and Rowland 2012). Measuring these high molecular weight compounds on GC-IRMS is being experimented as this entry is written in 2016.

Site-Specific Isotope Measurements

The conversion of C, H, N, or O to analyte gases is required by CSIA based on the traditional gas source IRMS. The isotopic value, however, is an average over all elemental positions within its molecular structure. Intramolecular variations in isotopic signatures are missing in this approach.

Innovations in the technology, including the utilizations of high-sensitivity detectors capable to quantify low-intensity multiply substituted ion beams using both improved IRMS (Eiler et al. 2013) or IR absorption spectroscopy (Ono et al. 2014). Position-specific intramolecular isotopic distributions are now being reported from several molecules, including ethane (Webb et al. 2013) and propane (Piasecki et al. 2016).

Selected Applications in Geoscience

The Alkenone-δ^{13}C Method for *p*CO$_2$

One of the earliest applications of CSIA was to measure the δ^{13}C of biomarkers associated with photosynthesis, such as porphyrins (Hayes et al. 1989; Popp et al. 1989) and alkenones (Jasper and Hayes 1990), as a proxy for atmospheric CO$_2$ levels. This methodology stems through the isotopic fractionation models of C3 plants during photosynthesis (Farquhar et al. 1982, 1989). Compared with the traditional bulk organic carbon measurements, CSIA provides isotopic evidence from the substance with a clear photosynthetic origin. Alkenones are then favored over porphyrins because they are only produced by a few species of the haptophyte algea in the modern ocean (Conte et al. 1994).

The alkenone-^{13}C based *p*CO$_2$ estimates have covered most of the Cenozoic era, which reveals a long-term decline of the greenhouse gas forcing from the Paleogene into the Neogene (Pagani et al. 2005; Zhang et al. 2013). Specific time intervals are also targeted, with *p*CO$_2$ often found to be tightly coupled to major climate change events (Bijl et al. 2010; Pagani et al. 2011). Alkenone-derived reconstructions largely agree with other proxy-based CO$_2$ estimates (Palmer et al. 2010), but occasionally show low sensitivity to CO$_2$ changes (Badger et al. 2013). Efforts are being made to constrain the physiology of the haptophyte algae and how they are going to affect carbon isotope fractionations (Bolton et al. 2016; Henderiks and Pagani 2007).

^{13}C–Depleted Biomarkers and Methane Cycling

CSIA is widely used to trace biogeochemical processes (Freeman et al. 1990). For example, massive amount of methane produced in the deep ocean are oxidized anaerobically before they can reach the sea surface. Anaerobic oxidation of methane (AOM) has been suggested by geochemical data in the 1970s (Reeburgh 1976). However, for a long time the microorganisms responsible for this process could not been identified. In 1999, Hinrichs et al. noticed that the biomarkers associated with archaea in a gas hydrate site offshore of northern California are extremely depleted in ^{13}C. The δ^{13}C of these biomarkers, including archaeol, hydroxyarchaeol, and *sn*-2-hydroxyarchaeol, ranges between −100 and −110‰, indicating that the carbon source of the archaea has a methenotrophic origin (Hinrichs et al. 1999). Later, microscopic evidence was provided to confirm the role of archaea in the AOM process, and showed that a consortium of archaea and sulfate reducing bacteria that commonly perform sulfate reduction – anaerobic methane oxidation in marine sediment (Boetius et al. 2000).

Summary

Compound-specific isotope analysis has broad utilities in tracing sources and revealing the biogeochemical processes that involves isotopic fractionation. The field has greatly expanded from measuring carbon isotopes of GC-amendable compounds to employing a variety of approaches to separate and purify compounds, including those that cannot be separated by the traditional GC, for isotope measurements of C, N, H, O, S, and other light elements. Position-specific isotope analysis is also being explored that adds a whole new dimension to CSIA. CSIA is widely applied in organic geochemistry, biogeochemistry, geobiology, paleoclimatology, forensic geoscience, and petroleum science and technology.

Cross-References

References

Badger MPS, Schmidt DN, Mackensen A, Pancost RD (2013) High-resolution alkenone palaeobarometry indicates relatively stable pCO_2 during the Pliocene (3.3–2.8 ma). Phil Trans R Soc A 371(2001):20130094

Bijl PK, Houben AJP, Schouten S, Bohaty S, Sluijs A, Reichart GJ, Damste JSS, Brinkhuis H (2010) Transient middle eocene atmospheric CO_2 and temperature variations. Science 330:819–821

Boetius A, Ravenschlag K, Schubert CJ, Rickert D, Widdel F, Cleseke A, Amann R, Jorgensen BB, Witte U, Pfannkuche O (2000) A marine microbial consurtium apparently mediating anaerobic oxidation of methane. Nature 407:623–626

Bolton CT, Hernandez-Sanchez MT, Fuertes M-A, Gonzalez-Lemos S, Abrevaya L, Mendez-Vicente A, Flores J-A, Probert I, Giosan L, Johnson J, Stoll HM (2016) Decrease in coccolithophore calcification and CO_2 since the middle Miocene. Nat Commun 7:10284

Burgoyne TW, Hayes JM (1998) Quantitative production of H_2 by pyropysis of gas chromatographic effluents. Anal Chem 70:5136–5141

Conte M, Volkman JK, Eglinton G (1994) Lipid biomarkers of the haptophyta. In: Green JC, Leadbeater BSC (eds) The haptophyte algae. Clarendon Press, Oxford, pp 351–377

Eiler JM, Clog M, Magyar P, Piasecki A, Sessions AL, Stolper D, Deerberg M, Schlueter H-J, Schwieters J (2013) A high-resolution gas-source isotope ratio mass spectrometer. Int J Mass Spectrom 335:45–56

Farquhar GD, O'Leary MH, Berry JA (1982) On the relationship between carbon isotope discrimination and the intercellular carbon dioxide concentration in leaves. Aust J Plant Physiol 9:121–137

Farquhar GD, Ehleringer JR, Hubick KT (1989) Carbon isotope discrimination and photosynthesis. Annu Rev Plant Physiol Plant Mol Biol 40:503–537

Freeman KH, Hayes JM, Trendel J-M, Albrecht P (1990) Evidence from carbon isotope measurements for diverse origins of sedimentary hydrocarbons. Nature 343:254–256

Hayes JM, Freeman KH, Popp BN, Hoham CH (1989) Compound-specific isotopic analyses: a novel tool for reconstruction of ancient biogeochemical processes. Org Geochem 16:1115–1128

Henderiks J, Pagani M (2007) Refining ancient carbon dioxide estimates: significance of coccolithophore cell size for alkenone-based pCO_2 records. Paleoceanography 22:PA3202

Hinrichs KU, Hayes JM, Sylva SP, Brewer PG, DeLong EF (1999) Methane-consuming archaebacteria in marine sediments. Nature 398:802–805

Jasper JP, Hayes JM (1990) A carbon isotope record of CO_2 levels during the late quaternary. Nature 347:462–464

Leckrone KJ, Hayes JM (1997) Efficiecy and temperature dependence of water removal by membrane dryers. Anal Chem 1997:911–918

Matthews DE, Hayes JM (1978) Isotope-ratio-monitoring gas chromatography mas spectrometry. Anal Chem 50:1465–1473

Merritt DA, Hayes JM (1994) Nitrogen isotopic analysis by isotope-ratio-monitoring gas chromatography-mass spectrometry. J Am Soc Mass Spectrom 5:387–397

Merritt DA, Freeman KH, Ricci MP, Studley SA, Hayes JM (1995) Performance and optimization of a combustion interface for isotope ratio monitoring gas chromatography/mass spectrometry. Anal Chem 67:2461–2473

Ono S, Wang DT, Gruen DS, Sherwood Lollar B, Zahniser MS, McManus BJ, Nelson DD (2014) Measurement of a doubly substituted methane isotopologue, $^{13}CH\,^3D$, by tunable infrared laser direct absorption spectroscopy. Anal Chem 86:6487–6494

Pagani M, Zachos JC, Freeman KH, Tipple B, Bohaty S (2005) Marked decline in atmospheric carbon dioxide concentrations during the Paleogene. Science 309:600–603

Pagani M, Huber M, Liu ZH, Bohaty S, Henderiks J, Sijp W, Krishnan S, DeConto R (2011) The role of carbon dioxide during the onset of Antarctic glaciation. Science 334:1261–1264

Palmer MR, Brummer GJ, Cooper MJ, Elderfield H, Greaves MJ, Reichart GJ, Schouten S, Yu JM (2010) Multi-proxy reconstruction of surface water pCO_2 in the northern Arabian Sea since 29 ka. Earth Planet Sci Lett 295:49–57

Pearson A, Hurley S, Shah Walter SR, Kusch S, Lichtin S, Zhang YG (2016) Stable carbon isotope ratios of intact GDGTs indicate heterogeneous sources to marine sediments. Geochim Cosmochim Acta 181:18–35

Piasecki A, Sessions AL, Lawson M, Ferreira AA, Santos Neto EV, Eiler JM (2016) Analysis of the site-specific carbon isotope composition of propane by gas source isotope ratio mass spectrometer. Geochim Cosmochim Acta 188:58–72

Polissar PJ, Fulton JM, Junium CK, Turich CC, Freeman KH (2009) Measurement of ^{13}C and ^{15}N isotopic composition on nanomolar quantities of C and N. Anal Chem 81:755–763

Popp BN, Takigiku R, Hayes JM, Louda JW, Baker EW (1989) The post-Paleozoic chronology and mechanism of ^{13}C depletion in primary marine organic matter. Am J Sci 289:436–454

Reeburgh WS (1976) Methane comsumption in Cariaco trench waters and sediments. Earth Planet Sci Lett 28:337–344

Sessions AL (2006) Isotope-ratio detection for gas chromatography. J Sep Sci 29:1946–1961

Sessions AL, Burgoyne TW, Hayes JM (2001) Correction of H_3^+ contributions in hydrogen isotope ratio monitoring mass spectrometry. Anal Chem 73:192–199

Sessions AL, Sylva SP, Hayes JM (2005) Moving-wire device for carbon isotopic analyses of nanogram quantities of nonvolatile organic carbon. Anal Chem 77:6519–6527

Sigman DM, Casciotti KL, Andreani M, Barford C, Galanter M, Bohlke JK (2001) A bacterial method for the nitrogen isotopic analysis of nitrate in seawater and freshwater. Anal Chem 73:4145–4153

Summons R (2000) Compound-specific isotope analysis. In: Marshall CP, Fairbridge RW (eds) Encyclopedia of geochemistry. Springer, Amsterdam, Netherlands, p 100

Sutton PA, Rowland SJ (2012) High temperature gas chromatography-time-of-flight-mass spectrometry (HTGC-ToF-MS) for high-bioling compounds. J Chromatogr A 1243:69–80

Webb M, Wang Y, Braams BJ, Bowman JM, Miller TF III (2013) Equilibrium clumped-isotope effects in doubly substituted isotopologues of ethane. Geochimi Cosmochimi Acta 197:14–26

Zhang YG, Pagani M, Liu Z, Bohaty SM, DeConto R (2013) A 40-million-year history of atmospheric CO_2. Phil Trans R Soc A 371:20130096

Copper

Xingcheng Liu and Xiaolin Xiong
Guangzhou Institute of Geochemistry, Chinese Academy of Sciences, Guangzhou, China

Element Data
Atomic Symbol: Cu
Atomic Number: 29
Atomic Weight: 63.546 u
Isotopes and Abundances: ^{63}Cu 69.15%, ^{65}Cu 30.85%
1 Atm Melting Point: 1084.6 °C
1 Atm Boiling Point: 2562 °C
Common Valences: 2+, 1+
Ionic Radii: 1+: fourfold: 60 pm, sixfold: 77 pm; 2+:
Fourfold: 57 pm, sixfold: 73 pm
Pauling Electronegativity: 1.9
First Ionization Energy: 745.5 kJ mol^{-1}
Chondritic (CI) Abundance: 131 ppm
Silicate Earth Abundance: 20–30 ppm
Crustal Abundance: 27 ppm
Seawater Abundance: 0.4–5 nmol/kg
Core Abundance: 125 ppm

Properties

Copper (Cu) is a reddish metal with an atomic number 29, standard atomic weight of 63.546, and melting point of 1357.8 K at 1 atm. It was moderately volatile during the Earth formation by accretion of solid material condensed from the solar nebula. As a siderophile element, it partitioned into the core during the separation of metallic core from molten silicate mantle. In the silicate Earth, it behaves as a chalcophile element and usually forms stable sulfides; chalcopyrite ($CuFeS_2$) is the most common copper-bearing sulfide. In nature, copper is the 26th most abundant element in the Earth's crust, with concentrations ranging from 26 ppm in the lower continental crust to 28 ppm in the upper continental crust; the concentration in the oceanic crust is lower at 44 ppm. Concentrations in MORB range from 60 to 80 ppm, in arc basalts from 50 to 100 ppm, and in oceanic island basalts from 80 to 120 ppm (White 2013).

History and Use

Cu was the first metal people learned to smelt and this discovery ended the Stone Age in many parts of the world. The discovery that alloying it with tin produced bronze, a stronger metal, led to the Bronze Age.

Due to its high electrical conductivity, tensile strength, ductility, creep resistance, corrosion resistance, low thermal expansion, and high thermal conductivity, copper is extensively used in building construction, power generation and transmission, electronic product manufacturing, and the production of industrial machinery and transportation vehicles nowadays (Doebrich 2009). Besides the pure metal, copper is often alloyed with zinc, tin, gold, and nickel in industrial applications.

The US Geological Survey estimates the global mine production and consumption of Cu is over 18 and 20 million metric tons in 2015, respectively. Major producing countries include Chile, China, and Peru.

Geochemical Behavior: Magmatic Processes

Copper dissolves in silicate melts (natural magmas) dominantly as Cu^{1+} and perhaps in very minor amounts as Cu^{2+}. Copper is believed to dissolve in silicate melts mainly as $CuO_{0.5}$. The solubility of Cu in sulfur-free silicate melts increases with increasing temperature and increasing oxygen fugacity (Liu et al. 2015 and references therein). Zajacz et al. (2012, 2013) also suggest that Cu dissolves in silicate melts dominantly as Cu–O complex, while Cu–S and Cu–Cl complexes are not significant; thus, its solubility is enhanced only slightly by the presence of chlorine (Cl) and sulfur (S) in the melts.

In magmatic evolution, the geochemical behavior of Cu is controlled by the partition coefficients between silicate minerals, Fe–Ti oxides, sulfides, and magmas. The partition coefficients (given in Table 1) suggest that Cu is highly incompatible in silicate minerals (generally <0.2), incompatible to moderately compatible in Fe–Ti oxides, and highly compatible in sulfides. It should be noted that the partition coefficients are generally controlled by compositions of silicate melts, temperature, pressure, and oxidation state. Thus it's important to know the chemical and physical environmental conditions while applying the partition coefficients to predict the geochemical behavior of Cu.

Geochemical Behavior: Hydrothermal Processes

In contrast, the behavior of Cu in fluids (volatile phases) is a different story. The presences of S and Cl significantly enhance the solubility of Cu in the geological fluids. According to direct Cu K-edge X-ray absorption near-edge structure (XANES) spectra, Berry et al. (2006) suggest that Cu^+ is stable in high-temperature brines in synthetic

Copper, Table 1 Partition coefficients of Cu between mineral and silicate melts

Minerals	Liu et al.	F & C	Lee et al.	A & P	Recommended
Olivine	0.04–0.20	0.06–0.21	0.03–0.16	0.02–0.07	0.1
Orthopyroxene	0.04–0.24	0.15–0.82	0.03		0.1
Clinopyroxene	0.04–0.45		0.04	0.01–0.07	0.2
Garnet	0.01–0.06		0.004		0.04
Amphibole	0.04–0.20		0.05		0.1
Plagioclase	0.02–0.12				0.08
Spinel	0.18–1.3		0.22		0.5
Fe–Ti oxides	0.2–1.8			0.17–0.63	1
Sulfides	L & A	K & W	Zajacz et al.	M & B	
MSS (pyrrhotite)	280–42,000		50–9400		
Sulfide liquid	800–4600	38–675		1060–2130	

Data are from Liu et al. (2014, 2015); F & C, Fellows and Canil (2012); Lee et al. (2012); A & P, Audétat and Pettke (2006); L & A, Li and Audétat (2012, 2015); K & W, Kiseeva and Wood (2013); Zajacz et al. (2013); M & B, Mungall and Brenan (2014).
MSS monosulfide solid solution.

fluid inclusions. In addition, Cu typically occurs as $CuCl_2^-$ ($\pm Cu(HS)_2^-$) in natural hydrothermal systems, in which the partition coefficients of Cu between volatile phases and silicate melts range from dozens to several hundreds (Simon and Ripley 2011; Pokrovski et al. 2013). This means that Cu will be transported into brines or vapors from ascending magma in magmatic–hydrothermal processes if the magmatic aqueous fluids are present. The mass transfer of Cu from magmas to volatile phase(s) is the most important process in the development of a porphyry Cu deposit (Audétat and Simon 2012, and references therein).

Ore Deposits

Most copper is extracted from ore deposits as copper sulfides. Porphyry Cu deposits and sediment-hosted Cu deposits contain most portions of the world's Cu resources. Porphyry ore deposits supply over 70% of the world's copper. They dominantly formed above subduction zones and most of them are genetically related to intermediate to felsic calc-alkaline magmas, which provide metals and fluids (e.g., H_2O, CO_2, Cl, and S) for the ore formation. However, the most important controlling factor(s) is still debated.

Individual copper deposits may contain millions of tons of copper and generally are developed by using open-pit mining methods (Doebrich 2009).

Natural Waters

Copper exists in natural waters mainly as Cu^{2+} and is readily complexed by hydroxyl and carbonate. Surface water concentrations of dissolved Cu are 63.55 ppt in the open ocean

and 1.48 ppb in the rivers (global average) (Bruland et al. 2014; Gaillardet et al. 2014). The Cu^{2+} in surface waters is buffered by a strong Cu-binding class of organic ligands, called L_1, which chelates nearly 99.8% Cu^{2+} and reduces the Cu^{2+} concentration to a nontoxic condition for phytoplankton. Without organic complexation, the dominant species of Cu would be $Cu(CO_3)^0$ and approximately a factor of 20 lower than the total dissolved concentration (Bruland et al. 2014 and references therein).

Biological Utilization and Toxicity

Cu^{2+} and Cu^+ can participate in a wide spectrum of interactions with proteins to drive diverse structures and biochemical reactions. As life evolved, more complex roles for Cu arose, concurrent with the elaboration of mechanisms to tightly regulate acquisition and distribution of Cu and provide protection against Cu toxicity (Festa and Thiele 2011). It is an essential and required trace element in plants and animals but can be toxic to some microorganisms at relatively low concentrations. Defects in Cu homeostasis lead to human disease. On the other hand, excess Cu intake induces toxicity for human.

Summary

Humans have been using copper for several thousands of years. As an industrial material, it is significant and widely used in modern society. As a trace element in Earth, it also provides insight into the crust–mantle differentiation, the formation of ore deposits, and the redox history of magmas.

Cross-References

▶ Chalcophile Elements
▶ Copper Isotopes
▶ Ore Deposits
▶ Partitioning and Partition Coefficients
▶ Sulfide Minerals

References

Audetat A, Pettke T (2006) Evolution of a porphyry-Cu mineralized magma system at Santa Rita, New Mexico (USA). J Petrol 47 (10):2021–2046

Audétat A, Simon A (2012) Magmatic controls on porphyry copper deposits. Soc Econ Geol Spec Publ 16:573–618

Berry AJ, Hack AC, Mavrogenes JA, Newville M, Sutton SR (2006) A XANES study of Cu speciation in high-temperature brines using synthetic fluid inclusions. Am Mineral 91(11–12):1773–1782

Bruland KW, Middag R, Lohan MC (2014) 8.2 – controls of trace metals in seawater. In: Turekian HDHK (ed) Treatise on geochemistry, 2nd edn. Elsevier, Oxford, pp 19–51

Doebrich J (2009) Copper–A metal for the ages: U.S. Geological Survey fact sheet 2009–3031, 4 p. Available at http://pubs.usgs.gov/fs/2009/3031/

Fellows SA, Canil D (2012) Experimental study of the partitioning of Cu during partial melting of Earth's mantle. Earth Planet Sci Lett 337:133–143

Festa RA, Thiele DJ (2011) Copper: an essential metal in biology. Curr Biol 21(21):R877–R883

Gaillardet J, Viers J, Dupré B. 7.7 – trace elements in river waters. In: Turekian HDHK (ed) Treatise on geochemistry, 2nd edn. Elsevier, Oxford, pp 195–235

Kiseeva ES, Wood BJ (2013) A simple model for chalcophile element partitioning between sulphide and silicate liquids with geochemical applications. Earth Planet Sci Lett 383:68–81

Lee C-TA, Luffi P, Chin EJ, Bouchet R, Dasgupta R, Morton DM, Le Roux V, Yin Q-Z, Jin D (2012) Copper systematics in arc magmas and implications for crust-mantle differentiation. Science 336 (6077):64–68

Li Y, Audétat A (2012) Partitioning of V, Mn, Co, Ni, Cu, Zn, As, Mo, Ag, Sn, Sb, W, Au, Pb, and Bi between sulfide phases and hydrous basanite melt at upper mantle conditions. Earth Planet Sci Lett 355:327–340

Li Y, Audétat A (2015) Effects of temperature, silicate melt composition, and oxygen fugacity on the partitioning of V, Mn, Co, Ni, Cu, Zn, As, Mo, Ag, Sn, Sb, W, Au, Pb, and Bi between sulfide phases and silicate melt. Geochim Cosmochim Acta 162:25–45

Liu X, Xiong X, Audétat A, Li Y, Song M, Li L, Sun W, Ding X (2014) Partitioning of copper between olivine, orthopyroxene, clinopyroxene, spinel, garnet and silicate melts at upper mantle conditions. Geochim Cosmochim Acta 125:1–22

Liu X, Xiong X, Audetat A, Li Y (2015) Partitioning of Cu between mafic minerals, Fe-Ti oxides and intermediate to felsic melts. Geochim Cosmochim Acta 151:86–102

Mungall J, Brenan J (2014) Partitioning of platinum-group elements and Au between sulfide liquid and basalt and the origins of mantle-crust fractionation of the chalcophile elements. Geochim Cosmochim Acta 125:265–289

Pokrovski GS, Borisova AY, Bychkov AY (2013) Speciation and transport of metals and metalloids in geological vapors. Rev Mineral Geochem 76(1):165–218

Simon AC, Ripley EM (2011) The role of magmatic sulfur in the formation of ore deposits. Rev Mineral Geochem 73(1):513–578

White WM (2013) Geochemistry. Wiley-Blackwell, Oxford, UK

Zajacz Z, Candela PA, Piccoli PM, Wälle M, Sanchez-Valle C (2012) Gold and copper in volatile saturated mafic to intermediate magmas: Solubilities, partitioning, and implications for ore deposit formation. Geochim Cosmochim Acta 91:140–159

Zajacz Z, Candela PA, Piccoli PM, Sanchez-Valle C, Wälle M (2013) Solubility and partitioning behavior of Au, Cu, Ag and reduced S in magmas. Geochim Cosmochim Acta 112:288–304

Copper Isotopes

Paul Savage
Department of Earth and Environmental Sciences,
University of St Andrews, St Andrews, UK

Synonyms

Copper stable isotopes; Cu isotopes

Introduction

Copper has two stable isotopes, ^{63}Cu and ^{65}Cu, with relative abundances of 69.15% and 30.85%, respectively. A transition metal, Cu is moderately siderophile and strongly chalcophile (around 2/3 of Earth's Cu is thought to be stored in its core). Copper is redox-sensitive and is present in three oxidation states in terrestrial environments: native Cu^0, Cu^+ and Cu^{2+}. Copper is both economically important and an essential micronutrient. For all these reasons, isotopic variations of Cu have the potential to inform us of processes, sources, and phenomena in all disciplines of the geosciences. A more detailed review of the myriad applications of Cu isotopes is given by Moynier et al. (in press).

Analysis

As with many other stable isotope systems, accurate, precise, and routine measurement of Cu isotope ratio was made possible with the advent of Multi-collector Inductively-Coupled-Plasma Mass Spectrometry (MC-ICPMS) and precisions of <50 ppm are now attainable. This is usually by solution analysis, whereby copper is isolated from a dissolved sample using ion exchange chromatography (Marechal et al. 1999); however, some in-situ laser ablation isotope analyses has been made (Ikehata and Hirata 2013). Variations in Cu isotopes are represented using the delta notation as $\delta^{65}Cu$ in permil (‰; Eq. 1), relative to the pure Cu standard NIST976:

C

$$\delta^{65}Cu = \left[\frac{(^{65}Cu/^{63}Cu)_{sample}}{(^{65}Cu/^{63}Cu)_{NIST976}} - 1 \right] \times 1000 \qquad (1)$$

(N.B. while this standard is still utilized in Cu isotope analysis, it is now commercially unavailable and a number of replacements have been characterized, e.g., Moeller et al. 2012; however, $\delta^{65}Cu$ values should remain relative to NIST976 using a precalibrated standard, to allow for direct comparison of all Cu isotope data).

Meteorites

The chondritic meteorites display significant variability in Cu isotope abundances. Carbonaceous chondrites (CC) define the largest range, from CI (0.02 ± 0.12) to CV (-1.45 ± 0.04) and each group has a distinct average (Fig. 1; Luck et al. 2003). Ordinary chondrites (OC) define a smaller range; nevertheless, the groups H, L, and LL again have distinct $\delta^{65}Cu$, becoming more enriched in ^{65}Cu with decreasing Fe content (Fig. 1). Both CC and OC $\delta^{65}Cu$

Copper Isotopes, Fig. 1 *Box* and *whisker plot* showing representative ranges of various Cu isotope reservoirs – see text for data sources. *Top panel* – high-temperature and extra-terrestrial samples. *Bottom panel* – impact-generated and critical zone (low temperature) samples
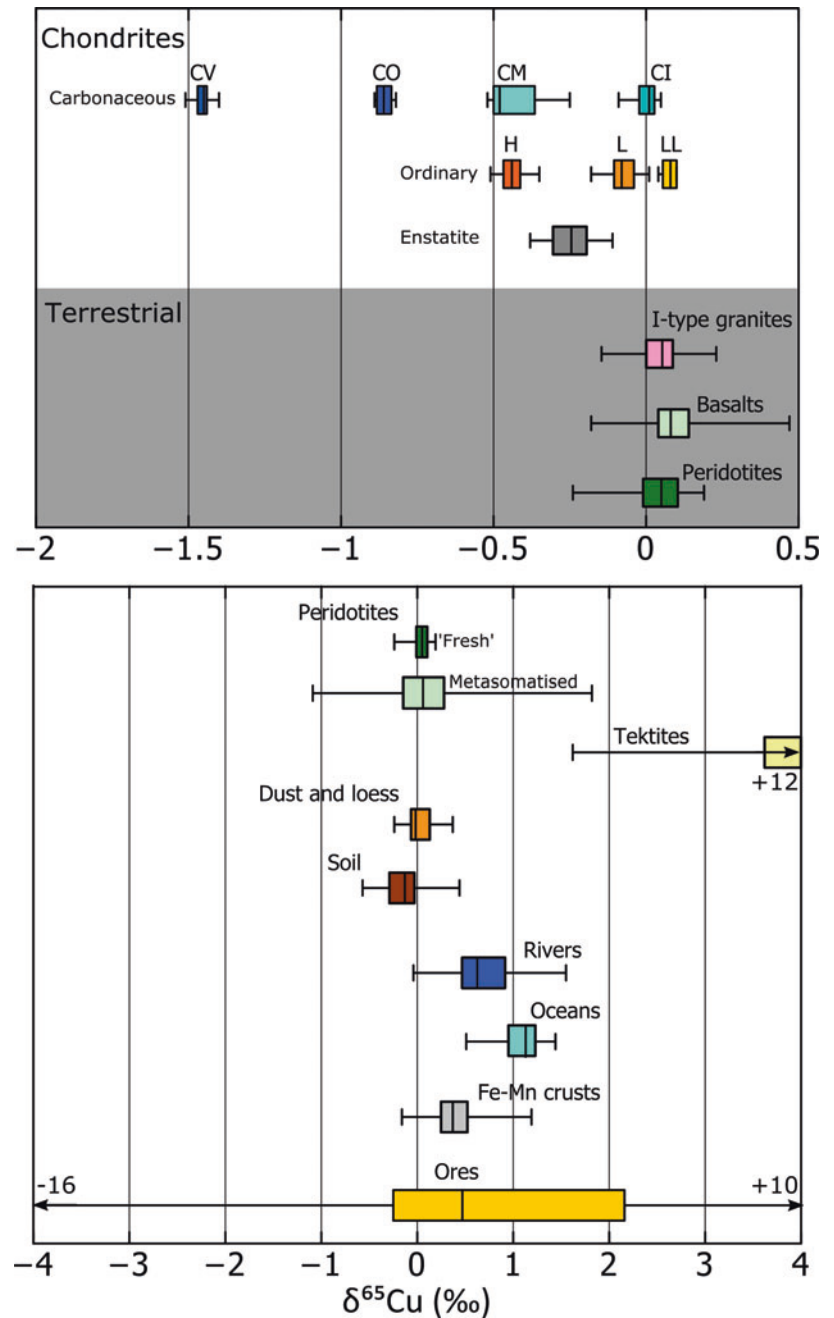
values vary systematically with oxygen isotope anomaly ($\Delta^{17}O$), which Luck et al. (2003) interpreted as revealing the presence of two, possibly three, distinct Cu isotope reservoirs in the early solar system, which mixed in varying proportions by nebula processing. Unlike carbonaceous and ordinary, enstatite chondrite groups (EH and EL) have similar Cu isotope compositions, which fall in the middle of the primitive meteorite range (-0.25 ± 0.09; Fig. 1). Savage et al. (2015a) used these data, in part, to define the bulk Earth $\delta^{65}Cu$ based on the observation that for many other isotope systems, enstatite chondrites and terrestrial materials appear identical.

In terms of iron meteorites, the first Cu isotope analyses by Luck et al. (2005) showed that IIIAB (magmatic), IA, and IIICD (silicate-bearing) iron meteorites showed similar, limited compositional ranges which broadly fell within the chondrite array ("magmatic" irons are thought to represent the cores of asteroids, and "silicate-bearing" possibly represent impact-generated melt-pools). A subsequent study by Bishop et al. (2012) showed that the silicate-bearing irons' Cu isotope and $\Delta^{17}O$ compositions correlate – as with the chondrites. The same could be true for the magmatic irons; as these meteorites have no silicates (and thus minimal oxygen to measure), Bishop et al. (2012) suggested that their Cu isotope compositions could instead be used to indicate genetic links with other meteorites. Most recently, large (negative) Cu isotope variations (-5.84 to -0.24) have been measured in the volatile element-poor IVB meteorites (Chen et al. 2016). These meteorites have high Ni/Cu ratios, and these negative enrichments are interpreted as resulting from variable exposure to galactic cosmic rays, whereby neutron capture forms excesses of ^{63}Ni, which decays quickly to ^{63}Cu.

Igneous Rocks

Two recent estimates of the copper isotope composition of the bulk silicate Earth (BSE; i.e. the mantle and crust) place it at 0.07 ± 0.10 and 0.06 ± 0.20 (Savage et al. 2015a; Liu et al. 2015, respectively). Both estimates were based on representative suites of mantle peridotites and ultra-mafic and mafic mantle-derived melts (e.g. komatiites, mid-ocean ridge basalts, ocean-island basalts) and are identical within error. Copper isotopes do not appear to fractionate greatly as a result of magmatic differentiation, even in systems where sulfide fractionation is occurring (Savage et al. 2015b). There appears to be a small enrichment (+0.1 ‰) in heavy Cu as differentiation approaches rhyolitic compositions, which agrees with the few analyses of I-type granites available in the literature (Li et al. 2009; Fig. 1). Metasomatism appears to have a strong effect on Cu isotope compositions, as evinced by much larger Cu isotope variations seen in metasomatized

peridotites (Savage et al. 2015b; Liu et al. 2015; Fig. 1). This raises the possibility that Cu isotopes could be used to characterize the nature of a metasomatic agent.

Planetary Accretion and Differentiation

Savage et al. (2015a) noted that the Cu isotope composition of BSE is heavy compared to estimates for bulk Earth and suggested that fractionation occurred during Earth's differentiation. This isotope difference could reflect metal-silicate equilibration during core formation; however, experiments performed by Savage et al. (2015a), as well as analyses of individual metal, silicate, and sulphide grains from iron meteorites (Williams and Archer 2011) suggest that metal-hosted Cu is isotopically heavier than co-evolving silicates. This seems to rule out core formation as explaining the positive $\Delta^{65}Cu_{BSE\text{-}bulk\ Earth}$ ($\delta^{65}Cu_{BSE} - \delta^{65}Cu_{bulk\ Earth}$), as an isotopically heavier core implies a negative $\Delta^{65}Cu_{BSE\text{-}bulk\ Earth}$. Savage et al. (2015a) argued that either 1) the $\Delta^{65}Cu_{BSE\text{-}bulk\ Earth}$ implies that the majority of mantle Cu was delivered post-core formation, by a CI-like impactor (cf. Schönbachler et al. 2010); or 2) this missing light Cu is stored in sulfides, either in the mantle or a reservoir that was subsequently admixed into the core. Further experimental constraints on the partitioning behavior of Cu isotopes are required, but there is great potential for Cu isotopes to reveal information about the formation of Earth and other rocky bodies.

Impact-Driven Loss of Cu

Some of the largest Cu isotope variations measured in natural samples are recorded in tektites, glasses formed by high-energy (i.e., meteorite) impact events. Values up to 12.5 ‰ have been measured in tektites from the across the globe (Fig. 1; Moynier et al. 2010; Rodovská et al. 2015), which have been interpreted as an effect of kinetic isotope fractionation – whereby the lighter isotope can escape to the gas phase more easily – in a diffusion-limited regime. Anomalously high Cu isotope compositions have also been measured in lunar soils (Moynier et al. 2006; Herzog et al. 2009), caused by micro-meteorite "gardening" and, potentially, lunar basalts (~0.5 ‰). Because igneous processes do not fractionate Cu isotopes resolvably, the isotopically heavy composition of the latter sample group relative to Earth could be induced by volatile Cu loss, reflecting the violent nature of the Moon's birth (Day and Moynier 2014).

Low Temperature Environments

Mechanical weathering (to form dust, loess, clastic sediments) does not appear (as would be expected) to fractionate Cu isotopes – with aeolian dust samples showing limited Cu isotope variation and compositions close to BSE (Fig. 1;

Dong et al. 2013). However, compared to that seen in high-temperature terrestrial settings, a much wider range of Cu isotope compositions have been measured in such systems affected by chemical weathering and biological activity that occur in the "critical zone".

Weathering/leaching of primary Cu-bearing minerals generally involves oxidation (from Cu^+ to Cu^{2+}) and results in the release of isotopically heavier Cu (by ∼0.5–4.0 ‰) relative to the source. This has been shown via experiments (Fernandez and Borrok 2009) as well as measurements of soils and corresponding pore waters (Fig. 1; Mathur et al. 2012). Acid mine drainage solutions also have relatively heavy Cu isotope compositions, thought to be related to the oxidation of the source Cu (Kimball et al. 2009). These observations have been corroborated by ab initio calculations (Fujii et al. 2013). Biological utilization of Cu can also involve oxidation (i.e. through the reductase enzyme in the plant root system), and where this occurs, the biologically-complexed Cu is heavier than the source (Jouvin et al. 2012).

Redox reactions are thought to be the main control over the extremely large range of Cu isotope compositions seen in ore minerals. Specifically, "primary" (igneous) ore minerals have compositions close to that of BSE (∼0.0 ± 0.5 ‰), whereas supergene ores show huge variability (−16.5 to +10 ‰; Mathur et al. 2009; Fig. 1). These large variations are likely due to multiple cycles of oxidation and reduction in the supergene environment, although Rayleigh fractionation, kinetic effects, and complexing ligand (Fujii et al. 2013) could also play a role.

Most Cu in the "critical zone" is organically complexed or sorbed onto the surface of Fe (oxy)-hydroxides (Vance et al. 2009). In regards to organically complexed Cu, experiments show that this pool is isotopically heavier than the free Cu ion and that the magnitude of isotope fractionation between the two pools increases as the stability constant of the complex increases (e.g. Ryan et al. 2014) – again, corroborated by ab initio calculations (Sherman 2013). Like organic complexation, sorbtion onto Fe-oxides causes a positive isotope effect, with the sorbed Cu showing around a 1 ‰ enrichment compared to the free metal pool (Pokrovsky et al. 2008).

Vegetation also has an impact on Cu isotopes in the critical zone. In general, plant material has an isotopically light Cu isotope composition compared to the surface pool. In a study by Weinstein et al. (2011) on lentil plants, light Cu was seen to be preferentially transferred up the plant, such that the youngest leaves were isotopically lighter than the root system. Comparison experiments between Strategy I plants (which involve a reduction step during Cu utilization) and Strategy II (no reduction), reveal that the latter have lighter isotope compositions than the former, identifying the importance of the reduction step in controlling Cu isotope compositions under Strategy I (Jouvin et al. 2012; Ryan et al. 2013). Any organic-rich soil horizon should therefore be isotopically light, and this has been observed in natural settings where decaying plant material was present (e.g., Bigalke et al. 2011).

In summary, weathering and Cu bio-utilization in the critical zone release isotopically heavy Cu to the solution – via oxidation of primary minerals, organic complexation, and/or preferential storage of light Cu in biomass. This suggests that the riverine and ocean Cu isotope compositions should be heavier than the continents – and this is indeed the case. Measurements of the isotope composition of dissolved riverine Cu give an average composition of ∼0.7 ‰ (Fig. 1; Vance et al. 2008) and, given that riverine input dominates oceanic Cu, this will be close to average ocean $\delta^{65}Cu$. The recent study of Little et al. (2014) modeled both the elemental and isotopic ocean Cu cycle and revealed a missing, isotopically heavy, Cu sink. One explanation could be that ^{65}Cu is preferentially sorbed on Mn-Fe oxides (e.g. Pokrovsky et al. 2008); however, Little et al. (2014) went on to measure such samples and found that they were isotopically light (∼0.2 ‰; Fig. 1) relative to the oceans. This issue, as of writing, remains unresolved.

Biomedical Applications

The application of traditionally geochemical techniques to biomedicine is a new and exciting topic (Albarède 2015). Copper plays a vital role in the human body, thus Cu isotopes may be extremely important in this new field. Arguably the most promising application for Cu isotopes is in the early detection of some cancers. In patients with cancer, blood serum Cu is known to be anomalously high; however, changes in serum [Cu] are typically too ambiguous to be usable as a biomarker. However, Telouk et al. (2015) found a significant difference in the Cu isotope composition of blood serum from cancer patients compared to healthy patients, which, in their pilot study, was more explicit than the canonical cancer biomarker.

Cross-References

▶ Chalcophile Elements
▶ Chemical Weathering
▶ Copper
▶ Formation and Evolution of the Earth
▶ Inductively Coupled Plasma Mass Spectrometry (ICP-MS)

References

Albarède F (2015) Metal stable isotopes in the human body: a tribute of geochemistry to medicine. Elements 11:265–269

Bigalke M, Weyer S, Wilcke W (2011) Stable Cu isotope fractionation in soils during oxic weathering and podzolization. Geochim Cosmochim Acta 75:3119–3134

Bishop MC, Moynier F, Weinstein C, Fraboulet JG, Wang K, Foriel J (2012) The Cu isotopic composition of iron meteorites. Meteorit Planet Sci 47:268–276

Chen H, Moynier F, Humayun M, Bishop MC, Williams J (2016) Cosmogenic effects on Cu isotopes in IVB iron meteorites. Geochim Cosmochim Acta 182:145–154

Day JM, Moynier F (2014) Evaporative fractionation of volatile stable isotopes and their bearing on the origin of the Moon. Philos Transact A 372:20130259

Dong S, Weiss DJ, Strekopytov S, Kreissig K, Sun Y, Baker AR, Formenti P (2013) Stable isotope ratio measurements of Cu and Zn in mineral dust (bulk and size fractions) from the Taklimakan Desert and the Sahel and in aerosols from the eastern tropical North Atlantic Ocean. Talanta 114:103–109

Fernandez A, Borrok DM (2009) Fractionation of Cu, Fe and Zn isotopes during weathering of sulfide-rich rocks. Chem Geol 264:1–12

Fujii T, Moynier F, Abe M, Nemoto K, Albarède F (2013) Copper isotope fractionation between aqueous compounds relevant to low temperature geochemistry and biology. Geochim Cosmochim Acta 110:29–44

Herzog GF, Moynier F, Albarède F, Berezhnoy AA (2009) Isotopic and elemental abundances of copper and zinc in lunar samples, Zagami, Pele's hairs, and a terrestrial basalt. Geochim Cosmochim Acta 73:5884–5904

Ikehata K, Hirata T (2013) Evaluation of UV-fs-LA-MC-ICP-MS for precise in situ copper isotopic microanalysis of cubanite. Anal Sci 29:1213–1217

Jouvin D, Weiss D, Mason T, Bravin M, Louvat P, Zhao F, Ferec F, Hinsinger P, Benedetti M (2012) Stable isotopes of Cu and Zn in higher plants: evidence for Cu reduction at the root surface and two conceptual models for isotopic fractionation processes. Environ Sci Technol 46:2652–2660

Kimball BE, Mathur R, Dohnalkova AC, Wall AJ, Runkel RL, Brantley SL (2009) Copper isotope fractionatin in acid mine drainage. Geochim Cosmochim Acta 73:1247–1263

Li W, Jackson S, Pearson NJ, Alard O, Chappell BW (2009) The Cu isotopic signature of granites from the Lachlan Fold Belt, SE Australia. Chem Geol 258:38–49

Little SH, Vance D, Walker-Brown C, Landing WM (2014) The oceanic mass balance of copper and zinc isotopes, investigated by analysis of their inputs, and outputs to ferromanganese oxide sediments. Geochim Cosmochim Acta 125:673–693

Liu S-A, Huang J, Liu J, Woerner G, Yang W, Tang Y-J, Chen Y, Tang L, Zheng J, Li S (2015) Copper isotopic composition of the silicate Earth. Earth Planet Sci Lett 427:95–103

Luck JM, Othman DB, Barrat JA, Albarède F (2003) Coupled ^{63}Cu and ^{16}O excesses in chondrites. Geochim Cosmochim Acta 67:143–151

Luck JM, Othman DB, Albarède F (2005) Zn and Cu isotopic variations in chondrites and iron meteorites: early solar nebula reservoirs and parent-body processes. Geochim Cosmochim Acta 69:5351–5363

Maréchal C, Télouk P, Albarède F (1999) Precise analysis of copper and zinc isotopic compositions by plasma-source mass spectrometry. Chem Geol 156:251–273

Mathur R, Titley S, Barra F, Brantley S, Wilson M, Phillips A, Munizaga F, Maksaev V, Vervoort J, Hart G (2009) Exploration potential of Cu isotope fractionation in porphyry copper deposits. J Geochem Explor 102:1–6

Mathur R, Jin L, Prush V, Paul J, Ebersole C, Fornadel A, Williams JZ, Brantley S (2012) Cu isotopes and concentrations during weathering of black shale of the Marcellus formation, Huntingdon County, Pennsylvania (USA). Chem Geol 304:175–184

Moeller K, Schoenberg R, Pedersen R-B, Weiss D, Dong S (2012) Calibration of the new certified reference materials ERM-AE633 and ERM-AE647 for copper and IRMM-3702 for zinc isotope amount ratio determinations. Geostand Geoanal Res 36(2): 177–199

Moynier F, Albarede F, Herzog GF (2006) Isotopic composition of zinc, copper and iron in lunar samples. Geochim Cosmochim Acta 70:6103–6117

Moynier F, Koeberl C, Beck P, Jourdan F, Telouk P (2010) Isotopic fractionation of Cu in tektites. Geochim Cosmochim Acta 74:799–807

Moynier F, Vance D, Fujii T, Savage PS (2017) The isotope geochemistry of zinc and copper. In: Teng F-Z, Watkins J, Dauphas N (eds), Reviews in mineralogy and geochemistry, vol 82, Non-traditional stable isotopes, pp 543–600. https://doi.org/10.2138/rmg.2017.82.13

Pokrovsky OS, Viers J, Emnova EE, Kompantseva EI, Freydier R (2008) Copper isotope fractionation during its interaction with soil and aquatic microorganisms and metal oxy(hyd)oxides: possible structural control. Geochim Cosmochim Acta 72:1742–1757

Rodovská Z, Magna T, Kato C, Savage PS, Moynier F, Žák K (2015) Zinc and copper isotopes in central European tektites and sediments from the Ries impact area – implications for material sources and loss of volatile elements during tektite formation. In: 46th lunar and planetary science conference, vol 1832, p 1951

Ryan BM, Kirby JK, Degryse F, Harris H, McLaughlin MJ, Scheiderich K (2013) Copper speciation and isotopic fractionation in plants: uptake and translocation mechanisms. New Phytol 199:367–378

Ryan BM, Kirby JK, Degryse F, Scheiderich K, McLaughlin MJ (2014) Copper isotope fractionation during equilibration with natural and synthetic ligands. Environ Sci Technol 48:862–866

Savage P, Moynier F, Chen H, Shofner G, Siebert J, Badro J, Puchtel IS (2015a) Copper isotope evidence for large-scale sulphide fractionation during Earth's differentiation. Geochem Perspect Lett 1:53–64

Savage P, Moynier F, Harvey J, Burton K (2015b) The behavior of copper isotopes during igneous processes. In: AGU conference, San Francisco

Schonbachler M, Carlson RW, Horan MF, Mock TD, Hauri EH (2010) Heterogeneous accretion and the moderately volatile element budget of Earth. Science 328:884–887

Sherman DM (2013) Equilibrium isotopic fractionation of copper during oxidation/reduction, aqueous complexation and ore-forming processes: predictions from hybrid density functional theory. Geochim Cosmochim Acta 118:85–97

Telouk P, Puisieux A, Fujii T, Balter V, Bondanese VP, Morel A-P, Clapisson G, Lamboux A, Albarède F (2015) Copper isotope effect in serum of cancer patients. A pilot study. Metallomics 7:299–308

Vance D, Archer C, Bermin J, Perkins J, Statham PJ, Lohan MC, Ellwood MJ, Mills RA (2008) The copper isotope geochemistry of rivers and the oceans. Earth Planet Sci Lett 274:204–213

Vance D, Teagle DAH, Foster GL (2009) Variable quaternary chemical weathering fluxes and imbalances in marine geochemical budgets. Nature 458:493–496

Weinstein C, Moynier F, Wang K, Paniello R, Foriel J, Catalano J, Foriel J (2011) Cu isotopic fractionation in plants. Chem Geol 286:266–271

Williams HM, Archer C (2011) Copper stable isotopes as tracers of metal-sulphide segregation and fractional crystallisation processes on iron meteorite parent bodies. Geochim Cosmochim Acta 75:3166–3178

C

Cosmic Elemental Abundances

Herbert Palme
Forschungsinstitut und Naturmuseum Senckenberg,
Frankfurt am Main, Germany

Definition

The average chemical composition of the solar system is identical to the composition of the Sun, representing more than 99.8% of the mass of the solar system. Solar abundance data obtained from absorption spectroscopy and complemented by the more accurate chemical data on CI chondrites, a small group of meteorites with solar abundances of non-volatile elements, define the *solar system element abundances*, which are known to within a few percent for most elements. Many stars have compositions similar to the average solar system composition, justifying the term cosmic element abundances. Solar system abundances are, however, much better known than the more loosely defined cosmic element abundances.

The Concept of Cosmic Abundances

Three lines of evidence lead to the concept of cosmic abundances. (1) Since about 1920, it is possible to determine the abundances of most chemical elements in the photosphere of the Sun by using the absorption lines in the solar emission spectrum. Although this only allows determining the composition of the outer 200 km of the Sun, it is believed that the interior of the Sun has essentially the same composition. The same procedure can be applied to stars. Thus the chemical composition of numerous stars is known. (2) Undifferentiated or chondritic meteorites come from planetesimals that were never fully molten. These meteorites have compositions not very different from that of the solar photosphere. A precise match, i.e., agreement of most elements within the error bars between solar abundances and meteoritic abundances, is found for one specific group of meteorites, the CI chondrites. The agreement is for all elements heavier than oxygen and excluding the very volatile rare gases. Other groups of undifferentiated or chondritic meteorites deviate somewhat from the solar or CI abundances. (3) The Big Bang produced hydrogen (H), helium (He), and some lithium (Li), about 13.8 billion years ago. All other chemical elements were made later in stars by nuclear reactions. As a result the heavy element abundances in the universe increase continually with time. The parameter [Fe/H] of a star is called metallicity. It is the logarithm of the ratio of iron atoms divided by hydrogen atoms divided by the same ratio in the Sun. The metallicity of the 4.67 billion-year-old Sun is 1, and stars older than the Sun have metallicities lower than 1 and younger stars above 1. The relative abundances of metals (all elements heavier than H and He in the jargon of astronomers) are in most stars very similar to those in the Sun. This element pattern is in agreement with nucleosynthetic calculations. An important parameter is the stability of a nucleus or its binding energy. Elements with even mass or atomic number gaining stability from pairing energy of neutrons and/or protons are more stable and therefore more abundant than elements with uneven mass or atomic numbers. This is visible in Fig. 1, displaying the abundances of elements in the Sun versus atomic number.

The convergence of solar-observed photospheric abundances, measured meteoritic abundances, and calculations of nucleosynthesis to a single more or less constant element pattern is a strong indication for well-defined solar system abundances, which when extended to other stars become cosmic abundances. The only variable is the metallicity, the ratio of heavy elements to hydrogen, which continually increases with time.

Historical Background

During the 1920s and 1930s of the last century, Victor Moritz Goldschmidt and his colleagues measured and compiled chemical data of terrestrial rocks, meteorites, and individual phases of meteorites. Based on these data Goldschmidt set up a cosmic abundance table. Goldschmidt realized that most meteorites should be representative of average cosmic matter because they have not been affected by melting and crystallization, whereas the crust of the Earth, a product of mantle melting, is not representative of the Earth's bulk composition. Goldschmidt calculated the average concentrations of elements in cosmic matter by using a weighted mean of element abundances in meteorite phases: metal (2 parts), sulfide (1 part), and silicates (10) parts.

The German physicist Joseph von Fraunhofer (1787–1826) was the first to observe dark lines in the spectrum of the light emitted from the Sun. Some 50 years later, G. Kirchhoff (1824–1887) recognized that these lines are characteristic of chemical elements, and he correctly concluded that the outer cooler layers of the Sun absorb radiation from the hotter underlying parts. At the beginning of the twentieth century, C.H. Payne made the first attempts to

Cosmic Elemental Abundances, Fig. 1 Elemental solar system abundances as function of atomic number normalized to 10^6 Si atoms. The preponderance of H and He is obvious. The stability of ^{56}Fe and the higher stability of elements with even atomic numbers are clearly visible (Figure is from Lodders et al. 2009)
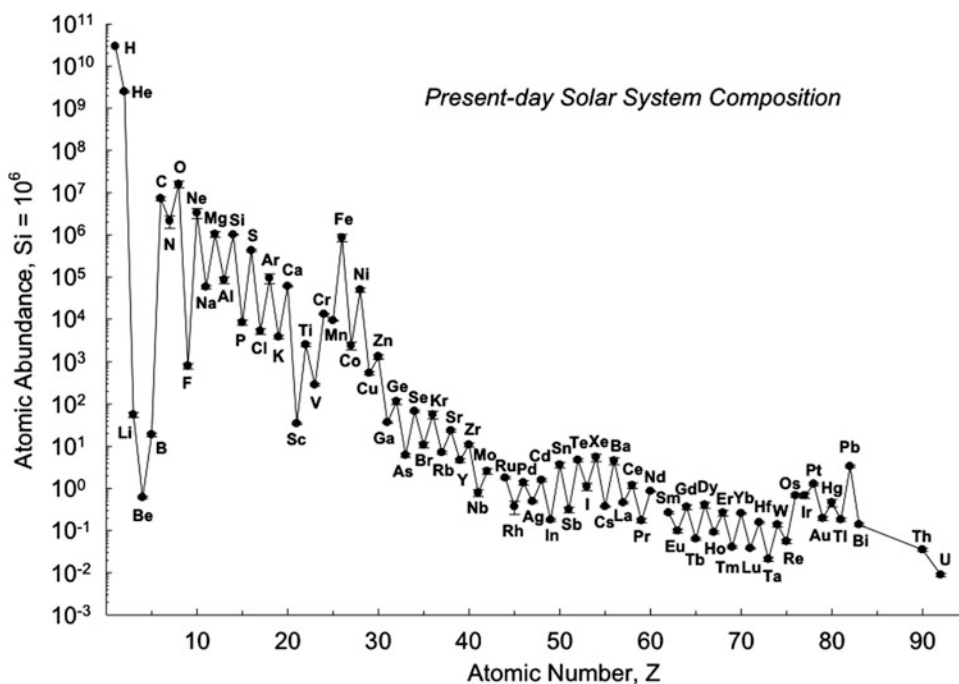
quantify the information contained in stellar and solar absorption lines. She recognized the large abundance of H in stars and gave the first estimates of the chemical composition of stellar atmospheres. Later N. H. Russell published the elemental abundances of 56 elements in the solar photosphere.

Goldschmidt's and Russell's lists had most of the major features of the solar system abundances as we know them today: the dominance of H and He; the strong decrease in abundance with increasing atomic number; the very low abundances of Li, Be, and B; and the pronounced abundance peak at ^{56}Fe (see Fig. 1).

Later compilations took into account improved analytical data of meteorites and of the solar photospheric spectrum (see Lodders et al. 2009 and Palme et al. 2014 for references).

Abundances of Elements in the Sun and in Meteorites

In Table 1, we have listed elemental abundances of the Sun and compare them to the abundances in CI chondrites which closely match the solar abundances for heavy elements. Solar and meteoritic abundances are calculated relative to 10^{12} hydrogen atoms, the scale used in astronomy. The Table is

from Palme et al. (2014), and from Lodders et al. (2009). The solar abundances listed here are very similar to those in Asplund et al. (2009).

Table 2 contains the abundances of elements by mass in CI meteorites, chiefly the Orgueil meteorite. The table is from Palme et al. (2014), largely based on earlier compilations (Lodders et al. 2009). In the last column data are converted to atoms and normalized to 10^6 atoms of Si. The conversion from the astronomical scale (A_{ast}) based on 10^{12} H atoms to the meteoritical scale (A_{met}) based on 10^6 atoms of Si is according to Palme et al. (2014):

$$\log A_{ast} = \log A_{met} + 1.533$$

The CI chondrites match the solar element abundances within analytical uncertainties. Other groups of chondritic meteorites deviate somewhat from the solar composition. This is demonstrated in Fig. 2, where several abundance ratios are plotted for members of the major chondrite classes and compared with solar abundance ratios.

The major chondrite classes shown in Fig. 2 are carbonaceous chondrites with CI, CM, CO, and CV groups; ordinary chondrites with H, L, and LL groups; and enstatite chondrites with EH and EL groups. These are the most populated chondrite groups (e.g., Krot et al. 2003).

The element ratios plotted in Fig. 2 are representative of different cosmochemical components. Each of these

Cosmic Elemental Abundances, Table 1 Solar photospheric abundances and meteorite-derived solar system abundances

		Solar photosphere	s.d. dex	Meteorite (CI)	s.d. dex	Sun/meteorite N_{sun}/N_{met}
1	H	12		8.24	0.04	5.70E + 03
2	He	10.925	0.02	1.31		3.86E + 09
3	Li	1.10	0.10	3.28	0.04	0.01
4	Be	1.38	0.09	1.32	0.03	1.10
5	B	2.70	0.17	2.81	0.04	0.78
6	C	8.39	0.04	7.42	0.04	9.44
7	N	7.86	0.12	6.28	0.06	38.2
8	O	8.73	0.07	8.42	0.04	2.09
9	F	4.56	0.30	4.44	0.06	1.32
10	Ne	8.05	0.10	−1.1		1.40E + 09
11	Na	6.30	0.03	6.29	0.04	1.03
12	Mg	7.54	0.06	7.55	0.02	0.98
13	Al	6.47	0.07	6.45	0.03	1.06
14	Si	7.52	0.06	7.53	0.01	1.01
15	P	5.46	0.04	5.45	0.03	1.01
16	S	7.14	0.01	7.18	0.02	0.92
17	Cl	5.50	0.30	5.25	0.06	1.79
18	Ar	6.50	0.10	−0.48		9.61E + 06
19	K	5.12	0.03	5.10	0.04	1.05
20	Ca	6.33	0.07	6.32	0.03	1.12
21	Sc	3.10	0.10	3.07	0.03	1.09
22	Ti	4.90	0.06	4.93	0.03	1.25
23	V	4.00	0.02	3.98	0.03	1.04
24	Cr	5.64	0.01	5.66	0.02	0.96
25	Mn	5.37	0.05	5.50	0.03	0.75
26	Fe	7.45	0.08	7.47	0.02	0.94
27	Co	4.92	0.08	4.89	0.02	1.06
28	Ni	6.23	0.04	6.22	0.03	0.99
29	Cu	4.21	0.04	4.27	0.06	0.86
30	Zn	4.62	0.15	4.65	0.02	0.98
31	Ga	2.88	0.10	3.10	0.03	0.61
32	Ge	3.58	0.05	3.61	0.04	0.94
33	As			2.32	0.04	
34	Se			3.37	0.03	
35	Br			2.56	0.06	
36	Kr	3.28	0.08	−2.25		3.41E + 05
37	Rb	2.60	0.10	2.39	0.03	1.63
38	Sr	2.92	0.05	2.90	0.03	1.04
39	Y	2.21	0.02	2.19	0.02	1.10
40	Zr	2.58	0.02	2.56	0.02	1.06
41	Nb	1.42	0.06	1.43	0.04	0.96
42	Mo	1.92	0.05	1.96	0.04	0.93
44	Ru	1.84	0.07	1.79	0.02	1.13
45	Rh	1.127	0.12	1.08	0.02	1.14
46	Pd	1.66	0.04	1.67	0.02	0.97
47	Ag	0.94	0.30	1.22	0.04	0.52
48	Cd	1.77	0.11	1.73	0.03	1.09
49	In	<1.50	UL	0.78	0.02	5.97
50	Sn	2.00	0.30	2.09	0.06	0.81
51	Sb	1.00	0.30	1.04	0.06	0.94
52	Te			2.20	0.03	0.01
53	I			1.57	0.08	0.03
54	Xe	2.27	0.08	−1.92		1.56E + 04

(continued)

Cosmic Elemental Abundances, Table 1 (continued)

		Solar photosphere	s.d. dex	Meteorite (CI)	s.d. dex	Sun/meteorite N_{sun}/N_{met}
55	Cs			1.10	0.03	0.08
56	Ba	2.17	0.07	2.20	0.02	0.94
57	La	1.14	0.03	1.20	0.01	0.86
58	Ce	1.61	0.06	1.60	0.01	0.96
59	Pr	0.76	0.04	0.78	0.01	0.86
60	Nd	1.45	0.05	1.47	0.01	0.96
62	Sm	1.00	0.05	0.96	0.01	1.09
63	Eu	0.52	0.04	0.53	0.01	0.95
64	Gd	1.11	0.05	1.07	0.01	1.09
65	Tb	0.28	0.10	0.34	0.01	0.89
66	Dy	1.13	0.06	1.15	0.01	0.98
67	Ho	0.51	0.10	0.50	0.01	1.05
68	Er	0.96	0.06	0.94	0.01	1.03
69	Tm	0.14	0.04	0.14	0.01	0.72
70	Yb	0.86	0.10	0.94	0.01	1.37
71	Lu	0.12	0.08	0.11	0.01	0.89
72	Hf	0.88	0.08	0.73	0.01	1.42
73	Ta			−0.15	0.04	1.34
74	W	1.11	0.15	0.67	0.04	2.75
75	Re			0.28	0.02	0.52
76	Os	1.45	0.11	1.37	0.02	1.21
77	Ir	1.38	0.05	1.34	0.02	1.10
78	Pt	1.74	0.30	1.64	0.02	1.29
79	Au	1.01	0.18	0.82	0.05	1.52
80	Hg			1.19	0.18	0.06
81	Tl	0.95	0.20	0.79	0.05	1.45
82	Pb	2.00	0.06	2.06	0.03	0.88
83	Bi			0.67	0.04	0.21
90	Th	<0.08	UL	0.08	0.03	1.04
92	U	<−0.47	UL	−0.52	0.03	1.11

s.d. standard deviation, *dex* decimal exponent on a $\log_{10}$ scale, e.g., a s.d. of 0.1 dex indicates an uncertainty of about 25%

Cosmic Elemental Abundances, Table 2   Solar system abundances based on CI meteorites

Element		Mean CI abundance (by mass)		Estimated accuracy in (%)	Atoms per $1.00E + 06$ atoms of Si
1	H	1.97	%	10	5.13E + 06
2	He	0.00917	ppm		0.601
3	Li	1.45	ppm	10	54.8
4	Be	0.0219	ppm	7	0.638
5	B	0.775	ppm	10	18.8
6	C	3.48	%	10	7.60E + 05
7	N	0.295	%	15	5.53E + 04
8	O	45.90	%	10	7.53E + 06
9	F	58.2	ppm	16	804
10	Ne	0.00018	ppm		0.0023
11	Na	4962	ppm	9	5.67E + 04
12	Mg	9.54	%	4	1.03 E + 06
13	Al	0.840	%	6	8.17E + 04
14	Si	10.70	%	3	1.00E + 06
15	P	985	ppm	8	8.34 + 03
16	S	5.35	%	5	4.38E + 05
17	Cl	698	ppm	15	5.17E + 03
18	Ar	0.00133	ppm		0.0096

Cosmic Elemental Abundances, Table 2 (continued)

Element		Mean CI abundance (by mass)		Estimated accuracy in (%)	Atoms per 1.00E + 06 atoms of Si
19	K	546	ppm	9	3.67E + 03
20	Ca	0.911	%	6	5.97E + 04
21	Sc	5.81	ppm	6	33.9
22	Ti	447	ppm	7	2.43E + 03
23	V	54.6	ppm	6	281
24	Cr	2623	ppm	5	1.32E + 04
25	Mn	1916	ppm	6	9.15 + 03
26	Fe	18.66	ppm	4	8.77E + 05
27	Co	513	ppm	4	2.28E + 03
28	Ni	1.091	%	7	4.83E + 04
29	Cu	133	ppm	14	549
30	Zn	309	ppm	4	1.24E + 03
31	Ga	9.62	ppm	6	36.2
32	Ge	32.6	ppm	9	118
33	As	1.74	ppm	9	6.10
34	Se	20.3	ppm	7	67.53
35	Br	3.26	ppm	15	10.7
36	Kr	5.22E − 5	ppm		1.64E − 4
37	Rb	2.32	ppm	8	7.13
38	Sr	7.79	ppm	7	23.3
39	Y	1.46	ppm	5	4.31
40	Zr	3.63	ppm	5	10.4
41	Nb	0.283	ppm	10	0.800
42	Mo	0.961	ppm	10	2.66
44	Ru	0.690	ppm	5	1.79
45	Rh	0.127	ppm	5	0.337
46	Pd	0.560	ppm	4	1.38
47	Ag	0.201	ppm	9	0.489
48	Cd	0.674	ppm	7	1.49
49	In	0.0778	ppm	5	0.168
50	Sn	1.63	ppm	15	3.35
51	Sb	0.145	ppm	14	0.300
52	Te	2.28	ppm	7	4.56
53	I	0.53	ppm	20	1.05
54	Xe	1.74E − 4	ppm		3.48E − 4
55	Cs	0.188	ppm	6	0.371
56	Ba	2.42	ppm	5	4.63
57	La	0.2414	ppm	3	0.4561
58	Ce	0.6194	ppm	3	1.160
59	Pr	0.09390	ppm	3	0.1749
60	Nd	0.4737	ppm	3	0.8621
62	Sm	0.1536	ppm	3	0.2681
63	Eu	0.05883	ppm	3	0.1016
64	Gd	0.2069	ppm	3	0.3453
65	Tb	0.03797	ppm	3	0.06271
66	Dy	0.2558	ppm	3	0.4132
67	Ho	0.05644	ppm	3	0.08982
68	Er	0.1655	ppm	3	0.2597
69	Tm	0.02609	ppm	3	0.04054
70	Yb	0.1687	ppm	3	0.2559
71	Lu	0.02503	ppm	3	0.03755
72	Hf	0.1065	ppm	3	0.1566
73	Ta	0.015	ppm	10	0.0218

Cosmic Elemental Abundances, Table 2 (continued)

Element		Mean CI abundance (by mass)		Estimated accuracy in (%)	Atoms per 1.00E + 06 atoms of Si
74	W	0.096	ppm	10	0.137
75	Re	0.0400	ppm	5	0.0554
76	Os	0.495	ppm	5	0.683
77	Ir	0.469	ppm	5	0.640
78	Pt	0.925	ppm	5	1.24
79	Au	0.148	ppm	12	0.197
80	Hg	0.35	ppm	50	0.41
82	Tl	0.140	ppm	11	0.184
82	Pb	2.62	ppm	8	3.32
83	Bi	0.110	ppm	9	0.138
90	Th	0.0300	ppm	7	0.0339
92	U	0.00810	ppm	7	0.00893

C
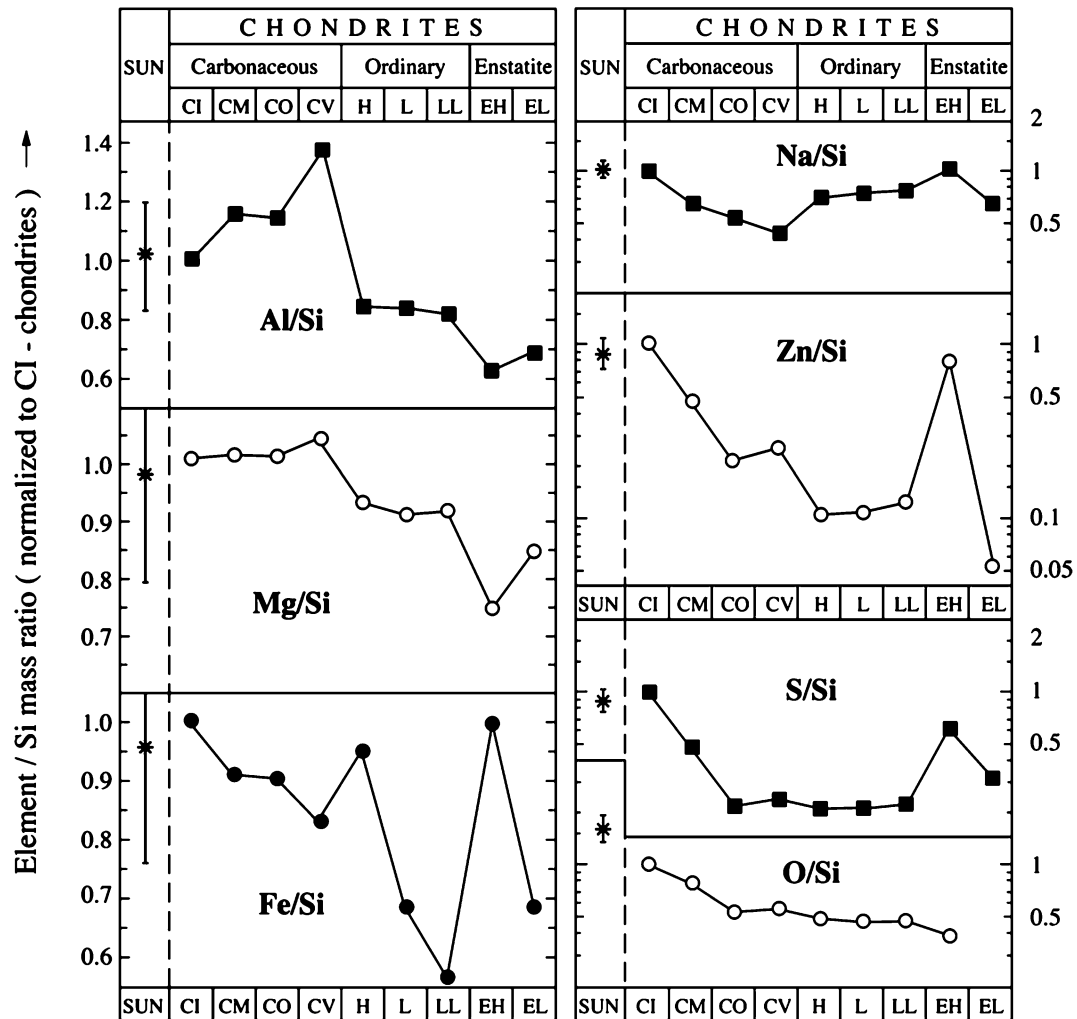
Cosmic Elemental Abundances, Fig. 2 Element/Si mass ratios of characteristic elements in various groups of chondritic (undifferentiated) meteorites. The refractory component is represented by Al; Mg represents the Mg silicates, Fe the metal component, and Na, Zn, and S the moderately volatile elements. Only CI chondrites fit with photospheric abundances indicated on the left side (Figure is from Lodders et al. 2009)

components has a characteristic formation temperature indicated by condensation temperatures of elements and phases involved. Condensation temperatures are calculated by assuming thermodynamic equilibrium between solids and a cooling gas of solar composition (see Lodders 2003, for details). The various cosmochemical components are in order of decreasing condensation temperatures:

Refractory component: The first phases to condense from a cooling gas of solar composition are Ca,Al-oxides, and silicates associated with many trace elements, such as the REE (rare earth elements), Zr, Hf, and Sc, and additionally refractory metals, e.g., W, Os, and Ir. The refractory component makes up about 5% of the total condensable matter. Variations in, e.g., Al/Si and Ca/Si ratios of bulk chondrites may be ascribed to the incorporation of variable amounts of early condensed refractory phases.

Mg silicates: The major fraction of condensable matter is associated with the three most abundant elements heavier than oxygen: Si, Mg, and Fe. In the relatively reducing environment of the solar nebula, Fe condenses almost entirely as metal alloy (FeNi), while Mg and Si form forsterite (Mg_2SiO_4) which converts to enstatite ($MgSiO_3$) at lower temperatures by reaction with gaseous SiO. Variations in Mg/Si ratios of bulk meteorites are produced by the incorporation of various amounts of early-formed forsterite.

Metallic iron condenses as a FeNi alloy at about the same temperature as forsterite, the sequence depending on total pressure. Variations in the concentrations of Fe and other siderophile elements in meteorites are produced by the incorporation of variable fractions of metal.

Moderately volatile elements have condensation temperatures between those of Mg silicates and FeS (troilite). The most abundant element of the moderately volatile elements is sulfur. The amount and the relative abundances of these elements in meteorites are probably the result of removal of volatiles during condensation.

Highly volatile elements have condensation temperatures below FeS and above water ice The group of highly volatile elements comprises elements with very different geochemical affinities, such as the chalcophile Pb and the lithophile I. Similar processes as those invoked for the depletion of moderately volatile elements are responsible for variations in these elements. In addition, heating on small parent bodies may lead to loss of highly volatile elements by evaporation.

Ultra volatile elements have condensation temperatures below that of water ice. This group includes H, C N, O, and the noble gases.

In summary, Fig. 2 gives some indication for the range of elemental variations in chondritic meteorites. We assume that minor compositional variations among chondritic meteorites are produced by nebular processes that occurred before accretion of planetesimals. Planetary melting processes, such as core formation or partial melting, lead to rocks with completely different compositions.

The bulk composition of the terrestrial planets is essentially solar with similar numbers of Mg, Si, and Fe atoms and about one tenth of Al atoms. This characteristic composition prevails, with more or less variability in kilometer-sized asteroids, meter-sized chondritic meteorites, submillimeter- to millimeter-sized micrometeorites, micrometer-sized interplanetary dust particles, and sub-micrometer-sized particles, possibly interstellar dust. The major variables are the ratio of metallic to oxidized Fe and variations in the depletion of volatile elements.

Summary

The abundance pattern of chemical elements in the Sun and many other stars is determined by the Big Bang making H and He and by later production of heavy elements in the interior of stars, a process that is still active. The pattern of heavy, non-volatile elements in unmelted, chondritic meteorites is the same as in the Sun, with one group of meteorites the CI chondrites fitting best. Other undifferentiated, chondritic meteorites have compositions deviating somewhat from solar. These meteorites were modified by solar nebula processes before planetesimal accretion. The solar system abundances, a combination of solar photospheric and meteoritic abundances, are known to within a few percent for each element. Extension to other stars leads to heavy element cosmic abundances which are less well known.

Cross-References

▶ Chondrites
▶ Formation and Evolution of the Earth
▶ Meteorites

References

Asplund M, Grevesse N, Sauval J, Scott P (2009) The chemical composition of the Sun. Annu Rev Astron Astrophys 47:481–522

Krot AN, Keil K, Goodrich CA, Scott ERD, Weisberg MK (2003) Classification of meteorites. In: Davis AM, Holland HD, Turekian KK (eds) Meteorites, comets and planets, Treatise on geochemistry, vol Vol. 1. Elsevier, Oxford, pp 83–128

Lodders K (2003) Solar system abundances and condensation temperatures of the elements. Astrophys J 591:1220–1247

Lodders K, Palme H, Gail HP (2009) Abundances in the solar system., Chap. 4.4. In: Trümper JE (ed) Landolt-Börnstein, new series, vol VI/4B. Springer, Berlin/Heidelberg/New York, pp 560–598

Palme H, Lodders K, Jones A (2014) Solar system abundances of the elements. In: Holland HD, Turekian KK (eds) Treatise on geochemistry, vol 2, 2nd edn. Elsevier, Oxford, pp 15–36

Cosmogenic Nuclides

Rainer Wieler
Department of Earth Sciences, Institute of Geochemistry and
Petrology, ETH Zürich, Zürich, Switzerland

Definition

Cosmogenic nuclides are produced when primary or secondary particles of the galactic (or in some cases also the solar) cosmic radiation interact with atomic nuclei in extraterrestrial or terrestrial material. Cosmogenic nuclides are observable mainly for noble gas isotopes and radioactive nuclides, whose abundances in the target materials are otherwise extremely low. In this article, we discuss production and applications of cosmogenic nuclides in meteorites and other extraterrestrial samples (Wieler 2002; Eugster et al. 2006; Herzog and Caffee 2014) as well as in terrestrial samples (Gosse and Phillips 2001; Dunai 2010; Granger et al. 2013). In solid matter, the cosmic-ray flux has a mean attenuation length of roughly 50 cm. Hence, cosmogenic nuclides in meteorites are primarily used to determine exposure ages, i.e., the time spent as meter sized or smaller body in interplanetary space before falling on Earth or in some cases also the residence time in the uppermost few meters of their larger parent body. Cosmogenic nuclides in terrestrial rocks allow determining ages or erosion rates of geologic surfaces and nuclides produced in the atmosphere and subsequently being deposited in terrestrial archives provide records of, e.g., past solar activity and geomagnetic field variations.

Introduction

On Earth, cosmogenic nuclides are produced both in the atmosphere and in situ in solid samples at the Earth's surface. Cosmogenic radionuclides produced in the atmosphere (together with contributions from nuclear power plants and nuclear bombs) are used to study atmospheric dynamics and the hydrological cycle. Nuclides produced in the atmosphere will eventually also be deposited in the geosphere or hydrosphere as "meteoric nuclides." Meteoric nuclides which found their way into archives such as ice or sediment cores allow us to determine the past flux of the cosmic radiation entering the Earth's atmosphere. Such archives are therefore used to investigate the physics of the sun, the heliosphere, and the geomagnetic field. Meteoric radionuclides also allow us to study processes near the Earth's surface such as subduction of oceanic crust or sediment dynamics. A particularly important cosmogenic nuclide produced in the atmosphere is ^{14}C, which ultimately may find its way into organic matter. The nuclide

^{14}C is the basis of the most widely used radiometric dating method. On the Earth's surface, the cosmic-ray flux is several orders of magnitude lower than in interplanetary space. Production rates and concentrations of cosmogenic nuclides produced at the Earth's solid surface are thus much lower than in meteorites, which presents considerable analytical challenges. Nevertheless, cosmogenic radionuclides and noble gases produced in situ in terrestrial surface rocks have become a very widely used tool in Earth surface sciences, allowing, e.g., to determine the time since a rock has been exposed on the Earth's surface or long-term erosion rates of landscapes.

Production of Cosmogenic Nuclides

Cosmogenic nuclides are produced either when target atoms interact with high-energy cosmic-ray particles (mainly between 100 MeV–10 GeV) or when they capture low-energy neutrons ("thermal" or "epithermal" neutrons, i.e., ~0.025 eV and 0.5 eV–0.1 MeV, respectively). A detailed account of cosmogenic nuclide production is given by Gosse and Phillips (2001). Primary cosmic-ray particles (mostly protons and alpha particles) need to be distinguished from secondary particles, the latter being created in the cascade of nuclear reactions initiated by primary particles. Secondary particles include high-energy protons and neutrons as well as thermal and epithermal neutrons. On the Earth also secondary cosmic-ray muons are of some importance. These can be considered as heavier brothers of the electron with a half-life on the order of a microsecond. In meteorites production by primary and secondary particles is important (Eugster et al. 2006; Herzog and Caffee 2014). In contrast, the cosmogenic nuclide production in terrestrial rocks is largely dominated by secondary neutrons, since hardly any cosmic-ray protons arrive at the Earth's surface. Muon-induced reactions become important at depths below several meters, because the mean attenuation length of muons in matter is much larger than that of neutrons. As discussed further down, the analysis of several cosmogenic nuclides in the same or adjacent samples will often allow us to constrain the "shielding" of a meteorite sample during cosmic-ray exposure, i.e., the size of the meteorite before it becomes ablated upon passage through the Earth's atmosphere and the depth of the sample within this "meteoroid." This is because production rates of different cosmogenic nuclides vary with depth in different ways. Analyses of several nuclides are also used to better constrain exposure and erosional histories of terrestrial samples. Most widely studied nuclides are the rare isotopes of helium, neon and argon (^{3}He, ^{21}Ne, ^{38}Ar) and the radioactive nuclides ^{10}Be (T$_{1/2}$ = 1.387 Ma), ^{14}C (5730 a), ^{26}Al (0.717 Ma), ^{36}Cl (0.301 Ma) and ^{53}Mn (3.74 Ma). Complete lists of nuclides measured in meteorites and terrestrial samples are given by Eugster et al. (2006) and Dunai (2010), respectively.

In meteorites, important parameters governing production rates are energy-dependent particle fluxes at the sample site, energy-dependent cross sections of all important reactions, and the major target element composition of the sample (e.g., Leya and Masarik 2009). The particle flux depends on the primary cosmic-ray proton flux, which varies with the solar cycle but usually is assumed to be constant over longer time scales. The flux seen by a sample also depends on its shielding and on the composition of the meteorite as a whole. A high Fe concentration, for example, leads to a higher production of secondary neutrons, while neutrons are more efficiently slowed down in meteorites relatively rich in H and C. Production rates are usually considerably higher from target elements with only a slightly higher mass than the product nuclide. For example, the production of ^{21}Ne from Mg is about 2.5–3 times higher than that from Si and some two orders of magnitude higher than that from Fe (Leya and Masarik 2009). A good knowledge of the major target element composition of a given sample is thus a prerequisite for an accurate production rate estimate.

Production rates on the Earth depend largely on the shielding of a sample by the atmosphere (i.e., the sample's altitude) and the modulation of the primary proton flux by the Earth's magnetic field (the geomagnetic latitude). For example, at a given latitude, production rates at sea level are some 15–20 times lower than at 4000 m altitude, and at the equator, production rates are ~2.5 times lower than at latitudes >60° (Lal 1991; Balco et al. 2008; Lifton et al. 2014). This is because near the poles virtually all cosmic-ray protons reach the upper atmosphere unhindered by the Earth's magnetic field, whereas at lower latitudes lower energy protons will be deflected (Gosse and Phillips 2001; Beer et al. 2012). For the relatively short-lived nuclide ^{14}C (which is also produced in situ in rocks) and for samples with high erosion rates, the position of the geomagnetic poles in the past (polar wandering) may have to be considered. For longer-lived nuclides, it is usually assumed that the average position of the geomagnetic poles coincides with the geographic poles, as these nuclides integrate production over at least several ten thousand years unless erosion rates are very high (see below). Time-integrated production rates of a sample will crucially depend on the rock's erosion history, as a sample now at the immediate rock surface will in the past have been shielded by overlying material. The production rate in the past will therefore have been lower than the present day surface value, and this effect will be more pronounced with higher erosion rates (Lal 1991; Gosse and Phillips 2001; Dunai 2010, see Fig. 1). This is the reason why cosmogenic nuclides very often are used to constrain erosion rates rather than exposure ages.
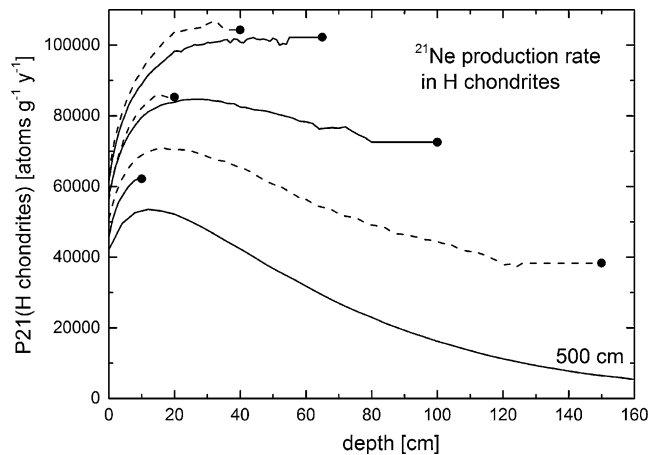
Models to calculate production rates in meteorites are based on large libraries of measured cross sections for proton- and neutron-induced reactions as well as nuclear model codes used to extend or interpolate measured data (Leya and
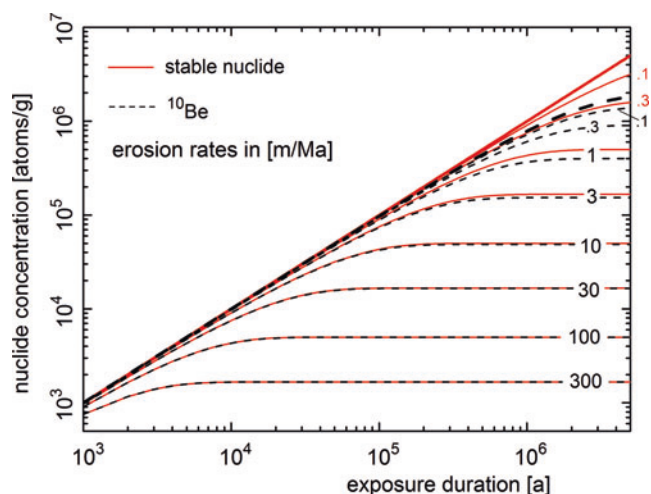
Cosmogenic Nuclides, Fig. 1 Nuclide concentrations at the top of eroding surfaces. Exposure duration in years since onset of erosion with constant rate [m/Ma]. *Red solid lines* are valid for stable nuclides, *dashed lines* for ^{10}Be. The two *thick lines* represent non-eroding surfaces. A hypothetical production rate of 1 atom per gram per year is adopted; hence concentrations need to be multiplied with the actual local production rate. Concentrations of ^{10}Be are only sizably affected due to radioactive decay for erosion rates not exceeding ~3 m/Ma. In eroding surfaces also stable nuclides reach a steady-state concentration which depends on the erosion rate (Figure adapted from Lal (1991) and Dunai (2010))

Masarik 2009). This needs especially to be done for neutron-induced reactions to compensate for the many gaps in the measured data. The spectra of primary and secondary protons and neutrons as function of meteorite radius and sample depth are calculated by nuclear codes using Monte Carlo techniques (Leya and Masarik 2009). The primary galactic cosmic-ray proton flux is calibrated by fitting modelled concentrations of radionuclides (e.g., ^{10}Be) to measured values in well-studied meteorites, for which the preatmospheric geometry can be reliably reconstructed and which have exposure ages long enough for the radionuclide concentration to have reached its equilibrium value, where production and radioactive decay match (in practice after some 4–5 half-lives of the nuclide). Figure 2 shows modelled production rates of ^{21}Ne (P21) as a function of depth in spherical meteorites of H-chondritic composition and radii between 10 and 500 cm. The increase of P21 from the meteorite surface up to depths varying between ~15 and 40 cm reflects the development of the cascade of secondary protons and neutrons. At large depths, the decrease of P21 approximately reflects the mean attenuation length of the cosmic-ray flux of ~50 cm.
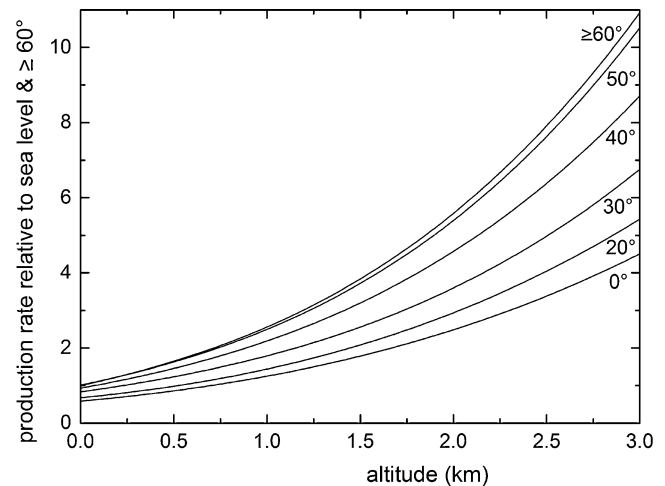
Because meteorites suffer large ablation losses or split into multiple fragments upon atmospheric passage, pre-atmospheric meteorite size and sample depth will hardly ever be known a priori. However, analyses of several cosmogenic nuclides on the same sample (or a series of samples) combined with model calculations may allow one to constrain the shielding of a given sample and hence its production rates.

Cosmogenic Nuclides, Fig. 2 Production rate of ^{21}Ne in meteorites of H-chondritic composition with radii of 10, 20, 40, 65, 100, 150, and 500 cm, calculated with the nuclide production model by Leya and Masarik (2009). Wiggles near the centers of the meteorites are the result of poor statistics in the model calculations due to relatively low volumes considered

Cosmogenic Nuclides, Fig. 3 Cosmogenic nuclide production rates relative to values at sea level and high latitude ($\geq$60°, SLHL) according to the classical scaling scheme proposed by Lal (1991). Production rates at 3000 m altitude and high latitude are ~11 times higher than the SLHL values; production rates at sea level and the equator are ~60% of the SLHL values. Other scaling schemes are mentioned in the text

A widely used shielding parameter is the ratio ^{22}Ne/^{21}Ne, which decreases with increasing shielding, since production of ^{21}Ne by secondary neutrons is higher than that of ^{22}Ne. Other shielding indicators are based on ratios of a stable to a radioactive nuclide, which may vary little over a certain shielding range (Herzog and Caffee 2014). If the radionuclide can be assumed to be in saturation, the production rate of the stable nuclide can be determined. A well-known such combination is ^{26}Al-^{21}Ne. The combination of radioactive ^{81}Kr with stable Kr isotopes even yields shielding-corrected exposure ages by a single Kr isotope analysis (e.g., Leya et al. 2015). None of these shielding corrections is perfect, however. They may be valid over a limited size and depth range only, some of them require multiple analyses and analytical precision is often also a problem. ^{81}Kr concentrations, for example, are very low, and in many cases, also corrections for non-cosmogenic stable Kr isotopes are very substantial. In summary, production rates usually have considerable uncertainties, in favorable cases perhaps 10%, but often 20% or more.

A major issue when studying cosmogenic nuclide production at the Earth's surface is proper "scaling" of production rates determined at one geographical location to altitude and latitude of any sample site of interest. In contrast to meteorites, the moment in time when a sample at the Earth's surface had been freshly exposed to cosmic rays can independently be deduced in favorable cases (Dunai 2010; Granger et al. 2013). For example, the eruption age of a lava flow can be determined by radiometric dating. Production rates of cosmogenic nuclides at the sample site can then be deduced, although care is required to properly assess potential erosion of the calibration sample or effects such as episodic cover by snow or vegetation. Also partial shielding from cosmic rays by

surrounding mountains, other obstacles or inclined surfaces need to be considered (Gosse and Phillips 2001; Dunai 2010). Fortunately, topographic shielding is only significant in "rather spectacular" landscapes (Dunai 2010), because the angular cosmic-ray flux seen by a sample strongly decreases towards the horizon. For relatively young samples, also the paleopole positions may have to be taken into account. In the case of in situ ^{14}C, it may not even be necessary to know the actual exposure age of a sample. Similar to production rate determinations of radionuclides in meteorites, it may suffice if one reliably can assume the sample to have been exposed for longer than some four or five half-lives of ^{14}C, i.e., for more than ~25 ka. Potential uplift of a calibration sample – leading to increasing production rates with time – should hardly be a concern, since suitable calibration samples mostly have rather low exposure ages in order to minimize uncertainties due to erosion. By convention, production rates determined at a calibration site are scaled to sea level and high latitude (>60°) as described in the next paragraph, and these "SLHL" values are reported. At 60° or higher, production rates will not increase with latitude any further.

Scaling schemes are largely based on measured neutron fluxes in the atmosphere. Figure 3 shows scaling factors according to the classical study by Lal (1991). A recent model uses analytical approximations to fluxes of cosmic-ray neutrons as well as protons and muons modeled by Monte Carlo techniques (Lifton et al. 2014). Various online calculators and computer codes are available to scale production rates to latitude and altitude of samples of interest (Vermeesch 2007; Balco et al. 2008; Lifton et al. 2014). It is highly recommended to always report the scaling scheme

used in a particular study. Dunai (2010) provides a checklist of further information recommended to be reported. Because pressure regimes are not identical to standard atmospheric values everywhere on Earth, corrections for such persistent anomalies may be required. The best-known case is Antarctica, where today pressures at all elevations are a few ten hPa lower than standard values and production rates accordingly some 25–30% higher (Stone 2000). When calculating exposures ages of antarctic samples, it is usually assumed that this anomaly has persisted over millions of years.

Production rates of cosmogenic nuclides in the atmosphere are also calculated with physical models. Required proton and neutron flux spectra are obtained with extensive computer codes (Masarik and Beer 2009; Kovaltsov and Usoskin 2010; Beer et al. 2012). Similar to the Earth's surface, production rates increase with geomagnetic latitude. However, because of atmospheric mixing, concentrations of atmosphere-derived cosmogenic nuclides in terrestrial archives such as ice cores depend much less on the latitude than is the case for in situ produced nuclides.

Analytical Aspects

Cosmogenic noble gases are measured by noble gas mass spectrometry; radionuclides are mostly analyzed by accelerator mass spectrometry (AMS) (Christl et al. 2014). For routine analyses of meteorites, often whole-rock samples are measured, whereas mineral separates are the rule in terrestrial studies, with quartz being the most important by far. A major reason for this is that meteoric radionuclides can be removed in a controlled way from quartz by etching off grain surface layers (Kohl and Nishiizumi 1992). Meteoric ^{10}Be in an untreated quartz separate is orders of magnitude more abundant than in situ produced ^{10}Be. Noble gases are usually extracted by heating samples in single or multiple steps, sometimes combined with in vacuo crushing, e.g., to partly remove or correct for non-cosmogenic ^{3}He or ^{21}Ne (Niedermann 2002). Preparation for radionuclide analyses of rock samples requires several steps of chemical treatment, first to obtain clean mineral separates (Kohl and Nishiizumi 1992) and next to extract the nuclides (Gosse and Phillips 2001). Similar procedures – though nuclide and sample specific – are used for meteoric radionuclide separation from terrestrial archives (Beer et al. 2012). Cosmogenic and non-cosmogenic noble gases can usually not be separated quantitatively from each other, or in many cases are not separated at all, e.g., in meteorite analyses. Corrections for non-cosmogenic contributions may be minor in many cases, e.g., for meteorites with low concentrations of primordial or solar-wind-implanted noble gases, but often non-cosmogenic noble gases are the limiting factor deciding whether or not concentrations of cosmogenic noble gases in a sample may be

determined. This is particularly a problem for terrestrial samples and is the main reason why often much lower exposure ages can be determined with radionuclides than with noble gases. On the other hand, stable noble gas isotopes are useful to determine very old exposure ages in very slowly eroding arid landscapes.

Cosmogenic Nuclides in Extraterrestrial Samples

Two classical applications of cosmogenic nuclides in meteorites are to determine their cosmic-ray exposure age and their terrestrial age, i.e., the time they spent in interplanetary space as roughly meter-sized objects and the time they fell on Earth and became essentially shielded from cosmic rays by the atmosphere. Exposure ages longer than ~5–6 Ma (some 4–5 half-lives of ^{10}Be) are determined with stable noble gas isotopes, often together with radionuclide analyses to constrain shielding of and hence production rate in a sample, as explained above. With some exceptions, exposure ages of stony meteorites fall in the range of below one Ma to about hundred Ma, whereas iron meteorites often have exposure ages of several hundred Ma, with a highest value of some two Ga (Marti and Graf 1992; Herzog and Caffee 2014). Figure 4 shows the exposure age distribution of the H chondrites, one of the largest stony meteorite classes.

In arid areas meteorites weather only slowly, hence terrestrial ages of meteorites from hot deserts are often in the ten to several ten thousand year range, whereas many meteorites found in Antarctica have been on Earth since several hundred
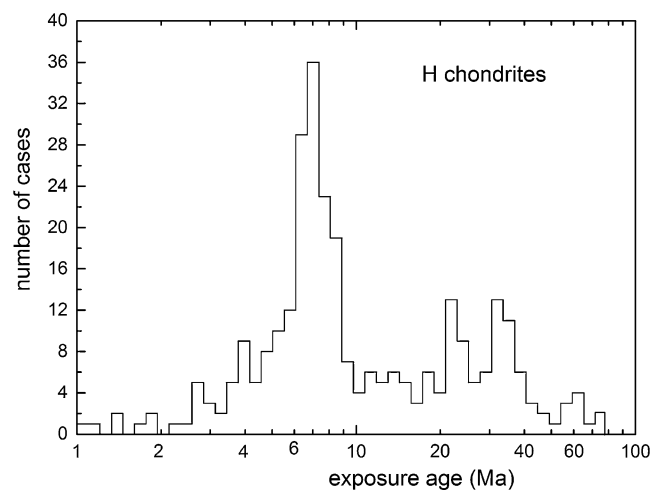
Cosmogenic Nuclides, Fig. 4 Cosmic-ray exposure age distribution of H chondrites (Graf and Marti 1995). About 45% of all H chondrites show an exposure age of 7–8 Ma, indicating one (or perhaps two) major collision(s) in the asteroid belt 7–8 Ma ago. Minor peaks at ~24 Ma and 33 Ma are the result of further major collisions in the asteroid belt. Exposure age distributions of other meteorite classes are shown by Herzog and Caffee (2014). Often also these histograms show a clustering of ages typical for the respective class

thousand years, with the highest reported values being ~3 Ma (Jull 2006; Herzog et al. 2015). Terrestrial ages are determined with radionuclides of suitable half-lives. An additional noble gas analysis may confirm that the exposure age of the sample had been long enough to bring the radionuclide concentration in saturation at the time of fall. Carbon-14 is the main nuclide used for stony meteorites; ^{36}Cl is used for iron meteorites and for stony meteorites with long terrestrial ages. Also pairs of radionuclides are used for shielding corrections, e.g., ^{14}C–^{10}Be or ^{36}Cl–^{41}Ca (Jull 2006; Herzog et al. 2015). The atmosphere can be assumed to completely shield a fallen meteorite from further cosmogenic nuclide production, since production rates on Earth are very much lower than in space.

Meteorites from the asteroid belt are delivered to Earth through resonances, for example, the 3:1 mean-motion resonance with Jupiter. A meteorite with a semimajor axis of ~2.5 astronomical units will complete three orbits in the time Jupiter revolves around the sun once. Such resonances result in chaotic eccentricities and inclinations, and the meteorite may collide with the Earth within one Ma or so (Wisdom 1987; Gladman et al. 1997). Since most meteorites have much longer exposure ages, they must therefore spend most of their lifetime as meter-sized bodies in the asteroid belt. After having been released from larger parent bodies by a collision, they slowly move towards a resonance largely due to non-gravitational forces, e.g., the Yarkovsky effect, the anisotropic emission of infrared photons (Bottke et al. 2002).

Cosmic-ray exposure ages are important to evaluate whether meteorites may be paired or source paired, i.e., whether they belonged to the same meteoroid prior to breakup in the atmosphere or were ejected from their parent body by the same event, respectively. Identification of paired meteorites is especially important for the numerous desert finds. Identical terrestrial ages are a further pairing criterion, and in some cases, short-lived cosmogenic radionuclides (half-lives on the order of months or years) provide evidence for a (common) recent fall date. Care is required not to overinterpret cosmogenic nuclide data, however. Identical exposure ages of two meteorites are by far not a sufficient pairing criterion by themselves. For example, about 20% of all H chondrites – belonging to many hundred different falls - have an exposure age of about 7–8 Ma (Fig. 4). On the other hand, the 7–8 Ma H chondrites indeed very likely originate from one (or perhaps two) major collisions in the asteroid belt (Graf and Marti 1995).

By now, exposure age distributions of most major meteorite classes are known, and it is clear that different classes have different distributions (Herzog and Caffee 2014). Most of them show clusters similar to the 7–8 Ma peak in the H chondrite histogram. This means that a small number of collisions produced a very large fraction of the known meteorites, which indicates that we sampled only a tiny portion of the potential meteorite parent bodies in the asteroid belt (Wieler and Graf 2001).

Sometimes, exposure ages derived for different samples of the same meteorite or by different nuclides in the same sample are clearly discrepant. This often indicates a "complex" exposure history, which means that not all cosmogenic nuclides were acquired during the recent exposure stage prior to fall but that some of them testify of earlier irradiations in different settings (Herzog and Caffee 2014). For example, a meteorite may have been broken up on its way to Earth. Particularly interesting are complex exposure histories where the first stage happened near the surface of the parent body. In such cases, cosmogenic nuclides allow us to study the dynamics of the parent body regolith. This can often only be done with stable noble gas nuclides, as radionuclides potentially acquired on the parent body may have completely decayed during the transfer of the meteorite to Earth. Differences in nominal cosmic-ray exposure ages indicate that different samples from a regolith breccia had spent variable times near the surface of their parent body (perhaps at different depths) before compaction into the present-day meteorite (Wieler 2002). Complex exposure histories are also reported for single grains or single chondrules in some meteorites, which contain sometimes orders of magnitude higher concentrations of cosmogenic noble gases than the parent meteorite as a whole. It remains controversial whether this indicates – at least in some cases – an irradiation by a high fluence of solar energetic particles from the very early sun (Woolum and Hohenberg 1993) or simply a prolonged irradiation by galactic cosmic rays in the parent body regolith (Roth et al. 2011). Most lunar meteorites contain cosmogenic noble gases acquired on the parent body, indicating a shallow excavation depth (Herzog and Caffee 2014; Herzog et al. 2015). In contrast, martian meteorites show hardly any signs of a parent body exposure, hence must have been excavated from larger depths (Herzog and Caffee 2014). Also in situ analyses of cosmogenic nuclides by spacecraft have a considerable potential to study the evolution of the morphology of planetary surfaces, in essence similar to what is now routinely done on Earth (e.g., Farley et al. 2014).

Not only noble gases and radionuclides but essentially the isotopes of all other elements are also produced by cosmic-ray interactions. Until recently, however, the resulting shifts in isotopic composition have in most cases remained unnoticed. Exceptions were gadolinium and samarium which both contain isotopes with very large cross sections for thermal neutron capture. These elements have been used to study the depositional history of the lunar regolith with samples from Apollo drill cores (Russ et al. 1972; Hidaka and Yoneda 2007) and cosmic-ray exposure histories of large meteorites (Bogard et al. 1995). The very high precision of present-day analyses now reveal tiny isotopic anomalies in several other elements as results of cosmic-ray effects. Some of these elements are important for cosmochemistry, and the cosmogenic isotopic shifts are large enough to require a proper

C

correction. The foremost example is tungsten, measured to date early solar system events by the Hf-W method (Kleine et al. 2009). Cosmic rays modify not only the abundances of the radiogenic isotope ^{182}W (from decay of ^{182}Hf) but also W isotopes used to correct for instrumental mass fractionation (or sometimes to study potential primordial isotopic anomalies). The effects are largest in samples with long exposure ages, especially lunar samples and iron meteorites (Leya et al. 2000). The knowledge of an exposure age alone does often not permit a proper correction, however, because the magnitude of isotopic shifts may also substantially depend on the shielding of the sample. Isotopes of platinum are an excellent monitor to correct tungsten isotopes in iron meteorites for cosmic-ray effects, because W and Pt are both modified by thermal and epithermal neutrons (Kruijer et al. 2013).

Cosmogenic Nuclides in Terrestrial Rocks

Considerably later than in meteoritics in situ produced cosmogenic nuclides also became an important tool in Earth surface sciences. This delay is due to the fact that nuclide concentrations on Earth are orders of magnitude lower than in meteorite samples. Yet, since the late 1980s terrestrial applications proliferate and led to what is often called a revolution in Earth surface science. Publication and citation rates of Earth science studies involving cosmogenic nuclides increased by orders of magnitude in the past 20–25 years (Dunai 2010). Cosmogenic nuclides allow us to study and quantify processes and timescales in geomorphology in a qualitatively new way.

Two major applications are dating the ages of geologic surfaces (exposure dating) and determinations of erosion or denudation rates. The two questions are often intertwined, as is illustrated in Fig. 1. Concentrations of stable nuclides (e.g., ^{21}Ne) and the radionuclide ^{10}Be ($T_{1/2} = 1.38$ Ma) in a sample presently at the immediate surface of the Earth are shown as a function of exposure duration and for different (time-independent) erosion rates. A hypothetical production rate of 1 atom per gram per year is adopted. Concentrations as displayed therefore need to be multiplied with the actual local production rate at a sample site. The concentration of a stable nuclide in a non-eroding surface increases linearly with time, but in an eroding surface, also stable nuclides will eventually reach equilibrium. The higher the erosion rate, the sooner the equilibrium concentration will be reached and the lower it will be. This is because the cosmic-ray neutron flux seen by the sample had always been lower than the present-day value at the very surface as long as it was shielded by overlying material (Lal 1991). For erosion rates larger than some 3 m/Ma, radioactive decay has no discernible additional effect on the ^{10}Be concentration. For very high erosion rates of 300 m/Ma (0.3 mm/a), erosional saturation is reached already after some 7000 a, whereas for low erosion rates of 0.3 m/Ma,

stable nuclides will not have reached their steady-state concentrations even after ~5 Ma and ^{10}Be hardly so. The figure also illustrates that with a single nuclide, essentially only a minimum exposure age (assuming no erosion) or a maximum erosion rate (assuming an infinite exposure age) can be determined. Analyses of two nuclides with different half-lives (e.g., ^{10}Be and stable ^{21}Ne or ^{10}Be and ^{26}Al) in principle allow the determination of both erosion rate and exposure age. Such data pairs also permit to recognize "complex" exposure histories, i.e., when a sample already contained "inherited" nuclides from a previous exposure stage under a different geometry or when a sample had been buried for a certain time (Lal 1991; Granger 2006; Dunai 2010). However, analytical uncertainties often limit the accuracy of erosion rate/exposure age data pairs.

Some of the numerous studies using in situ produced cosmogenic nuclides to determine exposure ages and erosion rates are reviewed, e.g., by Morris et al. (2002), Dunai (2010), Balco (2011) and Granger et al. (2013). Classical examples include dating of glacial moraines and other glacially overprinted landscapes, studies of other erosional surfaces such as river terraces or slowly eroding desert landscapes, and dating of lava flows or fault scarps induced, e.g., by earthquakes. Careful fieldwork is obviously crucial, and sampling strategies need to take into account the specific requirements for cosmogenic nuclide studies.

Cosmogenic radionuclides may not only allow us to derive the time when a rock became exposed to the cosmic radiation but also the moment a sample became completely shielded from cosmic rays. This can occur when sediments are washed into caves or when rocks are covered by water, ice, sediment deposits, volcanic flows, etc. The principle of "burial dating" is somewhat analogous to terrestrial age determinations of meteorites with cosmogenic radionuclides, except that in the terrestrial case, two radionuclides with different half-lives are required (Granger 2006; Dunai 2010). If the concentration ratio of the two nuclides at the time the sample became buried can be assumed to be known, the measured ratio will yield the burial duration. Well suited is the couple ^{10}Be-^{26}Al, since their preburial concentration ratio can often reliably be assumed to be close to the production rate ratio. While for samples that experienced a simple exposure history followed by a rapid burial, the burial event can be dated, for samples that experienced repeated episodes of exposure and burial, cosmogenic nuclides can only provide a lower limit for the total near-surface exposure (Granger 2006).

Cosmogenic nuclides do not only constrain erosion rates at a specific site but can also be used to derive erosion rates averaged over entire river catchments (von Blanckenburg 2005; Portenga and Bierman 2011; Willenbring et al. 2013). This is done by analyzing sediment samples from active river channels at the low end of a catchment of interest. To obtain accurate results, several conditions need to be fulfilled (Dunai 2010). These include that (i) erosion rates in the catchment are constant over

the period reflected by a nuclide studied, i.e., mass wasting processes did not contribute significantly to the overall erosion, (ii) all lithologies in the catchment are equally well represented in the sample analyzed (often a quartz grain separate), and (iii) transit times of sediments through the catchment are short compared to the erosional timescale. Even if not all these conditions are met, however, the method may still usefully constrain catchment wide erosion rates, though with limited accuracy (Dunai 2010). Relevant production rates averaged over the entire catchment are derived either from digital elevation models or – more simply – are taken to be equal to the production rate at the mean altitude (and latitude) of a catchment.

Catchment-wide erosion rates in the past are reflected in cosmogenic nuclide concentrations in sediment cores (Schaller et al. 2002; Charreau et al. 2011; Savi et al. 2014). These data may require a – sometimes large – correction for in situ nuclide production after sediment deposition. Limited knowledge of variables such as the extent of the paleo source region may also lead to considerable uncertainties, but the method can provide important data not to be obtained otherwise (Granger et al. 2013).

Meteoric ^{10}Be (and ^{14}C)

The two most important cosmogenic nuclides produced in the atmosphere and eventually incorporated into solid or liquid inventories are ^{14}C and ^{10}Be. Here we concentrate on meteoric ^{10}Be but also discuss ^{14}C in tree rings independently dated by dendrochronology. Beryllium-10 is produced mainly from atmospheric nitrogen and oxygen, ^{14}C from nitrogen, with a production maximum at ~10–12 km altitude (Masarik and Beer 2009; Kovaltsov and Usoskin 2010; Beer et al. 2012). Carbon-14 atoms combine with oxygen to form CO_2, the major fraction of which becoming dissolved in the ocean while a smaller part quickly gets incorporated into plants. This carbon cycle is explained in more detail by Beer et al. (2012) and an understanding of its basics is required to properly use ^{14}C as dating tool or environmental tracer. Beryllium-10 atoms get adsorbed on aerosol particles which are deposited at the Earth's surface typically within less than a year (Morris et al. 2002; Beer et al. 2012). About two orders of magnitude more ^{10}Be is produced in the atmosphere than in situ in rocks. Therefore, in terrestrial samples, meteoric ^{10}Be usually completely dominates in situ produced ^{10}Be and needs to be removed carefully when the latter is of interest, as discussed above. The large amounts of meteoric ^{10}Be require, on the other hand, much lower sample sizes than in situ studies, or – alternatively – can be detected even when strongly diluted, e.g., upon subduction and recycling of sediment at convergent margins (Morris et al. 2002).

Because intensity and energy spectrum of the cosmic radiation entering the Earth's atmosphere are influenced by both the heliospheric and the geomagnetic fields, analyses of meteoric ^{10}Be in ice cores and ^{14}C in tree rings provide a paleo-cosmic-ray record, which is used to investigate the physics of the sun, the heliosphere, and the geomagnetic field in the past several ten thousand to several hundred thousand years (Beer et al. 2012). High solar activity leads to stronger cosmic-ray attenuation and hence lower nuclide production and vice versa. Six "Grand minima" (several consecutive solar cycles with very low activity maxima such as the "Maunder Minimum" in the seventeenth century) are recorded both in ^{14}C and ^{10}Be records over the last 1200 years. Such minima occur in clusters, and four clusters in the past ~7.5 ka are revealed by the ^{10}Be data (Steinhilber et al. 2010). The ^{14}C and ^{10}Be records over the last 10 ka agree very well with each other, which means that the observed variations are indeed caused by periodic changes in the cosmic-ray intensity in the past and are not a "transport" effect, i.e., caused by variations in atmospheric transport processes of ^{14}C and ^{10}Be or ocean storage of ^{14}C (Beer et al. 2012).

To derive solar magnetic field intensity changes over timescales of more than a few hundred years, variations in radionuclide concentrations caused by variations in the geomagnetic field need to be corrected for, as the latter dominate the overall variability on these timescales. This can be done by conventional paleomagnetic techniques, e.g., by measuring the magnetic properties of dated samples. A second method is to combine ^{14}C and ^{10}Be data, which helps to reduce the effects of noise in the data. While this is far from trivial, the overall agreement between the two different paleofield reconstructions in the past 50 ka is satisfying (Beer et al. 2012). Beryllium-10 data from ice or sediment cores (sometimes stacked data from many cores) are also used to derive the geomagnetic field intensity in the past several ten thousand to several hundred thousand years (Frank et al. 1997; Beer et al. 2012). Even the Brunhes-Matuyama magnetic field reversal ~780 ka ago has been observed in the Epica Dome C ice core in Antarctica (Raisbeck et al. 2006).

Meteoric ^{10}Be is also used to date sediments, for example, ferromanganese crusts at ocean floors. Beryllium-10 in sediments is used to derive paleodenudation rates over millions of years and catchment-wide modern erosion rates (Willenbring and von Blanckenburg 2010a, b; von Blanckenburg et al. 2012; Granger et al. 2013). In these cases, also the concentration of the non-cosmogenic stable ^{9}Be isotope needs to be determined. One of the first applications of meteoric ^{10}Be has been its use as tracer of subduction zone processes: cosmogenic ^{10}Be found in island-arc volcanic rocks and other mantle-derived rocks has been recycled from marine sediments incorporated into arc lavas during subduction (Morris et al. 2002). In such studies, ^{10}Be is also combined with U-series studies to better constrain timescales and mechanisms of the transfer from the slab to the mantle.

Beer et al. (2012) give an overview of further applications of radionuclides in studies of the atmosphere, hydrosphere,

and geosphere. Such work includes analyses of many nuclides not discussed so far, with a wide range of half-lives, e.g., Tritium, ^{36}Cl, ^{39}Ar, ^{81}Kr, ^{85}Kr, and ^{129}I. Some of these nuclides are predominantly anthropogenic, produced during nuclear bomb testing or deriving from nuclear power or reprocessing plants.

Summary

Cosmogenic nuclides are very widely studied in cosmochemistry and geochemistry. They allow us to study the transport of meteorites from their parent bodies to Earth and sometimes their previous history near the parent body surface. Cosmogenic nuclides are a tool to judge whether different meteorite specimens, e.g., found in a desert, may belong to a common fall or may have been released from their parent body by the same event. While in the past mostly bulk meteorite samples were analyzed, more recently much attention is given to single phases, such as individual chondrules or calcium-aluminum-rich inclusions. It is still debated whether or not such studies allow us to recognize irradiation of meteoritic matter by an intense flux of solar particles in the early solar system. Analytical advances also allow us to analyze cosmogenic nuclides in other tiny samples such as single presolar grains in meteorites, interplanetary dust particles, and material from sample return missions, e.g., from the regolith of the asteroid Itokawa sampled by the Japanese Hayabusa probe. Since some three decades, cosmogenic nuclides are having a tremendous impact in Earth surface sciences. Fields such as geomorphology, glaciology, paleoseismology, or volcanology profit from the unprecedented possibility to quantify geomorphic processes and timescales. Progress is driven by continuous analytical developments, allowing, in particular, the analysis of ever smaller amounts of cosmogenic radionuclides by new generations of accelerator mass spectrometers. Apart from cosmogenic nuclides produced in situ in rock samples, meteoric radionuclides – produced in the atmosphere before being deposited at the Earth's surface – have long since been and continue to be important tools in paleoclimatology and paleomagnetic studies. More recently, the potential of meteoric radionuclides as tracers and as tools to study large scale erosion has been recognized. A continuing challenge in many applications of cosmogenic nuclides in cosmochemistry and geochemistry is a reliable and accurate determination of relevant production rates. Further progress depends on both theoretical and experimental work.

Cross-References

► Beryllium Isotopes

► Meteorites

References

Balco G, Stone JO, Lifton NA, Dunai TJ (2008) A complete and easily accessible means of calculating surface exposure ages or erosion rates from ^{10}Be and ^{26}Al measurements. Quat Geochronol 3:174–195

Balco G. (2011) Contributions and unrealized potential contributions of cosmogenic-nuclide exposure dating to glacier chronology, 1990–2010. Quaternary Science Reviews 30:3–27

Beer J, McCracken K, von Steiger R (2012) Cosmogenic radionuclides - theory and applications in the terrestrial and space environments. Springer, Berlin/Heidelberg

Bogard DD, Nyquist LE, Bansal BM, Garrison DH, Wiesmann H, Herzog GF, Albrecht AA, Vogt S, Klein J (1995) Neutron-capture ^{36}Cl, ^{41}Ca, ^{36}Ar, and ^{150}Sm in large chondrites: evidence for high fluences of thermalized neutrons. J Geophys Res Planets 100:9401–9416

Bottke WF, Vokrouhlický D, Rubinkam DP, Broz M (2002) The effect of Yarkovsky thermal forces on the dynamical evolution of asteroids and meteoroids. In: Bottke WF et al (eds) Asteroids III. University of Arizona Press, Tucson, pp 395–408

Charreau J, Blard PH, Puchol N, Avouac JP, Lallier-Vergès E, Bourlès, D, Braucher R, Gallaud, A, Finkel R, Jolivet M, Chen Y, Roy P (2011) Paleo-erosion rates in Central Asia since 9 Ma: A transient increase at the onset of Quaternary glaciations? Earth Planet Sci Lett 304:85–92

Christl M, Wieler R, Finkel RC (2014) Measuring one atom in a million billion with mass spectrometry. Elements 10:330–332

Dunai TJ (2010) Cosmogenic nuclides – principles, concepts and applications in the earth surface sciences. Cambridge University Press, Cambridge, MA, 187pp

Eugster O, Herzog GF, Marti K, Caffee MW (2006) Irradiation records, cosmic ray exposure ages, and transfer times of meteorites. In: auretta DS, McSween HY (eds) Meteorites and the early solar system II. University Arizona Press, Tucson, pp 829–851

Farley KA et al (2014) In situ radiometric and exposure age dating of the Martian surface. Science 343:1247166

Frank M, Schwarz B, Baumann S, Kubik PW, Suter M, Mangini A (1997) A 200 kyr record of cosmogenic radionuclide production rate and geomagnetic field intensity from ^{10}Be in globally stacked deep-sea sediments. Earth Planet Sci Lett 149:121–129

Gladman BJ, Migliorini F, Morbidelli A, Zappalà V, Michel P, Cellino A, Froeschlé C, Levison HF, Bailey M, Duncan M (1997) Dynamical lifetimes of objects injected into asteroid belt resonances. Science 277(5323):197–201

Gosse JC, Phillips FM (2001) Terrestrial in situ cosmogenic nuclides: theory and application. Quaternary Sci Rev 20:1475–1560

Graf T, Marti K (1995) Collisional history of H chondrites. J Geophys Res Planets 100:21247–21263

Granger DE (2006) A review of burial dating methods using ^{26}Al and ^{10}Be. In: Siame LL, Bourlès DL, Brown ET (eds) In situ-produced cosmogenic nuclides and quantification of geological processes. Geological Society of America Special Paper 415:1–16

Granger DE, Lifton NA, Willenbring JK (2013) A cosmic trip: 25 years of cosmogenic nuclides in geology. Geol Soc Am Bull 125:1379–1402

Herzog GF, Caffee MW (2014) Cosmic-ray exposure ages of meteorites. In: Davis AM (ed) Treatise in geochemistry, 2nd edn. Elsevier, Oxford, pp 419–454

Herzog GF, Caffee MW, Jull AJT, (2015) Cosmogenic nuclides in antarctic meteorites. In: Righter K, Corrigan CM, McCoy TJ, Harvey RP (eds) 35 seasons of U.S. Antarctic meteorites (1976–2010): a pictorial guide to the collection. American geophysical union, special publication series. Wiley, Hoboken, 320pp

Hidaka H, Yoneda S (2007) Sm and Gd isotopic shifts of Apollo 16 and 17 drill stem samples and their implications for regolith history. Geochim Cosmochim Acta 71:1074–1086

Jull AJT (2006) Terrestrial ages of meteorites. In: Lauretta DS, McSween HY (eds) Meteorites and the early solar system II. University Arizona Press, Tucson, pp 889–905

Kleine T, Touboul M, Bourdon B, Nimmo F, Mezger K, Palme H, Jacobsen SB, Yin QZ, Halliday AN (2009) Hf-W chronology of the accretion and early evolution of asteroids and terrestrial planets. Geochim Cosmochim Acta 73:5150–5188

Kohl CP, Nishiizumi K (1992) Chemical isolation of quartz for measurement of in-situ produced cosmogenic nuclides. Geochim Cosmochim Acta 56:3583–3587

Kovaltsov GA, Usoskin IG (2010) A new 3D numerical model of cosmogenic nuclide Be-10 production in the atmosphere. Earth Planet Sci Lett 291:182–188

Kruijer TS, Fischer-Gödde M, Kleine T, Sprung P, Leya I, Wieler R (2013) Neutron capture on Pt isotopes in iron meteorites and the Hf-W chronology of core formation in planetesimals. Earth Planet Sci Lett 361:162–172

Lal D (1991) Cosmic ray labeling of erosion surfaces: in situ nuclide production rates and erosion models. Earth Planet Sci Lett 104:424–439

Leya I, Masarik J (2009) Cosmogenic nuclides in stony meteorites revisited. Meteoritics Planet Sci 44:1061–1086

Leya I, Wieler R, Halliday AN (2000) Cosmic-ray production of tungsten isotopes in lunar samples and meteorites and its implications for Hf-W cosmochemistry. Earth Planet Sci Lett 175:1–12

Leya I, Dalcher N, Vogel N, Wieler R, Caffee MW, Welten KC, Nishiizumi K (2015) Calibration of cosmogenic noble gas production based on ^{36}Cl-^{36}Ar ages. Part 2. The ^{81}Kr-Kr dating technique. Meteorit Planet Sci 50:1863–1879

Lifton N, Sato T, Dunai TJ (2014) Scaling in situ cosmogenic nuclide production rates using analytical approximations to atmospheric cosmic-ray fluxes. Earth Planet Sci Lett 386:149–160

Marti K, Graf T (1992) Cosmic-ray exposure history of ordinary chondrites. Annu Rev Earth Planet Sci 20:221–243

Masarik J, Beer J (2009) An updated simulation of particle fluxes and cosmogenic nuclide production in the Earth's atmosphere. J Geophys Res Atmos 114: Article Number D11103

Morris JD, Gosse J, Brachfeld S, Tera F (2002) Cosmogenic ^{10}Be and the solid earth: studies in geomagnetism, subduction zone processes, and active tectonics. Rev Mineral Geochem 50:207–270

Niedermann S (2002) Cosmic-ray-produced noble gases in terrestrial rocks: dating tools for surface processes. Rev Min Geochem 47:731–784

Portenga EW, Bierman PR (2011) Understanding Earth's eroding surface with ^{10}Be. GSA Today 21: 4–10

Raisbeck GM, Yiou F, Cattani O, Jouzel J (2006) Be-10 evidence for the Matuyama-Brunhes geomagnetic reversal in the EPICA Dome C ice core. Nature 444:82–84

Roth ASG, Baur H, Heber VS, Reusser E, Wieler R (2011) Cosmogenic helium and neon in individual chondrules from Allende and Murchison: implications for the precompaction exposure history of chondrules. Meteoritics Planet Sci 46:989–1006

Russ GP, Burnett DS, Wasserburg GJ (1972) Lunar neutron stratigraphy. Earth Planet Sci Lett 15:172–186

Savi S, Norton KP, Picotti V, Akcar N, Delunel R, Brardinoni F, Kubik P, Schlunegger F (2014) Quantifying sediment supply at the end of the last glaciation: Dynamic reconstruction of an alpine debris-flow fan. Geol Soc Am Bull 126:773–790

Schaller M, von Blanckenburg F, Veldkamp A, Tebbens LA, Hovius N, Kubik PW (2002) A 30 000 yr record of erosion rates from cosmogenic ^{10}Be in Middle European river terraces. Earth Planet Sci Lett 204:307–320

Steinhilber F, Abreu JA, Beer J, McCracken KG (2010) Interplanetary magnetic field during the past 9300 years inferred from cosmogenic radionuclides. J Geophys Res-Space Phys 115: Article Number A 01101

Stone J (2000) Air pressure and cosmogenic isotope production. J Geophys Res-Solid Earth 105:23753–23759

Vermeesch P (2007) CosmoCalc: an Excel add-in for cosmogenic nuclide calculations. Geochem Geophys Geosyst 8:Q08003

Von Blanckenburg F (2005) The control mechanisms of erosion and weathering at basin scale from cosmogenic nuclides in river sediment. Earth Planet Sci Lett 237:462–479

von Blanckenburg F, Bouchez J, Wittmann H (2012) Earth surface erosion and weathering from the ^{10}Be (meteoric)/^{9}Be ratio. Earth Planet Sci Lett 351:295–305

Wieler R (2002) Cosmic-ray-produced noble gases in meteorites. Rev Mineral Geochem 47:125–170

Wieler R, Graf T (2001) Cosmic ray exposure history of meteorites. In: Peucker-Ehrenbrink B, Schmitz B (eds) Accretion of extraterrestrial matter throughout Earth's history. Kluwer, New York, pp 221–240

Willenbring JK, von Blanckenburg F (2010a) Long-term stability of global erosion rates and weathering during late-Cenozoic cooling. Nature 465:211–214

Willenbring JK, von Blanckenburg F (2010b) Meteoric cosmogenic Beryllium-10 adsorbed to river sediment and soil: applications for earth-surface dynamics. Earth Sci Rev 98:105–122

Willenbring JK, Codilean AT, McElroy B (2013) Earth is (mostly) flat: Apportionment of the flux of continental sediment over millennial time scales. Geology 41:343–346

Wisdom J (1987) Chaotic dynamics in the solar system. Icarus 72:241–275

Woolum DS, Hohenberg C (1993) Energetic particle environment in the early solar system – extremely long pre-compaction meteoritic ages or an enhanced early particle flux. In: Levy EH, Lunine JI (eds) Protostars and planets III. University Arizona Press, Tucson, pp 903–919

C

Critical Points

William H. Casey[1] and Peter A. Rock[2]
[1]Department of Chemistry and Department of Earth and Planetary Sciences, University of California, Davis, CA, USA
[2]College of Math and Physical Sciences, Department of Chemistry, University of California, Davis, CA, USA

Definition

The point in phase space where the distinction between liquid and vapor disappears.

Elaboration

If you heat water in a closed volume, the temperature and pressure are initially fixed by equilibrium between a liquid and vapor. Beyond a certain temperature and pressure, however, the meniscus that separates the two phases disappears, and they become indistinguishable. If one draws a curve in

---

Prof. Peter A. Rock is deceased.

P-V space that identifies the region where both a liquid and vapor coexist, the *critical point* lies at the maximum where the slope is zero:

$$\left(\frac{\partial P}{\partial V}\right)_{T=T_c} = 0 \quad \text{and} \quad \left(\frac{\partial^2 P}{\partial V^2}\right)_{T=T_c} = 0 \qquad (1)$$

As this point is approached, the two phases, gas and liquid, begin to closely resemble one another on a molecular scale. The critical point for pure water is at 374.2 °C and 218.3 atm.

Near the critical point, the structure of these phases is very sensitive to small changes in temperature and pressure, and these changes are reflected in the macroscopic properties. Density, for example, changes considerably with small variations in pressure and temperature because the relative proportions of the two phases, liquid and vapor, fluctuate widely.

To illustrate the sensitivity of fluid properties near the critical point, consider that the critical point for pure CO_2 is at 31.8 °C and 72.9 atm, which are easily accessible in a laboratory. At these conditions a change in pressure of 1 part in 50,000 causes the CO_2 fluid density to increase by 10%. The density of critical CO_2 is 0.5 g/cm^3 so that 1 torr of CO_2 corresponds to an inch-thick layer. This one-inch-thick layer of CO_2 exhibits a 10% greater density at the bottom of the column than at the top simply due to the weight of the gas.

Likewise, the enthalpy of vaporization goes to zero at the critical point, and it can be seen that the isothermal compressibility

$$\beta \equiv -\frac{1}{V}\left(\frac{\partial V}{\partial P}\right)_T \qquad (2)$$

becomes infinite at the critical point. Correspondingly, the heat capacity, C_p, for the substance reaches large values near the critical point. Near-critical fluids also exhibit curious properties, such as critical opalescence, where light scatters into a dazzling display as the fluid reaches a certain molecular density because the molecular structures reach a characteristic length similar to the wavelength of visible light. Stated differently, the refractive index varies widely near the critical point along with the other bulk properties.

Addition of other components, such as CO_2, NaCl, or H_2, to H_2O dramatically affects the critical point of the solution. For these systems, a curve of critical points is defined in *P-T-X* space (*X* is a composition variable) that is generally nonlinear. The critical curve for the CO_2-H_2O system, for example, is a saddle with two maxima near end-member compositions and a minimum at intermediate values. The critical point for a saturated NaCl-H_2O mixture is at almost 600 °C and approximately 390 bars pressure, significantly higher than the value for pure H_2O.

Understanding the thermodynamic properties of mixed volatile fluids (e.g. CO_2-H_2O; H_2-H_2O) is important for predicting phase assemblages in rocks, for interpreting the compositions of fluid inclusions in minerals, and for predicting the effect of volatile gases on magma. Establishing these thermodynamic properties has been a major success in geochemistry during the last 50 years, and thermodynamic models have recently been extended to 6.0 GPa and 1200 °C based upon molecular-dynamic estimates of the dielectric constant of water (Sverjensky et al. 2014).

Cross-References

▶ Geochemical Thermodynamics
▶ Hydrothermal Vents
▶ Phase Equilibria

References

Sverjensky DA, Harrison B, Azzolini D (2014) Water in the deep earth: the dielectric constant and the solubilities of quartz and corundum to 60 kb and 1200 °C. Geochim Cosmochim Acta 129:125–145

Critical Zone

Justin B. Richardson
Dept. of Earth and Atmospheric Sciences, Cornell University, Ithaca, NY, USA

Synonyms

Earth's critical zone

Definition

The critical zone, the near-surface terrestrial environment from the bottom of circulating groundwater to the top of vegetation, hosts the complex interactions involving rock, soil, water, air, and living organisms that regulate life-sustaining resources.

Introduction

The term "critical zone" was first applied to the surface terrestrial environment by Dr. Gail Ashley (1998) in a presentation at the Geological Society of America. In her work, Dr. Ashley introduced the concept of the critical zone when

she wrote that a "holistic approach is needed to understand the three-dimensional complex linkages involving physical, chemical, and biological processes" and a study of geologic and surface processes that are "crucial for life" (Ashley 1998). In 2001, the United States National Research Council's Committee on Basic Research Opportunities in the Earth Sciences noted the future importance of the critical zone concept as integrative of disciplines and required to address interconnected problems (NRC 2001). The National Research Council defined the critical zone as "*the heterogeneous, near surface environment in which complex interactions involving rock, soil, water, air and living organisms regulate the natural habitat and determine availability of life sustaining resources*." Brantley et al. (2007) provided an alternative definition of the critical zone as "*the fragile skin of the planet defined from the outer extent of vegetation down to the lower limits of groundwater*," and many others have followed. In all definitions, the critical zone is recognized as a location of complex biogeochemical and physical processes that supports the terrestrial biosphere (Fig. 1) (White and Sharkey 2016). Study of the structure and function of the critical zone explicitly includes study of processes evolving at all timescales from that of the geologist to that of the meteorologist, and explicitly includes atmospheric (i.e., climate), geologic (e.g., volcanic, tectonic), and biologic (e.g., microbes, plants, organisms, humans) changes throughout Earth's deep and recent history (NRC 2001). Critical zone science can provide

Critical Zone, Fig. 1 An illustration of the Critical zone conceptual model modified from Chorover et al. (2007) (Artwork by R. Kindlimann)

information for sustainable adaptation to human perturbations (e.g., intensive land use and climate change).

Essential Concepts

The critical zone paradigm is a new integration of existing fields of natural sciences (Fig. 1). One of the essential aspects of this paradigm is that the term "critical" reflects that nearly all terrestrial life, including humans, depends on the critical zone (Giardino and Houser 2015; NRC 2001), establishing a clear link between Earth's surface processes and geosystems with humans (Brantley et al. 2007; Richter and Billings 2015). Land use and climatic impacts are affecting processes that govern biomass productivity, soil formation, geochemical cycling of elements, and water resources (Hooke et al. 2012). For this reason, it is essential for developing predictive abilities of how attributes, processes, and outputs of the critical zone will respond to projected climate and land-use changes. Some of the central scientific concepts that have been investigated through critical zone science are: (1) formation and distribution of weathered bedrock, (2) sustainability of water and soil resources, (3) tracing the movement of energy and reactive material, and (4) integration of processes across spatial and time scales and with respect to anthropogenic uses and perturbations.

Understanding the biological, chemical, and physical properties controlling bedrock and surficial deposit weathering is a central topic for critical zone science and for parallel efforts in geobiology and geochemistry (Pope 2015). The formation of weathered bedrock has been investigated by Earth scientists for more than 170 years (see Ebelmen 1845; Gilbert 1909). Critical zone science has generated renewed interest in the distribution, structure, and residence of weathered rock, features whose spatial distribution are generally considered to be difficult to measure (Holbrook et al. 2014). The architecture of the weathered bedrock of the critical zone has been shown to be a combination of tectonic, topographic, and weathering processes combined (e.g., Brantley and Lebedeva 2011; St. Clair et al. 2015). Weathering of bedrock may influence sustainability issues, in particular, the feedback between weathering rates and atmospheric CO_2 concentrations (Raymo 1989). Bedrock composition can also directly control the aboveground ecosystem. Hahm et al. (2014) found differences in forest productivity were directly linked to major and minor element composition of the underlying bedrock. The architecture and distribution of fractures is not only important for element cycling, but is also key for reservoirs of materials and energy in the critical zone. For example, the thickness and structure of the weathered bedrock in the critical zone controls many hydrologic properties such as water table elevation, plant-available water, and discharge rates to streams and rivers (Brooks et al. 2015).
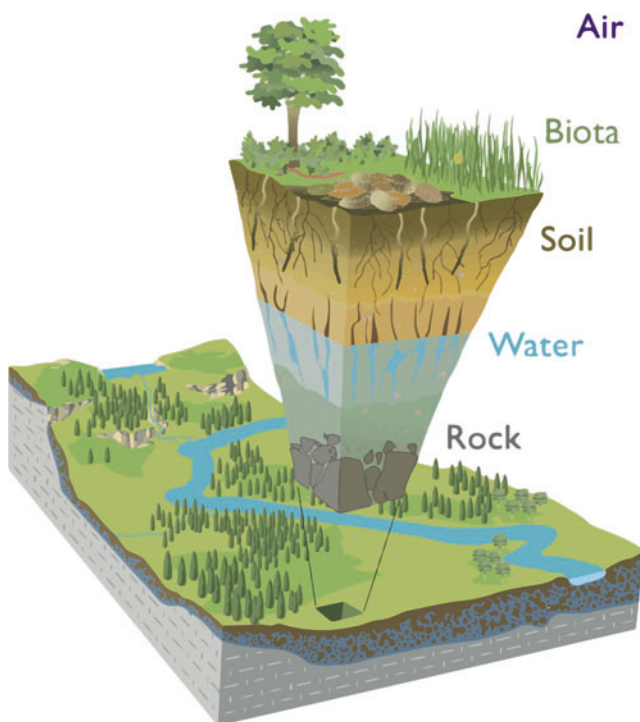
Soil and water sustainability is a fundamental component of critical zone science. Much of the framework of critical zone science is built upon principal themes of soil science (e.g., state factor model of Hans Jenny 1941) and hydrology (e.g., subsurface and surface flow by Freeze 1972). Critical zone science focuses on soil sustainability through estimating soil formation rates (e.g., soil formation on a hillslope by Riggins et al. 2011), modeling nutrient cycling (e.g., soil-vegetation cycling rates in a temperate forest by Kraepiel et al. 2015), and quantifying erosion and denudation rates (e.g., sediment transport from following a storm by Foster and Anderson 2016). In addition, water sustainability is considered through snowpack (e.g., snow accumulation in the southern Sierra Nevada by Kirchner et al. 2014), belowground water storage (e.g., water table recharge along a hillslope by Dralle et al. 2014), surface and subsurface flow (e.g., depth of preferential flow rates through soils by Thomas et al. 2013), plant-availability (e.g., plant ecohydrological strategies in seasonally dry ecosystems by Vico et al. 2015), and evapotranspiration losses (e.g., evapotranspiration along an elevation gradient in southern Sierra Nevada mountains by Goulden et al. 2012). While many of these efforts run parallel with traditional soil and hydrological sciences, their integration with other disciplines for broader theoretical understanding and quantitative modeling is pivotal for critical zone science. For an example of greater integration, Bales et al. (2011) observed that during severe droughts in the Sierra Nevada Mountains, California, the majority of water lost from soils and trees can be sourced from water stored in weathered bedrock. In addition, Wilson et al. (2016) linked tillage practices in agroecosystems with soil erosion, which influences crop productivity, carbon storage, and net income from a parcel of land. Critical zone science has built upon existing soil and water sustainability concepts with greater integration as a holistic system (Richter and Billings 2015).

Tracing the movement of material and energy is important for quantifying and modeling local and global critical zone processes, particularly those that are reactive. The movement of materials through soil and unconsolidated material has been a topic of concern for many disciplines. Materials of interest include nutrients (e.g., Davis et al. 2014), inorganic colloids (e.g., Trostle et al. 2016), organic carbon (e.g., Stielstra et al. 2015), trace metals and metalloids (e.g., Ma et al. 2011), and pollutants (e.g., Ma et al. 2014). The movement of these materials through the critical zone controls natural phenomena such as chemical weathering, erosion, nutrient cycling, and anthropogenic issues, such as acid-mine drainage, eutrophication of surface waters, atmospheric CO_2 concentrations, and contamination of drinking water (Li et al. 2017). Studies of material movement range from empirical studies and process-based models to quantify their movement. Li et al. (2017) described four areas in which reactive transport models may substantially

contribute to critical zone science as testable hypotheses: (1) evapotranspiration-chemical weathering controlled by reactive gases, (2) water availability-chemical weathering-atmospheric CO_2-temperature linkages at the global scale, (3) soil moisture influences on carbon stabilization in soil, and (4) plant root controls on soil formation and function. Understanding the movement of energy in the critical zone is important for investigating thermodynamic controls from climate on physical, biological, and chemical processes. Rasmussen et al. (2011) proposed the structure and evolution of the critical zone can be described using climatic and biotic forcings as a single environmental energy and mass transfer (EEMT) parameter with energy flux units (e.g., $J\ m^{-2}\ s^{-1}$). This concept has many potential applications and may be applied across any chosen spatial and temporal scales. Further coupling the movement of materials and energy are current areas of study with many future implications for understanding the critical zone.

Linking critical zone processes across time and spatial scales is a principal goal of critical zone science. Many chemical reactions occur at molecular microsystems (mineral surfaces, root surfaces, macropores, rock fractures), and critical zone scientists are working to measure their effect on larger scale processes (soil formation, hillslopes development, watersheds ecosystem services). For example, Brantley et al. (2011) notes that as rocks and minerals weather, their size decreases and surface area increases, exerting a control on the rate of chemical weathering in the soil profile with potential influences at the watershed scale in Puerto Rico and Pennsylvania. Moreover, mechanisms occurring in a soil profile or at an acre scale can be coupled with regional and global scale estimates. In addition to size and spatial scales, the other most arduous endeavors for Earth Scientists has been linking short-term processes (hours, days, years) with longer-term changes (decades, centuries, and millennia). Monitoring efforts have been fundamental for quantifying short- and long-term biogeochemical and physical processes of the critical zone. For example, a short-term observation may be daily monitoring for peak streamflow during melt season in a snow-dominated watershed (Chen et al. 2016). As a long-term example, Richter et al. (2000) observed that the impact of atmospheric nitrogen was dominant in biological nitrogen fixation over 40 years, by comparing soils collected and archived from 1962 through 1997 at the Calhoun Experimental Forest. Coupled numerical models, such as Flux-Penn State Integrated Hydrologic Model (Flux-PIHM) (Shi et al. 2013) and Terrestrial Integrated Modeling System (TIMS) (Niu et al. 2014), are the leading edge on combining processes over multiple time scales to evaluate the relative influences of different critical zone parameters, and hold out the capacity to support predictions of critical zone processes in the past and future. Furthermore, coupled numerical models are capable of using contemporary processes to

investigate changes over geologic time scales (thousands to millions of years).

Current Investigations

The critical zone is studied at a number of Critical Zone Observatories (CZOs), where multiple scientific communities work in tandem to understand coupled processes, through both field and theoretical approaches. Teams of researchers monitor surface and subsurface water, meteorological conditions, soil properties, and vegetation. In addition, researchers undertake sampling campaigns of vegetation, soils, sediments, regolith, and bedrock. Information generated through monitoring and from sampling campaigns is synthesized to investigate complex systems at CZOs.

While individual CZOs each develop novel approaches to quantify critical zone processes, observatories aim to complete comparable measurements as a network. A key aspect is to use common measurements in which sampling is guided by overarching hypotheses and further developed to reflect site conditions, but materials and methods are implemented in a similar manner across the CZO network (White et al. 2015). Although cross-CZO data comparisons are a substantial goal, many lines of inquiry are site-specific and utilize approaches based on the principal of "best technique and sampling design" at each individual CZO. Thus, even though CZOs are individual entities, data is collected to be comparable with local, regional, and global monitoring efforts. Cross-CZO comparisons that are generalizable across space and time may be modeled using common measurement data and are paramount for creating integrated processes theories needed to expand predictive modeling (i.e., Earth-casting) (White et al. 2015; Richter and Billings 2015).

The United States National Science Foundation (NSF) has funded 10 CZOs across the United States and nine of these still receive funding (White et al. 2015). The NSF CZO program began in 2007 with support of three CZOs: Susquehanna-Shale Hills CZO in Pennsylvania, the Southern Sierra CZO in California, and the Boulder Creek CZO in Colorado. In 2009, three additional observatories were added: Luquillo Mountains CZO in Puerto Rico, Christina River Basin CZO in Delaware and Pennsylvania, and the Jemez River Basin/Santa Catalina Mountains CZO in Arizona and New Mexico. In 2013, four new observatories were selected for funding: Eel River CZO in northern California; Reynolds Creek CZO in Idaho; the Intensively Managed Landscape CZO in Illinois, Iowa, and Minnesota, and the Calhoun CZO in northern South Carolina. Measurements at the NSF-funded CZOs include a common set of variables that quantify Critical zone architecture and evolution, fluxes across the Critical zone boundaries, and changes in storage of the major critical zone reservoirs. The CZOs have recognized that many of the details of overarching science questions can best be addressed if a core set of variables is measured across the CZOs, and if those core measurements are made using the same or readily comparable methods. In 2014, the CZO National Office was created to spur network level research and outreach activities.

There have been many international projects to conduct critical zone research globally. Although some observatories worldwide are not called CZOs, scientists across the international research communities have adopted the framework and nomenclature of "critical zone science," because the paradigm is compelling for addressing environmental sustainability and accelerating interest in Earth surface sciences (White et al. 2015; Richter and Billings 2015). International CZOs and similar projects have identified objectives of determining changes to the critical zone in response to human pressures, and each program has its own approach and strategy. The European Commission funded SoilTrEC in 2009. The SoilTrEC network consisted of four CZOs: Koilaris River Basin in Crete, Damma Glacier in Switzerland, Slavka Forest in the Czech Republic, and in Fuchsenbigl, Austria. Germany has also established the TERENO network, a set of four observatories: Eifel/Lower Rhine Valley, Harz/Central German Lowland, Northeastern German Lowland, and Bavarian Alps/pre-Alps Observatories. Additional CZOs in France and through a United Kingdom-China partnership are in development. Through internationally funded meeting and workshops, there are 60 countries conducting research at 21 funded CZOs as of 2015 (White et al. 2015).

Conclusions

Critical zone science is a new paradigm focusing on integration of existing fields of natural sciences: a systems approach needed to understand the three-dimensional complex linkages involving physical, chemical, and biological processes at the Earth's surface. The term "critical" reflects that nearly all terrestrial life depends on the critical zone. Critical zone science aims to develop predictive abilities, which are essential to understand the past and future effects of climate and land-use. The central scientific concepts investigated through critical zone science are the formation of weathered bedrock, water and soil resources, the movement of energy and reactive material, and integration of natural processes across spatial and time scales. The critical zone is studied at Critical Zone Observatories (CZOs), where multiple scientific communities monitor and conduct sampling campaigns to synthesize the complex interactions systems. Critical zone research is conducted globally as international research communities have adopted the framework and nomenclature to renew interest in Earth surface processes and their sustainability.

Cross-References

References

Ashley GM (1998) Where are we headed? "Soft" rock research into the new millennium. Geo Soc Am Ab/Pro 30:A-148

Bales RC, Hopmans JW, O'Geen AT, Meadows M, Hartsough PC, Kirchner P, Hunsaker CT, Beaudette D (2011) Soil moisture response to snowmelt and rainfall in a Sierra Nevada mixed-conifer forest. Vadose Zone J 10:786–799

Brantley SL, Lebedeva M (2011) Learning to read the chemistry of regolith to understand the critical zone. Annu Rev Earth Planet Sci 39:387–416

Brantley SL, Goldhaber MB, Ragnarsdottir KV (2007) Crossing disciplines and scales to understand the critical zone. Elements 3:307–314

Brantley SL, Buss HL, Lebedeva M, Fletcher RC, Ma L (2011) Investigating the complex interface where bedrock transforms to regolith. Appl Geochem 26:S12–S15. https://doi.org/10.1016/j.apgeochem.2011.03.017

Brooks PD, Chorover J, Fan Y, Godsey SE, Maxwell RM, McNamara JP, Tague C (2015) Hydrological partitioning in the critical zone: recent advances and opportunities for developing transferable understanding of water cycle dynamics. Water Resour Res 51:6973–6987

Chen X, Kumar M, Wang R, Winstral A, Marks D (2016) Assessment of the timing of daily peak streamflow during the melt season in a snow-dominated watershed. J Hydrometeorol 17:2225–2244

Chorover J, Kretzschmar R, Garcia-Pichel F, Sparks DL (2007) Soil biogeochemical processes within the critical zone. Elements 3:321–326

Davis CA, Ward AS, Burgin AJ, Loecke TD, Riveros-Iregui DA, Schnoebelen DJ, Just CL, Thomas SA, Weber LJ, St. Clair MA (2014) Antecedent moisture controls on stream nitrate flux in an agricultural watershed. J Environ Qual 43:1494–1503. https://doi.org/10.2134/jeq2013.11.0438

Dralle DN, Boisramé G, Thompson SE (2014) Spatially variable water table recharge and the hillslope hydrologic response: analytical solutions to the linearized hillslope Boussinesq equation. Water Resour Res 50:8515–8530

Ebelmen JJ (1845) Sur les produits de la décomposition des espèces minérales de la famille des silicates. In Annales des Mines 7:66

Foster MA, Anderson RS (2016) Assessing the effect of a major storm on 10 BE concentrations and inferred basin-averaged denudation rates. Quat Geochronol 34:58–68

Giardino JR, Houser C (2015) Introduction to the Critical zone. In: Principles and Dynamics of the Critical zone, vol 19, Elsevier, Amsterdam, Netherlands, pp 1–14

Gilbert GK (1909) The convexity of hilltops. J Geol 17:344–350

Goulden ML, Anderson RG, Bales RC, Kelly AE, Meadows M, Winston GC (2012) Evapotranspiration along an elevation gradient in California's Sierra Nevada. J Geophys Res Biogeo 117(G3)

Hahm WJ, Riebe CS, Lukens CE, Araki S (2014). Bedrock composition regulates mountain ecosystems and landscape evolution. Proceedings of the National Academy of Sciences, 111:3338-3343

Holbrook WS, Riebe CS, Elwaseif M, Hayes JL, Basler-Reeder K, Harry DL, Malazian A, Dosseto A, Hartsough PC, Hopmans JW (2014) Geophysical constraints on deep weathering and water storage potential in the Southern Sierra Critical zone Observatory. Earth Surf Process Landf 39:366–380

Hooke RL, Martín-Duque JF, Pedraza J (2012) Land transformation by humans: a review. GSA Today 22:4–10

Jenny H (1941) Factors of soil formation: a system of quantitative pedology. McGraw-Hill Book Company, Inc., New York

Kirchner PB, Bales RC, Molotch NP, Flanagan J, Guo Q (2014) LiDAR measurement of seasonal snow accumulation along an elevation gradient in the southern Sierra Nevada. California Hyd Earth Sys Sci 18:4261–4275. https://doi.org/10.5194/hess1842612014

Kraepiel AML, Dere AL, Herndon EM, Brantley SL (2015) Natural and anthropogenic processes contributing to metal enrichment in surface soils of central Pennsylvania. Biogeochemistry 123:265–283

Li L, Maher K, Navarre-Sitchler A, Druhan J, Meile C, Lawrence C, Moore J, Perdrial J, Sullivan P, Thompson A, Jin L, Bolton EW, Brantley SL, Dietrich WE, Mayer KU, Steefel CL, Valocci A, Zachara J, Kocar B, Mcintosh J, Tutolo BM, Kumar M, Sonnenthal E, Bao C, Beisman J (2017) Expanding the role of reactive transport models in critical zone processes. Earth Sci Rev 165:280–301

Ma L, Jin L, Brantley SL (2011) Geochemical behaviors of different element groups during shale weathering at the Susquehanna/Shale Hills Critical zone Observatory. Appl Geochem 26:S89–S93. https://doi.org/10.1016/j.apgeochem.2011.03.038

Ma L, Konter J, Herndon E, Jin L, Steinhoefel G, Sanchez D, Brantley S (2014) Quantifying an early signature of the industrial revolution from lead concentrations and isotopes in soils of Pennsylvania, USA. Anthropocene 7:16–29

Niu GY, Paniconi C, Troch PA, Zeng X, Durcik M, Huxman T (2014) An integrated modeling framework of catchment-scale ecohydrological processes: 1. Model description and tests over an energy-limited watershed. Ecohydrolog 7:427–439. https://doi.org/10.1002/eco.1362

NRC, National Research Council (2001) Basic research opportunities in earth sciences. National Academies Press, Washington, DC

Pope GA (2015) Regolith and weathering (rock decay) in the critical zone. In: Principles and dynamics of the critical zone, vol 19, Elsevier, Amsterdam, Netherlands, pp 113–146

Rasmussen C, Troch PA, Chorover J, Brooks PD, Pelletier JD, Huxman TE (2011) An open system framework for integrating critical zone structure and function. Biogeochemistry 102:15–29. https://doi.org/10.1007/s10533-010-9476-8

Raymo ME (1989) Geochemical evidence supporting T.C. Chamberlin's theory of glaciation. Geology 19(4):344–347

Richter DD, Billings SA (2015) 'One physical system': Tansley's ecosystem as Earth's critical zone. New Phytol 206:900–912

Richter DD, Markewitz D, Heine PR, Jin V, Raikes J, Tian K, Wells CG (2000) Legacies of agriculture and forest regrowth in the nitrogen of old-field soils. For Ecol Manag 138:233–248

Riggins SG, Anderson RS, Anderson SP, Tye AM (2011) Solving a conundrum of a steady-state hillslope with variable soil depths and production rates, Bodmin Moor, UK. Geomorphology 128:73–84. https://doi.org/10.1016/j.geomorph.2010.12.023

Shi Y, Davis KJ, Duffy CJ, Yu X (2013) Development of a coupled land surface hydrologic model and evaluation at a critical zone observatory. J Hydrometeorology 14:1401–1420

St. Clair J, Moon S, Holbrook WS, Perron JT, Riebe CS, Martel SJ, Carr B, Harman C, Singha K, Richter DD (2015) Geophysical imaging reveals topographic stress control of bedrock weathering. Science 350:534–538. https://doi.org/10.1126/science.aab2210

Stielstra CM, Lohse KA, Chorover J, McIntosh JC, Barron-Gafford GA, Perdrial JN, Litvak M, Barnard HR, Brooks PD (2015) Climatic and landscape influences on soil moisture are primary determinants of soil carbon fluxes in seasonally snow-covered forest ecosystems. Biogeochemistry 123:447–465. https://doi.org/10.1007/s10533-015-0078-3

Thomas EM, Lin H, Duffy CJ, Sullivan PL, Holmes GH, Brantley SL, Jin L (2013) Spatiotemporal patterns of water stable isotope compositions at the Shale Hills Critical zone Observatory: Linkages to subsurface hydrologic processes. Vadose Zone J 12:1–16

Trostle KD, Ray Runyon J, Pohlmann MA, Redfield SE, Pelletier J, McIntosh J, Chorover J (2016) Colloids and organic matter complexation control trace metal concentration-discharge relationships in Marshall Gulch stream waters. Water Resour Res 52:7931–7944

Vico G, Thompson SE, Manzoni S, Molini A, Albertson JD, Almeida-Cortez JS, Fay PA, Feng X, Guswa AJ, Liu H, Wilson TG (2015) Climatic, ecophysiological, and phenological controls on plant ecohydrological strategies in seasonally dry ecosystems. Ecohydrology 8:660–681

White T, Sharkey S (2016) Critical zone Oxford bibliography. Oxford Bibliographies. https://doi.org/10.1093/OBO/9780199363445-0055

White T, Brantley S, Banwart S, Chorover J, Dietrich W, Derry L, Lohse K, Anderson S, Aufdenkampe A, Bales R, Kumar P (2015) The role of critical zone observatories in critical zone science. Dev Earth Sur Proc 19:15–78

Wilson CG, Wacha KM, Papanicolaou AN, Sander HA, Freudenberg VB, Abban BK, Zhao C (2016) Dynamic assessment of current management in an intensively managed agroecosystem. J Contemp Water Res Edu 158:148–171

Crystal Chemistry

Dana T. Griffen
Geology Department, Brigham Young University, Provo, UT, USA

Definition

Crystalline materials consist of periodically repeating arrays of atoms with compositions that can be represented by definite chemical formulas (which may be variable within certain compositional limits). Crystal chemistry addresses the interdependence of crystallography and chemistry and the attendant consequences and phenomena. Thus, crystal chemistry is concerned with the symmetry and dimensions of the unit cell, the positions of atoms within the unit cell, the kinds of atoms found at each crystallographic site, and relationships with similar phases through such phenomena as solid solution, exsolution, polymorphism, and so forth. For earth

scientists, the crystals of interest are minerals. Although the boundaries between crystal chemistry, materials science, and certain areas of solid-state physics and solid-state chemistry are quite blurry, we shall approach the subject from the viewpoint of geology – that is, mineralogical crystal chemistry.

Stereochemistry

Atoms

Virtually everything of interest in crystal chemistry is related in some way to the spatial and chemical relationships among atoms or ions in a crystal. (The terms "cation" and "anion" are used hereafter to suggest atoms with lesser or greater electronegativity, respectively. No implication of fully ionic charges or fully ionic bonds is intended. Ionic size is discussed under ▶ ionic radii.) In general, ions may be viewed as soft spheres, with cations smaller than anions and surrounded by them; the number of ions bonded to a cation or anion is the coordination number. That the coordination numbers of cations should depend on their sizes relative to the surrounding anions and that bond lengths should equal the sums of the ionic radii are ideas formalized early in the twentieth century. They were stated in the first of five rules by Linus Pauling (1929), and these came to be known as Pauling's rules. For decades, they were taken as the basis for understanding inorganic crystal structures. Because they are often cited even in current literature, it is worthwhile to consider them as relevant concepts that are discussed in the paragraphs below.

Coordination Polyhedra

Imagining cations surrounded by anions leads to the concept of coordination polyhedra, envisioned by connecting the anions about a cation (Gibbs 1982). Figure 1 illustrates this concept using the crystal structure of the common mineral, titanite ($CaTiSiO_5$). Figure 1a is a "ball-and-stick" depiction of the structure and has the advantage of showing the positions of each atom; even so, it is somewhat confusing, and the coordination numbers and geometric relationships can be extracted only by careful study. Figure 1b is a polyhedral drawing, anions are assumed to be at each corner of each polyhedron, cations are presumed to lie within (although not necessarily at the precise center of) each polyhedron, and the coordination numbers and geometric relationships are immediately obvious. For atoms that have large coordination numbers and/or irregular coordination polyhedra, such as the Ca atoms in titanite, it is often advantageous to show them simply as independent spheres.

The frequent occurrence of 3-, 4-, 6-, 8-, and 12-coordination in crystalline solids leads to the recognition of regular coordination polyhedra (see Table 1 and Fig. 2). "Regular coordination" need not mean geometrically ideal, indeed, coordination polyhedra are most often distorted in
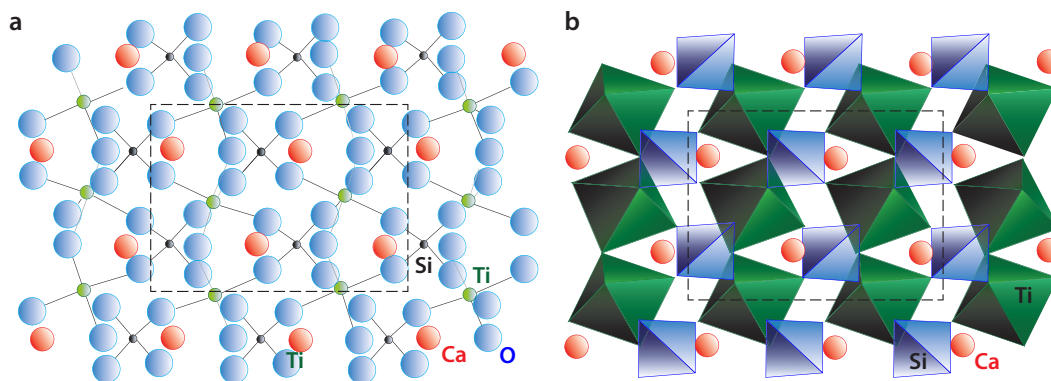
Crystal Chemistry, Fig. 1 (**a**) The crystal structure of titanite ($CaTiSiO_5$) represented as a "ball-and-stick" illustration. (**b**) The same crystal structure represented as a polyhedral diagram with the SiO_4 tetrahedra and TiO_6 octahedra shaded; the Ca polyhedra are irregular, and the Ca atoms are left as independent spheres for clarity

some way, but it implies representation by some type of regular solid. Coordination numbers such as 5, 7, 9, and 10 do occur, although much less frequently for cations with radii below about 1.0 Å, and with some exceptions, no attempt is made to represent these by polyhedra with simple shapes.

Figure 2e, f look very similar, but note that the triangles of anions on the top are rotated 60° with respect to one another. Figure 2e represents hexagonal close packing of anions (the layer sequence is . . .ABABA. . .), and Fig. 2f represents cubic close packing (. . .ABCABC. . .). Many minerals have crystal structures that are based on one of the two types of close packing. For example, olivine is based on a distorted hexagonal close packed array of oxygens with Si in some of the tetrahedral interstices and Mg or Fe^{2+} in some of the octahedral interstices; the pyroxene structure is based on very distorted cubic close packing.

Polyhedral Arrangements

Representing crystal structures, or parts thereof, as assemblages of linked polyhedra not only simplifies envisioning the structure but leads to crystallochemically useful ways of classifying minerals. Silicates, for example, are classified on the basis of tetrahedral polymerization – that is, the extent to which tetrahedra are linked (or "share corners") in the structure. (See ▸ Silicate Minerals)

Consideration of the extent to which corners can be shared, that is, the number of cations bonded to an anion, leads to another important crystallochemical principle. Pauling's second rule states that the sum of electrostatic bond strengths reaching an anion is equal to the charge (oxidation number) of the anion with the sign reversed. Electrostatic bond strength is defined as

$$EBS = \frac{cation\,oxidation\,number}{cation\,coordination\,number} \qquad (1)$$

Crystal Chemistry, Table 1 The regular coordination polyhedra

Type	No. of corners	No. of edges
Triangle	3	3
Tetrahedron	4	6
Octahedron	6	12
Cube	8	12
Cuboctahedron	12	24

and is the proportion of the formal charge of the cation allotted to each coordinating anion. The rule seems a reasonable requirement, and there are many structures for which it works perfectly. Consider the common garnet, grossular, $Ca_3Al_2Si_3O_{12}$. There is only one crystallographically unique oxygen atom, and it is bonded to one Si, one Al, and two Ca atoms, which are 4-, 6-, and 8-coordinated, respectively. The bond strengths are therefore

$$EBS_{Si} = \frac{4}{4} = 1; \quad EBS_{Al} = \frac{3}{6} = \frac{1}{2}; \quad EBS_{Ca} = \frac{2}{8} = \frac{1}{4}$$

Thus,

$$\sum EBS = 1 + \frac{1}{2} + 2\left(\frac{1}{4}\right) = 2$$

which is the oxidation number of oxygen with the sign reversed.

Very often, Pauling's second rule fails, however. Sometimes the failure is minor, in that the deviations in Σ EBS are not large, and the average over the anions is correct. In other cases, the deviations are quite large. The problem is that the rule tacitly assumes that all of the bond lengths about a cation are identical, and this is most often not the case. Because shorter bonds are obviously stronger than longer ones for the same cation–anion pair, dividing the oxidation number by the

Crystal Chemistry, Fig. 2 Regular coordination polyhedra. (**a**) Triangular coordination. (**b**) Tetrahedral coordination. (**c**) Octahedral coordination. (**d**) Cubic coordination. (**e, f**) Two types of 12-coordination, one based on hexagonal close packing (**e**) and one on cubic close packing (**f**)
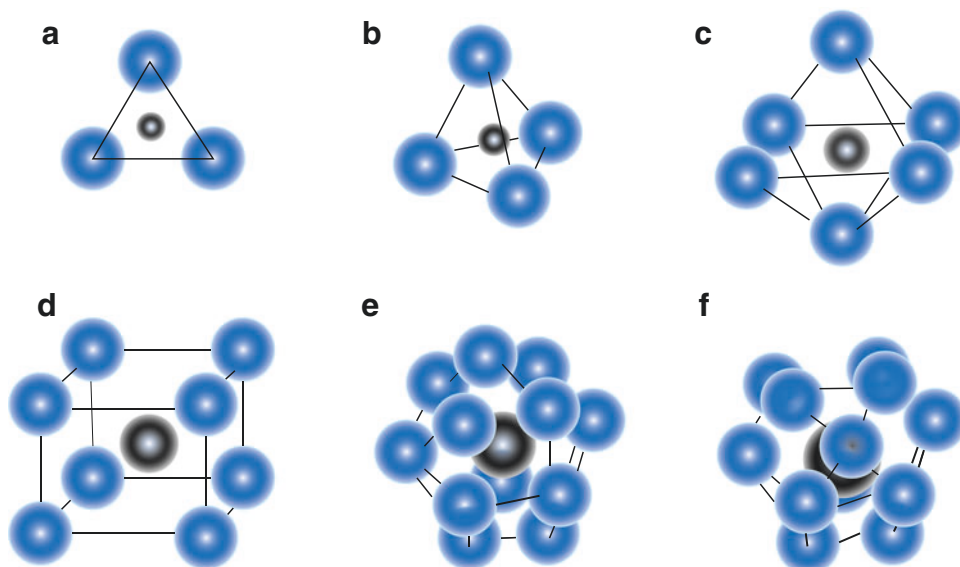
Crystal Chemistry, Fig. 3 The effects on cation–cation distances of sharing polyhedral elements. (**a**) Shared octahedral corner (one anion). (**b**) Shared octahedral edge (two anions). (**c**) Shared octahedral face (three anions)
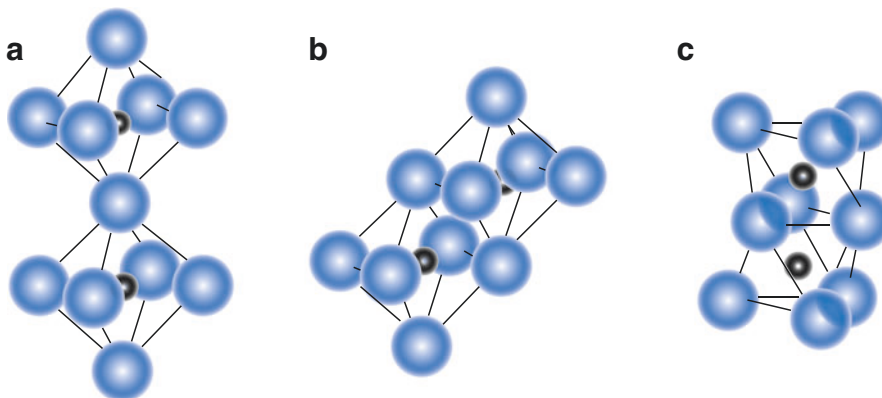
coordination number does not yield a proper bond strength. A popular approach to "correcting" this problem has been the development of empirical bond-strength–bond-length relationships of the form

$$s = e^{(r-r_0)/B} \qquad (2)$$

or

$$s = \left(\frac{r}{r_0}\right)^{-N} \qquad (3)$$

where s is often called bond valence, r is bond length, and r_0, B, and N are adjustable parameters (e.g., Brown and Shannon 1981). Using this approach, it is generally possible to obtain bond–valence sums that are very close to the oxidation number of the anion. It also facilitates the recognition of hydroxyls in a structure that has been refined by X-ray diffraction; the bond–valence sum about a hydroxyl should be close to 1 rather than 2. Even using a refinement such as the

bond–valence approach, the sums are often not quite perfect, for the same reasons that the first rule of Pauling lacks rigor: Variations in bond strength, like variations in bond length, result not only from the ionic effects assumed by the models but also from the effects of covalence.

Shared Polyhedral Elements

Figure 3 shows pairs of octahedra sharing a corner (i.e., one anion), an edge (two anions), and a face (three anions). It is evident that the cation–cation distance decreases in the order shared corner-edge-face. The third and fourth of Pauling's rules state that the sharing of polyhedral edges and (particularly) faces tends to decrease the stability of a structure and that this effect is largest for small, highly charged cations, which tend not to share polyhedral elements with one another. The usual rationale is based on cation–cation repulsions, which, it will be seen from Fig. 3, increase as edges and faces are shared.

The sharing of polyhedral elements is extremely common, however. It is true that the size and charge of the cations have an

Crystal Chemistry, Fig. 4
(**a**) The direction in which the shortening of shared polyhedral edges increases the cation–cation distances, thereby reducing cation–cation repulsion. (**b**) A part of the octahedral sheet in muscovite. The shared octahedral edges are shown by heavy *lines*
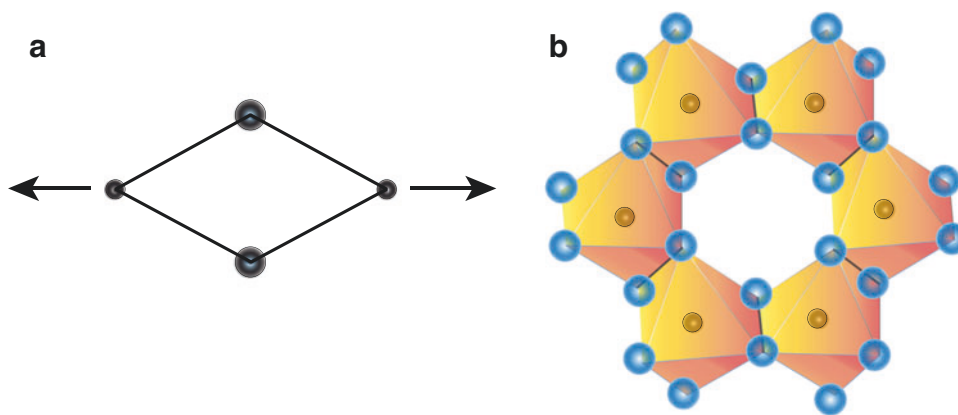
effect (e.g., SiO_4 tetrahedra never share faces, although BeO_4 tetrahedra are known to), but the sharing of octahedral edges occurs in many minerals (olivines, pyroxenes, amphiboles, micas, and many more), and octahedral faces are even shared in some (e.g., corundum, hematite, and dumortierite). In the case of shared edges, one structural compensation that occurs is that the shared edges tend to shorten, thereby lengthening the cation–cation distance and perhaps positioning the anions so as to increase the negative charge density between the cations (Fig. 4a). Figure 4b shows part of a sheet of octahedra in muscovite. Note that the shared octahedral edges (heavy lines) are shorter than the unshared edges. In the case of shared faces, not only do edges shorten, but the cations typically move away from the shared face if it is opposite to an unshared face.

Pauling's fifth and last rule is known as the rule of parsimony and states that the number of essentially different kinds of constituents in a crystal structure tends to be small. If "constituents" are interpreted as coordination polyhedra, and if "essentially different kinds" means that differently distorted polyhedra with the same number of anions are considered "the same kind," then this rule is acceptable, although of doubtful practical significance. Consider this example: Anorthite contains eight symmetrically unique sites containing Si, eight containing Al, and eight containing Ca. Each of the Si sites is geometrically somewhat different from all of the others, and the same is true for each Al and each Ca site. Twenty-four unique kinds of coordination polyhedra are not a small number. Nevertheless, if it is conceded that all of the tetrahedral (Si and Al) sites are very similar, as are all of the Ca sites, then there are only two kinds of "constituents" in anorthite – tetrahedra of oxygens with either Si or Al in the centers and an irregular Ca polyhedron.

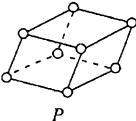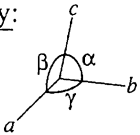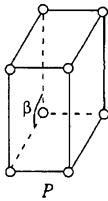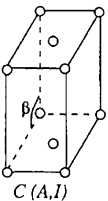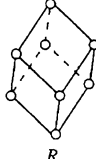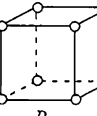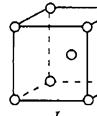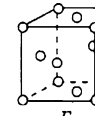### Why Are Some Structures Stable While Others Do Not Occur?
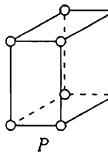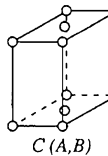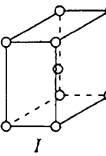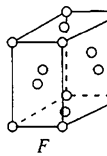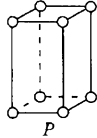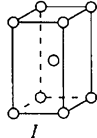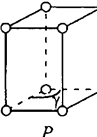
Pauling's rules served for many years as the basis for rationalizing the steric details of crystal structures. Even with the recognition of their important limitations, they have proven too useful to crystal chemists to be abandoned altogether.

Nonetheless, they and the various modifications and amendments that have been added over the years are tools for rationalization of what is observed, not for prediction of what might be observed. At least two kinds of crystallochemical predictions are of interest: (1) Given a certain type of structure, what are the limits of chemical substitution that the structure will tolerate, and (2) given a certain proposed stoichiometry, what kinds of crystal structures are stable? The first is perhaps the easier to approach, because the atomic substitutions envisioned will impose roughly predictable variations on bond lengths, nonbonded distances, and interatomic bond angles, and there is a substantial body of literature documenting the acceptable ranges of values for these sorts of parameters. The second question is more interesting and much more difficult to deal with. Recent and current research, both on the general question and on predictions for specific minerals and other inorganic compounds, has focused on bond topology (connectivity, particularly of the strongest bonds in a structure), the predictive use of bond–valence theory, the application of molecular orbital theory (at various levels of approximation, applied both qualitatively and quantitatively) to "molecular" fragments of crystal structures, band theory, experimental methods such as vibrational spectroscopy (Berry and Vaughan 1985), Landau theory (Tolédano and Tolédano 1987), and others.

Crystallography and Crystal Symmetry

By definition, a crystal consists of an arrangement of atoms that is periodically repeated in three dimensions. The smallest parallelepiped that possesses within both the symmetry and stoichiometry of the overall arrangement is called the unit cell, and the entire crystal consists of unit cells related to one another by translation alone. The corners of the unit cell are surrounded by identical groups of atoms, and form a lattice, the definition of which is an array of points in space arranged such that each one has an identical and indistinguishable environment. There may be other points that are surrounded

Crystal Chemistry, Fig. 5 The
14 Bravais lattices, arranged by
crystal system

Triclinic		$a \neq b \neq c$ $\alpha \neq \beta \neq \gamma$
	P	

Key:

P	primitive
C,A,B	end centered
I	body centered
F	face centered

Monoclinic — $a \neq b \neq c$, $\alpha = \gamma = 90°$, $\beta > 90°$ — P, C (A,I)

Orthorhombic — $a \neq b \neq c$, $\alpha = \beta = \gamma = 90°$ — P, C (A,B), I, F

Tetragonal — $a = b \neq c$, $\alpha = \beta = \gamma = 90°$ — P, I

Hexagonal — $a = b \neq c$, $\alpha = \beta = 90°$, $\gamma = 120°$ — P; Rhombohedral $a = b = c$, $\alpha = \beta = \gamma \neq 90°$ — R

Cubic (Isometric) — $a = b = c$, $\alpha = \beta = \gamma = 90°$ — P, I, F

by groups of atoms identical to those around the corners of the unit cell; if so, the lattice is referred to as a centered lattice, and if not it is called a primitive lattice. Combining both primitive and centered lattices, there are only 14 symmetrically unique possibilities. These are called the Bravais lattices, after Auguste Bravais (1811–1863), and they are illustrated in Fig. 5. Note that each lattice is represented in Fig. 5 by a single unit cell, the edges of which define three crystallographic axes *a*, *b*, and *c* separated by three interaxial angles α, β, and γ.

Rotational Symmetry

Consideration of the data in Fig. 5 reveals that each type of lattice can be mapped into itself by at least one symmetry operation. Depending upon the arrangement of the atoms about the lattice points, this will be true also of the unit cells (i.e., of the entire crystal structure). Although it is easy to conceive of an atomic arrangement that would yield no

symmetry, there are very few minerals that fall into that category; the overwhelming majority show symmetry of some sort.

Rotational symmetry elements are lines (axes of symmetry) around which an arrangement of atoms may be rotated so as to exactly reproduce itself. Proper rotation axes are those that map right-handed objects into right-handed objects, and improper rotation axes map right-handed objects into left-handed ones. Proper symmetry operations are represented symbolically by Arabic numerals, and improper symmetry operations are represented by Arabic numerals with a bar over them. The constraints imposed by the definition of a lattice (given above) limit the types of rotations that may occur in a crystal structure (and in the resulting macroscopic crystal) to those shown in Table 2. It can be shown that the sixfold rotoinversion is equivalent to a triad with a mirror plane perpendicular to it (symbolized 3/*m*), but $\bar{6}$ is usually used. The symbol *m* (rather than $\bar{2}$) is used for a mirror plane.

Crystal Classes

Not only are the types of rotational symmetry in crystals limited but so are the compatible combinations of symmetry elements. First, it is possible for a crystalline atomic arrangement or a macroscopic crystal to have only one kind of rotational symmetry. If there are two symmetrically different kinds, however, then there must also be a third that is symmetrically distinct from the other two. Symmetrically distinct or different here means that the operation of any one of the symmetry elements does not map the other two into each other. Among these three symmetry elements, all may be proper, or one can be proper and two improper. Given these constraints, there are only 32 permissible groups of symmetry elements (including those groups made up of but a single symmetry element), and these are called the crystal classes or crystallographic point groups. They are a subset of the infinite set of noncrystallographic point groups that are not restricted to one-, two-, three-, four-, and sixfold symmetry. The 32 crystal classes are given in Table 3. The symbols in the table are called Hermann–Mauguin symbols, and they specify the particular symmetry required for the class. A fuller explanation is beyond the scope of this article but may be found in any introductory text on mineralogy or crystallography or in Hahn (1987).

Table 3 also lists the defining symmetry for each of the crystal systems; this is the minimum symmetry that must be possessed by a crystal to place it in a particular crystal system.
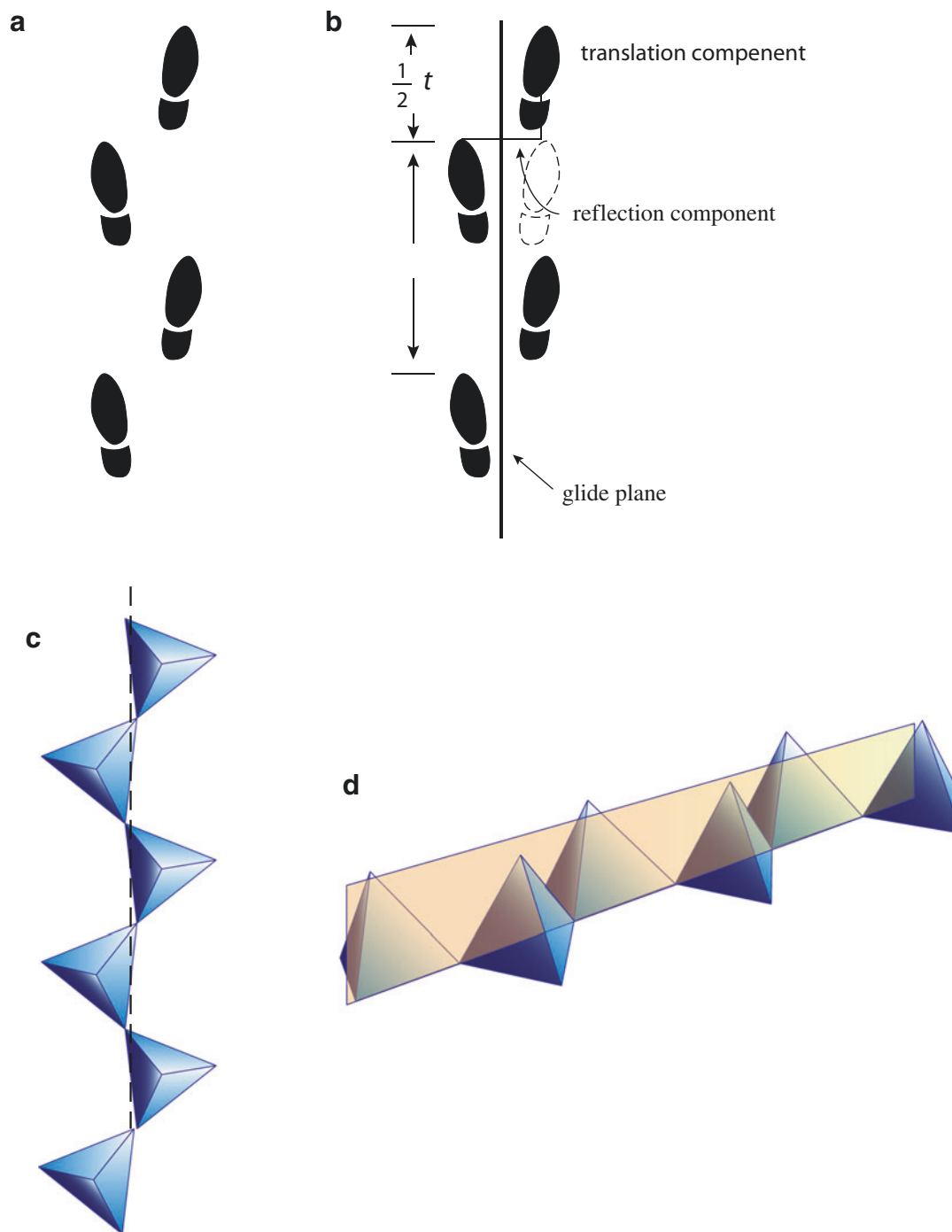
Symmetry is a more rigorous requirement for membership in a crystal system than is the geometry of the unit cell (Fig. 5). To illustrate, it is possible to superimpose on a cubic lattice a periodic arrangement of atoms that negates all of the inherent symmetry of the lattice; thus one would have a metrically cubic unit cell with no symmetry, and it would belong to the triclinic system. Although this is highly unlikely, because the non-cubic arrangement of atoms would impose asymmetrical atomic interactions that would lower the symmetry of the lattice, it does sometimes happen that experimental measurements of a unit cell (by, e.g., X-ray diffraction) show it to be within experimental error of the geometry of a higher crystal system than the atomic arrangement allows.

The external symmetry of a macroscopic crystal is completely described by the rotational symmetry elements of the 32 crystal classes. For the crystal chemist, the more interesting issue is the symmetry of the arrangement of atoms, and this sometimes involves symmetry elements that combine both rotation and translation.

Translational Symmetry Elements

Figure 6a shows a set of footprints. It is obvious that there is some symmetrical relationship between the set of right footprints and the set of left ones, but it is more complicated than a simple reflection. Figure 6b shows the symmetry relationship to be a reflection followed by a translation of one-half the repeat distance parallel to the mirror plane. This is called a glide plane, and the glide plane that relates successive tetrahedra in the pyroxene chain is shown in Fig. 6c, d. Because the translation component of the glide plane is parallel to the c crystallographic axis in the case of pyroxenes, it is called a c-glide; the other axial glide planes are a-glides and b-glides. Two other types of glide planes may be found in some atomic arrangements: diagonal glides, in which the glide component is one-half the vector sum of two axial translations, and diamond glides, in which the glide component is one-fourth the vector sum or difference of either two or three of the axial translations; they are labeled n-glides and d-glides, respectively.

The final type of translational symmetry element is the screw axis, which is a rotation (two-, three-, four-, or sixfold) followed by a translation. Figure 7 illustrates a screw axis.

Crystal Chemistry, Table 2 Permissible rotational symmetry operations

Symbol	Names	Rotation angle
1	Onefold rotation axis monad	0°, 360°
2	Twofold rotation axis diad	180°
3	Threefold rotation axis triad	120°
4	Fourfold rotation axis tetrad	90°
6	Sixfold rotation axis hexad	60°
$\overline{1}$	Center of symmetry inversion center	0° or 360° + inversion
$\overline{2} = m$	Mirror plane of reflection	180° + inversion
$\overline{3}$	Threefold rotoinversion bar-three	120° + inversion
$\overline{4}$	Fourfold rotoinversion bar-four	90° + inversion
$\overline{6}$	Sixfold rotoinversion bar-six	60° + inversion

Crystal Chemistry, Table 3 The 32 crystal classes

System	Minimum symmetry			Hermann-Mauguin symbols for crystal classes				
Triclinic	None	1	$\overline{1}$					
Monoclinic	1 diad[a]	2	m	$\frac{2}{m}$				
Orthorhombic	3 $\perp$ diads[a]	222	mm^2	$\frac{2}{m}\frac{2}{m}\frac{2}{m}$				
Tetragonal	1 tetrad[a]	4	$\overline{4}$	$\frac{4}{m}$	422	4 mm	$\overline{4}2m$	$\frac{4}{m}\frac{2}{m}\frac{2}{m}$
Hexagonal	1 hexad[a]	6	$\overline{6}$	$\frac{6}{m}$	622	6 mm	$\overline{6}m2$	$\frac{6}{m}\frac{2}{m}\frac{2}{m}$
(Trigonal)	(1 triad[a])		3	$\overline{3}$	32	3 m	$\overline{3}\frac{2}{m}$	
Cubic	4 triads[a]		23	$\frac{2}{m}\overline{3}$	432	$\overline{4}32$	$\frac{4}{m}\overline{3}\frac{2}{m}$	

[a]May include a permissible combination of proper and improper axes

Crystal Chemistry, Fig. 6 (**a**) Although there is clearly some symmetry relationship between the right and left footprints, it is not pure reflection. (**b**) A reflection followed by a translation of one-half the repeat distance parallel to the mirror plane is called a glide reflection, and the symmetry element is a glide plane. (**c**) The tetrahedral chain of Si-containing tetrahedra in pyroxene (diopside, in this case). Oxygen atoms are implied at the corners of the tetrahedra. The chain runs parallel to the *c* crystallographic axis, so this is a *c*-glide (*dashed*). (**d**) The *c*-glide in diopside seen in perspective

The types of possible screw axes are 2_1, 3_1, 3_2, 4_1, 4_2, 4_3, 6_1, 6_2, 6_3, 6_4, and 6_5. If the subscript is less than one-half of the Arabic numeral representing the rotation, the screw axis is right-handed (i.e., a rotation to the right followed by translation); if it is greater than one-half of the rotation numeral, the screw axis is left-handed; if it is equal to one-half of the rotation numeral, the screw axis is neutral, because right- and left-handed rotations yield identical results. Table 4 shows the translation distances, in fractions of the repeat distance along the axis, for each type of screw axis.
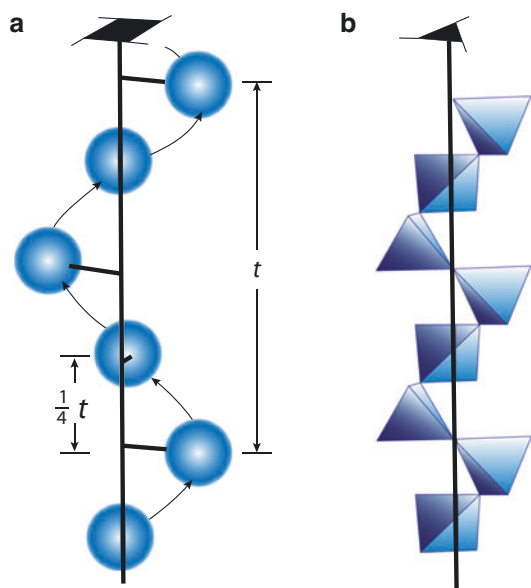
Crystal Chemistry, Fig. 7 (**a**) A schematic 4_1 screw axis consisting of successive 90° right-handed rotations followed by translations of one-fourth the repeat distance parallel to the rotation axis. (**b**) The helical chain of tetrahedra found in quartz; tetrahedra are related by a 3_2 screw axis

Crystal Chemistry, Table 4 Translational components of screw axes

Rotation	Translation[a]			
	$\frac{c}{2}$	$\frac{c}{3}$	$\frac{c}{4}$	$\frac{c}{6}$
180°	2_1			
120°		$3_1, 3_2$		
90°	4_2		$4_1, 4_3$	
60°	6_3	$6_2, 6_4$		$6_1, 6_5$

[a] 2_1 screw axes may be in other directions than parallel to c, depending on crystal system. All three-, four-, and sixfold screw axes are parallel to c; in the cubic system, a fourfold screw axis parallel to c requires one parallel to a and b as well

Space Groups

The combination of 14 Bravais lattices, 32 crystal classes, and glide planes and screw axes leads to 230 unique combinations of crystallographic symmetry elements that describe the symmetry of crystals on the atomic level (Burns and Glazer 1990). They are called space groups and are enumerated, diagrammed, and thoroughly explained in Hahn (1987). The determination of the space group of a particular mineral does not specify its atomic arrangement (i.e., crystal structure) but places limitations and requirements on the possible locations of atoms. For example, although tremolite and sanidine have entirely different crystal structures, they crystallize in the same space group and therefore possess identical symmetry properties.

The notation used for space groups provides the type of Bravais lattice, the crystal system, the crystal class, and the translational symmetry elements present and is best understood by analyzing an example. The space group of the clinopyroxenes, such as diopside, is $C2/c$. The first letter, always in upper case, is the Bravais lattice type – a C-centered lattice in this case. $2/c$ is the crystal class with translational symmetry elements replacing rotational symmetry elements, if applicable; in this case, a c-glide replaces the mirror plane that is normal to the diad. Thus the crystal class is $2/m$ and the crystal is monoclinic, but the atoms that would be related by a mirror plane are instead related by a glide operation.

Crystallochemical Phenomena

Polymorphism and Phase Transformations

Polymorphism is the existence of two or more different crystal structures with identical chemical compositions. (Technically, if only two structures exist for a given composition, they should be referred to as dimorphs, but the almost universal practice is to call them polymorphs.) Transformations between phases provide important information about the conditions of formation or the thermobaric history of a rock, and they can be described in several different ways (Price and Ross 1992; Hazen and Finger 1982):

1. Transformations in which atomic bonds are broken and rearranged (i.e., in which the topology is changed) are called reconstructive transformations. They are generally sluggish, often leading to the metastable persistence of phases under conditions of thermodynamic instability (Lasaga and Kirkpatrick 1981). For example, Al_2SiO_5 exists as the minerals kyanite, andalusite, and sillimanite, all of which have fields of stability in pressure–temperature (P–T) space and each of which possesses a quite different bond topology; nevertheless, all of these can be found in rocks that have been exposed at the Earth's surface, because the energy required to break and reform the bonds is unavailable under ambient conditions. Transformations that involve only shifts in atomic positions without the breaking of bonds leave bond topology unchanged and are called displacive transformations. These phase transitions are typically rapid and easily reversible. A good example is the β–α quartz transformation, which occurs around 573 °C at atmospheric pressure. When that temperature is reached from either above or below, the atomic transformation occurs immediately, regardless of the rate of temperature change; thus, β-quartz does not exist in rocks under surface conditions.

2. Another way of characterizing phase transformations is to examine changes in coordination polyhedra. If the number of anions around a cation changes as a result of the transition, then it is a change in primary coordination. Again, the Al_2SiO_5 polymorphs provide an example, and the change is apparent if the coordination numbers are written as upper

left superscripts in the chemical formulas: Kyanite is $^{[6]}Al^{[6]}Al^{[4]}SiO_5$, andalusite is $^{[6]}Al^{[5]}Al^{[4]}SiO_5$, and sillimanite is $^{[6]}Al^{[4]}Al^{[4]}SiO_5$. If no primary coordination numbers change, but the dispositions of polyhedra are altered (i.e., if the numbers and/or types of atoms in the second coordination sphere change), then this is a change in secondary coordination. The transition between quartz and tridymite, wherein all Si atoms in both phases are tetrahedrally coordinated, but the arrangements of tetrahedra are quite different, is of this type. If coordination numbers do not change, but the chemical species within polyhedra are rearranged, then the change is an ordering transformation. For example, two polymorphs of $KAlSi_3O_8$ are sanidine and microcline; they differ in the way in which Al and Si are ordered within the available tetrahedral sites.

3. Phase transformations can also be defined in thermodynamic terms based on the behavior of derivatives of the Gibbs free energy (G), defined as

$$G - H - TS \qquad (4)$$

where H is enthalpy, T is temperature, and S is entropy. Molar volume and entropy are first derivatives of G, and heat capacity, compressibility, and thermal expansion coefficient are second derivatives. If the first derivatives of G are discontinuous at the transformation temperature, the transformation is a first-order transition. If the first derivatives are continuous but the second derivatives are discontinuous, the transformation is of second order. If the second derivatives (particularly heat capacity, C_P) tend to infinity at the transition temperature, it is called a lambda transformation. Reconstructive transformations tend to be first order, displacive transformations are often second order, and the α–β quartz transition may be a lambda transformation.

4. If the new phase nucleates at discrete locations in the host phase and grows from these, the transformation is called a discontinuous phase transition. If, on the other hand, the transformation occurs simultaneously throughout the host by structural modulation of the parent atomic arrangement, the transformation is a continuous phase transition.

A single example of the information available from the study of phase transformations must suffice. Consider the Ca-poor clinopyroxene, pigeonite. At high temperature, it crystallizes in space group $C2/c$, so that all of the tetrahedral chains (see Fig. 6c, d) are identical. As the temperature decreases, the site in which the small amount of Ca present is concentrated contracts, causing different rotations in what had previously been two symmetrically identical tetrahedral chains. This yields symmetrically different SiA and SiB chains and lowers the symmetry to $P2_1/c$. The transformation is rapid and displacive. Because either chain in the $C2/c$ structure can become the SiB chain in the $P2_1/c$ structure, the "choice" is made differently in different parts of the crystal, and when the microdomains of consistent "choice" meet, they are out of phase with one another. This antiphase domain texture can be observed by transmission electron microscopy and provides information on the thermal history of the sample.

Solid Solution and Exsolution

Many minerals exist in ranges of compositions that are limited by three factors:

1. The crystal structures of all compositions exhibited by a mineral must be topologically identical (i.e., they may differ only by small distortions).
2. The atoms (or ions) that substitute for one another must have roughly the same radii.
3. Electrostatic neutrality must be retained by the substitutions.

If all three requirements are met and a range of compositions is in fact observed, the mineral is said to exhibit solid solution. The requirement for similarity in radii is important but only approximate; a rule of thumb often stated is that the radii should be within 15% of each other. Electrostatic neutrality may be maintained either by substituting ions that have identical oxidation numbers or by substituting ions in combination with one another (coupled substitutions) so that overall neutrality is maintained.

Consider, for example, the feldspars. The plagioclase feldspars consist of the solid solution series $NaAlSi_3O_8$–$CaAl_2Si_2O_8$ (albite to anorthite). The crystal structures are topologically identical; the effective ionic radii of Na and Ca in 7-coordination are 1.12 Å and 1.06 Å, respectively; and the substitution $Na^+Si^{4+} \leftrightarrow Ca^{2+}Al^{3+}$ meets the requirement for electrostatic neutrality. Thus, to a first approximation, the plagioclase feldspars display a complete solid solution series between the two end members. The alkali feldspars are those with compositions between albite and $KAlSi_3O_8$ (compositionally called orthoclase, although it can exist in several polymorphs). Like Na, K is monovalent, but its radius is 1.46 Å. At high temperature, atomic vibrations make the effective sizes of Na and K similar, and complete solid solution occurs. As temperature decreases, however, the size difference becomes important, and at low temperatures, there is only limited solid solution; that is, a small amount of K can substitute in crystals of albite-rich composition, and a small amount of Na can substitute in crystals of K-rich composition. Between the K and Ca end members, solid solution is even more restricted.

If alkali feldspar crystallizes at high temperature as a homogenous phase in a magma, and then the temperature is slowly lowered (as, e.g., in a cooling pluton), the feldspar becomes unstable because of the substantial crystallographic

strains required to accommodate both K and Na in the same lattice. The result is a solid-state migration of K and Na, which separate into regions of high K and regions of high Na concentration. If the bulk composition is nearer the K end member, then a K-rich feldspar becomes the host to exsolution "stringers" or lamellae of an Na-rich phase; if it is nearer the Na end member, then the reverse occurs. Although feldspars have been used for illustration, solid solution is extremely common for many important mineral families, and exsolution occurs when solid solution behavior for end members differs significantly over the temperature range experienced by the mineral.

Other Phenomena

Among the many other phenomena that arise from the crystal chemistry of minerals are color, elastic and vibrational properties, ordering of atomic species in preferred crystallographic sites, polytypism, twinning, compositional zoning, hydration and surface phenomena, and others. Space does not permit more than this brief enumeration, but the bibliographic listings include works that delve into all of these areas and more (Boisen and Gibbs 1985; Burdett 1995; Deer et al. 2013; Griffen 1992; Kieffer and Navrotsky 1985; Jaffe 1988; Vaughan and Pattrick 1985).

Cross-References

▶ Atomic Absorption, Inductively Coupled Plasma Optical Emission Spectroscopy, and Infrared Spectroscopy
▶ Crystal Chemistry
▶ Crystal Field Theory
▶ Diffusion
▶ Dolomite and Dolomitization
▶ Electron Probe Microanalysis (EPMA)
▶ Geochemical Thermodynamics
▶ Ionic Radii
▶ Kinetics of Geochemical Processes
▶ Mineral Defects
▶ Mineralogy
▶ Phase Equilibria
▶ Solid Solution/Exsolution
▶ Stoichiometry
▶ Surface Geochemistry
▶ X-Ray Diffraction

References

Berry FJ, Vaughan DJ (eds) (1985) Chemical bonding and spectroscopy in mineral chemistry. Chapman and Hall, New York. 325 pp
Boisen MB Jr, Gibbs GV (1985) Mathematical crystallography, Reviews in Mineralogy, vol 15. Mineralogical Society of America, Washington, DC. 460 pp
Brown ID, Shannon RD (1981) The bond–valence method: an empirical approach to chemical structure and bonding. In: O'Keefe M, Navrotsky A (eds) Structure and bonding in crystals, vol 2. Academic, New York, pp 1–31
Burdett JK (1995) Chemical bonding in solids. Oxford University Press, New York. 319 pp
Burdett JK, McLarnen TM (1984) An orbital interpretation of Pauling's rules. Am Mineral 69:601–621
Burns G, Glazer AM (1990) Space groups for solid state scientists. Academic, San Diego. 343 pp
Deer WA, Howie RA, Zussman J (2013) An introduction to the rock-forming minerals. The Mineralogical Society, London. 498 pp
Gibbs GV (1982) Molecules as models for bonding in silicates. Am Mineral 67:421–450
Griffen DT (1992) Silicate crystal chemistry. Oxford University Press, New York. 442 pp
Hahn T (ed) (1987) International tables for crystallography, vol A. D. Reidel Publishing Company, Dordrecht. 878 pp
Hazen RM, Finger LW (1982) Comparative crystal chemistry: temperature, pressure, composition, and the variation of crystal structure. Wiley, New York. 231 pp
Jaffe HW (1988) Crystal chemistry and refractivity. Cambridge University Press, Cambridge. 335 pp
Kieffer SW, Navrotsky A (eds) (1985) Microscopic to macroscopic, Reviews in mineralogy, vol 14. Mineralogical Society of America, Washington, DC. 428 pp
Lasaga AC, Kirkpatrick RJ (eds) (1981) Kinetics of geochemical processes, Reviews in mineralogy, vol 8. Mineralogical Society of America, Washington, DC. 398 pp
Megaw HD (1973) Crystal structures: a working approach. Saunders, Philadelphia. 563 pp
Pauling L (1929) The principles determining the structure of complex ionic crystals. J Am Chem Soc 51:1010–1026
Price GD, Ross NL (eds) (1992) The stability of minerals. Chapman and Hall, London. 368 pp
Putnis A, McConnell JDC (1980) Principles of mineral behaviour. Elsevier, New York. 257 pp
Tolédano J, Tolédano P (1987) The Landau theory of phase transitions. World Scientific Publishing Co., Singapore. 451 pp
Vaughan DJ, Pattrick RAD (eds) (1985) Mineral surfaces. Chapman and Hall, London. 370 pp

Crystal Field Theory

Hans Keppler
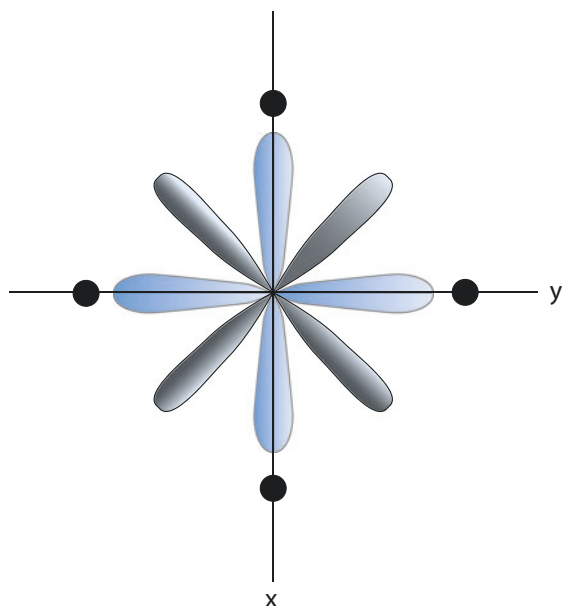Bayerisches Geoinstitut, University of Bayreuth, Bayreuth, Germany

Crystal field theory is a model describing the interaction between the electric charges of a cation and the surrounding anions. A more sophisticated version of this model, which includes covalent bonding effects, is the ligand field theory. Very frequently, however, the terms crystal field theory and ligand field theory are used synonymously. Crystal field

theory can be used to extract thermodynamic properties (crystal field stabilization energies) from optical spectra of minerals and other substances. By considering crystal field stabilization energies, many features of the geochemistry of transition metals can be explained.
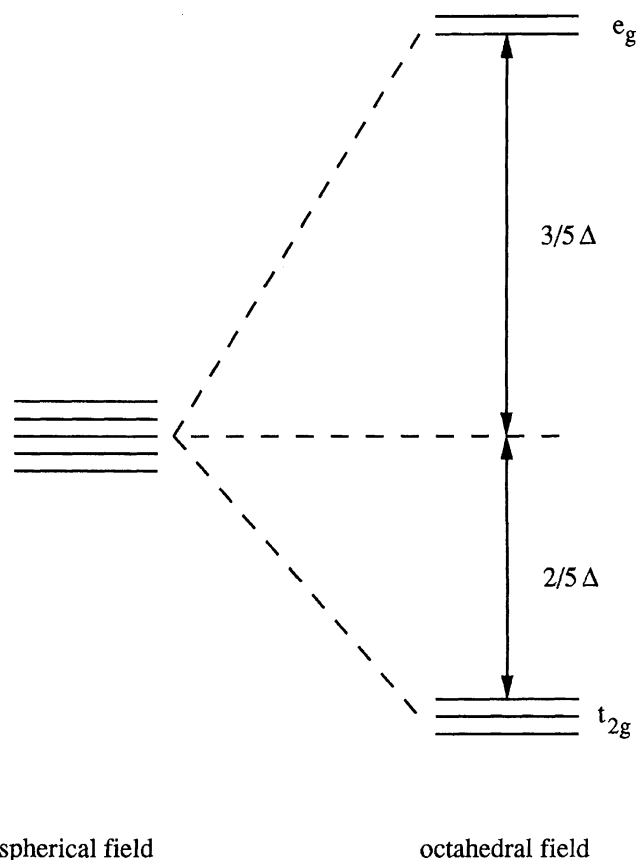
The basic idea of crystal field theory is related to the fact that the charge distribution of the d- and f-orbitals in cations is not spherically symmetrical. This means that the repulsive electrostatic forces between the electrons in these orbitals and the surrounding anions (ligands) depend on the relative orientations of the anions. This is shown schematically in Fig. 1. If one considers the charge density of d-orbitals in the xy-plane of a Cartesian coordinate system, the d_{xy} orbital has maximum charge density (maximum probability to find an electron) between the coordinate axes. The $d_{x^2-y^2}$ orbital, on the other hand, has the maximum charge in the direction of the coordinate axes. If the cation is surrounded by six anions in octahedral coordination, these anions can be grouped in the directions of the coordinate axes (four in the xy-plane, one in $+z$, and one in $-z$ direction), as shown in Fig. 1. Obviously, the electrostatic repulsion between these anions and the $d_{x^2-y^2}$ orbital will be stronger than the repulsion between the anion and the d_{xy} orbital. Therefore, the energy of an electron in the $d_{x^2-y^2}$ orbital will be higher than in the d_{xy} orbital. In vacuum or in a spherically symmetrical field, however, the energies of these orbitals are equal – they are said to be degenerate. Therefore, the effect of the electrical field of the anions is to split the d-orbitals into groups of different energies. The

magnitude of this splitting is called the crystal field splitting Δ. A detailed analysis shows that an octahedral field splits the five d-orbitals into two levels, the t_{2g} level (d_{xy}, d_{xz}, d_{yz} orbital) and the e_g level ($d_{x^2-y^2}$, d_{z^2} orbital). The magnitude of the splitting follows the so-called center of gravity rule, which means that the average energy of the five orbitals must equal the energy of the orbitals in a spherically symmetric field. This condition is only fulfilled if relative to a spherically symmetrical field the t_{2g} levels are lowered in energy by $2/5\Delta$ while the e_g levels are raised by $3/5\Delta$. This situation is schematically depicted in Fig. 2.

The type and magnitude of the crystal field splitting depend on the geometry of the coordination polyhedron. It can be shown, for example, that in a tetrahedral environment, the effect of the crystal field splitting is opposite to the octahedral case, i.e., the energies of d_{xy}, d_{xz}, and d_{yz} are raised, while the energies of $d_{x^2-y^2}$ and d_{z^2} are lowered. Other things being equal, the magnitude of the crystal field splitting in a tetrahedral field will be 4/9 of that in an octahedral field. Furthermore, if the symmetry of the coordination polyhedron is lower than cubic, i.e., if the coordination tetrahedron or octahedron is distorted, additional splittings of energy levels can be induced. For example, $d_{x^2-y^2}$ and d_{z^2} orbitals no longer

Crystal Field Theory, Fig. 1 Orientation of the $d_{x^2-y^2}$ (*light blue*) and d_{xy} (*dark*) orbitals of a cation relative to the xy-plane of a Cartesian coordinate system. The positions of anions surrounding the cation in octahedral coordination are indicated as *black dots*. Four of these anions are in the xy-plane, one is above in $+z$, and one below in $-z$ direction

Crystal Field Theory, Fig. 2 Splitting of the energies of d-orbitals in an octahedral environment. Δ is the crystal field splitting

need to have the same energy in a distorted octahedral or tetrahedral environment.

Crystal field theory was originally derived for cations in a crystal lattice (Bethe 1929). However, exactly the same formalism can be applied to cations in liquids (silicate melts, aqueous solutions) and even gases. The effects described by crystal field theory are almost completely due to interactions within the first coordination shell, so that the medium and long-range order in the phase considered is not important.

The splitting of d-orbital levels by interaction with the charges in the first coordination sphere has important consequences if the d-orbital shell is not completely filled. Consider, for example, an ion with three d-electrons, such as Cr^{3+}, in an octahedral environment. In the ground state of the ion, the three electrons will occupy the d_{xy}, d_{xz}, and d_{yx} orbitals (the t_{2g} level, Fig. 2). The $d_{x^2-y^2}$ and d_{z^2} orbitals are empty. This has the following consequences:

1. Relative to Cr^{3+} in a spherically symmetric electrostatic field, the energy of the octahedrally coordinated Cr^{3+} ion will be lowered. Since the t_{2g} level is lowered by 2/5Δ and there are three electrons in this level, this effect stabilizes the octahedral Cr^{3+} by 6/5Δ. This energy is called the crystal field stabilization energy (CFSE). CFSE is often in the order of the free energy of chemical reactions (several 10 or 100 kJ/mol). In the case of ions which have very large CFSE, such as octahedral Cr^{3+} or Ni^{2+}, one can often predict the direction of a reaction or the approximate value of an equilibrium constant by considering the CFSE of the ions in the phases involved. Such considerations have been very fruitful for predicting the partitioning of transition metal ions between different sites in a crystal (e.g., tetrahedral and octahedral sites in spinel) as well as for predicting the partitioning between different phases (minerals and silicate melts). However, it is important to note that the CFSE amounts only to a maximum of 20–30% of the total bonding energy, which means that other effects can also be important.

2. Since the three electrons in Cr^{3+} occupy those orbitals which have the weakest interaction with the anions, while the orbitals that are closest to the anions are empty the effective ionic radius of octahedral Cr^{3+} is lower than expected for a spherically symmetrical charge distribution. Crystal field theory can therefore explain irregularities in the ionic radii of transition metal ions.

3. If the Cr^{3+} ion interacts with electromagnetic radiation, electrons can be promoted from the t_{2g} into the e_g level. This gives rise to absorption bands in the near-infrared, visible, and ultraviolet region of the electromagnetic spectrum. These spectra can be used to detect the oxidation state and coordination number of transition metals.

Moreover, the crystal field splitting and crystal field stabilization energy can easily be obtained from such spectra. A fully quantitative interpretation of the spectra requires a modification of the simple electrostatic model of crystal field theory that allows for some covalent bonding effects. This model is often called ligand field theory. Covalent bonding implies that the electrons are not completely localized at the cation any more, but they can be "smeared out" over the anions. This effect will reduce the interelectronic repulsion, because the average distance between the electrons increases. The Racah parameter B is a measure for interelectronic repulsion and can be obtained from optical absorption spectra. If there is some covalent bonding, the Racah parameter will be reduced relative to the value for the free ion in vacuum. In order to obtain both the crystal field splitting and the Racah parameter from spectroscopic data, the Tanabe–Sugano diagrams (Tanabe and Sugano 1954) are used which are plots of the energies of the possible states of an ion as a function of Δ and B.

If the d-electron levels are completely filled, the CFSE is zero, and no optical absorption due to transitions within the d-orbital levels can occur. Ions with incompletely filled f-orbitals (lanthanides and actinides) are in principle subjected to crystal field effects. These effects, however, are relatively small, since the f-electrons are strongly shielded from the surrounding electrostatic fields. Therefore, crystal field theory is primarily a tool for understanding the chemistry and geochemistry of transition metal ions which contain partially filled d-orbitals.

A special situation can arise, for example, for octahedrally coordinated cations having four d-electrons, such as Cr^{2+} or Mn^{3+}. In these cations, three electrons will occupy the t_{2g} level, while one electron is in the e_g level, i.e., either in the $d_{x^2-y^2}$ or the d_{z^2} orbital (see Fig. 2). In an undistorted octahedron, the energies of the $d_{x^2-y^2}$ orbital and the d_{z^2} orbital are identical. This means that there are two possible ground states (states with lowest energy) of the ion, depending on which one of the two e_g orbitals contains an electron. This is often expressed by saying that the ground state of these ions is degenerate. However, if the octahedron is slightly distorted, the degeneracy is lifted, since then the two orbitals will have different energy. Since the e_g electron can then reside in the orbital with the lower energy ($d_{x^2-y^2}$ or d_{z^2}, depending on the type of distortion), generally this effect will lower the total energy of the system. Therefore, the coordination polyhedron of ions with a degenerate ground state, such as octahedral Cr^{2+} or Mn^{3+}, will always be distorted. This is known as the Jahn–Teller effect. As a consequence of this effect, cations such as Cr^{2+} or Mn^{3+} will prefer the more distorted sites in

crystal structures, if several sites of approximately equal size are available.

In most coordination environments, the crystal field splitting is small compared to the energy necessary to cause spin pairing of electrons. This means that if five electrons are present in an octahedrally coordinated cation, three will occupy the t_{2g} and two the e_g-level (Fig. 2). Any additional electrons will then enter these orbitals with antiparallel spin. However, in some cases the crystal field splitting can become so large that spin pairing is induced. In this case, up to six electrons will first enter the t_{2g} level, and only after that the e_g level can be filled with additional electrons. This means that for some cations, two different electronic configurations are possible, depending on the magnitude of the crystal field splitting: the high-spin configuration (where the vectorial sum of the electron spins is maximum) for low Δ and the low-spin configuration for high Δ. Certain ligands, such as sulfide, can cause Δ to be very large; therefore, many transition metal sulfides are in the low-spin state. Oxides and silicates under normal conditions are in the high-spin state. It is possible, however, that they convert into the low-spin state at extreme pressures prevailing in the lower mantle. Since the high-spin to low-spin transition changes the configuration of the outer electron shell, this could completely change the geochemical behavior of the elements involved.

A good introduction into the theoretical background of crystal field theory is the book by Figgis (1966). Symmetry aspects are discussed by Cotton (1971). Geochemical applications can be found in Burns (1985, 1993) and Rossman (1988).

Cross-References

▶ Atomic Absorption, Inductively Coupled Plasma Optical Emission Spectroscopy, and Infrared Spectroscopy
▶ Crystal Chemistry
▶ Free Energy
▶ Geochemical Thermodynamics
▶ Mineral Defects
▶ Mineralogy
▶ Solid Solution/Exsolution
▶ Transition Elements

References

Bethe H (1929) Termaufspaltung in Kristallen. Ann Phys 3:133–206
Burns RG (1985) Thermodynamic data from crystal field spectra. Rev Mineral 14:277–316
Burns RG (1993) Mineralogical applications of crystal field theory, 2nd edn. Cambridge University Press, Cambridge. 551 pp
Cotton FA (1971) Chemical applications of group theory, 2nd edn. Wiley, New York. 386 pp
Figgis BN (1966) Introduction to ligand fields. Wiley, New York. 351 pp
Rossman GR (1988) Optical spectroscopy. Rev Mineral 18:207–254
Tanabe Y, Sugano S (1954) On the absorption spectra of complex ions. J Phys Soc Jpn 9:753–779